UNIVERSITA' DEGLI STUDI DI VERONA

DIPARTIMENTO DI BIOTECNOLOGIE

SCUOLA DI DOTTORATO IN SCIENZE DELLA VITA E DELLA SALUTE

DOTTORATO DI RICERCA IN
BIOTECNOLOGIE MOLECOLARI INDUSTRIALI ED AMBIENTALI

CICLO XXVII / 2012-2014

Photoprotection in oxygenic photosynthesis: A reverse genetic study

S.S.D. BIO/04

Coordinatore:: Ch.mo Prof. Roberto Bassi

Supervisore: Ch.mo Prof. Roberto Bassi

Dottorando: Dott. Stefano Cazzaniga

Contents

Summary

Light is essential for photosynthesis and life on earth and yet it is harmful for plants. When photons are absorbed in excess with respect to the capacity of photosynthetic electron transport, reactive oxygen species are produced that causes photoinhibition, limiting plant growth and productivity. Oxygenic photosynthetic organisms have evolved photoprotective mechanisms to prevent/avoid photodamage. Among these, the Non-Photochemical Quenching (of chlorophyll fluorescence) or NPQ is of particular interest. NPQ has been reported to quench the chlorophyll excited states thus catalyzing the thermal dissipation of energy absorbed in excess. Over the past decades many efforts have been made to elucidate the mechanisms underlying these processes. Besides academic curiosity, manipulation of thermal dissipation rate and its regulation in response to environmental cues appears to be the key for both enhancing stress resistance and productivity for food and fuels.

In my PhD I used a reverse genetic approach on the model organism *Arabidopsis thaliana* to disentangle and characterize the role of different components of photoprotective mechanisms as well as their contribution to acclimation to abiotic stresses. Of particular interest have been the generation and analysis of mutants defective in carotenoids biosynthesis, specific xanthophyll binding proteins and in the chloroplast light avoidance mechanism.

Section A. Role of carotenoids in photoprotection and composition of photosynthetic complexes.

Carotenoids fulfill several important functions in photosynthesis. They have a major role in photoprotection, contribute to the assembly and stability of photosynthetic complexes and act as photoreceptors. Photoprotection is catalyzed through (i) the quenching of chlorophyll triplets, (ii) the scavenging of singlet oxygen and other ROS, and (iii) the heat dissipation of excess singlet excited states (NPQ). In higher plants carotenoids can be grouped in two major classes: **carotenes** which are polyenes with cyclic groups in both ends and **xanthophylls,** oxygenated derivatives of carotenes. I studied biosynthesis mutants with altered levels of individual carotenoid species.

A1. A quadruple mutant of *Arabidopsis thaliana* reveals a β-carotene hydroxylation activity for LUT1/CYP97C1 and a regulatory role of xanthophylls on determination of the PSI/PSII ratio.

Xanthophylls play a crucial role in the photosynthetic apparatus of higher plants. Their composition is remarkably conserved and consists of five major xanthophylls: lutein, violaxanthin, neoxanthin, antheraxanthin and zeaxanthin.

Xanthophylls biosynthesis in plants is organized in two distinct branches: the α branch leads to the formation of the ε-β-hydroxylated xanthophyll lutein from α-carotene, while the β branch leads to the production of β-β-hydroxylated xanthophylls (zeaxanthin, antheraxanthin, violaxanthin and neoxanthin) from β-carotene. The first step consists into the hydroxylation of α- and β-carotene. Two different classes of enzymes are involved: the ferredoxin-dependent di-iron oxygenases (CHY1 and CHY2) which are active in β-ring hydroxylation, and the cytochromes P450 (LUT1/CYP97C1, LUT5/CYP97A3), which are active in hydroxylation of both the ε-ring and β-ring of α-carotene.

We have introduced the *lut2* mutation in the *chy1chy2lut5* background of *A. thaliana*. LUT2 is the lycopene epsilon-cyclase enzyme that converts lycopene to α-carotene; the mutant *lut2* is thus blocked in lutein biosynthesis.

Surprisingly, the *chy1chy2lut2lut5* mutant showed increased abundance of β-β-xanthophylls with respect to *chy1chy2lut5*. This evidenced that the LUT1 protein, previously reported to act in α-carotene hydroxylation only, in fact had a major β-carotene hydroxylation activity in the absence of α-carotene.

The *chy1chy2lut2lut5 showed a higher photosensitivity with respect to chy1chy2lut5.* NPQ amplitude was strongly reduced in the *chy1chy2lut2lut5* mutant, its amplitude being close to zero, supporting the correlation between xanthophyll content and the efficiency of quenching reactions.

The analysis of the pigment-protein complexes in the *chy1chy2lut2lut5* mutant showed that while LHCB proteins are strongly decreased with respect to PSII, the LHCI proteins are maintained with the same stoichiometry with respect to PSI reaction center. Unexpectedly, in spite of its correct folding, the abundance of PSI reaction center is drastically reduced in *chy1chy2lut2lut5* with respect to wild type. Upon analysis of genotypes having different xanthophyll/carotenoid ratios, we showed that xanthophyll availability correlates with PSI/PSII ratio within a wide range, controlling either PSI synthesis or degradation.

A2. The *Arabidopsis thaliana nox* mutant lacking carotene hydroxylase activity reveals a critical role for xanthophylls in photosystem I biogenesis.

Each xanthophyll species has a specific role in photoprotection but their collected importance as a class of compounds distinct from carotenes had not been assessed. During my PhD, we isolated and characterized the *A. thaliana chy1chy2lut1lut5* quadruple mutant (referred to as *nox*), which lacks all xanthophylls but retains carotenes.

Knockout of the four hydroxylase genes completely abolished xanthophyll biosynthesis, thus confirming that CHY1, CHY2, LUT1, and LUT5 constitute the full complement of carotenoids hydroxylases in

A. thaliana. The phenotype included depletion of light-harvesting complex subunits and impairment of NPQ, two effects consistent with the location of xanthophylls in photosystem II antenna. The biogenesis of the photosynthetic apparatus was strongly affected in *nox* plants, and this resulted in reduced photosynthetic electron transport and increased photosensitivity. The *nox* was unable to sustain photoautotrophic growth in low light and rapidly underwent photoinhibition in moderate light. Thus, xanthophylls appeared to be essential not only for photoprotection but also for biogenesis of the photosynthetic machinery.

In section A1 the decrease in the xanthophylls/carotenoids ratio was shown to cause a proportional decrease in the abundance of PSI core units with respect to PSII. We showed that *nox* leaves fail to accumulate PSI complexes, thus confirming the need for xanthophylls in PSI biogenesis. This result was surprising, since there is no evident reason for the preferential effect of xanthophyll depletion on PSI versus PSII core complexes; PSI core complexes bind chlorophyll *a* and β-carotene as the only pigments, which are not limited in *nox*. Biochemical analysis revealed that the *nox* mutant was specifically depleted in photosystem I function due to a severe deficiency in PSAA/B subunits. While the stationary level of PSAA/B transcripts showed no major differences between genotypes, the stability of newly synthesized PSAA/B proteins was decreased and translation of PSAA/B mRNA was impaired in *nox* with respect to wild type plants. Xanthophylls, besides their role in photoprotection and LHC assembly, are also needed for photosystem I core translation and stability. We suggest that a linear relation between the abundance of LHCB proteins connected to PSII, controlling its antenna size, and the total amount of PSI-LHCI complex is functional to the maintenance of physiological redox poise of plastoquinone pool during acclimative response to light intensity.

A3. The *Arabidopsis thaliana szl1* Mutant Reveals a Critical Role of β-Carotene in Photosystem I Photoprotection.

While xanthophyll biosynthesis mutants of *A. thaliana* and *Chlamydomonas reinhardtii* have revealed distinct photoprotective roles in vivo for xanthophyll species, until recently no photoautotrophic mutant had been described showing a selective β-carotene loss, thus hampering the elucidation of function for this species. Recently, the *A. thaliana* mutant *szl1*, that carries a point mutation of lcyB gene, decreasing lycopene β-cyclase activity with respect to the wild type, was identified. Due to the cooperative action of the four carotene hydroxylase enzymes that catalyze the downstream reactions leading to xanthophylls synthesis, a depletion in β-carotene with respect to wild type plants is produced in the mutant, offering the opportunity of specifically probing carotene function *in vivo* in the presence of a level of xanthophylls similar to wild type.

The *szl1* plants, besides lower carotene content, also showed a lower β,β/ε,β-xanthophylls and a slight accumulation of α-carotene with respect to wild type. For these reasons we included the *chy1chy2*

and *lut5* genotypes in this characterization as controls. The *chy1chy2* double mutant has a reduced conversion of β-carotene into β,β-xanthophylls, yielding the same β,β/ε,β-xanthophylls ratio as the *szl1* plants. The *lut5* genotype had a level of carotenes similar to wild type but accumulates α-carotene.

When exposed to High Light (HL) at low temperature, *szl1* plants showed the highest levels of photodamage measured as pigment bleaching and lipid peroxidation. This effect was not due to β,β-xanthophylls content or α-carotene accumulation, since *szl1* was more photoinhibited than *chy1chy2* and *lut5.* The increased photoinhibition was specifically due to the decreased β-carotene content.

The *szl1* plants were specifically affected in PSI complex, leading to a dramatic photosensitivity of PSI activity at all light intensities. It is particularly remarkable that PSI, which in the literature has been considered to be far more resistant than PSII, was preferentially affected by the deficiency of carotenes. In fact, while the PSII photoinhibition and PSII repair efficiency were very similar for the different genotypes, the *szl1* was far more sensitive to PSI photoinhibition, as shown by a 6-fold-faster PSI photoinhibition rate. The $^1O_2$ yield was 2-fold higher in the PSI-LHCI from *szl1* with respect to that from the wild type, while PSII core complexes from all genotypes showed a similar yield in $^1O_2$.

The regulation of PSI Chl excited states under HL and cold stress is crucial for protection of the photosynthetic apparatus. While PSII has an efficient repair machinery, the recovery of PSI from photoinhibition takes several days and the damage to PSI is considered to be essentially irreversible thus involving degradation and re-synthesis of the whole complex. Taken together, the above results showed that carotene ligands to PSI are crucial in ensuring its photoprotection.

A4. Zeaxanthin protects plant photosynthesis by modulating chlorophyll triplet yield in specific light-harvesting antenna subunits.

Xanthophylls are involved in a number of photoprotection mechanisms, being active in preventing over-excitation of reaction centers by quenching ^{1}Chl* states and quenching ^{3}Chl* by carotenoid triplet (^{3}Car*) formation, thus avoiding $^1O_2$ generation. Moreover, they scavenge ROS whenever formed. Among xanthophylls, zeaxanthin (Zea) is of particular interest because it is accumulated in the excess light only and it increase high light stress resistance.

Earlier reports have emphasized some effect of zeaxanthin accumulation, including the enhancing effect on NPQ, the PSBS-dependent thermal dissipation of ^{1}Chl* excited states. However, genetic dissection showed that thermal dissipation of excess energy accounts for a relatively small fraction of Zea photoprotection activity as assessed by comparing *npq1npq4* to *npq4* (*npq1* constitutively lacks Zea, *npq4* lacks PSBS). Thus, understanding the Zea-dependent photoprotection mechanism(s), their location and dependence on ^{1}Chl*/^{3}Chl* quenching, ROS scavenging or other factors was to be obtained.

First, we evaluated the photoprotective effect of lipid-free versus LHC-bound Zea using a mutant, *ch1*, which cannot accumulate LHC antenna proteins. We showed that the ROS scavenging activity of free

Zea had a small effect on photoprotection which was strongly enhanced by Zea binding to LHC proteins. In this condition a strong negative effect on $^1O_2$ production was observed.

By using time-resolved differential spectroscopy *in vivo*, we studied ^{3}Car* optical spectra and identified a Zea-dependent spectral form red shifted in triplet-minus-singlet spectra of leaves and, upon fractionation, on specific pigment-binding LHC proteins. This signal was found in the sub-family of monomeric CP24, CP26 and CP29 subunits of PSII and the LHCA1–4 subunits of PSI but it was not present in the major LHCII antenna proteins. The red spectral shift was correlated to resistance to excess light conditions, i.e. with the dominant component of Zea-dependent photoprotection: monomeric LHCB, without Zea, were preferentially destroyed in excess light. The hypothesis that Zea could quench chlorophyll triplets specifically in the monomeric antenna complexes of Photosystem II was confirmed by fluorescence-detected magnetic resonance spectroscopic analysis. These results showed that the high light-induced binding of Zea to key proteins located in between the major antenna proteins and PSII reaction centers plays a major role in enhancing photoprotection by modulating the yield of potentially dangerous chlorophyll-excited states and preventing the production of singlet oxygen *in vivo*.

Section B. Disturbed excitation energy transfer in *Arabidopsis thaliana* mutants lacking minor antenna complexes of photosystem II.

The “minor” antenna protein of PSII, CP24, CP26 and CP29, have been proposed to be involved in the mechanism of thermal dissipation of excitation energy in excess. Elucidating the molecular details of NPQ induction in higher plants has proven to be a major challenge. The role of individual subunits has been investigated using reverse genetics but depletion of single monomeric LHCB proteins could not completely abolish NPQ, implying redundancy within the subfamily members. The making of a mutant lacking all three monomeric proteins was important in order to verify whether NPQ can be sustained in the absence of this class of gene products sharing the common properties of binding Zea in site L2 and having intermediate location between LHCII and the Core Complex.

Upon extensive breeding, we were able to isolate a mutant completely deleted of minor antenna that we called *NoM* for **No M**inor antenna. In order to isolate knock-out lines of *A. thaliana* lacking two or three minor antennae, *kolhcb4.1*, *kolhcb4.2* (CP29), *kolhcb5* (CP26) and *kolhcb6* (CP24) homozygous KO lines were identified in seed pools using specific antibodies raised against single antenna proteins. KO double mutants *kolhcb5kolhcb6* retained CP29 as the only minor antenna, while deletion of both CP29 isoforms in the *kolhcb4.1kolhcb4.2* double mutant results in a plant retaining CP26 as the only minor antenna, since accumulation of CP24 is hampered in this genotype. Triple mutant *kolhcb4.1kolhcb4.2kolhcb5* actually lacked all minor antennae: indeed, deletion of both lhcb4.1 and lhcb4.2 yielded a plant devoid of CP29, and lack of CP29 hampered CP24 stability and accumulation; thus the triple

KO only retains subunits of the major antenna complex LHCII. In this section I present preliminary results on this genotype.

When grown in control conditions *NoM* plants were much smaller than wild type. The pigment content of mutant thylakoids showed a significant decrease in the Chl *a*/Chl *b* ratio with respect to the membranes from wild type, reflecting the relative decrease in outer antenna. The PSI/PSII ratio was essentially the same as in the wild type, while the LHCII/PSII showed an increase by ~45%. The *NoM* mutant lacked the antenna complex CP29–CP24–LHCII and was completely devoid of PSII supercomplexes. The missing minor complexes are not replaced by other LHCs, implying that they are unique among the antenna subunits and crucial for the functioning and macro-organization of PSII.

Thylakoid membranes of wild type, the double knock-out mutants *koCP26/24* and *koCP29/24* (as controls) and *NoM* were been studied by time-resolved fluorescence spectroscopy. The lifetime of PSI component was similar in all the mutants while that of PSII-LHCII was far slower in the three mutants and, especially, in the *NoM*. Using a two excitation wavelength analysis of the fluorescence decay upon picoseconds excitation, it was possible to determine that a large part of the LHCII trimer was detached from PSII core and was found in a quenched state in the *NoM*, possibly aggregated in LHCII-only clusters. The same measure, when performed on *koCP26/24* and *koCP29/24* mutants, showed that only one LHCII trimer was directly (specifically) connected to the PSII core (or two LHCII trimers per PSII core dimer) in these genotypes whereas all other trimers are interspersed between the supercomplexes and still lead to relatively good excitation energy transfer, not hampering plant growth.

A key consideration for the efficiency of primary productivity in plants and algae is the size of the light-harvesting system: theoretical simulation of net CO_2 uptake suggested that a smaller antenna size would significantly improve photosynthetic efficiency on crop canopies. However, strategies to improve light penetration must ensure that truncated antenna mutants are not photosynthetically impaired. The present results showed that depletion of even a sub-group of LHCs strongly affects the PSII light-harvesting efficiency and thus limits photoautotrophic growth.

Section C. Role of Chloroplast relocation in photoprotection and its contribution in defining NPQ kinetic.

Besides relying in dissipative mechanisms located within the chloroplasts, plants can also avoid over-excitation by decreasing light absorption. This is obtained by relocating chloroplasts within the cell: the ‘avoidance response’ relocates chloroplasts alongside cell walls where they shade each other and decrease overall leaf photon absorption. In low light, instead, the ‘accumulation response’ directs chloroplasts toward the cytosolic layer along the periclinal cell walls maximizing light harvesting. In *A. thaliana,* accumulation and avoidance responses are mediated by phototropins PHOT1 and PHOT2. The

phot2 mutant lacks PHOT2, a membrane-bound serine/threonine kinase receptor activated by blue light: its chloroplasts remains always aligned on periclinal cell walls regardless of light intensity, making *phot2* plants more susceptible to photodamage than wild type when exposed to HL. Although the photoprotective actions of chloroplast avoidance, NPQ or Zea synthesis have been previously investigated, their relative contribution to photosynthetic efficiency in HL is unknown. We evaluated their relative photoprotective effect under excess light. During these analyses we also found out new insight for the interpretation of the fluorescence decay kinetics of leaves.

NPQ curves identified three kinetic components: qE, the fast phase ($\tau_{½}$ ~1 min); a middle phase ($\tau_{½}$ ~10–20 min); qI, the slow phase of relaxation ($\tau_{½}$ > 1 h). As the rapidly-reversible qE component provides a major contribution to NPQ amplitude, it has been investigated more thoroughly than the other components. It depends on ΔpH gradient across the membrane, PSBS protein and Zea. The intermediate kinetic component was alternatively attributed to state transitions and PSBS-independent Zea quenching. I found out that the intermediate phase of the apparent NPQ kinetics strongly depended on the chloroplast avoidance movement rather than on genuine fluorescence quenching effects.

C1. Interaction between avoidance of photon absorption, excess energy dissipation and zeaxanthin synthesis against photooxidative stress in *Arabidopsis thaliana*.

In order to evaluate the relative photoprotective effect of NPQ and chloroplast relocation, we have produced double mutants impaired in the chloroplast avoidance movement (*phot2*) and in either the qE activity (*npq4)*, or the Zea synthesis (*npq1)*, and analyzed their photoprotection performance *in vivo*. Suppression of avoidance response resulted in oxidative stress under excess light at low temperature, while removing either Zea or PSBS had a milder effect. The double mutant *phot2npq1* and *phot2npq4* showed the highest sensitivity to photooxidative stress, indicating that xanthophyll cycle and qE have additive effects over the avoidance response. Our results highlight a crucial role of chloroplast photorelocation response as compared to other protective mechanisms.

The interactions between non-photochemical quenching and avoidance responses were studied by analyzing fluorescence decay and recovery at different light intensities in wild type and *phot2*. The rapidly induced qE activity was the same in both genotypes but the NPQ kinetics evidenced that *phot2* fluorescence decay lacked the intermediate ($\tau_{½}$ ~10–20 min) component. The same component was induced in wild type by white light but not by red actinic light. We showed that the intermediate phase of NPQ kinetics strongly depended on the chloroplast avoidance movement, while it was not affected by Zea synthesis, photoinhibition or state1-state2 transitions. On these bases, we suggested that chloroplast photorelocation, rather than xanthophyll cycle, is the main process contributing to the quenching component previously described as qT or qZ. This decay kinetic component represented a light-induced decrease in photon absorption which leads to a decrease in fluorescence yield rather than the building up

of a genuine quenching process. During illumination, chloroplast movement towards the anticlinal cell walls changed the distribution of pigments with the formation of areas with extremely high absorption due to the formation of localized chloroplast stacks. This produces a 'sieve effect' which reduces the photon dose absorbed by the ensemble of chloroplasts, thus yielding into a reduced Chl fluorescence emission. When using fluorometry this event can easily be interpreted as a fluorescence quenching. Thus, we decided to rename the intermediate component of NPQ decay curves as "qM", for chloroplast **M**ovement.

C2. On the origin of a slowly reversible fluorescence decay component in the *Arabidopsis thaliana npq4* mutant.

We proceeded to a further characterization of qM using the mutant *npq4*. The *npq4* mutant lacks the qE component but maintain the same qM of wild type thus allowing dissecting qM without the qE "background". The middle phase component is not related to PSII photoinhibition or ΔpH slow relaxation after illumination. Instead, we found that it was uncoupler-sensitive and that the fluorescence decline was prevented in leaves infiltrated with the ionophore nigericin.

In order to search for the molecular basis of this process, the *npq4* genotype was crossed with others, which blocked different mechanisms known to alter NPQ activity, and the fluorescence quenching kinetic was analyzed on the double mutants obtained. Zea and Lute did not affect the amplitude of qM. Mutants depleted in LHC proteins showed the same fluorescence decay as *npq4*. The *npq4stn7* mutant (blocked in state transition) had the same qM as *npq4*.

The *npq4phot2* mutant confirmed that qM is affected by chloroplast relocation and absent when using red light actinic excitation. Light microscopy analysis confirmed that movement of chloroplasts was inhibited in the presence of nigericin, consistent with the depletion in qM. Nigericin wrecks all the transmembrane electrochemical gradients, thus blocking several signal transduction events. The double effect of nigericin in collapsing the thylakoid pH gradient and in blocking chloroplast relocation can easily lead to misinterpretation of qM as a slow qE response in the absence of PSBS. Although chloroplast relocation is the major factor affecting the amplitude of qM in *npq4*, the fluorescence recovery kinetics of *npq4phot2* were not completely devoid of qM. The residual component accounts for about 18% of total reversible quenching in wild type and reflects a mechanism sensitive to uncouplers and yet distinct from the avoidance response.

Previous reports had hypothesized that *npq4* plants lacking PSBS were nevertheless competent in quenching, although the process was slower than in wild type plants. Our results showed that no qE occurs in *npq4* leaves within a wide range of actinic light intensities. Moreover, light-induced fluorescence decline was always far lower in *npq4* than in wild type plants, even upon one hour of exposure to high light. Overall, these results point to a crucial role of PSBS in the modulation of NPQ and show that sensing of

trans-thylakoid ΔpH by protonatable residues in the LHC is not enough to induce wild type levels of NPQ in the absence of PSBS.

While most of my thesis work focused on fundamental aspects of photosynthesis, I devoted a fraction of my time to attempt exploiting the concepts established in basic research to applied problems: the utilization of biomass from microalgae for feed and fuel production. This is one of the key elements for the development of a sustainable and secure energy supply and I would greatly be satisfied by contributing to solving such a crucial problem for society.

Appendix A. Domestication of the green alga *Chlorella sorokiniana*: reduction of antenna size improves light-use efficiency in a photobioreactor.

Among the different microalgae, *Chlorella* species are of interest because of their high productivity, high lipid content, and resistance to the high light conditions typical of photobioreactors. However, the economic feasibility of growing algae at an industrial scale is yet to be realized, in large part because of biological constraints that limit biomass yield. A key issue is the inefficient use of light due to uneven light distribution in photobioreactors, and the dissipation of excess absorbed light as heat. The successful implementation of biofuel production facilities requires the development of algal strains with enhanced light use efficiency in photobioreactors. Such domestication strategies include decreasing the absorption cross section in order to enhance light penetration, increasing the size of metabolic sinks per chlorophyll and minimizing feedback energy dissipation.

During my PhD we applied random mutagenesis and phenotypic selection to *Chlorella* species *C. sorokiniana*. Truncated antenna mutants (TAMs) were selected that exhibited a lower fluorescence yield than the wild type strain. Six putatively interesting mutants were selected by high throughput fluorescence video imaging, two of which, *TAM-2* and *TAM-4*, were found to have approximately half the chlorophyll content per cell and LHCII complement per PSII with respect to the wild type. In batch culture, *TAM-2* showed an increased photon use efficiency, yielding a higher P_{max} at saturating irradiances with respect to the wild type. Cultivation of *TAM-2* in both laboratory-scale and outdoor photobioreactors showed higher productivity than wild type, with a 30% higher biomass yield in dense cell suspensions typical of industrial photobioreactors.

Appendix B. Biogenesis of photosynthetic complexes in the chloroplast of *Chlamydomonas reinhardtii* requires ARSA1, a homolog of prokaryotic arsenite transporter and eukaryotic TRC40 for guided entry of tail-anchored proteins.

The generation and screening of pale green mutant was also performed in *C. reinhardtii*, a model organism for microalgae that is suitable for random genetic transformation and which genome sequence is available, thus allowing the identification of the mutations. Random insertion mutagenesis of *C. reinhardtii* and phenotype screening identified a mutant severely affected in chlorophyll content, down to about 8% of the wild type level, named *as1*, for **a**ntenna **s**ize mutant ***1***. The mutant was found to carry an insertion into a gene homologous to prokaryotic arsenite transporter (ARSA), whose yeast and mammal counterparts were found to be involved in the targeting of tail-anchored (TA) proteins to cytosol-exposed membranes, essential for several cellular functions. During my PhD we characterized the first insertion mutant in an ARSA-homolog gene and showed it has a strong effect on photosynthesis.

This mutant showed a light-harvesting antenna size of both photosystems significantly reduced with respect to wild type and a smaller chloroplast size. It showed a general reduced level of photosynthetic polypeptides.

ARSA1 protein was localized in the cytosol and we demonstrated that it is necessary for the insertion of the TA-protein TOC34 into the outer chloroplast membrane. TOC34 is a key component of the outer chloroplast membrane translocon complex that performs the physical task of translocating the nuclear proteins across the double membrane envelope of the chloroplast. In the *as1* mutant, no trace of TOC34 can be detected thus explaining the extreme pale phenotype since many genes of photosynthetic complexes are nuclear encoded.

Introduction

1.1 Oxygenic Photosynthesis

Photosynthesis is the process that converts the light energy of the sun into chemical energy in plants, green algae and cyanobacteria. In oxygenic photosynthesis, the initial substrates are water, used as electron donor, and carbon dioxide that is converted in carbohydrates like sucrose, glucose or starch, following this reaction:

$$nH2O + nCO2 + light \rightarrow (CH2O)n + nO2$$

Oxygen is generated as secondary product. This is one of the most important chemical processes on Earth: the production of oxygen and assimilation of carbon dioxide into organic matter determines the composition of our atmosphere and provides all heterotrophic organisms with essential food and fuel. All organisms depend directly or indirectly from the solar energy conversion.

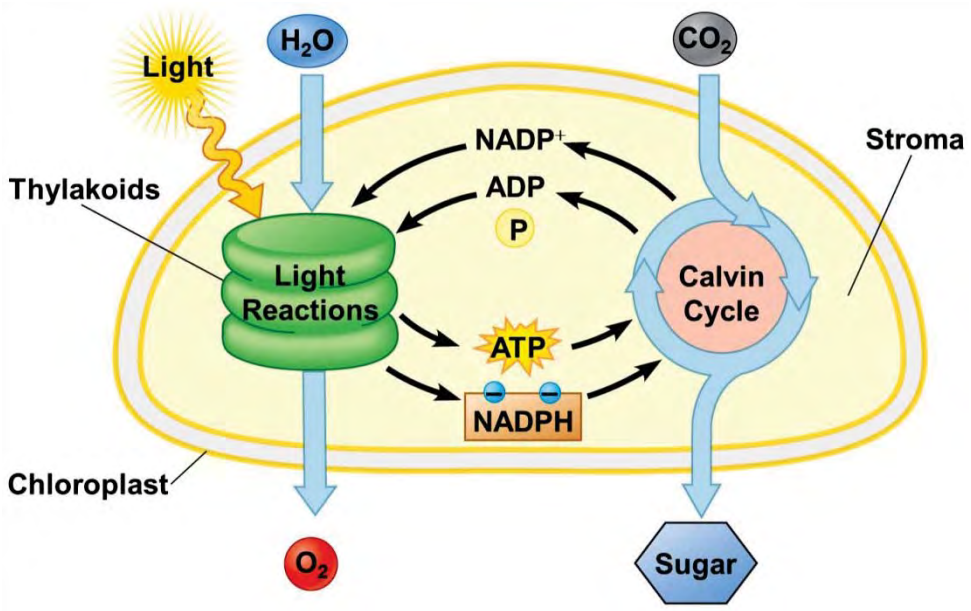

Figure 1. *Schematic representation of light and dark reactions in photosynthesis (Pearson Education 2012).*

Photosynthesis consists of both light-dependent and light-independent reactions (fig. 1). In the light-depended phase, sunlight is absorbed by pigment molecules and the energy was transferred to the reaction centre of the two photosystems where charge separation occurs. This event induces a set of electron transfer reactions leading to the formation of a proton gradient across the thylakoid membrane and finally to the generation of free energy and reducing power, in the form of ATP and NADPH.

Meanwhile, each chlorophyll molecule replaces its lost electron with an electron from water, generating oxygen as consequence:

$$2\ NADP^{+} + 2H_2O + light \rightarrow 2\ NADPH + O_2 + 2H^{+}$$

$$ADP + Pi + energy \rightarrow ATP$$

In the light-independent phase energy from the ATP and NADPH molecules generated by the light reactions are used to reduce carbon dioxide from the atmosphere to a three-carbon sugar called glyceraldehyde-3-phosphate (GAP). Cells then use GAP to build a wide variety of other sugars (such as glucose) and organic molecules:

$$3\ CO_2 + 9\ ATP + 6\ NADPH \rightarrow GAP + 9\ ADP + 8\ Pi + 6\ NADP+$$

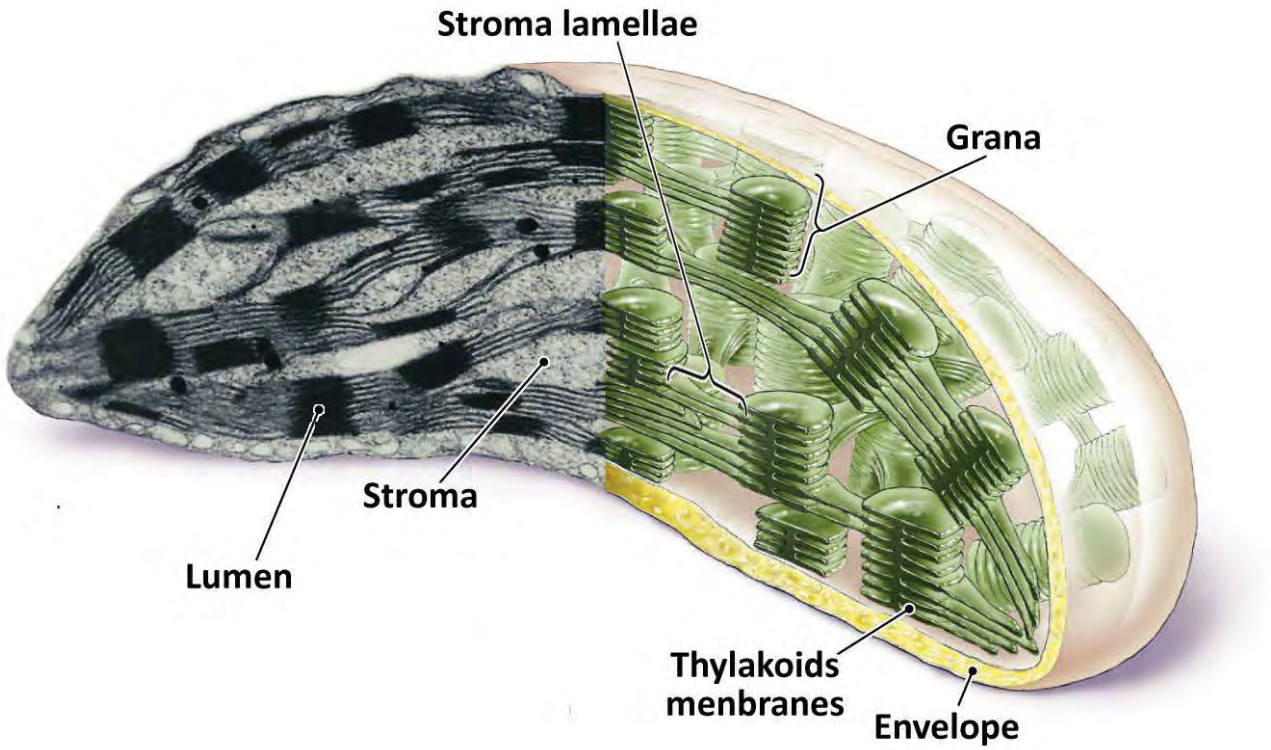

Figure 2. *Transmission Electron Microscopy merged to a schematic reconstruction of a chloroplast structure (Pearson Education 2006).*

In photosynthetic eukaryotes, photosynthesis occurs in organelles called chloroplasts in which both light-dependent and independent phases take place. Chloroplasts have a diameter of 5-10 µm and a depth of 3-4 µm. They are limited by two membranes (together called envelope): the first one is highly permeable, while the second one contains specific transporters which mediate the flux with the cytoplasm. The soluble phase delimited by the envelope membranes is called stroma and contains all enzymes

catalyzing the light-independent reactions and the plastidial DNA, RNA and ribosomes. A third membrane system, the thylakoids, is found in the stroma and it confines a second compartment, the lumen. This membrane presents an extensive folding and an inhomogeneous structure. They consist of two main domains: the grana, which are stacks of thylakoids, and the stroma lamellae, which are unstacked thylakoids and connect the grana stacks (fig. 2) (Barber 1980). Complexes that catalyze the light reaction, embedded into thylakoid membrane, are not evenly distributed throughout it: PSII and LHCII reside mainly in the grana membranes, while PSI and ATPase reside predominantly in the stroma and the cytochrome b6/f complex is distributed in grana and grana margins (fig. 3). Protein–protein interactions determine for a major part the shape and folding pattern of the thylakoid membrane.

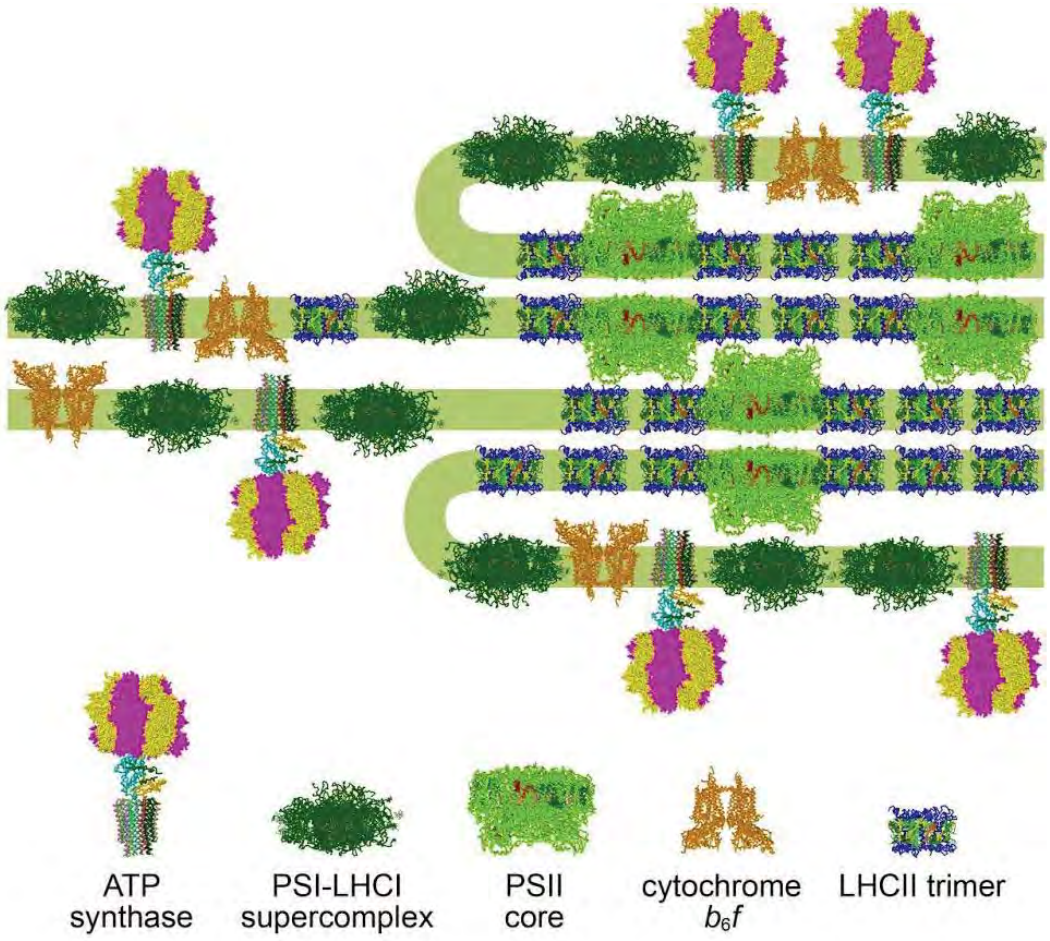

Figure 3. *Organization of protein complexes in thylakoid membranes (Nagy et al. 2014).*

1.1.1 The light-dependent phase

In thylakoid membranes there are four large membrane-protein complexes called photosystem I (PSI), photosystem II (PSII), cytochrome b6/f (Cyt-b6/f) and ATP synthase (ATPase) that drive light-dependent phase of oxygenic photosynthesis (fig. 4). These complexes catalyze the processes of light harvesting, electron transport and photo-phosphorylation, leading to the conversion of light energy to chemical free energy (ATP and NADPH). According to the partial reactions that they catalyze, PSII is defined

as a water–plastoquinone oxidoreductase, the cytochrome b6/f complex as a plastoquinone-plastocyanin oxidoreductase, PSI as a plastocyanin-ferredoxin oxidoreductase and the ATPase as a pmf (proton motive force) driven ATP synthase.

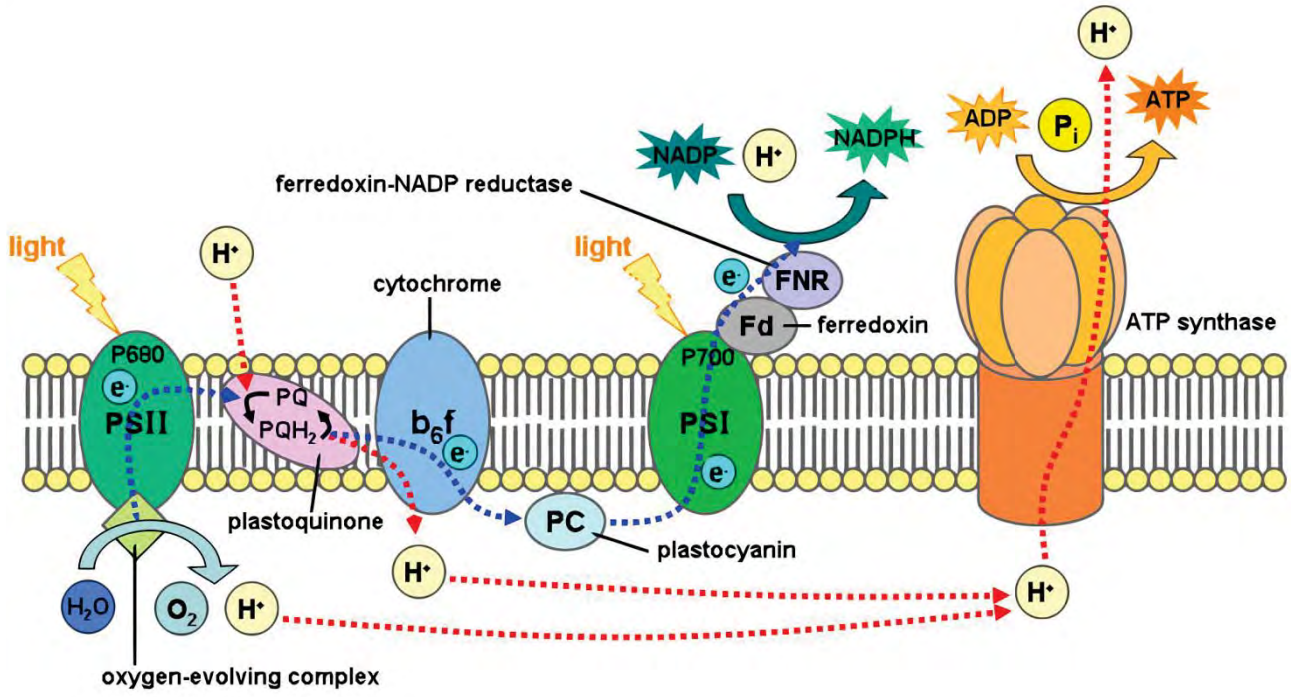

Figure 4. *The light phase of photosynthesis. A schematic organization of the major protein complexes in thylakoid membranes and electron transport chain is shown.*

PSI and PSII binds a large number of pigments that harvest light within the visible region. The excitation energy is transferred among individual pigment molecules via a mechanism called “Forster’s transfer”. The energy transfer requires that pigment molecules are in close contact with each other. This is an energetically down-hill reaction, and energy is thus preferentially transferred from chlorophyll *b* (max≈647 nm) to chlorophyll *a* (max≈663 nm). Due to difference in the redox potential, larger than the energy content of a red photon, between the electron donor (oxygen in a water molecule) and final electron acceptor during the light phase of photosynthesis (NADP+), two photosystems work in series in order to accumulate the energy of two photons, as described in the so called Z-scheme (fig. 5)(Hill and Bendall 1960).

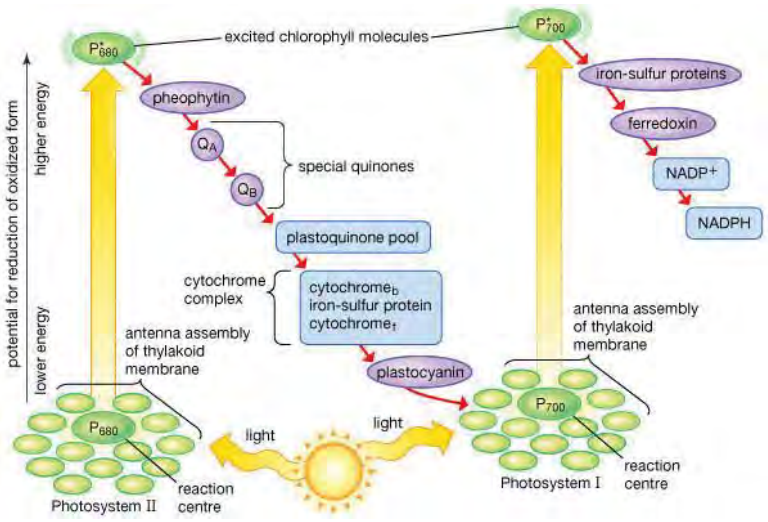

Figure 5. *The Z-scheme of Bendall and Hill. Cofactors involved in electron translocation between H_2O and NADP+ are indicated*

After absorption of light by light-harvesting antenna of PSII, the excitation energy is transferred to a special pair of chlorophylls in the reaction centre (RC), named P680 (Primary electron donor absorbing at 680 nm) (fig. 5). Upon receiving the first energy quantum, an electron is released from P680 through an accessory chlorophyll and a pheophytin (Pheo) molecule to the tightly bound quinone Q_A, and this is followed by the reduction of a mobile quinone PQ at the Q_B site. $P680^+$, which has a high redox potentials, oxidizes a nearby tyrosine (Tyr_z); Tyr_z extracts an electron from a cluster of four manganese ions (OEC, oxygen-evolving complex), which binds two substrate water molecules (fig. 6A) (Zouni et al. 2001). After another photochemical cycle, the doubly reduced plastoquinone (PQ^{2-}) takes up two protons from the stromal space to form plastoquinol (PQH_2), which diffuses into the membrane toward the Cyt-b6/f complex and it's replaced by an oxidized quinone from the pool (fig. 7A). After two more photochemical cycles, the manganese cluster accumulates a total of four oxidizing equivalents, which are used to oxidize two water molecules leading to the formation of O_2, the release of protons in the inner thylakoid space and the return of manganese cluster to the reduced state (Ferreira et al. 2004).

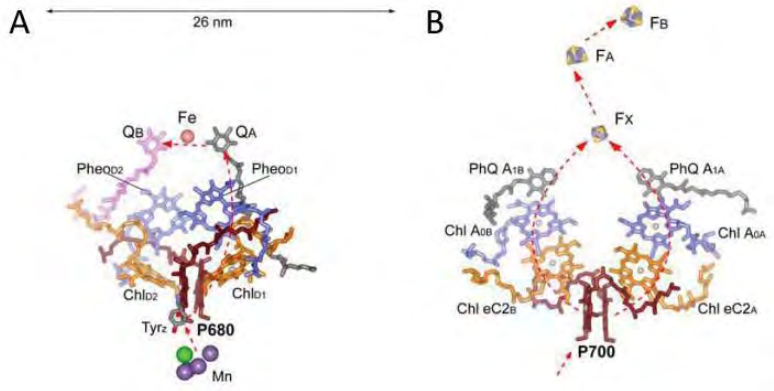

Figure 6. *Electron transfer reactions of PSII (A) and PSI (B) reaction centre (Caffarri et al. 2014)*

In Cyt-b6/f the electrons from the PQH_2 are transferred to plastocyanin (PC), a small, copper-containing protein (fig. 7). The resulting PQ is recycled to PSII while two protons are released into the inner thylakoid space increasing the pmf formed across the membrane. These reactions are called Q-cycle. The Q-cycle oxidizes two plastoquinols, reduces one PQ and one PC, and translocates 4 H^+ for every 2 electrons transported to PSI (Trumpower 1990).

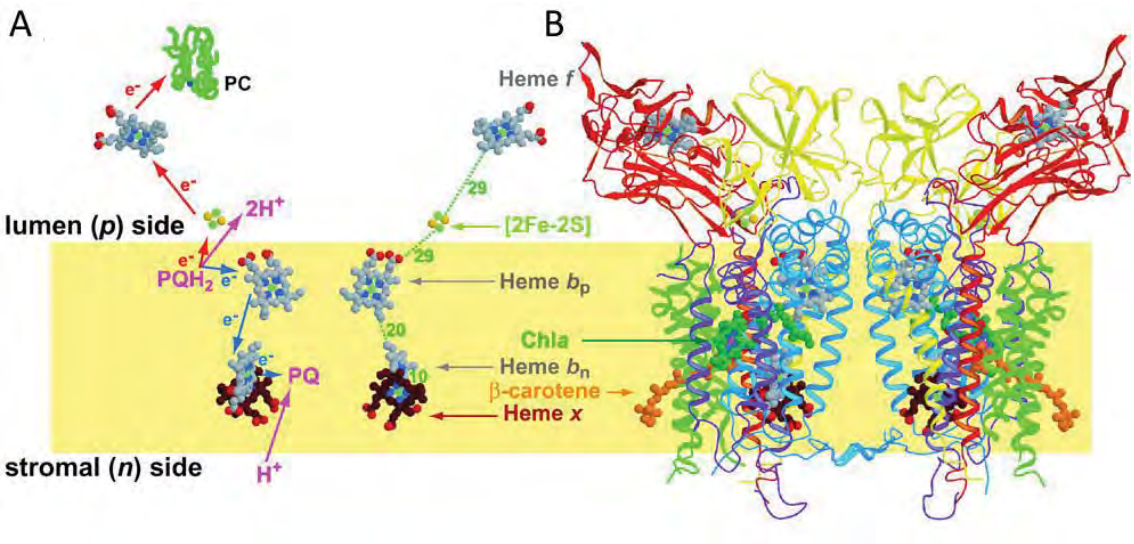

Figure 7. *Cytochrome b_6f complex. (A) Electron and proton transfer pathway through the b_6f complex and distances between redox cofactors. (B) Side view showing bound cofactors and protein subunits (Kurisu et al. 2003)*

In PSI, light is absorbed by the antenna pigments and the excitation energy is transferred to the RC. As in PSII, a special pair of Chls is present in the PSI-RC defined as P700 (Primary electron donor absorbing at 700 nm) (fig. 6B). P700 upon excitation releases an electron that reduces ferredoxin (Fd) on the stroma side. Reduced Fd is subsequently used in numerous regulatory cycles and reactions, like nitrate and CO_2 assimilation, fatty-acid desaturation and NADPH production through a $NADP^+$ oxidoreductase (Buchanan 1991). Both photosystems operate with a very high quantum yield but while PSII operates with a lower efficiency (about 0.85), PSI works with an almost perfect quantum yield of 1.0. Cyclic electron flow (CEF) or cyclic photophosphorylation is an alternative electron-transfer pathway that, unlike the prevailing linear flow (LEF), does not involve PSII (Harbinson and Foyer 1991). In this process, electrons are circled around PSI, Fd and the Cyt-b6/f complex; no NADPH is formed in this pathway but a pmf is generated by plastocyanin reduction.

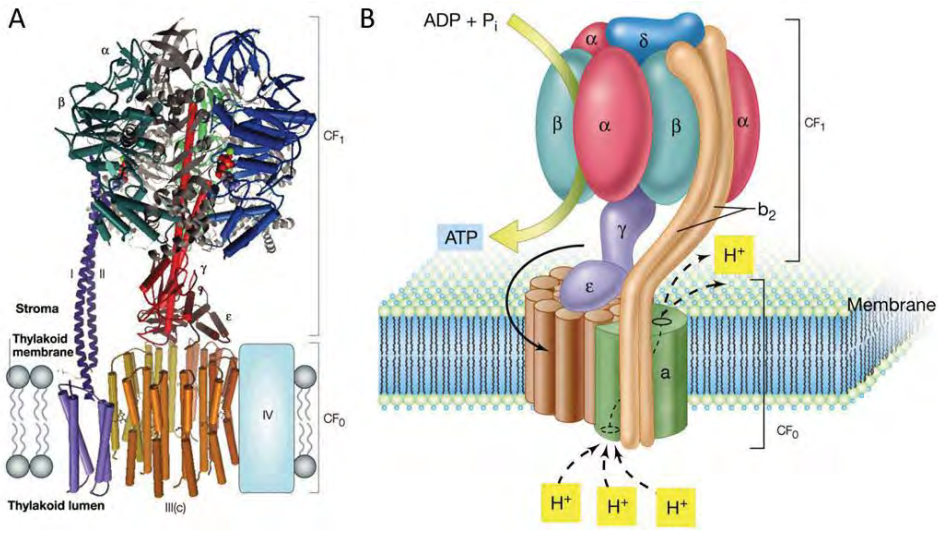

Figure 8. *Structure of ATPase. (A) 3D model created using available structural data for mitochondrial F-ATPase subcomplexes (Nelson and Ben Shem 2004). (B) Schematic model of ATPase.*

The charge separation in PSI and PSII, together with the electron transfer through the Cyt-b6/f and cyclic electron transport, leads to the formation of an electrochemical potential gradient, between the stromal and the lumenal side of the membrane, which powers ATP synthesis by the ATPase (Mitchell 1961). The ATPase enzyme is a multimeric complex with a stromal (CF1) and transmembrane regions (CF0). Proton transport through CF0 is coupled to ATP synthesis/hydrolysis in the β-subunits of CF1. The whole CF0-CF1 complex is thought to function as a rotary proton-driven motor, in which the stationary subunits are I, II, IV, δ, α and β, and the rotary subunits are III (c), γ and ε (fig. 8)(McCarty et al. 2000).

1.1.2 The dark phase

The dark phase of photosynthesis includes different reactions, on the whole indicated as Calvin cycle (Benson and Calvin 1950): through these reactions, atmospheric CO_2 is reduced to carbohydrates, using the chemical free energy (ATP and NADPH) produced during the light reactions (fig. 9).

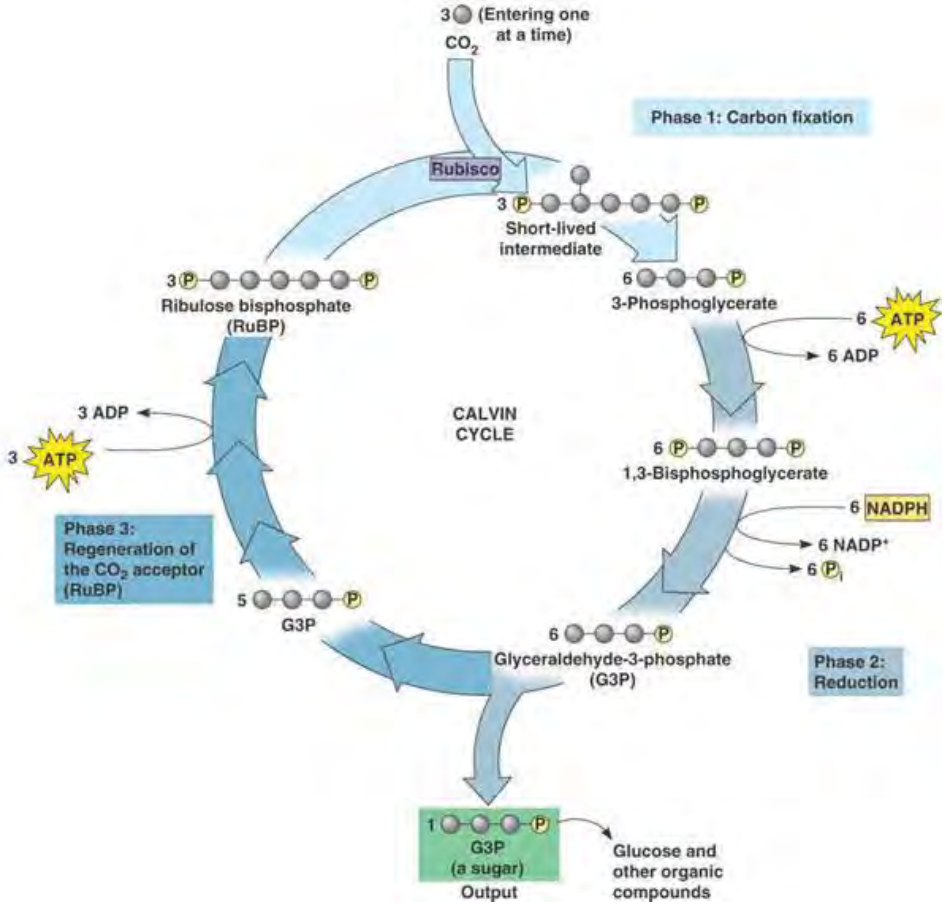

Figure 9. *Enzymatic steps involved in Calvin cycle.*

1.2 Photosynthetic pigments

Photosynthetic pigments are categorized into two chemical groups or “chromophores”: the chlorophylls (Chls) and carotenoids (Cars). The Chls are the pigments of the RCs and also occur in the core and light harvesting antennae. Specialized Chls at the reaction centre serve to trap the excitation energy and convert the electronic energy to chemical energy through charge separation. The Cars are accessory pigments that help collecting light and serve to protect Chls against photodamage.

1.2.1 Chlorophylls

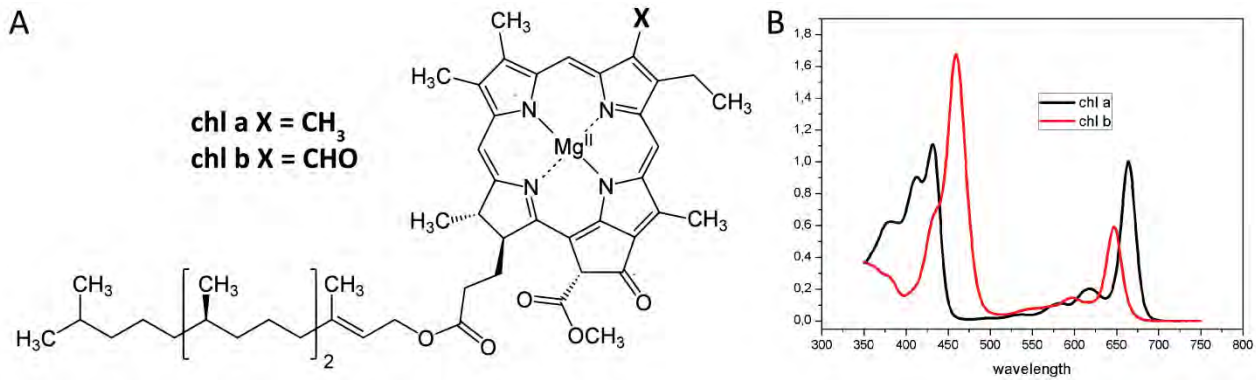

Figure 10. *Chlorophyll a and b. (A) Structure and (B) absorption spectra in acetone 80%.*

The most abundant light-harvesting pigments are Chls. Their structure consists of a cyclic tetrapyrrole (porphyrin) in which the four nitrogen atoms of the pyrroles coordinate an Mg atom and a long phytol chain esterified to the ring (fig. 10). The characteristic ability of Chls to absorb light in the visible region is due to the high number of conjugated double bonds present in these molecules. Chls are synthesized starting from the amino acid glutamic acid. In the first phase glutamic acid is converted to 5-aminolevulinic acid (ALA) than two molecules of ALA are then condensed to form porphobilinogen (PBG), which ultimately form the pyrrole rings in Chls. The next phase is the assembly of a porphyrin structure from four molecules of PBG. This phase consists of six distinct enzymatic steps, ending with the product protoporphyrin IX. Then the insertion of an Mg atom and the attachment of a fifth ring and of a phytol tail completes the biosynthesis (fig. 11).

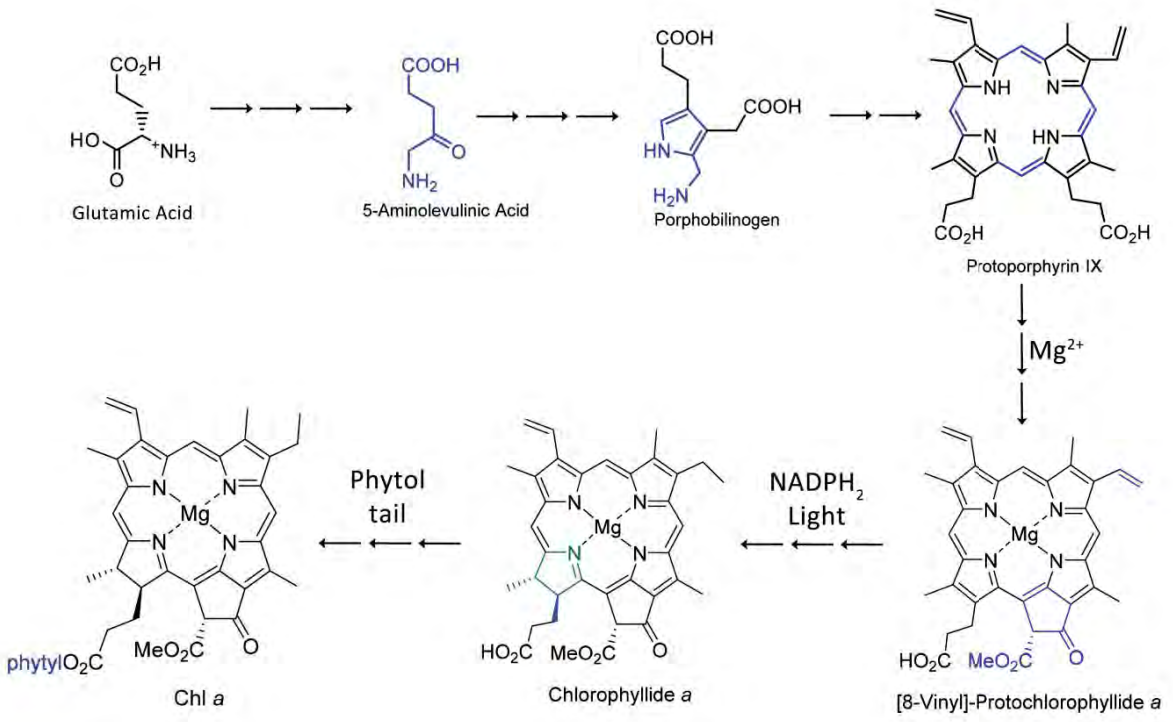

Figure 11. *Main steps of biosynthetic pathway of chlorophyll a.*

In photosynthetic organism 5 different types of Chls are present differing in their substitutions but in vascular plants only Chl *a* and Chl *b* are present. These two pigments are almost identical but Chl *a* has a methyl group on second pyrrole ring while Chl *b* has a formil group (fig. 10A). The Chl *a* and Chl *b* absorption spectra in solution do not completely overlap, this increase the spectral range over which light is absorbed, thus increasing the efficiency of light-harvesting (fig. 10B). The absorption spectra of the Chls present two main bands: the Qy transition is the red-most band, which peaks around 640-670 nm, respectively in Chl *b* and Chl *a* in organic solvent. It corresponds to the transition of an electron from S_0 to S_1 (the first excited state). The Soret band, on the contrary, corresponds to transitions to higher states. Its maximum is around 430 and 460 nm for Chl *a* and Chl *b,* respectively. The last absorption band of the spectrum is the weak Qx transition that appears around 580-640 nm and is partly masked by the Qy vibronic transitions. It corresponds to the transition from a ground state (S_0) electron to the second excited state (S_2). The strong absorption of both red and blue/violet light by Chls causes the green colors of most plants. The absorbance spectra of Chls is influenced by the protein complexes in which they are bound, such that there can be variations in the same type of pigment and the peak absorbance *in vivo* tend to be broadened and shifted compared to those of the pure pigments extracted in solution.

1.2.2 Carotenoids

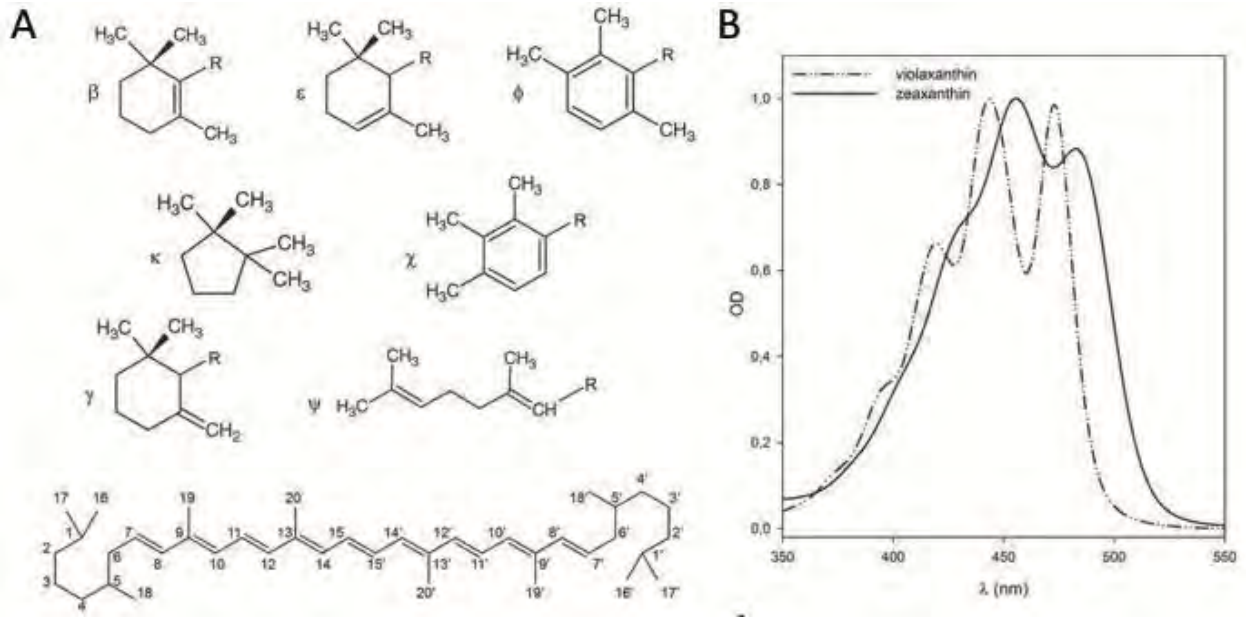

Figure 12. *Carotenoid structure. (A) Characteristic end groups of carotenoids and structure of a generic carotenoid with common numbering system. (B) Visible absorption spectra of violaxanthin and zeaxanthin in acetone.*

Cars are a class of more than 600 naturally occurring pigments synthesized by all photosynthetic organisms and some non-photosynthetic bacteria and fungi (Kull and Pfander 1995). They absorb in the blue-green region with pronounced absorption bands between 450 and 550 nm, where Chls do not absorb efficiently (fig. 12). Cars fulfill several important functions in photosynthesis. They contribute to the assembly and stability of photosynthetic complexes (Plumley and Schmidt 1987, Paulsen et al. 1993), act as photoreceptors (Mimuro and Katoh 1991, Gradinaru et al. 2000), and have a main role in photoprotection (Havaux and Niyogi 1999). Carotenoids protect the photosynthetic apparatus in different ways, including the quenching of chlorophyll triplets, scavenging of singlet oxygen, and the dissipation of excess light energy absorbed by the antenna pigments by non-photochemical quenching of chlorophyll fluorescence.

Plant carotenoids are tetraterpenes derived from the 40-carbon isoprenoid phytoene. These molecules consist of a polyene chain of alternating single and double bonds, with two rings at the end of the molecule (fig 12). Different levels of hydrogenation and introduction of oxygen-containing functional groups create a large family of carotenoids. In higher plants, they can be grouped in two major classes: carotenes which are hydrocarbons with linear structure and with cyclic groups in one or both extremities and xanthophylls which are oxygenated derivatives of carotenes. The conjugated double bond system of carotenoid molecules determines their photochemical properties. The π-electrons delocalization in the conjugated double bonds system leads to the light absorption in the visible range 400-500 nm. When Cars absorb light, electrons are transferred from ground state S_0 to the second excited singlet state S_2; this strongly dipole-

dipole allowed transition is responsible for the characteristic absorption spectrum. The first excited singlet state S_1 cannot be populated from the ground state by photon absorption due to symmetry reasons. The absorption spectra of Cars are strongly red-shifted *in vivo*, compared to their spectra in organic solvents. This shift represents a lowering of the S_2 energy level, which has been ascribed to the mutual polarizability of the carotenoid and protein environment (Andersson et al. 1991). In higher plants the most abundant carotenoids associated with thylakoid membranes are the α- and β-Carotene (α-Car, β-Car) and the xanthophylls Lutein (Lute), Violaxanthin (Viola), Neoxanthin (Neo) and Zeaxanthin (Zea). Chloroplasts have a remarkably similar carotenoid composition in all plants, with Lute (45% of the total), β-Car (25–30%), Viola (10–15%) and Neo (10–15%) as the most abundant carotenoids (Britton 1995). Carotenes (mainly β-Car) are enriched in the photosystem reaction centre, whereas xanthophylls are most abundant in the light-harvesting complexes (Niyogi et al. 1997, Dall'Osto et al. 2007).

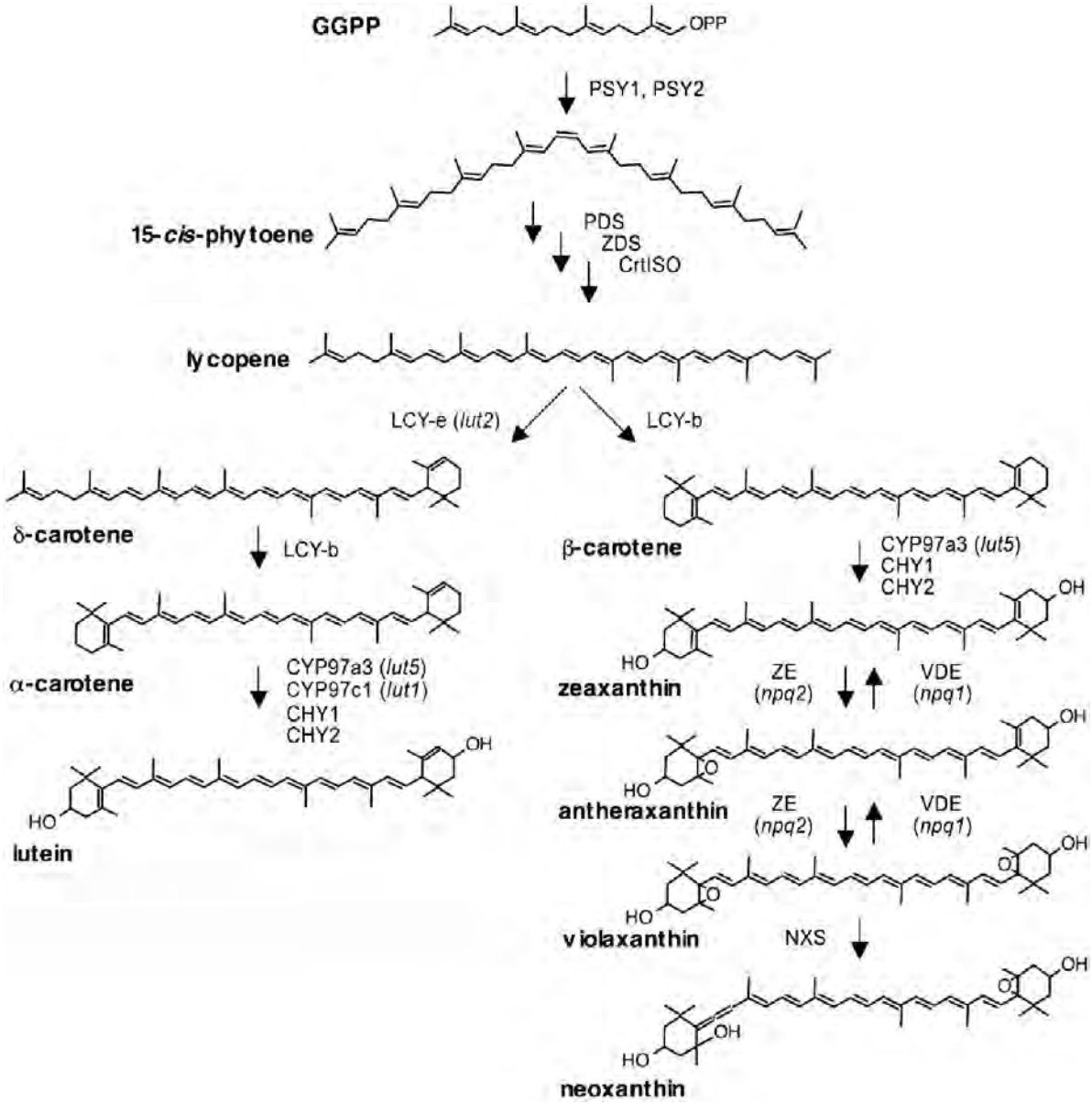

Figure 13. *Biosynthetic pathway of carotenoids in higher plants, with enzymes involved.*

Like all isoprenoids, Cars are synthesized from the five-carbon units isopentenyl diphosphate (IPP) and its double-bond isomer dimethylallyl diphosphate (DMAPP) (fig. 13). Addition of three IPP molecules to DMAPP generates geranylgeranyl diphosphate (GGPP). The condensation of two GGPP molecules produces the 40-carbon phytoene. Phytoene is then desaturated to create the chromophore-bearing chain of conjugated double bonds that forms the backbone of plant carotenoids and determines their physical and biological properties (Britton 1995). Desaturation and isomerization of uncolored phytoene eventually results in the production of lycopene, a red carotenoid. The cyclization of the ends of the lycopene polyene chain is the first branch point in the pathway and results in the production of carotenes either with one ß ring and one ε ring (α-Car) or with two β rings (β-Car). Carotenoids with two ε rings do not exist in *A. thaliana* and are uncommon in plants. Hydroxylation of the carotene rings generates xanthophylls such as Lute (from α-Car) and Zea (from β-Car). Zea is epoxidated twice to make Viola, which can be subsequently modified to make Neo. In Arabidopsis four enzymes provide for Chls hydrogenation: CHY1 and CHY2, two non-heme di-iron monoxygenase, which catalyze the hydroxylation of β ring only and CYP97A3 and CYP97C1, two heme-containing cytochrome P450 hydroxylases, which catalyze the hydroxylation of β and ε ring respectively.

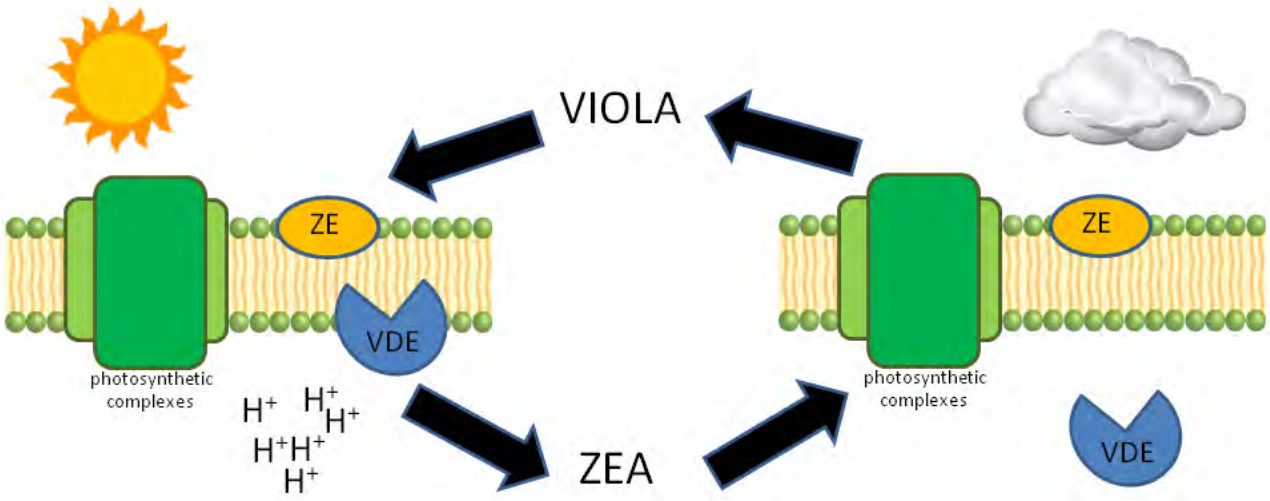

Figure 14. *Schematic representation of xanthophyll cycle.*

While hydroxylation of α-Car produces Lute, a carotenoid end-product that accumulates at high levels, hydroxylation of β-Car produce zeaxanthin that, under light conditions that do not saturate photosynthesis or in the dark, is readily converted to violaxanthin via antheraxanthin in a two-step reaction catalyzed by the enzyme zeaxanthin epoxidase (ZE). When light is strong and exceeds the photosynthetic capacity, Viola is de-epoxidated back into Zea by the activity of the enzyme violaxanthin de-epoxidase (VDE) (Yamamoto and Kamite 1972, Demmig-Adams et al. 1996) (fig. 14). The interconversion of Zea and Viola is known as the xanthophyll cycle and has a key role in the adaptation of plants to different light intensities (Dall'Osto et al. 2005). VDE is activated when light-driven proton translocation across the thylakoid membrane exceeds the dissipation rate of the proton gradient by ATPase, leading to a decrease

in pH in the thylakoid lumen while ZE is always active. The xanthophyll cycle is uniquely separated on opposite sides of the thylakoid membrane; VDE activity takes place on the thylakoid lumen side of the membrane, whereas ZE occurs on the chloroplast stromal side (Hieber et al. 2000). Xanthophyll cycle is a key component of several photo-protective mechanisms as scavenging of ROS, thermal dissipation of excitation energy in excess or Chls triplets excited state quenching (Niyogi 1999, Holt et al. 2004).

1.3 Photosystems

PSI and PSII are multi-protein complexes binding the pigments responsible for light harvesting and charge separation. Both are composed of a core complex, where Chls special pairs and cofactors involved in electron transport are located and a peripheral antenna system, composed by Chls binding proteins responsible for light harvesting and energy transfer to the reaction centre (RC). Chls and Cars are bound both by core complex and antenna system; core complexes bind only Chl *a* and carotenes, while antenna proteins bind Chl *a*, Chl *b* and xanthophylls. The core complexes have been well conserved during the evolution, as most of the subunits are similar in prokaryotic and eukaryotic photosystems and only a few are specific to each group. On the contrary, the peripheral antenna system displays great variability, being composed of peripheral associated membrane proteins in cyanobacteria, the phycobilisomes, and integral light harvesting complexes (LHC) membrane proteins in eukaryotic cells.

1.3.1 PSII Core complex

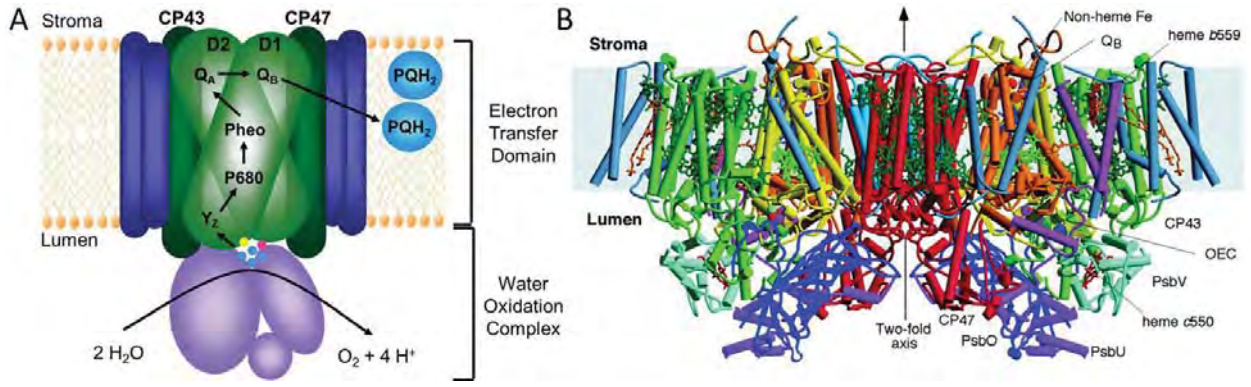

Figure 15. *(A) Schematic model for PSII and (B) 3D crystal structure of PSII core complex (Ferreira et al. 2004).*

Core complex of PSII is composed by the polypeptides denominated PSB encoded from both nuclear and plastidial genes. The core of PSII is a multi-subunit complex composed of about 25-30 subunits; it contains four large membrane-intrinsic subunits (PSBA-D), three membrane-extrinsic subunits (PSBO–Q) and a large number of small subunits (fig. 15), most of which span the membrane once and are involved in the dimerization or in Chls and Cars binding stabilization, but they do not all have a well-clarified function (Shi et al. 2012). PSBA (D1) and PSBD (D2) bind six Chl *a* and two Pheo *a* molecules and constitute the photochemical reaction centre in which the charge separation and primary electron transfer reactions take place. PSBB (CP47) and PSBC (CP43) bind 16 and 14 Chl *a* molecules respectively and have a light-harvesting function: they absorb light and transfer the excitation energy to the reaction centre and also accept excitation energy from the peripheral antenna and transfer this to the reaction centre (Barber et al. 2000). There are no indications yet that any of the extrinsic or small proteins binds chlorophyll. On the lumenal

side of the complex, three extrinsic proteins of 33, 23 and 17 KDa (OEC1-3) compose the OEC, and have a calcium, chloride and bicarbonate ion as necessary cofactors (Zouni et al. 2001).

1.3.2 PSII peripheral antenna

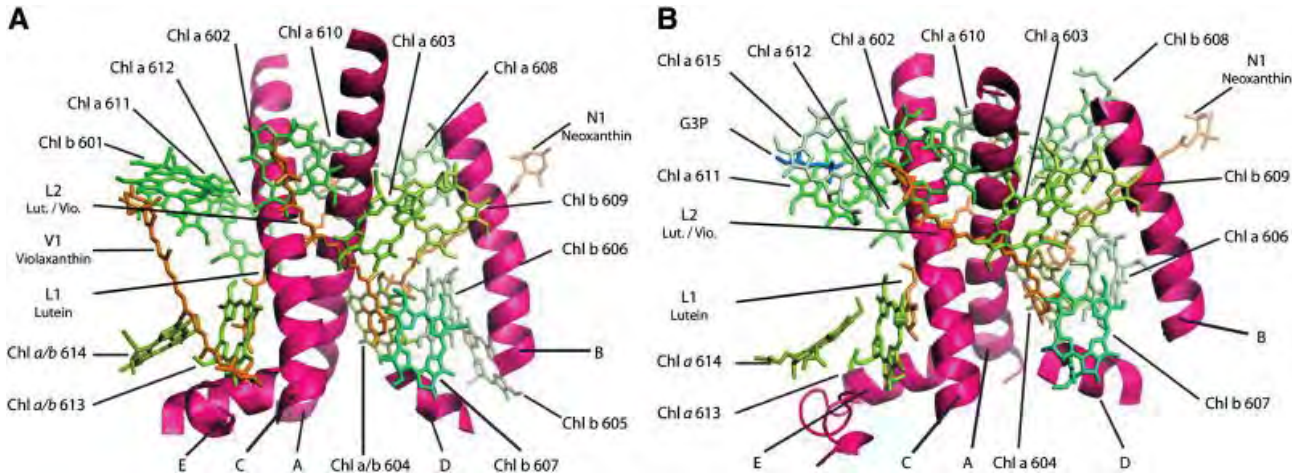

Figure 16. *Molecular model of LHCII monomer (A) and CP29 (B) showing chlorophyll and xanthophyll chromophores bound to different binding sites (Ballottari et al. 2012).*

In higher plants and eukaryotic algae, the peripheral antenna of PSII consists of a number of pigment-protein complexes belonging to the LHC super-gene family. In green plants two types of peripheral antenna proteins associated to PSII can be distinguished: the “major” LHCII antenna complex (Thornber et al. 1967) and the minor antenna complexes (Bassi et al. 1996). LHCII occurs in a trimeric association state and is not unique in composition; it consists of various combinations of three very similar proteins named LHCB1-3. In addition, there are three “minor” antenna complexes, which are called LHCB4 (CP29), LHCB5 (CP26) and LHCB6 (CP24) and usually occur in monomeric aggregation states. All these complexes bind various molecules of Chl *a* and Chl *b* and of the xanthophylls Lute, Viola and Neo (fig. 16). All the peripheral antennae are encoded by nuclear genes. In *Arabidopsis thaliana* LHCB3 is encoded by a single gene while LHCB1 and LHCB2 are encoded by high homologous multiple genes. Single genes encode CP26 and CP24, while three lhcb4 genes are present (lhcb4.1-3) (Jansson 1999). Recently the expression profile of the third gene coding for CP29, lhcb4.3, was shown to be different from lhcb4.1 and lhcb4.2 and was then renamed lhcb8. An additional isoform for minor complexes was identified and named LHCB7 (Klimmek et al. 2006). However LHCB8 and LHCB7 proteins are not present in detectable amount into thylakoids membranes and their role is still unclear.

LHCII trimers are heterotrimers constituted by the subunits LHCB1, LHCB2 and LHCB3; the three polypeptides, however, are not equimolar, with LHCB1 found in larger amounts (Caffarri et al. 2004, Dekker and Boekema 2005). High resolution structural models of antenna complexes have been obtained for LHCII

(Liu et al. 2004) (fig. 16A). In the trimeric complex of LHCII, each monomer is constituted of 3 transmembrane domains with α-helix conformation (helices A, B and C). The N-terminal is fully hydrophilic, thus protruding into the stroma space and the C-terminal peptides is exposed on the lumenal space. Two amphipathic helixes, named D and E, were found respectively on the C-terminal peptide and in the BC loop region; both helices lie on the lumenal surface. The trimerization domain covers: the amino-terminal domain, the carboxyl terminus, the stromal end of helix B, several hydrophobic residues from helix C and also pigments and lipid as phosphatidylglycerol (PG), bound to these parts of the polypeptide chain. Six Chl *a* (two from each monomer) constitute the core of the trimer (Liu et al. 2004). Each monomer binds 14 Chls and 4 xanthophylls. Part of the chlorophylls binding sites are selective for Chl *a* or Chl *b*, while in other cases Chls binding sites with mixed occupancy are present. Two central lutein molecules are bound in the grooves on both sides of the helices A and B cross-brace, forming the internal L1 and L2 carotenoid binding sites (Caffarri et al. 2001); the polyene chains are firmly fixed in two hydrophobic cavities, providing strong linkage between helices A and B. The third xanthophyll, Neo is located in the Chl *b*-rich region around helix C in the carotenoid binding site N1 (Remelli et al. 1999); side chains from helices B and C as well as phytyl chains form a hydrophobic space that accommodates the hook-shaped polyene chain of Neo, while ring on the other ends stretches into the exterior solvent region. The fourth carotenoid is located in a peripheral site named V1 (Ruban et al. 1999). V1 site is constituted by a hydrophobic pocket at the interface monomer-monomer, formed by several Chls, hydrophobic residues and the PG; part of the xanthophyll is located inside this pocket, while the opposite end group is located outside, toward the stromal surface.

Three Chl *a*, *b*-and xanthophyll-binding proteins constitute monomeric minor antennae: CP29, CP26 and CP24, named from their apparent mass in non-denaturing SDS-PAGE gels (Bassi et al. 1987). The transcription levels of minor antennae are similar and the proteins are found in equimolar amounts in the thylakoids (Nield et al. 2000).

CP29 is composed by 256-258 amino acids in its mature form in *A. thaliana*, and it is the largest among LHC encoded proteins. The overall sequence identity between CP29 and LHCII is 34%, but most of the substitutions are conservative, especially in the helix regions. It is necessary for PSII organization and a key component for the stability of the PSII-LHCII supercomplex (van Oort et al. 2010). And since is located between the outmost antenna LHCII and the inner antenna CP47, CP29 plays a bridging-type role in transferring the excitation energy to the reaction centre (Caffarri et al. 2009). A recent crystal structure of spinach CP29 (Pan et al. 2011) shows that it contains 13 Chl-binding sites: eight Chls *a*, four Chls *b* and one possible mixture of Chl *a* and Chl *b* (fig. 16B). Moreover, the purified CP29 sample used for crystallization contains three species of carotenoids: Lute, Viola and Neo. Each carotenoid molecule occupies a separate site in CP29: Lute at L1 site, Viola at L2 site and Neo at the N1 site. Compared to LHCII, CP29 does not bind any pigments at Chls b601 and b605 sites that are located at the periphery of the LHCII monomer. Instead,

a new Chl-binding site, a615, which is absent in LHCII, has been discovered on the surface of CP29 and close to the previous Chl b601 site in LHCII. Regarding the Cars binding sites, CP29 and LHCII show great differences at site L2, which binds Lute in LHCII but Viola in CP29. In addition, CP29 does not contain the fourth Car-binding site at the monomer-monomer interface of the LHCII trimer (V1). The L1 and N1 sites are conserved between CP29 and LHCII. Nevertheless, the Neo at the N1 site in CP29 rotates slightly and forms an increased angle between its transition dipole moment and the membrane normal (60.2° versus 58° in LHCII). The structural differences between CP29 and LHCII, especially their pigment composition and spatial arrangement, may account for their different functions in photosynthetic light harvesting and regulatory processes. CP29 can be phosphorylated, especially when plants are exposed to low temperature and high light stress (Croce et al. 1996). CP29 phosphorylation is supposed to induce conformational rearrangement or modification in the PSII supercomplex that could facilitate thermal energy dissipation.

CP26 is 243 amino acids long in *A. thaliana*, shows 48% identity with respect to LHCII and coordinates 7 Chl *a*, 3 Chl *b* and 2-3 xanthophylls (Lute, Viola and Neo) (Bassi et al. 1996, Croce et al. 2002). CP26, as LHCB1 and CP29, presents a Tyr residue which is suggested to stabilize the third carotenoid binding site N1 (Caffarri et al. 2007).

CP24 is the smallest of LHC proteins (211 amino acids in *A. thaliana*), due to the lack of the major part of the C-terminal region of the protein. Sequence homology and absorption spectra suggest that 5 Chl *a*, 5 Chl *b* and 2 xanthophylls are bound (Bassi et al. 1996, Pagano et al. 1998). CP24, differently from other LHCB proteins does not bind neo; indeed the Tyr residue involved in N1 stabilization is absent.

1.3.4 PSII supercomplex

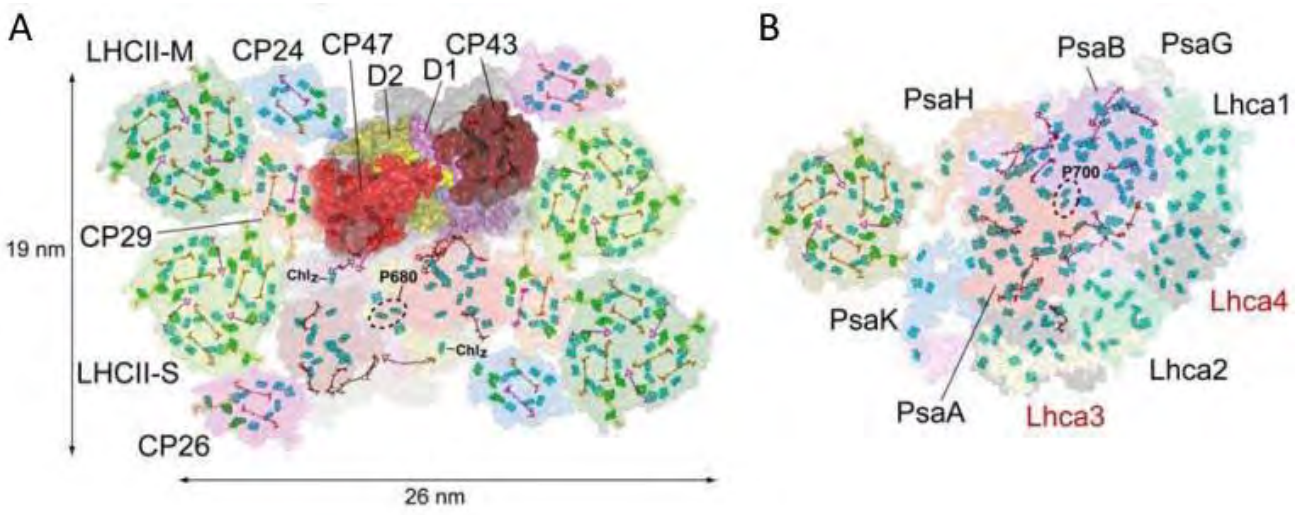

Figure 17. *(A) PSII-LHCII supercomplex ($C_2S_2M_2$) and of the (B) PSI-LHCII supercomplex in State II (Caffarri et al. 2014)*

A variable number of peripheral antenna proteins can associate with dimeric PSII core complexes to form PSII-LHCII supercomplexes (fig. 17A). A dimeric core (C_2) associate with up to four copies of peripheral LHCII trimers. Connection of the first two LHCII-S trimers (strongly bound) extends a C_2 complex to a C_2S_2 supercomplex, and two further M trimers (moderately strong bound) are bound in a $C_2S_2M_2$ supercomplex. Spinach supercomplexes may bind a third type of L trimer (loosely bound), but the resulting $C_2S_2M_2L_{1-2}$ supercomplexes are rare. Recent studies suggest that LHCII-L trimer may migrate between PSII and PSI to balance the excitation level of two photosystems in response to light fluctuations (Galka et al. 2012). The $C_2S_2M_2$ supercomplex of *A. thaliana* was analyzed by single particle electron microscopy at 12 Å resolution (Caffarri et al. 2009), permitting a more accurate fitting of the peripheral antenna proteins, based on the known LHCII structure. $C_2S_2M_2$ contains a dimeric core (C_2), four LHCII trimers, two strongly bound (S) and two moderately strongly bound (M) to the core, and two monomeric copies each of CP29, CP26, and CP24. In particular, LHCII-S trimers are attached to a dimeric PSII via CP29 to one PSII core monomer and CP26 to the other and LHCII-M trimers are attached via CP24 and CP29. Biochemical experiments show that LHCB3 is present in trimer M only; instead, LHCB2 is a specific component of trimer S. LHCB1 is present in both trimers (Dekker and Boekema 2005). CP24 and LHCB3 are necessary for binding the M trimer; *A. thaliana* plants depleted of one of these subunits do not form $C_2S_2M_2$ supercomplexes or the small pentameric complex LHCII-M/CP24/CP29 (Kovacs et al. 2006). In the absence of CP26 no bands containing high molecular weight supercomplexes are visible and the amount of the fractions containing the smaller supercomplexes (C_2S, C_2M, C_2S_2, C_2SM) is extremely reduced (Caffarri et al. 2009). $C_2S_2M_2$ were still

detectable in a mutant without CP29, albeit their amounts were reduced compared with the wild type. An empty space was observed within this supercomplex at the CP29 position, implying that the missing CP29 was not replaced by other LHC subunits. This suggests that CP29 is unique among PSII antenna proteins and determinant for its macro-organization and photoprotection (de Bianchi et al. 2011).

1.3.5 PSI core

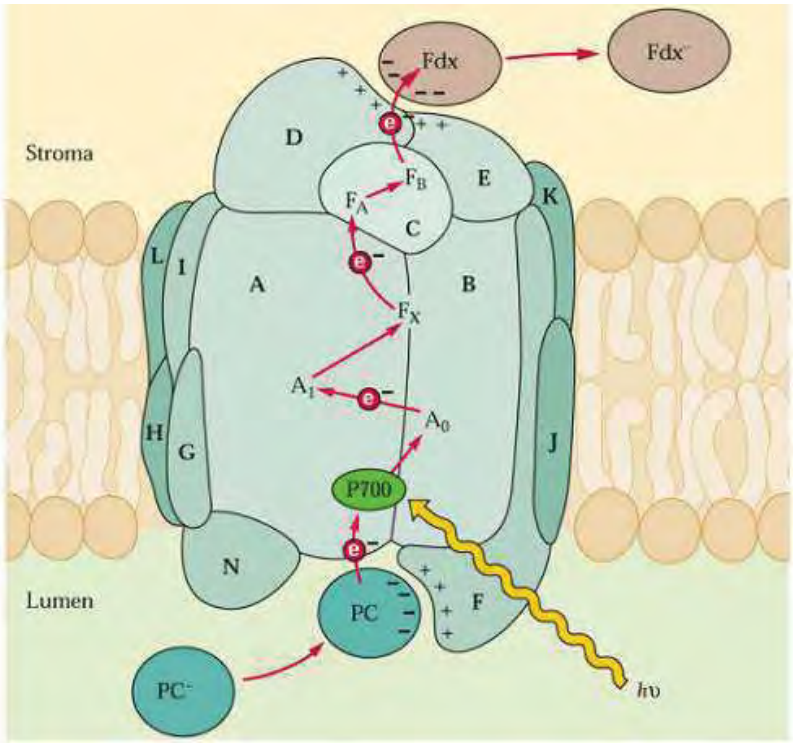

Figure 18. *Schematic model of photosystem I. Subunits organization and cofactors involved in electron transfer are indicated.*

Core complex of PSI is composed by the polypeptides denominated PSA encoded from both nuclear and plastidial genes. PSI core is responsible for light-driven charge separation and electron transfer. It coordinates around 100 Chls and 20 β-Car molecules. Its primary and tertiary structures are highly conserved among green algae and plants; 14 subunits are present in both types of organisms (PSAA-PSAL and PSAN-PSAO), whereas PSAP is present in plants but so far seems to be absent in algae (Jensen et al. 2007). The PSAA-PSAB heterodimer forms the inner core of PSI, binding the P700 special Chl pair where the light-driven charge separation occurs (fig. 18) They bind all of the cofactors of the electron transfer chain (Jordan et al. 2001), except for the last 2 Fe_4S_4 clusters (FA and FB). These are bound to the peripheral subunit PSAC, which together with PSAD and PSAE forms the docking site for FD on the stromal side of the membrane (Scheller et al. 2001). PSAF and PSAN are important for electron transfer from PC to P700 (Haldrup et al. 1999). PSAJ is a hydrophobic protein located close to PSAF and plays a role in the

stabilization of this subunit conformation (Fischer et al. 1999). PSAH, PSAI, PSAL, and PSAO form a cluster of integral membrane proteins, placed on one side of the core, where they are involved in interactions with LHCII during state transitions (Lunde et al. 2000, Zhang and Scheller 2004). PSAG and PSAK are located near PSAA and PSAB respectively and have been proposed to be important for the association of the outer antenna with the core (Ben Shem et al. 2004).

1.3.6 PSI peripheral antenna

PSI of green plants and green algae binds peripheral antenna, called LHCI. In green plants, this antenna consists of four different polypeptides from the LHC super-gene family, called LHCA1-4, with protein mass of around 25 KDa. These complex show structural homology with PSII peripheral antenna: LHCI polypeptide has three transmembrane α-helices and coordinates Chls *a*, Chls *b*, and different Cars molecules (Jansson 1999, Croce et al. 2002). The PSI crystal structure revealed 12 chlorophylls for LHCA1, LHCA2 and LHCA4, 11 for LHCA3, as well as 9 "linker" Chls between the LHCI complexes. LHCI are assembled in two heterodimer LHCA1-LHCA4 and LHCA2-LHCA3 (Ben Shem et al. 2004). In *A. thaliana* two additional LHCA have been identified named LHCA5 and LHCA6 but their expression level is low (Ganeteg et al. 2004, Peng et al. 2009). Recent results showed a peripherally interaction between LHCA5 and LHCA2-3 dimer and possibly a presence of LHCA5 homodimer as substitute of LHCA1-4 eterodimer (Lucinski et al. 2006). LHCA6 polypeptide has been detected and together with LHCA5 it is required for the formation of the full-size NAD(P)H dehydrogenase-PSI supercomplex formation (NDH-PSI supercomplex) (Peng et al. 2011).

PSI is characterized by the presence of Chls adsorbing at lower energies with respect to the reaction centre P700 named "red forms" (Gobets and van Grondelle 2001). While they are still red forms in the core complex, the red-most Chls are found in the antenna complex LHCI (Mullet et al. 1980). In vitro reconstitution, together with biochemical and spectroscopic analysis of LHCA proteins, has shown that the 'red forms' are mainly associated to LHCA3 and LHCA4 and derived from the binding site, via an asparagine, for the Chl A5 (Castelletti et al. 2003). The function of the red forms is still not fully understood. It has been suggested that they focus the energy to the primary electron donor, have a role in protection against light-stress, or absorb light efficiently in a dense vegetation system where light is enriched in wavelengths above 690 nm (Rivadossi et al. 1999, Wientjes and Croce 2011). Plants depleted in LHCA polypeptides showed a reduced capacity for photoprotection and an increased production of reactive oxygen species upon high light exposure. Preferential degradation of LHCI upon illumination of isolated PSI-LHCI is effective in protecting the catalytic activity of the complex (Alboresi et al. 2009).

1.3.7 PSI supercomplex

While the PSII supercomplexes are dimeric and contain usually from two to four copies of trimeric LHCII complexes, the PSI consists of a monomeric core complex with single copies of four different LHCI proteins. The structure of PSI-LHCI complex from higher plants was resolved at 4.4 Å and 3.4 Å resolution (Ben Shem et al. 2004, Amunts et al. 2007) giving details on the supramolecular organization of the complex. It shows that the LHCI subunits bind in one cluster at the side occupied by the PSAF and PSAJ subunits of the core complex. PSAH, L, O, and I are located on the opposite side with respect to LHCI. These proteins are involved in state transition forming the docking site for LHCII (Lunde et al. 2000, Zhang and Scheller 2004) (fig. 17B).

1.4 Photoprotection

1.4.1 Generation of reactive oxygen species

Light energy is required for photosynthesis but it is also harmful for plants. In fact, light intensity and spectral quality are highly variable in space and time according to the time of day, season, geography, climate, and the position of leaf within canopy and cell within leaf. In these conditions the absorbed light energy can exceed the capacity for its utilization by photochemistry and the excess light can generate highly reactive intermediates and by-products that can cause oxidative damage to the photosynthetic apparatus. Potentially damaging molecules are generated at three major sites in the photosynthetic apparatus: the LHC, the PSII RC, and the PSI.

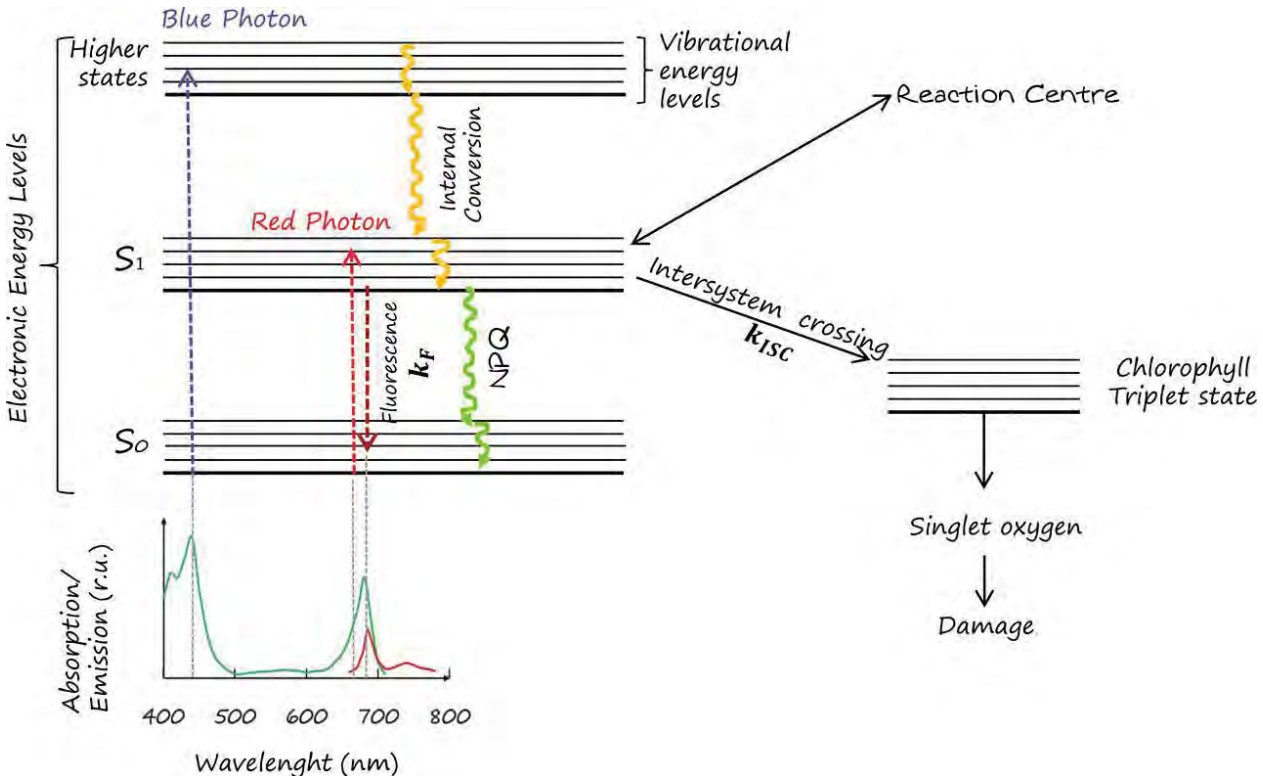

Figure 19. *Jablonski's diagram illustrating the energy partitioning of absorbed photons in a chlorophyll a molecule. Image modified from Porcar-Castellet et al. (Porcar-Castell et al. 2014)*

In the LHC upon absorption of blue light, an electron from the ground state is raised to a higher energy state and the energy is rapidly dissipated non-radiatively as heat mainly by internal conversion, and the electron rapidly relaxes to the first excited state. Absorption of a red photon causes Chl to enter directly the singlet excited state (^{1}Chl*) (fig. 19). From there the ^{1}Chl* can relax to the ground state via different pathways: the excitation energy can be emitted as fluorescence, it can be transferred to RC for photosynthetic reactions or it can dissipate non-radiatively as thermal emission (NPQ). The prevalence of a

mechanism with respect to another depends on the required time for dissipation energy. Before ^{1}Chl* is relaxed back to its ground state by one of these mechanism, triplet Chl (^{3}Chl*) can be formed from ^{1}Chl* through intersystem crossing. The yield of ^{3}Chl* formation depends on the average lifetime of ^{1}Chl*. In excess light conditions there is an accumulation of excitation energy in the antennae; photochemical reaction are saturated and thermal dissipation processes is not able to deal with all the energy absorbed, thereby increasing the lifetime of ^{1}Chl* and the probability to conversion into ^{3}Chl*. In contrast to ^{1}Chl*, ^{3}Chl* is relatively long-lived and can interact with O_2 to produce singlet oxygen ($^1O_2$) an highly reactive species that it is harmful for plant causing oxidation of lipids, proteins and pigments (Tardy and Havaux 1996).

In the PSII reaction centre, after primary charge separation $P680^+$ and $Pheo^-$ species are formed. $Pheo^-$ is reconverted to Pheo after electron transfer to Q_A, while $P680^+$ is reconverted to P680 through Tyr oxidation. However, in excess light the Q_A is already reduced and electron transport is blocked; the $P680^+$/ $Pheo^-$ radical can revert and the charge recombination can generate triplet P680 (^{3}P680*) (Vass et al. 1992, Aro et al. 1993). ^{3}P680* can generate $^1O_2$. Furthermore, the high pH that builds up in excessive light can inhibit electron donation to $P680^+$ from the oxygen-evolving complex, resulting in longer-lived $P680^+$.

Because the average lifetime of ^{1}Chl* in the PSII-LHCII is several times longer than in the PSI-LHCI, the potential for generation of $^1O_2$ is greater in the PSII-LHCII. In contrast to $P680^+$ of PSII, $P700^+$ is a very efficient quencher of excitation energy from the PSI-LHCI (Dau 1994). Nevertheless, at the acceptor side of PSI, FD can reduce molecular oxygen to the superoxide anion (O_2^-) (Mehler 1951). This short-living specie can be metabolized to hydrogen peroxide (H_2O_2) or hydroxyl radical (OH•), the latter one being an extremely aggressive ROS .

Plant had developed several mechanisms to protect themselves from photodamage both directing at decreasing the light absorption and at decreasing ^{1}Chl* lifetime.

1.4.2 Leaf movement

Several plant species are able to move their leaves in response to direct sunlight (Ehleringer and Forseth 1980). This leaf movement is also affected by ambient growth conditions, such as light intensity, temperature, water and nutrient availability. The heliotropism displays two forms: (i) diaheliotropism (the leaf lamina becomes oriented at an angle perpendicular to the direction of light); and (ii) paraheliotropism (the leaf lamina becomes oriented at an angle parallel to the direction of light). Paraheliotropism is associated with minimizing the absorption of solar radiation and avoids absorbing excessive light energy for

photosynthesis. Interruption of the diurnal heliotropic leaf movement causes acceleration of photoinhibition in bean plants (Pastenes et al. 2005).

1.4.3 Chloroplast Avoidance Movement

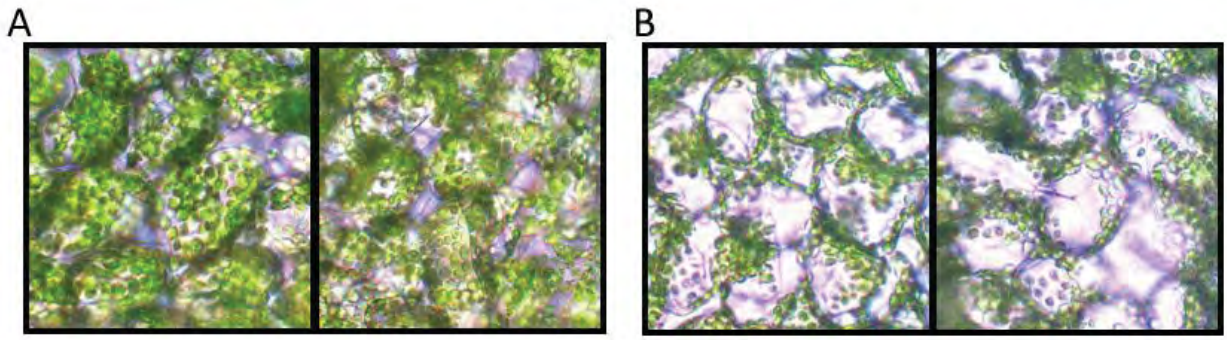

Figure 20. *Distribution of chloroplasts in the mesophyll cells of A. thaliana determined by light microscopy. (A) Low light-adapted leaves. (B) Leaves illuminated with high light.*

At a cellular level, plants can avoid over-excitation by relocating chloroplasts. Under high light, chloroplasts move to the sides of a plant cell so that they are positioned parallel to the direction of incident light to avoid absorption of excessive light and thereby minimize photodamage (Kasahara et al. 2002). This response is called chloroplast avoidance movement. In low light instead, the chloroplasts move toward the cytosolic layer along the periclinal cell walls maximizing light harvesting (fig. 20). In most plants chloroplasts movement is mediated by blue light and a blue light photoreceptor called phototropin (Wada et al. 2003). Phototropin was first identified as a ~120 KDa plasma membrane protein that has blue light-dependent autophosphorylation activity (Christie 2007). *A. thaliana* contains two phototropins, PHOT1 and PHOT2, each of which consists of two tandem LOV (light-, oxygen-, and voltage-sensing) domains at the N terminus and a Ser/Thr kinase domain at the C terminus (Jarillo et al. 2001). LOV domains bind flavin mononucleotide (FMN) and are responsible for blue/UV-A light perception. PHOT2 is the photoreceptor that regulates the chloroplast avoidance movement; the mutant *phot2*, that cannot relocate chloroplast under high light, showed an higher damage of the photosynthetic apparatus and faster bleaching of leaf (Kasahara et al. 2002).

1.4.4 State1-state2 transitions

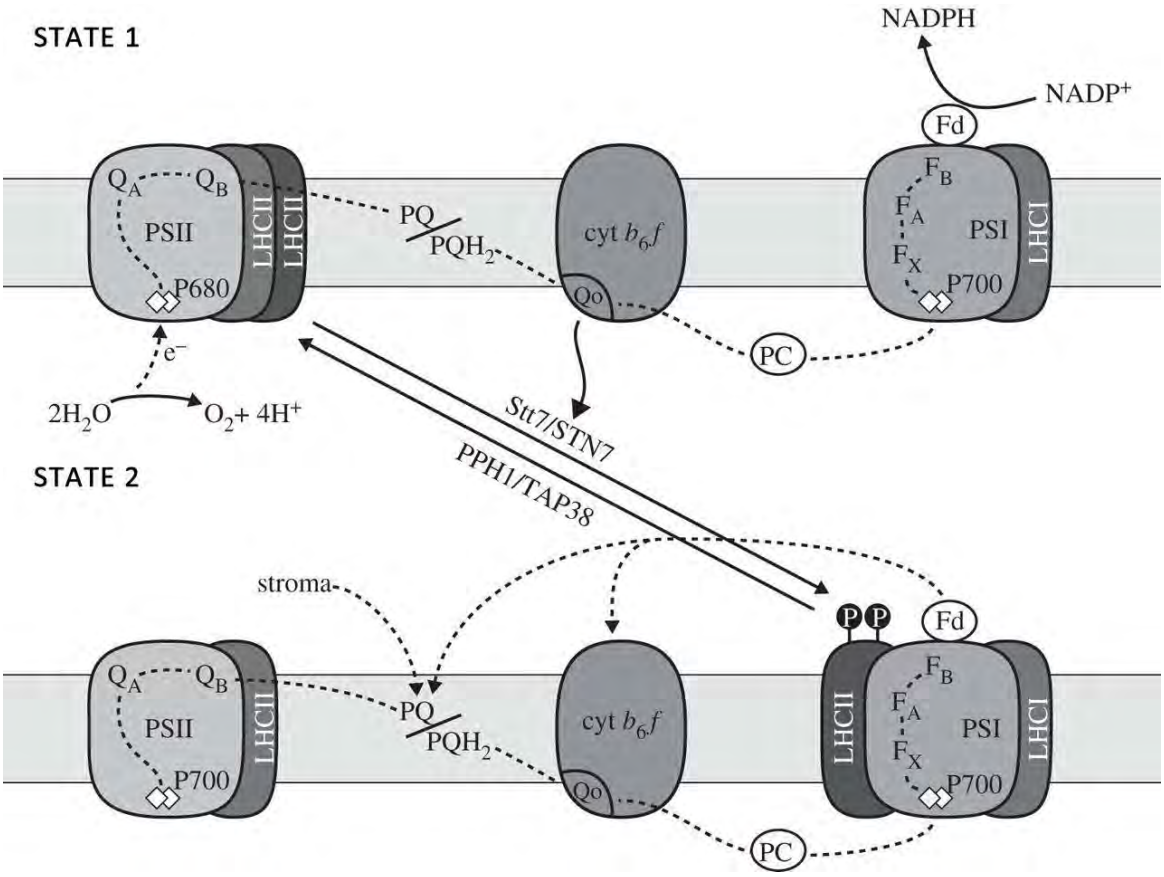

Figure 21. *Scheme of LHCII state transitions (Rochaix et al. 2012)*.

An important short term photoprotective mechanism is the "state1-state2 transitions" (Rochaix 2007). This phenomenon consists in the redistribution of excitation energy between PSI and PSII depending on the association of LHCII with PSII (State I) or PSI (State II). When PSII is preferably excited, LHCII is phosphorylated and moves towards the unstacked region of thylakoids where PSI is located. On the contrary, when PSI is preferentially excited, LHCII is dephosphorylated and migrates back to PSII (fig. 21) (Allen 1992). State transitions are principally observed under non saturating light conditions, where the redistribution of the antenna cross-section between the two photosystem can have a significant effect in increasing the overall thylakoid electron transport rate (Jennings and Zucchelli 1986). In higher plants the size of the mobile LHCII has been quantified in about 20-25% of the total LHCII pool. In *A. thaliana*, the STN7 kinase is responsible for the phosphorylation of LHCII (Bellafiore et al. 2005). In State II, the plastoquinone pool becomes more reduced (because of the light-limited turnover of PSI) and the reduced PQ is bound to the Q_0 site of the Cyt-b6/f, this leads to a conformational change in this complex that activates STN7 (Zito et al. 1999). It has been suggested that the phosphorylation at the N-terminus of LHCII causes a conformational change that lowers the affinity of LHCII for PSII and at the same time increase the affinity for PSI (Nilsson et al. 1997). In State I instead, a thylakoid peripheral protein (TAP38/PPH1)

dephosphorylates LHCII upon which it migrates back to PSII (Shapiguzov et al. 2010). Analyses of different PSI mutants showed that the PSAH subunit is essential for the docking of LHCII, but also other subunits are important (for instance PSAL, PSAO and PSAP) for the formation of the interaction (Lunde et al. 2000).

1.4.5 Non photochemical quenching

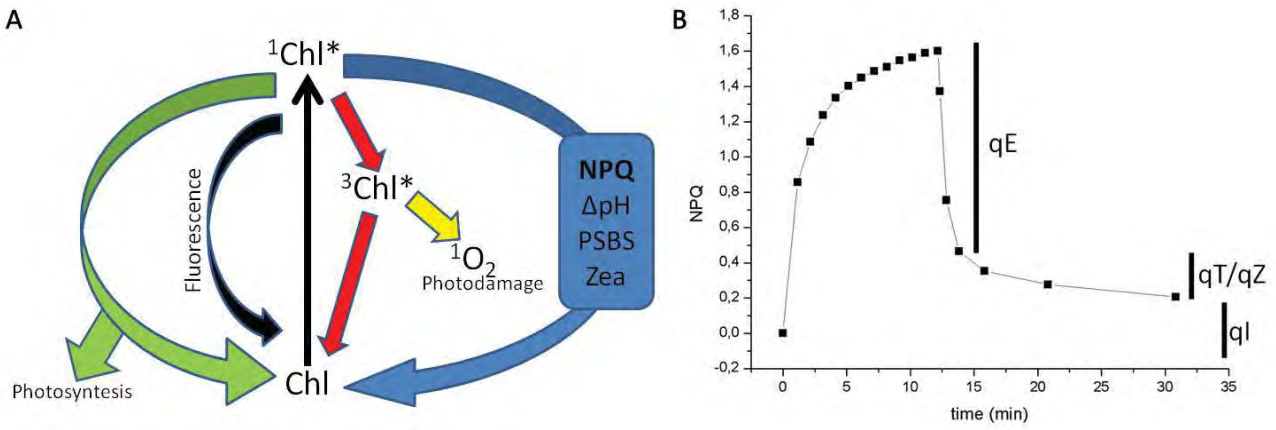

Figure 22. *(A) Scheme of NPQ photoprotective mechanism. (B) NPQ different components defined by dark relaxation kinetic*

The ability of plants to modulate light utilization efficiency in the fluctuating light is crucial for plant fitness. A major role for prevention of over-excitation is played by a set of inducible mechanisms referred to as Non-Photochemical Quenching (NPQ). NPQ allows for the harmless thermal dissipation of excess absorbed photons by PSII, thus preventing the formation of ^{3}Chl* (Frank et al. 2000) and can be monitored as a light-dependent quenching of leaf Chl fluorescence (Genty et al. 1989). According to kinetics of rise in the light and decay in darkness, NPQ can be dissected in three components (Horton and Hague 1988) (fig. 22):

- qE (energy quenching), the most rapid and predominant component of NPQ, yielding into dissipation of excess energy with half-time of ~1 min, it's triggered by ΔpH change across the thylakoid membrane induced by high light.

- qI, the slowest component, which is independent from lumenal pH and has been attributed to inactive PSII centres produced by HL stress. It has an half time above 60 minutes

- An additional quenching component with intermediate half-time of ~10-20 min which was originally attributed to state transitions, and more recently to Zea binding to the LHC proteins, hence the naming as qT or qZ.

1.4.5.1 qE

The activation of qE mechanism is dependent of three factors: proton gradient across thylakoid membranes, PSBS protein and it is modulated in amplitude by zeaxanthin (Niyogi 1999).

Absorption of sunlight that saturates plant capacity for photochemistry results in the build-up of a proton gradient across thylakoid membranes by photosynthetic electron transport and inhibition of ATPase for lack of Phosphate and ADP. The decrease in pH within the thylakoid lumen is an immediate signal of excess light that triggers NPQ. The control by lumen pH allows induction or reversal of qE within seconds of a change in light intensity, which is fast enough to cope with natural fluctuations in light intensity that are due to, for example, passing clouds on a partly sunny day (Muller et al. 2001). The requirement for low lumen pH is evidenced by the inhibition of qE by uncouplers such as nigericin. This ionophore collapses ΔpH and prevents the activation of NPQ otherwise activated within a few seconds of exposure to HL (Shikanai et al. 1999).

Signal transduction of lumen over-acidification involves the PSII subunit PSBS that is essential for qE induction, as demonstrated by the phenotype of the *npq4,* the mutant lacking PSBS, that show no fast component of NPQ (Li et al. 2000). PSBS belongs to the LHC protein superfamily, but differs from other members for having four transmembrane helices rather than the three generally found in most LHC proteins and for the absence of most conserved Chls-binding residues in its sequence (Dominici et al. 2002). Typical of this protein is the presence of two lumen-exposed glutamate residues, Glu122 and Glu226, that bind DCCD (N,N'-dicyclohexylcarbodiimide), a protein-modifying agent that covalently binds to protonatable residues in hydrophobic environments (Jahns et al. 1988). In *A. thaliana*, mutations of each glutamate to a non-protonatable residues, i.e. E122Q and E226Q, decreased by 50% both qE and DCCD binding capacity, whereas the double mutant has a qE-null phenotype like *npq4* (Li et al. 2004). These results suggest that these two glutamate residues are the target of protonation upon thylakoid lumen acidification and mediate the activation of PSBS-dependent qE. The exact localization of PSBS within PSII complexes is still not defined. Based on previous data, it was initially proposed that it could be localized at the interface between the reaction centre and the peripheral light harvesting antenna system. However, more recent studies highlight that PSBS cannot be purified with $C_2S_2M_2$ supercomplexes (Caffarri et al. 2009). As a consequence, PSBS must have a peripheral localization, although this has never been experimentally proven. Immunoaffinity and immunoprecipitation experiments showed that PSBS interacts with many different photosynthetic complexes (as CP29, LHCII, PSI, or Cyt-b6/f complexes), leading to the model suggesting that PSBS might be mobile in thylakoid membranes (Teardo et al. 2007).

The third factor needed for qE activation is Zea synthesis. The amount of Zea synthesized via the xanthophyll cycle is highly correlated with the level of qE (Demmig-Adams 1990). The requirement for Zea

in qE has been investigated in vivo by using inhibitors and mutants. Dithiothreitol blocks Zea synthesis in leaves and results in inhibition of qE (Demmig-Adams et al. 1990). Mutants that are unable to convert Viola to Zea have been isolated and show a lower level of qE. Although Zea is generally necessary for maximal qE in vivo, it is not sufficient. In mutants that accumulate it constitutively, qE must still be induced by a low pH (Niyogi 1999). This demonstrates that the low pH has an additional role in qE, besides activation of the xanthophylls cycle. In addition to Zea another xanthophyll, Lute, has also been implicated in qE. In *A. thaliana,* the mutant *lut2,* which is defective in the lycopene e-cyclase and therefore lacks Lute, has less qE with respect to wild type (Pogson et al. 1998). Double mutants of *A. thaliana* that lack Lute and Zea are totally devoid of any qE (Niyogi et al. 2001).

The detailed molecular mechanisms that give rise to qE are still a matter of intense debate. PSBS is able to sense the transmembrane pH induced by electron transport, through protonation of the two glutamic acid. Thus, protonation of PSBS leads to activation of a Lute and Zea-dependent quenching. Nevertheless, the mode of interaction is still obscure. Most of the experimental evidences and proposed models suggest that qE occurs at the level of LHCB proteins. In order for PSBS protonation to yield dissipation of ^{1}Chl* and fluorescence quenching, this event must affect a Chl-binding protein. Such a protein should also bind Lute and Zea as mentioned above or, at least, should interact tightly with a xanthophyll-binding protein, thus providing a quenching effect. Early work proposed that PSBS might bind both Chls and xanthophylls or Zea alone (Funk et al. 1995, Aspinall-O'Dea et al. 2002), making it a candidate for the role of quencher. Nevertheless, later analysis pointed to the non-conservation of Chl-binding residues in PSBS, while its properties both *in vivo* and *in vitro* are not consistent with binding of xanthophylls (Bonente et al. 2007) although coordination to new sites, different from those conserved in LHCs, cannot be excluded in principle. LHCB proteins appear to be ideal candidates for the role of quenching sites; the *ch1* mutant of *A. thaliana* that lacks Chl *b*, thus leading to degradation of LHC proteins, exhibits a strongly reduced capacity of NPQ in the presence of both Lute and Zea, suggesting that LHCs are needed for the quenching events (Andrews et al. 1995). The role of individual LHCs has been investigated using reverse genetics. Down-regulation of LHCB1 showed a decrease in qE while down-regulation LHCB2 and knockout of LHCB3 did not significantly decrease NPQ amplitude or slow down its kinetics (Andersson et al. 2003, Damkjaer et al. 2009, Pietrzykowska et al. 2014). *CP26* knockout plants retained qE (de Bianchi et al. 2008), whereas the qI component of NPQ was down-regulated (Dall'Osto et al. 2005). qE was affected in *CP24* and *CP29* knockout plants (Andersson et al. 2001, de Bianchi et al. 2008). In summary, depletion of a single monomeric LHCB protein could not completely abolish NPQ, implying redundancy within the subfamily members. The making of a mutant lacking all three monomeric proteins or alternatively LHCII is awaited in order to verify whether NPQ can be sustained in the absence of these gene products.

In LHCII the quenching was proposed as originating also from aggregation (Pascal et al. 2005, Ruban et al. 2007). This suggestion was supported by the evidence that low energy states emitting at ~700 nm can be induced in isolated LHCB complexes upon induction of aggregation *in vitro* (Ruban et al. 1994, Muller et al. 2010) and that similar fluorescence changes can be observed also *in vivo* at low temperature (Ruban et al. 2007). Aggregation was shown to be instrumental in catalyzing conformational change(s) within the LHCII protein, and the spectral signatures associated to this event were interpreted to indicate the formation of a tight interaction between Lute bound into the site L1 and terminal emitter Chl *a*. In this hypothesis PSBS would promote LHCII aggregation thought membrane reorganization (Miloslavina et al. 2008). Recently a significant Chl fluorescence quenching was observed *in vitro* when LHCII was reconstituted in proteoliposomes in the presence of PSBS and Zea, although neither Zea nor PSBS alone could induce the same quenching (Wilk et al. 2013).

The role of Zea has been much debated. Zea binding to minor LHCB results in a conformational change (Niyogi et al. 2001) and in a decrease in the fluorescence lifetime (Joliot et al. 1973, Butler and Kitajima 1975). The presence of a Zea-binding site effective in providing enhancement of NPQ is not a property of a specific LHC protein since enhancement of the quenching amplitude has been observed in plants depleted of different antennae (de Bianchi et al. 2008, de Bianchi et al. 2011). Although it is clear that the concentration of Zea increases at the expenses of Viola when leaves are illuminated by high light (Demmig-Adams 1990), qE was shown to develop in thylakoid in the absence of the xanthophyll cycle albeit with reduced value and different kinetics of formation and relaxation kinetics (Niyogi et al. 1998). It was therefore proposed that Zea acts indirectly as an allosteric modulator of qE (Horton 1996, Bassi and Caffarri 2000, Dall'Osto et al. 2005), probably controlling the organization of the antenna complexes and stabilizing a “dissipative” conformational state of the complexes.

Zea was also proposed to have a direct role in the quenching of chlorophyll excitation through the formation of a charge-transfer state with Chl *a* (Holt et al. 2005). In this model, qE activation involves a charge separation between a Chl-Zea heterodimer that produce a transient zeaxanthin radical cation ($Zea^{\cdot+}$) with a short relaxation time (50–200 ps). Interestingly, it was also shown that singlet excited state quenching can occur by the formation of $Chl^{-}/Lute^{+}$ state, although probably occurring at different sites within the LHC complexes (Avenson et al. 2009). Irrespective of the location of the quenching centers and the exact molecular mechanisms by which excited state quenching occurs, all models propose a change in interactions between the bound pigments, being either Chl-Chl or Chl-Car, which would promote the formation of a quenching centre. Such modification in the pigment-pigment interactions is thought to be associated with conformation of the protein structure, leading to alteration of either the inter-chromophore distances or mutual orientations.

A third observation about the triggering of qE is that PSBS action is able to affects the rigidity of grana membranes and the readjustment of the antenna organization that might result in the formation of quenching sites. High light induce dissociation of antenna from PSII core and the formation of two different quenching site; the Q1 site reflecting the functional detachment of part of the antenna of the PSII supercomplex, and the Q2 quenching site that is located in the antenna that remains attached to the PSII core under HL conditions (Miloslavina et al. 2011) (fig. 23).

This has been proposed on the basis of the observation that PSBS is needed for light induced dissociation of a pentameric complex, including CP29 and CP24, together with an LHCII. Thus the unquenched conformation of LHCB proteins is stabilized by their inclusion in this large complex, while its dissociation by PSBS would allow transition to the quenching state, also promoted by Zea binding (Betterle et al. 2009). Indeed, mutations inducing constitutive dissociation of the pentameric complex (designated as 'B4 complex' from its order of migration in sucrose gradients) show formation of two-dimensional arrays of C_2S_2 particles in the centre of grana discs, whereas LHCII is segregated out towards grana margins (Kovacs et al. 2006, de Bianchi et al. 2008).

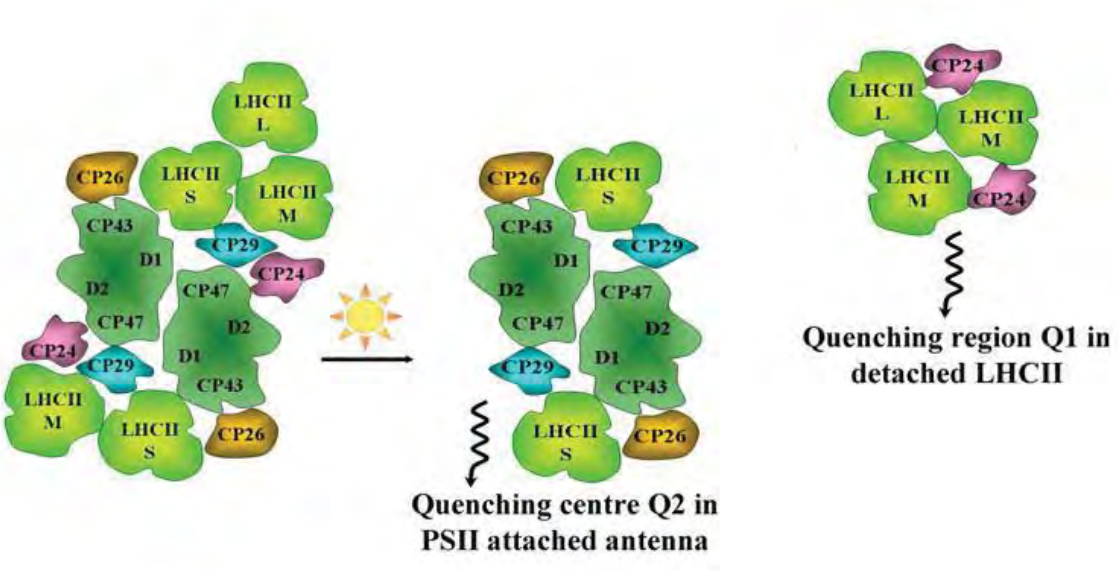

Figure 23. *Model of the PSII supercomplex reorganization under high light adaptation (Miloslavina et al. 2011).*

1.4.5.1 qI and the intermediate kinetic component

Photoinhibitory quenching, or qI, has been associated to a kinetic component whose relaxation is far slower than the decay of trans-thylakoid pH gradient upon light to dark transition and was attributed to processes involving damage of PSII and turnover, implying a reduction of the quantum yield of photosynthetic electron transport (Krause 1988). qI is much less characterized and might be due to a mix of photoprotection and photodamage. *In vivo* qI recovers with an half times of the order of several hours,

thus comparable with those of PSII turnover, whereas *in vitro* it is substantially irreversible. In the case of qI, the nature of the quencher has been less intensively investigated and therefore remains to be elucidated. However, the protective effect of qI appears to be modest (Sarvikas et al. 2010).

The intermediate kinetic component of NPQ was first defined as qT for its dependence form state transition; this part of the quenching was attributed to the shift of LHCII from PSII to PSI in state 2 induction and consequential decrease of PSII fluorescence that was measured as NPQ increase. Despite its name, is unlikely to be related to state1-state2 transitions since the *A. thaliana stn7* mutant blocked in state transitions showed an unaltered amplitude of the three kinetic components of NPQ (Bellafiore et al. 2005, Nilkens et al. 2010) and these state transitions occur only under low light only while they are inhibited at the excess light in which NPQ mechanism is active. (Rintamaki et al. 1997). More recently this component has been defined as qZ, for the Chl^{-}/Zea^{+} depending quenching, since results showed that Zea accumulation and its binding to LHC modulate the amplitude of the intermediate kinetic component of NPQ relaxation (Nilkens et al. 2010). Even if it is true that Zea accumulation and its binding to LHC modulate the amplitude of NPQ and influence qE, it is not easy to associate Zea with the intermediate component of NPQ. This component has half-relaxation time of 10-20 minutes while the Zea decrease in the dark is much more slower with a half-time higher than 1 hour. Thus further studies are needed to fully comprehend this component.

1.4.6 Photoprotection through photochemistry

Diversion of energy from the normal assimilative pathway can also be performed a role in consuming excess excitation energy. Oxygen can function as an electron acceptor either through the oxygenase reaction catalyzed by Rubisco (photorespiration) or by direct reduction of oxygen by electrons on the acceptor side of PSI (Mehler 1951).

In C3 plants, especially under conditions of CO_2 limitation, photorespiratory oxygen metabolism is capable of maintaining considerable linear electron transport and utilization of light energy. Blocking photorespiration with mutations or inhibitors leads to inhibition of photosynthesis and increase of photo-oxidative damage (Osmond 1981).

Direct reduction of O_2 by PSI is the first step in an alternative electron transport pathway known as pseudocyclic electron transport or water-water cycle. The O_2^{-} produced on the acceptor side of PSI by reduction of O_2 is efficiently metabolized by thylakoid-bound superoxide dismutase (SOD) and ascorbate peroxidase (APX) to generate H_2O and monodehydroascorbate, which can itself be reduced directly by PSI to regenerate ascorbate (Asada 1999). This pseudocyclic pathway generates a ΔpH for ATPase, but neither

NADPH nor net O_2 is produced. Like photorespiration, the water-water cycle may help to dissipate excitation energy through electron transport.

Cyclic electron transport around PSI is also suggested to have an important role in photoprotection. In addition to dissipating energy absorbed by PSI, cyclic electron transport may be involved in generating or maintaining the ΔpH that is necessary for down-regulation of PSII by thermal dissipation of excess absorbed light energy (Heber and Walker 1992).

1.4.7 Scavenging of reactive oxygen species

In the chloroplast several antioxidant species are present that can scavenge reactive oxygen species that are generated by photosynthesis (fig. 24).

Carotenoids are membrane-bound antioxidants that can protect photosynthetic apparatus quenching both ^{3}Chl* and $^1O_2$ and inhibiting lipid peroxidation and protein degradation. The lowest triplet energy level of Cars is lower in energy than singlet oxygen, and therefore they cannot react with oxygen to produce singlet oxygen. Xanthophylls bound to the LHC proteins are located in close proximity to Chls for efficient quenching of ^{3}Chl*. Cars can also scavenge $^1O_2$; the excitation energy transfer from ROS to Cars results in the formation of the ground triplet state of molecular oxygen ($^3O_2$) and the triplet excited state of carotenoid (^{3}Car*). The triplet carotenoid decays radiationless into the ground state, while the triplet excitation energy is converted effectively into heat. As discussed above, specific xanthophylls are also involved in quenching of ^{1}Chl* during thermal dissipation. β-carotene in the PSII reaction centre quenches $^1O_2$ produced from interaction of ^{3}P680 and O_2 (Telfer et al. 1994).

Another important thylakoid membrane antioxidant is α-tocopherol (vitamin E), which can physically quench or chemically scavenge $^1O_2$, $O2^-$ and OH^- to prevent lipid peroxidation (Fryer 1992). Whereas the xanthophylls are largely bound to proteins, α-tocopherol is free in the lipid matrix of the membrane and appears to have a role in controlling membrane fluidity and stability. Although α-tocopherol is the most abundant tocopherol in the chloroplast, other tocopherols such as β- and γ-tocopherols are also present at low levels.

The soluble antioxidant ascorbate (vitamin C) has a central role in preventing oxidative damage through direct quenching of $^1O_2$, O_2^- and OH-, and as a substrate in both the violaxanthin de-epoxidase and APX reactions (Smirnoff 1996).

Glutathione is capable of detoxifying $^1O_2$ and OH-. Glutathione protects thiol groups in stromal enzymes, and it is also involved in α-tocopherol and ascorbate regeneration through the glutathione-ascorbate cycle (Foyer et al. 1994).

The enzymes SOD and APX are involved in scavenging reactive oxygen species in the chloroplast. O_2^- generated by reduction of O_2 by PSI is metabolized enzymatically by SOD to produce H_2O_2. The subsequent reduction of H_2O_2 by APX produces the monodehydroascorbate radical, which can be directly reduced by PSI (via ferredoxin) in the water-water cycle (Asada 1999). Ascorbate can also be regenerated in the stroma by the set of enzymes comprising the glutathione-ascorbate cycle.

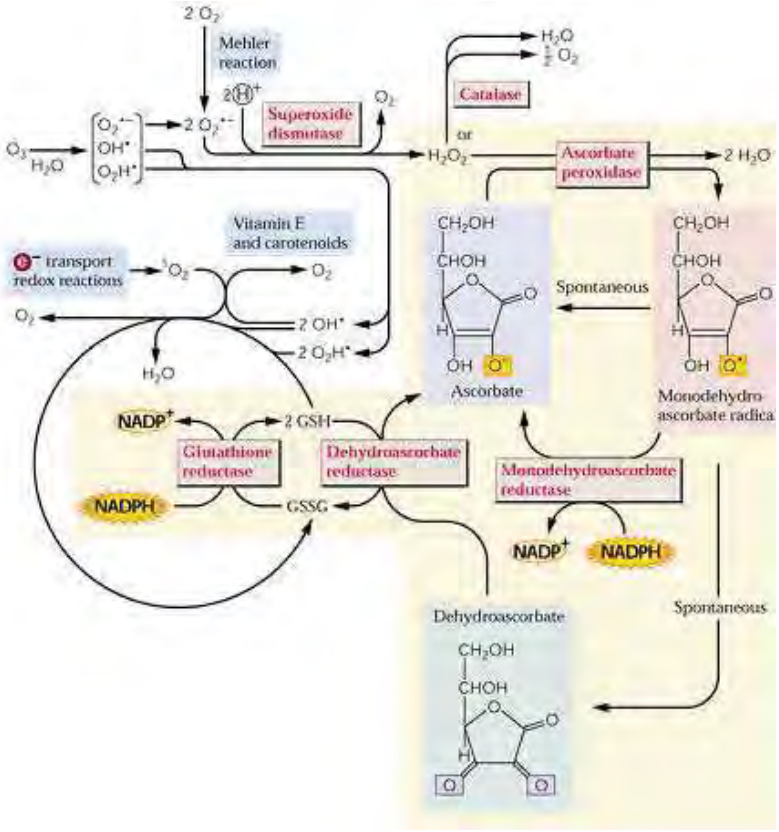

Figure 24. *Different pathways for reactive oxygen species (ROS) scavenging in plants.*

1.4.9 Repair of photodamage

Despite multiple lines of defense, damage to the photosynthetic apparatus is an inevitable consequence of oxygenic photosynthesis, and the PSII reaction centre is especially susceptible to photo-oxidative damage. Therefore, oxygenic photosynthetic organisms have evolved an elaborate but efficient system for repairing PSII that involves selective degradation of D1 and incorporation of newly synthesized proteins to functional PSII (Aro et al. 1993). The rate of repair must match the rate of damage to avoid photoinhibition resulting from net loss of functional PSII centres. Therefore, continual new synthesis is critical for photoprotection at all light intensities. Blocking chloroplast protein synthesis with inhibitors during exposure to light results in photoinhibition and net loss of D1 protein (Tyystjärvi et al. 1994).

1.4.9 Long-term photoprotective mechanisms

When plants are exposed for a long time to stress conditions, long-term photoprotective mechanisms are activated. Many plants compensate for changes in incident light quantity and quality by control of Chls content in leaves and by modification of plant architecture and composition. Plants change from an energy conserving organization typical of light-limiting conditions and towards an organization favoring photoprotection. For example, the size of photosynthetic antenna systems, particularly PSII, is reduced, the PSII/PSI ratio decreased and the stoichiometry of electron transport components and ATPase is up-regulated with respect to photosynthetic reaction centres and the enzymes of Calvin cycle is increased. In *A. thaliana*, this regulation is mediated directly by photoreceptors such as cryptochrome (Ruckle et al. 2007), or through biochemical and metabolic signals such as the plastoquinone redox state, the release of ROS, the redox state of the glutathione pool and the ATP/ADP ratio (Pfannschmidt et al. 1999, op den Camp et al. 2003).

Reference List

Alboresi, A., M. Ballottari, R. Hienerwadel, G. M. Giacometti and T. Morosinotto (2009). "Antenna complexes protect Photosystem I from photoinhibition." BMC.Plant Biol. **9**: 71.

Allen, J. F. (1992). "Protein phosphorylation in regulation of photosynthesis." Biochim Biophys Acta **1098**(3): 275-335.

Amunts, A., O. Drory and N. Nelson (2007). "The structure of a plant photosystem I supercomplex at 3.4 A resolution." Nature **447**(7140): 58-63.

Andersson, J., R. G. Walters, P. Horton and S. Jansson (2001). "Antisense inhibition of the photosynthetic antenna proteins CP29 and CP26: Implications for the mechanism of protective energy dissipation." Plant Cell **13**(5): 1193-1204.

Andersson, J., M. Wentworth, R. G. Walters, C. A. Howard, A. V. Ruban, P. Horton and S. Jansson (2003). "Absence of the Lhcb1 and Lhcb2 proteins of the light-harvesting complex of photosystem II - effects on photosynthesis, grana stacking and fitness." Plant J. **35**(3): 350-361.

Andersson, P. O., T. Gillbro, L. Ferguson and R. J. Cogdell (1991). "Absorption Spectral Shifts of Carotenoids Related to Medium Polarizability." Photochem.Photobiol. **54**: 353-360.

Andrews, J. R., M. J. Fryer and N. R. Baker (1995). "Consequences of LHC II deficiency for photosynthetic regulation in chlorina mutans of barley." Photosynth.Res. **44**: 81-91.

Aro, E.-M., S. McCaffery and J. M. Anderson (1993). "Photoinhibition and D1 protein degradation in peas acclimated to different growth irradiances." Plant Physiol. **103**: 835-843.

Aro, E.-M., I. Virgin and B. Andersson (1993). "Photoinhibition of Photosystem II - inactivation, protein damage and turnover." Biochim.Biophys.Acta **1143**: 113-134.

Asada, K. (1999). "The water-water cycle in chloroplasts: scavenging of active oxygens and dissipation of excess photons." Annu.Rev.Plant Physiol Plant Mol.Biol. **50**: 601-639.

Aspinall-O'Dea, M., M. Wentworth, A. Pascal, B. Robert, A. V. Ruban and P. Horton (2002). "In vitro reconstitution of the activated zeaxanthin state associated with energy dissipation in plants." Proc.Natl.Acad.Sci.U.S.A **99**(25): 16331-16335.

Avenson, T. J., T. K. Ahn, K. K. Niyogi, M. Ballottari, R. Bassi and G. R. Fleming (2009). "Lutein can act as a switchable charge transfer quencher in the CP26 light-harvesting complex." J Biol Chem **284**(5): 2830-2835.

Ballottari, M., J. Girardon, L. Dall'Osto and R. Bassi (2012). "Evolution and functional properties of Photosystem II light harvesting complexes in eukaryotes." Biochimica et Biophysica Acta-Bioenergetics **1817**(1): 143-157.

Barber, J. (1980). "Membrane surface charges and potentials in relation to photosynthesis." Biochim.Biophys.Acta **594**: 253-308.

Barber, J., E. Morris and C. Büchel (2000). "Revealing the structure of the photosystem II chlorophyll binding proteins, CP43 and CP47." Biochim.Biophys.Acta **1459**: 239-247.

Bassi, R. and S. Caffarri (2000). "Lhc proteins and the regulation of photosynthetic light harvesting function by xanthophylls." Photosynthesis Research **64**(2-3): 243-256.

Bassi, R., E. Giuffra, R. Croce, P. Dainese and E. Bergantino (1996). Biochemistry and molecular biology of pigment binding proteins. R. C. Jennings, G. Zucchelli, F. Ghetti and G. Colombetti. New York, Plenum Press. **287:** 41-63.

Bassi, R., G. Hoyer-hansen, R. Barbato, G. M. Giacometti and D. J. Simpson (1987). "Chlorophyll-proteins of the photosystem-II antenna system." J.Biol.Chem. **262**: 13333-13341.

Bellafiore, S., F. Barneche, G. Peltier and J. D. Rochaix (2005). "State transitions and light adaptation require chloroplast thylakoid protein kinase STN7." Nature **433**(7028): 892-895.

Ben Shem, A., F. Frolow and N. Nelson (2004). "Light-harvesting features revealed by the structure of plant Photosystem I." Photosynthesis Research **81**(3): 239-250.

Benson, A. A. and M. Calvin (1950). "Carbon Dioxide Fixation by Green Plants." Annual Review of Plant Physiology and Plant Molecular Biology **1**: 25-42.

Betterle, N., B. M., S. Zorzan, S. de Bianchi, S. Cazzaniga, L. Dall'Osto, T. Morosinotto and R. Bassi (2009). "Light-induced dissociation of an antenna hetero-oligomer is needed for non-photochemical quenching induction." Journal of Biological Chemistry **284**(22): 15255-15266.

Bonente, G., B. D. Howes, S. Caffarri, G. Smulevich and R. Bassi (2007). "Interactions between the photosystem II subunit psbs and xanthophylls studied in vivo and in vitro." J.Biol Chem. **283**(13): 8434-8445.

Britton, G. (1995). "Structure and properties of carotenoids in relation to function." Faseb j **9**(15): 1551-1558.

Buchanan, B. B. (1991). "Regulation of CO2 assimilation in oxygenic photosynthesis: the ferredoxin/thioredoxin system. Perspective on its discovery, present status, and future development." Arch Biochem Biophys **288**(1): 1-9.

Butler, W. L. and M. Kitajima (1975). "Fluorescence Quenching in Photosystem II of Chloroplasts." Biochim.Biophys.Acta **376**: 116-125.

Caffarri, S., R. Croce, J. Breton and R. Bassi (2001). "The major antenna complex of photosystem II has a xanthophyll binding site not involved in light harvesting." J.Biol.Chem. **276**(38): 35924-35933.

Caffarri, S., R. Croce, L. Cattivelli and R. Bassi (2004). "A look within LHCII: differential analysis of the Lhcb1-3 complexes building the major trimeric antenna complex of higher-plant photosynthesis." Biochemistry **43**(29): 9467-9476.

Caffarri, S., R. Kouril, S. Kereiche, E. J. Boekema and R. Croce (2009). "Functional architecture of higher plant photosystem II supercomplexes." EMBO J. **28**: 3052-3063.

Caffarri, S., F. Passarini, R. Bassi and R. Croce (2007). "A specific binding site for neoxanthin in the monomeric antenna proteins CP26 and CP29 of Photosystem II." FEBS Lett. **581**(24): 4704-4710.

Caffarri, S., T. Tibiletti, R. C. Jennings and S. Santabarbara (2014). "A comparison between plant photosystem I and photosystem II architecture and functioning." Curr Protein Pept Sci **15**(4): 296-331.

Castelletti, S., T. Morosinotto, B. Robert, S. Caffarri, R. Bassi and R. Croce (2003). "Recombinant Lhca2 and Lhca3 subunits of the photosystem I antenna system." Biochemistry **42**(14): 4226-4234.

Christie, J. M. (2007). "Phototropin blue-light receptors." Annu Rev Plant Biol **58**: 21-45.

Croce, R., J. Breton and R. Bassi (1996). "Conformational Changes Induced by Phosphorylation in the CP29 Subunit of Photosystem II." Biochemistry **35**: 11142-11148.

Croce, R., g. Canino, F. Ros and R. Bassi (2002). "Chromophore organization in the higher-plant photosystem II antenna protein CP26." Biochemistry **41**(23): 7334-7343.

Croce, R., T. Morosinotto, S. Castelletti, J. Breton and R. Bassi (2002). "The Lhca antenna complexes of higher plants photosystem I." Biochimica et Biophysica Acta-Bioenergetics **1556**(1): 29-40.

Dall'Osto, L., S. Caffarri and R. Bassi (2005). "A mechanism of nonphotochemical energy dissipation, independent from Psbs, revealed by a conformational change in the antenna protein CP26." Plant Cell **17**(4): 1217-1232.

Dall'Osto, L., A. Fiore, S. Cazzaniga, G. Giuliano and R. Bassi (2007). "Different roles of a- and b-branch xanthophylls in photosystem assembly and photoprotection." J.Biol.Chem. **282**(48): 35056-35068.

Damkjaer, J., S. Kereiche, M. P. Johnson, L. Kovacs, a. z. kiss, E. J. Boekema, A. V. Ruban, P. Horton and S. Jansson (2009). "The Photosystem II light-harvesting protein Lhcb3 affects the macrostructure of Photosystem II and the rate of state transitions in Arabidopsis." Plant Cell **21**: 3245-3256.

Dau, H. (1994). "Molecular mechanisms and quantitative models of variable photosystem II fluorescence." Photochem.Photobiol. **60**: 1-23.

de Bianchi, S., N. Betterle, R. Kouril, S. Cazzaniga, E. Boekema, R. Bassi and L. Dall'Osto (2011). "*Arabidopsis* mutants deleted in the light-harvesting protein Lhcb4 have a disrupted Photosystem II macrostructure and are defective in photoprotection." Plant Cell **23**(7): 2659-2679.

de Bianchi, S., L. Dall'Osto, G. Tognon, T. Morosinotto and R. Bassi (2008). "Minor antenna proteins CP24 and CP26 affect the interactions between photosystem II subunits and the electron transport rate in grana membranes of Arabidopsis." Plant Cell **20**: 1012-1028.

Dekker, J. P. and E. J. Boekema (2005). "Supramolecular organization of thylakoid membrane proteins in green plants." Biochim.Biophys.Acta **1706**(1-2): 12-39.

Demmig-Adams, B. (1990). "Carotenoids and photoprotection in plants: A role for the xanthophyll zeaxanthin." Biochim.Biophys.Acta **1020**: 1-24.

Demmig-Adams, B., W. W. Adams, U. Heber, S. Neimanis, K. Winter, A. Krüger, F.-C. Czygan, W. Bilger and O. Björkman (1990). "Inhibition of zeaxanthin formation and of rapid changes in radiationless energy dissipation by dithiothreitol in spinach leaves and chloroplasts." Plant Physiol. **92**: 293-301.

Demmig-Adams, B., A. M. Gilmore and W. W. Adams, 3rd (1996). "Carotenoids 3: in vivo function of carotenoids in higher plants." Faseb j **10**(4): 403-412.

Dominici, P., S. Caffarri, F. Armenante, S. Ceoldo, M. Crimi and R. Bassi (2002). "Biochemical properties of the PsbS subunit of photosystem II either purified from chloroplast or recombinant." J.Biol.Chem. **277**(25): 22750-22758.

Ehleringer, J. and I. Forseth (1980). "Solar tracking by plants." Science **210**(4474): 1094-1098.

Ferreira, K. N., T. M. Iverson, K. Maghlaoui, J. Barber and S. Iwata (2004). "Architecture of the photosynthetic oxygen-evolving center." Science **303**(5665): 1831-1838.

Fischer, N., E. Boudreau, M. Hippler, F. Drepper, W. Haehnel and J. D. Rochaix (1999). "A large fraction of PsaF is nonfunctional in photosystem I complexes lacking the PsaJ subunit." Biochemistry **38**(17): 5546-5552.

Foyer, C. H., P. Descourvieres and K. J. Kunert (1994). "PROTECTION AGAINST OXYGEN RADICALS - AN IMPORTANT DEFENSE-MECHANISM STUDIED IN TRANSGENIC PLANTS." Plant Cell and Environment **17**(5): 507-523.

Frank, H. A., J. A. Bautista, J. S. Josue and A. J. Young (2000). "Mechanism of nonphotochemical quenching in green plants: Energies of the lowest excited singlet states of violaxanthin and zeaxanthin." Biochemistry **39**: 2831-2837.

Fryer, M. J. (1992). "THE ANTIOXIDANT EFFECTS OF THYLAKOID VITAMIN-E(ALPHA-TOCOPHEROL)." Plant Cell and Environment **15**(4): 381-392.

Funk, C., G. Renger, I. Adamska, B. Andersson and P. Schröder (1995). The PS II-S polypeptide. An atypical CAB protein. From Light to Biophere Vol.I. Dordrecht, Kluwer**:** 339-342.

Galka, P., S. Santabarbara, T. T. H. Khuong, H. Degand, P. Morsomme, R. C. Jennings, E. J. Boekema and C. S (2012). "Functional analyses of the plant Photosystem I–Light-harvesting complex II supercomplex reveal that Light-harvesting complex II loosely bound to Photosystem II is a very efficient antenna for Photosystem I in state II." Plant Cell **24**(7): 2963-2978.

Ganeteg, U., F. Klimmek and S. Jansson (2004). "Lhca5 - an LHC-Type Protein Associated with Photosystem I." Plant Mol.Biol. **54**(5): 641-651.

Genty, B., J.-M. Briantais and N. R. Baker (1989). "The relationship between the quantum yield of photosynthetic electron transport and quenching of chlorophyll fluorescence." Biochim.Biophys.Acta **990**: 87-92.

Gobets, B. and R. van Grondelle (2001). "Energy transfer and trapping in Photosystem I." Biochim.Biophys.Acta **1057**(1-3): 80-99.

Gradinaru, C. C., I. H. M. van Stokkum, A. A. Pascal, R. van Grondelle and H. Van Amerongen (2000). "Identifying the pathways of energy transfer between carotenoids and chlorophylls in LHCII and CP29. A multicolor, femtosecond pump - probe study." J.Phys.Chem.B **104**: 9330-9342.

Haldrup, A., H. Naver and H. V. Scheller (1999). "The interaction between plastocyanin and photosystem I is inefficient in transgenic Arabidopsis plants lacking the PSI-N subunit of photosystem I." Plant J. **17**: 689-698.

Harbinson, J. and C. H. Foyer (1991). "Relationships Between the Efficiencies of Photosystem- I and Photosystem-II and Stromal Redox State in CO2- Free Air - Evidence for Cyclic Electron Flow In Vivo." Plant Physiol. **97**: 41-49.

Havaux, M. and K. K. Niyogi (1999). "The violaxanthin cycle protects plants from photooxidative damage by more than one mechanism." Proc.Natl.Acad.Sci.U.S.A **96**(15): 8762-8767.

Heber, U. and D. Walker (1992). "CONCERNING A DUAL FUNCTION OF COUPLED CYCLIC ELECTRON-TRANSPORT IN LEAVES." Plant Physiology **100**(4): 1621-1626.

Hieber, A. D., R. C. Bugos and H. Y. Yamamoto (2000). "Plant lipocalins: violaxanthin de-epoxidase and zeaxanthin epoxidase." Biochim.Biophys.Acta **1482**(1-2): 84-91.

Hill, R. and F. Bendall (1960). "Function of the two cytochrome components in chloroplasts: A working hypothesis." Nature **186**: 136-137.

Holt, N. E., G. R. Fleming and K. K. Niyogi (2004). "Toward an understanding of the mechanism of nonphotochemical quenching in green plants." Biochemistry **43**(26): 8281-8289.

Holt, N. E., D. Zigmantas, L. Valkunas, X. P. Li, K. K. Niyogi and G. R. Fleming (2005). "Carotenoid cation formation and the regulation of photosynthetic light harvesting." Science **307**(5708): 433-436.

Horton, P. (1996). Nonphotochemical quenching of chlorophyll fluorescence. Light as an Energy Source and Information Carrier in Plant Physiology. R. C. Jennings. Plenum Press, New York**:** 99-111.

Horton, P. and A. Hague (1988). "Studies on the induction of chlorophyll fluorescence in isolated barley protoplasts. IV. Resolution of non-photochemical quenching." Biochim.Biophys.Acta **932**: 107-115.

Jahns, P., A. Polle and W. Junge (1988). "The photosynthetic water oxidase: its proton pumping activity is short-circuited within the protein by DCCD." Embo j **7**(3): 589-594.

Jansson, S. (1999). "A guide to the Lhc genes and their relatives in Arabidopsis." Trends Plant Sci. **4**: 236-240.

Jarillo, J. A., H. Gabrys, J. Capel, J. M. Alonso, J. R. Ecker and A. R. Cashmore (2001). "Phototropin-related NPL1 controls chloroplast relocation induced by blue light." Nature **410**(6831): 952-954.

Jennings, R. C. and G. Zucchelli (1986). "Studies on thylakoid phosphorylation and noncyclic electron transport." Arch.Biochem.Biophys. **246**(1): 108-113.

Jensen, P. E., R. Bassi, E. J. Boekema, J. P. Dekker, S. Jansson, D. Leister, C. Robinson and H. V. Scheller (2007). "Structure, function and regulation of plant photosystem I." Biochim Biophys Acta **1767**(5): 335-352.

Joliot, P., P. Bennoun and A. Joliot (1973). "New Evidence Supporting Energy-Transfer Between Photosynthetic Units." Biochimica et Biophysica Acta **305**(2): 317-328.

Jordan, P., P. Fromme, H. T. Witt, O. Klukas, W. Saenger and N. Krauss (2001). "Three-dimensional structure of cyanobacterial photosystem I at 2.5 A resolution." Nature **411**(6840): 909-917.

Kasahara, M., T. Kagawa, K. Oikawa, N. Suetsugu, M. Miyao and M. Wada (2002). "Chloroplast avoidance movement reduces photodamage in plants." Nature **420**: 829-832.

Kovacs, L., J. Damkjaer, S. Kereiche, C. Ilioaia, A. V. Ruban, E. J. Boekema, S. Jansson and P. Horton (2006). "Lack of the light-harvesting complex CP24 affects the structure and function of the grana membranes of higher plant chloroplasts." Plant Cell **18**(11): 3106-3120.

Krause, G. H. (1988). "Photoinhibition of photosynthesis. An evaluation of damaging and protective mechanisms." Physiol.Plant. **74**: 566-574.

Kull, O. and H. Pfander (1995). List of new carotenoids. Carotenoids: Isolation and Analysis. S. L.-J. G.Britton, and H.Pfander,eds. Basel, Birkauser Publishing**:** 295-317.

Kurisu, G., H. Zhang, J. L. Smith and W. A. Cramer (2003). "Structure of the cytochrome b6f complex of oxygenic photosynthesis: tuning the cavity." Science **302**(5647): 1009-1014.

Li, X. P., O. Bjorkman, C. Shih, A. R. Grossman, M. Rosenquist, S. Jansson and K. K. Niyogi (2000). "A pigment-binding protein essential for regulation of photosynthetic light harvesting." Nature **403**(6768): 391-395.

Li, X. P., A. M. Gilmore, S. Caffarri, R. Bassi, T. Golan, D. Kramer and K. K. Niyogi (2004). "Regulation of photosynthetic light harvesting involves intrathylakoid lumen pH sensing by the PsbS protein." J.Biol.Chem. **279**(22): 22866-22874.

Liu, Z., H. Yan, K. Wang, T. Kuang, J. Zhang, L. Gui, X. An and W. Chang (2004). "Crystal structure of spinach major light-harvesting complex at 2.72 A resolution." Nature **428**(6980): 287-292.

Lucinski, R., V. H. R. Schmid, S. Jansson and F. Klimmek (2006). "Lhca5 interaction with plant photosystem I." FEBS Letters **580**(27): 6485-6488.

Lunde, C., P. E. Jensen, A. Haldrup, J. Knoetzel and H. V. Scheller (2000). "The PSI-H subunit of photosystem I is essential for state transitions in plant photosynthesis." Nature **408**(6812): 613-615.

McCarty, R. E., Y. Evron and E. A. Johnson (2000). "THE CHLOROPLAST ATP SYNTHASE: A Rotary Enzyme?" Annu Rev Plant Physiol Plant Mol Biol **51**: 83-109.

Mehler, A. H. (1951). "Studies on reactions of illuminated chloroplasts. I. Mechanism of the reduction of oxygen and other Hill reagents." Arch Biochem Biophys **33**(1): 65-77.

Miloslavina, Y., S. de Bianchi, L. Dall'Osto, R. Bassi and A. R. Holzwarth (2011). "Quenching in Arabidopsis thaliana mutants lacking monomeric antenna proteins of photosystem II." J.Biol.Chem. **286**(42): 36830-36840.

Miloslavina, Y., A. Wehner, P. H. Lambrev, E. Wientjes, M. Reus, G. Garab, R. Croce and A. R. Holzwarth (2008). "Far-red fluorescence: a direct spectroscopic marker for LHCII oligomer formation in non-photochemical quenching." FEBS Lett. **582**: 3625-3631.

Mimuro, M. and T. Katoh (1991). "Carotenoids in photosynthesis: Absorption, transfer and dissipation of light energy." Pure Appl.Chem. **63**: 123-130.

Mitchell, P. (1961). "Coupling of phosphorylation to electron and hydrogen transfer by a chemi-osmotic type of mechanism." Nature **191**: 144-148.

Muller, M. G., P. Lambrev, M. Reus, E. Wientjes, R. Croce and A. R. Holzwarth (2010). "Singlet energy dissipation in the photosystem II light-harvesting complex does not involve energy transfer to carotenoids." Chemphyschem. **11**(6): 1289-1296.

Muller, P., X. P. Li and K. K. Niyogi (2001). "Non-photochemical quenching. A response to excess light energy." Plant Physiol **125**(4): 1558-1566.

Mullet, J. E., J. J. Burke and C. J. Arntzen (1980). "Chlorophyll proteins of photosystem I." Plant Physiol. **65**: 814-822.

Nagy, G., R. Unnep, O. Zsiros, R. Tokutsu, K. Takizawa, L. Porcar, L. Moyet, D. Petroutsos, G. Garab, G. Finazzi and J. Minagawa (2014). "Chloroplast remodeling during state transitions in Chlamydomonas reinhardtii as revealed by noninvasive techniques in vivo." Proc Natl Acad Sci U S A **111**(13): 5042-5047.

Nelson, N. and A. Ben Shem (2004). "The complex architecture of oxygenic photosynthesis." Nature **5**: 1-12.

Nield, J., E. V. Orlova, E. P. Morris, B. Gowen, M. van Heel and J. Barber (2000). "3D map of the plant photosystem II supercomplex obtained by cryoelectron microscopy and single particle analysis." Nat.Struct.Biol. **7**(1): 44-47.

Nilkens, M., E. Kress, P. Lambrev, Y. Miloslavina, M. Muller, A. R. Holzwarth and P. Jahns (2010). "Identification of a slowly inducible zeaxanthin-dependent component of non-photochemical quenching of chlorophyll fluorescence generated under steady-state conditions in Arabidopsis." Biochim.Biophys.Acta **1797**(4): 466-475.

Nilsson, A., D. Stys, T. Drakenberg, M. D. Spangfort, S. Forsen and J. F. Allen (1997). "Phosphorylation controls the three-dimensional structure of plant light harvesting complex II." J.Biol.Chem. **272**: 18350-18357.

Niyogi, K. K. (1999). "Photoprotection revisited: genetic and molecular approaches." Annu.Rev.Plant Physiol.Plant Mol.Biol. **50**: 333-359.

Niyogi, K. K., O. Bjorkman and A. R. Grossman (1997). "The roles of specific xanthophylls in photoprotection." Proc.Natl.Acad.Sci.U.S.A **94**(25): 14162-14167.

Niyogi, K. K., A. R. Grossman and O. Björkman (1998). "Arabidopsis mutants define a central role for the xanthophyll cycle in the regulation of photosynthetic energy conversion." Plant Cell **10**: 1121-1134.

Niyogi, K. K., C. Shih, W. S. Chow, B. J. Pogson, D. DellaPenna and O. Björkman (2001). "Photoprotection in a zeaxanthin- and lutein-deficient double mutant of Arabidopsis." Photosynth.Res. **67**: 139-145.

op den Camp, R. G., D. Przybyla, C. Ochsenbein, C. Laloi, C. Kim, A. Danon, D. Wagner, E. Hideg, C. Gobel, I. Feussner, M. Nater and K. Apel (2003). "Rapid induction of distinct stress responses after the release of singlet oxygen in Arabidopsis." Plant Cell **15**(10): 2320-2332.

Osmond, C. B. (1981). "PHOTO-RESPIRATION AND PHOTOINHIBITION SOME IMPLICATIONS FOR THE ENERGETICS OF PHOTOSYNTHESIS." Biochimica Et Biophysica Acta **639**(2): 77-98.

Pagano, A., G. Cinque and R. Bassi (1998). "

In vitro reconstitution of the recombinant photosystem II light-harvesting complex CP24 and its spectroscopic characterization." J.Biol.Chem. **273**(27): 17154-17165.

Pan, X., M. Li, T. Wan, L. Wang, C. Jia, Z. Hou, X. Zhao, J. Zhang and W. Chang (2011). "Structural insights into energy regulation of light-harvesting complex CP29 from spinach." Nat.Struct.Mol.Biol. **18**(3): 309-315.

Pascal, A. A., Z. Liu, K. Broess, B. van Oort, H. Van Amerongen, C. Wang, P. Horton, B. Robert, W. Chang and A. Ruban (2005). "Molecular basis of photoprotection and control of photosynthetic light-harvesting." Nature **436**(7047): 134-137.

Pastenes, C., P. Pimentel and J. Lillo (2005). "Leaf movements and photoinhibition in relation to water stress in field-grown beans." J Exp Bot **56**(411): 425-433.

Paulsen, H., B. Finkenzeller and N. Kuhlein (1993). "PIGMENTS INDUCE FOLDING OF LIGHT-HARVESTING CHLOROPHYLL ALPHA/BETA-BINDING PROTEIN." Eur.J.Biochem. **215**(3): 809-816.

Peng, L. W., Y. Fukao, M. Fujiwara, T. Takami and T. Shikanai (2009). "Efficient Operation of NAD(P)H Dehydrogenase Requires Supercomplex Formation with Photosystem I via Minor LHCI in Arabidopsis." Plant Cell **21**(11): 3623-3640.

Peng, L. W., Y. Fukao, F. Myouga, R. Motohashi, K. Shinozaki and T. Shikanai (2011). "A Chaperonin Subunit with Unique Structures Is Essential for Folding of a Specific Substrate." Plos Biology **9**(4).

Pfannschmidt, T., A. Nilsson and J. F. Allen (1999). "Photosynthetic control of chloroplast gene expression." Nature **397**(6720): 625-628.

Pietrzykowska, M., M. Suorsa, D. A. Semchonok, M. Tikkanen, E. J. Boekema, E. M. Aro and S. Jansson (2014). "The Light-Harvesting Chlorophyll a/b Binding Proteins Lhcb1 and Lhcb2 Play Complementary Roles during State Transitions in Arabidopsis." Plant Cell **Epub ahead of print**.

Plumley, F. G. and G. W. Schmidt (1987). "Reconstitution of chloroform a/b light-harvesting complexes: Xanthophyll-dependent assembley and energy transfer." Proc.Natl.Acad.Sci.U.S.A **84**: 146-150.

Pogson, B. J., K. K. Niyogi, O. Bjorkman and D. DellaPenna (1998). "Altered xanthophyll compositions adversely affect chlorophyll accumulation and nonphotochemical quenching in Arabidopsis mutants." Proc.Natl.Acad.Sci.U.S.A **95**(22): 13324-13329.

Porcar-Castell, A., E. Tyystjarvi, J. Atherton, C. van der Tol, J. Flexas, E. E. Pfundel, J. Moreno, C. Frankenberg and J. A. Berry (2014). "Linking chlorophyll a fluorescence to photosynthesis for remote sensing applications: mechanisms and challenges." J Exp Bot **65**(15): 4065-4095.

Remelli, R., C. Varotto, D. Sandona, R. Croce and R. Bassi (1999). "Chlorophyll binding to monomeric light-harvesting complex. A mutation analysis of chromophore-binding residues." J.Biol.Chem. **274**(47): 33510-33521.

Rintamaki, E., M. Salonen, U. M. Suoranta, I. Carlberg, B. Andersson and E. M. Aro (1997). "Phosphorylation of light-harvesting complex II and photosystem II core proteins shows different irradiance-dependent regulation in vivo. Application of phosphothreonine antibodies to analysis of thylakoid phosphoproteins." J.Biol.Chem. **272**(48): 30476-30482.

Rivadossi, A., G. Zucchelli, F. M. Garlaschi and R. C. Jennings (1999). "The importance of PSI chlorophyll red forms in light-harvesting by leaves." Photosynt.Res. **60**: 209-215.

Rochaix, J. D. (2007). "Role of thylakoid protein kinases in photosynthetic acclimation." FEBS Lett **581**(15): 2768-2775.

Rochaix, J. D., S. Lemeille, A. Shapiguzov, I. Samol, G. Fucile, A. Willig and M. Goldschmidt-Clermont (2012). "Protein kinases and phosphatases involved in the acclimation of the photosynthetic apparatus to a changing light environment." Philos Trans R Soc Lond B Biol Sci **367**(1608): 3466-3474.

Ruban, A. V., R. Berera, C. Ilioaia, I. H. van Stokkum, J. T. Kennis, A. A. Pascal, H. Van Amerongen, B. Robert, P. Horton and R. van Grondelle (2007). "Identification of a mechanism of photoprotective energy dissipation in higher plants." Nature **450**(7169): 575-578.

Ruban, A. V., P. J. Lee, M. Wentworth, A. J. Young and P. Horton (1999). "Determination of the stoichiometry and strength of binding of xanthophylls to the photosystem II light harvesting complexes." J.Biol.Chem. **274**: 10458-10465.

Ruban, A. V., A. Young and P. Horton (1994). "Modulation of chlorophyll fluorescence quenching in isolated light harvesting complex of Photosystem II." Biochim.Biophys.Acta **1186**: 123-127.

Ruckle, M. E., S. M. DeMarco and R. M. Larkin (2007). "Plastid signals remodel light signaling networks and are essential for efficient chloroplast biogenesis in Arabidopsis." Plant Cell **19**(12): 3944-3960.

Sarvikas, P., T. Tyystjarvi and E. Tyystjarvi (2010). "Kinetics of prolonged photoinhibition revisited: photoinhibited Photosystem II centres do not protect the active ones against loss of oxygen evolution." Photosynth Res **103**(1): 7-17.

Scheller, H. V., P. E. Jensen, A. Haldrup, C. Lunde and J. Knoetzel (2001). "Role of subunits in eukaryotic Photosystem I." Biochim.Biophys.Acta **1507**: 41-60.

Shapiguzov, A., B. Ingelsson, I. Samol, C. Andres, F. Kessler, J. D. Rochaix, A. V. Vener and M. Goldschmidt-Clermont (2010). "The PPH1 phosphatase is specifically involved in LHCII dephosphorylation and state transitions in Arabidopsis." Proc Natl Acad Sci U S A **107**(10): 4782-4787.

Shi, L. X., M. Hall, C. Funk and W. P. Schroder (2012). "Photosystem II, a growing complex: updates on newly discovered components and low molecular mass proteins." Biochim Biophys Acta **1817**(1): 13-25.

Shikanai, T., Y. Munekage, K. Shimizu, T. Endo and T. Hashimoto (1999). "Identification and characterization of Arabidopsis mutants with reduced quenching of chlorophyll fluorescence." Plant Cell Physiol. **40**: 1134-1142.

Smirnoff, N. (1996). "The function and metabolism of ascorbic acid in plants." Annals of Botany **78**(6): 661-669.

Tardy, F. and M. Havaux (1996). "Photosynthesis, chlorophyll fluorescence, light-harvesting system and photoinhibition resistance of a zeaxanthin- accumulating mutant of Arabidopsis thaliana." J.Photochem.Photobiol.B **34**: 87-94.

Teardo, E., P. P. De Laureto, E. Bergantino, V. F. Dalla, F. Rigoni, I. Szabo and G. M. Giacometti (2007). "Evidences for interaction of PsbS with photosynthetic complexes in maize thylakoids." Biochim.Biophys.Acta **1767**(6): 703-711.

Telfer, A., S. Dhami, S. M. Bishop, D. Phillips and J. Barber (1994). "b-carotene quenches singlet oxygen formed by isolated photosystem II reaction centers." Biochemistry **33**: 14469-14474.

Thornber, J. P., J. C. Stewart, M. W. Hatton and J. L. Bailey (1967). "Studies on the nature of chloroplast lamellae. II. Chemical composition and further physical properties of two chlorophyll-protein complexes." Biochemistry **6**(7): 2006-2014.

Trumpower, B. L. (1990). "The protonmotive Q cycle. Energy transduction by coupling of proton translocation to electron transfer by the cytochrome bc1 complex." J Biol Chem **265**(20): 11409-11412.

Tyystjärvi, E., R. Kettunen and E.-M. Aro (1994). "The rate constant of photoinhibition in vitro is independent of the antenna size of Photosystem II but depends on temperature." Biochim.Biophys.Acta **1186**: 177-185.

van Oort, B., M. Alberts, S. de Bianchi, L. Dall'Osto, R. Bassi, G. Trinkunas, R. Croce and H. Van Amerongen (2010). "Effect of antenna-depletion in Photosystem II on excitation energy transfer in Arabidopsis thaliana." Biophysical Journal **98**: 922-931.

Vass, I., S. Styring, T. Hundal, A. Koivuniemi, E.-M. Aro and B. Andersson (1992). "Reversible and irreversible intermediates during photoinhibition of photosystem II: Stable reduced QA species promote chlorophyll triplet formation." Proc.Natl.Acad.Sci.USA **89**: 1408-1412.

Wada, M., T. Kagawa and Y. Sato (2003). "Chloroplast movement." Ann.Rev.Plant Biol. **54**: 455-468.

Wientjes, E. and R. Croce (2011). "The light-harvesting complexes of higher-plant Photosystem I: Lhca1/4 and Lhca2/3 form two red-emitting heterodimers." Biochemical Journal **433**: 477-485.

Wilk, L., M. Grunwald, P. N. Liao, P. J. Walla and W. Kuhlbrandt (2013). "Direct interaction of the major light-harvesting complex II and PsbS in nonphotochemical quenching." Proc Natl Acad Sci U S A **110**(14): 5452-5456.

Yamamoto, H. Y. and L. Kamite (1972). "The effects of dithiothreitol on violaxanthin deepoxidation and absorbance changes in the 500nm region." Biochim.Biophys.Acta **267**: 538-543.

Zhang, S. and H. V. Scheller (2004). "Photoinhibition of Photosystem I at chilling temperature and subsequernt recovery in Arabidopsis thaliana." Plant and Cell Physiology **45**(11): 1595-1602.

Zito, F., G. Finazzi, R. Delosme, W. Nitschke, D. Picot and F. A. Wollman (1999). "The Qo site of cytochrome b6f complexes controls the activation of the LHCII kinase." EMBO J. **18**(11): 2961-2969.

Zouni, A., H. T. Witt, J. Kern, P. Fromme, N. Krauss, W. Saenger and P. Orth (2001). "Crystal structure of photosystem II from Synechococcus elongatus at 3.8 A resolution." Nature **409**(6821): 739-743.

Section A.
Role of carotenoids in photoprotection and composition of photosynthetic complexes.

A1. A quadruple mutant of *Arabidopsis thaliana* reveals a β-carotene hydroxylation activity for LUT1/CYP97C1 and a regulatory role of xanthophylls on determination of the PSI/PSII ratio.

Fiore et al. BMC Plant Biology 2012, 12:50
http://www.biomedcentral.com/1471-2229/12/50

BMC Plant Biology

RESEARCH ARTICLE Open Access

A quadruple mutant of Arabidopsis reveals a β-carotene hydroxylation activity for LUT1/CYP97C1 and a regulatory role of xanthophylls on determination of the PSI/PSII ratio

Alessia Fiore[1†], Luca Dall'Osto[2†], Stefano Cazzaniga[2], Gianfranco Diretto[1], Giovanni Giuliano[1] and Roberto Bassi[2,3,4*]

Abstract

Background: Xanthophylls are oxygenated carotenoids playing an essential role as structural components of the photosynthetic apparatus. Xanthophylls contribute to the assembly and stability of light-harvesting complex, to light absorbance and to photoprotection. The first step in xanthophyll biosynthesis from α- and β-carotene is the hydroxylation of ε- and β-rings, performed by both non-heme iron oxygenases (CHY1, CHY2) and P450 cytochromes (LUT1/CYP97C1, LUT5/CYP97A3). The Arabidopsis triple *chy1chy2lut5* mutant is almost completely depleted in β-xanthophylls.

Results: Here we report on the quadruple *chy1chy2lut2lut5* mutant, additionally carrying the *lut2* mutation (affecting lycopene ε-cyclase). This genotype lacks lutein and yet it shows a compensatory increase in β-xanthophylls with respect to *chy1chy2lut5* mutant. Mutant plants show an even stronger photosensitivity than *chy1chy2lut5*, a complete lack of qE, the rapidly reversible component of non-photochemical quenching, and a peculiar organization of the pigment binding complexes into thylakoids. Biochemical analysis reveals that the *chy1chy2lut2lut5* mutant is depleted in Lhcb subunits and is specifically affected in Photosystem I function, showing a deficiency in PSI-LHCI supercomplexes. Moreover, by analyzing a series of single, double, triple and quadruple Arabidopsis mutants in xanthophyll biosynthesis, we show a hitherto undescribed correlation between xanthophyll levels and the PSI-PSII ratio. The decrease in the xanthophyll/carotenoid ratio causes a proportional decrease in the LHCII and PSI core levels with respect to PSII.

Conclusions: The physiological and biochemical phenotype of the *chy1chy2lut2lut5* mutant shows that (i) LUT1/CYP97C1 protein reveals a major β-carotene hydroxylase activity *in vivo* when depleted in its preferred substrate α-carotene; (ii) xanthophylls are needed for normal level of Photosystem I and LHCII accumulation.

Background

Carotenoids are a group of C_{40} pigments that contain a conjugated double-bond system, leading to strong absorption of visible light and antioxidant properties. They are widely distributed among taxa, ranging from cyanobacteria and fungi to red and green algae and land plants [1]. Xanthophylls are oxygenated carotenoids that play a crucial role in the photosynthetic apparatus of higher plants [2]. Their composition in plants is remarkably conserved and consists of five major xanthophylls, the most abundant being the β-ε-xanthophyll lutein, and the four β-β-xanthophylls violaxanthin, neoxanthin, antheraxanthin and zeaxanthin [3]. Xanthophylls act both as photoreceptors, absorbing light energy which is used in photosynthetic electron transport, and as photoprotectants of the photosynthetic apparatus from excess light and from the reactive oxygen species (ROS) generated during photosynthesis [4-7]. Moreover, they are structural elements of the photosynthetic apparatus: LHCII, the major light-harvesting complex (LHC) of Photosystem (PS) II, binds lutein, violaxanthin and

* Correspondence: roberto.bassi@univr.it
† Contributed equally
[2]Dipartimento di Biotecnologie, Università di Verona, Strada Le Grazie 15, 37134 Verona, Italy
Full list of author information is available at the end of the article

neoxanthin at four distinct binding sites called respectively L1, L2, N1 and V1 [8]; the occupancy of L1 site was shown to be essential for protein folding [9].

Xanthophyll biosynthesis in plants is divided in two distinct branches: the α branch leads to the formation of the ε-β-hydroxylated xanthophyll lutein from α-carotene, while the β branch leads to the production of β-β-hydroxylated xanthophylls (zeaxanthin, antheraxanthin, violaxanthin and neoxanthin) from β-carotene (Figure 1E). Recent studies on carotenoid biosynthetic mutants of *Arabidopsis thaliana* have improved our understanding on xanthophyll accumulation at the molecular level. The first steps in plant xanthophyll biosynthesis are the hydroxylation of α- and β-carotene. Two different classes of enzymes are involved: the ferredoxin-dependent di-iron oxygenases (CHY1 and CHY2) which are active in β-ring hydroxylation, and the cytochromes P450 (LUT1/CYP97C1, LUT5/CYP97A3) [10-14] which are active in hydroxylation of both the ε-ring and β-ring of α-carotene, although the activity of LUT5 on ε-rings is low [13]. It has been suggested that a third chloroplast-targeted member of the CYP97 family, CYP97B3 might have a role in carotenoid biosynthesis [14]. This hypothesis is however in contrast with the complete lack of xanthophylls in the quadruple *chy1chy2lut1lut5* mutant [14], suggesting that CHY1, CHY2, LUT1/CYP97C1 and LUT5/CYP97A3 are the complete complement of carotene hydroxylases in *A. thaliana*.

The strong phenotypes of mutants with altered xanthophyll composition imply that the presence and relative amounts of these pigments have a key role for plant fitness. The *lut2* mutant, affected in ε-ring formation, lacks lutein [15] and shows a complex phenotype with reduced antenna size, photodamage in high light (HL) due to impaired chlorophyll triplet quenching [16] and decrease of non-photochemical quenching (NPQ) [17]. Additional features include over-accumulation of zeaxanthin in HL with respect to wild-type and monomerization of LHCII. Lack of both lutein and zeaxanthin further decreases the capacity for photoprotection in both Arabidopsis and Chlamydomonas [16,18-20]. The double *chy1chy2* mutant, in which the two non-heme β-hydroxylases are deleted, shows reduced levels of β-β-xanthophylls and decreased resistance to photooxidation [10]. Introduction of the *lut5* mutation in the *chy1chy2* background leads to the almost complete disappearance of β-xanthophylls and strong photosensitivity [6,12,14]. Neoxanthin preserves PSII from photoinactivation by superoxide anions [21] while violaxanthin and zeaxanthin show enhanced activity in singlet oxygen scavenging [6]. In order to further detail the effects of altered xanthophyll composition on the organization of photosynthetic complexes and gain understanding on the regulatory events controlling xanthophyll biosynthesis in Arabidopsis, we have introduced the *lut2* mutation in the semi-lethal *chy1chy2lut5* background. Surprisingly, the *chy1chy2lut2lut5* mutant shows increased presence of β-β-xanthophylls with respect to *chy1chy2lut5*. The PSI/PSII ratio in this mutant is severely decreased as well as the level of total xanthophyll accumulation,

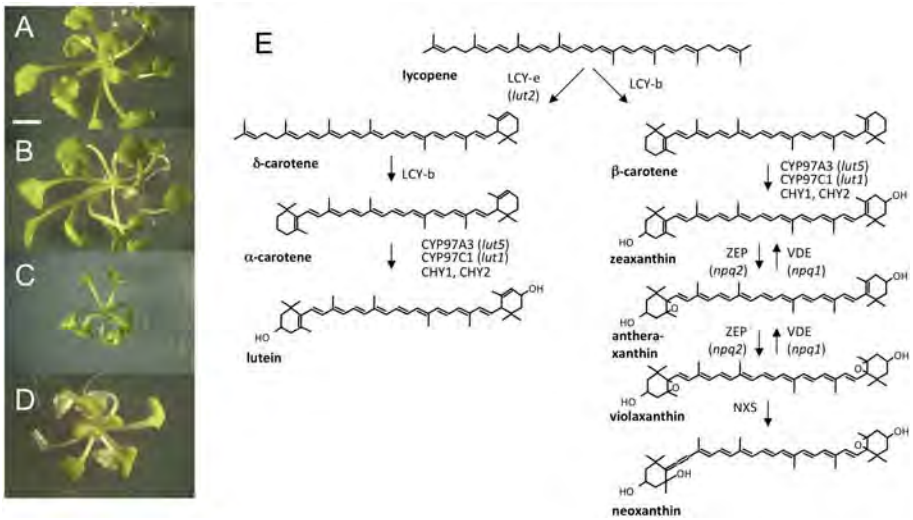

Figure 1 Growth and morphology of wild-type and carotenoid biosynthesis mutant plants. Phenotypes of 6-weeks-old wild type (**A**), *lut2* (**B**), *chy1chy2lut5* (**C**), and *chy1chy2lut2lut5* (**D**) plantlets, grown at 30 μmol photons m^{-2} s^{-1}. (**E**) Biosynthetic pathway of carotenoids in *A. thaliana;* names of the enzymes controlling each step are indicated: lycopene ε-cyclase (LCY-ε); lycopene β-cyclase (LCY-β); β-carotene hydroxylase (CYP97A3); ε-β-carotene hydroxylase (CYP97C1); β-carotene hydroxylase 1 and 2 (CHY1, CHY2); zeaxanthin epoxidase (ZEP); violaxanthin deepoxidase (VDE); neoxanthin synthase (NXS). Names of Arabidopsis knock-out mutants are indicated in parentheses. Scale bar = 5 mm.

suggesting that the latter have a key role, beside photoprotection, in regulating photosystem stoichiometry.

Results

Construction of the chy1chy2lut2lut5 quadruple mutant

To generate the quadruple mutant *chy1chy2lut2lut5*, the homozygous triple mutant *chy1chy2lut2* was crossed with the homozygous single mutant *lut5* [12]. All T-DNA insertions were in the Columbia background and appropriate oligonucleotides were used to confirm the presence of the insertions and their homozygous *vs.* heterozygous state (Additional file 1: Figure S1 and Additional file 1: Table S1) [12]. The mutant was maintained as a triple homozygous, single heterozygous stock: two different parental genotypes were used, heterozygous for either *LUT5/CYP97A3* or *CHY2*, with similar results (Additional file 1: Figure S2). The *lut2* and *chy1chy2lut5* lines were included in this characterization, representing respectively the lutein-less and β-xanthophyll-less controls. When selfed, the progeny of each single heterozygous stock, as well as wild-type, *chy1chy2lut5* and *lut2* seeds, were grown under low light conditions (30 μmol photons m^{-2} s^{-1}) both in agar plates containing sucrose (see Methods) and in soil. No quadruple homozygous mutants were recovered in soil after 1 week of growth, while the progeny segregated in a 1:3 ratio for white: green seedlings in agar plates. Wild type and *lut2* plants did not display a visible phenotype after 6 weeks of growth in agar plates, whereas mutants *chy1chy2lut5* and *chy1chy2lut2lut5* showed, respectively, reduced growth and paler leaves (Figure 1A-D).

Pigment composition

We analyzed by HPLC-DAD-MS the pigment content of six-week-old leaves of wild type, *lut2, chy1chy2lut5* and *chy1chy2lut2lut5* plants grown on agar plates (Tables 1, 2 and Additional file 1: Table S2). Pigments were resolved on a C-30 column, able to separate *cis-* from *trans*-carotenoids and their identity was confirmed by co-migration with authentic standards and high resolution MS (Additional file 1: Table S2). *chy1chy2lut5* and *chy1chy2lut2lut5* plants showed an increase in chlorophyll a/b ratio, as well as a reduced chlorophyll (Chl) and carotenoids (Car) content per fresh weight, with respect to both wild-type and *lut2*; the effects were more severe in the quadruple mutant, that showed a significant reduction of Chl/Car ratio (2.1) with respect to the other genotypes (~3.3, Table 1). Wild-type leaves accumulate four major carotenoids (neoxanthin, violaxanthin, lutein and β-carotene) and trace amounts of α-carotene. Mutants show distinct composition of the xanthophyll fractions: lutein represents > 98% of total xanthophylls in *chy1chy2lut5* plants; *lut2* and *chy1chy2lut2lut5* do not contain lutein and accumulate violaxanthin, antheraxanthin, zeaxanthin and neoxanthin; *chy1chy2lut2lut5* shows a higher content of β-β-xanthophylls (24% of total carotenoids) with respect to *chy1chy2lut5* (0.7% of total carotenoids). β-carotene content is strongly increased in *chy1chy2lut2lut5* with respect to the wild-type and the other mutants (Table 2). As a result, the xanthophyll/carotene ratio changes dramatically, ranging from 2.5 ± 0.7 in wild-type to 0.3 ± 0.1 in *chy1chy2lut2lut5*.

β-carotene accumulation is expected in *chy1chy2lut2lut5*, in which the biosynthetic flux is diverted towards the β-β-branch by the lack of three out of four β-carotene hydroxylases (CHY1, CHY2 and CYP97A3/LUT5) (Figure 1E); however, β-β-xanthophyll accumulation in this mutant suggests that the fourth hydroxylase (CYP97C1/LUT1) is more active toward β-carotene in this background than in the *chy1chy2lut5* parent, resulting in 28-fold higher levels of β-β-xanthophylls.

Table 1 Pigment content of leaf tissue from wild-type and mutant genotypes

	chl a/b	chl/car	Chl content (μg/g FW)	Car content (μg/g FW)
WT	3.2 ± 0.5[a,b]	3.3 ± 0.8[a,b]	801 ± 88[a]	244 ± 51[a]
lut2	3.2 ± 0.2[a]	3.3 ± 0.7[a,b]	742 ± 79[a]	222 ± 38[a]
chy1chy2lut5	3.9 ± 0.3[b]	3.4 ± 0.7[a]	569 ± 76[b]	166 ± 25[b]
chy1chy2lut2lut5	7.9 ± 0.3[c]	2.1 ± 0.4[b]	303 ± 42[c]	146 ± 21[b]

Pigment composition was quantified via LC-DAD-MS in dark-adapted leaves from 6-weeks-old plants. Data are expressed as mean ± SD (n = 4). FW, fresh weight. Values marked with the same letters are not significantly different from each other within a column ($P > 0.05$).

Gene expression

We measured the *LUT1, LUT5, CHY1 and CHY2* mRNA levels by real time PCR in the different mutants (Figure 2). All mRNAs are almost completely absent in the corresponding mutants; *LUT5, CHY1 and CHY2* are induced in the *lut2* mutant, that accumulates higher levels of β-carotene; *LUT1* is induced in the *chy1chy2lut5* and, even more, in the *chy1chy2lut2lut5* mutant, which shows drastically reduced xanthophyll/carotene ratios; however, the increase of *LUT1* levels between the two mutants is only 1.3-fold, while the increase of β-β-xanthophylls is 28-fold.

Photosynthesis-related functions: PSII quantum efficiency and non-photochemical quenching of chlorophyll fluorescence

The impact of xanthophyll depletion on photosynthesis was investigated by room temperature chlorophyll fluorescence measurements (Table 3). The variable/maximum fluorescence yield (F_v/F_m) of dark-adapted

Table 2 HPLC analysis of leaf carotenoid content (μg/g FW) in dark-adapted plants

	Carotenoid content (μg/g FW)								
	neoxanthin	violaxanthin	antheraxanthin	lutein	zeaxanthin	α-carotene	β-carotene	β-β-xantophylls	xanthophylls/carotenes
WT	18.6 ± 1.6[a]	44.1 ± 5.8[a]	nd	105.6 ± 22.4[a]	nd	4.4 ± 0.6[a]	62.1 ± 14.8[a]	62.7 ± 6.0[a]	2.5 ± 0.7[a]
lut2	22.1 ± 0.7[b]	94.7 ± 4.9[b]	14.6 ± 1.4[a]	nd	5.0 ± 0.6[a]	nd	74.9 ± 5.1[a]	136.4 ± 5.1[b]	1.8 ± 0.1[a]
chy1chy2lut5	0.3 ± 0.2[c]	0.9 ± 0.6[c]	nd	69.1 ± 4.7[b]	nd	51.0 ± 2.7[b]	42.8 ± 1.4[b]	1.2 ± 0.6[c]	0.7 ± 0.1[b]
chy1chy2lut2lut5	8.4 ± 0.1[d]	13.6 ± 0.2[d]	8.5 ± 0.1[b]	nd	3.4 ± 0.1[b]	nd	109.4 ± 2.3[c]	33.9 ± 0.3[d]	0.3 ± 0.1[c]

Plants grown at 30 μmol photons m^{-2} s^{-1} for 6 weeks were dark-adapted, then carotenoids were extracted and quantified via LC-DAD-MS. Data are expressed as mean ± SD (n = 4). nd, not detectable; FW, fresh weight. Values marked with the same letters are not significantly different from each other within a column ($P > 0.05$).

leaves reflects changes in PSII photochemical efficiency [22]. *lut2* had the same F_v/F_m ratio as wild-type (0.80), while the triple *chy1chy2lut5* and quadruple *chy1chy2-lut2lut5* mutants scored, respectively, values of 0.68 and 0.51 (Table 3). The efficiency of PSII photochemistry (Φ_{PSII}) gives a measure of the rate of linear electron transport, an indication of the photosynthetic activity [23]. Chlorophyll fluorometry revealed a significant reduction in Φ_{PSII} in both *chy1chy2lut5* and *chy1chy2lut2lut5* (0.07 and 0.08 respectively, with respect to 0.17 in wild-type plants, Table 3), confirming that efficient light use is compromised by β-β-xanthophyll depletion.

Non-photochemical quenching (NPQ) of chlorophyll fluorescence is the fastest photoprotective mechanism in the chloroplast: thermal dissipation is activated within

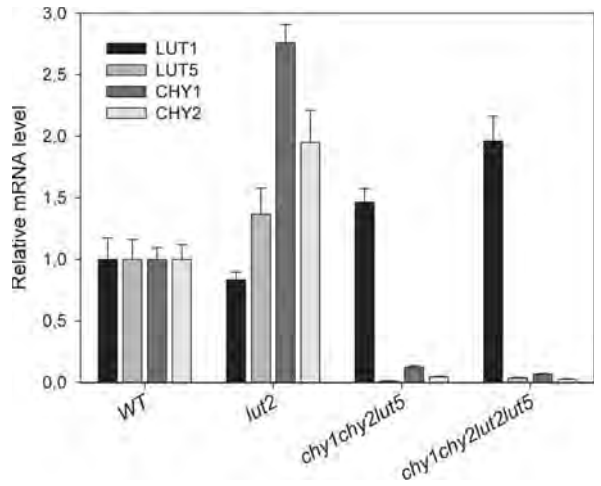

Figure 2 Real-time PCR expression profile of Arabidopsis carotenoid hydroxylase genes. For individual genes, the relative mRNA levels were normalized with respect to the *TUBULIN* housekeeping transcript and then to wild-type levels. RNA was extracted from dark-adapted, 6-weeks-old plants (see Methods for details). Data are expressed as mean ± SD (n = 3).

few seconds upon exposure to excess light and it protects photosynthesis by decreasing the lifetime of singlet chlorophylls [24] in order to minimize generation of ROS in the PSII [4]. NPQ was measured on detached leaves, in saturating CO_2 (Figure 3). Wild-type plants, upon short illumination at saturating light intensity (1000 μmol photons m^{-2} s^{-1}, 7 min), showed a rapid rise of NPQ, reaching a maximum value of 0.8. Most of this NPQ relaxed rapidly in the dark, thus reflecting the ΔpH-dependent de-excitation of excess energy measured as qE, the rapidly-reversible component of NPQ. *lut2* showed NPQ kinetics in agreement with published results [6,19], with lower amplitude and slower rise than wild-type plants (Figure 3A). The other mutants showed a strong reduction in NPQ, scoring 0.30 in *chy1chy2lut5* and 0.22 in *chy1chy2lut2lut5;* furthermore, upon correction for residual quenching after dark relaxation (photoinhibitory quenching, qI), both mutants showed very little recovery (Figure 3A), suggesting that the measured fluorescence quenching was mainly due to photoinhibition, and the capacity for qE was strongly reduced in mutant leaves (Figure 3A). Furthermore, NPQ kinetics were measured during steady-state photosynthesis, upon a prolonged illumination with increasing light intensities (ranging from 70 to 1500 μmol photons m^{-2} s^{-1}, 20 min). All genotypes showed chlorophyll fluorescence quenching, whose magnitude increased with irradiance. However, fluorescence quenching in wild-type and *lut2* leaves was mainly due to the qE-type of NPQ (Figure 3B), while in both *chy1chy2lut5* and *chy1chy2lut2lut5* the main component of NPQ was qI-type, irreversible quenching (Figure 3C). These data confirm that both the reduction of β-β-xanthophylls and the lack of lutein are responsible for impaired NPQ kinetics.

Photosensitivity under short-term stress conditions

When photosynthetic organisms are exposed to light in excess, photo-oxidative stress occurs within the chloroplast, with production of ROS such as singlet oxygen

Table 3 Analysis of room temperature chlorophyll fluorescence during steady-state photosynthesis

	Fv/Fm	ΦPSII
WT	0.81 ± 0.03[a]	0.17 ± 0.05[a]
lut2	0.80 ± 0.02[a]	0.12 ± 0.01[a, b]
chy1chy2lut5	0.68 ± 0.02[b]	0.07 ± 0.01[c]
chy1chy2lut2lut5	0.51 ± 0.10[c]	0.08 ± 0.05[b, c]

Detached leaves of wild-type and mutant plants grown at 30 μmol photons m^{-2} s^{-1} for 6 weeks were given 20 min of illumination (1000 μmol photons m^{-2} s^{-1}), then photosynthetic parameters were provided by analysis of RT chlorophyll fluorescence: maximum quantum yield of PSII (F_v/F_m) and efficiency of PSII photochemistry (Φ_{PSII}). Data are expressed as mean ± SD (n = 4). Values marked with the same letters are not significantly different from each other within a column ($P > 0.05$).

($^1O_2$), leading to oxidative damages to a large variety of biomolecules.

The β-xanthophyll-depleted mutants *chy1chy2lut5* and *chy1chy2lut2lut5*, even upon growth in low light (30 μmol photons m^{-2} s^{-1}), showed signs of photooxidation: lower chlorophyll content and PSII quantum yield, retarded growth and paler leaves with respect to wild-type and *lut2* plants (Tables 1, 3). Therefore, in order to assess whether lower xanthophyll levels affect the capacity to prevent chloroplast photooxidation, leaves from wild-type and mutant plants grown in low light were transferred to strong light (900 μmol photons m^{-2} s^{-1}) and low temperature (5°C) for 3.5 h; the combination of low temperature and high light intensity is known to enhance the induction of both PSII photoinhibition and membrane photooxidation in leaves, since the enzymes of the Calvin cycle are slowed down and the light harvested by photosystems rapidly exceed the capacity of plants to use this energy. Thus, the treatment produces a photooxidative stress, which can be measured as a decrease in the chlorophyll content and an increase in oxidation of membrane lipids. HL treatment was effective in producing higher pigment bleaching in *chy1chy2lut5* (40% reduction) and *chy1chy2lut2lut5* (57% reduction), while wild-type and *lut2* leaves were less affected, loosing around 25% of their chlorophyll content (Figure 4A). To investigate the level of membrane lipid peroxidation, the same leaves were analyzed for MDA content (malondialdehyde, a byproduct of lipid peroxidation): *chy1chy2lut2lut5* and *chy1chy2lut5* leaves showed higher accumulation of MDA upon stress treatment (+120% and +45%, respectively), thus a far higher level of lipid peroxidation with respect to wild-type and *lut2* plants (+25%); *chy1chy2lut2lut5* plants showed a far higher photosensitivity in high-light than *chy1chy2lut5* (Figure 4B); the latter was the xanthophyll mutant with the highest light sensitivity described so far [6]. Results clearly show an unprecedented level of photosensitivity in *chy1chy2lut2lut5* plants, thus implying a severe impairment of the photoprotection mechanisms in this xanthophyll-depleted mutant.

Organization and stoichiometry of pigment binding complexes

The extreme sensitivity to photo-oxidative stress of the *chy1chy2lut2lut5* mutant could be due to altered pigment composition, to altered protein composition of photosystems, or to both. This mutant showed the highest Chl *a/b* ratio, and the lowest chlorophyll content and xanthophyll/carotene ratio of all analyzed genotypes (Tables 1, 2). Since both Chl *b* and xanthophylls are associated with LHC, their decrease suggests a decrease in antenna size. We investigated the organization of pigment-protein complexes in thylakoids by non-denaturing Deriphat-PAGE and by sucrose density gradient fractionation of solubilized thylakoids, followed by SDS-PAGE of the fractions (Figures 5, 6). Seven major green bands were resolved upon solubilization of wild-type thylakoid membranes with 0.8% dodecyl-α-D-maltoside (α-DM) on Deriphat-PAGE [25]. The PSI-LHCI complex was the major band (B6) in the upper part of the gel, while the components of the PSII-LHCII complex migrated as multiple bands, namely the PSII core (B5) and the antenna moieties, including the CP29-CP24-LHCII-M supercomplex (B4) [26], LHCII trimer (B3) and monomeric Lhcb (B2). Bands with high apparent masses were detected in the upper part of the gel (B7) containing non-dissociated PSII supercomplexes.

The *chy1chy2lut5* pattern was very similar to that of wild-type, showing no major qualitative changes in the organization of the photosynthetic apparatus: the main differences consisted in a higher PSII core/Lhcb ratio and a lower content in PSII supercomplexes (B7) [6]. In the genotypes lacking lutein, namely *lut2* and *chy1chy2lut2lut5*, the trimeric organization of LHCII was disrupted, as previously described [17]. However, thylakoid membranes isolated from *chy1chy2lut2lut5* plants showed additional features, namely the complete absence of bands 3, 4 and 7; bands 2 and 6 were much less represented than in wild-type, while PSII core complex was the most abundant among pigment-protein complexes (Figure 5A).

In order to obtain sufficient amounts of pigment-protein complexes for further analysis, solubilized thylakoids from wild type and mutants were fractionated by sucrose gradient ultracentrifugation (Figure 5B); the results confirmed that trimeric LHCII band, as well as the CP29-CP24-LHCII supercomplex completely disappeared in the *chy1chy2lut2lut5* mutant; further differences consisted into reduced levels of monomeric Lhcb (band 2) and a much higher PSII/PSI ratio (band 5 *vs.* band 6) with respect to the other genotypes. The

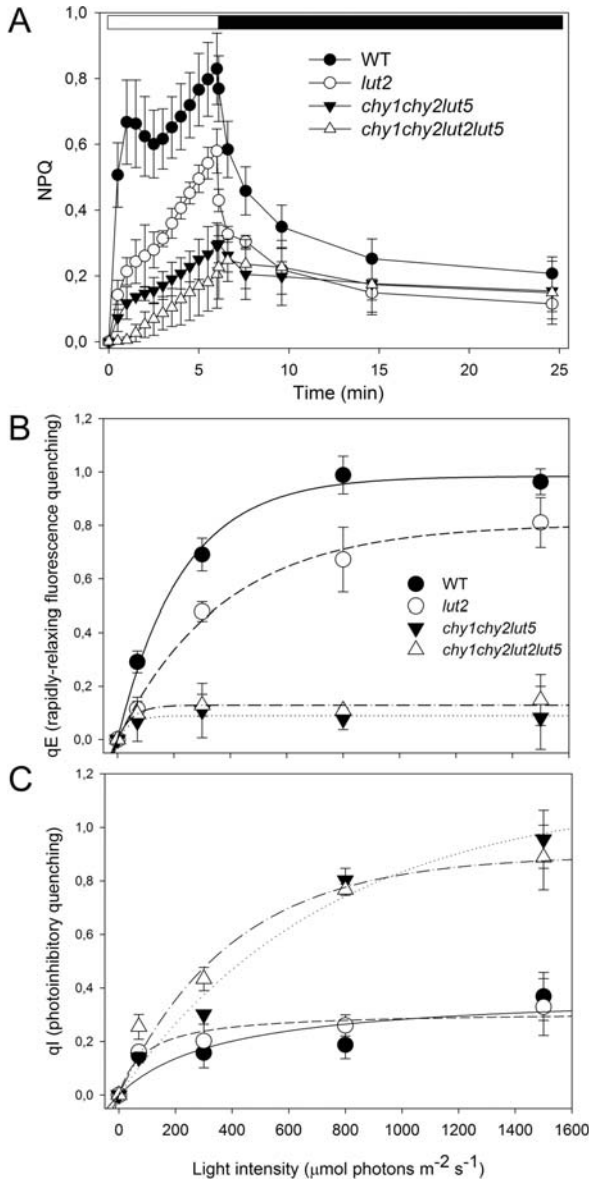

Figure 3 NPQ analysis of wild-type and mutant genotypes. (**A**) Kinetics of NPQ induction and relaxation were recorded with a pulse amplitude modulated fluorometer. Chlorophyll fluorescence was measured in dark-adapted leaves, during 7 min of illumination at 1000 µmol photons m^{-2} s^{-1} followed by 18 min of dark relaxation. (**B**) Amplitude of the reversible energy dissipation (qE). (**B, C**) Extent of feed-back de-excitation (qE, panel B) and photoinhibitory quenching (qI, panel C) determined at a series of irradiances as a difference between NPQ values upon illumination and following 15 min dark relaxation. Symbols and error bars show means ± SD (n = 4).

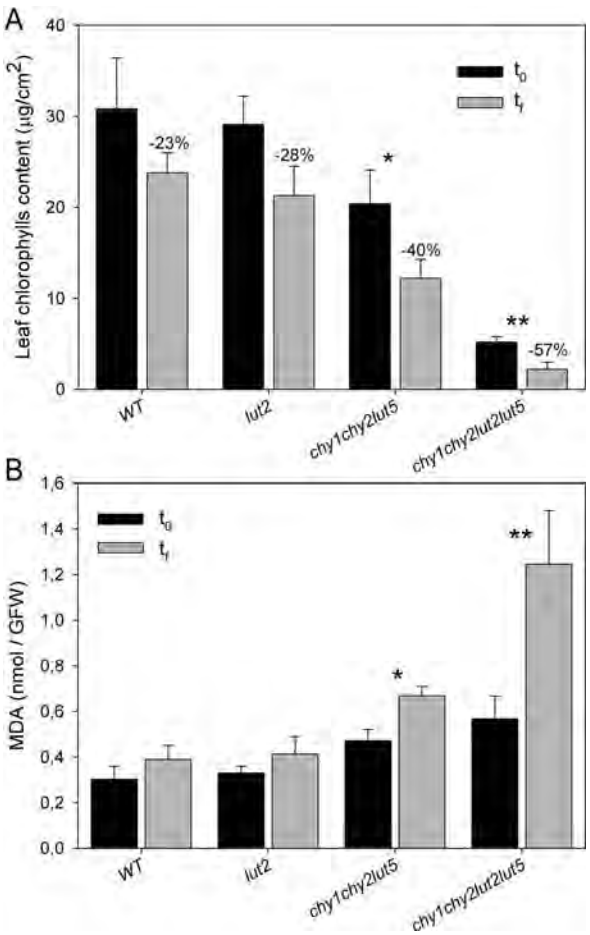

Figure 4 Photo-oxidation of Arabidopsis wild-type and mutant genotypes under photoxidative stress. Detached leaves on wet paper were treated at 900 µmol photons m^{-2} s^{-1} at 5°C for 3.5 h, then chlorophyll bleaching (**A**) and MDA formation (**B**) were recorded. Data are expressed as means ± SD (n = 4). Significant difference ($P < 0.05$ (*) or $P < 0.02$ (**)) against wild type within each treatment are marked. Chlorophyll and MDA contents were quantified before (t_0) or after (t_f) the high-light stress.

reduction of monomeric Lhcbs in the *chy1chy2lut2lut5* mutant occurs in spite of the presence of the *lut2* mutation, which favors LHCII monomerization (compare band 2 in wild type *vs*. *lut2* and in *chy1chy2lut5 vs*. *chy1chy2lut2lut5*, Figure 5B).

Fractions collected from the sucrose gradients of wild-type and *chy1chy2lut2lut5* (bands 2-6) were further characterized by SDS-PAGE using two buffer systems (Figure 6A) and by absorption spectroscopy (Additional file 1: Figure S3). According to previous results with α-DM, SDS-PAGE analyses of wild-type fractions showed that band 2 contained the minor antennae CP29, CP26 and CP24 as well as components of monomerized LHCII, while band 3 contained Lhcb1-3 polypeptides only (Figure 6A, left panel) [27]. Band 5 was enriched in PSII core complex (Figure 6A, right panel) [28], nevertheless the Chl *b* absorption (Additional file 1: Figure S3) suggests it retains Lhcb proteins; band 6 contained almost exclusively the PSI-LHCI complex (Figure 6A, right panel and Additional file 1: Figure S3) [29]. Band 2

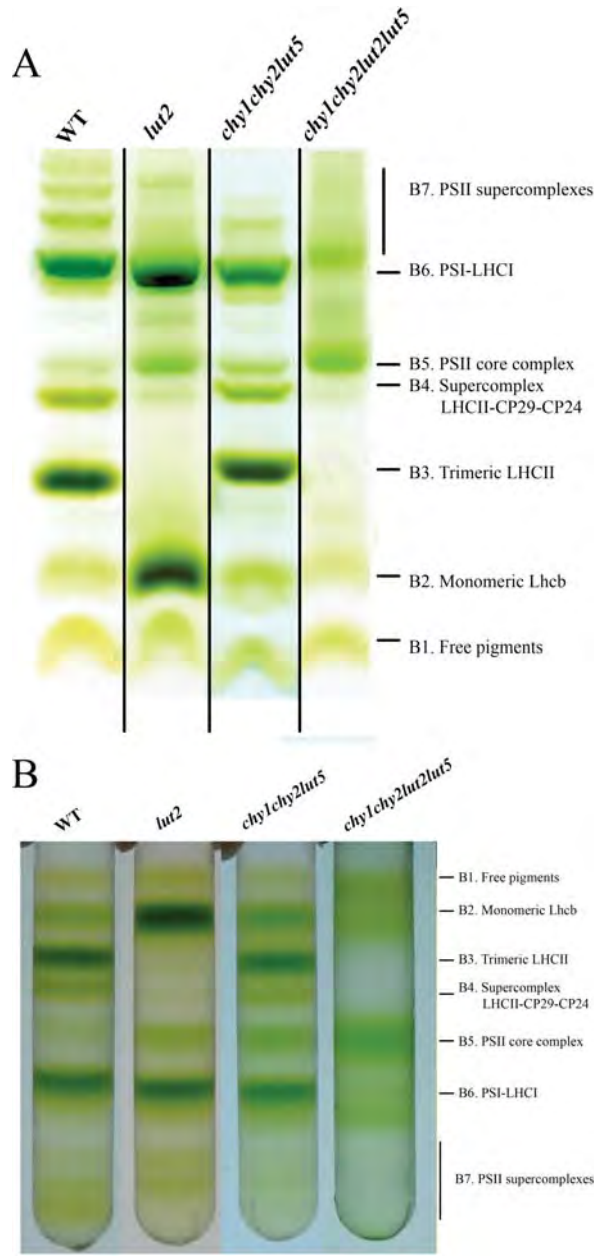

Figure 5 Analysis of pigment-protein complexes of wild-type and mutants. (**A**) Thylakoid pigmented complexes were separated by non-denaturing Deriphat-PAGE (**A**) or by sucrose density gradient fractionation (**B**) upon solubilization with 0.8% α-DM.

from *chy1chy2lut2lut5* contained the same polypeptides as the corresponding band from wild-type, although the relative amounts of the Lhcb1-3 polypeptides and CP26 were decreased (Figure 6A, left panel). The data confirm that LHCII is present in the mutant, however in far lower amounts than in wild-type, and is in its monomeric aggregation state. Band 5 from the mutant contained almost exclusively PSII core complex polypeptides (Figure 6A and Additional file 1: Figure S3), band 6 from the mutant contained PSI-LHCI.

The levels of selected proteins in wild-type and *chy1chy2lut2lut5* thylakoids were determined by quantitative western-blot analysis using PsbB (CP47) as internal control (Figure 6B): all Lhcb subunits were reduced in *chy1chy2lut2lut5* with respect to wild-type thylakoids; PsbA (D1), OEC-33 and PsbS, subunits of the PSII core complex, were present in the same level in both genotypes, while cytochrome *f* and ATPase β-subunit were in higher amounts in *chy1chy2lut2lut5*. Immunoblotting using PsaA as internal standard showed that each Lhca protein was present in wild-type amounts, thus suggesting that the Lhca/PSI ratio is conserved in the mutant. In contrast, the PSI/PSII ratio was extremely low in *chy1chy2lut2lut5*, reaching approximately 22% of wild-type value (Figure 6B).

The data shown above indicate that xanthophyll depletion in the *chy1chy2lut2lut5* plants causes a strong reduction in the amount of Lhcb proteins per PSII reaction center, and has a negative impact on the total amount of the PSI-LHCI supercomplex. The latter result is unexpected, since xanthophylls are mainly bound to Lhc complexes while core complexes of both photosystems only bind carotenes, implying that xanthophyll abundance should not affect their folding or stability.

A key question is whether the lower PSI/PSII ratio found in *chy1chy2lut2lut5* thylakoids is peculiar to this genotype or is a general consequence of altered xanthophyll content. To answer this question, the abundance of LHCII and PSI core with respect to CP47 was assessed by quantitative immunotitration, in thylakoids isolated from 12 Arabidopsis mutants with altered xanthophyll content [6,12]. Figure 7 shows the distribution of LHCII (A) and PSI core (B) amounts, relative to CP47, in the different mutants with different xanthophyll/carotenoid ratios: both distributions show an increase of LHCII/PSII and PSI/PSII at increasing xanthophyll/carotenoid ratios, and the data can be fitted with an exponential function ($y = y_o + a \cdot e^{bx}$). The results display a clear correlation between parameters ($R_{LHCII/PSII}^2 = 0.76$; $R_{PSI/PSII}^2 = 0.78$). Furthermore, quantitative data for the individual pigment-protein complexes accumulation level per fresh weight (namely PSI core, PSII core and LHCII) were plotted *vs.* xanthophyll/carotenoid content in the different mutants (Additional file 1: Figure S4). The distributions show a lower LHCII content per fresh weight at decreasing xanthophyll/carotenoid ratios (panel C), while PSII core (CP47 subunit) content per fresh weight was essentially unaffected by xanthophylls depletion (panel B). Unlike PSII, the PSI core (PsaA subunit) content decreases at decreasing xanthophyll/carotenoid ratios (panel A). These results suggest that xanthophyll depletion not only causes a marked

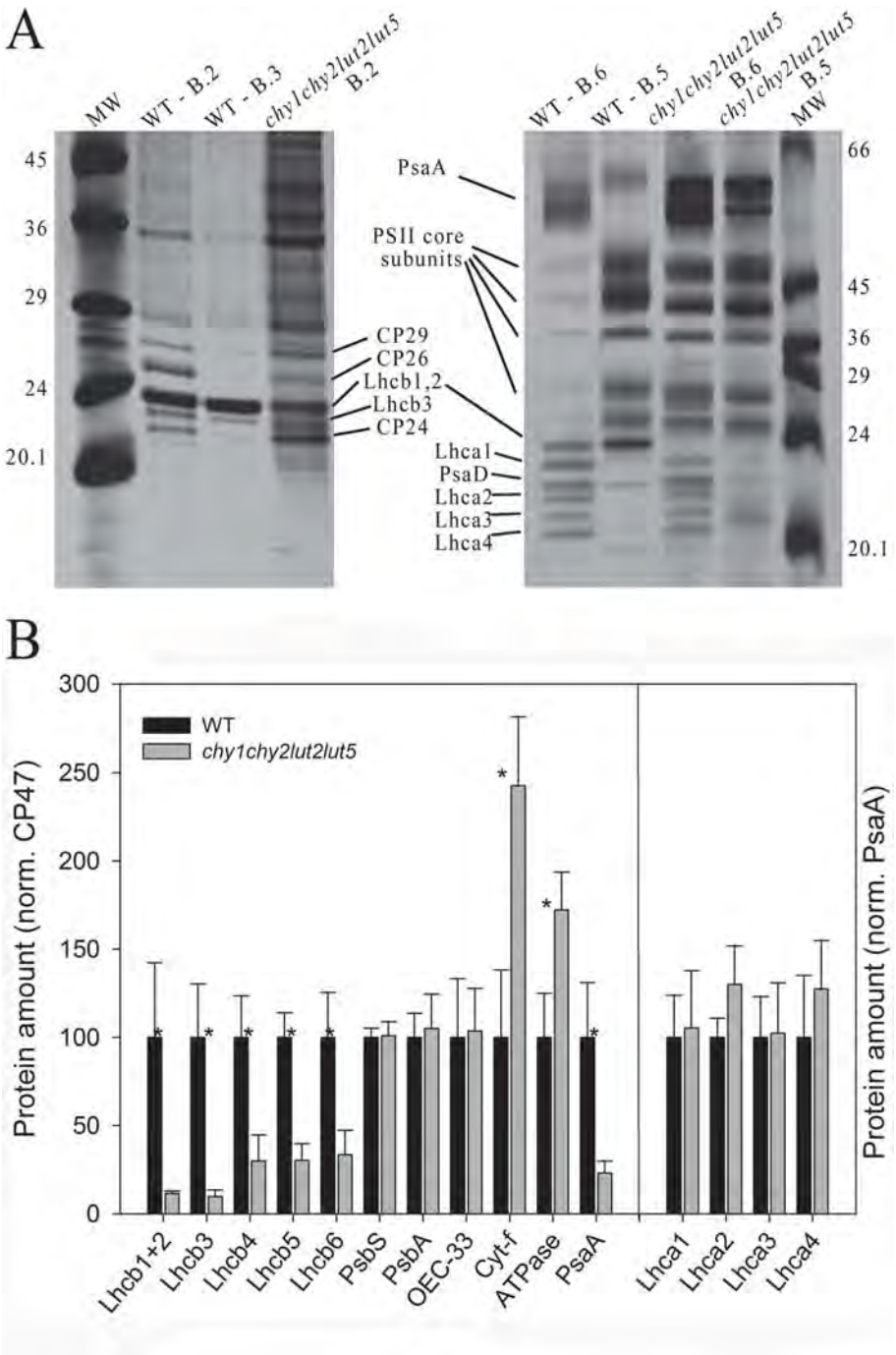

Figure 6 Analysis of polypeptide composition of wild-type and *chy1chy2lut2lut5* thylakoid membrane. (**A**) Pigment-protein complexes isolated by sucrose density gradient fractionation (Figure 5B) were analyzed by Tris-tricine (*left panel*) of Tris-glycine (*right panel*) SDS-PAGE. Main protein components of each fraction are indicated. MW, molecular weight marker. (**B**) Results of the immuno-titration of thylakoid proteins. Immunoblot analyses were performed with antibodies directed against individual gene products. Data of PSII subunits were normalized to the PsbB content, that of Lhca to the PsaB content, and expressed as a percentage of the corresponding wild-type content. Significantly different values in protein amount than the corresponding wild-type, according to Student's *t* test ($P < 0.05$), are marked (*).

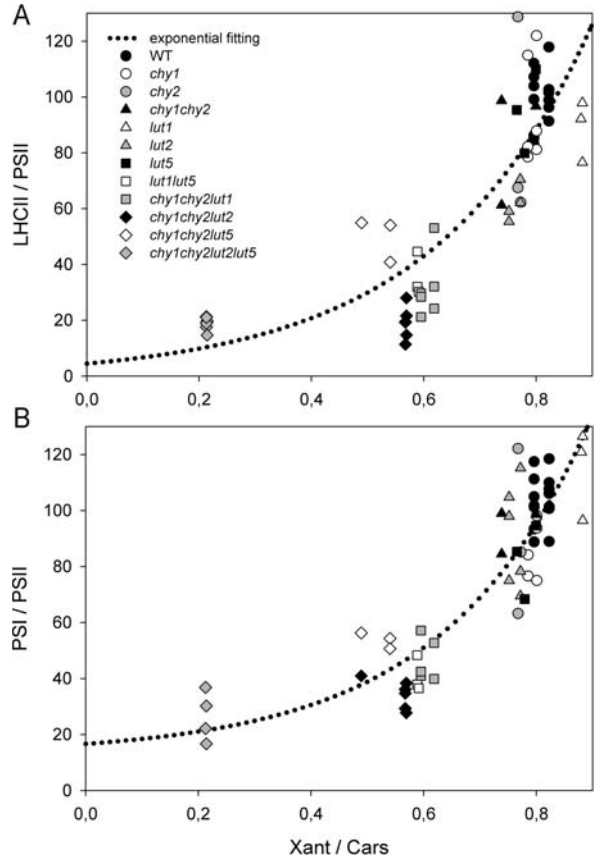

Figure 7 Relations between LHCII/PSII (A) and PSI/PSII (B) ratios and the relative content of xanthophylls on thylakoids. Parameters were measured for wild-type and 11 xanthophyll biosynthesis mutants plants previously described ([12]; present ms). LHCII/PSII and PSI/PSII ratios were determined on thylakoid membranes by quantitative western blot, while xanthophyll/carotenoid ratios were quantified by HPLC. Both distributions were fitted with exponential functions ($y = y_o + a \cdot e^{bx}$); $R_{LHCII/PSII}^2 = 0.76$; $R_{PSI/PSII}^2 = 0.78$.

depletion in LHC proteins, as expected from the xanthophylls being ligands of Lhcs, but also modulates the ratio between PSI/PSII, despite β-carotene rather than xanthophylls is the ligand for PSI and PSII core complexes.

Discussion

In this work, we analyzed the modifications of the photosynthetic apparatus in the Arabidopsis mutant *chy1chy2lut2lut5*, that accumulates β-xanthophylls despite disruption of the three *chy1, chy2* and *lut5* genes encoding carotene hydroxylases. In this mutant the only carotene hydroxylase activity is provided by the LUT1 gene product, which allows for accumulation of only 20% of the wild-type xanthophylls. In these conditions, biogenesis of the photosynthetic apparatus was strongly affected yielding into a reduction of PSII antenna size, a decrease of PSI/PSII ratio and an increased photosensitivity.

LUT1 as a β-carotene hydroxylase

LUT1 was originally reported to be only gene product required for the ε-ring hydroxylation of α-carotene [11]. The first indication of a possible involvement of LUT1 in β-ring hydroxylation came from the analysis of the *chy1chy2lut5* triple mutant, which accumulates lutein (β-ε-dihydroxy-carotene), providing genetic evidence that LUT1 must be also active in the hydroxylation of the β-ring of α-carotene [12]. Introduction of the *lut1* mutation in the *chy1chy2lut5* triple mutant completely abolished xanthophyll biosynthesis, indicating that CHY1, CHY2, LUT1 and LUT5 constitute the full complement of carotenoid hydroxylases in Arabidopsis [14]. A number of studies [11-14] have shown a functional redundancy amongst the carotene hydroxylase enzymes. However, the extent of recovery in xanthophyll content by mutants carrying a single carotene hydroxylase activity gave insights on the substrate preference of residual activity. As an example, trace amounts of β-β-xanthophylls, present in the *chy1chy2lut5* triple mutant and abolished by the introduction of the *lut1* mutation [14], led to the conclusion that LUT1 has a low level of activity toward the β-rings of β-carotene. Overall, *in vivo* analysis clearly showed that CHY1 and CHY2 are most active in β-carotene hydroxylation, while LUT1 and LUT5 enzymes catalyze preferentially the biosynthesis of α-xanthophylls [14]. Here we show that, in the absence of α-carotene (whose synthesis is prevented by the *lut2* mutation), LUT1 shows a major β-carotene hydroxylase activity, leading to the accumulation of substantial amounts of β-β-xanthophylls. Indeed, when considering the moles of hydroxylated β-rings accumulated in *chy1chy2lut5* and *chy1chy2lut2lut5* mutants, total amount is maintained upon introduction of the *lut2* mutation into the *chy1chy1lut5* background: ~0.125 μmol of hydroxylated β-rings/gFW in *chy1chy2lut5 vs*. ~0.118 μmol/gFW in *chy1chy2lut2lut5* (Table 2). However, the total amount of xanthophylls per fresh weight is reduced significantly in *chy1chy2lut2lut5* (-52%, see Table 2), while the carotene/xanthophyll ratio is increased (+57%). The most likely scenario is that LUT1 has a higher affinity towards ε-rings *vs*. β-rings and that, when α-carotene is available, LUT1 performs mainly ε-ring hydroxylation; however, since no ε-ring-substrates are available in the *chy1chy2lut2lut5*, the β-ring substrates are processed, thus bringing out this minor activity of the enzyme. Conversely, in the absence of the main hydroxylases for β-rings CHY1, CHY2 and LUT5, all β-rings become available for LUT1 activity in *chy1chy2lut2lut5*. A consequence of LUT1 operation on a less preferred substrate (i.e., β-carotene over α-carotene) is its reduced overall

catalytic rate that limits the level of xanthophylls accumulated in the *chy1chy2lut2lut5* genotype. It is worth noting that the β-hydroxylase activity does not discriminate between β-rings of α- and β-carotene; indeed, the total amount of hydroxylated β-rings per fresh weight is the same in both *chy1chy2lut5* and *chy1chy2lut2lut5*. This evidence updates our knowledge on the molecular details of carotenoid hydroxylases, with respect to the view that LUT1 has only a low level of *in vivo* hydroxylase activity toward the β-carotene and a stronger activity towards α-carotene [14].

The concentration of β-carotene increased in the quadruple *chy1chy2lut2lut5* mutant to a level higher than in the wild type (Table 2). This is the result of the combination of several factors: first, the *lut2* mutation redirects the flux in the pathway towards the β-β-branch; this mutation alone is sufficient to cause a slight increase in β-carotene (Table 2). Moreover, the reduced hydroxylase activity due to the *chy1, chy2 and lut5* mutations, reduces the rate of β-carotene processing into downstream xanthophylls (Figure 1E), favoring its accumulation. The almost 2-fold increase of the *LUT1* transcript in the quadruple mutant with respect to the wild type (Figure 2) is insufficient to fully compensate for the disappearance of the CHY1, CHY2 and LUT5 hydroxylases, likely due to the low catalytic efficiency of LUT1 for β-rings.

Reduced xanthophyll content negatively affects energy-dependent quenching qE and photoprotection

The excess energy dissipation into heat (NPQ) is strongly depleted in the *chy1chy2lut2lut5* mutant, its amplitude being close to zero (Figure 3). Since the level of PsbS, the pH sensitive trigger for NPQ [30] is similar to wild-type, this effect can be attributed to the low level of the interacting partners of PsbS where the actual quenching occurs, i.e. the Lhcb proteins [31-34], and to the lack of lutein which limit NPQ [16,35]. All together these results support the correlation between xanthophyll content and amplitude of qE, previously indicated on the basis of antisense inhibition of beta hydroxylation [36]. However, the high photosensitivity of *chy1chy2lut2lut5* plants is likely to be caused by the failure of additional photoprotection mechanisms, since the *npq4* mutant, although depleted in NPQ, only showed minor increase in photosensitivity [30].

The fast leaf chlorophyll bleaching (Figure 4A) and high levels of lipid peroxidation (Figure 4B) in *chy1chy2lut2lut5* with respect to wild-type, *lut2 and chy1chy2lut5* are likely due to the strong depletion in Lhcb proteins (Figure 6B). Xanthophylls are needed for folding of Lhc proteins *in vitro* [37], thus it is not surprising that a strong decrease in their availability leads to a decreased content in LHC. However, only Lhcb proteins are affected, while Lhca proteins are maintained with the same stoichiometry with respect to PSI reaction center, as shown by the identical migration rate of PSI-LHCI supercomplexes in sucrose gradients and native gels (Figure 5B) and by quantitative immunotitration of Lhca versus PsaA content (Figure 6B). As a result of the higher stability of Lhca *vs*. Lhcb proteins, PSI antenna function is maintained, while PSII antenna function is impaired. We conclude that *in vivo* carotenes cannot replace xanthophylls in stabilizing Lhcb proteins, thus leading to their strong reduction. Furthermore, this implies that functional Lhcb proteins are essential for photoprotection, in agreement with a previous report [38]. Extreme reduction in Lhc proteins is obtained with the *ch1* mutation in Arabidopsis, that impairs Chl *b* synthesis and prevents assembly of functional LHC [39]. Although this mutant undergoes severe photoinhibition in high light, it can grow on soil and is not photoinhibited in moderate light [7]. Thus *ch1*, with a PSII antenna size even smaller than that of *chy1chy2lut2lut5*, can survive in the absence of a reduced carbon source, a lethal condition for *chy1chy2lut2lut5*. We conclude that reduced LHC content, although likely contributing to sensitivity, cannot be the only reason for the extreme phenotype of *chy1chy2lut2lut5*.

Limitation in total xanthophyll availability affects light-harvesting complex content and PSI/PSII ratio

The analysis of the pigment-protein complexes in the *chy1chy2lut2lut5* mutant shows that Lhcb proteins are strongly decreased with respect to PSII, while Lhca assembly into PSI-LHCI are much less, or not at all, affected (Figures 5, 6). A reduction in Lhcb proteins is also observed in the *chy1chy2lut5* mutant, albeit to a lesser extent than in *chy1chy2lut2lut5* [6]. This effect is likely due to the incapacity of Lhcb proteins to fold in the absence of xanthophylls [37], while Lhca proteins can also bind small amounts of β-carotene [40,41]. Instead, there is no evident reason for the 5-fold decrease in PSI/PSII ratio (Figure 7): since Lhca proteins are maintained with the same stoichiometry with respect to PSI reaction center and thus likely contribute to the complex stability (Figures 5 and 6B), such a strong decrease of PSI is not expected. The dependence of PSI/PSII ratio on the xanthophyll/carotenoid ratio of different genotypes contrasts with the fact that both PSI core and PSII core complexes bind β-carotene [42] which is fully available in *chy1chy2lut2lut5*, as well as in the other genotypes carrying mutations in xanthophyll biosynthesis (Figure 7).

Alternatively, it can be hypothesized that PSI level might be limited by the amount of LHCI available.

However, three lines of evidence are against the hypothesis that PSI depletion is a secondary effect of a limitation in LHCI:

1) Several Arabidopsis mutants showing a strong depletion of LHCI, including Lhca antisense lines [43] or the *ch1* mutant [7,44] still accumulate a functional PSI core complex in moderate light [38].

2) $P700^+$ is not such a strong oxidizer as $P680^+$, therefore photooxidative damages to PSI require very strong irradiance [45]. We have grown *chy1chy2lut2lut5* and other genotypes (Figure 7) under moderate light, a condition that did not affect PSI activity in *ch1* mutants [38]. Thus it is unlikely that a fraction of assembled PSI core complexes are destroyed due to lack of the LHCI moiety.

3) The capacity of LHCI to fold by binding both xanthophylls and β-carotene [41] makes these subunits less limited in their possibility to fold into pigment-protein complexes than Lhcb proteins.

We conclude that a tight correlation exists in plant thylakoids between PSI accumulation and xanthophyll availability which is not due to either direct stabilization of the complex by xanthophylls or by photoxidative stress. PSI and PSII core complex steady state level could be limited by chlorophyll availability, while a co-regulation of chlorophyll and carotenoid accumulation has been reported [46]. Nevertheless, the reduced amount of Chls in carotenoid biosynthesis mutants appears to be mainly due to de-stabilization of the carotenoid/chlorophyll-binding proteins [47]. Analysis of chlorophyll biosynthesis mutants [48] showed that PSI accumulation is less reduced than PSII accumulation, suggesting that the strong effect on PSI we observed in *chy1chy2lut2lut5* is not due to limitation in Chls supply. The effect of norflurazon treatment, which shows a preferential effect on PSII activity [49], further suggests that the phenotype we observe is specific for PSI core and is specifically caused by xanthophyll depletion. The lack of xanthophylls in PSI core, however, suggests this specific effect must be indirect. One possibility is that xanthophylls, or their metabolites, control either PSI synthesis or degradation. A number of factors are involved in the synthesis of PSI and PSII subunits, either bound to the thylakoid membrane or soluble in the chloroplast stroma, that could be considered as tentative targets of regulation, including *srp* and *ftsy* [50,51] or *ATAB2* protein [52]. Alternatively, carotenoid catabolites with regulatory roles [53] could be responsible for this effect. However, while the identification of the mechanisms underlying the down-regulation of PSI synthesis under limiting xanthophylls is beyond the scope of this manuscript, it is interesting to consider the implications that such a regulation would have on the function of the photosynthetic apparatus:

a) the regulation of xanthophyll/carotene level in high-light would reflect into a modulation of PSI level [54-56], thus alleviating PQ over-reduction and protecting from photoinhibition;

b) while PSII reaction centers are subjected to rapid turn-over and their level readily adjusted to environmental conditions, PSI is much more stable, thus requiring specific mechanisms for its down-regulation in limiting light. Lhcbs bind large amounts of xanthophylls and are strongly regulated depending on light intensity. Coupling PSI to xanthophyll levels would provide a mechanism for coordinated regulation of PSII antenna size and PSI/PSII ratio, a phenomenon observed in many species [57].

Conclusions

One of the most noticeable results of recent work on the plant carotenoid biosynthesis pathway is the high level of redundancy in carotene hydroxylation, which is found to be catalyzed by 4 different enzymes. Here we show that the LUT1 protein, previously reported to act in α-carotene hydroxylation, has a major β-carotene hydroxylation activity, which is evidenced in the α-carotene-less genetic background of the *chy1chy2lut2lut5*. Surprisingly, in this mutant LHCI proteins are maintained with the same stoichiometry with respect to PSI reaction center. Unexpectedly, in spite of its correct folding, PSI reaction center is drastically reduced in *chy1chy2lut2lut5* with respect to wild type, a condition that cannot be explained by a limitation in the availability of its LHCI moiety. Upon analysis of genotypes having different xanthophyll/carotenoid ratios, we show that xanthophyll availability correlates with PSI/PSII ratio within a wide range. The molecular mechanism(s) underlying regulation of both PSII antenna size and PSI/PSII ratio, alleviating PQ over-reduction during acclimation to excess light conditions, are being investigated.

Methods

Plant material and growth conditions

T-DNA insertion mutants were identified in the Syngenta and Salk collections. The knock-out lines mentioned in the article can be obtained from the NASC under the stock numbers N862308 (CHY1), N845663 (CHY2), N629724 (LUT1), N505018 (LUT2), N616660 (LUT5). Double and triple mutants were obtained as described [6]. To generate the quadruple mutant *chy1chy2lut2lut5*, the triple mutant *chy1chy2lut2* and the single mutant *lut5* were crossed, and F1 seeds were grown and self-fertilized to obtain the F2 generation. The genotype of the F2 individual seeds was checked by PCR using gene-specific and T-DNA primers [12]. We used two different parental genotypes for selection of the quadruple gene knockout (*chy1chy1chy2CHY2lut2lut2lut5lut5* and

chy1chy1chy2chy2lut2lut2lut5LUT5) identified by PCR from a segregating F_2 population of a *chy1chy1chy2chy2-lut2lut2LUT5LUT5* x *CHY1CHY1CHY2CHY2LUT2LU-T2lut5lut5* cross. Progeny from each quadruple mutant parent genotype were analyzed on Petri plates containing 0.5× MS medium, 3.0% sucrose and 0.9% agar under a photoperiod of 16 h light (30 μmol photons m^{-2} s^{-1}). The genotypes of putative quadruple mutants were confirmed by PCR [12].

In vivo fluorescence and NPQ measurements

Non-photochemical quenching of chlorophyll fluorescence (NPQ), its components qE and qI, and PSII yield (Φ_{PSII}) was measured on whole leaves at RT (room temperature, 22°C) with a PAM 101 fluorometer (Walz, Germany). Leaves were given either 7 or 20 min of illumination in saturating CO_2, and 15 min of dark-relaxation. Parameters were calculated during steady state photosynthesis according to [58].

LC-MS analysis of leaf pigments

Chlorophyll/carotenoid extraction, LC separation and photodiode array were performed as previously described with slight modifications (Fraser *et* al., 2000). Briefly, 2-3 mg of ground lyophilized leaf powder were extracted with chloroform (spiked with 100 mg/l α-tocopherol acetate as internal standard) and methanol (2:1 by volume), 1 volume of 50 mM Tris buffer (pH 7.5, containing 1 M NaCl) was added and samples were kept 20 min on ice. After centrifugation (15,000 g for 10 min at 4°C), the organic hypophase was removed and the aqueous phase was re-extracted with spiked chloroform (2 by volume). Combined organic phases were then dried by speedvac and resuspended in 100 μl of ethyl acetate. For each genotype, at least four independent extractions were performed. LC-MS analyses were carried out using a Discovery LTQ-Orbitrap mass spectrometry system (Thermo Fischer Scientific) operating in negative mode-atmospheric pressure chemical ionization (APCI), coupled to an Accela U-HPLC system (Thermo Fischer Scientific, Waltham, MA). LC separations were performed using a C30 reverse-phase column (250 × 4.6 mm) purchased from YMC (YMC Europe GmbH, Schermbeck, Germany). The mobile phases used were methanol (A), water/methanol (20/80 by volume), containing 0.2% ammonium acetate (B), and tert-methyl butyl ether (C). The gradient was: 95%A:5%B for six minutes, followed by 80%A:5%B:15%C for 14 min and by a linear gradient to 30%A:5%B:65%C over 16 min. Detection was performed continuously from 220 to 700 nm with an online Accela Surveyor photodiode array detector (PDA, Thermo Fischer Scientific, Waltham, MA). All solvents used were LC-MS grade quality (CHROMASOLV® from Sigma-Aldrich). Carotenoids were quantified on the basis of the internal standard amounts, obtained by through comparison with peak areas of known amounts of external standard LC-MS runs; data were then normalized on spectrophotometric chlorophyll contents. For APCI-MS ionization of xanthophylls (0-14 min of LC-MS run), nitrogen was used as sheath and auxiliary gas which were set to 25 and 5 units, respectively while the vaporizer temperature was 350°C, the capillary temperature was 250°C, the discharge current was set to 6.5 μA, the capillary voltage and tube lens settings were -2050 V and -77 V, respectively. APCI-MS ionization of carotenes (14-30 min of LC-MS runs) was performed with the following parameters: 40 and 10 unites of, respectively, nitrogen sheath and auxiliary gas; 250°C for vaporizer and capillary temperatures, 5.0 μA as discharge current, -30 and -110 as, respectively, capillary voltage and tube lens settings. Identification was performed by through comparison of chromatographic and spectral properties of authentic standards and reference spectra (Britton *et* al., 2004), and on the basis of the m/z accurate masses, as reported on Pubchem database http://pubchem.ncbi.nlm.nih.gov/ for monoisotopic masses identification, or on Metabolomics Fiehn Lab Mass Spectrometry Adduct Calculator http://fiehnlab.ucdavis.edu/staff/kind/Metabolomics/MS-Adduct-Calculator/ in case of adduct ion detection.

Thylakoid isolation

Thylakoids were isolated from leaves as previously described [59]. Membranes (70 μg of chlorophylls) were washed twice with 5 mM EDTA, 20 mM Hepes pH 7.8, then solubilized in 150 μl of 0.8% α-Dodecyl-maltoside (α-DM), 10 mM HEPES pH 7.5. Solubilized samples were then fractionated by ultracentrifugation (5.5 h at 60,000 rpm, 4°C) in a 0.1-1 M sucrose gradient containing 0.06% α-DM.

Gel electrophoresis

SDS-PAGE analysis was performed with either the Tris-Tricine or the Tris-Glycine buffer systems as previously described [60]. Non-denaturing Deriphat-PAGE was performed as described by [61]. For immunotitration, thylakoid samples corresponding to 0.05, 0.1, 0.25 and 0.5 μg of chlorophyll were loaded for each sample and electroblotted on nitrocellulose membranes. Filters were incubated with specific antibodies and were detected with alkaline phosphatase-conjugated antibody [62]. Gel images were quantified using GelPro 3.2 (Bio-Rad). Samples compared were loaded in the same slab gel.

Spectroscopy

Spectra were recorded on samples in 10 mM HEPES pH 7.5, 0.06% α-DM, 0.2 M sucrose, using an SLM-Aminco DW-2000 spectrophotometer at RT.

Determination of the sensitivity to photooxidative stress

Photooxidative stress was induced in detached leaves by a strong light treatment at low temperature. Detached leaves on wet filter paper were exposed to high light (900 μmol photons m^{-2} s^{-1}, 5°C) for 3.5 h, then immediately frozen in liquid nitrogen. Photooxidative stress was assessed by measuring malondialdehyde (MDA) formation [63]; the thiobarbituric acid adduct MDA-$(TBA)_2$ was quantified by HPLC [21].

Real-time PCR

Total RNA was isolated from frozen tissue and analyzed through Real Time RT-PCR using previously published methods [64]. Three independent RNA extractions (from three pools of at least ten plants each) and three cDNAs (one for each RNA extraction) were used for the analyses; first strand cDNA was synthesized from 0.5 μg of RNA in 20 μl with oligo-dT(16) and Superscript II (Invitrogen). Real Time PCR was performed using an ABI PRISM 7000 instrument and the SYBR Green Master Mix kit (Applera). Standard dilution curves were performed for each gene fragment and all data were normalized for the β-TUBULIN transcript and for wild-type expression levels. Primers for Real Time experiments (Additional file 1: Table S1) were designed using the Primer Express v2.0 software and validated with the Amplify v3.1 software.

Statistics

Significance analyses were performed using an analysis of variance with a pair-wise multiple comparison procedure in Origin. Error bars represent the standard deviation.

Additional material

Additional file 1: Figure S1. Genomic structure of the different mutants utilized. Figure S2. PCR confirmation of the different mutants. Figure S3. Isolation and characterization of the pigment-protein complexes from wild-type and *chy1chy2lut2lut5* thylakoid membrane. Figure S4. Distribution of the PSI core (**A**), PSII core (**B**) and LHCII (**B**) amount per fresh weight *vs*. the relative content of xanthophylls on thylakoids. Table S1. Sequences of oligonucleotides used for RT-PCR measurement of transcripts. Table S2. LC-DAD-MS analysis of wild-type and mutant Arabidopsis leaves.

Abbreviations

PSI and PSII: Photosystem I and II: respectively; α-DM: *n*-dodecyl-α-D-maltoside; Car: carotenoids; Chl *a* and *b*: chlorophyll *a* and b: respectively; F_v/F_m: maximal PSII photochemical efficiency; gFW: gram of fresh weight; HL: high-light; HPLC-DAD-MS: high pressure liquid chromatography - diode array detector - mass spectrometry; Lhca and Lhcb: light-harvesting complexes of PSI and PSII: respectively; LHCI: antenna complex of photosystem I; LHCII: major light-harvesting complex of PSII; MDA: malondialdehyde; NPQ: non-photochemical quenching; PQ: plastoquinone; qE: ΔpH-dependent component of NPQ; qI: photoinhibition quenching; qP: photochemical quenching; ROS: reactive oxygen species; RT: room temperature; TBA: thiobarbituric acid; Φ_{PSII}: efficiency of PSII photochemistry.

Acknowledgements

Work supported by the Italian ministry of Research, special fund for basic research (PRIN 2008XB774B), and by the European Commission, Metapro project.

Author details

[1]Italian National Agency for New Technologies, Energy and Sustainable Development (ENEA), Casaccia Research Center, Via Anguillarese 301, 00123 Rome, Italy. [2]Dipartimento di Biotecnologie, Università di Verona, Strada Le Grazie 15, 37134 Verona, Italy. [3]ICG-3: Phytosphäre Forschungszentrum Jülich, 52425 Jülich, Germany. [4]Dipartimento di Biotecnologie, Università di Verona, Strada Le Grazie 15, 37134 Verona, Italy.

Authors' contributions

AF performed identification and isolation of all the genotypes used, carried out the molecular genetic studies and drafted the manuscript; LD and SC carried out the biochemical and photosynthetic characterization of plants under control and photoxidative conditions, performed western-blot analysis and drafted the manuscript; GD performed mass-spectrometry analysis; GG and RB conceived the study, participated in its design and coordination and edited the manuscript. All authors read and approved the final manuscript.

Received: 27 November 2011 Accepted: 18 April 2012
Published: 18 April 2012

References

1. Kull O, Pfander H: **List of new carotenoids.** In *Carotenoids: Isolation and Analysis*. Edited by: Britton SL-JaHPe G. Basel: Birkauser Publishing; 1995:316-317.
2. Baroli I, Niyogi KK: **Molecular genetics of xanthophyll-dependent photoprotection in green algae and plants.** *Philos Trans R Soc Lond B Biol Sci* 2000, **355**:1385-1394.
3. Demmig-Adams B, Adams WW: **Photoprotection and other responses of plants to high light stress.** *Ann Rev Plant Physiol Plant Mol Biol* 1992, **43**:599-626.
4. Niyogi KK: **Safety valves for photosynthesis.** *Curr Opin Plant Biol* 2000, **3**:455-460.
5. Dall'Osto L, Caffarri S, Bassi R: **A mechanism of nonphotochemical energy dissipation, independent from Psbs, revealed by a conformational change in the antenna protein CP26.** *Plant Cell* 2005, **17**:1217-1232.
6. Dall'Osto L, Fiore A, Cazzaniga S, Giuliano G, Bassi R: **Different roles of α- and β-branch xanthophylls in photosystem assembly and photoprotection.** *Journal of Biological Chemistry* 2007, **282**:35056-35068.
7. Havaux M, Dall'Osto L, Bassi R: **Zeaxanthin has Enhanced Antioxidant Capacity with Respect to All Other Xanthophylls in Arabidopsis Leaves and functions independent of binding to PSII antennae.** *Plant Physiol* 2007, **145**:1506-1520.
8. Liu Z, Yan H, Wang K, Kuang T, Zhang J, Gui L, *et al*: **Crystal structure of spinach major light-harvesting complex at 2.72 A resolution.** *Nature* 2004, **428**:287-292.
9. Croce R, Weiss S, Bassi R: **Carotenoid-binding sites of the major light-harvesting complex II of higher plants.** *J Biol Chem* 1999, **274**:29613-29623.
10. Tian L, Magallanes-Lundback M, Musetti V, DellaPenna D: **Functional analysis of beta- and epsilon-ring carotenoid hydroxylases in Arabidopsis.** *Plant Cell* 2003, **15**:1320-1332.
11. Tian L, Musetti V, Kim J, Magallanes-Lundback M, DellaPenna D: **The Arabidopsis LUT1 locus encodes a member of the cytochrome p450 family that is required for carotenoid epsilon-ring hydroxylation activity.** *Proc Natl Acad Sci USA* 2004, **101**:402-407.
12. Fiore A, Dall'Osto L, Fraser PD, Bassi R, Giuliano G: **Elucidation of the beta-carotene hydroxylation pathway in Arabidopsis thaliana.** *FEBS Lett* 2006, **580**:4718-4722.
13. Kim J, DellaPenna D: **Defining the primary route for lutein synthesis in plants: the role of Arabidopsis carotenoid beta-ring hydroxylase CYP97A3.** *Proc Natl Acad Sci USA* 2006, **103**:3474-3479.
14. Kim J, Smith JJ, Tian L, DellaPenna D: **The evolution and function of carotenoid hydroxylases in Arabidopsis.** *Plant Cell Physiol* 2009, **50**:463-479.
15. Pogson B, McDonald KA, Truong M, Britton G, DellaPenna D: **Arabidopsis carotenoid mutants demonstrate that lutein is not essential for photosynthesis in higher plants.** *Plant Cell* 1996, **8**:1627-1639.

16. Dall'Osto L, Lico C, Alric J, Giuliano G, Havaux M, Bassi R: **Lutein is needed for efficient chlorophyll triplet quenching in the major LHCII antenna complex of higher plants and effective photoprotection in vivo under strong light.** *Bmc Plant Biology* 2006, **6**:32.
17. Lokstein H, Tian L, Polle JE, DellaPenna D: **Xanthophyll biosynthetic mutants of Arabidopsis thaliana: altered nonphotochemical quenching of chlorophyll fluorescence is due to changes in Photosystem II antenna size and stability.** *Biochim Biophys Acta* 2002, **1553**:309-319.
18. Gilmore AM: **Xanthophyll cycle-dependent nonphotochemical quenching in Photosystem II: mechanistic insights gained from Arabidopsis thaliana L. mutants that lack violaxanthin deepoxidase activity and/or lutein.** *Photosynthesis Research* 2001, **67**:89-101.
19. Niyogi KK, Shih C, Chow WS, Pogson BJ, DellaPenna D, Bjorkman O: **Photoprotection in a zeaxanthin- and lutein-deficient double mutant of Arabidopsis.** *Photosynth Res* 2001, **67**:139-145.
20. Baroli I, Do AD, Yamane T, Niyogi KK: **Zeaxanthin accumulation in the absence of a functional xanthophyll cycle protects Chlamydomonas reinhardtii from photooxidative stress.** *Plant Cell* 2003, **15**:992-1008.
21. Dall'Osto L, Cazzaniga S, North H, MArion-Poll A, Bassi R: **The arabidopsis aba4-1 mutant reveals a specific function for neoxanthin in protection against photoxidative stress.** *Plant Cell* 2007, **19**:1048-1064.
22. Maxwell K, Johnson GN: **Chlorophyll fluorescence - a practical guide.** *J Exp Bot* 2000, **51**:659-668.
23. Genty B, Briantais J-M, Baker NR: **The relationship between the quantum yield of photosynthetic electron transport and quenching of chlorophyll fluorescence.** *Biochim Biophys Acta* 1989, **990**:87-92.
24. Horton P, Ruban A: **Molecular design of the photosystem II light-harvesting antenna: photosynthesis and photoprotection.** *J Exp Bot* 2005, **56**:365-373.
25. Caffarri S, Croce R, Breton J, Bassi R: **The major antenna complex of photosystem II has a xanthophyll binding site not involved in light harvesting.** *J Biol Chem* 2001, **276**:35924-35933.
26. Bassi R, Dainese P: **A Supramolecular Light-Harvesting Complex from Chloroplast Photosystem-II Membranes.** *Eur J Biochem* 1992, **204**:317-326.
27. de Bianchi S: **Dall'Osto L, Tognon G, Morosinotto T, Bassi R: Minor antenna proteins CP24 and CP26 affect the interactions between Photosystem II subunits and the electron transport rate in grana membranes of Arabidopsis.** *Plant Cell* 2008, **20**:1012-1028.
28. Caffarri S, Kouril R, Kereiche S, Boekema EJ, Croce R: **Functional architecture of higher plant photosystem II supercomplexes.** *EMBO J* 2009, **28**:3052-3063.
29. Ballottari M, Govoni C, Caffarri S, Morosinotto T: **Stoichiometry of LHCI antenna polypeptides and characterisation of gap and linker pigments in higher plants Photosystem I.** *Eur J Biochem* 2004, **271**:4659-4665.
30. Li XP, Muller-Moule P, Gilmore AM, Niyogi KK: **PsbS-dependent enhancement of feedback de-excitation protects photosystem II from photoinhibition.** *Proc Natl Acad Sci USA* 2002, **99**:15222-15227.
31. Ahn TK, Avenson TJ, Ballottari M, Cheng YC, Niyogi KK, Bassi R, *et al*: **Architecture of a charge-transfer state regulating light harvesting in a plant antenna protein.** *Science* 2008, **320**:794-797.
32. Avenson TJ, Ahn TK, Zigmantas D, Niyogi KK, Li Z, Ballottari M, *et al*: **Zeaxanthin radical cation formation in minor light-harvesting complexes of higher plant antenna.** *J Biol Chem* 2008, **283**:3550-3558.
33. Teardo E, De Laureto PP, Bergantino E, Dalla VF, Rigoni F, Szabo I, *et al*: **Evidences for interaction of PsbS with photosynthetic complexes in maize thylakoids.** *Biochim Biophys Acta* 2007, **1767**:703-711.
34. Betterle N, Ballottari M, Zorzan S, de Bianchi S, Cazzaniga S, Dall'Osto L, *et al*: **Light-induced dissociation of an antenna hetero-oligomer is needed for non-photochemical quenching induction.** *Journal of Biological Chemistry* 2009, **284**:15255-15266.
35. Pogson BJ, Niyogi KK, Bjorkman O, DellaPenna D: **Altered xanthophyll compositions adversely affect chlorophyll accumulation and nonphotochemical quenching in Arabidopsis mutants.** *Proc Natl Acad Sci USA* 1998, **95**:13324-13329.
36. Pogson B, Rissler HM: **Genetic manipulation of carotenoid biosynthesis and photoprotection.** *Phil Trans R Soc Lond B* 2000, **355**:1395-1403.
37. Plumley FG, Schmidt GW: **Reconstitution of chloroform a/b light-harvesting complexes: Xanthophyll-dependent assembley and energy transfer.** *Proc Natl Acad Sci USA* 1987, **84**:146-150.
38. Dall'Osto L, Cazzaniga S, Havaux M, Bassi R: **Enhanced photoprotection by protein-bound vs free xanthophyll pools: a comparative analysis of chlorophyll b and xanthophyll biosynthesis mutants.** *Molecular plant* 2010, **3**:576-593.
39. Espineda CE, Linford AS, Devine D, Brusslan JA: **The AtCAO gene, encoding chlorophyll a oxygenase, is required for chlorophyll b synthesis in Arabidopsis thaliana.** *Proc Natl Acad Sci USA* 1999, **96**:10507-10511.
40. Mozzo M, Morosinotto T, Bassi R, Croce R: **Probing the structure of Lhca3 by mutation analysis.** *Biochim Biophys Acta* 2006, **1757**:1607-1613.
41. Morosinotto T, Castelletti S, Breton J, Bassi R, Croce R: **Mutation analysis of Lhca1 antenna complex.** *Low energy absorption forms originate from pigment-pigment interactions. J Biol Chem* 2002, **277**:36253-36261.
42. Nelson N: **Ben Shem A: The complex architecture of oxygenic photosynthesis.** *Nature* 2004, **5**:1-12.
43. Klimmek F, Ganeteg U, Ihalainen JA, van Roon H, Jensen PE, Scheller HV, *et al*: **The structure of higher plant LHCI: in vivo characterisation and structural interdependence of the Lhca proteins.** *Biochemisty* 2005, **44**:3065-3073.
44. Tanaka A, Ito H, Tanaka R, Tanaka NK, Yoshida K, Okada K: **Chlorophyll a oxygenase (CAO) is involved in chlorophyll b formation from chlorophyll a.** *Proc Natl Acad Sci USA* 1998, **95**:12719-12723.
45. Havaux M, Kloppstech K: **The protective functions of carotenoid and flavonoid pigments against excess visible radiations at chilling temperature investigated in Arabidopsis npq and tt mutants.** *Planta* 2001, **213**:953-966.
46. Härtel H, Lokstein H, Dörmann P, Grimm B, Benning C: **Changes in the composition of the photosynthetic apparatus in the Galactolipid-deficient dgd1 mutant of Arabidopsis thaliana.** *Plant Physiol* 1997, **115**:1175-1184.
47. Paulsen H: **Pigment ligation to proteins of the photosynthetic apparatus in higher plants.** *Physiol Plant* 1997, **100**:760-768.
48. Meinecke L, Alawady A, Schroda M, Willows R, Kobayashi MC, Niyogi KK, *et al*: **Chlorophyll-deficient mutants of Chlamydomonas reinhardtii that accumulate magnesium protoporphyrin IX.** *Plant Mol Biol* 2010, **72**:643-658.
49. Dong H, Deng Y, Mu J, Lu Q, Wang Y, Xu Y, *et al*: **The Arabidopsis Spontaneous Cell Death1 gene, encoding a zeta-carotene desaturase essential for carotenoid biosynthesis, is involved in chloroplast development, photoprotection and retrograde signalling.** *Cell Res* 2007, **17**:458-470.
50. Asakura Y, Hirohashi T, Kikuchi S, Belcher S, Osborne E, Yano S, *et al*: **Maize mutants lacking chloroplast FtsY exhibit pleiotropic defects in the biogenesis of thylakoid membranes.** *Plant Cell* 2004, **16**:201-214.
51. Grudnik P, Bange G, Sinning I: **Protein targeting by the signal recognition particle.** *Biol Chem* 2009, **390**:775-782.
52. Barneche F, Winter V, Crevecoeur M, Rochaix JD: **ATAB2 is a novel factor in the signalling pathway of light-controlled synthesis of photosystem proteins.** *EMBO J* 2006, **25**:5907-5918.
53. Gomez-Roldan V, Fermas S, Brewer PB, Puech-Pages V, Dun EA, Pillot JP, *et al*: **Strigolactone inhibition of shoot branching.** *Nature* 2008, **455**:189-194.
54. Ballottari M: **Dall'Osto L, Morosinotto T, Bassi R: Contrasting behavior of higher plant photosystem I and II antenna systems during acclimation.** *Journal of Biological Chemistry* 2007, **282**:8947-8958.
55. Kim JH, Glick RE, Melis A: **Dynamics of Photosystem Stoichiometry Adjustment by Light Quality in Chloroplasts.** *Plant Physiol* 1993, **102**:181-190.
56. Chow WS, Melis A, Anderson JM: **Adjustments of photosystem stoichiometry in chloroplasts improve the quantum efficiency of photosynthesis.** *Proc Natl Acad Sci USA* 1990, **87**:7502-7506.
57. Dietzel L, Brautigam K, Pfannschmidt T: **Photosynthetic acclimation: state transitions and adjustment of photosystem stoichiometry-functional relationships between short-term and long-term light quality acclimation in plants.** *FEBS J* 2008, **275**:1080-1088.
58. Van Kooten O, Snel JFH: **The use of chlorophyll fluorescence nomenclature in plant stress physiology.** *Photosynt Res* 1990, **25**:147-150.
59. Casazza AP, Tarantino D, Soave C: **Preparation and functional characterization of thylakoids from Arabidopsis thaliana.** *Photosynth Res* 2001, **68**:175-180.
60. Schägger H, von Jagow G: **Tricine-sodium dodecyl sulfate-polyacrylamide gel electrophoresis for the separation of proteins in the range from 1 to 100 kDa.** *Anal Biochem* 1987, **166**:368-379.

61. Peter GF, Thornber JP: **Electrophoretic Procedures for Fractionation of Photosystem-I and Photosystem-II Pigment-Proteins of Higher Plants and for Determination of Their Subunit Composition.** In *Methods in Plant Biochemistry. 5.* Edited by: Rogers LJ. New York: Academic Press; 1991:195-210.
62. Towbin H, Staehelin T, Gordon J: **Electrophoretic transfer of proteins from polyacrylamide gels to nitrocellulose sheets: Procedure and some applications.** *Proc Natl Acad Sci USA* 1979, **76**:4350-4354.
63. Vavilin DV, Ducruet J-M, Matorin DN, Venediktov PS, Rubin AB: **Membrane lipid peroxidation, cell viability and photosystem II activity in the green alga Chlorella pyrenoidosa subjected to varius stress conditions.** *J Photochem Photobiol B* 1998, **42**:233-239.
64. Carbone F, Pizzichini D, Giuliano G, Rosati C, Perrotta G: **Comparative profiling of tomato fruits and leaves evidences a complex modulation of global transcript profiles.** *Plant Science* 2005, **169**:165-175.

doi:10.1186/1471-2229-12-50
Cite this article as: Fiore *et al.*: A quadruple mutant of Arabidopsis reveals a β-carotene hydroxylation activity for LUT1/CYP97C1 and a regulatory role of xanthophylls on determination of the PSI/PSII ratio. *BMC Plant Biology* 2012 **12**:50.

Additional results

Additional Figure 1

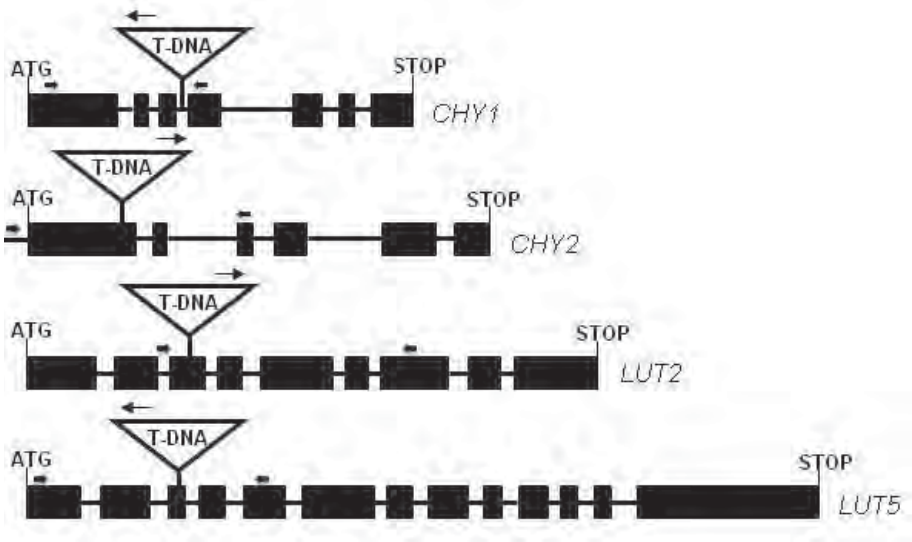

Additional Figure 1. Genomic structure of the different mutants utilized. The T-DNA insertions are indicated as triangles. Thick arrows represent gene-specific primers, thin arrows represent the T-DNA-specific primer.

Additional Figure 2.

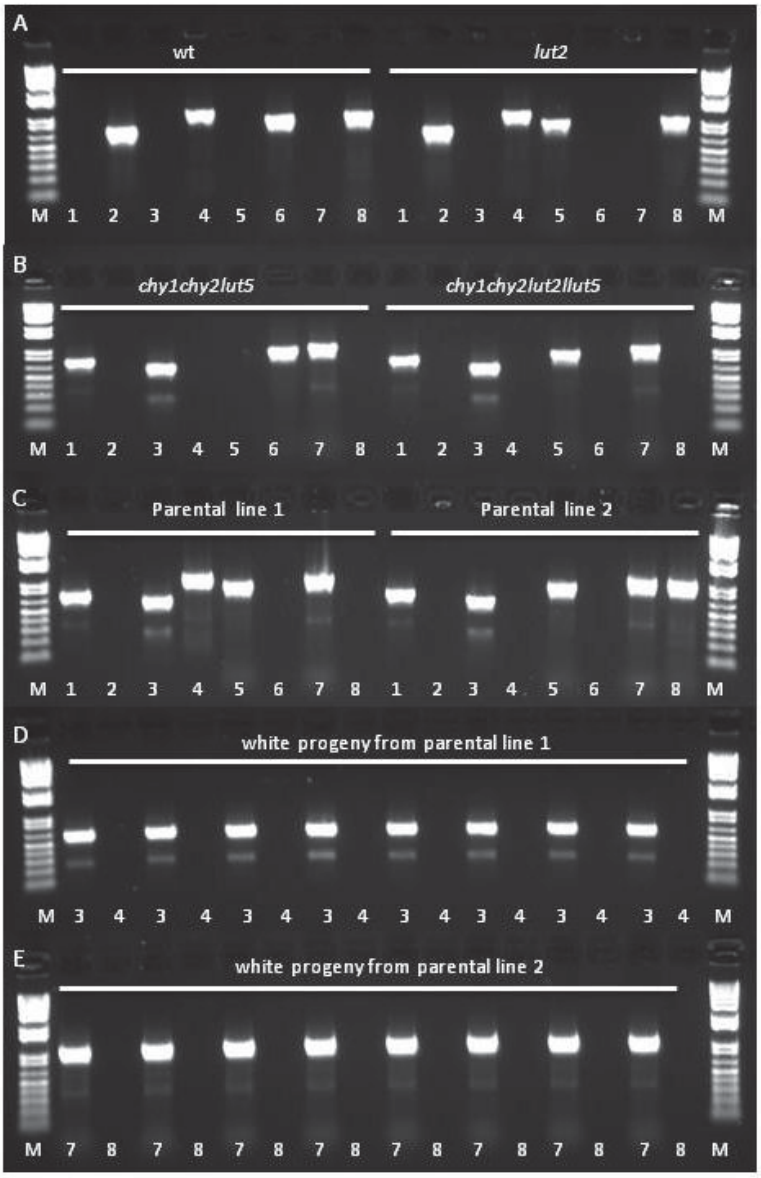

Additional Figure 2. PCR confirmation of the different mutants. (A) Wild-type and *lut2* mutant. (B) *chy1chy2lut5* (triple) and *chy1chy2lut2lut5* (quadruple) mutants. (C) Parental line 1 (*chy1lut2lut5* triple mutant, heterozygous for the *chy2* mutation) and parental line 2 (*chy1chy2lut2* triple mutant, heterozygous for the *lut5* mutation) for the *chy1chy2lut2lut5* quadruple mutant. (D) Analysis of the *CHY2* gene in eight white seedlings deriving from parental line 1; all seedlings are *chy2*/*chy2*. (E) Analysis of the *LUT5* gene in eight white seedlings deriving from parental line 2; all seedlings are *lut5/lut5*. M: molecular weight marker. 1: *CHY1*:T-DNA amplicon. 2: *CHY1* gene-specific amplicon. 3: *CHY2*: T-DNA amplicon. 4: *CHY2* gene-specific amplicon. 5: *LUT2*: T-DNA amplicon. 6: *LUT2* gene-specific amplicon. 7: *LUT5*:T-DNA amplicon. 8: *LUT5* gene-specific amplicon.

Additional Figure 3

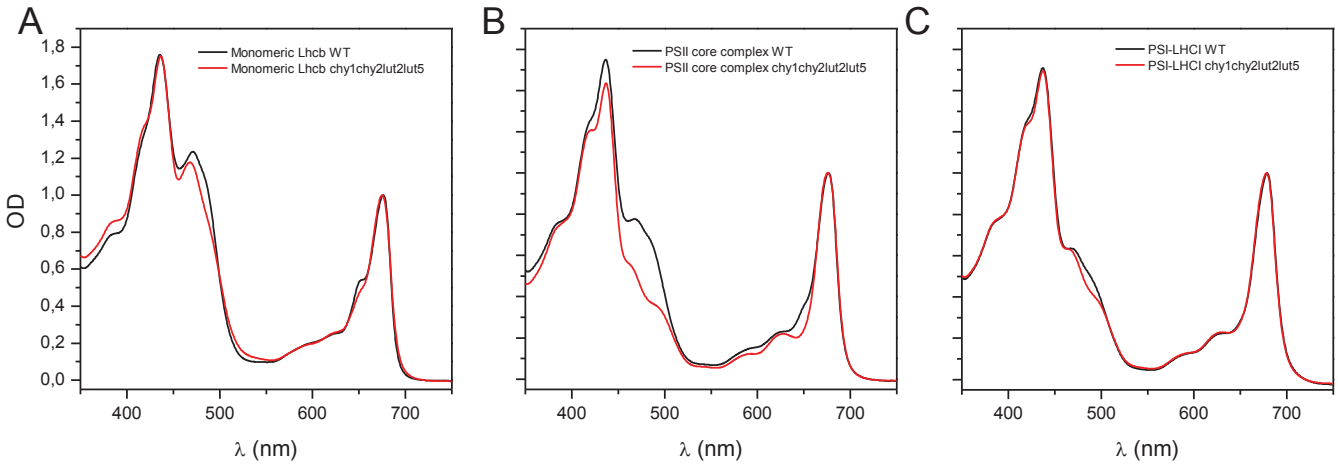

Additional Figure 3. Isolation and characterization of the pigment-protein complexes from wild-type and *chy1chy2lut2lut5* thylakoid membrane. Absorption spectra of the monomeric Lhcb (band 2, panel A), PSII core complex (band 5, panel B) and PSI-LHCI complexes (band 6, panel C) isolated by sucrose gradient ultracentrifugation from wild-type and *chy1chy2lut2lut5* thylakoids (see Figure 5B). The spectra are normalized to the maximum in the red region. The Chl *b* content, which is proportional to the Lhc antenna content, is obtained from the amplitude of the absorption components at 470 and 650 nm.

Additional Figure 4.

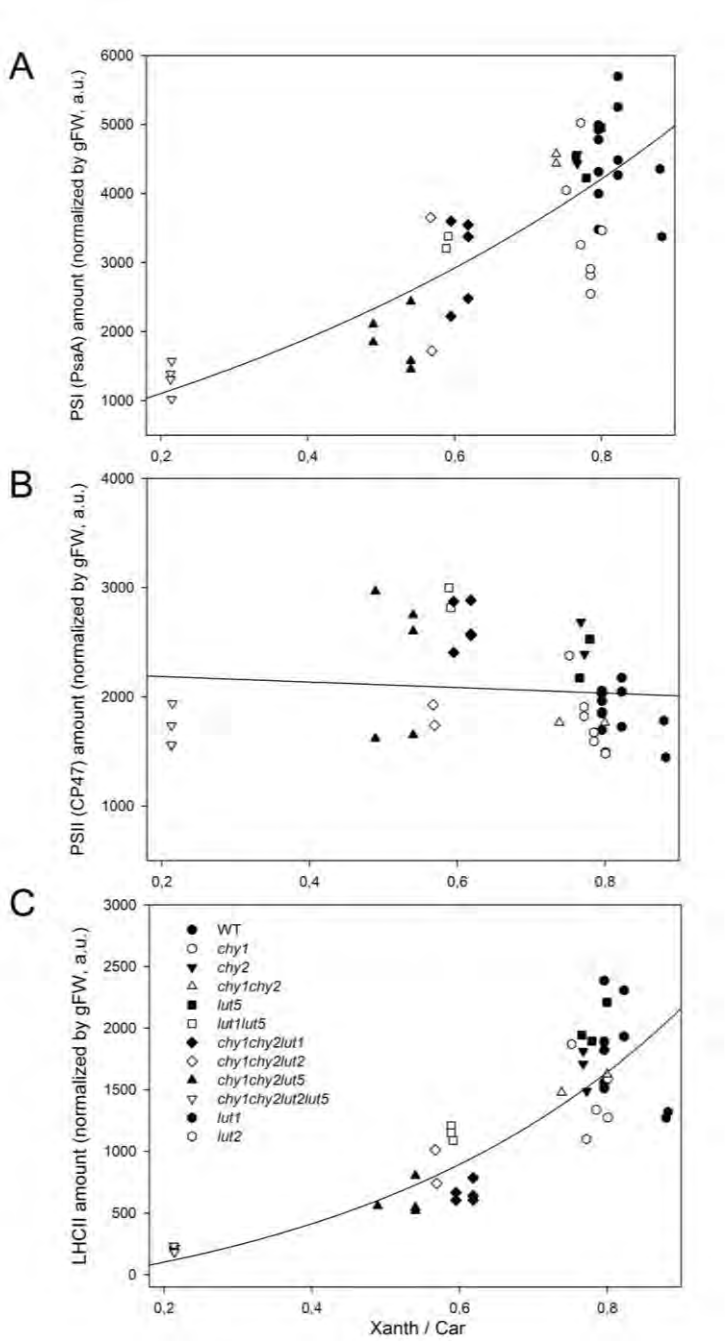

Additional Figure 4. Distribution of the PSI core (A), PSII core (B) and LHCII (B) content per gram of fresh weight *vs.* the xanthophyll/carotenoid ratio. Protein amounts were measured for wild-type and 11 xanthophyll biosynthesis mutants plants previously described (Fiore *et al.*, 2006; Dall'Osto *et al.*, 2007b; present ms). Protein amounts per fresh weight were determined on leaf extracts by quantitative western blot, while xanthophyll/carotenoid ratios were quantified by HPLC. gFW, gram of fresh weight. $R^2_{\text{PSI amount}}$ = 0.65; $R^2_{\text{PSII amount}}$ = 0.01; $R^2_{\text{LHCII amount}}$ = 0.73.

Additional Tables

Additional Table 1

Genes	Oligonucleotides
CHY1 forward	GCTCTCTCTGTTGGTGCTGCT
CHY1 reverse	AGCCCATCTTGCCCAGAAT
CHY2 forward	TTTGCTCTTTCCGTTGGTGC
CHY2 reverse	CCATCTTGCCCAAAACTCCAT
LUT1 forward	ACATAGATGGCGCAATCCCT
LUT1 reverse	CTACACATTTTCTAGGCCCTCCA
LUT2 forward	GTATTGAGCATGTTTGGAG
LUT2 reverse	TCGTAAGTCTTTAGAATTCG
LUT5 forward	CGGCGGCAGTATTAACATGG
LUT5 reverse	CACTTGGTTCCGTTGTTAAAAGG
TUB forward	GGTGTTCCCTTCACCAAAGGT
TUB reverse	GCGTTGTAAGGCTCCACCAC

Additional Table 1. Sequences of oligonucleotides used for RT-PCR measurement of transcripts. TUB, tubulin.

Additional Table 2

Metabolite	RT (minutes)	Abs (nm)	Formula	Theoretical mass (m/z)	Experimental mass (m/z)	Experimental formula	Theoretical adduct mass (m/z)	Authentic Standard
Neoxanthin	11,22	417, **440**, 468	$C_{40}H_{56}O_4$	600,4178	659,4234	$C_{42}H_{58}O_6$ (M+Hac-H)	659,4317	yes
Violaxanthin	11,87	416, **439**, 469	$C_{40}H_{56}O_4$	600,4178	659,4320	$C_{42}H_{58}O_6$ (M+Hac-H)	659,4317	yes
9-cis-Violaxanthin	12,94	413, **436**, 464	$C_{40}H_{56}O_4$	600,4178	659,4280	$C_{42}H_{58}O_6$ (M+Hac-H)	659,4317	yes
Antheraxanthin	15,59	416, **446**, 475	$C_{40}H_{56}O_3$	584,4229	643,4268	$C_{42}H_{58}O_5$ (M+Hac-H)	643,4367	no
Lutein	18,03	422, **445**, 472	$C_{40}H_{56}O_2$	568,4280	568,4298	$C_{40}H_{56}0_2$	-	yes
Zeaxanthin	20,01	**450**, 480	$C_{40}H_{56}O_2$	568,4280	627,4459	$C_{42}H_{58}O_4$ (M+Hac-H)	627,4418	yes
cis-α-carotene	26,15	428, **444**, 468	$C_{40}H_{56}$	536,4382	536,4377	$C_{40}H_{56}$	-	yes
α-carotene	26,9	428, **448**, 475	$C_{40}H_{56}$	536,4382	536,4354	$C_{40}H_{56}$	-	yes
β-carotene	28,72	433, **452**, 478	$C_{40}H_{56}$	536,4382	536,4367	$C_{40}H_{56}$	-	yes
cis-β-carotene	29,92	**447**, 473	$C_{40}H_{56}$	536,4382	536,4317	$C_{40}H_{56}$	-	yes
chlorophyll *a*	20,28	416	$C_{55}H_{72}MgN_4O_5$	892,5353	892,5279	$C_{55}H_{72}MgN_4O_5$	-	no
chlorophyll *b*	15,99	467	$C_{55}H_{70}MgN_4O_6$	906,5145	906,5108	$C_{55}H_{70}MgN_4O_6$	-	no

Additional Table 2. LC-DAD-MS analysis of wild-type and mutant Arabidopsis leaves. Retention time (RT), maximum absorbance wavelenghts, chemical formula and theoretical (as reported on Pubchem:http://pubchem.ncbi.nlm.nih.gov/) and experimental accurate masses for each metabolite are reported. Experimental formula was obtained using the Metabolomics Fiehn Lab Mass Spectrometry Adduct Calculator (http://fiehnlab.ucdavis.edu/staff/kind/Metabolomics/MS-Adduct-Calculator/). M: monoisotopic mass; Hac: acetic acid. For more details, see Methods.

A2. The *Arabidopsis thaliana nox* mutant lacking carotene hydroxylase activity reveals a critical role for xanthophylls in photosystem I biogenesis.

The Plant Cell, Vol. 25: 591–608, February 2013, www.plantcell.org

The *Arabidopsis nox* Mutant Lacking Carotene Hydroxylase Activity Reveals a Critical Role for Xanthophylls in Photosystem I Biogenesis[C][W]

Luca Dall'Osto,[a,1] Maria Piques,[b] Michela Ronzani,[a] Barbara Molesini,[a] Alessandro Alboresi,[a] Stefano Cazzaniga,[a] and Roberto Bassi[a,c]

[a] Dipartimento di Biotecnologie, Università di Verona, 37134 Verona, Italy
[b] Max Planck Institute of Molecular Plant Physiology, 14474 Potsdam-Golm, Germany
[c] Institute for Chemistry and Dynamics of the Geosphere, Phytosphaere Forschungszentrum Jülich, 52425 Juelich, Germany

Carotenes, and their oxygenated derivatives xanthophylls, are essential components of the photosynthetic apparatus. They contribute to the assembly of photosynthetic complexes and participate in light absorption and chloroplast photoprotection. Here, we studied the role of xanthophylls, as distinct from that of carotenes, by characterizing a *no xanthophylls* (*nox*) mutant of *Arabidopsis thaliana*, which was obtained by combining mutations targeting the four carotenoid hydroxylase genes. *nox* plants retained α- and β-carotenes but were devoid in xanthophylls. The phenotype included depletion of light-harvesting complex (LHC) subunits and impairment of nonphotochemical quenching, two effects consistent with the location of xanthophylls in photosystem II antenna, but also a decreased efficiency of photosynthetic electron transfer, photosensitivity, and lethality in soil. Biochemical analysis revealed that the *nox* mutant was specifically depleted in photosystem I function due to a severe deficiency in PsaA/B subunits. While the stationary level of psaA/B transcripts showed no major differences between genotypes, the stability of newly synthesized PsaA/B proteins was decreased and translation of psaA/B mRNA was impaired in *nox* with respect to wild-type plants. We conclude that xanthophylls, besides their role in photoprotection and LHC assembly, are also needed for photosystem I core translation and stability, thus making these compounds indispensable for autotrophic growth.

INTRODUCTION

Carotenoids are a group of C_{40} pigments that contains extended conjugated double-bond systems conferring strong absorption of light and antioxidant properties. These compounds are widely distributed among taxa, including fungi, cyanobacteria, red and green algae, and land plants (Kull and Pfander, 1995; Britton et al., 2004). More than 700 different carotenoids have been described, and this structural diversity has likely evolved in relation to their many functions: They act as vitamins and hormones, as substrate for the synthesis of volatile products, and as colors in flowers and fruits (DellaPenna and Pogson, 2006; Cuttriss and Pogson, 2006). Furthermore, carotenoids play essential roles in higher plant photosynthesis, as components of the photosynthetic apparatus (Nelson and Ben Shem, 2004).

Carotenoids are composed of two major groups, namely, carotenes and their oxygenated derivatives, the xanthophylls. In higher plants, β-carotene binds to reaction center subunits of both photosystems, while xanthophylls are accessory pigments and structural elements of light-harvesting complexes (LHCs) (Bassi et al., 1993). Together with β-carotene, xanthophylls act as photoreceptors, absorbing light energy, which is used in photosynthetic electron transport. Also, they are photoprotectants of the photosynthetic apparatus from excess light (EL) and from the reactive oxygen species (ROS) generated during oxygenic photosynthesis (Niyogi, 2000; Dall'Osto et al., 2005; Havaux et al., 2007).

The xanthophyll composition of higher plants is remarkably conserved and includes four major xanthophylls: the β,ε-xanthophyll lutein and the three β,β-xanthophylls, violaxanthin (Viola), neoxanthin (Neo), and zeaxanthin (Zea; Demmig-Adams and Adams, 1992b). Recent studies on carotenoid biosynthetic mutants of *Arabidopsis thaliana* have improved our understanding of the biosynthetic pathway (Pogson et al., 1998; Fiore et al., 2006; Kim and DellaPenna, 2006; North et al., 2007; Dall'Osto et al., 2007b; Kim et al., 2009) (see Supplemental Figure 1 online). β-Carotene, the precursor of β,β-xanthophylls, is formed from lycopene by the symmetrical action of β-cyclase, while the β,ε-carotenoid α-carotene is formed by the combined action of both β-cyclase and ε-cyclase on lycopene (DellaPenna and Pogson, 2006), thus making a bifurcation in the pathway between the β,β- and β,ε-xanthophyll branches.

Hydroxylation of α-carotene produces lutein, the most abundant xanthophyll in leaves, while hydroxylation of β-carotene yields Zea, which is rapidly epoxidized to antheraxanthin and Viola and then converted to Neo (North et al., 2007). However, EL activates the deepoxidation of Viola, leading to the

[1] Address correspondence to luca.dallosto@univr.it.
The author responsible for distribution of materials integral to the findings presented in this article in accordance with the policy described in the Instructions for Authors (www.plantcell.org) is: Luca Dall'Osto (luca.dallosto@univr.it).
[C] Some figures in this article are displayed in color online but in black and white in the print edition.
[W] Online version contains Web-only data.
www.plantcell.org/cgi/doi/10.1105/tpc.112.108621

accumulation of Zea (Yamamoto et al., 1962; Demmig-Adams and Adams, 1992b). Biosynthesis of lutein requires one β- and one ε-ring hydroxylation of α-carotene, while synthesis of β-xanthophylls needs hydroxylation of both β-carotene β-rings. *Arabidopsis* mutants impaired in carotenoid biosynthesis showed that heme-containing cytochrome P450 hydroxylases CYP97A3 (LUT5) express a major β-carotene hydroxylase activity in vivo, while CYP97C1 (LUT1) is primarily involved in the hydroxylation of the ε ring of α-carotene (Tian et al., 2004; Kim and DellaPenna, 2006; Fiore et al., 2012). Non-heme di-iron monoxygenases CHY1 and CHY2 primarily catalyze the hydroxylation of β-carotene. Indeed, the *chy1 chy2* double mutant showed an 80% reduction in β-carotene–derived xanthophylls (Tian et al., 2003; DellaPenna and Pogson, 2006). Recently, the expression of each carotenoid hydroxylase, as well as their biochemical activity, was assessed in vivo using knockout genotypes (Kim et al., 2009; Fiore et al., 2012).

A remarkable characteristic of higher plant xanthophylls is their similar spectral properties in the visible region (Kull and Pfander, 1995), implying that a similar light-harvesting activity operates across species. This evidence is apparently incoherent with the conservation of composition and relative abundance across plant taxa (Demmig-Adams and Adams, 1992a; Koniger et al., 1995), suggesting that each xanthophyll species serves a specific biological function. The phenotypes of *Arabidopsis* carotenoid biosynthetic mutants with altered xanthophyll composition suggest that the combination of constitutive contributions of lutein, Viola, and Neo, integrated by the action of Zea in EL, is the most functional solution for facing oxidative stress in highly variable natural conditions. Indeed, lack of lutein and/or Zea decreases the capacity for photoprotection in EL (Niyogi et al., 2001), while lack of Neo increases sensitivity to superoxide anions, formed in the Mehler's reaction (Dall'Osto et al., 2007a). Depletion of Viola, as in the *chy1 chy2 lut5* mutant, caused extreme photosensitivity (Dall'Osto et al., 2007b). Lutein bound to site L1 of all LHC proteins is essential for protein folding and for chlorophyll triplet quenching (Croce et al., 1999; Formaggio et al., 2001). Viola binds to L2 and/or V1 sites, while Neo has its own specific binding site called N1 (Liu et al., 2004; Caffarri et al., 2007; Pan et al., 2011). Zea is produced in EL and replaces Viola in LHC protein structure (Dall'Osto et al., 2005), leading to (1) enhancement of nonphotochemical quenching (NPQ) (Holt et al., 2005) and (2) the protection of thylakoid lipids from peroxidation (Baroli et al., 2003).

Although the above observations support the notion that each xanthophyll species has a specific role in photoprotection, their collected importance as a class of compounds distinct from carotenes has not been assessed so far. In this work, we isolated and characterized the *Arabidopsis chy1 chy2 lut1 lut5* quadruple mutant (hereafter referred to as *nox* for the sake of brevity), which lacks all xanthophylls but retains carotenes. The *nox* mutant showed a complete depletion of LHC proteins, inactivation of NPQ, and high sensitivity to photooxidative stress with respect to the wild type. Besides, *nox* plants showed decreased photosynthetic electron transport and depletion of photosystem I (PSI), an unexpected feature, since β-carotene, the only carotenoid ligand in the core complex, is conserved in the mutant. PSI content declined due to enhanced protein turnover and impaired translation of the PsaA/PsaB messengers. Thus, carotenes alone were unable to sustain photosynthetic electron transport even in dim light. These findings imply that xanthophylls, besides their well-known role in light harvesting and photoprotection, are also essential for the biogenesis of the PSI core complex.

RESULTS

nox, a Quadruple Knockout Mutant of *Arabidopsis*, Accumulates α- and β-Carotene as the Only Carotenoids

nox plants were obtained by crossing homozygous T-DNA mutants carrying insertions in genes encoding the two non-heme hydroxylases (*chy1* and *chy2*), the ε-ring hydroxylase (*lut1*), and its paralog (*lut5*) (Fiore et al., 2006). Absence of the transcripts for the mutated genes was verified via RT-PCR (Figure 1A), while pigment composition of *nox* plants was verified by HPLC (Figure 1B): *nox* plants contained α- and β-carotene as the only carotenoids, but lacked xanthophylls. Homozygous knockout mutant seedlings developed white cotyledons and were lethal when grown on soil. They could only be maintained on medium supplemented with 3% Suc under low light (20 μmol photons m^{-2} s^{-1}) (Figures 1C and 1D). Under sterile heterotrophic conditions, leaf morphology and size were unaltered in *nox* in comparison to wild-type plants (Figure 1C). Mutant seedlings were paler, with strongly reduced (~17%) chlorophyll content per leaf area compared with wild-type plants; the chlorophyll *a*/*b* ratio was 7.5 in *nox* versus 2.9 in wild-type seedlings, while the chlorophyll/carotenoid ratio was less affected (Table 1).

Chloroplast ultrastructure was observed by transmission electron microscopy. Wild-type chloroplasts showed the characteristic organization with grana stacks interconnected by stroma membranes and small starch granules in most sections (see Supplemental Figures 2A and 2B online). Instead, the *nox* plastids were ~2 times smaller and were depleted in thylakoids and starch granules. The plastids of the mutant had rudimentary thylakoids, lacking grana stacks, and consisted of stroma lamellae only, arranged into concentric monovesicles (see Supplemental Figures 2C and 2D online), resembling a sliced onion in section. It appears that thylakoid development was arrested at an early developmental stage of two disks grana.

nox Is Impaired in Photoprotection and Photosynthetic Electron Transport

When photosynthetic organisms are exposed to EL, photooxidative stress occurs with the production of ROS in the chloroplast; in particular, singlet oxygen ($^1O_2$) derives from the reaction of chlorophyll triplets with molecular oxygen (Krieger-Liszkay, 2005). A feature of ROS is their high reactivity, leading to oxidative damage of biomolecules. To analyze the effect of missing xanthophylls on the yield of different ROS, we quantified the release of $^1O_2$ directly in wild-type and *nox* leaves, infiltrated with singlet oxygen sensor green (SOSG), a $^1O_2$-specific fluorescent probe. After illumination with moderate light intensity (200 μmol photons m^{-2} s^{-1}, 22°C), *nox* leaves showed, at each time point, a far higher release of $^1O_2$ per chlorophyll with respect to the wild type (Figure 2A). These results showed that xanthophyll-depleted *nox* leaves were impaired in the capacity of preventing

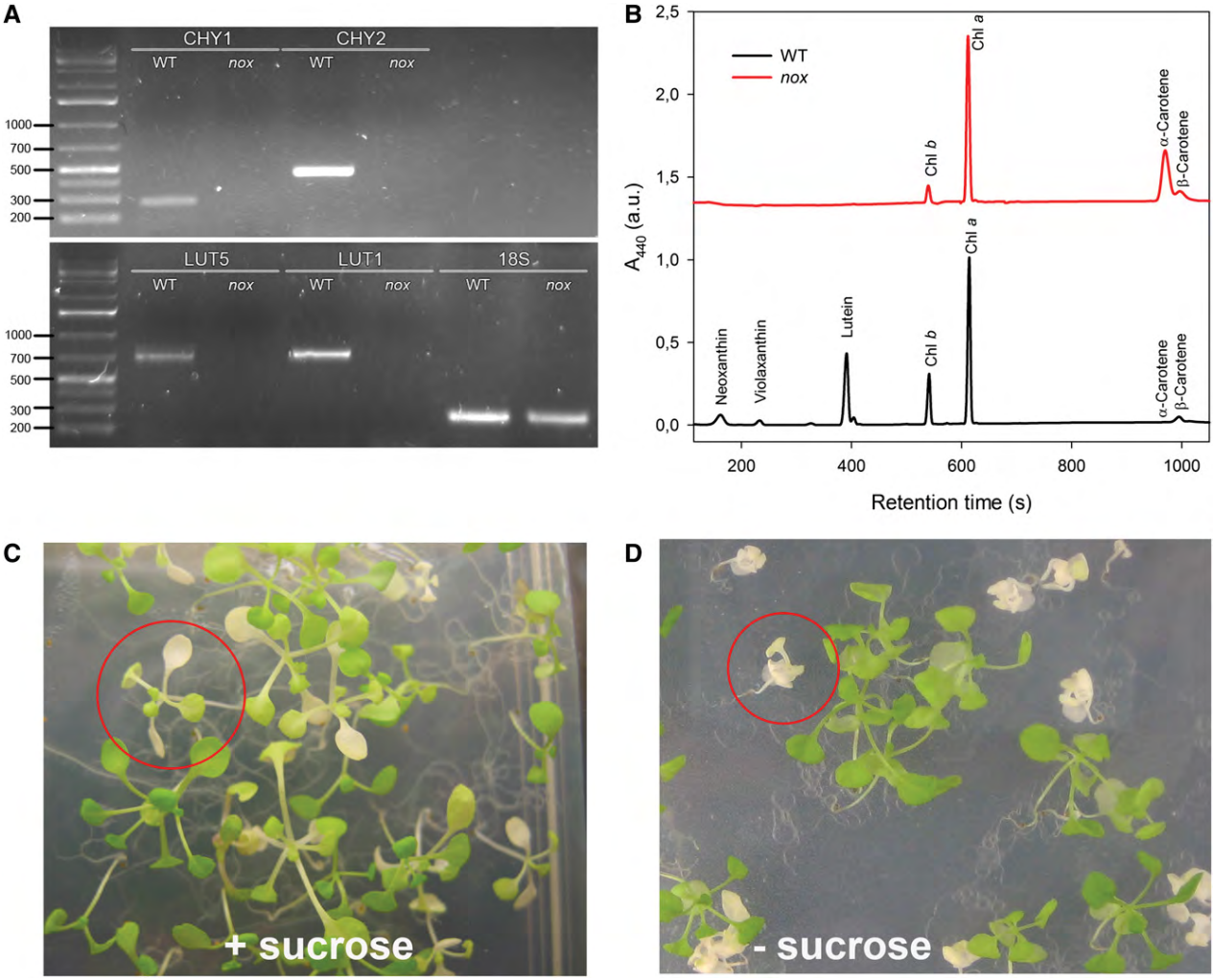

Figure 1. Genetic and Biochemical Characterization of Wild-Type and *nox Arabidopsis* Plants.

(A) RT-PCR amplification pattern of gene-specific transcripts. The 18S transcript was used as a control for the reverse transcriptase reaction. Details of primer sequences and expected sizes of the PCR products have been reported (Fiore et al., 2006). DNA ladder, 1 kb plus (75 to 20,000 bp). WT, the wild type.

(B) Analysis of pigment content of leaves from wild-type and *nox* plants. Separation of lipid-soluble pigments was based on HPLC analysis. Each chromatogram represents absorbance at 440 nm (A_{440}) of pigments extracted from a dark-adapted leaf. Chromatograms were vertically shifted for better comparison. a.u., arbitrary units.

(C) and **(D)** Phenotype of mutant plants, grown either heterotrophically **(C)** or autotrophically **(D)** for 2 weeks. Representative mutant plants are circled. [See online article for color version of this figure.]

$^1O_2$ release compared with xanthophyll-containing wild-type leaves.

nox plants accumulate both α- and β-carotene, while wild-type leaves accumulate β-carotene only. Since both α- and β-carotene can bind to photosynthetic core complexes, it might be asked whether photosensitivity could be ascribed to the accumulation of α-carotene into PSI and photosystem II (PSII) core complexes. To address this question, $^1O_2$ production (see Supplemental Figures 3A to 3C online) and photobleaching kinetics under EL (see Supplemental Figures 3D to 3F online) were measured on PSII and PSI complexes isolated from either wild-type and *lut5* leaves, which accumulate β-carotene and α-carotene, respectively (Dall'Osto et al., 2007b). β-Carotene substitution in *lut5* did not affect $^1O_2$ yield or photobleaching kinetics when compared with complexes isolated from the wild type at all light intensities tested. On this basis, we can exclude that the enhanced sensitivity of the photosynthetic apparatus of *nox* is due to α-carotene accumulation, implying that it is rather attributed to the absence of xanthophylls.

Photosynthetic activity was investigated by measuring both PSII and PSI function in wild-type and *nox* leaves. The $t_{2/3}$ of the chlorophyll fluorescence rise in DCMU-treated leaves was

Table 1. Pigment Content and PSII/PSI Functionality, Determined on the Leaves of Wild-Type and *nox Arabidopsis* Plants

Genotypes	Chlorophyll *a/b*	Chlorophyll/Carotenoid	Chlorophyll/m^2 (mg)	F_v/F_m	$t_{2/3}^{-1}$ ($\cdot 10^{-3}$, ms^{-1})	ΔA_{max} (705 nm, a.u.)
The wild type	2.9 ± 0.1	3.5 ± 0.2	171.2 ± 4.2	0.77 ± 0.02	6.1 ± 1.1	68.1 ± 6.6
nox	7.5 ± 0.6*	3.0 ± 0.3	31.3 ± 4.1*	0.44 ± 0.09*	1.8 ± 0.3*	4.9 ± 1.2*

Data are expressed as mean ± SD ($n > 5$), and significantly different values (Student's t test, $P < 0.05$) with respect to the wild type are marked with an asterisk. a.u., arbitrary units.

taken as a measure of the functional antenna size of PSII (Malkin et al., 1981). It was reduced by 70% in *nox* with respect to the wild type (Table 1), implying that the light-harvesting function is severely reduced in the absence of xanthophylls.

Further chlorophyll fluorescence analysis yielded insight into PSII function. Upon growth at 20 μmol photons m^{-2} s^{-1}, *nox* mutants had F_v/F_m ratios (the maximal photochemical yield of PSII) of 0.44 versus 0.77 for the wild type (Table 1). Also, *nox* plants showed a decrease in the PSII photochemical efficiency (Φ_{PSII}) at all light intensities tested (Figure 2B); this parameter is equivalent to the quantum yield of linear electron flux through PSII and is linearly related to the yield of O_2 evolution. The fraction of oxidized PSII acceptor Q_A (qL) was lower in *nox* compared with the wild type (Figure 2C). Finally, the capacity for

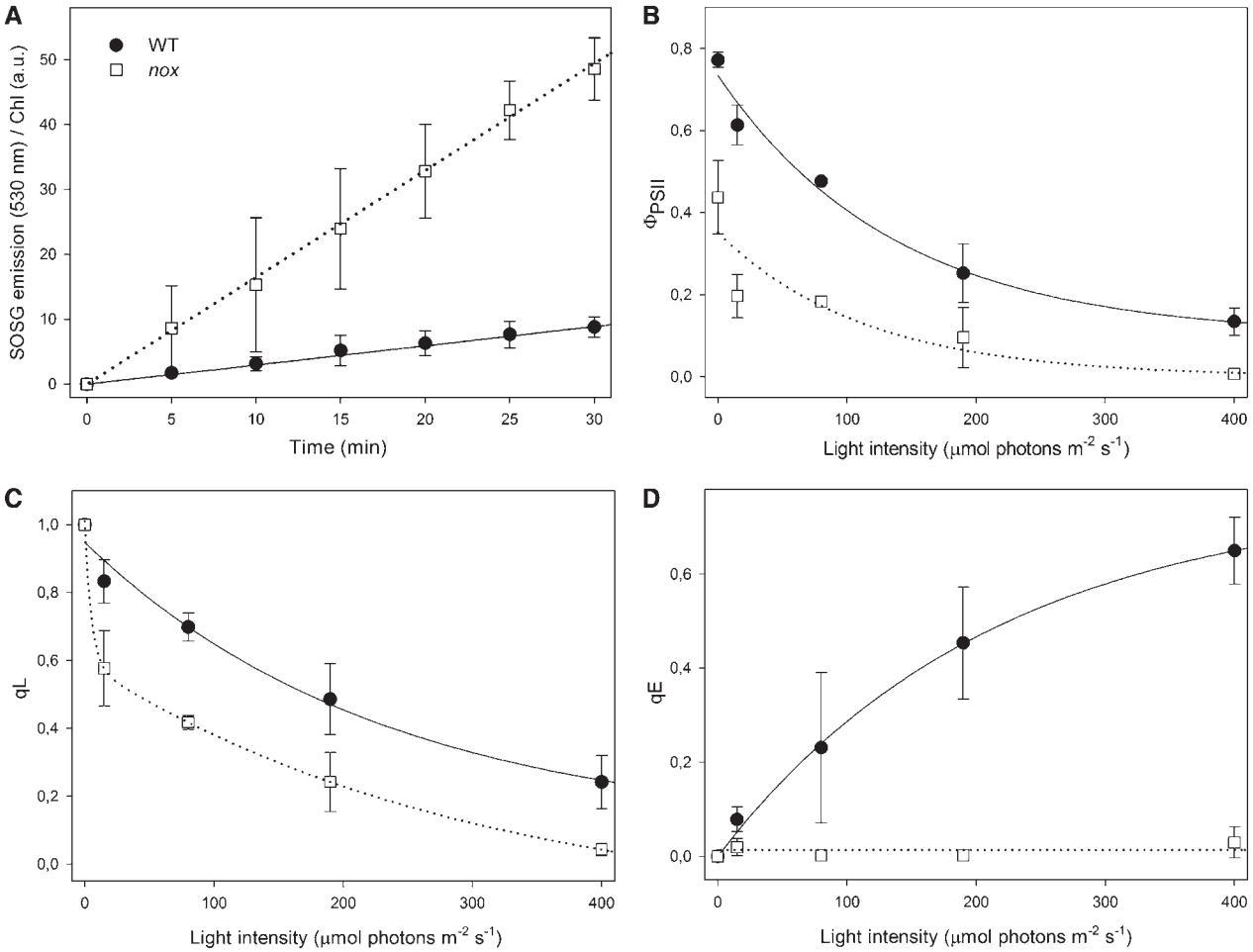

Figure 2. Analysis of $^1O_2$ Release and Chlorophyll Fluorescence during Photosynthesis in Wild-Type and *nox* Leaves.

(A) Wild-type and mutant leaves were infiltrated with SOSG, a fluorogenic probe that exhibits increased fluorescence yield upon reaction with $^1O_2$. The increase in probe signal was monitored during illumination with red actinic light (200 μmol photon m^{-2} s^{-1}, 600 < λ < 750 nm, 22°C); at each time point, the fluorescence signal was normalized to the leaf chlorophyll content. a.u., arbitrary units; WT, the wild type.

(B) to **(D)** Chlorophyll fluorescence was monitored in dark-adapted leaves during photosynthesis by following photosynthetic efficiency (Φ_{PSII}) **(B)**, PQ pool redox state (qL) **(C)**, and the ΔpH-dependent component (qE) of thermal energy dissipation (NPQ) **(D)**. Leaves were illuminated for 20 min, and parameters were determined during steady state photosynthesis. Symbols and error bars show mean ± SD ($n > 3$). Statistical analysis confirmed that parameters of *nox* leaves were always significantly different with respect to that of the wild type (Student's t test, $P < 0.05$).

heat dissipation (qE; measured as the rapidly reversible component of NPQ) was null at a light intensity up to 400 μmol photons m^{-2} s^{-1}, while the wild type showed an increase in qE with increasing light intensity, implying that xanthophylls are needed for qE activity (Figure 2D).

It should be noted that, although reduced, a qL activity was detected in *nox* leaves, implying that photosynthetic electron flow through PSII was active, while a bottleneck is likely to be localized at later electron transfer steps. Further insight into the light-harvesting efficiency and electron transport activity downstream of Q_A was obtained by analyzing the fluorescence induction and relaxation in dark-adapted leaves. To test the hypothesis that electron transport is restricted in the Q_A to Q_B step in *nox* plants, Q_A reoxidation kinetics upon a single turnover flash were analyzed in order to assess the capacity for Q_A reoxidation by the plastoquinone (PQ) pool. In short, when PSII is excited by a very short flash of saturating light, Q_A is fully reduced to reach F_m and then the kinetic of F_v recovery in the dark is determined, which depends on PQ diffusing from the surrounding membrane domains to the PSII Q_B site and on the total amount of reducible PQ (Sane et al., 2003). Since similar fluorescence decay kinetics were measured in wild-type and *nox* leaves (see Supplemental Figure 4A online), no restrictions to the accessibility of the Q_B site to PQ are likely to be present in either genotype.

Comparison of the fluorescence induction curves showed that, upon switching from dark to light, the time needed for reaching the F_{max} was longer in the mutant versus the wild type, consistent with the lower functional antenna size of *nox* plants (Table 1, $t_{2/3}^{-1}$). Nevertheless, fluorescence decline from F_{max} to stationary fluorescence, evident after ~10 s of continuous illumination in the wild type as a consequence of the activation of the Benson-Calvin cycle, was slower in the mutant (see Supplemental Figure 4B online). Taken together, these results suggest that the nonphotoautotrophic mutant phenotype is the consequence of a block in light-driven electron transport, which appears to occur at the level of cytochrome b_6f, plastocyanin, or PSI. To further detail the origin of electron transport restriction, we proceeded to monitor PSI activity in vivo, by measuring the total amount of photooxidizable P700 in intact leaves. Thus, absorbance changes at 705 nm (ΔA_{max}) were measured upon far-red illumination, clearly showing that PSI efficiency was severely reduced in the *nox* mutant compared with the wild type (Table 1), suggesting that xanthophyll depletion might affect either PSI activity and/or accumulation of the complex.

nox Is Primarily Defective in PSI Accumulation

To investigate the state of PSI, pigment-protein complexes were separated in wild-type and mutant plants by nondenaturing Deriphat-PAGE, upon solubilization of thylakoid membranes with 0.6% dodecyl-α-D-maltoside (α-DM). Several major green bands were resolved in the wild type (Figure 3A): Four green bands with high apparent molecular mass were detected in the upper part of the gel (collectively marked as B7) containing undissociated PSII supercomplexes with different Lhcb complements; the PSI-LHCI complex was a major band (B6), while the components of the PSII-LHCII complexes migrated as multiple green bands with increasing mobility in the gel, namely, PSII core monomers (B5), the Lhcb4/Lhcb6/LHCII-M supercomplex (B4) (Dainese et al., 1992), the LHCII trimer (B3), and the Lhcb monomeric band (B2). Finally, a band (B1) migrated with the front and contained free pigments. The electrophoretic profile of *nox* thylakoid membranes was markedly different (Figure 3A): Only two green bands could be distinguished, corresponding to bands B5 and B1 of the wild type. To characterize their polypeptide composition, the green lanes from the first dimension were excised and further fractionated by denaturing SDS-PAGE in a second dimension (Figure 3B). LHC apoproteins, well resolved in the gel containing the wild-type sample, were not detectable in the case of *nox*. From the major band (B5) in *nox*, PSII subunits were separated, namely, D1/D2 and CP43/CP47. PSI core complex subunits (PsaA/PsaB) were not evident. Fluorometric measurements of wild-type and *nox* chloroplasts at 77K showed that the PSII emission band at 685 nm was present in the mutant, implying it originated from the PSII core rather than from Lhcb components. Moreover, the PSI-specific fluorescence band, the largest in amplitude in the wild-type spectrum, was strongly reduced in *nox* (see Supplemental Figure 5 online); the 733-nm peak emission was shifted to 728 nm in *nox*, while the band at 733 nm was reduced to a shoulder of the spectrum.

The level of selected thylakoid proteins, relative to the wild type on a chlorophyll basis, was determined by immunoblot analysis (Figure 3C): All Lhcb subunits were undetectable in *nox*, while the Lhca content was strongly reduced, amounting to ~35% of wild-type values for Lhca2/3 and ~15% for Lhca1/4. Plastocyanin content was the same in both genotypes, while subunits of the PSII core complex (D1, OEC33, and CP47), cytochrome b_6f complex, and PsbS were present in higher amounts in *nox* with respect to the wild type. By contrast, the two major plastid-encoded PSI core subunits (PsaA and PsaB) were strongly decreased in *nox*, reaching ~6% with respect to the wild-type level. One possible reason for the downregulation of protein level is destabilization due to missing cofactors, such as Fe-S centers, which was shown to be important for the accumulation of the PSI core complex (Amann et al., 2004; Yabe et al., 2004). To investigate whether the *nox* mutation affects iron-sulfur cluster assembly, we measured the amount of plastid Fe-S cluster-containing proteins. Ferredoxin (which contains a 2Fe-2S cluster), NDH-L and NDH-K (subunits of the NADPH-dependent dehydrogenase, a 4Fe-4S cluster protein), and the chloroplast HCF101 subunits (a scaffold protein for 4Fe-4S cluster assembly) were present in the same amount in wild-type and *nox* leaves (see Supplemental Figure 6 online).

To verify whether this dramatic effect on the steady state level of LHC and PSI pigment proteins was due to the presence of an unrelated mutation, we analyzed single knockout mutants for carotene hydroxylases by Deriphat-PAGE (see Supplemental Figure 7 online). Each of these mutants clearly exhibited a PSI-LHCI band.

Photoinhibition of PSI Is Enhanced during Short-Term EL Treatments of *nox*

To investigate whether PSI depletion in *nox* plants was caused by an increased photosensitivity of PSI complexes under photooxidation, leaf discs from wild-type and mutant plants, grown in low light, were transferred to higher light (200 μmol photons m^{-2} s^{-1}, room temperature) for 2.5 h; then, PSII and PSI

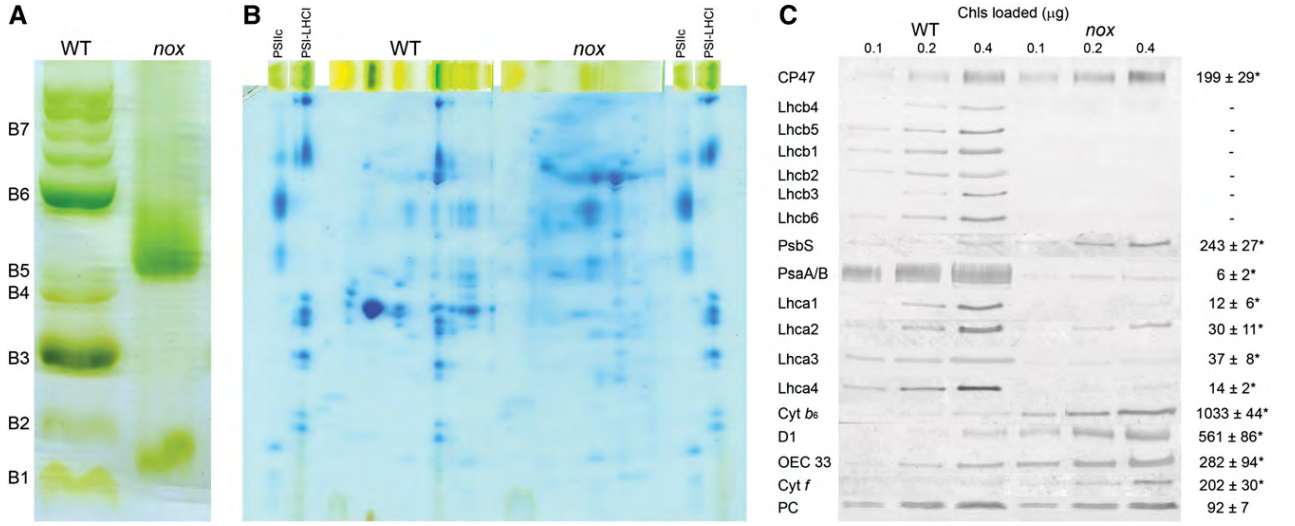

Figure 3. Biochemical Characterization of Thylakoid Membranes from Wild-Type and *nox* Plants.

(A) Nondenaturing Deriphat-PAGE separation of pigmented thylakoid complexes from wild-type (WT) and *nox* plants. Numbering of green bands (B1 to B7) is reported.

(B) Two-dimensional resolution of thylakoid protein complexes. α-DM–solubilized thylakoid protein complexes purified from wild-type and *nox* leaves were fractionated by Deriphat-PAGE in the first dimension and SDS-PAGE (Tris-Tricine system) in the second. Gel slices containing purified PSII core complex (PSIIc) and PSI-LHCI complexes were loaded as reference.

(C) Immunotitration of photosynthetic subunits. Amounts of chlorophylls loaded on the gel were 0.1, 0.2, and 0.4 μg. The abundance of each subunit in *nox* (right column) was expressed as a percentage of the corresponding content in the wild type. The *Arabidopsis* genome encodes two plastocyanin isoforms (PetE1/2), which were resolved both in the wild type and *nox* and detected in the same relative abundance. Data are reported as mean ± SD ($n = 3$), and significantly different values (Student's t test, $P < 0.05$) are marked (asterisk). Cyt, cytochrome; OEC 33, oxygen-evolving complex 33-kD subunit; PC, plastocyanin.

[See online article for color version of this figure.]

activities were assessed by measuring the decrease in maximal quantum yield of PSII (F_v/F_m) or maximum photooxidizable P700 (ΔA_{max}) upon the treatment. Figure 4A shows that 2.5 h of treatment was effective in producing a faster PSII photoinhibition on *nox* leaves with respect to the wild type (photoinhibition half-time: 7.5 h for the wild type and 2.7 for *nox*). The results are consistent with the well-established role of xanthophylls in ensuring photoprotection of thylakoids. Surprisingly, PSI photoinhibition rate was even faster than that of PSII in the *nox* mutant (Figure 4B): At 200 μmol photons m^{-2} s^{-1}, the half-time of PSI photoinhibition was 8.5 and 0.6 h for wild-type and *nox* leaves, respectively. Taken together, the above results show that *nox* plants are specifically affected in the PSI complex, leading to a strong downregulation of PSI core components and to a dramatic photosensitivity of PSI activity. It is particularly remarkable that PSI, normally the more stress resistant of the two photosystems, was indeed preferentially affected by light in the absence of xanthophylls.

Lower Abundance of PSI in *nox* Leaves Resulted from a Combination of Slower Synthesis and Faster Degradation

The low PSI content could be caused by increased degradation, as suggested by the above reported photodamage, or by impaired assembly, but also by a lower rate of synthesis, which in turn could be limited at different levels from transcription, to transcript maturation and/or translation. To determine the reasons for low PSI, the rate of these processes was determined. The level of transcripts encoding the main PSI subunits A, B, and C, as well as that encoding the PSII subunit D1 as a reference, was measured by quantitative real-time RT-PCR (qRT-PCR). Results are reported in Figure 5A: The transcript level of genes encoding PsaA, PsaB (PSI core subunits), and PsbA (PSII core subunit) were not significantly different in *nox* with respect to the wild type, while the PsaC transcript was upregulated in the mutant. Accumulation of transcripts of the nuclear-encoded subunits PsaD, E, and F, the depletion of which severely affected PSI accumulation (Haldrup et al., 2000; Varotto et al., 2000; Ihnatowicz et al., 2004), did not show any downregulation in *nox* with respect to the wild type (Figure 5B). Since KO of all other subunits of PSI (namely, PsaG-PsaL, PsaN, and PsaO) resulted in less severe PSI defects (Schöttler et al., 2011), these PSI subunits were not investigated in this study.

In addition, mRNA levels of genes encoding regulatory or assembly proteins for PSI biogenesis, such as hypothetical chloroplast RF3 (Ycf3, Boudreau et al., 1997; Albus et al., 2010), high chlorophyll fluorescence 101 (HCF101, Lezhneva et al., 2004), pale yellow green 7 (PYG7, Stöckel et al., 2006), *Arabidopsis* translation of PsaB mRNA (ATAB2, Barneche et al., 2006), Ycf3-interacting protein 1 (Y3IP1, Albus et al., 2010), and accumulation of photosystem one1 (APO1, Amann et al., 2004; Watkins et al., 2011), was the same in *nox* plants as in the wild

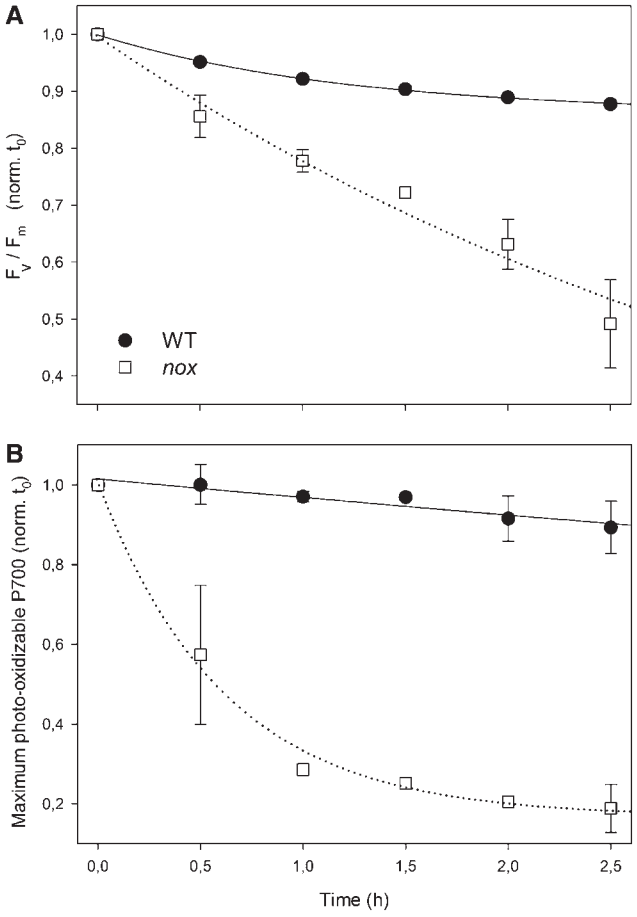

Figure 4. PSII and PSI Photoinhibition under Photooxidative Stress of the Wild-Type and *nox* Mutant Plants.

(A) Leaves excised from wild-type (WT) and *nox* and floating on water were treated at 200 μmol photons m^{-2} s^{-1} for 2.5 h, and the kinetics of the F_v/F_m decrease (PSII photoinhibition) was measured.
(B) PSI photoinhibition was quantified by measuring the decay kinetics of maximum photooxidizable P700 (ΔA_{max} at 705 nm) on detached leaves under high-light intensity (200 μmol photons m^{-2} s^{-1}, 2.5 h). The maximum contents of P700 was determined on methyl viologen–treated leaves using a saturating flash (3000 μmol photons m^{-2} s^{-1}) under a 520-μE far-red light background (Munekage et al., 2002). t_0, time zero. Data are expressed as means ± SD ($n > 3$). Statistical analysis shows that values measured for *nox* leaves were always significantly different with respect to those for the wild type (Student's *t* test, $P < 0.05$).

type, or even higher (Figure 5B). Moreover, the amount of Ycf3 and Ycf4, assembly factors for PSI (Boudreau et al., 1997; Krech et al., 2012), was similar in both genotypes (see Supplemental Figure 6 online).

Levels of all transcripts analyzed remained unaffected or were upregulated by the *nox* mutation; thus, additional analysis through RNA gel blot hybridization was performed to investigate whether the PSI deficiency was related to altered mRNA maturation. Indeed, the chloroplast genome is mainly organized in polycistronic transcription units, and primary transcripts undergo a number of processing events that yield a population of RNA sequences. Mutations that affect the maturation pattern of the *psaA/B* operon (Meurer et al., 1998) or the pre-mRNA splicing of the PSI assembly factor *ycf3* (Watkins et al., 2011) were shown to lead to a proportional loss of PSI.

A set of probes for plastid-encoded structural subunits of both PSI (*psaA* and *psaB*) and PSII (*psbA*) were used as well as probes for chloroplast genes involved in the PSI assembly process (*ycf3* and *ycf4*) and for the ribosomal protein S14 (Figure 6). The transcripts that contain sequences of *psaA/rps14*, *psaC*, *psbA*, and *ycf3/4* showed no major changes in abundance and/or length pattern in the wild type versus *nox*, thus ruling out the hypothesis of a lower maturation efficiency of these sequences upon xanthophyll depletion.

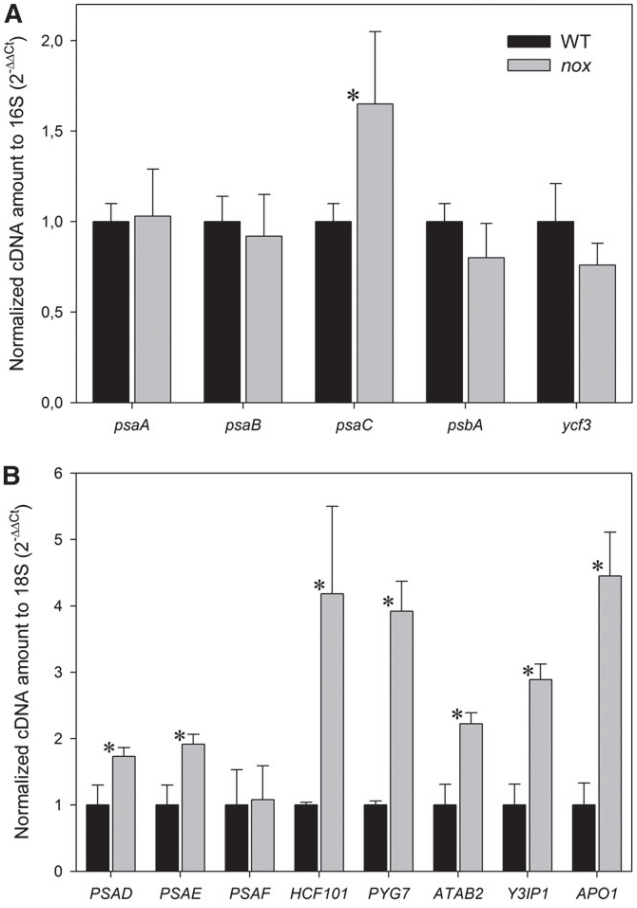

Figure 5. qRT-PCR Transcript Profiles of *Arabidopsis* Genes Involved in PSI Biogenesis.

Transcript levels of genes encoding either PSI and PSII structural subunits or subunits involved in PSI assembly were determined using specific primers and random primers for cDNA production (see Methods for details). For individual genes, relative mRNA levels were normalized with respect to either the 16S **(A)** or the 18S **(B)** rRNA housekeeping transcript and then to wild-type (WT) levels. qRT-PCR was performed with three RNAs isolated independently from three different batches of mutant and wild-type plants. Data are expressed as mean ± SD ($n = 3$). Values significantly different ($P < 0.05$) from the wild type are marked with an asterisk.

Furthermore, we monitored the synthesis and degradation rate of chloroplast-encoded thylakoid proteins by pulse labeling leaves with [^{35}S]Met in the presence of cycloheximide, an inhibitor of cytoplasmic protein synthesis. As shown in Figure 7A, the incorporation of radioactivity into the α- and β-subunits of chloroplast ATP synthase was increased in the mutant with respect to the wild type; labeling of the PSII protein D1 was slightly reduced in the wild type, while incorporation of radioactivity in the proteins CP43 and CP47 was similar in *nox* and the wild type. As for PSI, accumulation of PsaA/PsaB proteins was strongly reduced. Pulse labeling for 30 min was followed by a chase with unlabeled Met to monitor the turnover rate of the chloroplast-encoded proteins (Figure 7B). Plotting the kinetics of decrease in ^{35}S labeling during the chase showed that the turnover rates of PSII core protein D1 (Figure 7D) were similar in the wild type and *nox* mutant, whereas turnover of PsaA/PsaB was 3 times faster in the mutant with respect to the wild type (Figure 7C).

The above results suggest that impaired translation of PSI transcripts might contribute to limiting PSI accumulation. This was investigated by polysome analysis (Mathews et al., 2007) that consists of fractionating polysomes from wild-type and *nox* plants on Suc gradients by ultracentrifugation and assessing the partitioning of individual messages between fractions containing ribosome-free messages (plus monosomes) versus polysomal fractions. Figure 8 shows absorption profiles of ribonucleoprotein material that was extracted from wild-type (A) and *nox* (B) plants and harvested at the midpoint of the light period.

Based on the absorption readings (Figures 8A and 8B), no major differences were apparent in the polysome profiles, implying that the level of translation was comparable in the wild-type and *nox* plants (~34% of ribosomes were on polysomes for both). When using the ribosome concentration determined by qRT-PCR (Figure 8C), the wild-type and *nox* plants showed no significant difference in the total ribosome levels and on polysomes (39 and 46%, respectively). These results indicate that the global translational activity is similar in wild-type and *nox* plants. Also, the significant amount of free ribosome subunits and monosomes indicates that the availability of ribosomes does not seem to be a limiting factor for the global translation efficiency in *nox* and wild-type plants. A key parameter of the translational status of a gene is the fraction of its transcripts engaged in translation, defined as the transcript's ribosomal occupancy (Mathews et al., 2007): The greater the percentage of an mRNA that is associated with polysomes, the greater its translational efficiency. When the polysome occupancy of *psaA*, *psaB*, *psbA*, and *psaC* was analyzed, a strong reduction of the *psaA*/*psaB* transcripts (38%) and a weak but significant reduction of the *psbA* transcript (15%) was evidenced in the case of *nox* samples with respect to the wild type (Figure 8D), while the *psaC* transcript level was similar in the two genotypes. These results suggest that the translation initiation of PSI core subunits in *nox* plants is downregulated in response to xanthophyll depletion.

DISCUSSION

In this work, we analyzed the modifications of the photosynthetic apparatus in the *Arabidopsis* carotenoid biosynthetic mutant *chy1 chy2 lut1 lut5* (*nox*) that accumulates α- and β-carotene only. Knockout of the four hydroxylase genes completely abolished xanthophyll biosynthesis, thus confirming that CHY1, CHY2, LUT1, and LUT5 constitute the full complement of carotenoid hydroxylases in *Arabidopsis* (Kim et al., 2009). The biogenesis of the photosynthetic apparatus was strongly affected in *nox* plants, and this resulted in reduced photosynthetic electron transport and increased photosensitivity. This was mainly due to depletion in Lhcb proteins and of the PSI complex in mutant plants, to such an extent that *nox* is unable to sustain photoautotrophic growth in low light and rapidly undergoes photoinhibition in moderate light. Thus, xanthophylls appear to be essential not only for photoprotection but also for biogenesis of the photosynthetic machinery.

Reduced Xanthophyll Content Negatively Affects Photoprotection

The photoprotective role of carotenoids in photosynthesis has been widely investigated (Havaux and Niyogi, 1999; Davison et al., 2002; Baroli et al., 2003; Dall'Osto et al., 2007b). Photoprotection is performed both by carotenes (Wang et al., 2004; Telfer, 2005) and xanthophylls (Formaggio et al., 2001). A complete lack of xanthophylls in *nox* plants results in a strongly enhanced photosensitivity with respect to wild-type plants, as evidenced by the higher release of $^1O_2$ in high light (Figure 2A) and faster photoinhibition (Figure 4) in mutant leaves. A major feature of this mutant is the depletion in LHC proteins (Figure 3), consistent with the evidence that xanthophylls are needed for folding of LHC in vitro (Paulsen 1997). However, immunotitration of pigment-protein complexes in *nox* shows that a reduced level of Lhca proteins is maintained in the mutant, as also supported by the red-shifted fluorescence emission spectra at 77K, typical of LHCI complexes (see Supplemental Figure 5 online), while Lhcb proteins are virtually absent. This effect is likely due to the inability of carotenes to replace xanthophylls in stabilizing Lhcb (Plumley and Schmidt, 1987). Instead, Lhca can bind carotenes and form functional complexes (Morosinotto et al., 2002; Mozzo et al., 2006).

The photosensitive phenotype of *nox* plants implies that functional LHC complexes are essential for photoprotection, consistent with previous reports (Havaux et al., 2007; Dall'Osto et al., 2010). Indeed, while $^1O_2$ production from purified PSII core complexes is independent from the xanthophyll content, LHC from wild-type thylakoids produce far less $^1O_2$ with respect to that from xanthophyll-depleted mutants (Dall'Osto et al., 2007b), implying that LHC proteins folded in the presence of sufficient xanthophyll levels act in preventing production and/or in scavenging $^1O_2$ (Dall'Osto et al., 2010). One might wonder if the lack of antenna proteins alone could explain the impaired photoautotrophic growth in *nox* plants. An extreme reduction in LHC proteins is also obtained with the *ch1* mutation (Espineda et al., 1999), in which assembly of LHC is prevented. The *ch1* mutant can still grow on soil and is not photoinhibited in moderate light (Havaux et al., 2007); thus, despite a reduction in antenna size comparable to that of *nox*, *ch1* can perform photoautotrophic growth. We conclude that reduced LHC content cannot be the only reason for the extreme light sensitivity of *nox*.

The capacity for excess energy dissipation into heat (qE mechanism) is strongly reduced in the mutant (Figure 2D). Since the level of PsbS (Li et al., 2002) is not reduced in *nox* plants

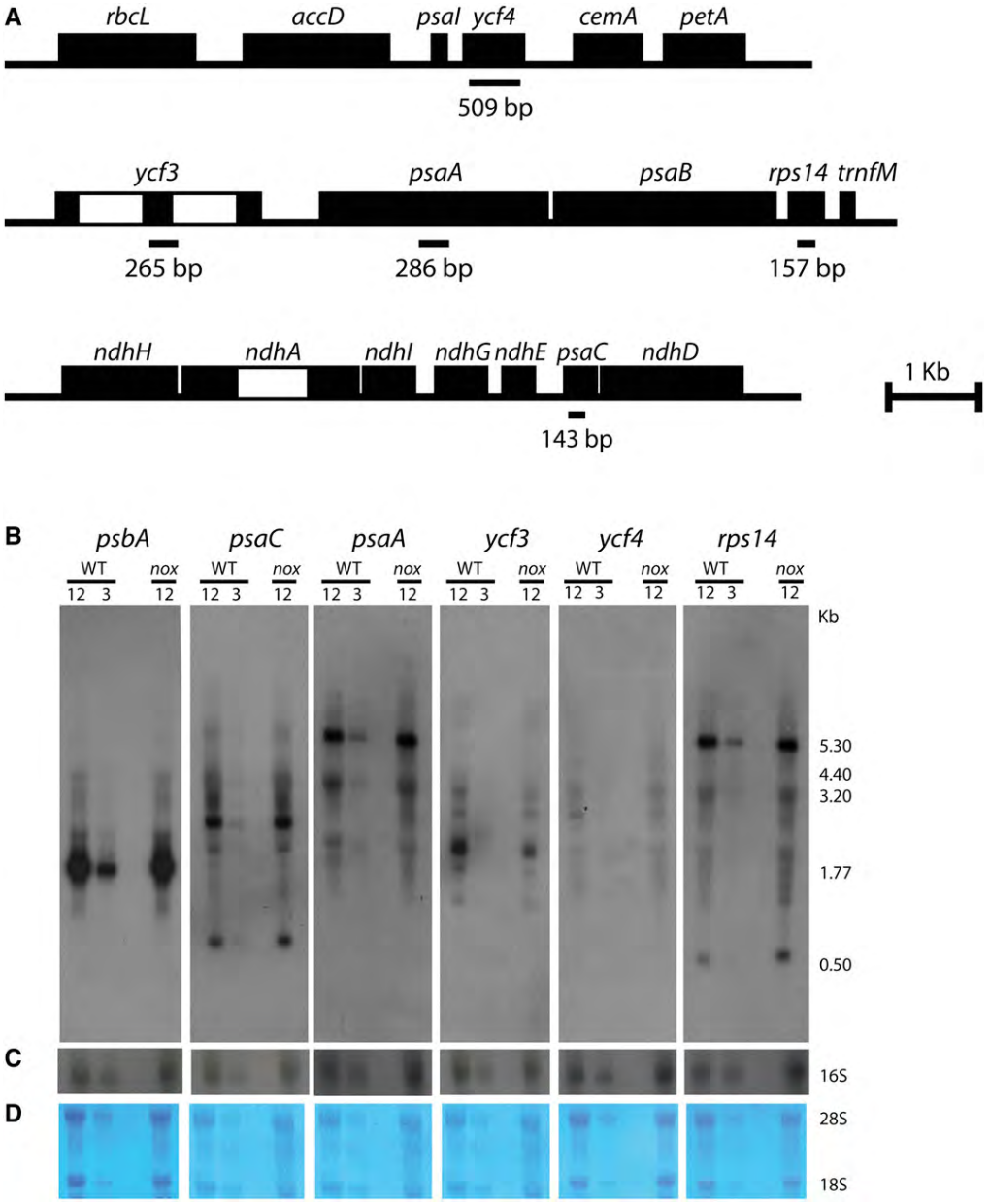

Figure 6. RNA Gel Blot Analysis of Plastid-Encoded Transcripts in the Wild Type and *nox*.

(A) Genetic maps of the plastid operons and gene clusters analyzed. Introns of *ycf3* and *ndhA* are shown as open boxes. The locations of probes used for RNA hybridization are marked below the genetic map together with their length in base pairs. Probes were cloned using primers described in Methods.

(B) RNA gel blot analysis of plastid-encoded genes of PSII (*psbA*), PSI (*psaC* and *psaA*), molecular chaperone-like factors involved in PSI assembly (*ycf3* and *ycf4*), and of the ribosomal protein S14 (*rps14*) in the *psaA*/*psaB*/*rps14* tricistronic transcript. Total RNA from the wild type (WT) and *nox* was electrophoresed under denaturing conditions, transferred to nylon membrane, and hybridized with the ^{32}P-labeled probes described in **(A)**, resulting in patterns similar to what was already reported in the literature (Lezhneva et al., 2004a; Meurer et al., 1998).

(C) Control hybridization with a probe for the plastid-encoded 16S rRNA.

(D) Staining with 0.1% toluidine blue of the cytoplasmic 28S and 18S rRNA on nylon membranes as a control of complete and homogenous transfer. For quantification, a dilution of wild-type RNA (corresponding to 12 and 3 μg of leaf RNA) were loaded and compared with transcripts in *nox* (12 μg RNA loaded per lane). The numbers indicate the size of the detected RNA species (in kilobases).

[See online article for color version of this figure.]

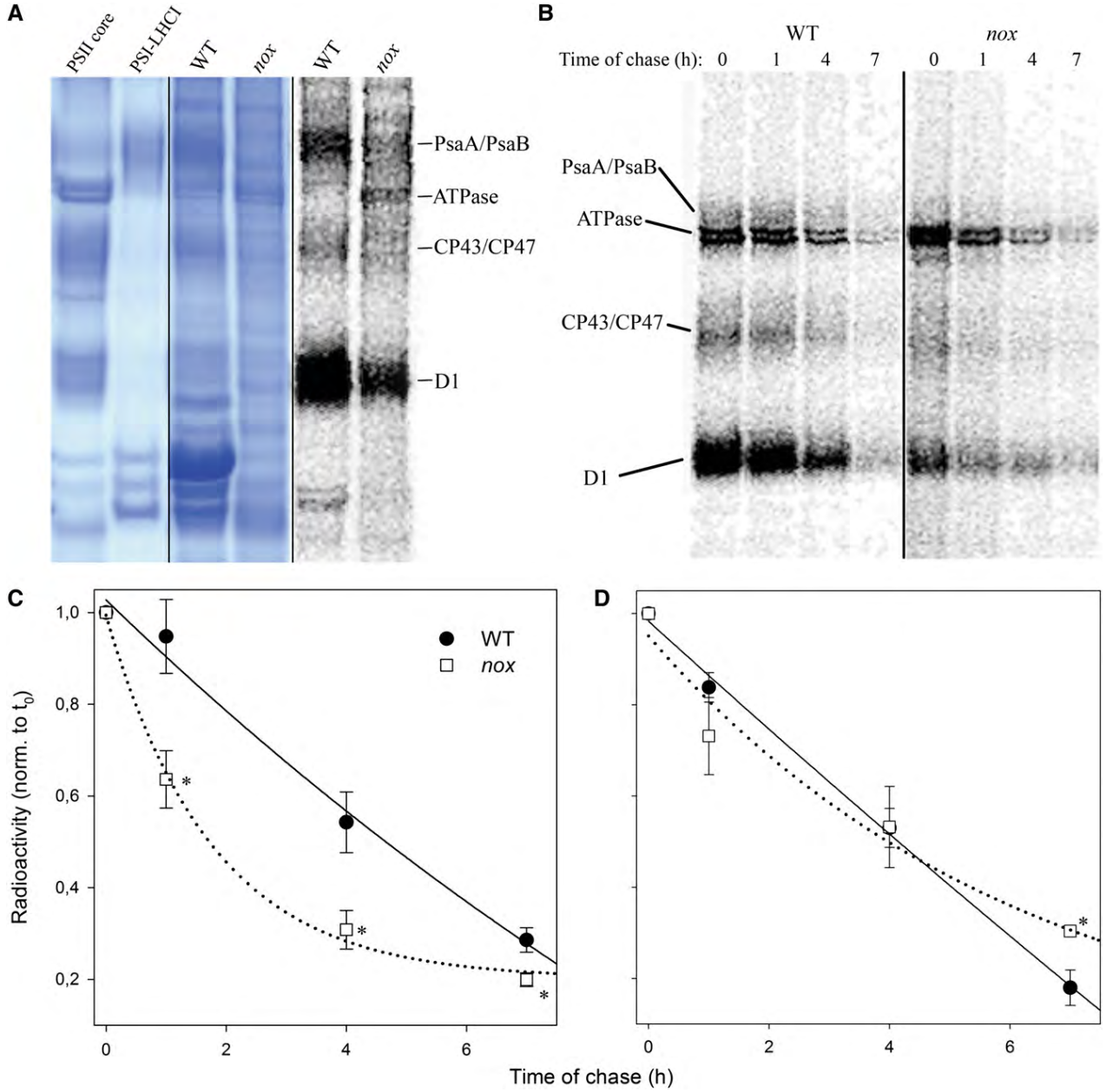

Figure 7. In Vivo Protein Synthesis and Turnover of Chloroplast-Encoded Membrane Proteins from Wild-Type and *nox* Plants.

(A) Pulse labeling of thylakoid proteins. After pulse labeling of *Arabidopsis* leaves with [^{35}S]Met in the presence of cycloheximide under low-light intensity (20 μmol photons m^{-2} s^{-1}, room temperature), thylakoid membranes were isolated and proteins were separated by SDS-PAGE. The resolved proteins were visualized by autoradiography (left panel); image of Coomassie blue–stained gel is reported (central panel); unlabeled PSI core and PSI-LHCI complexes were separated on an SDS-PAGE gel as reference (right panel). WT, the wild type.

(B) Pulse and chase labeling of thylakoid proteins. A [^{35}S]Met pulse labeling as in **(A)** (lane 0) was followed by chase in unlabeled medium for 1, 4, and 7 h under low light (20 μmol photons m^{-2} s^{-1}, room temperature).

(C) and **(D)** Time course of PsaA/PsaB **(C)** and D1/D2 **(D)** turnover. Data are expressed as means ± SD ($n > 3$). Values significantly different (Student's *t* test, $P < 0.05$) from the wild type are marked with an asterisk. norm., normalized.

[See online article for color version of this figure.]

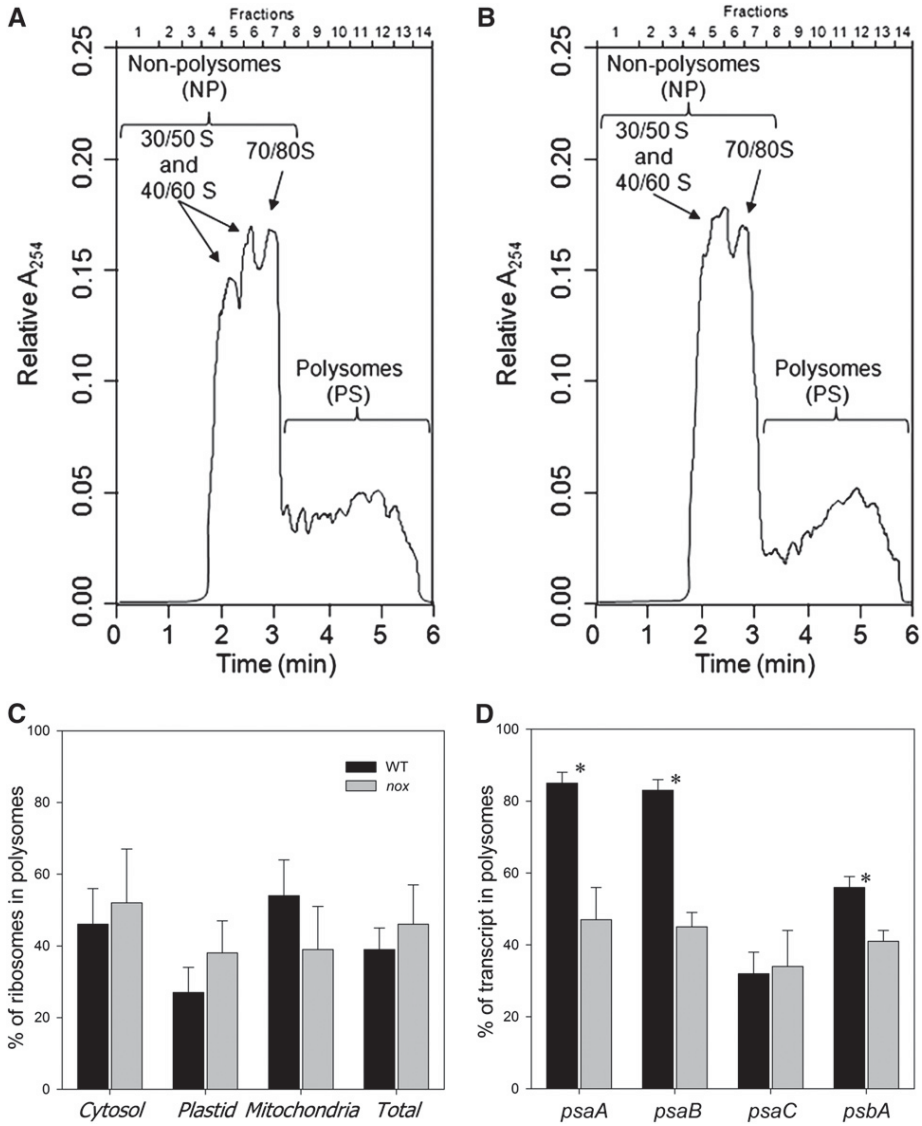

Figure 8. Polysome Loading Analysis of Wild-Type and *nox* Mutant Plants.

(A) and **(B)** Representative examples of the distribution of ribosomes in a Suc gradient for the wild type **(A)** and *nox* **(B)**. RNA was measured as absorbance at 254 nm (A_{254}). Ribosome subunits, free ribosomes, and monosomes are on the left and increasingly large polysomes toward the right of the display.

(C) Estimated proportion of ribosomes on polysomes for the wild type (WT; black bars) and *nox* (gray bars). The ribosome number in each fraction was calculated by determining the amount of the small subunit rRNA transcript for cytosolic, plastid, and mitochondrial ribosomes.

(D) Ribosome occupancy for the *psaA*, *psaB*, *psaC*, and *psbA* transcripts for the wild type (black bars) and *nox* (gray bars). The percentage of each transcript in the polysomes fractions was calculated using the absolute concentration of the transcript in the NP and PS fractions as (PS/[NP+PS]) and are given as numbers in the figures. The concentration of the transcripts was measured by qRT-PCR using random primers for cDNA production and specific PCR primers for the transcripts (see Methods for details). The results are given as mean ± SD (n = 4). Values significantly different (Student's t test, $P < 0.05$) from the wild type are marked with an asterisk.

relative to the wild type (Figure 3), qE depletion can thus be attributed to a lack of PsbS interacting partners, namely, the Lhcb proteins (Ahn et al., 2008; Avenson et al., 2008; Betterle et al., 2009). All together, these results support the correlation between xanthophyll content and qE amplitude, previously suggested on the basis of antisense inhibition of β-hydroxylation (Pogson and Rissler, 2000). As for the role in photoprotection, the *npq4* mutation abolished qE in *Arabidopsis* (Li et al., 2000) but has a modest impact on the photosensitivity in vivo (Li et al., 2002), just a fraction of the effect observed upon decreasing the level of xanthophylls (Niyogi et al., 2001; Dall'Osto et al., 2007b). We thus conclude that the differential resistance of wild-type versus

nox plants cannot be attributed to qE depletion. Rather, the decreased efficiency of photosynthetic electron transport, higher photoinhibition, and lethality in soil of the *nox* plants are to be ascribed to a severe deficiency in PSI.

nox Plants Fail to Accumulate Normal Levels of PSI Core Complexes

The immunotitration of pigment-protein complexes in mutant thylakoids showed that PSII core subunits and cytochrome b_6f accumulated in *nox*, while PsaA/B subunits were almost absent (Figure 3). The decrease in the xanthophyll/carotenoid ratio was shown to cause a proportional decrease in the abundance of PSI core units with respect to PSII (Fiore et al., 2012). Here, we show that *nox* leaves fail to accumulate PSI complexes, thus confirming that xanthophylls are needed for PSI biogenesis. This result is surprising, since (1) there is no evident reason for the preferential effect of xanthophyll depletion on PSI versus PSII core complexes, and (2) PSI core complexes bind chlorophyll *a* and carotene as the only pigments (Nelson and Ben Shem, 2004), which are not limited in *nox* thylakoids (Figure 1B).

Therefore, how does xanthophyll depletion contribute to the lower accumulation of PSI in *nox* plants with respect to the wild type?

One possibility is that the assembly/stability of the PSI core might be limited by the amount of LHCI available, which has a photoprotective role on PSI (Alboresi et al., 2009) and modulates plant fitness (Ganeteg et al., 2004). Since xanthophyll depletion in *nox* plants limits the total amount of LHC, this might enhance photooxidative stress, consistent with the increased PSI core degradation in *nox* mutant (Figure 7). Nevertheless, several *Arabidopsis* mutants strongly depleted in LHCI have been described (Klimmek et al., 2005; Havaux et al., 2007), and all of them maintain a functional PSI core complex.

Alternatively, the steady state level of PSI and PSII core complexes could be limited by chlorophyll availability; indeed, a coregulation of chlorophyll and carotenoid biosynthesis has been reported (Härtel et al., 1997). Nevertheless, the lower content of chlorophylls in carotenoid biosynthesis mutants is mainly due to destabilization of LHC (Paulsen, 1997), while chlorophyll biosynthesis mutants showed that the PSI level is less affected than in *nox* (Tottey et al., 2003). Therefore, we conclude that the *nox* phenotype is unlikely to be due to limitation in chlorophyll supply, and the contribution of xanthophylls to the modulation of PSI level might be substantially different from the indirect control of the chlorophyll biosynthetic rate.

Comparison between *nox* and Other Mutants Affected in the Biogenesis of PSI

The phenotype of *nox* leads to the conclusion that xanthophyll depletion might have further targets that interfere with thylakoid development, since additional features than that expected from xanthophyll depletion became evident, namely, (1) the *albino* phenotype of *nox* and the inability to grow photoautotrophically (Figure 1); (2) the poor development of the thylakoid membrane system; (3) the small size of the chloroplasts (Figure 2); and (4) the depletion in PSI core complex (Figure 3). The above phenotypic traits are consistent with a primary lesion leading to PSI depletion. In fact, similar symptoms are found in PSI-deficient mutants (Lezhneva and Meurer, 2004; Stöckel et al., 2006; Schöttler et al., 2011).

The PSI supercomplex has a chimeric nature: Some of its subunits are encoded by the nuclear genome and others by the chloroplast genome. The initial event in PSI assembly involves subunits encoded by the plastome: The formation of the heterodimer PsaA/PsaB is followed by association of PsaC, which is needed for further binding of PsaD and PsaE (Antonkine et al., 2003) and then a number of smaller subunits are added. While PSI in plants can accumulate in the absence of most small subunits, it is well known that mutants devoid of the PsaA/B dimer are unable to assemble a functional PSI core complex, although some peripheral subunits or detached Lhca can accumulate in the thylakoids (Redding et al., 1999; Lezhneva and Meurer, 2004).

Some of the available PsaA/B mutants are either defective in the transcription of the *psaA-psaB-rps14* operon (Hein et al., 2009) or in its stability (Lezhneva and Meurer, 2004); others are impaired in the translation of the dimeric complex or cannot accumulate a stable heterodimer (Stöckel et al., 2006; Albus et al., 2010) or are affected in intron splicing of chloroplast mRNAs, including those encoding molecular chaperone-like complexes, such as Ycf3 (Landau et al., 2009; Ye et al., 2012); others are defective in the stable assembly of several [4Fe-4S] cluster–containing complexes of chloroplasts, including the PsaA/B dimer (Schwenkert et al., 2010).

Several lines of evidence suggest that the accumulation of the chloroplast-encoded PSI subunits is mainly controlled at the level of translation (Lezhneva and Meurer, 2004; Schöttler et al., 2011). Indeed, only severe reductions in the amount of the *psaA/B* transcript lead to reduced PSI accumulation. Even in *nox* plants, the lower accumulation of PsaA/B subunits appears to be related to posttranscriptional regulatory events, since the *psaA* and *psaB* messenger levels are not affected with respect to the wild type (Figure 5).

Moreover, maturation of plastid mRNAs was shown to have a regulatory role in plastid gene expression (Stern et al., 2010), as suggested by mutations such as *pac-2*, that affect the maturation pattern of *psaA/B* messenger and lead to strong depletion of PSI (Meurer et al., 1998). However, the polycistronic transcripts analyzed (Figure 6) showed no major changes in abundance and distribution pattern in the wild type versus *nox*, thus ruling out the hypothesis of an effect of xanthophyll depletion on the maturation efficiency of these sequences.

Rather, a reduction in PsaA/B synthesis (Figure 8) and its accelerated degradation (Figure 7) both appear to be the major reasons for the absence of the PSI core complex in *nox*.

At present, the functional basis for the relation between impaired translation of PsaA/B and the lack of xanthophylls is unclear. Among mutants affected in PsaA/B synthesis, *nox* has common features with the maize (*Zea mays*) mutant *cps2*, which shows an impaired association of the *psaA/B* transcripts into functional polysomes (Barkan, 1993; Amann et al., 2004) or to *Arabidopsis atab2*, in which *psaA/B* transcripts are poorly associated with polysomes (Barneche et al., 2006). Expression of the translation initiation factor ATAB2 is upregulated in the mutant (Figure 5), thus ruling out its involvement in the *nox* phenotype. Thus, it seems

reasonable to speculate that xanthophylls might be needed for the initiation/elongation phases of *psaA* and *psaB* translation or targeting of the nascent chains to the thylakoid membranes.

However, even assuming that PSI accumulation is mainly regulated by the translation of the two subunits PsaA/B, a 50% reduction in the *psaA/B* ribosome occupancy in *nox* chloroplasts relative to the wild type is unlikely to account for a 95% reduction in PSI accumulation. Rather, the faster degradation rate of radiolabeled PsaA/PsaB (Figure 7) suggests a further block at the level of PSI assembly: In fact, if newly synthesize polypeptides are not assembled into a functional complexes, they are rapidly degraded, even though their synthesis proceeds at normal levels (Barkan et al., 1995).

Moreover, PSI is one of the most elaborate macromolecular complexes of the chloroplast, having 17 protein subunits and nearly 200 cofactors (Amunts et al., 2010) that need to be assembled in a concerted manner. Although a number of auxiliary factors involved in these tasks have been described, a complete understanding on how the molecular machinery works is still lacking. The transcription of genes encoding auxiliary proteins for PSI assembly described to date (Schöttler et al., 2011) was found to occur at similar levels in wild-type and *nox* plants or to be upregulated in the mutant (Figure 5). Otherwise, xanthophyll depletion in *nox* could impair the capacity for the biogenesis or assembly of [4Fe-4S] clusters (Amann et al., 2004; Lezhneva et al., 2004), possibly as a side effect of the enhanced release of ROS in *nox* chloroplasts. However, the mutant accumulates normal amounts of other [2Fe-2S] and [4Fe-4S] cluster–containing proteins, such as ferredoxin and the NDH complex (see Supplemental Figure 6 online). Finally, ribosomal loading of *psaC* is similar in wild-type and *nox* chloroplasts (Figure 7), despite the fact that the PsaC protein contains two [4Fe-4S] clusters (Amunts et al., 2010).

At the moment, we can only speculate as to which specific steps of PSI biogenesis are supported by xanthophylls. One possibility is that xanthophylls have a role in mediating (transitory) molecular interactions between photosystem subunits or with their putative chaperones (e.g., Ycf3, Ycf4, and Y3IP1). Alternatively, early events of cotranslational insertion in the thylakoid membrane of the PsaA subunit might require that a complex forms with xanthophylls, which is missing in *nox*.

Evidence for carotenoid-derived, mobile signaling molecules that regulate several aspects of plant physiology has emerged in recent years: Abscisic acid, strigolactone, and β-cyclocitral (Gomez-Roldan et al., 2008; Ramel et al., 2012) are examples of water-soluble carotenoids catabolites that have been previously found to regulate nuclear gene expression, apical dominance, and branching. Whether or not these signals affect the expression of the molecular mechanism underlying PSI assembly is currently unknown. Application of analytical approaches for the identification of protein interaction partners present in wild-type *psaA-psaB-rps14* polysomes and absent in *nox* will be crucial to identify xanthophyll-dependent assembly subunits involved in PSI biogenesis.

METHODS

Plant Materials and Growth Conditions

Wild-type plants of *Arabidopsis thaliana* ecotype Columbia and mutants *lut1*, *lut5*, *chy1*, and *chy2* were obtained from NASC (The European Arabidopsis Stock Centre). The T-DNA knockout lines used are *lut1* (Salk 129724), *lut5* (Salk 116660), *chy1* (SAIL 49A07), and *chy2* (SAIL 1242B12). The *chy1 chy2 lut1 lut5* quadruple mutant (*nox*) was isolated by crossing single mutant plants. Surface-sterilized seeds were sown on Petri dishes containing 0.3% (w/v) solidified plant-agar supplemented with 0.5% Murashige and Skoog nutrients and 2% (w/v) Suc. Seedlings were grown for 3 weeks with a 16-h photoperiod at a photon flux density of ~20 μmol photons m^{-2} s^{-1}, at 22°C. Since *nox* seedlings were unable to produce a mature inflorescence, the mutation was maintained in the heterozygous state.

Thylakoid Isolation and Sample Preparation

Unstacked thylakoid membranes were isolated as previously described (Bassi et al., 1988). Membranes from wild-type and *lut5* plants, corresponding to 400 μg of chlorophyll, were solubilized with 0.7% β-dodecylmaltoside and then fractionated by ultracentrifugation in a 0.1 to 1 M Suc gradient (Caffarri et al., 2009).

Pigment Analyses

Pigments were extracted from leaves with 80% acetone and then separated and quantified by HPLC (Gilmore and Yamamoto, 1991).

Gel Electrophoresis and Immunoblotting

SDS-PAGE analysis was performed with the Tris-Tricine buffer system (Schägger and von Jagow, 1987). For immunotitration, thylakoid samples corresponding to 0.1, 0.2, and 0.4 μg of chlorophylls were loaded for each sample and electroblotted on nitrocellulose membranes. Filters were incubated with specific antibodies and were detected with alkaline phosphatase–conjugated antibody. To avoid any deviation between different immunoblots, samples were compared only when loaded in the same gel. Nondenaturing Deriphat-PAGE was performed following the method described previously (Peter et al., 1991) with modifications reported by Havaux et al. (2004). Thylakoids concentrated at 1 mg/mL chlorophylls were solubilized with 0.8% α-DM, and 10 or 25 μg of chlorophylls was loaded in each lane.

Analysis of Chlorophyll Fluorescence and P700 Redox State

NPQ of chlorophyll fluorescence, PQ redox state (qL), and PSII yield (Φ_{PSII}) were measured at room temperature (22°C) with a PAM 101 fluorometer (Walz) according to the equation defined by Van Kooten and Snel (1990). Calculation of the ΔpH-dependent component of chlorophyll fluorescence quenching (qE) was performed as described previously (Walters and Horton, 1995). Fluorescence kinetics were measured with a home-built setup, in which leaves were vacuum infiltrated with 10^{-5} M DCMU 3.0 and excited with green light at 520 nm (Luxeon, Lumileds), and the emission was measured in the near far red (Rappaport et al., 2007). The $t_{2/3}$ of the fluorescence rise was taken as a measure of the functional antenna size of PSII (Malkin et al., 1981). The reoxidation kinetics of Q_A were measured as the decay of chlorophyll *a* fluorescence with the PAM fluorometer. Saturating single-turnover flashes obtained from a single-turnover flash unit (Heinz Walz XE-ST) were used to convert all Q_A to Q_A^-; the variable fluorescence decay, reflecting the reoxidation of Q_A^-, was detected at a 20-μs resolution. Data from 12 recordings were averaged. Changes in the redox state of P700 were measured on leaves vacuum infiltrated with methyl viologen (2 mM), by monitoring absorbance at 705 nm with a JTS-100 (BioLogic Instruments); the maximum content of photooxidizable P700 (ΔA_{max}) was determined on methyl viologen–treated leaves using a saturating flash (3000 μmol photons m^{-2} s^{-1}) under a 520 μmol m^{-2} s^{-1} far-red light background (Munekage et al., 2002).

Electron Microscopy

Intact leaf fragments from wild-type and *nox* mutant leaves were fixed, embedded, and observed in thin section as previously described (Sbarbati et al., 2004).

Spectroscopy

Steady state spectra were obtained using samples in 10 mM HEPES, pH 7.5, 0.06% α(β)-DM, and 0.2 M Suc. Absorption measurements were performed using a SLM-Aminco DW-2000 spectrophotometer. Fluorescence emission spectra were measured using a Jobin-Yvon Fluoromax-3 spectrofluorometer.

Measurements of ROS Production

ROS production in leaves was measured with SOSG, a fluorescent probe highly selective for $^1O_2$ (Flors et al., 2006). Analysis of $^1O_2$ release in leaves or purified complexes was performed as previously described (Dall'Osto et al., 2010).

Photobleaching Assay

The photobleaching kinetics of pigment-protein complexes was measured as described (Croce et al., 1999). Samples were cooled at 10°C. Initial and maximal absorbance was set in order to have the same absorbance area (corresponding to ~5 μg chlorophylls/mL) in the wavelength range of the actinic light ($600 < \lambda < 750$ nm).

Determination of the Sensitivity to Photooxidative Stress

High light treatment was performed for 2.5 h at 200 μmol photons m^{-2} s^{-1}, room temperature, on detached leaves floating on water. Light was provided by 150-W halogen lamps (Focus3; Prisma). Decay kinetics of F_v/F_m (Havaux et al., 2004) and maximum content of photooxidizable P700 (ΔA_{max} at 705 nm) (Sonoike, 2011) were recorded during illumination to assess the photoinhibition of PSII and PSI, respectively.

qRT-PCR

qRT-PCR was performed using 0.5 μg total RNA from each sample. The RNA was reverse transcribed using random primers with MoMLV reverse transcription reagents (Promega protocol). The cDNA was quantified using a Qbit fluorometer (Invitrogen), diluted, and used for quantitative PCR amplifications with specific primers. Each qRT-PCR was performed with SYBR Green fluorescence detection in a quantitative PCR thermal cycler (ABI Prism 7300; Applied Biosystems). Each reaction was prepared using 5 μL from a 0.2 ng/μL dilution of cDNA derived from the reverse transcription, 10 μL of SYBR Green PCR Master Mix (Applied Biosystems), and 0.5 μM forward and reverse primers in a total volume of 25 μL. The cycling conditions were as follows: 10 min at 95°C, followed by 40 cycles of 95°C for 15 s and 60°C for 1 min. Melting curve analysis was performed to identify nonspecific PCR products and primer dimers. Transcript levels of genes coding for PsaD, E, and F were determined with the following primers: PSAD-f, 5′-AACAGGAGGAGCTGCGATAA-3′; PSAD-r, 5′-CTCCATCTTTCGGGTGAAGA-3′; PSAE-f, 5′-CCGCTAAGGCTAAACCTCCT-3′, PSAE-r, 5′-ATTCGCGTAATTCACCTTGG-3′; PSAF-f, 5′-GACGGTTTACCGCACTTGAT-3′; and PSAF-r, 5′-CGGAAGATGATCCGACTAGC-3′. Transcript levels of genes coding for either PSI and PSII structural subunits, or subunits involved in PSI assembly, were determined using specific primers reported previously (Amann et al., 2004; Lezhneva and Meurer, 2004; Barneche et al., 2006; Stöckel et al., 2006; Albus et al., 2010).

In Vivo Protein Synthesis of Chloroplast-Encoded Membrane Proteins

In vivo labeling of leaf proteins was performed as previously described (Sun et al., 2010). Leaves from 3-week-old plants were preincubated in 20 μg/mL cycloheximide for 30 min and radiolabeled with 100 μCi/mL [^{35}S] Met in 20 μg/mL cycloheximide, at a light intensity of 20 μmol photons m^{-2} s^{-1} for 30 min at room temperature, followed by a chase with cold Met. Thylakoid membranes were isolated and the proteins were separated by SDS-PAGE, and then the gels were stained and dried and the radioactivity was quantified using ImageMaster (Pharmacia Biotech).

RNA Gel Blot Analysis

Total RNAs were isolated using the RNeasy mini kit (Qiagen). RNAs were quantified and their quality was assessed using a 2100 Bioanalyzer (Agilent). Approximately 12 μg of RNAs from the wild type and *nox* (a dilution of 3 μg for the wild type was also loaded) were fractionated on 1% agarose-formaldehyde denaturing gels. The gels were blotted on positively charged Hybond N^+ membranes (GE Healthcare) in 10× SSC (1× SSC is 0.15 M NaCl and 0.015 M sodium citrate). Total RNAs were immobilized on membranes by UV cross-linking and then stained with 0.1% toluidine blue. The DNA probes were labeled with [^{32}P]CTP by random priming using Ready to Go DNA labeling beads (-dCTP) (GE Healthcare). Unincorporated nucleotides were removed with an Illustra AutoSeq G-50 Dye Terminator Removal Kit (GE Healthcare). The membranes were hybridized overnight at 42°C in ULTRAhyb buffer (Ambion) in the presence of 10^6 cpm/mL of labeled probe. After hybridizations, unhybridized probes were removed by washing the membranes in 2× SSC containing 0.1% SDS at 42°C. Autoradiography was then performed using Kodak XAR-5 films. DNA probes were stripped by incubating the membranes in boiling 0.1% aqueous SDS solution. All the filters were reprobed with the 16S rRNA probe. The DNA sequences corresponding to the probes adopted for the hybridizations were cloned in pGEM-T Easy (Promega) and sequenced. The probes were obtained by PCR amplification with the following primers: ycf3-F, 5′-ATGTCGGCTCAATCTGAAGG-3′, and ycf3-R, 5′-CTCCTTGTTGAATGGCCTGT-3′ for the *ycf3* probe; and ycf4-F, 5′-TAACGGGGTCTCGAAAAACA-3′, and ycf4-R, 5′-TTCAATTGGTACACGCAAGAA-3′, for *ycf4*. The probes for *psaA*, *psaC*, *psbA*, and *rps14* were all cloned as previously described (Lezhneva and Meurer, 2004).

Ribosome Loading Analysis

Polysomes were fractionated from crude leaf extracts as described (Piques et al., 2009) but using 100 to 150 mg fresh weight. The gradients were fractionated using a programmable density gradient fractionation system (Teledyne Isco) to continuously record absorbance at 254 nm. Polysome levels were determined from the area under the polysome profile after subtracting gradient baseline absorbance. The area of each polysome profile was normalized to an equal value to account for differences in sample loading. Levels of nonpolysomes (NPs; gradient region containing mRNP complexes, 40/60S and 30/50S ribosome subunits, and 70/80S monosomes) and polysomes (PSs; gradient region containing more than two ribosomes per mRNA) were determined by calculating the corresponding peak areas of gradient regions. Areas corresponding to the NP and PS fractions were reported as a percentage of the total area under the profile.

Purification of Polysomal RNA and Quantification of Transcript Levels by qRT-PCR

Fractions corresponding to NS (1 to 8) and PS (9 to 14) were combined, and the total RNA was purified from these fractions separately by ethanolic precipitation using the RNeasy plant mini kit (Qiagen) as described (Piques et al., 2009). For absolute quantification of the transcript levels in the NP and PS fractions, a mix of six artificial poly(A)$^+$ RNAs (ArrayControl RNA spikes; Applied Biosystems/Ambion) were spiked into the NP and PS fractions before RNA purification. The concentrations of the spike-in controls were adjusted to make a calibration curve with a dynamic range from $9.0E^{+11}$ to $6.0E^{+07}$ copy number per gram fresh

weight. RNA concentration and integrity were measured with a NanoDrop ND-1000 UV-Vis spectrophotometer (NanoDrop Technologies) and an Agilent-2100 bioanalyzer using RNA 6000 NanoChip (Agilent Technologies). The cDNA synthesis, using 200 ng of total RNA, quality control of the synthesized cDNA, the qRT-PCR reactions, and data analysis were performed as described (Piques et al., 2009). All standard curves, derived from the six spike-in controls, had R^2 values higher than 0.99 and were used to calculate the concentration of the transcripts as copy g^{-1} fresh weight. The primers for the *PsaA*, *PsaB*, *PsaC*, and *PsbA* were designed according to Lezhneva and Meurer (2004), and the list of the primers for the other genes used is in Supplemental Table 1 online.

Estimation of the Ribosome Content

The ribosome number within NP and PS fractions was calculated by determining the amounts of cytosolic, plastid, and mitochondrial rRNA small subunits by qRT-PCR on the basis that each of these rRNAs corresponds to one ribosome (Piques et al., 2009).

Accession Numbers

Sequence data from this article can be found in the GenBank/EMBL data libraries under accession numbers At4G25700 (*chy1*), At5G52570 (*chy2*), At3G53130 (*lut1*), and At1G31800 (*lut5*).

Supplemental Data

The following materials are available in the online version of this article.

Supplemental Figure 1. Biosynthetic Pathway of Carotenoids in *Arabidopsis thaliana*.

Supplemental Figure 2. Transmission Electron Micrographs of Plastids from Leaf Mesophyll Cells of the *Arabidopsis* Wild-Type and *nox* Mutant Plants.

Supplemental Figure 3. Photoprotection Capacity of α- versus β-Carotene Binding Complexes.

Supplemental Figure 4. Decay and Induction Kinetics of PSII Fluorescence.

Supplemental Figure 5. Low-Temperature Fluorescence Emission Spectra of Chloroplasts.

Supplemental Figure 6. Analysis of Polypeptide Composition of Wild-Type and *nox* Thylakoid Membranes.

Supplemental Figure 7. Biochemical Characterization of Single Knockout Mutants of *Arabidopsis*.

Supplemental Table 1. Quantification of Transcript Levels on Polysomal RNA by qRT-PCR.

ACKNOWLEDGMENTS

This work was supported by the Marie Curie Actions–Networks for Initial Training Harvest (Grant PITN-GA-2009-238017) and by Ministero delle Politiche Agricole, Alimentari e Forestali BioMassVal (Grant 2/01/140). We thank Paolo Bernardi and Andrea Sbarbati (University of Verona) for help in sample preparation for electron microscopy. We thank Anita Zamboni (University of Verona) for help on PCR analysis and Nicola Tamassia (University of Verona) for valuable advice regarding ImageMaster. Antibodies against HCF101, NdhH, and NdhK were kind gifts of Jörg Meurer (Ludwig-Maximilians-Universität, Munich, Germany) and Toshiharu Shiakani (Kyoto University, Kyoto, Japan). We thank Alejandra M. Landau (Instituto Nacional de Tecnologia Agropecuaria, Castelar, Argentina) and Ralph Bock (Max-Planck-Institut für Molekulare Pflanzenphysiologie, Potsdam-Golm, Germany) for providing antibodies against Ycf3 and Ycf4, respectively. We thank Mark Stitt for his support while conducting the polysome experimental work.

AUTHOR CONTRIBUTIONS

L.D. isolated single knockout *Arabidopsis* mutants, carried out the crossings, and performed a biochemical and physiological characterization of their photosynthetic apparatus. M.P. carried out ribosome loading analysis. S.C. was involved in the photooxidative treatments and stress measurements and in data analysis. M.R. and A.A. carried out qRT-PCR and the assay for protein synthesis of chloroplast-encoded membrane proteins. B.M. and A.A. performed RNA blot analysis. R.B. and L.D. conceived the study, participated in its design and coordination, and drafted the article.

Received December 16, 2012; revised January 15, 2013; accepted January 18, 2013; published February 8, 2013.

REFERENCES

Ahn, T.K., Avenson, T.J., Ballottari, M., Cheng, Y.C., Niyogi, K.K., Bassi, R., and Fleming, G.R. (2008). Architecture of a charge-transfer state regulating light harvesting in a plant antenna protein. Science **320:** 794–797.

Alboresi, A., Ballottari, M., Hienerwadel, R., Giacometti, G.M., and Morosinotto, T. (2009). Antenna complexes protect photosystem I from photoinhibition. BMC Plant Biol. **9:** 71.

Albus, C.A., Ruf, S., Schöttler, M.A., Lein, W., Kehr, J., and Bock, R. (2010). Y3IP1, a nucleus-encoded thylakoid protein, cooperates with the plastid-encoded Ycf3 protein in photosystem I assembly of tobacco and *Arabidopsis*. Plant Cell **22:** 2838–2855.

Amann, K., Lezhneva, L., Wanner, G., Herrmann, R.G., and Meurer, J. (2004). ACCUMULATION OF PHOTOSYSTEM ONE1, a member of a novel gene family, is required for accumulation of [4Fe-4S] cluster-containing chloroplast complexes and antenna proteins. Plant Cell **16:** 3084–3097.

Amunts, A., Toporik, H., Borovikova, A., and Nelson, N. (2010). Structure determination and improved model of plant photosystem I. J. Biol. Chem. **285:** 3478–3486.

Antonkine, M.L., Jordan, P., Fromme, P., Krauss, N., Golbeck, J.H., and Stehlik, D. (2003). Assembly of protein subunits within the stromal ridge of photosystem I. Structural changes between unbound and sequentially PS I-bound polypeptides and correlated changes of the magnetic properties of the terminal iron sulfur clusters. J. Mol. Biol. **327:** 671–697.

Avenson, T.J., Ahn, T.K., Zigmantas, D., Niyogi, K.K., Li, Z., Ballottari, M., Bassi, R., and Fleming, G.R. (2008). Zeaxanthin radical cation formation in minor light-harvesting complexes of higher plant antenna. J. Biol. Chem. **283:** 3550–3558.

Barkan, A. (1993). Nuclear mutants of maize with defects in chloroplast polysome assembly have altered chloroplast RNA metabolism. Plant Cell **5:** 389–402.

Barkan, A., Voelker, R., Mendel-Hartvig, J., Johnson, D., and Walker, M. (1995). Genetic analysis of chloroplast biogenesis in higher plants. Physiol. Plant. **93:** 163–170.

Barneche, F., Winter, V., Crèvecoeur, M., and Rochaix, J.D. (2006). ATAB2 is a novel factor in the signalling pathway of light-controlled synthesis of photosystem proteins. EMBO J. **25:** 5907–5918.

Baroli, I., Do, A.D., Yamane, T., and Niyogi, K.K. (2003). Zeaxanthin accumulation in the absence of a functional xanthophyll cycle protects *Chlamydomonas reinhardtii* from photooxidative stress. Plant Cell **15:** 992–1008.

Bassi, R., Pineau, B., Dainese, P., and Marquardt, J. (1993). Carotenoid-binding proteins of photosystem II. Eur. J. Biochem. **212:** 297–303.

Bassi, R., Rigoni, F., Barbato, R., and Giacometti, G.M. (1988). Light-harvesting chlorophyll a/b proteins (LHCII) populations in phosphorylated membranes. Biochim. Biophys. Acta **936:** 29–38.

Betterle, N., Ballottari, M., Zorzan, S., de Bianchi, S., Cazzaniga, S., Dall'osto, L., Morosinotto, T., and Bassi, R. (2009). Light-induced dissociation of an antenna hetero-oligomer is needed for non-photochemical quenching induction. J. Biol. Chem. **284:** 15255–15266.

Boudreau, E., Takahashi, Y., Lemieux, C., Turmel, M., and Rochaix, J.D. (1997). The chloroplast ycf3 and ycf4 open reading frames of *Chlamydomonas reinhardtii* are required for the accumulation of the photosystem I complex. EMBO J. **16:** 6095–6104.

Britton, G., Liaaen-Jensen, S., and Pfander, H. (2004). Carotenoids Hand Book. (Basel, Switzerland: Birkhauser Publishing).

Caffarri, S., Kouril, R., Kereïche, S., Boekema, E.J., and Croce, R. (2009). Functional architecture of higher plant photosystem II supercomplexes. EMBO J. **28:** 3052–3063.

Caffarri, S., Passarini, F., Bassi, R., and Croce, R. (2007). A specific binding site for neoxanthin in the monomeric antenna proteins CP26 and CP29 of photosystem II. FEBS Lett. **581:** 4704–4710.

Croce, R., Weiss, S., and Bassi, R. (1999). Carotenoid-binding sites of the major light-harvesting complex II of higher plants. J. Biol. Chem. **274:** 29613–29623.

Cuttriss, A.J., and Pogson, B.J. (2006). Carotenoids. In The Structure and Function of Plastids, R.R.Wise and J.K. Hoober, eds (Dordrecht, The Netherlands: Springer), pp. 315–334.

Dainese, P., Santini, C., Ghiretti-Magaldi, A., Marquardt, J., Tidu, V., Mauro, S., Bergantino, E., and Bassi, R. (1992). The organization of pigment-proteins within photosystem II. In Research in Photosynthesis, Vol. II, N. Murata, ed (Dordrecht, The Netherlands: Kluwer Academic Publishers), pp. 13–20.

Dall'Osto, L., Caffarri, S., and Bassi, R. (2005). A mechanism of nonphotochemical energy dissipation, independent from PsbS, revealed by a conformational change in the antenna protein CP26. Plant Cell **17:** 1217–1232.

Dall'Osto, L., Cazzaniga, S., Havaux, M., and Bassi, R. (2010). Enhanced photoprotection by protein-bound vs. free xanthophyll pools: A comparative analysis of chlorophyll b and xanthophyll biosynthesis mutants. Mol. Plant **3:** 576–593.

Dall'Osto, L., Cazzaniga, S., North, H., Marion-Poll, A., and Bassi, R. (2007a). The *Arabidopsis* aba4-1 mutant reveals a specific function for neoxanthin in protection against photooxidative stress. Plant Cell **19:** 1048–1064.

Dall'Osto, L., Fiore, A., Cazzaniga, S., Giuliano, G., and Bassi, R. (2007b). Different roles of α- and β-branch xanthophylls in photosystem assembly and photoprotection. J. Biol. Chem. **282:** 35056–35068.

Davison, P.A., Hunter, C.N., and Horton, P. (2002). Overexpression of beta-carotene hydroxylase enhances stress tolerance in *Arabidopsis*. Nature **418:** 203–206.

DellaPenna, D., and Pogson, B.J. (2006). Vitamin synthesis in plants: Tocopherols and carotenoids. Annu. Rev. Plant Biol. **57:** 711–738.

Demmig-Adams, B., and Adams, W.W. (1992a). Carotenoid composition in sun and shade leaves of plants with different life forms. Plant Cell Environ. **15:** 411–419.

Demmig-Adams, B., and Adams, W.W. (1992b). Photoprotection and other responses of plants to high light stress. Annu. Rev. Plant Physiol. Plant Mol. Biol. **43:** 599–626.

Espineda, C.E., Linford, A.S., Devine, D., and Brusslan, J.A. (1999). The AtCAO gene, encoding chlorophyll a oxygenase, is required for chlorophyll b synthesis in *Arabidopsis thaliana*. Proc. Natl. Acad. Sci. USA **96:** 10507–10511.

Fiore, A., Dallosto, L., Cazzaniga, S., Diretto, G., Giuliano, G., and Bassi, R. (2012). A quadruple mutant of *Arabidopsis* reveals a β-carotene hydroxylation activity for LUT1/CYP97C1 and a regulatory role of xanthophylls on determination of the PSI/PSII ratio. BMC Plant Biol. **12:** 50.

Fiore, A., Dall'osto, L., Fraser, P.D., Bassi, R., and Giuliano, G. (2006). Elucidation of the beta-carotene hydroxylation pathway in *Arabidopsis thaliana*. FEBS Lett. **580:** 4718–4722.

Flors, C., Fryer, M.J., Waring, J., Reeder, B., Bechtold, U., Mullineaux, P.M., Nonell, S., Wilson, M.T., and Baker, N.R. (2006). Imaging the production of singlet oxygen in vivo using a new fluorescent sensor, Singlet Oxygen Sensor Green. J. Exp. Bot. **57:** 1725–1734.

Formaggio, E., Cinque, G., and Bassi, R. (2001). Functional architecture of the major light-harvesting complex from higher plants. J. Mol. Biol. **314:** 1157–1166.

Ganeteg, U., Külheim, C., Andersson, J., and Jansson, S. (2004). Is each light-harvesting complex protein important for plant fitness? Plant Physiol. **134:** 502–509.

Gilmore, A.M., and Yamamoto, H.Y. (1991). Zeaxanthin formation and energy-dependent fluorescence quenching in pea chloroplasts under artificially mediated linear and cyclic electron transport. Plant Physiol. **96:** 635–643.

Gomez-Roldan, V., et al. (2008). Strigolactone inhibition of shoot branching. Nature **455:** 189–194.

Haldrup, A., Simpson, D.J., and Scheller, H.V. (2000). Down-regulation of the PSI-F subunit of photosystem I (PSI) in *Arabidopsis thaliana*. The PSI-F subunit is essential for photoautotrophic growth and contributes to antenna function. J. Biol. Chem. **275:** 31211–31218.

Härtel, H., Lokstein, H., Dörmann, P., Grimm, B., and Benning, C. (1997). Changes in the composition of the photosynthetic apparatus in the galactolipid-deficient dgd1 mutant of *Arabidopsis thaliana*. Plant Physiol. **115:** 1175–1184.

Havaux, M., Dall'osto, L., and Bassi, R. (2007). Zeaxanthin has enhanced antioxidant capacity with respect to all other xanthophylls in *Arabidopsis* leaves and functions independent of binding to PSII antennae. Plant Physiol. **145:** 1506–1520.

Havaux, M., Dall'Osto, L., Cuiné, S., Giuliano, G., and Bassi, R. (2004). The effect of zeaxanthin as the only xanthophyll on the structure and function of the photosynthetic apparatus in *Arabidopsis thaliana*. J. Biol. Chem. **279:** 13878–13888.

Havaux, M., and Niyogi, K.K. (1999). The violaxanthin cycle protects plants from photooxidative damage by more than one mechanism. Proc. Natl. Acad. Sci. USA **96:** 8762–8767.

Hein, P., Stöckel, J., Bennewitz, S., and Oelmüller, R. (2009). A protein related to prokaryotic UMP kinases is involved in psaA/B transcript accumulation in *Arabidopsis*. Plant Mol. Biol. **69:** 517–528.

Holt, N.E., Zigmantas, D., Valkunas, L., Li, X.P., Niyogi, K.K., and Fleming, G.R. (2005). Carotenoid cation formation and the regulation of photosynthetic light harvesting. Science **307:** 433–436.

Ihnatowicz, A., Pesaresi, P., Varotto, C., Richly, E., Schneider, A., Jahns, P., Salamini, F., and Leister, D. (2004). Mutants for photosystem I subunit D of *Arabidopsis thaliana*: Effects on photosynthesis, photosystem I stability and expression of nuclear genes for chloroplast functions. Plant J. **37:** 839–852.

Kim, J., and DellaPenna, D. (2006). Defining the primary route for lutein synthesis in plants: The role of *Arabidopsis* carotenoid

beta-ring hydroxylase CYP97A3. Proc. Natl. Acad. Sci. USA **103:** 3474–3479.

Kim, J., Smith, J.J., Tian, L., and Dellapenna, D. (2009). The evolution and function of carotenoid hydroxylases in *Arabidopsis*. Plant Cell Physiol. **50:** 463–479.

Klimmek, F., Ganeteg, U., Ihalainen, J.A., van Roon, H., Jensen, P.E., Scheller, H.V., Dekker, J.P., and Jansson, S. (2005). The structure of higher plant LHCl: In vivo characterisation and structural interdependence of the Lhca proteins. Biochemisty **44:** 3065–3073.

Koniger, M., Harris, G.C., Virgo, A., and Winter, K. (1995). Xanthophyll-cycle pigments and photosynthetic capacity in tropical forest species - A comparative field study on canopy, gap and understory plants. Oecologia **104:** 280–290.

Krech, K., Ruf, S., Masduki, F.F., Thiele, W., Bednarczyk, D., Albus, C.A., Tiller, N., Hasse, C., Schöttler, M.A., and Bock, R. (2012). The plastid genome-encoded Ycf4 protein functions as a non-essential assembly factor for photosystem I in higher plants. Plant Physiol. **159:** 579–591.

Krieger-Liszkay, A. (2005). Singlet oxygen production in photosynthesis. J. Exp. Bot. **56:** 337–346.

Kull, O., and Pfander, H. (1995). List of new carotenoids. In Carotenoids: Isolation and Analysis, S.L.-J.a.H.P.e.G. Britton, ed (Basel, Switzerland: Birkhauser Publishing), pp. 295–317.

Landau, A.M., Lokstein, H., Scheller, H.V., Lainez, V., Maldonado, S., and Prina, A.R. (2009). A cytoplasmically inherited barley mutant is defective in photosystem I assembly due to a temperature-sensitive defect in ycf3 splicing. Plant Physiol. **151:** 1802–1811.

Lezhneva, L., Amann, K., and Meurer, J. (2004). The universally conserved HCF101 protein is involved in assembly of [4Fe-4S]-cluster-containing complexes in *Arabidopsis thaliana* chloroplasts. Plant J. **37:** 174–185.

Lezhneva, L., and Meurer, J. (2004). The nuclear factor HCF145 affects chloroplast psaA-psaB-rps14 transcript abundance in *Arabidopsis thaliana*. Plant J. **38:** 740–753.

Li, X.P., Björkman, O., Shih, C., Grossman, A.R., Rosenquist, M., Jansson, S., and Niyogi, K.K. (2000). A pigment-binding protein essential for regulation of photosynthetic light harvesting. Nature **403:** 391–395.

Li, X.P., Muller-Moule, P., Gilmore, A.M., and Niyogi, K.K. (2002). PsbS-dependent enhancement of feedback de-excitation protects photosystem II from photoinhibition. Proc. Natl. Acad. Sci. USA **99:** 15222–15227.

Liu, Z., Yan, H., Wang, K., Kuang, T., Zhang, J., Gui, L., An, X., and Chang, W. (2004). Crystal structure of spinach major light-harvesting complex at 2.72 A resolution. Nature **428:** 287–292.

Malkin, S., Armond, P.A., Mooney, H.A., and Fork, D.C. (1981). Photosystem II photosynthetic unit sizes from fluorescence induction in leaves. Correlation to photosynthetic capacity. Plant Physiol. **67:** 570–579.

Mathews, M.B., Sonenberg, N., and Hershey, J.W.B. (2007). Origins and principles of translational control. In Translational Control in Biology and Medicine, M.B. Mathews, N. Sonenberg, and J.W.B. Hershey, eds (Cold Spring Harbor, NY: Cold Spring Harbor Laboratory Press), pp. 1–40.

Meurer, J., Grevelding, C., Westhoff, P., and Reiss, B. (1998). The PAC protein affects the maturation of specific chloroplast mRNAs in *Arabidopsis thaliana*. Mol. Gen. Genet. **258:** 342–351.

Morosinotto, T., Castelletti, S., Breton, J., Bassi, R., and Croce, R. (2002). Mutation analysis of Lhca1 antenna complex. Low energy absorption forms originate from pigment-pigment interactions. J. Biol. Chem. **277:** 36253–36261.

Mozzo, M., Morosinotto, T., Bassi, R., and Croce, R. (2006). Probing the structure of Lhca3 by mutation analysis. Biochim. Biophys. Acta **1757:** 1607–1613.

Munekage, Y., Hojo, M., Meurer, J., Endo, T., Tasaka, M., and Shikanai, T. (2002). PGR5 is involved in cyclic electron flow around photosystem I and is essential for photoprotection in *Arabidopsis*. Cell **110:** 361–371.

Nelson, N., and Ben Shem, A. (2004). The complex architecture of oxygenic photosynthesis. Nature **5:** 1–12.

Niyogi, K.K. (2000). Safety valves for photosynthesis. Curr. Opin. Plant Biol. **3:** 455–460.

Niyogi, K.K., Shih, C., Soon Chow, W., Pogson, B.J., Dellapenna, D., and Björkman, O. (2001). Photoprotection in a zeaxanthin- and lutein-deficient double mutant of *Arabidopsis*. Photosynth. Res. **67:** 139–145.

North, H.M., De Almeida, A., Boutin, J.P., Frey, A., To, A., Botran, L., Sotta, B., and Marion-Poll, A. (2007). The *Arabidopsis* ABA-deficient mutant aba4 demonstrates that the major route for stress-induced ABA accumulation is via neoxanthin isomers. Plant J. **50:** 810–824.

Pan, X., Li, M., Wan, T., Wang, L., Jia, C., Hou, Z., Zhao, X., Zhang, J., and Chang, W. (2011). Structural insights into energy regulation of light-harvesting complex CP29 from spinach. Nat. Struct. Mol. Biol. **18:** 309–315.

Paulsen, H. (1997). Pigment ligation to proteins of the photosynthetic apparatus in higher plants. Physiol. Plant. **100:** 760–768.

Peter, G.F., Takeuchi, T., and Thornber, J.P. (1991). Solubilization and two-dimensional electrophoretic procedures for studying the organization and composition of photosynthetic membrane polypeptides. Methods: A Companion to Methods in Enzymology **3:** 115–124.

Piques, M., Schulze, W.X., Höhne, M., Usadel, B., Gibon, Y., Rohwer, J., and Stitt, M. (2009). Ribosome and transcript copy numbers, polysome occupancy and enzyme dynamics in *Arabidopsis*. Mol. Syst. Biol. **5:** 314.

Plumley, F.G., and Schmidt, G.W. (1987). Reconstitution of chlorophyll a/b light-harvesting complexes: Xanthophyll-dependent assembly and energy transfer. Proc. Natl. Acad. Sci. USA **84:** 146–150.

Pogson, B.J., Niyogi, K.K., Björkman, O., and DellaPenna, D. (1998). Altered xanthophyll compositions adversely affect chlorophyll accumulation and nonphotochemical quenching in *Arabidopsis* mutants. Proc. Natl. Acad. Sci. USA **95:** 13324–13329.

Pogson, B.J., and Rissler, H.M. (2000). Genetic manipulation of carotenoid biosynthesis and photoprotection. Philos. Trans. R. Soc. Lond. B Biol. Sci. **355:** 1395–1403.

Ramel, F., Birtic, S., Ginies, C., Soubigou-Taconnat, L., Triantaphylidès, C., and Havaux, M. (2012). Carotenoid oxidation products are stress signals that mediate gene responses to singlet oxygen in plants. Proc. Natl. Acad. Sci. USA **109:** 5535–5540.

Rappaport, F., Béal, D., Joliot, A., and Joliot, P. (2007). On the advantages of using green light to study fluorescence yield changes in leaves. Biochim. Biophys. Acta **1767:** 56–65.

Redding, K., Cournac, L., Vassiliev, I.R., Golbeck, J.H., Peltier, G., and Rochaix, J.-D. (1999). Photosystem I is indispensable for photoautotrophic growth, CO2 fixation, and H2 photoproduction in *Chlamydomonas reinhardtii*. J. Biol. Chem. **274:** 10466–10473.

Sane, P.V., Ivanov, A.G., Hurry, V., Huner, N.P., and Oquist, G. (2003). Changes in the redox potential of primary and secondary electron-accepting quinones in photosystem II confer increased resistance to photoinhibition in low-temperature-acclimated *Arabidopsis*. Plant Physiol. **132:** 2144–2151.

Sbarbati, A., Merigo, F., Benati, D., Tizzano, M., Bernardi, P., and Osculati, F. (2004). Laryngeal chemosensory clusters. Chem. Senses **29:** 683–692.

Schägger, H., and von Jagow, G. (1987). Tricine-sodium dodecyl sulfate-polyacrylamide gel electrophoresis for the separation of

proteins in the range from 1 to 100 kDa. Anal. Biochem. **166:** 368–379.

Schöttler, M.A., Albus, C.A., and Bock, R. (2011). Photosystem I: Its biogenesis and function in higher plants. J. Plant Physiol. **168:** 1452–1461.

Schwenkert, S., Netz, D.J.A., Frazzon, J., Pierik, A.J., Bill, E., Gross, J., Lill, R., and Meurer, J. (2010). Chloroplast HCF101 is a scaffold protein for [4Fe-4S] cluster assembly. Biochem. J. **425:** 207–214.

Sonoike, K. (2011). Photoinhibition of photosystem I. Physiol. Plant. **142:** 56–64.

Stern, D.B., Goldschmidt-Clermont, M., and Hanson, M.R. (2010). Chloroplast RNA metabolism. Annu. Rev. Plant Biol. **61:** 125–155.

Stöckel, J., Bennewitz, S., Hein, P., and Oelmüller, R. (2006). The evolutionarily conserved tetratrico peptide repeat protein pale yellow green7 is required for photosystem I accumulation in *Arabidopsis* and copurifies with the complex. Plant Physiol. **141:** 870–878.

Sun, X.W., Ouyang, M., Guo, J.K., Ma, J.F., Lu, C.M., Adam, Z., and Zhang, L.X. (2010). The thylakoid protease Deg1 is involved in photosystem-II assembly in *Arabidopsis thaliana*. Plant J. **62:** 240–249.

Telfer, A. (2005). Too much light? How beta-carotene protects the photosystem II reaction centre. Photochem. Photobiol. Sci. **4:** 950–956.

Tian, L., Magallanes-Lundback, M., Musetti, V., and DellaPenna, D. (2003). Functional analysis of beta- and epsilon-ring carotenoid hydroxylases in *Arabidopsis*. Plant Cell **15:** 1320–1332.

Tian, L., Musetti, V., Kim, J., Magallanes-Lundback, M., and DellaPenna, D. (2004). The *Arabidopsis* LUT1 locus encodes a member of the cytochrome p450 family that is required for carotenoid epsilon-ring hydroxylation activity. Proc. Natl. Acad. Sci. USA **101:** 402–407.

Tottey, S., Block, M.A., Allen, M., Westergren, T., Albrieux, C., Scheller, H.V., Merchant, S., and Jensen, P.E. (2003). *Arabidopsis* CHL27, located in both envelope and thylakoid membranes, is required for the synthesis of protochlorophyllide. Proc. Natl. Acad. Sci. USA **100:** 16119–16124.

Van Kooten, O., and Snel, J.F.H. (1990). The use of chlorophyll fluorescence nomenclature in plant stress physiology. Photosynth. Res. **25:** 147–150.

Varotto, C., Pesaresi, P., Meurer, J., Oelmüller, R., Steiner-Lange, S., Salamini, F., and Leister, D. (2000). Disruption of the *Arabidopsis* photosystem I gene psaE1 affects photosynthesis and impairs growth. Plant J. **22:** 115–124.

Walters, R.G., and Horton, P. (1995). Acclimation of *Arabidopsis thaliana* to the light environment: Changes in photosynthetic function. Planta **197:** 306–312.

Wang, Y.L., Mao, L.S., and Hu, X.C. (2004). Insight into the structural role of carotenoids in the photosystem I: A quantum chemical analysis. Biophys. J. **86:** 3097–3111.

Watkins, K.P., Rojas, M., Friso, G., van Wijk, K.J., Meurer, J., and Barkan, A. (2011). APO1 promotes the splicing of chloroplast group II introns and harbors a plant-specific zinc-dependent RNA binding domain. Plant Cell **23:** 1082–1092.

Yabe, O.T., Morimoto, K., Kikuchi, S., Nishio, K., Terashima, I., and Nakai, M. (2004). The *Arabidopsis* chloroplastic NifU-like protein CnfU, which can act as an iron-sulfur cluster scaffold protein, is required for biogenesis of ferredoxin and photosystem I. Plant Cell **16:** 993–1007.

Yamamoto, H.Y., Nakayama, T.O., and Chichester, C.O. (1962). Studies on the light and dark interconversions of leaf xanthophylls. Arch. Biochem. Biophys. **97:** 168–173.

Ye, J.-W., Gong, Z.-Y., Chen, C.-G., Mi, H.-L., and Chen, G.-Y. (2012). A mutation of OSOTP 51 leads to impairment of photosystem I complex assembly and serious photo-damage in rice. J. Integr. Plant Biol. **54:** 87–98.

NOTE ADDED IN PROOF

The reader is cautioned that the *nox* mutant name used in this paper, short for "*no xanthophylls*", is being used for convenience to describe the *chy1 chy2 lut1 lut5* quadruple mutant, which has mutations in all four genes encoding carotenoid hydroxylases in *Arabidopsis* and is devoid of xanthophylls. It does not describe a new gene or protein name, and should not be confused with Arabidopsis NOX proteins, which are NADPH oxidases.

Supplemental Data

Figure S1

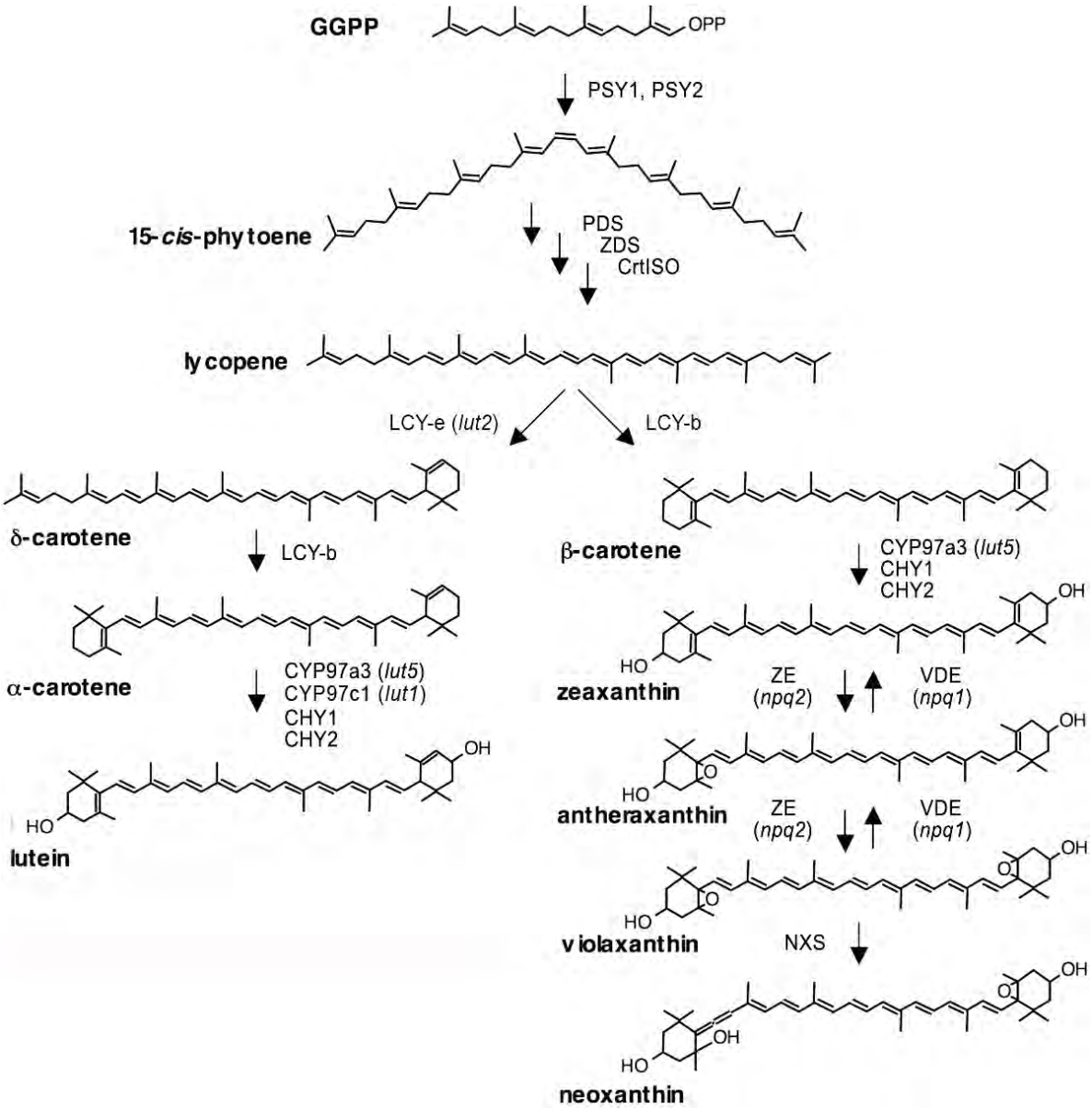

Figure S1. Biosynthetic pathway of carotenoids in *Arabidopsis thaliana.* Names of the enzymes catalyzing each step are indicated: phytoene synthase (PSY); phytoene desaturase (PDS); carotene desaturase (ZDS); carotenoid isomerase (CrtISO); lycopene ε-cyclase (LCY-e); lycopene β-cyclase (LCY-b); β-carotene hydroxylase (CYP97a3); ε-β-carotene hydroxylase (CYP97c1); β-carotene hydroxylase 1 and 2 (CHY1, CHY2); zeaxanthin epoxidase (ZEP); violaxanthin de-epoxidase (VDE); neoxanthin synthase (NXS). Names of *Arabidopsis* knock-out mutants are indicated in parentheses. GGPP, Geranylgeranyl pyrophosphate.

Figure S2

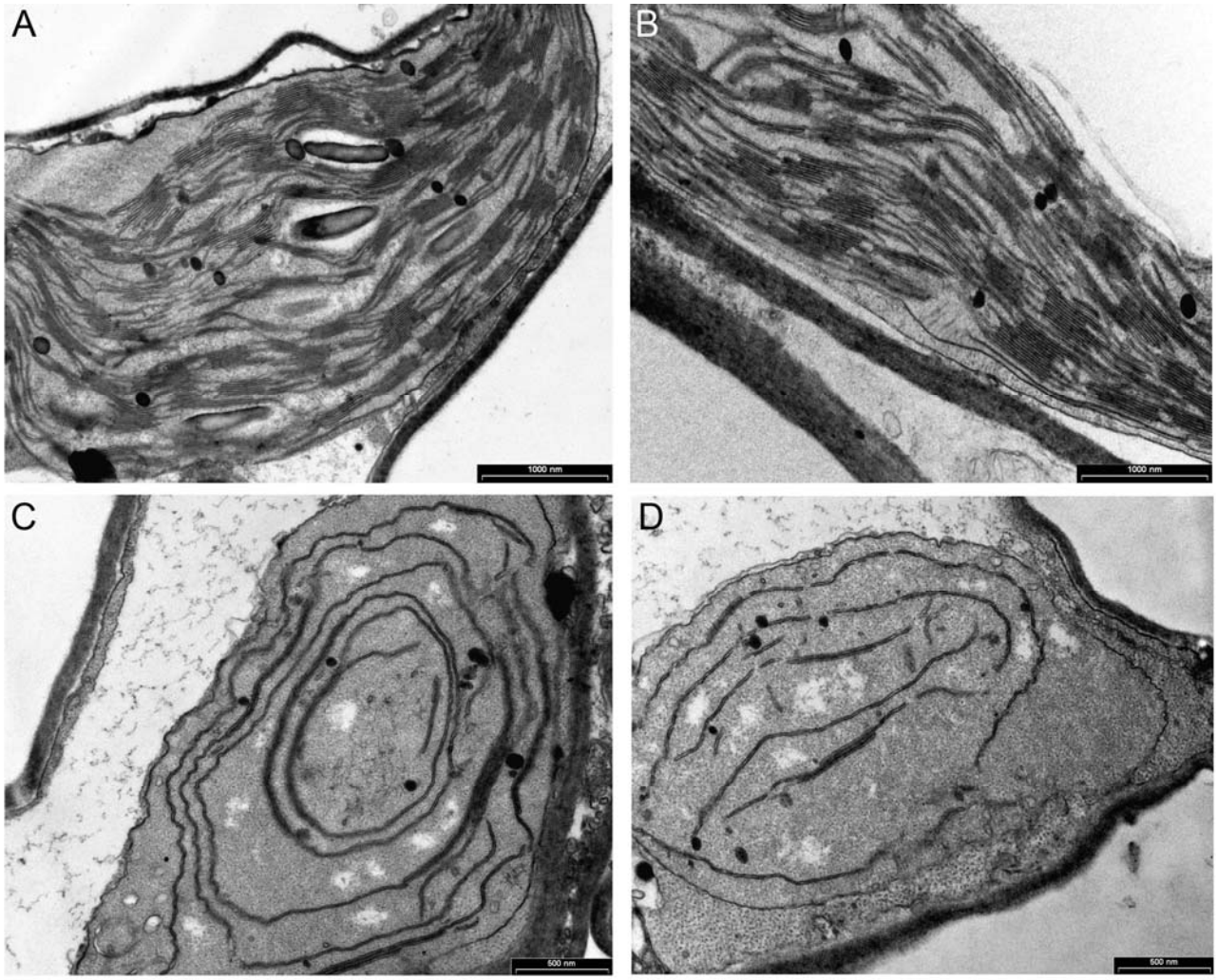

Figure S2. Transmission electron micrographs of plastids from leaf mesophyll cells of the *Arabidopsis* WT and *nox* mutant plants. Leaf samples from WT and *nox* were harvested at the midpoint of the light period, from three-week-old plants grown in long-day conditions (20 µmol photon m^{-2} s^{-1}, 24°C, 16/8 h day/night). The ultrastructure of chloroplasts from WT (A, B) and *nox* (C, D) plants was analyzed by electron microscopy. Representative thin sections are shown. The scale bars indicate 1 µm (WT) or 0.5 µm (*nox*).

Figure S3

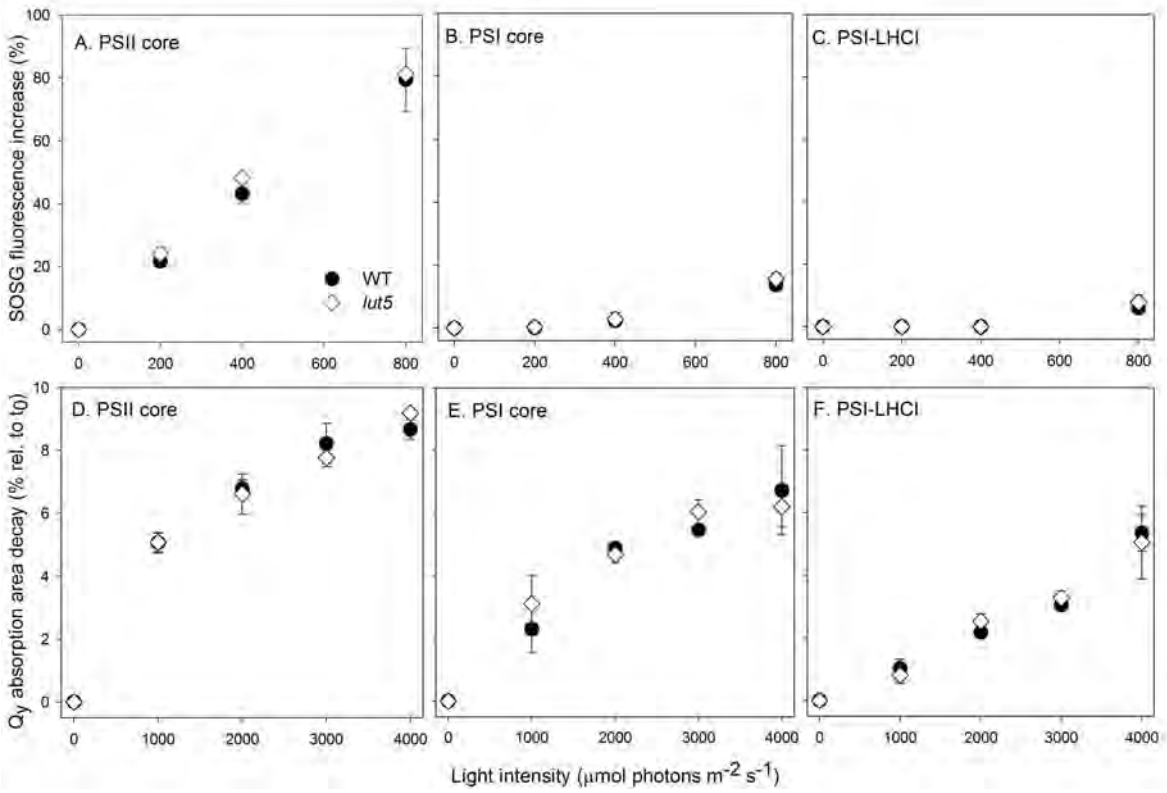

Figure S3. Photoprotection capacity of α- *vs.* β-carotene-binding complexes. Singlet oxygen yield (A-C) and Chl photobleaching (D-F) were measured in the PSII core, PSI core and PSI-LHCI complexes, purified from either WT or *lut5* leaves of *Arabidopsis*. Singlet oxygen ($^1O_2$) yield was measured on pigment-protein complexes upon illumination (200-800 μmol photons m^{-2} s^{-1}, 600<λ<750, 5 minutes, RT) by following SOSG (Singlet Oxygen Sensor Green) fluorescence emission increase as an effect of the light-dependent $^1O_2$ release by the complexes. Kinetics of light-dependent chlorophyll bleaching were analyzed in the same complexes, by following the Q_y transition absorbance decay during strong illumination (1000-4000 μmol photons m^{-2} s^{-1}, 600<λ<750, 10 minutes, 10°C). The photo-resistance of complexes was measured by quantifying the Q_y transition absorbance decay upon 10 min of strong illumination. The chlorophyll concentration of samples was set to have the same absorption area in the actinic wavelength range used. The symbols and error bars show mean ± SD (n = 3). Statistical analysis revealed that no complexes from *lut5* showed any significant difference with respect to the WT (Student's *t* test, $p < 0.05$) in both $^1O_2$ yield and photobleaching extent. t_0, time zero. Black dots, WT; unfilled diamonds, *lut5*. See Methods for details.

Figure S4

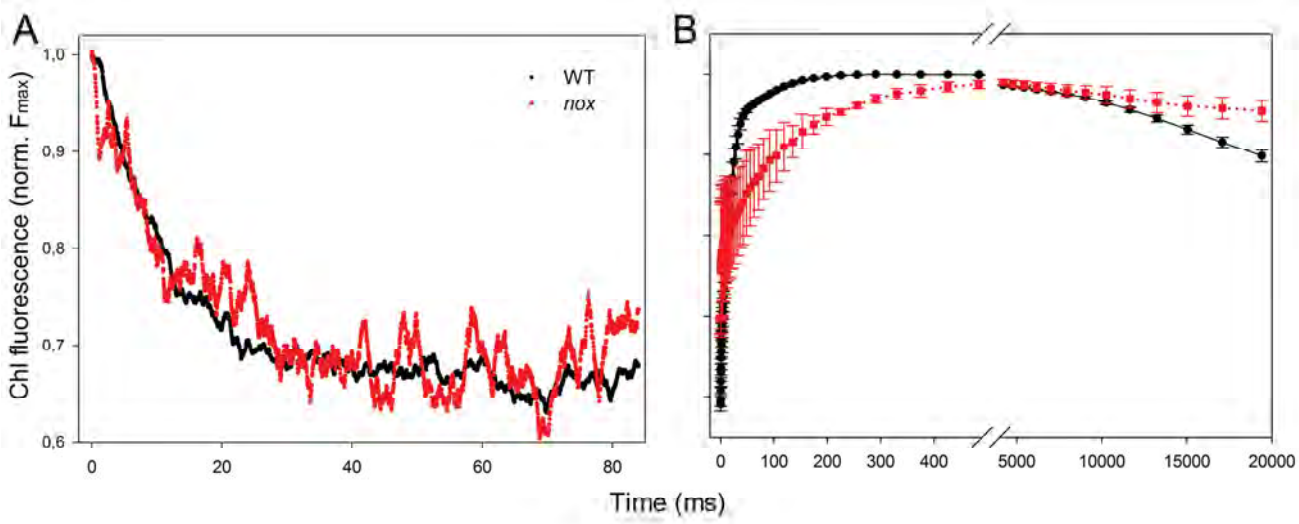

Figure S4. Decay and induction kinetics of PSII fluorescence. (A) Chlorophyll fluorescence decay kinetics were measured at room temperature on dark-adapted leaves after single-turnover flash illumination, as a measure of Q_A re-oxidation rate. (B) A fluorescence increase was induced in dark-adapted leaf, using a saturating pulse of green light (1200 μmol photons m^{-2} s^{-1}, 20 s, RT). Experimental fluorescence curves were normalized to the corresponding F_{max} values and represent the averages from 10 separate curves.

Figure S5

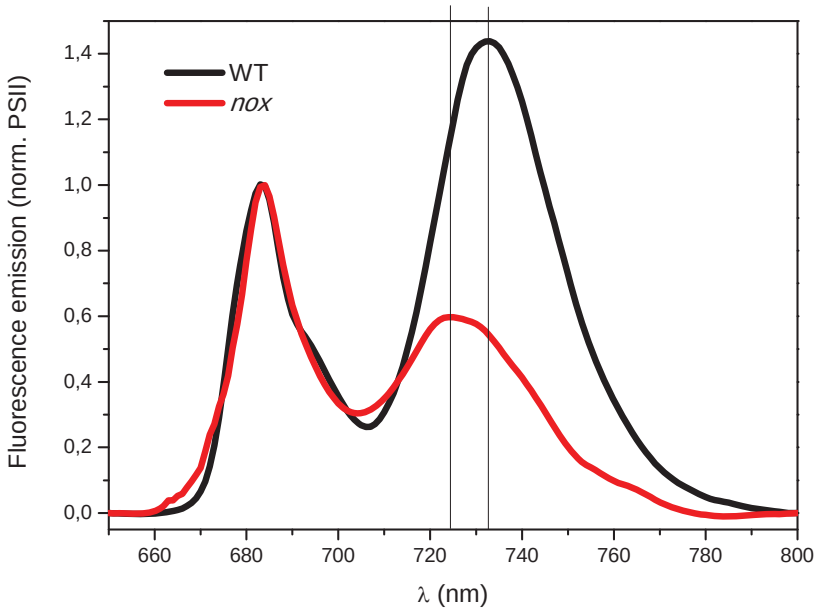

Figure S5. Low temperature fluorescence emission spectra of chloroplasts. Fluorescence emission spectra were determined for chloroplasts isolated from WT and *nox* dark-adapted leaves. Spectra were recorded at 77 K. Fluorescence emission spectra were normalized to the 682-nm emission peak emanating from PSII. Each curve is the mean of at least 10 replicates.

Figure S6

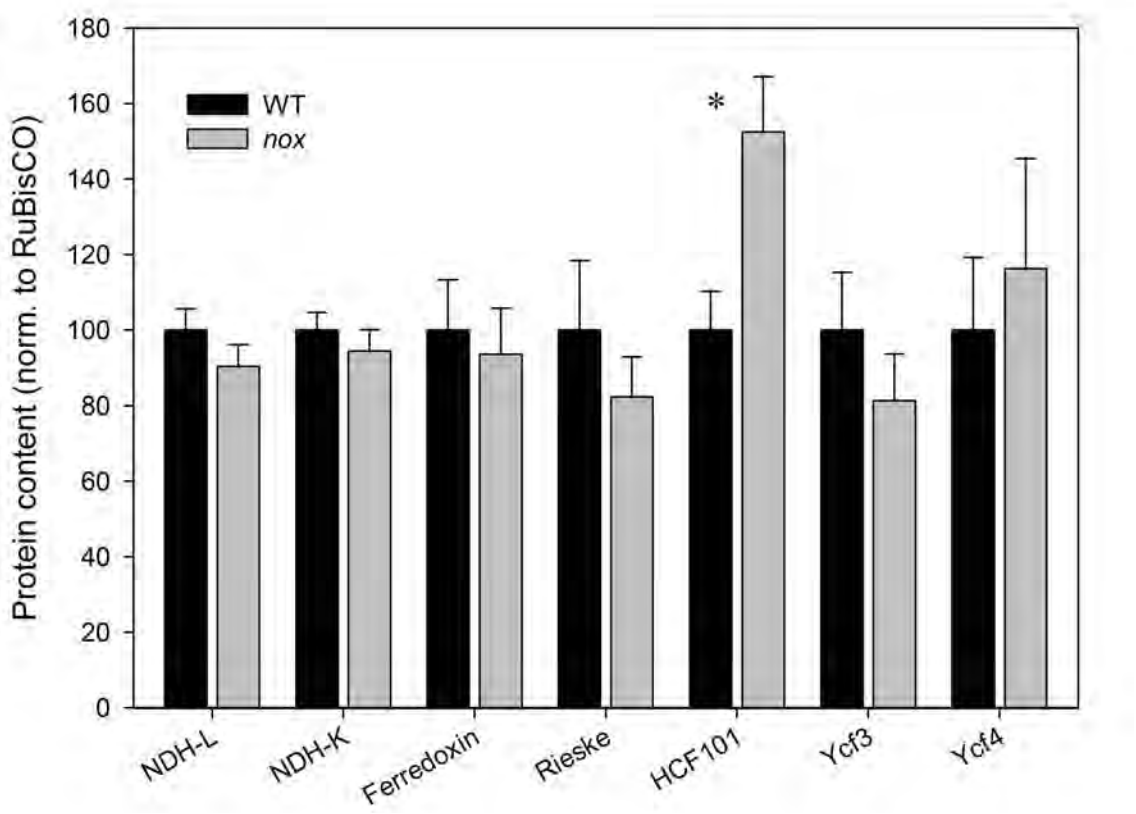

Figure S6. Analysis of polypeptide composition of WT and *nox* thylakoid membranes. Immunotitration of chloroplast proteins was performed on whole leaf extracts, with antibodies directed against individual gene products. The amount of each subunit was normalized to the content of the chloroplastic protein RuBisCO (large subunit) and expressed as a percentage of the corresponding WT content. The symbols and error bars show mean ± SD (n = 3). Significantly different values with respect to the corresponding WT, according to Student's *t* test ($P<0.05$), are marked (*). NDH-L/K, NADPH dehydrogenase subunits L/K.

Figure S7

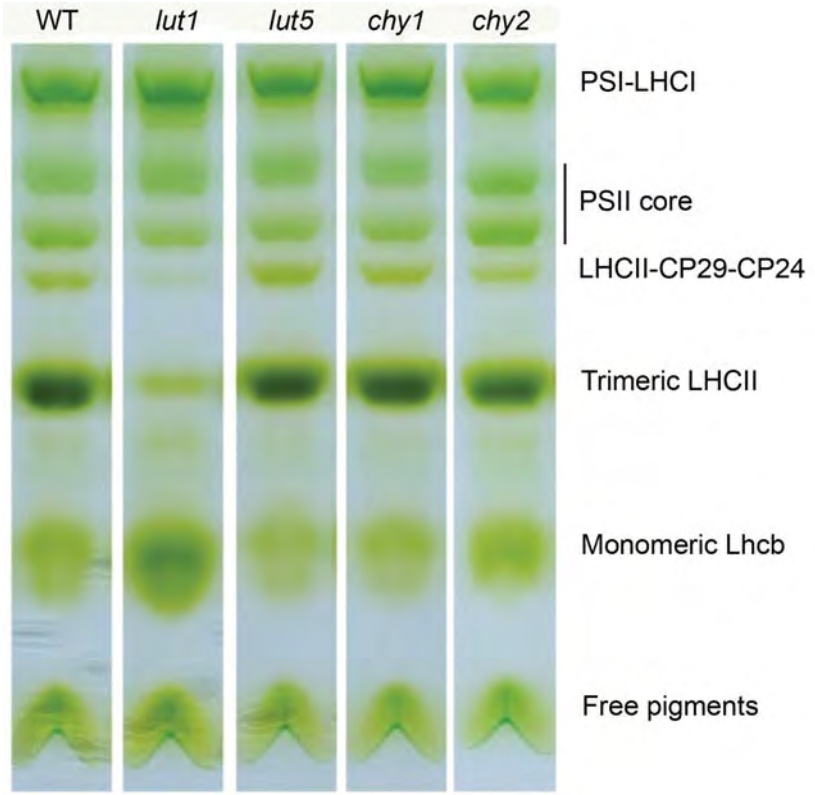

Figure S7. Biochemical characterization of single knock-out mutants of *Arabidopsis.* Thylakoid pigmented complexes isolated from WT and mutant *lut* and *chy* plants were separated by non-denaturing Deriphat-PAGE upon solubilization with 0.6% α-DM; 25 μg of chlorophyll were loaded in each lane. The composition of each green band is indicated.

Supplemental Table I

Gene/Control name	Locus	Gene Model	Forward Primer (5'-3') Length	Forward Primer Sequence	Reverse Primer (5'-3') length	Reverse Primer Sequence	Amplicon (bp)	Stock solution concentration (copies per µl)
Genes of interest								
Cytosolic rRNA small subunit (18S RRNA)	AT2G01010; AT3G41768	AT2G01010.1; AT3G41768.1	24	CCGTCCTAGTCTCAACCATAAACG	23	GGAGTCCTATAAGCAACATCCGC	64	-
Plastidic rRNA small subunit (RRN16S.1, RRN16S.2)	ATCG00920; ATCG01210	ATCG00920.1; ATCG01210.1	21	GCTTTTTAAGTCCGCCGTCAA	21	TTGGTAGTTTCCACCGCCTGT	62	-
Mitochondial rRNA small subunit (RRN18)	ATMG01390	ATMG01390.1	21	AGCGAAACCCTCGTCTTGTGT	21	GCTCACTTCGGTTTTCAAGCC	68	-
Check gDNA contamination								
Intron sequence of the MADS affecting flowering 5 (MAF5)	AT5G65080	AT5G65080.1	20	TTTTTTGCCCCCTTCGAATC	22	ATCTTCCGCCACCACATTGTAC	68	-
cDNA quality control								
GAPDH3'	AT1G13340	AT1G13340.1	26	GCAACATACGACGAAATCAAGAAGGC	26	ACACAACATCATCCTCAGTGTATCCC	91	-
GAPDH5'	AT1G13340	AT1G13340.1	23	CTCTCGATCTCAATTTCGCAAAA	22	GAAACCGTTGATTCCGATTCTG	61	-
Spikes for transcript quantification								
Spike3 (ArrayControl RNA Spikes; Applied Biosystems/Ambion, Darmstadt, Germany)	-	-	20	GATCGTTTGCCTGCATTACC	20	GAGAGCGTCAGCCATACCAC	103	9,0E+10
Spike5 (ArrayControl RNA Spikes; Applied Biosystems/Ambion, Darmstadt, Germany)	-	-	20	ACAAAGGCAGCGTTGAAAAC	20	TAGTGTCTGCACGCCATACC	132	2,4E+10
Spike6 (ArrayControl RNA Spikes; Applied Biosystems/Ambion, Darmstadt, Germany)	-	-	20	CGCAAAGTCTCTCCTCTTGG	20	CAGTAGCCATTGCGGAAGAT	115	3,0E+09
Spike7 (ArrayControl RNA Spikes; Applied Biosystems/Ambion, Darmstadt, Germany)	-	-	20	CTGAACCAGACTGCACATGG	20	ACGCTCATGGGCTTGTTTAT	111	5,0E+08
Spike8 (ArrayControl RNA Spikes; Applied Biosystems/Ambion, Darmstadt, Germany)	-	-	22	TCATTAAAGCGGAAGGCAAT	20	AAATCTTCCAGCACCGTCAG	145	6,5E+07
Alien (Alien qRT–PCR Inhibitor Alert; Stratagene-Agilent Technologies, Waldbronn, Germany)	-	-	-	-	-	-	-	1,0E+07

Supplemental Table I. Quantification of transcript levels on polysomal RNA by qRT-PCR. Information about the genes and controls primers, and spike concentrations used in this work, are reported. See Methods for further details.

A3. The *Arabidopsis thaliana szl1* mutant reveals a critical role of β-Carotene in photosystem I photoprotection.

The Arabidopsis *szl1* Mutant Reveals a Critical Role of β-Carotene in Photosystem I Photoprotection[1][C][W]

Stefano Cazzaniga, Zhirong Li, Krishna K. Niyogi, Roberto Bassi*, and Luca Dall'Osto

Dipartimento di Biotecnologie, Università di Verona, Verona 37134 Italy (S.C., R.B., L.D.'O.); Department of Plant and Microbial Biology, Howard Hughes Medical Institute, University of California, Berkeley, California 94720–3102 (Z.L., K.K.N.); Physical Biosciences Division, Lawrence Berkeley National Laboratory, Berkeley, California 94720 (Z.L., K.K.N.); and Pflanzenwissenschaften-2, Phytosphäre Forschungszentrum Jülich, 52425 Julich, Germany (R.B.)

Carotenes and their oxygenated derivatives, the xanthophylls, are structural determinants in both photosystems (PS) I and II. They bind and stabilize photosynthetic complexes, increase the light-harvesting capacity of chlorophyll-binding proteins, and have a major role in chloroplast photoprotection. Localization of carotenoid species within each PS is highly conserved: Core complexes bind carotenes, whereas peripheral light-harvesting systems bind xanthophylls. The specific functional role of each xanthophyll species has been recently described by genetic dissection, however the in vivo role of carotenes has not been similarly defined. Here, we have analyzed the function of carotenes in photosynthesis and photoprotection, distinct from that of xanthophylls, by characterizing the *suppressor of zeaxanthin-less* (*szl*) mutant of Arabidopsis (*Arabidopsis thaliana*) which, due to the decreased activity of the lycopene-β-cyclase, shows a lower carotene content than wild-type plants. When grown at room temperature, mutant plants showed a lower content in PSI light-harvesting complex I complex than the wild type, and a reduced capacity for chlorophyll fluorescence quenching, the rapidly reversible component of nonphotochemical quenching. When exposed to high light at chilling temperature, *szl1* plants showed stronger photoxidation than wild-type plants. Both PSI and PSII from *szl1* were similarly depleted in carotenes and yet PSI activity was more sensitive to light stress than PSII as shown by the stronger photoinhibition of PSI and increased rate of singlet oxygen release from isolated PSI light-harvesting complex I complexes of *szl1* compared with the wild type. We conclude that carotene depletion in the core complexes impairs photoprotection of both PS under high light at chilling temperature, with PSI being far more affected than PSII.

Carotenoids are polyisoprenoid pigments that are ubiquitously distributed among oxygenic photosynthetic organisms, from cyanobacteria to land plants (Britton et al., 2004). A molecular feature of these C_{40} molecules is a conjugated double-bond system, which is responsible for the strong absorption in the visible region of the spectrum and the antioxidant capacity of these pigments. In photosynthetic tissues of higher plants, carotenoids are mainly accumulated in the thylakoid membranes. Carotenoid composition is remarkably conserved among plant taxa, consisting of the hydrocarbons α- and β-carotene (accounting for one-fourth of total carotenoids) and their oxygenated derivatives called xanthophylls. The latter group include the β,ε-xanthophyll lutein, the most abundant plant carotenoid, and the β,β-xanthophylls violaxanthin, neoxanthin, antheraxanthin, and zeaxanthin (Demmig-Adams and Adams, 1992), whose biosynthesis is tightly controlled during plant acclimation to stressful conditions (Hirschberg, 2001; Alboresi et al., 2011). The carotenoid biosynthesis pathway from phytoene include a series of four desaturation reactions, leading to the formation of the C_{40} compound lycopene, which is then cyclized at both ends by β-cyclase (LCYB) to produce β-carotene. Alternatively, β-cyclization occurs at a single end, the other being processed by ε-cyclase (LUT2) to produce α-carotene. Thus, there exist two distinct branches in plant carotenoid biosynthesis, one leading to synthesis of β,β-hydroxylated xanthophylls from β-carotene, and the other to lutein from α-carotene. The hydroxylation of either α- or β-carotene is catalyzed by multiple enzymes with overlapping substrate specificity belonging to two different classes: CHY1 and CHY2 (ferredoxin-dependent diiron oxygenases) catalyze β-ring hydroxylation, while LUT1 and LUT5 (cytochromes P450) are involved in the hydroxylation of both ε-ring and β-ring of α-carotene (Tian et al., 2003, 2004; Fiore et al., 2006; Kim and DellaPenna, 2006; Kim et al., 2009). Complete lack of xanthophylls in the

[1] This work was supported by the Marie Curie Actions—Networks for Initial Training Harvest (grant no. PITN–GA–2009–238017) and by Ministero delle Politiche Agricole, Alimentari e Forestali BioMassVal (grant no. 2/01/140). Z.L. and K.K.N. were supported by a grant from the Chemical Sciences, Geosciences and Biosciences Division, Office of Basic Energy Sciences, Office of Science, U.S. Department of Energy (Field Work Proposal no. 449B).

* Corresponding author; e-mail roberto.bassi@univr.it.

The author responsible for distribution of materials integral to the findings presented in this article in accordance with the policy described in the Instructions for Authors (www.plantphysiol.org) is: Roberto Bassi (roberto.bassi@univr.it).

[C] Some figures in this article are displayed in color online but in black and white in the print edition.

[W] The online version of this article contains Web-only data.

www.plantphysiol.org/cgi/doi/10.1104/pp.112.201137

chy1chy2lut1lut5 mutant (Kim et al., 2009) confirms that these four genes encode the complete enzymatic complement catalyzing carotene hydroxylation in Arabidopsis (*Arabidopsis thaliana*).

The distribution of each carotenoid species between the different components of the photosynthetic machinery is the basis for their specific functions. Thus, a minor fraction is free in the lipid phase of thylakoids where it serves as antioxidant (Havaux et al., 2004) and modulates the fluidity of the lipid bilayer (Gruszecki and Strzałka, 2005). However, carotenoids are located mostly within specific binding sites of pigment-protein complexes, contributing to both light harvesting and photoprotection of these PS subunits. β-Carotene is bound to reaction center subunits of both PSI and PSII, whereas xanthophylls are bound to peripheral light-harvesting complexes (Lhc) subunits that comprise the antenna system. Core complexes of PSI and PSII bind, respectively, 15 and 11 β-carotenes (Amunts et al., 2010; Umena et al., 2011). Lhcb proteins, constituting the antenna system of PSII, bind lutein, violaxanthin, and neoxanthin at four distinct binding sites (Liu et al., 2004). Zeaxanthin, upon its synthesis from violaxanthin under excess light, can also bind to these antenna components in exchange for violaxanthin, in site V1 in the case of the major LHCII trimeric complex (Caffarri et al., 2001) or in site L2 in the case of the monomeric subunits CP26 (Lhcb5), CP29 (Lhcb4), and CP24 (Lhcb6; Croce et al., 2003; Betterle et al., 2010; Pan et al., 2011). PSI antenna proteins (Lhca1–4) and CP24 lack neoxanthin (Jensen et al., 2007; Passarini et al., 2009).

Besides their role as structural determinants, carotenoids are involved in photoprotective mechanisms. Indeed, they have coevolved with oxygenic photosynthesis to avoid photooxidative damage derived from photosensitizing action of porphyrins and reduction of oxygen by univalent photosynthetic electron transporters. This is particularly important under rapid fluctuations in light intensity, when photochemical quenching activity is exceeded, leading to photoinhibition (Külheim et al., 2002). Carotenoids protect chloroplasts from excess light by (1) modulating the nonradiative dissipation of excess excitation energy (Niyogi et al., 1998; Dall'Osto et al., 2005), and (2) by mediating direct quenching of chlorophyll (Chl) triplets (^{3}Chl*) or (3) by scavenging the reactive oxygen species (ROS) generated during photosynthesis (Niyogi, 2000; Dall'Osto et al., 2005, 2007b; Havaux et al., 2007). The essential role of carotenoids in photoprotection was evidenced by the phenotype of carotenoid-less plants, unable to perform photoautotrophic growth (Herrin et al., 1992; Trebst and Depka, 1997; Kim et al., 2009).

The roles of xanthophylls have been subjected to dissection through genetic analysis. Several mutants with altered xanthophyll composition are impaired in photoprotection, implying that these pigments have a key role in plant fitness. Lutein depletion in *lut2* plants resulted in higher photosensitivity in high light (HL) with respect to the wild type (Pogson et al., 1996), due to impaired ^{3}Chl* quenching within LHCII (Dall'Osto et al., 2006). Lack of both lutein and zeaxanthin further enhances the photodamage in both HL-treated plants and green algae (Niyogi et al., 1997, 2001; Gilmore, 2001; Baroli et al., 2003; Dall'Osto et al., 2006). Mutation of three β-carotene hydroxylases CHY1, CHY2, and LUT5 in Arabidopsis, yielded a plant with lutein as the only xanthophyll, revealing unprecedented photosensitivity (Fiore et al., 2006; Dall'Osto et al., 2007b; Kim et al., 2009) and implying that singlet oxygen ($^1O_2$) scavenging is a constitutive component of photoprotection in antenna proteins together with Chl triplet quenching. Finally, a neoxanthin-less mutant showed enhanced sensitivity to superoxide anion (Dall'Osto et al., 2007a).

While xanthophyll biosynthesis mutants of Arabidopsis and *Chlamydomonas* have revealed distinct photoprotective roles in vivo for xanthophyll species, until recently no photoautotrophic mutant showing a selective β-carotene loss has been described, to our knowledge. Therefore, the role of β-carotene has been more difficult to identify. Early reports showed that isolated PSII reaction centers form $^1O_2$ with high yield, thus causing photooxidation of P680 and other Chls (Barber et al., 1987; Telfer et al., 1994b). Indeed, the primary event upon PSII photoinhibition is the damage to the D1 subunit (Aro et al., 1993), and restoration of photosynthetic electron transport requires degradation and de novo synthesis of this subunit. These observations are consistent with the idea that the PSII reaction centers are a major source of $^1O_2$ within the chloroplasts (Krieger-Liszkay, 2005; Telfer, 2005), and led to the conclusion, although indirect, that β-carotene ligands in the core complex have a special role in scavenging $^1O_2$ (Telfer et al., 1994a; Telfer, 2005).

Recently, the Arabidopsis mutant *szl1* was identified (Li et al., 2009) that carries a point mutation of LCYB gene, and thus exhibits a less-active lycopene β-cyclase with respect to the wild type. Due to the activity of the four carotene hydroxylase enzymes that catalyze the subsequent reactions leading to xanthophyll synthesis, a depletion in carotene with respect to wild-type plants is produced (Li et al., 2009), offering the opportunity of specifically probing carotene function in vivo in the presence of xanthophylls.

In this work, we have addressed the question of the function for the carotene ligands of both PS, and their importance in the photoprotection of the chloroplast. To this aim, we have compared a panel of Arabidopsis mutants affected in the biosynthesis of either xanthophylls or carotenes, and analyzed the effect of their depletion on the photodamage of chloroplast in vivo. We show that, although the *szl1* mutation does not affect photosynthetic electron transport rate (ETR), mutant plants show a higher sensitivity to photoxidative stress with respect to the wild type when exposed to HL at low temperature (8°C). Interestingly, *szl1* plants revealed stronger photoinhibition of PSI compared with PSII. These findings imply that β-carotene ligands of PSI have a crucial role in

the photoprotection of the complex, especially in low-temperature conditions.

RESULTS

The *szl1* Mutant of Arabidopsis Has Lower Carotene and Higher Xanthophyll Content Than Wild-Type Plants

The *szl1* mutant (Li et al., 2009) showed, under our growth conditions (100 μmol photons m^{-2} s^{-1}, 8 h light, 23°C/16 h dark, 20°C), similar leaf morphology and development rate with respect to wild-type plants. Pigment content of leaves from both genotypes was analyzed through diode array HPLC of leaf acetone extracts (Table I). We tested dark-adapted plants, a condition in which wild-type leaves accumulate violaxanthin, and plants transferred for 60 min under HL (550 μmol photons m^{-2} s^{-1}), a condition in which violaxanthin is largely deepoxidated into zeaxanthin. Chl content, Chl *a*/*b*, and Chl/Car ratios were essentially the same in both genotypes (Table I), whereas β-carotene content was 60% lower in *szl1* leaves (Table II), as reported previously (Li et al., 2009). The *szl1* mutant showed a slight accumulation of α-carotene (a lutein precursor normally found in small amount in wild-type plants), a lower content in β,β-xanthophylls, and a higher content in lutein, thus a far lower β,β/ε,β-xanthophylls ratio than in the wild type. When plants were exposed to HL, deepoxidation was 30% lower in *szl1* with respect to the wild type (Table II).

The aim of this work was to address the function for carotene molecules bound to PS, and their relative importance in the photoprotection of the chloroplast. However, previous characterization of xanthophyll biosynthesis mutants (Dall'Osto et al., 2007b; Kim et al., 2009) clearly showed that xanthophyll composition of the LHCs also affects photoprotection. In particular, distinct roles were identified for β,β- and ε,β-xanthophylls. Relevant to this study, depletion of β,β-xanthophylls increased photosensitivity (Dall'Osto et al., 2007b). Since *szl1* plants, besides a lower carotene content, also have a lower β,β/ε,β-xanthophylls ratio than the wild type, it is important to distinguish the effect of carotene depletion in core complexes from the increased lutein to β,β-xanthophyll ratio in the antenna moiety of the PS. Therefore, we included the *chy1chy2* and *lut5* genotypes in this characterization as controls (Tables I and II). The *chy1chy2* double mutant has a reduced conversion of β-carotene into β,β-xanthophylls, yielding the same β,β/ε,β-xanthophylls ratio as the *szl1* plants. In addition, we analyzed the *lut5* genotype as a control with respect to the α-carotene accumulation. In fact, α-carotene competes with β-carotene binding sites on pigment-protein complexes (Dall'Osto et al., 2007b), and thus it might be responsible, in part, for changes in photoprotection activity. *chy1chy2* and *lut5* plants showed leaf Chl content and Chl *a*/*b* ratio identical to wild-type plants. Xanthophyll content per Chl was significantly lower than in the wild type (Table I), as expected from previous reports (Fiore et al., 2006; Kim et al., 2009).

Organization and Stoichiometry of Chl-Binding Proteins

The organization of pigment-protein complexes in wild-type and mutant genotypes was analyzed by nondenaturing Deriphat-PAGE (Fig. 1). In agreement with a previous report (de Bianchi et al., 2008), seven major green bands were resolved upon solubilization of thylakoid membranes with 0.8% dodecyl-α-D-maltoside (α-DM). The uppermost band contained the PSII-LHCII supercomplex whose dissociation into components yielded the PSII core and the antenna moieties, namely CP29-CP24-$(LHCII)_3$ supercomplex (Bassi and Dainese, 1992), trimeric LHCII, and monomeric Lhcb. The major green band just below the PSII supercomplex contained the PSI-LHCI supercomplex, which, different from PSII, is stable and does not yield dissociation products upon mild solubilization of wild-type thylakoids. Finally, the lowest band was composed of free pigments that dissociated during solubilization, mainly carotenoids. The distribution of Chl between PSI-LHCI, PSII core, and Lhcb components was determined from the densitometric analysis of the Deriphat-PAGE patterns. In *szl1*, the PSI-LHCI complex relative abundance was reduced versus wild-type thylakoids (−27%). Consistently, a higher PSII core/PSI-LHCI ratio was found in *szl1* (0.61) with respect to the wild type (0.41). Minor differences were observed in the Lhcb/PSII core ratio, which was slightly lower (approximately 4.0) in *chy1chy2* and *lut5* with respect to the wild type (5.5), accompanied by a higher PSII core/PSI-LHCI ratio (approximately 0.5 versus 0.4).

Table I. *Pigment content and Chl fluorescence induction parameters*

Measurements were done on dark-adapted leaves of Arabidopsis wild type and mutants *szl1*, *chy1chy2*, and *lut5*. Data are expressed as mean ± SD ($n \geq 4$). Chls, Total chlorophylls; Cars, total carotenoids; $T_{2/3}$, time corresponding to two-thirds of the induction fluorescence rise in DCMU-treated leaves; a.u., arbitrary units. Values marked with the same letters are not significantly different from each other within a column (Student's *t* test, $P < 0.05$).

Genotypes	Chls/cm^2	Chl *a*/*b*	Chls/Cars	Xanthophyll/Cars	Carotene/Cars	F_o	F_m	F_v/F_m	$T_{2/3}^{-1}$
	μg					a.u.			10^3, ms^{-1}
WT	20.8 ± 1.1[a]	3.0 ± 0.1[a]	3.7 ± 0.2[a,b]	0.7 ± 0.01[a]	0.3 ± 0.01[a]	388 ± 42[a]	2136 ± 149[a]	0.82 ± 0.01[a]	4.3 ± 0.4[a]
szl1	17.5 ± 1.6[a]	2.9 ± 0.1[a]	3.5 ± 0.1[a]	0.9 ± 0.01[b]	0.1 ± 0.01[b]	515 ± 39[b]	1858 ± 165[b]	0.72 ± 0.01[b]	4.6 ± 0.4[b]
chy1chy2	20.2 ± 1.9[a]	2.9 ± 0.1[a]	4.0 ± 0.2[b,c]	0.7 ± 0.01[c]	0.3 ± 0.01[c]	348 ± 35[a,c]	1766 ± 173[b]	0.80 ± 0.01[a]	3.7 ± 0.4[a]
lut5	19.4 ± 3.5[a]	3.0 ± 0.2[a]	4.1 ± 0.2[c]	0.6 ± 0.01[d]	0.4 ± 0.02[d]	388 ± 16[c]	1883 ± 131[b]	0.82 ± 0.01[a]	3.1 ± 0.3[c]

Table II. *Photosynthetic pigment content of the wild type and mutants*

Pigment content was determined before and after leaves were illuminated for 60 min at 550 μmol photons m^{-2} s^{-1}. Data are normalized to 100 Chl *a* + *b* molecules and are expressed as mean ± SD (*n* = 3). Values marked with the same letters are not significantly different from each other within a column and a light regime (Student's *t* test, $P < 0.05$).

Genotypes	Mol Pigment/100 Mol Chls							$\beta,\beta/\varepsilon,\beta$ Xanthophylls Ratio
	Neoxanthin	Violaxanthin	Antheraxanthin	Lutein	Zeaxanthin	α-Carotene	β-Carotene	
Dark adapted								
WT	4.4 ± 0.4[a]	2.8 ± 0.4[a]		13.0 ± 0.1[a]		0.2 ± 0.04[a]	6.9 ± 0.4[a]	0.6 ± 0.01[a]
szl1	1.3 ± 0.1[b]	0.8 ± 0.2[b]		22.3 ± 0.5[b]		1.2 ± 0.2[b]	2.7 ± 0.2[b]	0.1 ± 0.01[b]
chy1chy2	0.7 ± 0.2[b]	0.7 ± 0.1[b]		15.6 ± 0.8[c]		0.2 ± 0.1[a]	8.0 ± 0.2[c]	0.1 ± 0.03[b]
lut5	2.9 ± 0.4[c]	2.0 ± 0.2[c]		10.3 ± 0.5[d]		6.3 ± 0.4[c]	2.9 ± 0.2[b]	0.5 ± 0.01[c]
HL								
WT	4.2 ± 0.1[a]	1.4 ± 0.1[a]	0.3 ± 0.1[a]	12.6 ± 0.3[a]	1.1 ± 0.2[a]	0.2 ± 0.1[a]	6.1 ± 0.3[a]	0.6 ± 0.01[a]
szl1	1.3 ± 0.1[b]	0.6 ± 0.1[b]	0.1 ± 0.01[b]	20.8 ± 1.0[b]	0.8 ± 0.1[b]	1.1 ± 0.2[b]	2.4 ± 0.5[b]	0.1 ± 0.01[b]
chy1chy2	0.8 ± 0.2[c]	0.6 ± 0.1[b]	0.1 ± 0.01[b]	15.2 ± 0.4[c]	0.6 ± 0.1[b,c]	0.2 ± 0.1[a]	7.6 ± 0.4[c]	0.1 ± 0.02[b]
lut5	3.1 ± 0.4[d]	1.4 ± 0.1[a]	0.1 ± 0.04[b]	11.0 ± 0.7[d]	0.6 ± 0.04[c,d]	5.9 ± 0.4[c]	3.0 ± 0.1[b]	0.5 ± 0.04[c]

We first proceeded to determine whether the light harvesting and energy transfer to reaction center activity was affected by the mutations. The functional antenna size of PSII was measured on leaves by estimating the rise time of Chl florescence in the presence of 3-(3,4-dichlorophenyl)-1,1-dimethylurea (DCMU). *chy1chy2* and *lut5* leaves showed a significant reduction in the PSII antenna size with respect to the wild type (Table I), thus suggesting that carotenoid depletion did impair the overall light-harvesting capacity, as suggested by densitometric analysis of the Deriphat-PAGE. However, the PSII functional antenna size was not significantly affected by the *szl1* mutation.

Green bands were eluted from the gel, and their pigment composition was determined by HPLC (Table III). Monomeric and trimeric Lhcb complexes from mutant genotypes showed a lower content in carotenoids per unit Chl versus the corresponding fractions from the wild type (around −20%). Furthermore, antenna proteins isolated from *szl1* and *chy1chy2* thylakoids had a lower content in β,β-xanthophylls (−90% in monomeric Lhcb, −75% in trimeric LHCII) and a compensatory increase in lutein (+25% in monomeric Lhcb, +10% in trimeric LHCII), while the relative abundance of ε,β- and β,β-xanthophylls were similar in antenna proteins from the wild type and *lut5*. The PSII core complexes purified from wild-type and mutant thylakoids only bound Chl α,β-carotene and α-carotene. However, while the Chl/Car ratios were essentially the same in the wild type, *chy1chy2*, and *lut5*, the PSII core complex purified from *szl1* showed a far lower content in carotenes (−40%). Moreover, 33% of bound carotenes in the PSII core complex from *szl1*, are made by α-carotene, versus 72% in *lut5*; PSII core complexes bound almost exclusively β-carotene in both the wild type and *chy1chy2*.

A similar effect was observed on the pigment composition of the PSI-LHCI complexes purified from wild-type and mutant thylakoids: Carotenoid content per unit Chl was essentially the same in the wild type, *chy1chy2*, and *lut5*, while it was reduced in *szl1* due to a lower carotene content (−30%). The relative abundance of ε,β- and β,β-xanthophylls was similar in PSI-LHCI from the wild type and *lut5*, while complexes isolated from *szl1* and *chy1chy2* had a far lower content in β,β-xanthophylls and a compensatory increase in lutein. While β-carotene is the main carotene found in PSI-LHCI from the wild type and *chy1chy2*, α-carotene accounts for 28% and 62% of total carotenes of the complexes in *szl1* and *lut5*, respectively.

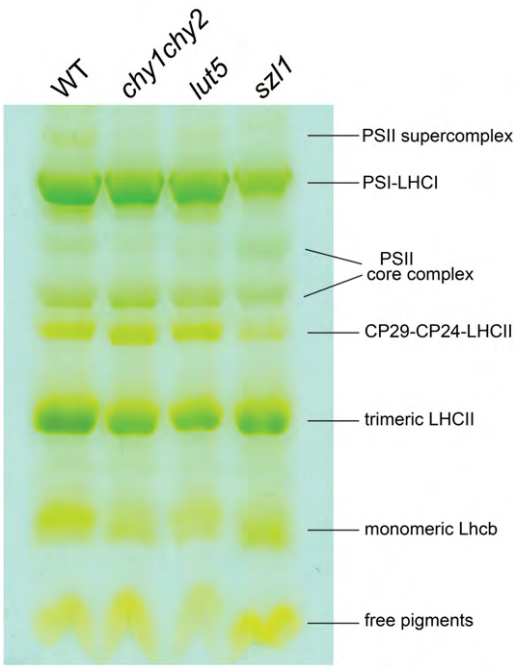

Figure 1. Analysis of pigment-protein complexes of the wild type and mutants. Thylakoid pigment-protein complexes were separated by nondenaturing Deriphat-PAGE upon solubilization with 0.8% α-DM. Thylakoids corresponding to 25 μg of Chls were loaded in each lane. Composition of each band is indicated. [See online article for color version of this figure.]

Table III. *Pigment composition of Chl proteins purified from thylakoids of the wild type, szl1, chy1chy2, and lut5*

Data are normalized to 100 Chl *a* + *b* molecules and are expressed as mean ± SD ($n = 3$). See "Materials and Methods" for details of purification. Abbreviations: Chls, Total Chl; Xanths, total xanthophylls; Cars, total carotenoids; ε-β,ε,β-xanthophylls, β-β,β,β-xanthophylls. Values marked with the same letters are not significantly different from each other within a column and a complex (Student's *t* test, $P < 0.05$).

Complexes	Mol Pigment/100 Mol Chls							Chls/Cars	ε,β/Xanths	β,β/Xanths
	Chl *a*	Chl *b*	Neoxanthin	Violaxanthin	Lutein	α-Carotene	β-Carotene			
Monomeric Lhcb										
WT	64.6 ± 0.3[a]	35.5 ± 0.2[a]	5.8 ± 0.4[a]	4.1 ± 0.2[a]	16.1 ± 0.1[a]			3.8 ± 0.01[a]	0.6 ± 0.01[a]	0.4 ± 0.01[a]
szl1	65.7 ± 0.1[b]	34.3 ± 0.1[b]	0.1 ± 0.01[b]	0.9 ± 0.02[b]	20.4 ± 0.6[b]			4.7 ± 0.1[b]	1.0 ± 0.01[b]	0.04 ± 0.01[b]
chy1chy2	60.3 ± 0.5[c]	39.7 ± 0.5[c]	0.2 ± 0.01[b]	1.1 ± 0.1[b]	20.0 ± 0.7[b]			4.7 ± 0.2[b]	1.0 ± 0.01[b]	0.06 ± 0.01[b]
lut5	62.4 ± 0.1[d]	37.6 ± 0.1[d]	3.0 ± 0.1[c]	4.4 ± 0.2[a]	15.5 ± 0.4[a]			4.4 ± 0.1[c]	0.7 ± 0.01[c]	0.3 ± 0.01[c]
Trimeric LHCII										
WT	58.0 ± 0.3[a]	42.0 ± 0.3[a]	7.3 ± 0.6[a]	1.7 ± 0.1[a]	21.1 ± 0.3[a]			3.3 ± 0.1[a]	0.7 ± 0.01[a]	0.3 ± 0.01[a]
szl1	59.7 ± 0.4[b]	40.3 ± 0.4[b]	1.7 ± 0.1[b]	0.8 ± 0.02[b]	22.5 ± 0.1[b]			4.0 ± 0.01[b]	0.9 ± 0.01[b]	0.1 ± 0.01[b]
chy1chy2	56.2 ± 0.2[c]	43.8 ± 0.2[c]	1.2 ± 0.1[b]	0.8 ± 0.04[b]	22.3 ± 0.1[b]			4.1 ± 0.01[c]	0.9 ± 0.01[b]	0.1 ± 0.01[b]
lut5	56.0 ± 0.8[a,c]	44.0 ± 0.8[a,c]	5.0 ± 0.4[c]	1.6 ± 0.1[a]	19.7 ± 0.3[c]			3.8 ± 0.01[d]	0.8 ± 0.01[c]	0.3 ± 0.01[c]
PSII core complex										
WT	100.0 ± 0.0					0.8 ± 0.1[a]	17.6 ± 1.6[a]	5.5 ± 0.5[a]		
szl1	100.0 ± 0.0					3.6 ± 0.1[b]	6.8 ± 0.4[b]	9.7 ± 0.3[b]		
chy1chy2	100.0 ± 0.0					0.7 ± 0.1[a]	16.4 ± 0.1[a]	5.9 ± 0.01[a]		
lut5	100.0 ± 0.0					12.5 ± 0.2[c]	5.0 ± 0.2[c]	5.7 ± 0.03[a]		
PSI-LHCI										
WT	88.8 ± 0.1[a]	11.3 ± 0.1[a]		3.2 ± 0.2[a]	6.2 ± 0.4[a,d]	0.5 ± 0.1[a]	14.1 ± 1.3[a]	4.2 ± 0.2[a]	0.7 ± 0.03[a]	0.3 ± 0.03[a]
szl1	88.4 ± 0.1[a]	11.6 ± 0.1[a]		0.7 ± 0.1[b]	7.4 ± 0.3[a,c]	2.7 ± 0.1[b]	7.2 ± 0.4[b]	5.6 ± 0.1[b]	0.9 ± 0.01[b]	0.1 ± 0.01[b]
chy1chy2	86.1 ± 0.3[b]	13.9 ± 0.3[b]		0.8 ± 0.1[b]	7.9 ± 0.1[c]	0.4 ± 0.02[a]	15.0 ± 0.5[a]	4.2 ± 0.1[a]	0.9 ± 0.01[b]	0.1 ± 0.01[b]
lut5	87.0 ± 0.2[c]	13.0 ± 0.2[c]		2.0 ± 0.1[c]	5.6 ± 0.4[d]	10.3 ± 0.4[c]	6.3 ± 0.3[c]	4.1 ± 0.1[a]	0.7 ± 0.03[c]	0.3 ± 0.03[c]

Photosynthesis-Related Functions: ETR and Excess Energy Dissipation

Analysis of the fluorescence yield in dark-adapted leaves (Butler, 1978) revealed a significant decrease of the PSII maximum quantum efficiency (F_v/F_m) in *szl1* with respect to the other genotypes (Table I). In all mutants, the absolute values of F_m is slightly reduced with respect to the wild type, while only in *szl1* the F_0 value is 35% higher than the corresponding wild type. Thus, the decline in F_v/F_m in *slz1* is mainly due to F_0 rise (Table I), meaning that a larger fraction of absorbed energy is lost as fluorescence in this mutant; it suggests either that the connection between the major LHC and PSII reaction center is less efficient in carotene-depleted plants, or that PSII reaction center trapping efficiency is reduced.

To test the hypothesis that carotene content might affect photosynthetic electron transport, PSII function during photosynthesis was analyzed by Chl fluorometry. *szl1*, *chy1chy2*, and *lut5* showed no major differences with respect to wild-type plants either in the linear ETR or in the Q_A redox state (qL), as measured on leaves at different light intensities in the presence of saturating CO_2 (Fig. 2, A and B).

Capacity for Chl fluorescence quenching (qE), the rapidly reversible component of nonphotochemical quenching (NPQ), was plotted as a function of light intensity (Fig. 2C), and a reduction in qE activity was measured in *chy1chy2* and *lut5* plants. These results are consistent with previous reports (Niyogi et al., 1998; Dall'Osto et al., 2007b; Kim et al., 2009) showing a correlation between xanthophyll content, accumulation of zeaxanthin, and amplitude of qE. *szl1* leaves were also analyzed for their fluorescence quenching capacity, to investigate if carotene depletion affected qE amplitude. *szl1* showed a maximum value of qE lower than the wild type but similar to that of the other mutants. Since PsbS content was the same in wild-type and *szl1* plants (Li et al., 2009), we determined the capacity of intact chloroplasts to produce changes in lumenal pH by following the light-induced quenching of 9-aminoacridine (AA; Johnson et al., 1994). All mutants performed similar to the wild type at all light intensities (Fig. 2D). This suggests that the reduction of qE in *szl1* can be attributed to its lower xanthophyll cycle pool size, similar to that of *chy1chy2* mutant, rather than to the lower content of carotenes in the core complex of both PS.

Photosensitivity under HL at Chilling Temperature

Treatment of plants with strong light produced photoxidative stress, whose severity was enhanced by low temperature. Under these conditions, enhanced release of $^1O_2$ caused bleaching of pigments, lipid peroxidation, and PSII photoinhibition (Zhang and Scheller, 2004). To analyze the effect of missing carotenoids on the sensitivity to photoxidative stress, leaf discs from the wild type and mutants were subjected to HL + cold stress (2,400 μmol photons m^{-2} s^{-1}, 8°C), then the time course of pigment photobleaching was measured (Fig. 3A). Results indicate that the Chl bleaching rate was higher in *szl1* leaves, lower in the wild type and *chy1chy2*, while *lut5* leaves showed an intermediate behavior.

The level of stress caused by HL + cold treatment in the wild type and mutants was further investigated by measuring the extent of lipid peroxidation as detected by thermoluminescence (TL; Ducruet and Vavilin,

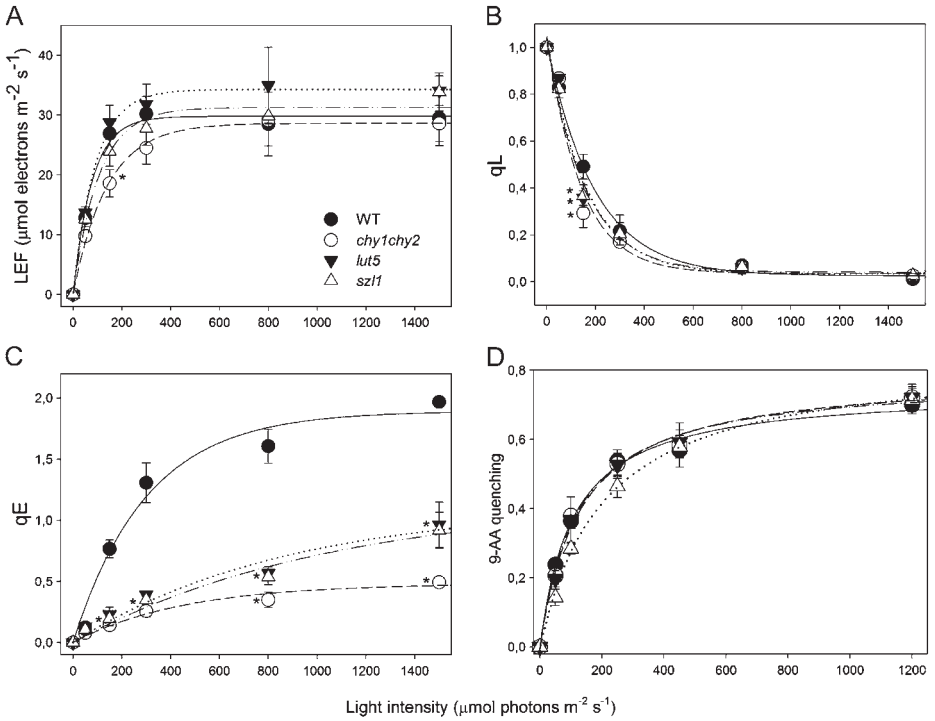

Figure 2. Analysis of room temperature Chl fluorescence during photosynthesis in wild-type and mutant plants. A, Dependence of the linear electron flow (LEF) on light intensity was measured in wild-type and mutant leaves. ETR was calculated as $\Phi_{PSII} \cdot PAR \cdot A_{leaf} \cdot fraction_{PSII}$ (see "Materials and Methods" for details). B, Amplitude of qL measured at different light intensities. qL reflects the redox state of the primary electron acceptor Q_A, thus the fraction of open PSII centers. C, Dependence of qE, the rapidly reversible component of NPQ, on light intensity. Data are expressed as means ± SD (n = 4). D, Amplitude of light-dependent quenching of 9-AA fluorescence, measured at different light intensities on intact chloroplasts. 9-AA fluorescence quenching is induced by actinic illumination of chloroplasts and reflects the amplitude of transthylakoid ΔpH buildup. Values that are significantly different ($P < 0.05$) from the wild type are marked with an asterisk (*).

1999). Figure 3B shows plots of TL amplitudes at different time points during exposure of leaf discs to HL + cold stress (800 μmol photons m^{-2} s^{-1}, 8°C). The highest levels of lipid peroxidation upon HL treatment was observed in *szl1*, followed by *lut5* while *chy1chy2* was only slightly more photosensitive than the wild type. Measurement of the $^1O_2$ production in leaves (Fig. 3C) was consistent with pigment bleaching and lipid peroxidation measurements: At the end of the treatment, the wild type showed the lowest level of singlet oxygen sensor green (SOSG) fluorescence, while *szl1* the highest; *chy1chy2* and *lut5* had intermediate behavior. Instead, after illumination with HL, *szl1* leaves showed significantly lower yield in reduced forms of ROS (namely, hydrogen peroxide, O_2^-, and OH·) with respect to all the other genotypes at each time point (Supplemental Fig. S1).

The enhanced photosensitivity of *szl1* plants could be caused by impaired photoprotection at either PSII, PSI, or both. To determine the primary target of photooxidation in *szl1* leaves upon exposure at HL and low temperature, kinetics of PSII and PSI photoinhibition were determined. The sensitivity to photoxidative stress in wild-type and mutant plants was assessed upon their transfer from control conditions to HL + cold stress (550 μmol photons m^{-2} s^{-1}, 8°C), upon which the levels of F_v/F_m, the maximal photochemical yield of PSII, were monitored for 9 h; results are reported on Figure 4A. In wild-type plants F_v/F_m gradually decreased from 0.8 to 0.6 during the treatment (halftime of PSII photoinhibition of approximately 20 h), similar to the behavior of *chy1chy2.* In *lut5*, however, F_v/F_m was more affected by the treatment, down to a value of 0.4 at the end of the treatment. The *szl1* plants were as photosensitive as *lut5*, since their F_v/F_m decreased to 0.35 at the end of the treatment, corresponding to a halftime for PSII photoinhibition of approximately 5.5 h. Measurements of F_v/F_m recovery after photoinhibitory treatment clearly showed the same rate of PSII quantum efficiency recovery in all genotypes (Supplemental Fig. S2), implying that the higher photosensitivity is due to a less-effective photoprotection rather than to impaired PSII repair mechanism (Aro et al., 1994).

Upon exposure to photoxidative stress, F_0 and F_m changes showed different kinetics in wild-type and mutant leaves (Supplemental Fig. S3). Stress treatment resulted in a decrease of F_m in all genotypes, likely due to photoinactivation of PSII reaction centers, which then dissipate excitation energy as heat rather than as photochemistry (Baker, 2008). Instead, while HL + cold stress was associated with an increase in F_0 in *chy1chy2*, *lut5*, and wild-type plants, as expected upon oxidative damage of PSII RC, *szl1* plants showed a slight reduction of F_0 value with time of treatment (Supplemental Fig. S3). The *szl1* F_0 changes could be traced back to the massive Chl bleaching of this genotype upon photoxidative stress (Fig. 3A) that are likely to affect the fluorescence emission per leaf surface area.

The kinetic of PSI photoinhibition was assessed by measuring the maximum content of photoxidizable P700 upon transfer of plants from control conditions to HL + cold stress. These stress conditions had a much more dramatic effect on photoinhibition of PSI with respect to that of PSII in Arabidopsis, in agreement with previous results (Zhang and Scheller, 2004).

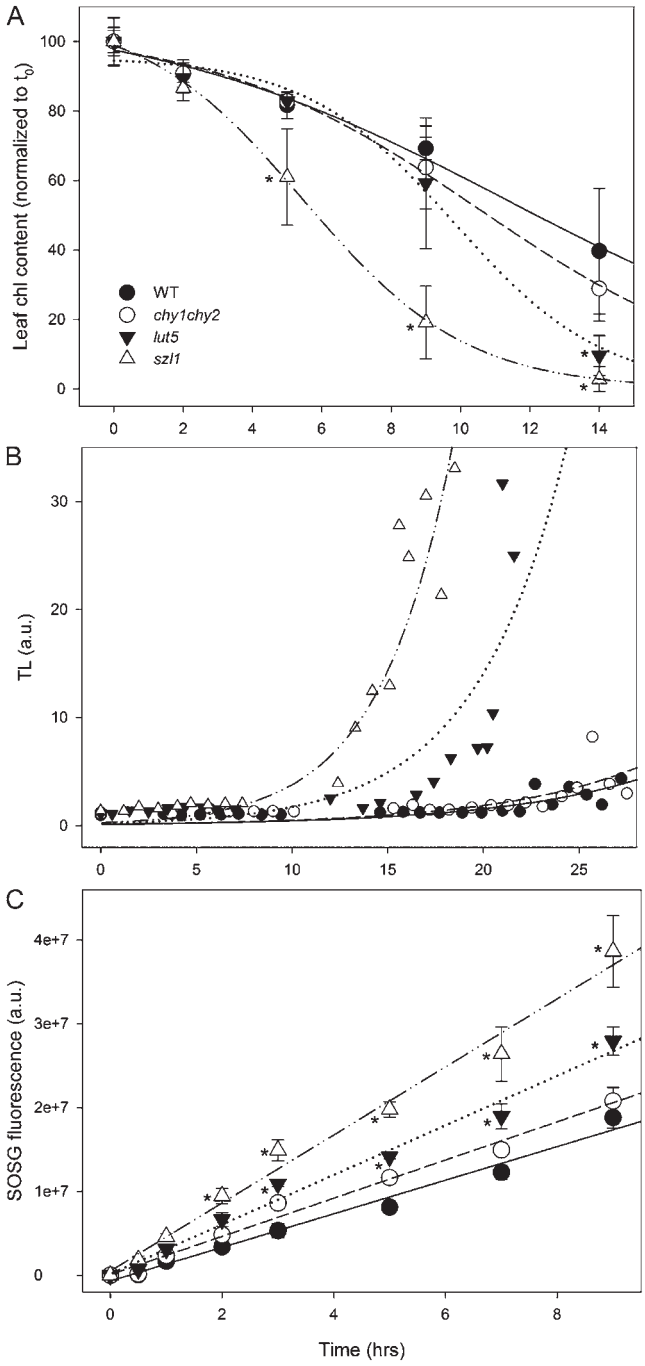

Figure 3. Photooxidation of Arabidopsis wild-type and mutant genotypes under photoxidative stress. A, Detached leaves floating on water were treated at 2,400 μmol photons m^{-2} s^{-1} at 8°C, and kinetics of Chl bleaching were recorded. Data are expressed as means ± SD ($n = 6$). B, Wild-type and mutant leaves floating on water were exposed to 800 μmol photons m^{-2} s^{-1} at 8°C, and photooxidation was estimated from the extent of lipid peroxidation measured by high-temperature TL. Each experimental point corresponds to a different sample. a.u., Arbitrary units. See "Materials and Methods" for details. C, Wild-type and mutant detached leaves were vacuum infiltrated with 5 μM SOSG, a $^1O_2$-specific fluorogenic probe. SOSG increases its fluorescence emission upon reaction with $^1O_2$. The increase in the probe emission was followed during illumination with red actinic light (550 μmol photons m^{-2} s^{-1}) at 8°C. a.u., Arbitrary units. Values that are significantly different ($P < 0.05$) from the wild type are marked with an asterisk (*).

Indeed, the photoxidizable P700 gradually decreased to 50% of its initial value in 4.5 h and to 30% at the end of the 9-h treatment in wild-type plants (Fig. 4B). The halftime of photoinhibition was shorter for *chy1chy2* and *lut5* genotypes (being 50% inhibited in 2.5 and 4 h, respectively). Surprisingly, the halftime of PSI photoinhibition was far shorter for *szl1* plants (approximately 0.6 h) than in the other genotypes.

To further quantify the PSI damage, the maximum level of $P700^+$ was measured upon a saturating flash under a far-red-light background, before and after HL treatment (Munekage et al., 2002). The decrease in the $P700^+$ level might be caused not only by PSI photoinhibition, but also by an overreduced state of acceptors and activation of cyclic electron flow (Sonoike, 2011; Rutherford et al., 2012). To evaluate the extent of PSI photoinhibition, leaves were vacuum infiltrated with methyl viologen upon the HL treatment; electron acceptance from PSI by methyl viologen restored the maximum oxidation of P700. Results (Supplemental Table S1) show that in the wild type less than 25% of PSI was damaged, whereas in *szl1* up to 80% of PSI was inactivated.

$^1O_2$ Production from Purified Pigment-Protein Complexes

The above results (Figs. 3 and 4) suggest a role for carotenes in photoprotection of both PSII and PSI reaction centers, possibly in limiting the $^1O_2$ release into the lipid phase. Although this result is consistent with carotene location in PSI-LHCI and PSII core complexes, it is relevant to experimentally assess whether photodamage is due to the properties of the pigment-binding proteins or is caused by pleiotropic factors. To this aim, we purified PSII core, Lhcb antenna proteins, and PSI-LHCI supercomplex and determined their $^1O_2$ production when illuminated with strong light (see "Materials and Methods" for details). When isolated Chl-binding complexes are exposed to strong light, $^1O_2$ is produced as the main ROS involved in the photoinhibition of both PS (Triantaphylidès et al., 2008) deriving from the reaction of excited Chl (^{3}Chl*) with molecular oxygen. The level of $^1O_2$ production by isolated complexes strongly depends on carotenoid composition and is inversely correlated with the capacity of ^{3}Chl* quenching and ROS scavenging by bound xanthophylls (Mozzo et al., 2008; Dall'Osto et al., 2010; de Bianchi et al., 2011).

Results of $^1O_2$ production at 20°C by the different complexes isolated from the wild type and *szl1* are reported in Figure 5. PSII core complexes from the wild type, *chy1chy2*, and *lut5* showed a similar yield of $^1O_2$ at each light intensity tested, up to 800 μmol photons m^{-2} s^{-1}. The complexes from *szl1* showed an

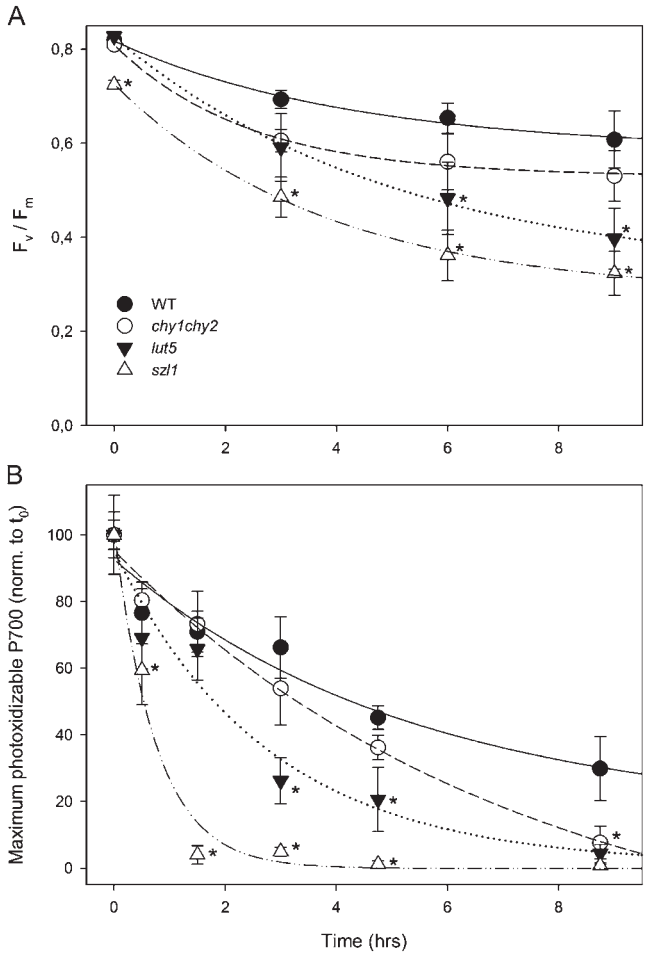

Figure 4. Photoinhibition of the wild type and mutants exposed to HL and low temperature. Kinetics of F_v/F_m decay (PSII photoinhibition) and maximum photoxidizable P700 decay (PSI photoinhibition) were measured on the wild type and mutants. Whole plants were exposed to 550 μmol photons m^{-2} s^{-1} at 8°C. Data are expressed as means ± SD ($n \geq 5$). Values that are significantly different ($P < 0.05$) from the wild type are marked with an asterisk (*). t_0, Time zero.

approximately 30% increase in $^1O_2$ production at low and moderate light intensities while the differences were less evident at higher light when the signal from all complexes tended to saturation (Fig. 5A). Measurements of Lhcb fractions (Fig. 5B) from the different genotypes did not show the same pattern. In fact, the complexes from *chy1chy2* and *szl1* showed an approximately 70% increase in $^1O_2$ production with respect to the corresponding fraction from the wild type and *lut5*, consistent with the lower β,β-xanthophyll content (Dall'Osto et al., 2007b). Similar results were obtained by measuring PSII-LHCII: Supercomplexes from *szl1* and *chy1chy2* showed an approximately 25% increase in $^1O_2$ production at moderate light intensities, with respect to both the wild type and *lut5*. In the case of PSI, the core complex and the antenna moieties form a stable complex that cannot be dissociated without some level of damage. We therefore measured $^1O_2$ production on PSI-LHCI supercomplexes. Clearly, the $^1O_2$ yield was 2-fold higher in the preparation from *szl1* with respect to that of the wild type (Fig. 5D). In contrast, $^1O_2$ yield from the PSI-LHCI complex of *chy1chy2* and *lut5* was only slightly higher than the wild type. Pigment-protein photoprotection was further evaluated from the ability to prevent Chl photobleaching via thermal deactivation of ^{3}Chl* by carotenoids under strong white light illumination in atmosphere. The PSII core complex from *szl1* did not show any reduction of its rate of bleaching ($t_{50\%}$ bleaching) with respect to the wild type. On the contrary, PSI-LHCI from *szl1* plants was less photoprotected, as shown by the 28% reduction in $t_{50\%}$ bleaching (Supplemental Fig. S4).

DISCUSSION

In this work, we have investigated the role of carotene versus xanthophyll ligands in the photosynthetic apparatus, focusing on their photoprotective capacity for both PS. A panel of Arabidopsis mutants affected in the carotenoid biosynthesis pathways was compared: In fact, due to the intermediate position of carotenes in the carotenoids biosynthesis pathway, it is impossible to affect their abundance without inducing changes in the xanthophylls, which are downstream in the metabolic pathway. The major target of our analysis was the mutant *szl1*, depleted in carotenes due to a lower β-cyclase activity (Li et al., 2009). When exposed to HL at low temperature, *szl1* plants showed the highest levels of pigment bleaching and lipid peroxidation among the genotypes considered in this study. Interestingly, carotene depletion in *szl1* plants preferentially affects PSI activity, since mutant plants revealed far stronger photoinhibition of PSI with respect to PSII. Thus, it appears that photoprotection efficiency strongly depends on carotene content of PS. It should be noted, however, that the *szl1* mutation, besides decreasing carotene content, also favors ε-branch versus β-branch xanthophylls, thus modifying the chromophore composition of the xanthophyll-binding Lhc subunits of the antenna system and increasing the α-carotene, usually a minor component, versus the normally found β-carotene. Comparison with the photoprotection phenotype of the *chy1chy2* and *lut5* is thus important to assess if the phenotype can be attributed in part to changes in xanthophyll composition, which is very similar in *szl1* and *chy1chy2*, or to the enrichment in α-carotene, a feature observed in both *szl1* and *lut5*.

Altered Xanthophyll Composition Affects Photoprotection Capacity

Photoprotection by carotenoids is performed by multiple mechanisms including quenching of Chl triplet states (Peterman et al., 1995; Mozzo et al., 2008), scavenging of both superoxide and hydroxyl radicals (Trevithick-Sutton et al., 2006), and quenching of $^1O_2$, thus preventing lipid peroxidation (Havaux and Niyogi, 1999). In addition, ROS production can be

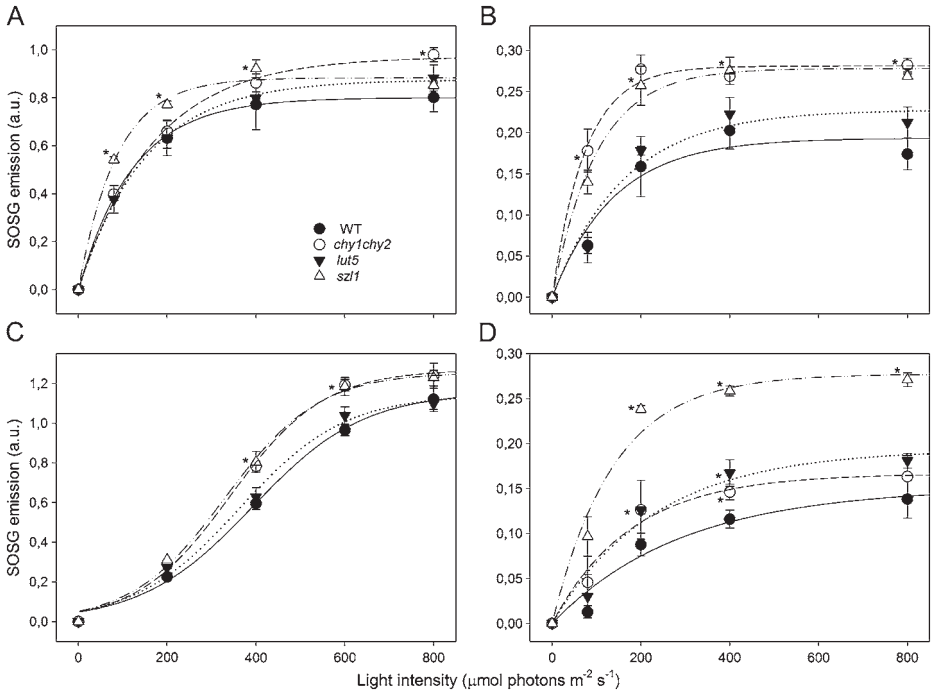

Figure 5. $^1O_2$ production from carotenoid-binding complexes. Dependence of $^1O_2$ release on light intensity was measured on purified PSII core (A), Lhcb (B), PSII-LHCII (C), and PSI-LHCI (D) supercomplexes. SOSG was used as $^1O_2$-specific fluorogenic probe, since it increases its fluorescence emission upon reaction with $^1O_2$ in solution. Symbols and error bars show means ± SD (n = 3). Values that are significantly different ($P < 0.05$) from the wild type are marked with an asterisk (*).

prevented by quenching of singlet Chl excited states, a function that is enhanced by lutein and zeaxanthin (Niyogi et al., 2001; Dall'Osto et al., 2005). The strong phenotypes of Arabidopsis mutants with altered xanthophyll composition (Niyogi et al., 2001; Dall'Osto et al., 2007b; Kim et al., 2009) showed that the presence and relative amounts of these pigments is relevant for plant fitness. We observed that *chy1chy2* plants are more sensitive to photoxidative stress than the wild type (Fig. 3). The total xanthophyll content is only slightly reduced in this mutant (Table II), and yet the β,β/ε,β-xanthophyll ratio is 8-fold decreased in the mutant, and in its LHC proteins (Table III). Previous work showed that optimal photoprotection of Lhc proteins depends on the balanced activity in ROS scavenging by β,β-xanthophylls and Chl triplet quenching by lutein (Dall'Osto et al., 2007b). Indeed, we observed an increased rate of $^1O_2$ release from antenna proteins purified from *chy1chy2*, with β,β-xanthophylls partially replaced by lutein, with respect to the corresponding preparation from the wild type (Fig. 5B). In particular, it appears that depletion in neoxanthin is a major factor, consistent with recent reports (Mozzo et al., 2008). Besides neoxanthin, violaxanthin and zeaxanthin are also effective in preventing photodamage since the effect of their depletion is observed in PSI-LHCI complex, which does not bind neoxanthin, isolated from *chy1chy2* plants (Table III). It should be noted that the assembly of PSI-LHCI supercomplexes is not impaired in *chy1chy2*, as shown by the migration rate of the supercomplex in the native PAGE identical to the wild type (Fig. 1).

Since Lhca and Lhcb proteins from *chy1chy2* and *szl1* have essentially the same β,β/ε,β-xanthophyll ratio and the same total xanthophyll content, the extreme sensitivity of *szl1* to excess light cannot be explained based on differences in the xanthophyll composition and/or organization of the antenna proteins, implying that additional sensitivity factors are present in *szl1* plants.

Altered Xanthophyll/Carotene Ratio Leads to Enhanced Photoxidation

Kinetics of pigment bleaching and lipid peroxidation clearly showed that *lut5* and *szl1* are much more sensitive to photoxidative stress with respect to both the wild type and *chy1chy2* (Fig. 3) while the discussion above led to the conclusion that this is not due to their xanthophyll composition. A striking difference between *lut5* and *szl1* plants is their carotenoid composition: a low xanthophyll content per Chl in the former (−25% with respect to the wild type, see Table II), and a high xanthophyll/carotene ratio in the latter (+50% compared with the wild type), and yet both conditions lead to a strong light sensitivity with respect to wild-type plants. We have shown above that the β,β/ε,β-xanthophyll ratio cannot be the cause for differential photosensitivity, since this is the same in *chy1chy2* and *szl1*, which exhibit very different levels of lipid peroxidation (Fig. 3). Overreduction of the plastoquinone pool is commonly associated with photoinhibition in wild-type plants, and yet the plastoquinone redox state was not significantly different in *lut5* or *szl1* with respect to *chy1chy2* (Fig. 2). Zeaxanthin accumulation in HL, which provides photoprotection by both modulating qE and scavenging $^1O_2$ in the lipid phase (Niyogi et al., 1998; Havaux and Niyogi, 1999), cannot account for the higher sensitivity of *szl1*

plants. Indeed, *szl1* showed a marked increase in both the accumulation of zeaxanthin (+40% compared with *lut5*, Table II) and rate of $^1O_2$ release in HL (Fig. 3C), while release of reduced ROS is far lower than in other genotypes (Supplemental Fig. S1).

Important differences between *szl1* and *lut5* are the strong depletion in Lhcb proteins (Fig. 1) and reduction in PSII functional antenna size (Table I) in *lut5*, while the PSII antenna size of *szl1* plants is the same as the wild type (Table I). It should be noted that only the abundance of Lhcb proteins is affected by the *lut5* mutation, whereas the Lhca assembly into PSI-LHCI supercomplexes is not disturbed, as shown by the identical migration of PSI-LHCI supercomplexes in native PAGE (Fig. 1; Dall'Osto et al., 2007b, 2010). We conclude that carotenes, although present in abundance, cannot replace xanthophylls in stabilizing Lhc proteins, and Lhcb proteins contribute to PSII photoprotection. Despite the observation that *lut5* and *szl1* are the most contrasting genotypes with respect to their Lhcb content (Fig. 1), *lut5* plants are still less photosensitive than *szl1* (Fig. 4), implying that the reason(s) for higher photosensitivity of *szl1* cannot be attributed to differences in composition or size of the antenna moiety of the PS.

Differences in the xanthophyll composition of Lhcb proteins from the wild type and mutants account for differential photosensitivity (Fig. 5), with proteins from *szl1* producing more $^1O_2$ at all light intensities with respect to both the wild type and *lut5*, and similar to the same fraction from *chy1chy2* (Tables II and III). Although caution should be applied when considering assays on isolated complexes as the reflection of an in vivo situation, it is worth noting that *szl1* is clearly more sensitive than *chy1chy2*, thus an additional source of sensitivity is present in *szl1*, deriving from a different component of the photosynthetic apparatus, specifically affected by the mutation. We observed that the $^1O_2$ production from purified PSII core complexes is similar in the complexes from all genotypes but *szl1* (Fig. 5A), which evolves more $^1O_2$, particularly at low-light intensity, a feature that correlates with the depletion in β-carotene content of PSII cores and strongly suggests this is a factor for increased photosensitivity of *szl1*. Yet, the increase in $^1O_2$ yield from the carotenoid-depleted PSII core is rather small (Fig. 5A) when compared with the effect of altered $\beta,\beta/\varepsilon,\beta$-xanthophyll ratio in the Lhc proteins (Fig. 5B).

β-Carotene depletion in *szl1* is evident not only in the PSII core but in PSI as well. Figure 5D shows that PSI-LHCI complex from *szl1* showed a marked increase in the rate of $^1O_2$ release (2-fold) in HL with respect to the wild-type complex, while PSI-LHCI from *chy1chy2* and *lut5* were less affected (Fig. 5C). Taken together, the above results show that *szl1* plants are specifically affected in PSI complex, leading to a dramatic photosensitivity of PSI activity at any light intensity. It is particularly remarkable that PSI, which in the literature has been considered to be the more resistant of the two PS, was preferentially affected by the deficiency of carotenes.

Besides carotene depletion, a further feature of *szl1* mutants is the presence of α-carotene in both PSI-LHCI and PSII core complexes, partially replacing β-carotene and potentially being a cause for photosensitivity (Table III). However, the *lut5* genotype has a far higher α/β-carotene ratio than *szl1* in both thylakoid (Table II) and isolated PSII core complexes (Table III), and yet isolated PSII core complexes and PSI-LHCI from this genotype did not show major differences in $^1O_2$ production with respect to the complexes from the wild type (Fig. 5A), implying that α-carotene is not the major cause of photosensitivity.

What Is the Origin of the Extreme PSI Photosensitivity in szl1 Plants?

In the PSII core complex, most of the β-carotene molecules are in close contact with Chls, as required for effective quenching of ^{3}Chl* (Ferreira et al., 2004). The only exception is represented by the two β-carotene ligands in the PSII reaction center, whose distance from the special pair P680 is higher, implying that they cannot quench ^{3}P680* by triplet-triplet transfer and rather, they likely act as scavengers for $^1O_2$ produced during charge recombination (Telfer et al., 1991, 1994b). PSII has been indicated as the primary target of photoinhibition (Andersson et al., 1992; Aro et al., 1993), since the D1 subunit is easily damaged in HL and rapidly turned over. Instead, $P700^+$ was reported to be protective for PSI, since it can quench excitation energy and oxidize the reduced electron acceptor of PSI and remove excess reducing power (Sonoike, 2011). However, ^{3}P680 and ^{3}P700 lie close in energy level, thus both are prone to react with oxygen and yield $^1O_2$. ^{3}P700 results from charge recombination, therefore its yield is increased by acceptor side limiting conditions (Rutherford et al., 2012). Furthermore, exposure of PSI-LHCI to HL generates ^{3}Car* mainly associated with LHCI (Santabarbara and Carbonera, 2005), while a selective bleaching of lutein molecules located in the outer antenna was observed (Andreeva et al., 2007), thus raising the question of what the role for carotene ligands is.

When comparing photoinhibition of *szl1* and *lut5* plants at HL + cold stress, the halftime of F_v/F_m decay (PSII photoinhibition, see Fig. 4A), as well as PSII repair efficiency (Supplemental Fig. S2), were very similar for both genotypes, while the *szl1* genotype was far more sensitive to PSI photoinhibition with respect to the other genotypes, as shown by a 6-fold-faster PSI photoinhibition rate (Fig. 4B). This is consistent with the quantification of $^1O_2$ released in HL by purified pigment-protein complexes: The $^1O_2$ yield was 2-fold higher in the PSI-LHCI from *szl1* with respect to that from the wild type (Fig. 5C), while PSII core complexes from all genotypes showed a similar yield of $^1O_2$ at each light intensity tested (Fig. 5A). What is the origin of the extreme PSI photosensitivity in *szl1* plants?

While PSII has an efficient repair machinery (Aro et al., 1993), a similar mechanism is not known for PSI:

After light-induced damage, recovery of PSI from photoinhibition takes several days (Sonoike and Terashima, 1994; Sonoike, 2011); indeed, the damage to PSI is considered to be essentially irreversible and involves degradation and resynthesis of the whole complex.

Because of its irreversibility, PSI photoinhibition must be specially avoided. This is accomplished by a number of protective mechanisms, namely cyclic electron transport (Munekage et al., 2002) and the stromal scavenging enzyme systems superoxide dismutase and ascorbate peroxidase, which scavenge reduced ROS released by PSI (Asada, 1999). In several plant species including Arabidopsis, PSI becomes more sensitive to photoinhibition under specific environmental conditions such as chilling temperature, likely because the protective mechanisms are less efficient at low temperature (Sonoike, 2011); furthermore, the sink of reductants is decreased at low temperature, thus overreduction of the electron chain occurs and the yield of ^{3}P700 and $^1O_2$ increases. Indeed, the primary target for PSI photoinhibition upon illumination was located in the iron-sulfur centers F_X, F_B, and F_A, and was caused by ROS (Inoue et al., 1986; Tjus and Andersson, 1993). Here, we show that HL + cold stress is effective in damaging PSI even in wild-type plants (Fig. 4B), and that this effect is greatly enhanced in carotene-depleted *szl1* plants, implying that carotene ligands in PSI are crucial in ensuring the maintenance of PSI activity under this condition.

When searching for the molecular mechanism(s) behind the preferential damage of PSI in *szl1*, it can be hypothesized that carotene composition might affect the susceptibility to photoinhibition of the mutant. Indeed, a clear difference between the wild type and *szl1* is the presence of α-carotene in PSI-LHCI of the mutant, partially replacing β-carotene. It is worth noting that PSI-LHCI from *lut5* plants has a higher α/β-carotene ratio than *szl1*, and roughly the same xanthophyll content (Table III). However, a faster PSI photoinhibition (Fig. 4B) and a higher release of $^1O_2$ from PSI-LHCI (Fig. 5C) were observed with respect to the wild type. On this basis, we cannot completely exclude the possibility that part of the PSI photosensitivity of *szl1* plants was related to the α-carotene content of either core complex or LHCI.

Moreover, PSI stability might be limited by the amount of carotene molecules available. Indeed, a recent improved model of plant PSI (Amunts et al., 2010) suggested that most of β-carotene molecules are coordinated by either different subunits or distant region of the same subunit; therefore, these pigments might have a key role for PSI structural integrity, and it is consistent with the high degree of conservation of their positions and coordination between plants and cyanobacteria (Amunts et al., 2010). In *szl1* plants, a general weakening of the PSI-LHCI structure would make the complex more susceptible to ROS attack thus causing degradation, as shown by native-PAGE analysis (Fig. 1). However, the photobleaching kinetics of PSI-LHCI complexes, challenged with strong light (Supplemental Fig. S4), show that this pigment-protein complex from *szl1* is rather stable.

Alternatively, rather than the PSI core complex, the peripheral light-harvesting system might be more affected by carotene depletion. Indeed, it should be stressed that β-carotene is a ligand not only of the wild-type PSI core complex, but also of LHCI antenna moiety (Wehner et al., 2004). A recent report (Alboresi et al., 2009) showed that preferential degradation of LHCI upon illumination of isolated PSI-LHCI is effective in protecting the catalytic activity of the complex. Recovery from PSI photoinhibition is an energetically demanding process, since it necessarily requires degradation and resynthesis of the whole complex; thus, sacrificing the antennae would be a photoprotective strategy evolved to limit photoxidative damage into LHCI moiety and preserve the integrity of iron-sulfur clusters. The role of LHCI proteins as safety valves for PSI is related to the red absorption forms (Carbonera et al., 2005; Alboresi et al., 2009), Chls of the outer antenna with low energy level that concentrate the excitation energy before transfer to the reaction center (Croce et al., 1996); ^{3}Chl* eventually formed by the red Chls are quenched by nearby carotenoids (Carbonera et al., 2005). This model implies that, as shown for Lhcb, Lhca proteins constitutively undergo formation of ^{3}Chl* and production of $^1O_2$. Carotenoid species bound to the LHCI, namely lutein, violaxanthin, and β-carotene, could be directly involved in triplet quenching and/or ROS scavenging, and likely occupy selective binding sites and serve distinct roles. Impairing one of these functions by changing the occupancy of specific carotenoid binding sites through mutations in the biosynthetic pathway leads to photosensitivity, similar to what observed previously within PSII antenna system (Dall'Osto et al., 2007b).

CONCLUSION

Here we show that the *szl1* plants, which carry a point mutation in the LCYB gene and thus a less-active β-cyclase than the wild type (Li et al., 2009), have a lower carotene content in both PS with respect to wild-type plants and altered xanthophyll composition of the light-harvesting component of the antenna systems. Physiological characterization of the *szl1* mutant offered the possibility of probing carotene function in vivo differentially from the effect on xanthophyll complement. When challenged with HL + cold stress, *szl1* mutant plants undergo more photodamage than the wild type, particularly within PSI-LHCI, despite the fact that PSI-LHCI was less depleted in carotenes than PSII. Comparison with the *chy1chy2* and *lut5* mutants, which respectively share with *szl1* alterations in xanthophyll composition and α-carotene accumulation, showed that these features were not the major factors causing enhanced susceptibility to photoinhibition and pointed to carotene depletion in photosynthetic core complexes as the major source of photodamage. It is

evident that regulation of PSI Chl excited states under HL + cold stress is crucial for protection of the photosynthetic apparatus.

MATERIALS AND METHODS

Plant Material and Growth Conditions

Wild-type plants of Arabidopsis (*Arabidopsis thaliana*) ecotype Columbia and mutants *chy1chy2*, *lut5*, and *szl1* were obtained as previously reported (Fiore et al., 2006; Li et al., 2009). T-DNA knockout lines used are: *chy1* (SAIL line 49A07), *chy2* (SAIL line 1242B12), and *lut5* (SALK line 116660). Plants were grown for 4 weeks on Sundermisch potting mix (Gramoflor) in controlled conditions of 8 h light, 23°C/16 h dark, 20°C, with a light intensity of 100 μmol photons m^{-2} s^{-1}.

Stress Conditions

For HL treatments, light was provided by 150-W halogen lamps (Focus 3, Prisma). Short-term HL treatment was performed for 1 h at 550 μmol photons m^{-2} s^{-1} at 8°C to measure maximum zeaxanthin accumulation on detached leaves floating on water. Samples for HPLC analysis were rapidly frozen in liquid nitrogen prior to pigment extraction. Photooxidative stress was induced in either whole plants or detached leaves by a strong light treatment. Whole Arabidopsis plants were exposed to HL (550 μmol photons m^{-2} s^{-1} with a photoperiod day/night of 16/8 h) at 8°C for 2 d; detached leaves were exposed to either 800 or 2,400 μmol photons m^{-2} s^{-1} at 8°C for 14 h.

Chloroplasts and Thylakoids Isolation

Chloroplasts and stacked thylakoid membranes were isolated from wild-type and mutant leaves as previously described (Casazza et al., 2001).

Pigment Analyses

Pigments were extracted from leaves with 80% acetone, then separated and quantified by HPLC (Gilmore and Yamamoto, 1991). Chl content was determined by fitting the spectrum of the sample's acetone extract with the spectra of individual pigments, as described previously (Croce et al., 2000).

Gel Electrophoresis

Nondenaturing Deriphat-PAGE was performed following the method described previously (Peter et al., 1991) but using 3.5% (w/v) acrylamide (38:1 acrylamide/bisacrylamide) in the stacking gel and in the resolving gel an acrylamide concentration gradient from 4.5% to 11.5% (w/v) stabilized by a glycerol gradient from 8% to 16%. Thylakoids concentrated at 1 mg/mL Chl were solubilized with either 0.8% α-DM or 1% β-DM, and 20 μg of Chls were loaded in each lane. Signal amplitude was quantified using the GelPro 3.2 software (BIORAD). Purified pigment-protein complexes were excised from gel and eluted with a pestle in a buffer containing 10 mM HEPES pH 7.5, 0.05% α-DM.

Analysis of Chl Fluorescence and P700 Redox Kinetics

PSII function during photosynthesis was measured through Chl fluorescence on whole leaves at room temperature with a PAM 101 fluorimeter (Heinz-Walz; Andersson et al., 2001), using a saturating light pulse of 4,500 μmol photons m^{-2} s^{-1}, 0.6 s, and white actinic light ranging from 50 to 1,100 μmol photons m^{-2} s^{-1}, supplied by a KL1500 halogen lamp (Schott). NPQ, ϕ_{PSII}, photochemical quenching (qP), qL, and ETR were calculated according to the following equations (Van Kooten and Snel, 1990; Baker, 2008): $NPQ = (F_m - F_m')/F_m'$, $\phi_{PSII} = (F_m' - F_s)/F_m'$, $qP = (F_m' - F_s)/(F_m' - F_0')$, $qL = qP \cdot F_0'/F_s$, $ETR = \phi_{PSII} \cdot PAR \cdot A_{leaf} \cdot fraction_{PSII}$, where F_0/F_0' is the minimal fluorescence from dark/light-adapted leaf, F_m/F_m' is the maximal fluorescence from dark/light-adapted leaves measured after the application of a saturating flash, F_s the stationary fluorescence during illumination, and PAR the photosynthetic active radiation; A_{leaf} (leaf absorptivity) was 0.67 ± 0.04 for the wild type, 0.59 ± 0.04 for *chy1chy2*, 0.61 ± 0.03 for *lut5*, 0.58 ± 0.05 for *szl1*; $fraction_{PSII}$ was measured by densitometric analysis of Deriphat-PAGE. Calculation of ΔpH-dependent component of qE was performed as described previously (Walters and Horton, 1995). Fluorescence kinetics were measured with a home-built setup, in which leaves were vacuum infiltrated with 3.0×10^{-5} M DCMU, 150 mM sorbitol, and were excited with green light at 520 nm (Luxeon, Lumileds), and emission was measured in the near far red (Rappaport et al., 2007). The halftime of the fluorescence rise was taken as a measure of the functional antenna size of PSII (Malkin et al., 1981).

P700 redox state measurements were performed using a LED spectrophotometer (JTS10, Biologic Science Instruments) in which absorption changes were sampled by weak monochromatic flashes (10-nm bandwidth).

Spectroscopy

Steady-state spectra were obtained using samples in 10 mM HEPES pH 7.5, 0.05% $\alpha(\beta)$-DM, 0.2 M Suc. Absorption measurements were performed using a SLM-Aminco DW-2000 spectrophotometer at room temperature. Fluorescence emission spectra were measured at room temperature using a Jobin-Yvon Fluoromax-3 spectrofluorimeter, equipped with a fiberoptic to measure emission of fluorogenic probes on vacuum-infiltrated leaves. Measure of ΔpH—the kinetics of ΔpH formation across the thylakoid membrane was measured using the method of 9-AA fluorescence quenching (Johnson et al., 1994) with modifications described in de Bianchi et al. (2008).

Measurements of ROS Production

Measurements of $^1O_2$ production from purified pigment-protein complexes were performed with a specific fluorogenic probes, SOSG (Invitrogen; Dall'Osto et al., 2010). SOSG is a $^1O_2$ highly selective fluorescent probe, that increases its 530-nm emission band in presence of this ROS species (Flors et al., 2006). Pigment-protein complexes were diluted in a reaction buffer (10 mM HEPES pH 7.5, 0.05% α-DM, 2 μM SOSG) to the same absorption area in the wavelength range 600 to 750 nm (about 2 μg Chls/mL), to measure $^1O_2$ yield for complexes having the same level of light-harvesting capacity. Isolated complexes were illuminated with red light ($\lambda > 600$ nm, 20°C, 5 min) and fluorescence yield of SOSG were determined before and after HL treatment (Dall'Osto et al., 2007a). Measurements of $^1O_2$ production from leaves were performed with leaf discs vacuum infiltrated with 200 μM SOSG in 50 mM phosphate buffer (pH 7.5), then illuminated with red light ($\lambda > 600$ nm, 550 μmol photons m^{-2} s^{-1}, 8°C) as previously described (Dall'Osto et al., 2010). At different times, leaf discs were harvested and SOSG fluorescence was measured. Measurements of reduced ROS (hydrogen peroxide, OH·, and O_2^-) production from leaves were performed with dichlorofluorescein diacetate, a specific fluorogenic ROS probe, and nitroblue tetrazolium. Leaf discs, after the different times of HL treatment, were infiltrated under vacuum with a solution of 200 μM dichlorofluorescein diacetate in 50 mM phosphate buffer (pH 7.5) and maintained in the dark for 30 min. Following excitation at 490 nm, the fluorescence emission at 530 nm was then detected. The NBT staining method was used for in situ detection and quantification of superoxide radical, as previously described (Ramel et al., 2009).

Determination of the Sensitivity to Photoxidative Stress

HL treatment was performed for 2 d at 550 μmol photons m^{-2} s^{-1}, 8°C on whole plants. Decay kinetics of maximal quantum yield of PSII photochemistry (F_v/F_m; Havaux et al., 2004) and maximum content of photooxidizable P700 (ΔA_{max} at 705 nm; Yang et al., 2010) were recorded on detached leaves during illumination to assess inhibition of PSII and PSI, respectively. Content of oxidizable P700 (ΔA_{max}) was recorded during far-red-light illumination (2,500 μmol photons m^{-2} s^{-1}, λ_{max} = 720 nm); to have a precise estimation of the PSI photoinhibition, ΔA_{max} has been determined in detached leaves, vacuum infiltrated with 50 μM dibromothymoquinone and 1 mM methyl viologen (Sonoike, 2011). The maximum contents of $P700^+$ was also determined on methylviologen-treated leaves using a saturating flash (3,000 μmol photons m^{-2} s^{-1}) under a 520 μE far-red-light background (Munekage et al., 2002). Photooxidative stress was measured on whole plants by thermoluminometry, with a custom-made apparatus that has been described (Ducruet, 2003). The amplitude of the TL peak at 135°C was used as an index of lipid peroxidation (Havaux, 2003). Chl bleaching was followed on 1-cm-diameter leaf discs, harvested from mature leaves. Leaf discs were kept floating on water and then exposed to white light (2,400 μmol m^{-2} s^{-1}, 8°C). Discs were rapidly frozen in liquid nitrogen prior to pigment extraction and quantification.

Statistics

Significance analyses were performed using an ANOVA with a pairwise multiple comparison procedure in Origin. Error bars represent the SD.

Sequence data from this article can be found in the EMBL/GenBank data libraries under accession numbers At4g25700 (*chy1*), At5g52570 (*chy2*), At1g31800 (*lut5*), and At2g32640 (*szl1*).

Supplemental Data

The following materials are available in the online version of this article.

Supplemental Figure S1. Production of reduced ROS in wild-type and mutant leaves.

Supplemental Figure S2. PSII repair efficiency under photoxidative stress.

Supplemental Figure S3. F_0 and F_m changes upon PSII photoinhibition.

Supplemental Figure S4. Photobleaching of pigment-protein complexes purified from wild-type and *szl1* plants.

Supplemental Table S1. Photosensitivity of PSI.

Received May 25, 2012; accepted June 20, 2012; published June 22, 2012.

LITERATURE CITED

Alboresi A, Ballottari M, Hienerwadel R, Giacometti GM, Morosinotto T (2009) Antenna complexes protect photosystem I from photoinhibition. BMC Plant Biol **9:** 71

Alboresi A, Dall'osto L, Aprile A, Carillo P, Roncaglia E, Cattivelli L, Bassi R (2011) Reactive oxygen species and transcript analysis upon excess light treatment in wild-type *Arabidopsis thaliana vs* a photosensitive mutant lacking zeaxanthin and lutein. BMC Plant Biol **11:** 62

Amunts A, Toporik H, Borovikova A, Nelson N (2010) Structure determination and improved model of plant photosystem I. J Biol Chem **285:** 3478–3486

Andersson B, Salter AH, Virgin I, Vass I, Styring S (1992) Photodamage to photosystem-II—primary and secondary events. J Photochem Photobiol B **15:** 15–31

Andersson J, Walters RG, Horton P, Jansson S (2001) Antisense inhibition of the photosynthetic antenna proteins CP29 and CP26: implications for the mechanism of protective energy dissipation. Plant Cell **13:** 1193–1204

Andreeva A, Abarova S, Stoitchkova K, Picorel R, Velitchkova M (2007) Selective photobleaching of chlorophylls and carotenoids in photosystem I particles under high-light treatment. Photochem Photobiol **83:** 1301–1307

Aro E-M, Virgin I, Andersson B (1993) Photoinhibition of photosystem II: inactivation, protein damage and turnover. Biochim Biophys Acta **1143:** 113–134

Aro EM, McCaffery S, Anderson JM (1994) Recovery from photoinhibition in peas (*Pisum sativum L.*) acclimated to varying growth irradiances (role of D1 protein turnover). Plant Physiol **104:** 1033–1041

Asada K (1999) The water-water cycle in chloroplasts: scavenging of active oxygens and dissipation of excess photons. Annu Rev Plant Physiol Plant Mol Biol **50:** 601–639

Baker NR (2008) Chlorophyll fluorescence: a probe of photosynthesis *in vivo.* Annu Rev Plant Biol **59:** 89–113

Barber J, Chapman DJ, Telfer A (1987) Characterisation of a PS II reaction centre isolated from the chloroplasts of *Pisum sativum.* FEBS Lett **220:** 67–73

Baroli I, Do AD, Yamane T, Niyogi KK (2003) Zeaxanthin accumulation in the absence of a functional xanthophyll cycle protects *Chlamydomonas reinhardtii* from photooxidative stress. Plant Cell **15:** 992–1008

Bassi R, Dainese P (1992) A supramolecular light-harvesting complex from chloroplast photosystem-II membranes. Eur J Biochem **204:** 317–326

Betterle N, Ballottari M, Hienerwadel R, Dall'Osto L, Bassi R (2010) Dynamics of zeaxanthin binding to the photosystem II monomeric antenna protein Lhcb6 (CP24) and modulation of its photoprotection properties. Arch Biochem Biophys **504:** 67–77

Britton G, Liaaen-Jensen S, Pfander H (2004) Carotenoids Hand Book. Birkhauser, Basel, Switzerland

Butler WL (1978) Energy distribution in the photochemical apparatus of photosynthesis. Annu Rev Plant Physiol **29:** 345–378

Caffarri S, Croce R, Breton J, Bassi R (2001) The major antenna complex of photosystem II has a xanthophyll binding site not involved in light harvesting. J Biol Chem **276:** 35924–35933

Carbonera D, Agostini G, Morosinotto T, Bassi R (2005) Quenching of chlorophyll triplet states by carotenoids in reconstituted Lhca4 subunit of peripheral light-harvesting complex of photosystem I. Biochemistry **44:** 8337–8346

Casazza AP, Tarantino D, Soave C (2001) Preparation and functional characterization of thylakoids from *Arabidopsis thaliana.* Photosynth Res **68:** 175–180

Croce R, Cinque G, Holzwarth AR, Bassi R (2000) The Soret absorption properties of carotenoids and chlorophylls in antenna complexes of higher plants. Photosynth Res **64:** 221–231

Croce R, Müller MG, Caffarri S, Bassi R, Holzwarth AR (2003) Energy transfer pathways in the minor antenna complex CP29 of photosystem II: a femtosecond study of carotenoid to chlorophyll transfer on mutant and WT complexes. Biophys J **84:** 2517–2532

Croce R, Zucchelli G, Garlaschi FM, Bassi R, Jennings RC (1996) Excited state equilibration in the photosystem I-light-harvesting I complex: P700 is almost isoenergetic with its antenna. Biochemistry **35:** 8572–8579

Dall'Osto L, Caffarri S, Bassi R (2005) A mechanism of nonphotochemical energy dissipation, independent from PsbS, revealed by a conformational change in the antenna protein CP26. Plant Cell **17:** 1217–1232

Dall'Osto L, Cazzaniga S, Havaux M, Bassi R (2010) Enhanced photoprotection by protein-bound vs free xanthophyll pools: a comparative analysis of chlorophyll b and xanthophyll biosynthesis mutants. Mol Plant **3:** 576–593

Dall'Osto L, Cazzaniga S, North H, Marion-Poll A, Bassi R (2007a) The *Arabidopsis* aba4-1 mutant reveals a specific function for neoxanthin in protection against photooxidative stress. Plant Cell **19:** 1048–1064

Dall'Osto L, Fiore A, Cazzaniga S, Giuliano G, Bassi R (2007b) Different roles of α- and β-branch xanthophylls in photosystem assembly and photoprotection. J Biol Chem **282:** 35056–35068

Dall'Osto L, Lico C, Alric J, Giuliano G, Havaux M, Bassi R (2006) Lutein is needed for efficient chlorophyll triplet quenching in the major LHCII antenna complex of higher plants and effective photoprotection *in vivo* under strong light. BMC Plant Biol **6:** 32

de Bianchi S, Betterle N, Kouril R, Cazzaniga S, Boekema E, Bassi R, Dall'Osto L (2011) *Arabidopsis* mutants deleted in the light-harvesting protein Lhcb4 have a disrupted photosystem II macrostructure and are defective in photoprotection. Plant Cell **23:** 2659–2679

de Bianchi S, Dall'Osto L, Tognon G, Morosinotto T, Bassi R (2008) Minor antenna proteins CP24 and CP26 affect the interactions between photosystem II subunits and the electron transport rate in grana membranes of *Arabidopsis.* Plant Cell **20:** 1012–1028

Demmig-Adams B, Adams WW (1992) Photoprotection and other responses of plants to high light stress. Annu Rev Plant Physiol Plant Mol Biol **43:** 599–626

Ducruet JM (2003) Chlorophyll thermoluminescence of leaf discs: simple instruments and progress in signal interpretation open the way to new ecophysiological indicators. J Exp Bot **54:** 2419–2430

Ducruet JM, Vavilin D (1999) Chlorophyll high-temperature thermoluminescence emission as an indicator of oxidative stress: perturbating effects of oxygen and leaf water content. Free Radic Res (Suppl) **31:** S187–S192

Ferreira KN, Iverson TM, Maghlaoui K, Barber J, Iwata S (2004) Architecture of the photosynthetic oxygen-evolving center. Science **303:** 1831–1838

Fiore A, Dall'osto L, Fraser PD, Bassi R, Giuliano G (2006) Elucidation of the beta-carotene hydroxylation pathway in *Arabidopsis thaliana.* FEBS Lett **580:** 4718–4722

Flors C, Fryer MJ, Waring J, Reeder B, Bechtold U, Mullineaux PM, Nonell S, Wilson MT, Baker NR (2006) Imaging the production of singlet oxygen in vivo using a new fluorescent sensor, singlet oxygen sensor green. J Exp Bot **57:** 1725–1734

Gilmore AM (2001) Xanthophyll cycle-dependent nonphotochemical quenching in photosystem II: mechanistic insights gained from *Arabidopsis thaliana L.* mutants that lack violaxanthin deepoxidase activity and/or lutein. Photosynth Res **67:** 89–101

Gilmore AM, Yamamoto HY (1991) Zeaxanthin formation and energy-dependent fluorescence quenching in pea chloroplasts under artificially mediated linear and cyclic electron transport. Plant Physiol **96:** 635–643

Gruszecki WI, Strzałka K (2005) Carotenoids as modulators of lipid membrane physical properties. Biochim Biophys Acta **1740:** 108–115

Havaux M (2003) Spontaneous and thermoinduced photon emission: new methods to detect and quantify oxidative stress in plants. Trends Plant Sci **8:** 409–413

Havaux M, Dall'osto L, Bassi R (2007) Zeaxanthin has enhanced antioxidant capacity with respect to all other xanthophylls in Arabidopsis leaves and functions independent of binding to PSII antennae. Plant Physiol **145:** 1506–1520

Havaux M, Dall'Osto L, Cuiné S, Giuliano G, Bassi R (2004) The effect of zeaxanthin as the only xanthophyll on the structure and function of the photosynthetic apparatus in *Arabidopsis thaliana.* J Biol Chem **279:** 13878–13888

Havaux M, Niyogi KK (1999) The violaxanthin cycle protects plants from photooxidative damage by more than one mechanism. Proc Natl Acad Sci USA **96:** 8762–8767

Herrin DL, Battey JF, Greer K, Schmidt GW (1992) Regulation of chlorophyll apoprotein expression and accumulation: requirements for carotenoids and chlorophyll. J Biol Chem **267:** 8260–8269

Hirschberg J (2001) Carotenoid biosynthesis in flowering plants. Curr Opin Plant Biol **4:** 210–218

Inoue K, Sakurai M, Hiyama T (1986) Photoinactivation sites of photosystem I in isolated chloroplasts. Plant Cell Physiol **27:** 961–968

Jensen PE, Bassi R, Boekema EJ, Dekker JP, Jansson S, Leister D, Robinson C, Scheller HV (2007) Structure, function and regulation of plant photosystem I. Biochim Biophys Acta **1767:** 335–352

Johnson GN, Young AJ, Horton P (1994) Activation of non-photochemical quenching in thylakoids and leaves. Planta **194:** 550–556

Kim J, DellaPenna D (2006) Defining the primary route for lutein synthesis in plants: the role of Arabidopsis carotenoid beta-ring hydroxylase CYP97A3. Proc Natl Acad Sci USA **103:** 3474–3479

Kim J, Smith JJ, Tian L, Dellapenna D (2009) The evolution and function of carotenoid hydroxylases in Arabidopsis. Plant Cell Physiol **50:** 463–479

Krieger-Liszkay A (2005) Singlet oxygen production in photosynthesis. J Exp Bot **56:** 337–346

Külheim C, Agren J, Jansson S (2002) Rapid regulation of light harvesting and plant fitness in the field. Science **297:** 91–93

Li Z, Ahn TK, Avenson TJ, Ballottari M, Cruz JA, Kramer DM, Bassi R, Fleming GR, Keasling JD, Niyogi KK (2009) Lutein accumulation in the absence of zeaxanthin restores nonphotochemical quenching in the *Arabidopsis thaliana npq1* mutant. Plant Cell **21:** 1798–1812

Liu Z, Yan H, Wang K, Kuang T, Zhang J, Gui L, An X, Chang W (2004) Crystal structure of spinach major light-harvesting complex at 2.72 A resolution. Nature **428:** 287–292

Malkin S, Armond PA, Mooney HA, Fork DC (1981) Photosystem II photosynthetic unit sizes from fluorescence induction in leaves: correlation to photosynthetic capacity. Plant Physiol **67:** 570–579

Mozzo M, Dall'Osto L, Hienerwadel R, Bassi R, Croce R (2008) Photoprotection in the antenna complexes of photosystem II: role of individual xanthophylls in chlorophyll triplet quenching. J Biol Chem **283:** 6184–6192

Munekage Y, Hojo M, Meurer J, Endo T, Tasaka M, Shikanai T (2002) PGR5 is involved in cyclic electron flow around photosystem I and is essential for photoprotection in Arabidopsis. Cell **110:** 361–371

Niyogi KK (2000) Safety valves for photosynthesis. Curr Opin Plant Biol **3:** 455–460

Niyogi KK, Björkman O, Grossman AR (1997) The roles of specific xanthophylls in photoprotection. Proc Natl Acad Sci USA **94:** 14162–14167

Niyogi KK, Grossman AR, Björkman O (1998) *Arabidopsis* mutants define a central role for the xanthophyll cycle in the regulation of photosynthetic energy conversion. Plant Cell **10:** 1121–1134

Niyogi KK, Shih C, Soon Chow W, Pogson BJ, Dellapenna D, Björkman O (2001) Photoprotection in a zeaxanthin- and lutein-deficient double mutant of Arabidopsis. Photosynth Res **67:** 139–145

Pan X, Li M, Wan T, Wang L, Jia C, Hou Z, Zhao X, Zhang J, Chang W (2011) Structural insights into energy regulation of light-harvesting complex CP29 from spinach. Nat Struct Mol Biol **18:** 309–315

Passarini F, Wientjes E, Hienerwadel R, Croce R (2009) Molecular basis of light harvesting and photoprotection in CP24: unique features of the most recent antenna complex. J Biol Chem **284:** 29536–29546

Peter GF, Takeuchi T, Thornber JP (1991) Solubilization and two-dimensional electrophoretic procedures for studying the organization and composition of photosynthetic membrane polypeptides. Methods **3:** 115–124

Peterman EJ, Dukker FM, van Grondelle R, van Amerongen H (1995) Chlorophyll a and carotenoid triplet states in light-harvesting complex II of higher plants. Biophys J **69:** 2670–2678

Pogson B, McDonald KA, Truong M, Britton G, DellaPenna D (1996) *Arabidopsis* carotenoid mutants demonstrate that lutein is not essential for photosynthesis in higher plants. Plant Cell **8:** 1627–1639

Ramel F, Sulmon C, Bogard M, Couée I, Gouesbet G (2009) Differential patterns of reactive oxygen species and antioxidative mechanisms during atrazine injury and sucrose-induced tolerance in *Arabidopsis thaliana* plantlets. BMC Plant Biol **9:** 28

Rappaport F, Béal D, Joliot A, Joliot P (2007) On the advantages of using green light to study fluorescence yield changes in leaves. Biochim Biophys Acta **1767:** 56–65

Rutherford AW, Osyczka A, Rappaport F (2012) Back-reactions, short-circuits, leaks and other energy wasteful reactions in biological electron transfer: redox tuning to survive life in O(2). FEBS Lett **586:** 603–616

Santabarbara S, Carbonera D (2005) Carotenoid triplet states associated with the long-wavelength-emitting chlorophyll forms of photosystem I in isolated thylakoid membranes. J Phys Chem B **109:** 986–991

Sonoike K (2011) Photoinhibition of photosystem I. Physiol Plant **142:** 56–64

Sonoike K, Terashima I (1994) Mechanism of photosystem-I photoinhibition in leaves of *Cucumis-Sativus l.* Planta **194:** 287–293

Telfer A (2005) Too much light? How β-carotene protects the photosystem II reaction centre. Photochem Photobiol Sci **4:** 950–956

Telfer A, Bishop SM, Phillips D, Barber J (1994a) Isolated photosynthetic reaction center of photosystem II as a sensitizer for the formation of singlet oxygen: detection and quantum yield determination using a chemical trapping technique. J Biol Chem **269:** 13244–13253

Telfer A, De Las Rivas J, Barber J (1991) Beta-carotene within the isolated photosystem II reaction centre: photooxidation and irreversible bleaching of this chromophore by oxidised P680. Biochim Biophys Acta **1060:** 106–114

Telfer A, Dhami S, Bishop SM, Phillips D, Barber J (1994b) β-Carotene quenches singlet oxygen formed by isolated photosystem II reaction centers. Biochemistry **33:** 14469–14474

Tian L, Magallanes-Lundback M, Musetti V, DellaPenna D (2003) Functional analysis of beta- and epsilon-ring carotenoid hydroxylases in *Arabidopsis.* Plant Cell **15:** 1320–1332

Tian L, Musetti V, Kim J, Magallanes-Lundback M, DellaPenna D (2004) The Arabidopsis LUT1 locus encodes a member of the cytochrome p450 family that is required for carotenoid epsilon-ring hydroxylation activity. Proc Natl Acad Sci USA **101:** 402–407

Tjus SE, Andersson B (1993) Loss of the trans-thylakoid proton gradient is an early event during photoinhibitory illumination of chloroplast preparations. Biochim Biophys Acta **1183:** 315–322

Trebst A, Depka B (1997) Role of carotene in the rapid turnover and assembly of photosystem II in *Chlamydomonas reinhardtii.* FEBS Lett **400:** 359–362

Trevithick-Sutton CC, Foote CS, Collins M, Trevithick JR (2006) The retinal carotenoids zeaxanthin and lutein scavenge superoxide and hydroxyl radicals: a chemiluminescence and ESR study. Mol Vis **12:** 1127–1135

Triantaphylidès C, Krischke M, Hoeberichts FA, Ksas B, Gresser G, Havaux M, Van Breusegem F, Mueller MJ (2008) Singlet oxygen is the major reactive oxygen species involved in photooxidative damage to plants. Plant Physiol **148:** 960–968

Umena Y, Kawakami K, Shen JR, Kamiya N (2011) Crystal structure of oxygen-evolving photosystem II at a resolution of 1.9 Å. Nature **473:** 55–60

Van Kooten O, Snel JFH (1990) The use of chlorophyll fluorescence nomenclature in plant stress physiology. Photosynth Res **25:** 147–150

Walters RG, Horton P (1995) Acclimation of Arabidopsis thaliana to the light environment: changes in photosynthetic function. Planta **197:** 306–312

Wehner A, Storf S, Jahns P, Schmid VH (2004) De-epoxidation of violaxanthin in light-harvesting complex I proteins. J Biol Chem **279:** 26823–26829

Yang J-S, Wang R, Meng J-J, Bi Y-P, Xu P-L, Guo F, Wan S-B, He Q-W, Li XG (2010) Overexpression of Arabidopsis CBF1 gene in transgenic tobacco alleviates photoinhibition of PSII and PSI during chilling stress under low irradiance. J Plant Physiol **167:** 534–539

Zhang S, Scheller HV (2004) Photoinhibition of photosystem I at chilling temperature and subsequent recovery in Arabidopsis thaliana. Plant Cell Physiol **45:** 1595–1602

Supplemental Data

Figure S1

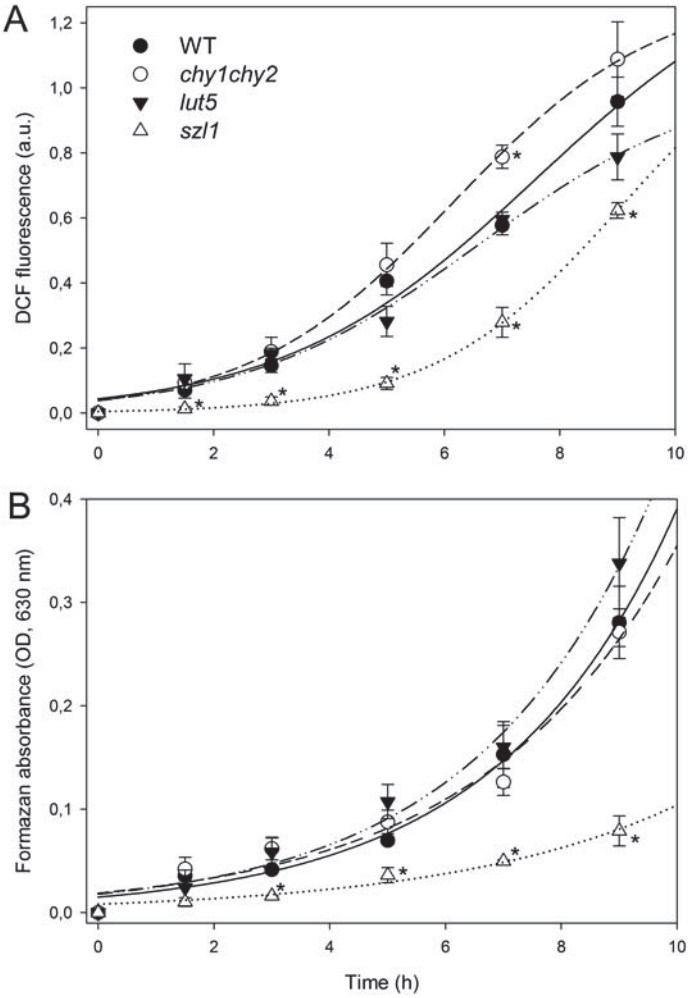

Figure S1. Production of reduced ROS in WT and mutant leaves. Leaf discs from WT and mutants were vacuum-infiltrated with ROS-specific probes, namely dichlorofluorescein (DCF, panel A) for hydrogen peroxide and hydroxyl radical detection, and nitroblue tetrazolium (NBT, panel B) for superoxide anion detection. *In vivo* ROS production was induced by illumination of discs with red actinic light (550 µmol photons m^{-2} s^{-1}) at 8°C. DCF increases its fluorescence emission upon reaction with a specific ROS; the increase in the probe emission was followed with a fiber-optic on the leaf surface. Superoxide production was visualized as a purple formazan deposit within leaf tissues, then extracted and quantified by measuring absorbance at 630 nm. See methods for details. The symbols and error bars show means ± SD (n = 4). Significantly different values ($P < 0.05$, Student's *t* test) from the WT are marked by an asterisk (*).

Figure S2

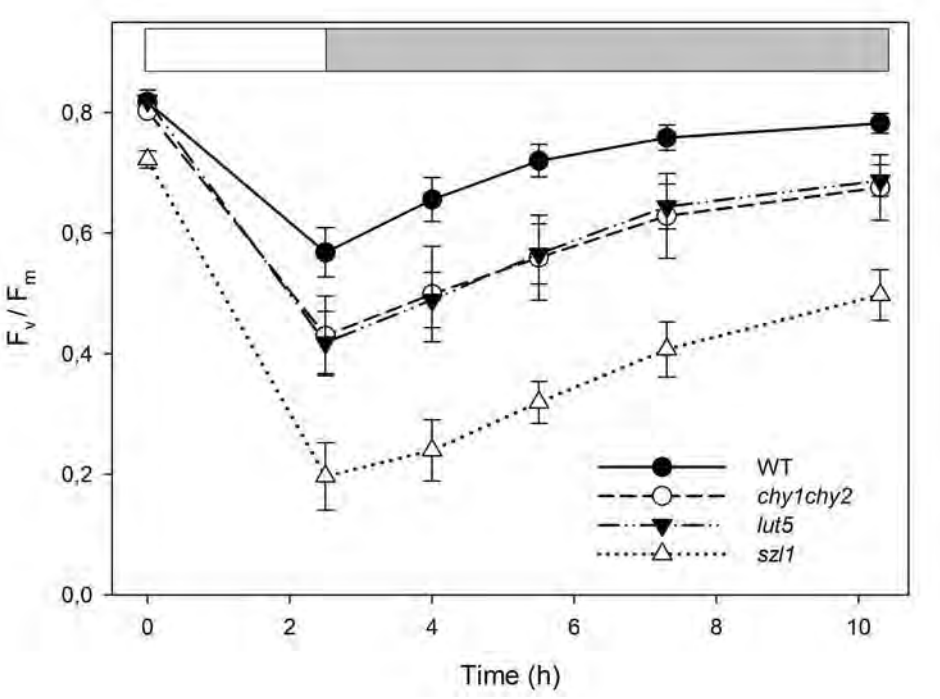

Figure S2. PSII repair efficiency under photoxidative stress. PSII repair was followed on WT, *chy1chy2*, *lut5* and *szl1* plants by measuring F_v/F_m recovery in low light (15 μmol photons m^{-2} s^{-1}, 8°C – gray bar) after photoinhibitory treatment (1100 μmol photons m^{-2} s^{-1}, 8°C – white bar). Data are expressed as means ± SD (*n* = 5).

Figure S3

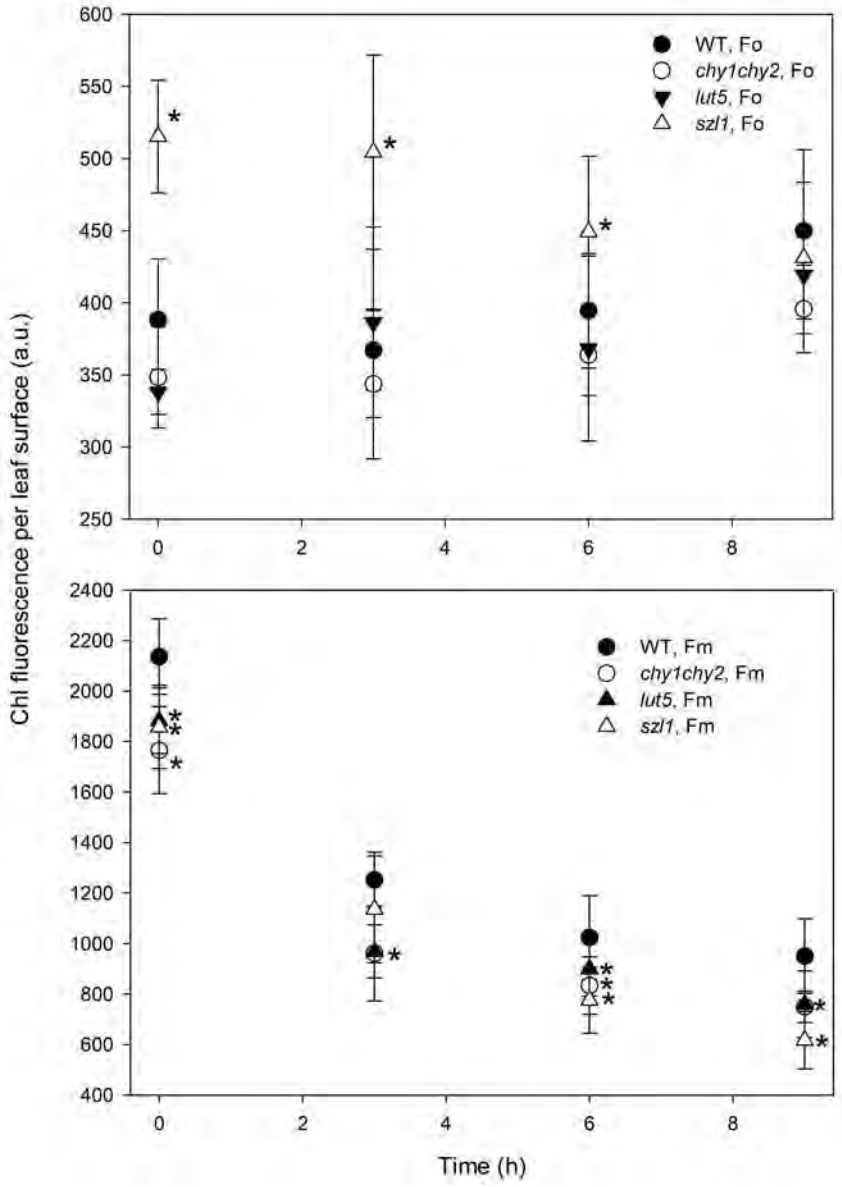

Figure S3. F_0 and F_m changes upon PSII photoinhibition. The same photoinhibitory treatment described in Figure 4A (550 µmol photons m^{-2} s^{-1}, 8°C) was repeated on WT and mutant leaves in order to follow the changes in the chlorophyll fluorescence parameters F_0 (upper panel) and F_m (lower panel) upon stress. Fluorescence values were normalized to leaf surface. Data are expressed as means ± SD ($n \geq 9$). Values that are significantly different ($P < 0.05$) from the wild-type are marked with an asterisk (*).

Figure S4

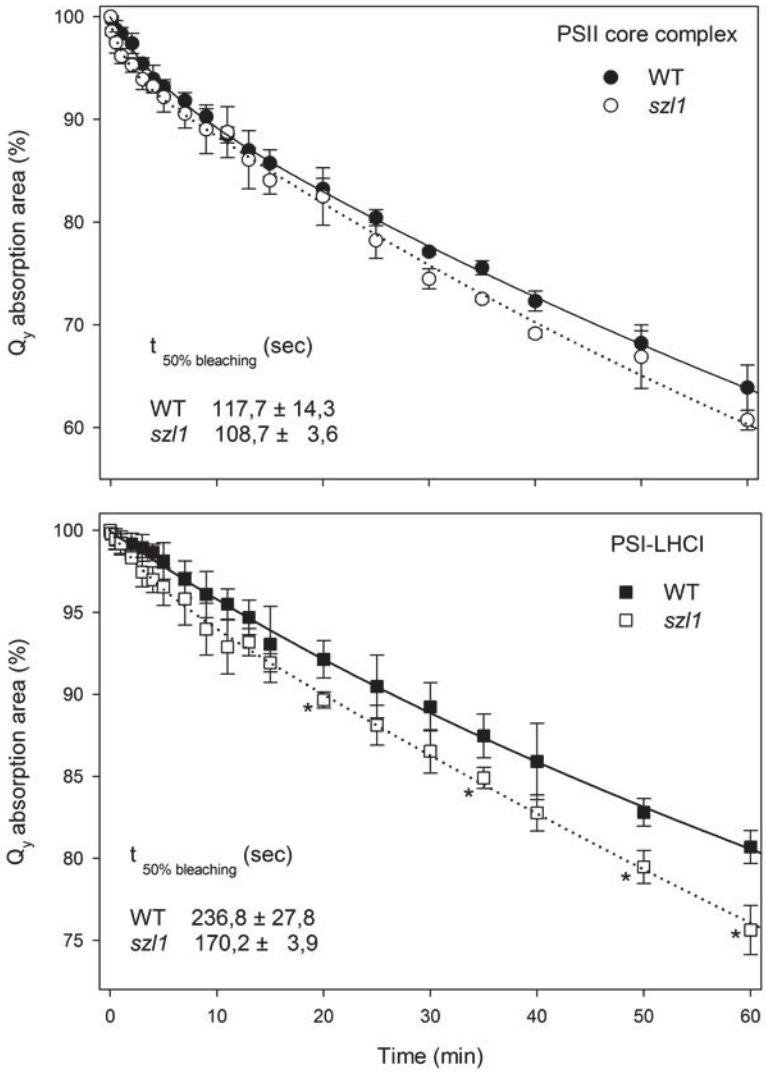

Figure S4. Photobleaching of pigment-protein complexes purified from WT and *szl1* plants. Photobleaching kinetics were recorded on PSII core (A) and PSI-LHCI complexes (B), by using a light intensity of 3000 µmol photons m^{-2} s^{-1} and samples cooled at 10°C. The decay curves show the total Q_y absorption relative to a 100% initial value; absorption decays were fittted in time according to an exponential law with the minimal requirement of two lifetime components ($A(t) = A_1e^{-yt/T1} + A_2e^{-yt/T2}$), after data normalization to 100% at time zero (initial and maximal absorbance = 0.6). In each panel, the photosensitivity of samples is quantified by the bleaching time ($t_{50\% \text{ bleaching}}$), a figure of merit describing the time necessary to bleach 50% of the total Chls. Data are expressed as means ± SD ($n \geq 9$). Values that are significantly different ($P < 0.05$) from the wild-type are marked with an asterisk (*).

Table S1

	WT	*chy1chy2*	*lut5*	*szl1*
maximum PSI activity (%)	77.8 ± 8.7	68.3 ± 14.3	65.8 ± 8.7	23.8 ± 12.2*

Table S1. Photosensitivity of Photosystem I. Plants were exposed to 550 μmol photons m^{-2} s^{-1} at 8°C for 60 min. The photoinhibition of PSI was calculated from the maximum content of $P700^{+}$ (ΔA_{max}). It was determined on intact leaves using a saturating flash (3 ms) under a far-red light background (720 nm, 700 μmol photons m^{-s} s^{-1}) in the presence of 1 mM methylviologen. Values represent the maximum activity of PSI after high light stress as relative values of the maximum activity before the stress (100%). Data are expressed as means ± SD (n= 5); values that are significantly different ($P < 0.05$) from the wild-type are marked with an asterisk (*).

A4. Zeaxanthin protects plant photosynthesis by modulating chlorophyll triplet yield in specific light-harvesting antenna subunits.

THE JOURNAL OF BIOLOGICAL CHEMISTRY VOL. 287, NO. 50, pp. 41820–41834, December 7, 2012

Zeaxanthin Protects Plant Photosynthesis by Modulating Chlorophyll Triplet Yield in Specific Light-harvesting Antenna Subunits*[S]

Received for publication, July 28, 2012, and in revised form, October 12, 2012 Published, JBC Papers in Press, October 12, 2012, DOI 10.1074/jbc.M112.405498

Luca Dall'Osto[‡], Nancy E. Holt[‡§], Shanti Kaligotla[¶], Marcel Fuciman[¶], Stefano Cazzaniga[‡], Donatella Carbonera[‖], Harry A. Frank[¶], Jean Alric[§], and Roberto Bassi[‡§‡‡1]**

*From the [‡]Dipartimento di Biotecnologie, Università di Verona, Strada Le Grazie 15, 37134 Verona, Italy, [§]Laboratoire de Genetique et Biophysique des Plantes, Faculté des Sciences de Luminy Case 901 136 Avenue de Luminy, 13288 Marseille Cedex 9, France, the [¶]Department of Chemistry, University of Connecticut, Storrs, Connecticut 06269, [‖]Dipartimento di Scienze Chimiche, Università di Padova, Via Marzolo 1, 35131 Padova, Italy, **Unité Mixte de Recherche 7141 CNRS-Université Paris 6, Institut de Biologie Physico-Chimique, 13 rue Pierre et Marie Curie, 75005 Paris, France, and [‡‡]Phytosphäre Forschungszentrum Jülich, 52425 Jülich, Germany*

Background: The plant carotenoid zeaxanthin is accumulated under excess light.
Results: Zeaxanthin induces a red shift in the carotenoid triplet excited state spectrum and reveals a higher efficiency in controlling chlorophyll triplet formation.
Conclusion: Binding of zeaxanthin to specific proteins modulates the yield of dangerous chlorophyll excited states and protects photosynthesis from over-excitation.
Significance: Functional dissection of zeaxanthin-dependent photoprotective mechanisms is crucial for understanding how plants avoid photoinhibition.

Plants are particularly prone to photo-oxidative damage caused by excess light. Photoprotection is essential for photosynthesis to proceed in oxygenic environments either by scavenging harmful reactive intermediates or preventing their accumulation to avoid photoinhibition. Carotenoids play a key role in protecting photosynthesis from the toxic effect of over-excitation; under excess light conditions, plants accumulate a specific carotenoid, zeaxanthin, that was shown to increase photoprotection. In this work we genetically dissected different components of zeaxanthin-dependent photoprotection. By using time-resolved differential spectroscopy *in vivo*, we identified a zeaxanthin-dependent optical signal characterized by a red shift in the carotenoid peak of the triplet-minus-singlet spectrum of leaves and pigment-binding proteins. By fractionating thylakoids into their component pigment binding complexes, the signal was found to originate from the monomeric Lhcb4–6 antenna components of Photosystem II and the Lhca1–4 subunits of Photosystem I. By analyzing mutants based on their sensitivity to excess light, the red-shifted triplet-minus-singlet signal was tightly correlated with photoprotection in the chloroplasts, suggesting the signal implies an increased efficiency of zeaxanthin in controlling chlorophyll triplet formation. Fluorescence-detected magnetic resonance analysis showed a decrease in the amplitude of signals assigned to chlorophyll triplets belonging to the monomeric antenna complexes of Photosystem II upon zeaxanthin binding; however, the amplitude of carotenoid triplet signal does not increase correspondingly. Results show that the high light-induced binding of zeaxanthin to specific proteins plays a major role in enhancing photoprotection by modulating the yield of potentially dangerous chlorophyll-excited states *in vivo* and preventing the production of singlet oxygen.

Plants are particularly prone to photo-oxidative damage for the same reasons that they are effective at photosynthesis, namely because the primary pigment chlorophyll (Chl)[2] is a very efficient sensitizer. The singlet excited states of Chl molecules (^{1}Chl*) are efficiently quenched by photochemical reaction centers. Nevertheless, environmental conditions easily unbalance the ratio between energy capture and utilization; *e.g.* at high photon flux densities, accumulation of excitons in the light-harvesting complexes (Lhc) of both photosystems (PS) increases the amount of ^{1}Chl*. This raises the probability of intersystem crossing to the Chl triplet state (^{3}Chl*), a species that reacts with molecular oxygen (O_2) to yield singlet oxygen ($^1O_2$) molecules (1). Because of the high reactivity and low diffusion radius of $^1O_2$, this reactive oxygen species (ROS) induces damage in its local environment by (2), destroying lipids and nucleic acids and proteins (3–5), thus leading to a loop of ever-

* This work was supported by grants from the Marie Curie Actions - Networks for Initial Training Harvest (Grant no. PITN-GA-2009-238017) and PRIN Programmi di Ricerca di Interesse Nazionale (Grant no. 2008XB774B) (to R. B.). Work in the laboratory of H. A. F. was supported by grants from the National Science Foundation (MCB-0913022) and the UConn Research Foundation.
[S] This article contains supplemental Tables S1–S3 and Fig. S1–S6.
The nucleotide sequence(s) reported in this paper has been submitted to the GenBank™/EBI Data Bank with accession number(s) At5G57030, At1G08550, At5G67030, and At1G44446.
[1] To whom correspondence should be addressed: University of Verona, Biotechnology Department, Strada Le Grazie 15, 37134 Verona, Italy. Tel.: 39-045-8027916; Fax: 39-045-8027929; E-mail: roberto.bassi@univr.it.

[2] The abbreviations used are: Chl, chlorophyll; Lhc, light-harvesting complex; PS, photosystem; ROS, reactive oxygen species; Car, carotenoid; Zea, zeaxanthin; EL, excess light; Vio, violaxanthin; qE, excitation quenching; TmS, triplet-minus-singlet; FDMR, fluorescence-detected magnetic resonance; EL, excess light; α-DM, α-dodecylmaltoside; SOSG, singlet oxygen sensor green; RT, room temperature; NPQ, non-photochemical quenching; qZ, Zea-dependent component of NPQ.

increasing $^1O_2$ production and further oxidation until photobleaching (6). This photooxidative damage leads to a dramatic depression of photosynthetic efficiency called photoinhibition (7–9).

A second pigment class essential for photosynthesis is represented by carotenoids (Car), whose photoprotective action in the photosynthetic apparatus is well established (10). Carotenoids are either carotenes, bound to PSI and PSII core complexes, or their oxygenated derivatives, xanthophylls, mainly bound to Lhc proteins. Xanthophylls are involved in a number of photoprotection mechanisms, being active in (i) preventing over-excitation of reaction centers by quenching ^{1}Chl* states (11), (ii) quenching ^{3}Chl* through carotenoid triplet (^{3}Car*) formation, thus avoiding ROS formation (12), and (iii) scavenging ROS (13). Among xanthophylls, zeaxanthin (Zea) is of particular interest because it is absent in dark or low light conditions and only accumulates in excess light (EL), where it is produced from the diepoxide xanthophyll violaxanthin (Vio) (14) through the action of the violaxanthin de-epoxidase enzyme (15, 16). Zea is known to be involved in several types of photoprotection events of the PSII reaction center, which occur on varying timescales. A number of these mechanisms quench ^{1}Chl*, namely (i) feedback de-excitation quenching (qE) (17, 18), which occurs on the timescale of seconds to minutes, (ii) a slowly inducible quenching or qZ (19), which is likely caused by Zea binding to Lhc upon exchange with Vio (20), and (iii) a long term, irreversible quenching that reflects a photoinhibitory state of PSII (21). An increase of thermal dissipation of ^{1}Chl* can effectively protect reaction centers from over-excitation, thus reducing the probability of intersystem crossing to ^{3}Chl* and $^1O_2$ formation in the Lhcs.

Previous results (22) demonstrated that the *npq1* mutant of *Arabidopsis thaliana*, which is defective in the light-dependent Vio to Zea interconversion, shows increased photoinhibition and lipid peroxidation with respect to wild type (WT) in EL, leading to a decreased fitness (23). Early suggestions pointed to the decreased capacity for quenching of singlet excited chlorophylls (qE) (11). Further work by comparing the *npq1* to the *npq4* mutant, the latter lacking qE but retaining the ability for Zea synthesis, showed that protection of thylakoid membrane lipids against photooxidation was provided by a mechanism different than ^{1}Chl* quenching (22). Moreover, besides its role in singlet energy dissipation, Zea has been proposed to act as an antioxidant by scavenging $^1O_2$ and thus preventing lipid peroxidation (24) upon its release from the pH-dependent V1 binding site of the major LHCII complex (25, 26) into the lipid phase. However, a fundamental understanding of the Zea-dependent photoprotection mechanism, its location and whether its significance in providing overall photoprotection *in vivo* is mainly dependent on either ^{1}Chl*/^{3}Chl* quenching or ROS scavenging remains and awaits a more detailed analysis of the contributions of the different mechanisms involved in photoresistance.

Once synthesized, Zea has a dual location; it can be either free into thylakoid membrane lipids or bound to the Lhc proteins (27, 28). The effect of the former pool was investigated in *Arabidopsis* showing that Zea has a distinct capacity for scavenging ROS with respect to other xanthophyll species (29). Furthermore, it has been reported (30, 31) that the photoprotective effect of xanthophylls is greatly enhanced by their binding to Lhc proteins. Therefore, besides ROS scavenging in the lipid phase (32) and enhancing of qE (11), a third photoprotective effect is provided by a mechanism specifically exerted by the Lhc-bound Zea pool.

Here, we show that Zea bound to specific Lhcs is directly involved in the modulation of ^{3}Chl*. By means of time-resolved spectroscopy *in vivo*, we found that the photoresistance of *Arabidopsis* to EL treatment tightly correlates with the detection of a red shift in the major carotenoid signal in triplet-minus-singlet (TmS) spectra upon Zea synthesis, as measured in intact leaves. Fractionation of thylakoid membranes from EL-treated plants allowed detection of the red-shifted TmS signal in the monomeric Lhcb subunits of PSII (Lhcb4–6) and the dimeric Lhca subunits of PSI but not in the major trimeric LHCII complex. In each case the Zea-dependent red shift correlates with a reduced yield of $^1O_2$ production from purified Lhc proteins or from photosynthetic supercomplexes containing these subunits. Analysis by fluorescence-detected magnetic resonance (FDMR) at 4 K showed decreased amplitude of ^{3}Chl* upon Zea binding, implying a Zea-specific effect in decreasing the yield of dangerous excited states. We conclude that, in addition to the previously described effects in quenching ^{1}Chl* and scavenging $^1O_2$, an additional photoprotection mechanism is elicited by Zea binding to specific Lhc protein subunits consisting of a reduction in the yield in harmful ^{3}Chl*.

EXPERIMENTAL PROCEDURES

Plant Material

WT plants of *A. thaliana* and mutants *lut2* (lacking lutein (Lut)), *npq1* (unable to synthesize zeaxanthin in high light), *npq2* (retaining lutein and zeaxanthin as only xanthophylls), and *ch1* (lacking chlorophyll *b*) were obtained from NASC (ecotype Col-0). Mutants *npq1lut2*, *npq2lut2*, *ch1npq1*, *ch1lut2* were isolated by crossing single mutant plants. Plants were grown for 4 weeks on Sondermisch potting mix (Gramoflor) in controlled conditions (~120 μmol of photons m^{-2} s^{-1}, 23 °C, 8 h light/16 h dark) before measurements.

Thylakoid Isolation and Sample Preparation

Stacked thylakoid membranes were isolated from either dark-adapted or excess light (EL)-treated leaves (33). Grana membranes have been isolated from dark- and EL-treated samples using α-dodecylmaltoside (α-DM) solubilization of stacked thylakoids, as described in Ref. 34. Membranes corresponding to 500 μg of chlorophylls were washed with 5 mM EDTA, solubilized with 0.6% α-DM, and then fractionated by ultracentrifugation in a 0.1–1 M sucrose gradient as previously described (25). Purified monomeric Lhcb proteins (band 2 in the sucrose gradient) were further fractionated by flat-bed isoelectric focusing at 4 °C (35). Purified LHCI complexes were obtained as described in Ref. 36.

Pigment Analysis

Pigments were extracted either from whole leaves, thylakoid membranes, or isolated antenna complexes with 80% acetone then separated and quantified by HPLC (37).

Determination of the Sensitivity to Photooxidative Stress

Short term EL treatment was performed for 1 h at 1200 μmol photons m^{-2} s^{-1} at RT (22 °C) to obtain the maximum Zea accumulation on detached leaves floating on water. Light was provided by 150 watt halogen lamps (Focus3, Prisma, Italy). Samples for HPLC analysis were rapidly frozen in liquid nitrogen before pigment extraction. EL-treated leaves used for thylakoid isolation were vacuum-infiltrated with 50 μM Norfluorazon (a zeaxanthin-epoxidase inhibitor) upon EL treatment to slow down Zea-Vio conversion (38) during thylakoid isolation procedure. Photo-destruction of pigment-protein complexes *in vivo* was induced by a strong light treatment; leaf discs floating on water were exposed to high light (2500 μmol of photon m^{-2} s^{-1}) at RT for 31 h. For the quantification of Lhcb subunits, frozen leaf discs were homogenized in liquid nitrogen, and protein was extracted in 62.5 mM Tris-HCl, pH 6.8, 10% glycerol, 2% SDS, 5% β-mercaptoethanol. For each sample, the same volume of leaf extract (corresponding to 0.5 μg of chlorophylls of t_0 sample) was loaded on SDS-PAGE. Immunoblot assays with antibodies against different polypeptides were performed as described previously (39). To avoid any deviation between different immunoblots, samples were compared only when loaded in the same slab gel.

Spectroscopy

Steady State Spectroscopy—Spectra were obtained using samples in 10 mM Hepes, pH 7.5, 0.06% α-DM, 0.2 M sucrose. Absorption measurements were performed using a SLM-Aminco DW-2000 spectrophotometer at RT.

Time-resolved Spectroscopy—absorbance changes were monitored in purified proteins or intact *Arabidopsis* leaves with a home-built pump and probe laser spectrophotometer basically described in Ref. 40) or with a laser flash photolysis spectrometer for isolated pigments. Transient absorption spectra were recorded in the laboratory of H. A. Frank at room temperature using an Edinburgh Instruments Model LP920KS flash photolysis spectrometer consisting of a Xe 920 450-watt arc lamp as a probe light source. The excitation pulse was generated by a Continuum Nd:YAG-pumped optical parametric oscillator laser tuned to excite selectively the Chl *a* Q_y band at 662 nm. The pump laser and probe light beams were configured perpendicular to each other. A Tektronix digital oscilloscope model TDS 3012B was used for signal averaging. All transient absorption profiles were the average of 20 scans. The solutions contained micromolar concentrations of Chl *a* (as a triplet donor), and the xanthophylls (as triplet acceptors) and were degassed using at least five freeze-pump-thaw cycles before the spectroscopic measurements.

Quantification of Singlet Oxygen Yield—Measurements of $^1O_2$ production on leaves and purified pigment-protein complexes were performed using Singlet Oxygen Sensor Green (SOSG, Invitrogen). SOSG is a fluorescent probe highly selective for $^1O_2$ that increase its 530-nm emission band in presence of this ROS; it was shown to be a useful and reliable probe for the detection of $^1O_2$ *in vivo* and in purified Lhcs (30, 41–43). Leaves were vacuum-infiltrated with the dye solution (SOSG 200 μM) and illuminated with red light ($\lambda > 600$ nm, 1200 or 400 μmol m^{-2} s^{-1}) at RT. The increase of SOSG-specific fluorescence emission was followed to quantify ROS release into leaves (λ_{exc} 480 nm, λ_{emis} 530 nm). Fluorescence emission spectra were measured at RT using a Jobin-Yvon Fluoromax-3 spectrofluorimeter equipped with a fiber optic to measure emission of fluorogenic probes on leaves. For the measurements of $^1O_2$ yield on either Lhc, PSII supercomplex, and PSI-LHCI, pigment-protein complexes were harvested from sucrose gradient and diluted in a reaction buffer (10 mM Hepes, pH 7.5, 0.06% α-DM, 2 μM SOSG) to the same absorption area in the wavelength range 600–750 nm (about 2.2 μg of Chls/ml). Isolated complexes were illuminated with red light ($\lambda > 600$ nm), and fluorescence yield of SOSG were determined before and during EL treatment to quantify $^1O_2$-dependent fluorescence increase (30). Upon EL treatment, we did not observe photobleaching of either chlorophyll or carotenoid in leaves or purified pigment-protein complexes.

FDMR—For all the experiments, the samples were dissolved in buffer to a concentration of 200 μg Chl/ml. Degassed glycerol was added (60% v/v) just before freezing the samples by direct immersion in liquid helium into the pre-cooled cryostat. FDMR experiments were performed in the laboratory-built apparatus, previously described in detail (44–46). In the specific experiments, the modulation frequency and the microwave power were chosen depending on the triplet state. The temperature of all the experiments performed was 1.8 K. All the FDMR spectra are presented as $\Delta I/I$, where ΔI is the fluorescence change induced by the resonant microwave field, and I is the steady state fluorescence detected by the photodiode. Because in all the experiments I remains substantially unmodified upon light treatments, the change of the intensity of $\Delta I/I$ signal after EL is a measure of the change in triplet yield.

Statistics

Significance analysis was performed using either Student's *t* test or analysis of covariance in GraphPad Prism (see the figure legends for details). *Error bars* represent the standard deviation.

Sequence data from this article can be found in the EMBL/GenBank™ data libraries under the following accession numbers: *lut2* (line N656231 with insertion into the lycopene-ϵ-cyclase gene, At5G57030); *npq1* (line N624757 with insertion into the violaxanthin-deepoxidase gene, At1G08550); *npq2* (line N559469 with insertion into the zeaxanthin-epoxidase gene, At5G67030); *ch1* (line N524295 with insertion into the chlorophyll-a oxygenase gene, At1G44446).

RESULTS

Effect of Zea-Lhc Interaction in Limiting $^1O_2$ Release from Arabidopsis Leaves under EL—When photosynthetic organisms are exposed to EL, photo-oxidative stress occurs with the production of $^1O_2$. Among the xanthophylls, Zea has been proposed to be the most active into scavenging of $^1O_2$ and preventing lipid peroxidation (29). To investigate the function of the Lhc-bound zeaxanthin pool, we analyzed the photoprotective efficacy of *A. thaliana* mutants that were deficient in their ability to synthesize Zea (*npq1*) either in a WT or *ch1* genetic background. The *ch1* mutation inactivates Chl *a* oxidase (47) and thus Chl *b* synthesis; see supplemental Table S1 for pigment

composition of these genotypes. Because Chl *b* is an essential co-factor for the assembly of Lhc pigment-protein complexes (48), a de-stabilization of Lhc proteins is obtained; the *ch1* mutation leads to a strong reduction of PS antenna size (49), whereas xanthophylls bound to Lhc in the WT are released into the membrane (29).

We evaluated $^1O_2$ release on leaf discs using SOSG (41), a $^1O_2$ highly selective fluorescence probe. After illumination of discs with EL (1200 μmol photons m^{-2} s^{-1}, RT), *ch1* leaves showed a far higher release of $^1O_2$ with respect to WT at each time point (supplemental Fig. S1) despite a 4-fold lower PSII antenna size (29). This observation is consistent with recent reports showing that the enhanced lipid peroxidation in *ch1* is due to $^1O_2$ attack on lipids (50) and that higher $^1O_2$ yield in *ch1* is attributed to the lack of xanthophyll binding complexes (30). To evaluate the photoprotection capacity of zeaxanthin in WT *versus ch1* background, intensity of EL was chosen for *npq1* and *ch1npq1* leaf discs to obtain the same $^1O_2$ yield; thus, WT and *npq1* discs were illuminated with 1200 μmol of photons m^{-2} s^{-1}, and *ch1* genotypes were illuminated with 400 μmol of photons m^{-2} s^{-1}. Results are reported in Fig. 1. The WT leaves exhibited a lower $^1O_2$ yield per chlorophyll relative to the *npq1* in EL (Fig. 1*A*), thus confirming the enhanced photoprotection capacity of Zea with respect to the other xanthophylls (29). However, Zea-dependent photoprotection is lower in *ch1* plants; clearly, the effect of the *npq1* mutation in increasing $^1O_2$ release was significant only in non-*ch1* genotypes (Fig. 1). These findings with *ch1* plants imply that, although Zea has a high photoprotective effect, its performance is strongly enhanced through binding to the Lhc proteins.

Measurements of Light-induced $^1O_2$ Yield on Purified Pigment-Protein Complexes—The results reported above suggest a role for Zea-Lhc interactions in the photoprotection of thylakoid membranes by preventing $^1O_2$ release into the lipid phase. Previous investigation on recombinant Lhcs (20) and *in vivo* (51) showed that Zea can bind to specific sites of Lhc subunits; in particular, xanthophyll exchange occurs in the inner L2 site of the minor antennae of Lhcb4 (CP29), Lhcb5 (CP26), Lhcb6 (CP24), and LHCI (51–53), whereas trimeric LHCII binds Zea to the external site V1 (25).

The differential level of $^1O_2$ production with *versus* without Zea is the signature of the Zea-dependent photoprotection mechanism and can be used for tracking the pigment-protein complexes responsible for this effect. To this aim, we compared the capacity for photoprotection of Lhcbs binding Vio or Zea by analyzing the amount of $^1O_2$ released by pigment-protein complexes isolated from either dark-adapted (Vio) or EL-treated (Zea) leaves. The $^1O_2$ yield was measured upon illumination of the complexes in the presence of SOSG. The pigment composition of purified complexes was analyzed by HPLC (supplemental Table S2). Binding of Zea to monomeric Lhcbs (a preparation of monomeric PSII antenna proteins that contains Lhcb4, Lhcb5, and Lhcb6 along with a fraction of monomerized LHCII complex) and LHCI (PSI antennae) significantly reduces the amount of $^1O_2$ produced in EL. Fig. 2, *A* and *C*, show that $^1O_2$ yield by monomeric Lhcb-Zea is reduced by 65% with respect to the Lhcb-Vio sample, the reduction being even greater in purified Lhcb5; likewise, the reduction in $^1O_2$ yield of

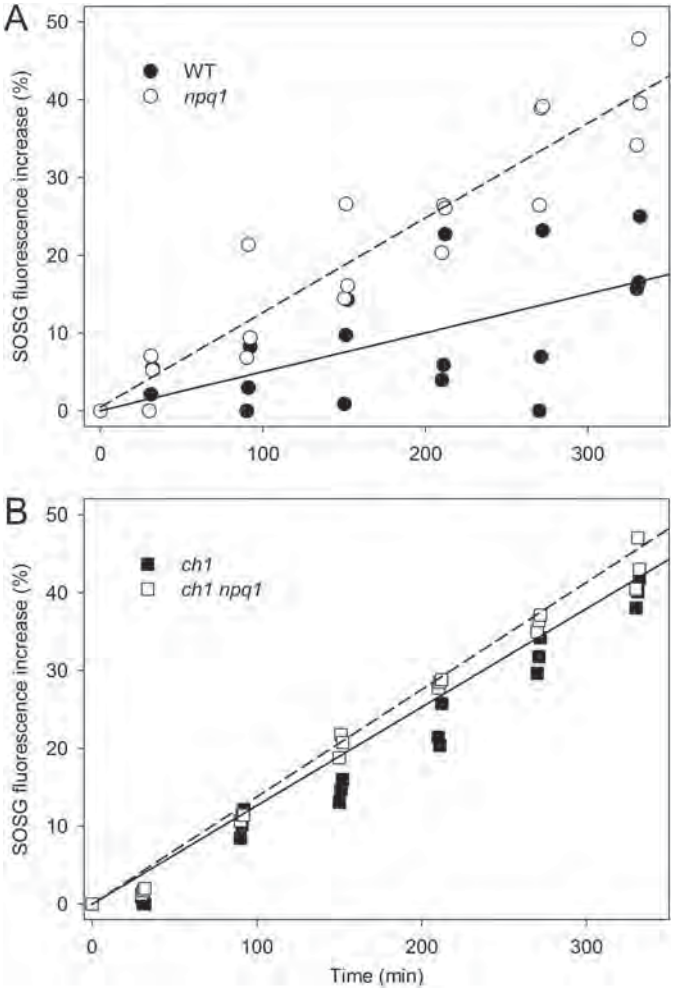

FIGURE 1. **Photoprotective role of Zea-Lhc interaction.** Singlet oxygen production from WT and xanthophyll mutants lacking Zea (*npq1*, *panel A*) and/or Lhc complexes (*ch1*, *panel B*) was measured on intact leaves upon illumination ($600 < \lambda < 750$ nm, RT, 1200 μmol of photons m^{-2} s^{-1} for WT and *npq1*, 400 μmol of photons m^{-2} s^{-1} for *ch1* background). The highly selective fluorescent probe SOSG was used to quantify light-dependent $^1O_2$ release, as its 530-nm emission band increases in proportion to the amount of this ROS released by the photosynthetic apparatus. Each experimental point corresponds to a different sample; these data are representative of two independent experiments. Experimental points were modeled with a linear regression. Statistical analysis (analysis of covariance) revealed that *npq1* leaves showed significantly higher $^1O_2$ production than wild type ($p = 0.0013$, *panel A*); instead, Zea-dependent photoprotection is less evident in *ch1* plants (differences between the slopes of *panel B* are not significant, $p = 0.55$).

LHCI-Zea *versus* LHCI-Vio is 40% at 700 μmol photons m^{-2} s^{-1} (Fig. 2*D*). These results imply that the Zea-containing complexes have a stronger capacity for photoprotection with respect to the same complexes binding Vio. Such an effect was not observed in trimeric LHCII, *i.e.* there was no change in $^1O_2$ yield based on its Vio or Zea content (Fig. 2*B*). When the production of $^1O_2$ was measured on both PSII supercomplexes (C_2S_2, see Ref. 54) and PSI-LHCI, complexes isolated from dark-adapted leaves (Vio binding) exhibited a 2-fold higher $^1O_2$ yield with respect to complexes isolated from EL-treated leaves (Zea binding) (Fig. 2, *E* and *F*, respectively). These results show that the lack of bound Zea to Lhc complexes negatively affects the photoprotective efficiency of the whole photosystem for both PSI and PSII.

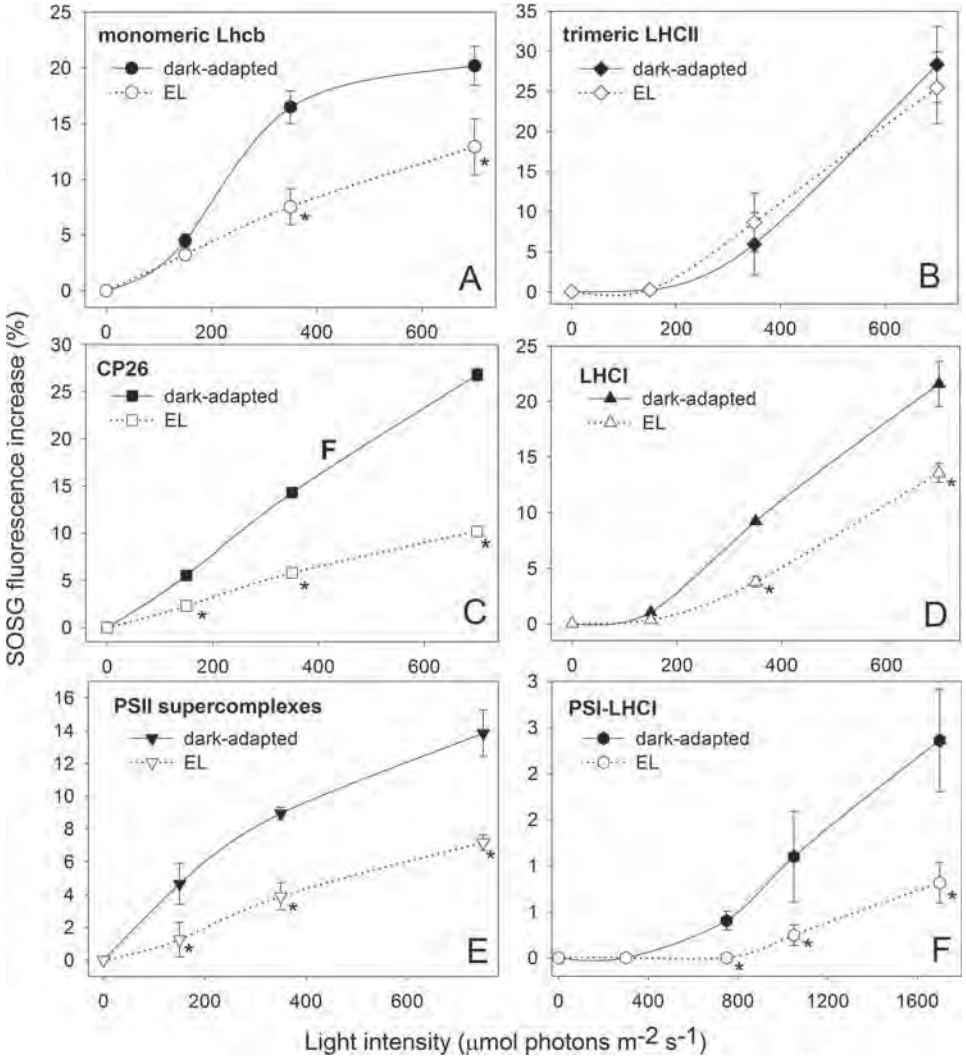

FIGURE 2. **Light-dependent singlet oxygen production from isolated pigment-proteins complexes.** SOSG was used to follow light-dependent $^1O_2$ release of pigment-protein complexes isolated from either dark-adapted or EL-treated leaves. Fluorescence of SOSG has been measured upon illumination of a solution containing monomeric Lhcb (*A*), trimeric LHCII (*B*), CP26 (*C*), and LHCI (*D*) with either Vio bound (*solid line*, *closed symbols*) or Zea bound (*dashed line*, *open symbols*) at different light intensities, 10 min each intensity. Trimeric LHCII isolated from either dark-adapted or EL-treated plants did not show significant differences in $^1O_2$ yield at all light intensities tested (*B*). Instead, Zea binding monomeric Lhcb, CP26, and LHCI showed significantly lower $^1O_2$ release than the Vio-binding complexes. Zea bound to these specific proteins plays a role in enhancing photoprotection by preventing the release of $^1O_2$ from either PSII (*E*) and PSI-LHCI (*F*) supercomplexes. *, $p < 0.05$ by Student's *t* test of Zea binding complexes relative to the corresponding Vio binding.

Among Lhcs, the components of the monomeric Lhcb fraction showed the highest reduction in $^1O_2$ yield upon binding Zea. To distinguish between the contributions of individual Lhc gene products, monomeric antennae fractions isolated from either dark-adapted and EL-treated WT leaves were further fractionated by preparative isoelectrofocusing; this purification procedure was shown to be affective in removing loosely bound pigments, such as xanthophyll bound to the external V1 site of LHCII, whereas xanthophylls of inner binding sites were retained (25). The pigment composition of purified complexes were analyzed by HPLC (supplemental Table S2); fraction 1 contained only monomeric LHCII and had a low content of Zea, whereas the fractions containing minor antennae had higher levels of Vio-Zea exchange. The fractions were further analyzed for their $^1O_2$ release upon EL treatment. Results are reported in Fig. 3; monomeric LHCII-Zea (fraction 1) did not show significant differences in $^1O_2$ yield with respect to LHCII-Vio (Fig. 3*A*); instead, fractions enriched in monomeric antennae (fractions 2–4) showed clear differences, with complexes from dark-adapted leaves yielding from 25% (CP29) to 65% (CP24) more $^1O_2$ with respect to the same complexes isolated from EL-treated leaves (Fig. 3, *B–D*).

Role of Zea-Lhc Interaction in the Photoprotection of PSII Antenna Subunits—The hypothesis that the lack of Zea might prevent activation of photoprotective mechanisms localized within monomeric Lhcs, thus enhancing ROS production specifically at the level of monomeric Lhcbs, was further investigated by analyzing WT and *npq1* genotypes for their capacity to resist degradation of Lhcb complexes *in vivo* upon exposure to EL. The kinetics of Lhcb photodegradation under strong light was quantified on total leaf extracts by immunoblotting with specific antibodies directed against different polypeptides supplemental Fig. S2). We observed that upon EL treatment the abundance in individual Lhcb polypeptides underwent a decay with rates that are affected by the presence/absence of Zea. A pronounced effect was clearly observed in the decay of minor

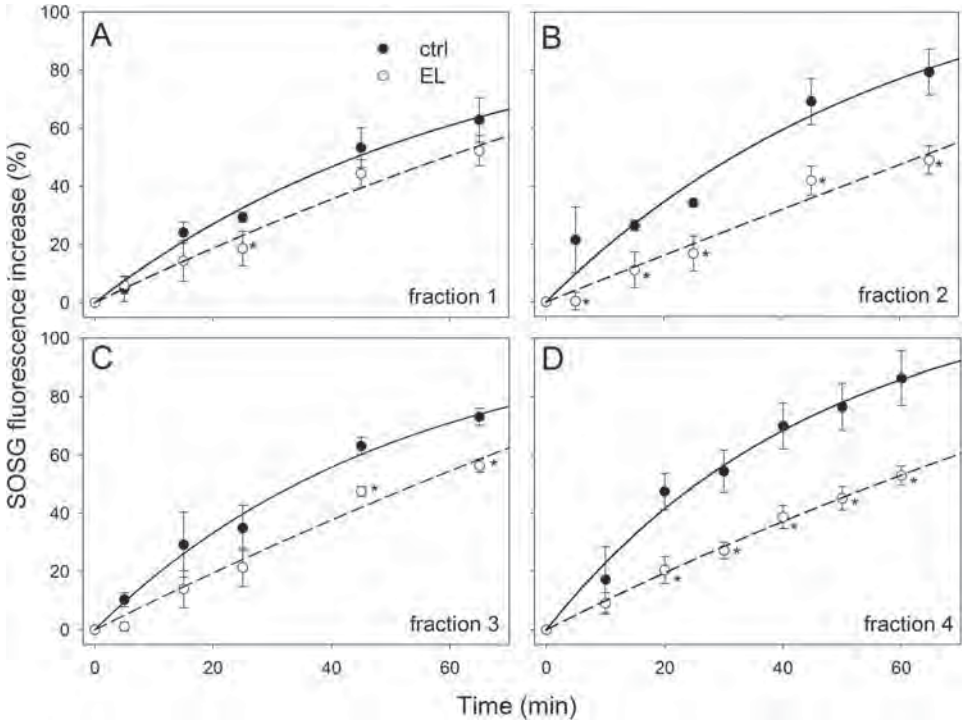

FIGURE 3. **Light-dependent $^1O_2$ release from monomeric Lhcb complexes.** SOSG was used to quantify light-dependent $^1O_2$ yield of monomeric Lhcb isolated by isoelectric focusing. Fluorescence of SOSG has been measured upon illumination of fractions containing monomeric LHCII (*A*) or enriched in minor antennae CP24 (*B*), CP29 (*C*), or CP26 (*D*) with either Vio bound (*closed symbols*) or Zea bound (*open symbols*) at 1000 μmol of photons m^{-2} s^{-1}. Monomeric LHCII isolated from either dark-adapted or EL-treated plants did not show any changes in $^1O_2$ yield (*A*). Zea binding monomeric Lhcbs (*B*, *C*, and *D*) showed significantly lower $^1O_2$ production than the Vio binding complexes. Thus, Zea bound to minor antennae plays a role in enhancing photoprotection by preventing the production of $^1O_2$. *, $p < 0.05$ by Student's *t* test of Zea binding complexes relative to the corresponding Vio binding.

antennae that depended on the WT or *npq1* genetic background, whereas the decay rate of the major LHCII polypeptides was only marginally affected if at all (supplemental Fig. S2). The decay for Lhcb4–6 degradation was clearly faster in *npq1* leaves (no Zea) than WT (+Zea) during EL stress, whereas no difference was observed in the case of LHCII (supplemental Fig. S2). We conclude that the Zea-dependent enhancement of photoprotection is located in monomeric Lhcs rather than in the major trimeric LHCII complex.

Time-resolved Laser Spectroscopy Measurements of the Car Triplet-excited States—Previous work has shown that ^{3}Chl* quenching and $^1O_2$ scavenging by xanthophylls ligands are the major determinants for the level of $^1O_2$ release by Lhc proteins upon EL treatment *in vitro* and *in vivo* (55, 56). To identify the physical mechanism(s) underlying the Zea-dependent photoprotective effect in plants, we measured the light-induced formation of triplet states (TmS spectra) upon excitation of Chl at 650 nm. These spectra are denoted TmS because they show the intersystem crossing of a pigment from its singlet state to its triplet state. The disappearance of the singlet state (S_0) and the appearance of the triplet state (T_1) are observed as a bleaching of the singlet absorbance bands ($S_2 \leftarrow S_0$) and the appearance of triplet absorbance bands ($T_2 \leftarrow T_1$). Such measurements of light-induced absorbance changes were done on a reconstituted *in vitro* suspension containing a mixture of Chl *a* and purified xanthophylls and *in vivo* on intact leaves from *Arabidopsis* genotypes differing in their capacity to synthesize Zea in EL (see supplemental Fig. S3, which compares the *in vivo* spectra with the triplet state spectra of Vio and Zea in solution, and supplemental Table S1 for pigment composition of the different genotypes). As expected, the kinetics and spectral response of the *in vitro* and *in vivo* systems were different because of the different environments (solvent or protein, respectively) surrounding the pigments. As commonly reported, the absorption peaks of pigments in solution are shifted toward shorter wavelengths as compared with what they are in the proteins, and due to diffusion, energy transfer between pigments in solution is slower than in their native environment. The data obtained on isolated pigments show that Zea is the "red-most carotenoid" (Table 1). It suggests that the substitution of Vio into Zea must translate into a red shift of the *in vivo* triplet spectrum of carotenoids.

On intact leaves a strong absorbance increase is instantly (<100 ns) observed at 520 nm after a flash of 650 ± 10-nm light (supplemental Fig. S3). The decay of this signal is biexponential, with half-times of ~2 μs and ~200 ms. Measurements of the dependence of each component on the intensity of the excitation light and the corresponding spectra at approximately maximum amplitude are shown in supplemental Fig. S3, C and D, respectively. The fast (~2 μs) component dominantly results from ^{3}Car*, whereas the slow component (~200 ms) is due to the electrochromic band-shift of carotenoids induced by transmembrane charge separation (57). Therefore, the TmS spectra of carotenoids can be deconvoluted from the electrochromic shift of carotenoids on the basis of their very different lifetimes. The amplitude of the triplet signal largely exceeds the amplitude of the bandshift signal, itself largely exceeding the $P700^+$ signal; indeed, in the spectral region 500–560 nm (Fig. 4) $P700^+$

TABLE 1

Singlet state, ϵ_S, and triplet state, ϵ_T, extinction coefficients of xanthophylls.

Extinction coefficients are at the wavelengths indicated in parentheses. The values are in units of L/mol·cm. The ϵ_S values were obtained from Britton *et al.* (80). The ϵ_T values were obtained as described in the text. ("Experimental Procedures - Spectroscopy")

Xanthophyll	ϵ_S	ϵ_T
	liters/mol·cm	*liters/mol·cm*
Violaxanthin	1.5×10^5 (440 nm)	4.2×10^5 (481 nm)
Zeaxanthin	1.4×10^5 (450 nm)	3.6×10^5 (510 nm)
Lutein	1.4×10^5 (445 nm)	3.2×10^5 (490 nm)
Neoxanthin	1.3×10^5 (440 nm)	3.6×10^5 (485 nm)

signal is very flat and of small amplitude (58). In the subsequent text, the fast microsecond component is referred as TmS (triplet-minus singlet) difference spectrum.

The TmS transition of WT, *npq1*, and *lut2* leaves, dark-adapted and after exposure to strong actinic light (to trigger the synthesis of Zea), in the 500–560-nm range that includes the ^{3}Car* transition are shown in Fig. 4. In comparing dark-adapted *versus* EL-treated leaves, a loss of signal was observed upon illumination in WT (Fig. 4*A*) and *lut2* (Fig. 4*C*) leaves between 500 and 520 nm (minimum at 505 nm), whereas a gain of signal was observed above 520 nm, with a maximum between 530 and 535 nm. Such an EL-induced red shift in ^{3}Car* transition level is expected from the de-epoxidation of Vio into Zea and from the red-most spectral contribution of the latter (supplemental Fig. S3). Consistently, the *npq1* mutation (Fig. 4*B*) abolished the red shift. It is worth noting that the amplitude of the ^{3}Car* red shift measured on intact leaves was proportional to the amount of Zea accumulated during EL treatment, which was not existent in *npq1*, greatest in *lut2*, and in-between the changes observed in *npq1* and *lut2* for WT leaves. These results show that Zea synthesis correlated with the formation of the red-shifted ^{3}Car* spectral form on intact leaves.

The red-shifted spectral form is likely to arise via ^{3}Chl* quenching rather than scavenging of $^1O_2$ because, although scavenging of $^1O_2$ by Zea occurs in the lipid phase (22, 29), it is very unlikely that it would be detected on timescales as short as 100 ns. To test this hypothesis, *ch1* mutants were investigated, as *ch1* plants lack Lhcb and have eight times more lipid-free xanthophylls than WT plants (30), implying that the red-shifted ^{3}Car* spectral form should be more evident in these mutants if it results from scavenging. Upon light-induced Zea synthesis, the *ch1lut2* plants (lacking both Lhcbs and Lut) did not undergo changes in the carotenoid TmS spectrum (Fig. 4*D*), although they do synthesize twice as much Zea than *lut2* plants (29). It seems plausible that β-carotene is the only carotenoid contributing to the TmS spectra of *ch1lut2* leaves; indeed in this genotype all xanthophylls are released into the thylakoid membrane, and β-carotene is the only carotenoid bound to chlorophyll-protein complexes, thus in condition to perform direct quenching of ^{3}Chl*. This is consistent with TmS spectrum reported for *ch1lut2* dark-adapted leaves, which showed a maximum even redder than that of EL-treated WT leaves; indeed, similar ^{3}Car* transition maxima have been reported for Zea and β-carotene (59). Additional measurements on mutants with different abilities for synthesizing Zea under EL treatment, namely *npq1lut2* and *npq2lut2*, showed that the formation of the red-shifted ^{3}Car* signal was associated with the extent of Vio to Zea conversion (Fig. 4, *E* and *F*). Moreover, TmS red shift still holds in a mutant lacking qE (*npq4lut2*, see supplemental Fig. S4) implying it is independent from PsbS, the protein essential for qE. Therefore, we conclude that the Car red shift observed is only due to Zea bound to the Lhc proteins serving as Chl *a*/*b*-xanthophyll binding antennas of photosystems.

Identification of Photosynthetic Subunits Involved in the Red Shift of Carotenoid Triplet Signal—To find the binding site for the Zea responsible for the red shift observed in the ^{3}Car* spectrum of leaves, we performed TmS spectroscopy measurements on proteins isolated from WT leaves that were either dark-adapted or treated with EL (Fig. 5; see supplemental Table S2 for pigment composition of purified complexes). Changes were observed in the monomeric Lhcb subunits (Fig. 5*A*) and LHCI (Fig. 5*D*)-containing fractions, whereas trimeric LHCII did not show any changes in the ^{3}Car* spectrum when isolated from EL-treated plants (Fig. 5*B*). These results suggest that both PSII and PSI have a specific Lhc target for Zea binding. A further fractionation of monomeric Lhcbs into antenna components revealed that changes in the ^{3}Car* spectrum were measured in all minor antennae (CP29, CP26, and CP24). Given by way of example, Fig. 5*C* compares TmS spectra from samples of CP26 containing either Vio or Zea (CP26 dark-adapted and CP26 EL, respectively) at the same Chl concentration. The peak amplitude of the CP26 dark-adapted sample is reduced by 45% with respect to CP26 EL, whereas the amount of absorption at wavelengths longer than 520 nm is ~60% higher in the CP26 EL sample containing Zea. In the LHCI samples containing either Vio or Zea (LHCI dark-adapted and LHCI EL, respectively) the peak was observed at 515 and 525 nm, respectively (Fig. 5*D*). We conclude that the TmS spectral shift observed *in vivo* tightly correlates with that detected in the LHCI and Lhcb4–6 subunits but not in the major trimeric LHCII complex. Moreover, both of these spectral features are associated with the major component of Zea-dependent photoprotection.

Investigation on the Chlorophyll-to-carotenoid Triplet Transfer—The mechanism(s) underlying the decreased production of $^1O_2$ upon Zea binding could be either (i) an increased efficiency in ^{3}Chl* quenching by xanthophylls bound to Lhc proteins or (ii) a direct down-regulation of the chlorophyll triplet yield, as compared with other de-excitation pathways. To distinguish between these two hypotheses, we assessed both the total amount of ^{3}Car* and the kinetics of ^{3}Car* formation in isolated pigment-protein complexes by time-resolved TmS spectroscopy. For this experiment, we chose the monomeric CP26 protein purified from dark-adapted or EL-treated WT leaves; in the latter, both (i) the Zea-dependent reduction of $^1O_2$ release (Fig. 2*C*) and (ii) the red shift in TmS spectra (Fig. 5*C*) were observed.

For an estimation of ^{3}Car* formed upon chlorophyll excitation, the TmS spectra of CP26 was fitted with ^{3}Car* spectral forms in a protein environment (Fig. 6), obtained by measuring recombinant LHC reconstituted with single xanthophyll species.[3] Although this deconvolution problem might have more

[3] R. Bassi, unpublished results.

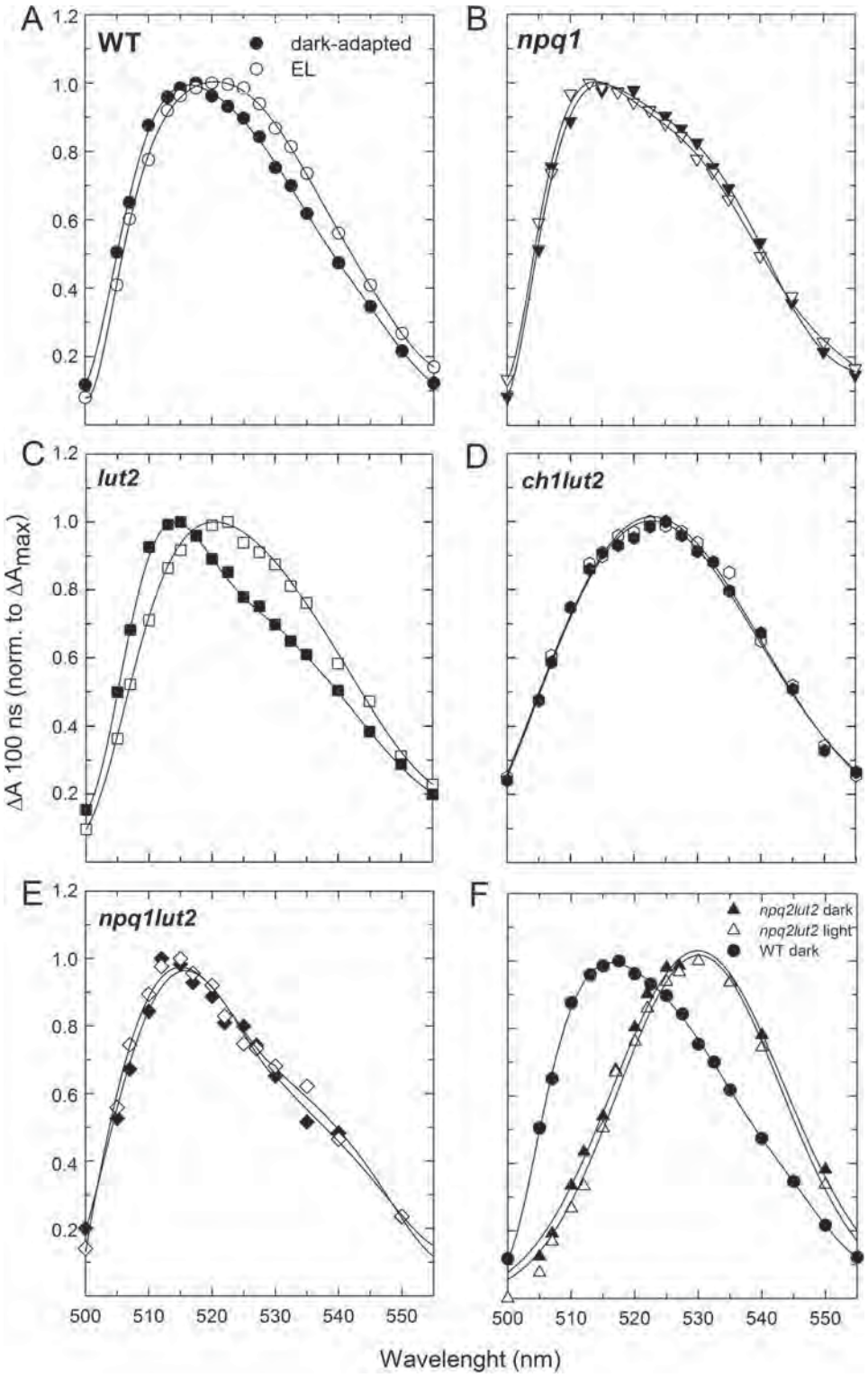

FIGURE 4. **Light-induced red shift of the carotenoid triplet transition on intact leaves.** Carotenoid triplet signal (difference between the spectra at 100 ns and 30 μs) was registered on *Arabidopsis* WT leaves either dark-adapted (*closed symbols*) or treated with EL (*open symbols*) upon vacuum infiltration with Norfluorazon to stabilize Zea content during measurements (see "Experimental Procedures" for details). Briefly, the same dark-adapted leaf, without being removed from the sample holder, was then illuminated with a continuous red light (630 nm $< \lambda <$ 700 nm, 1500 μmol of photons m^{-2} s^{-1}). After 15 min of exposure to the red light, the triplet signal was measured again. TmS spectra were recorded on leaves from WT (*A*), *npq1* (*B*), *lut2* (*C*), *ch1lut2* (*D*), and *npq1lut2* (*E*). In *panel F*, spectra of leaves from mutant *npq2lut2* (*triangles*), which constitutively accumulates Zea, are compared with the carotenoid triplet transition measured on dark-adapted WT leaves (*closed circles*).

than one solution, the fits given in Fig. 6 give a likely estimation of the total amount of ^{3}Car* formed upon excitation of Chls in the two samples. Both TmS spectra were described using single ^{3}Vio*, ^{3}Lutein* (^{3}Lut*), and ^{3}Zea* forms; the spectra of the CP26-Vio and CP26-Zzea complexes fit well by using similar spectral forms of ^{3}Vio* and ^{3}Lut*, whereas a

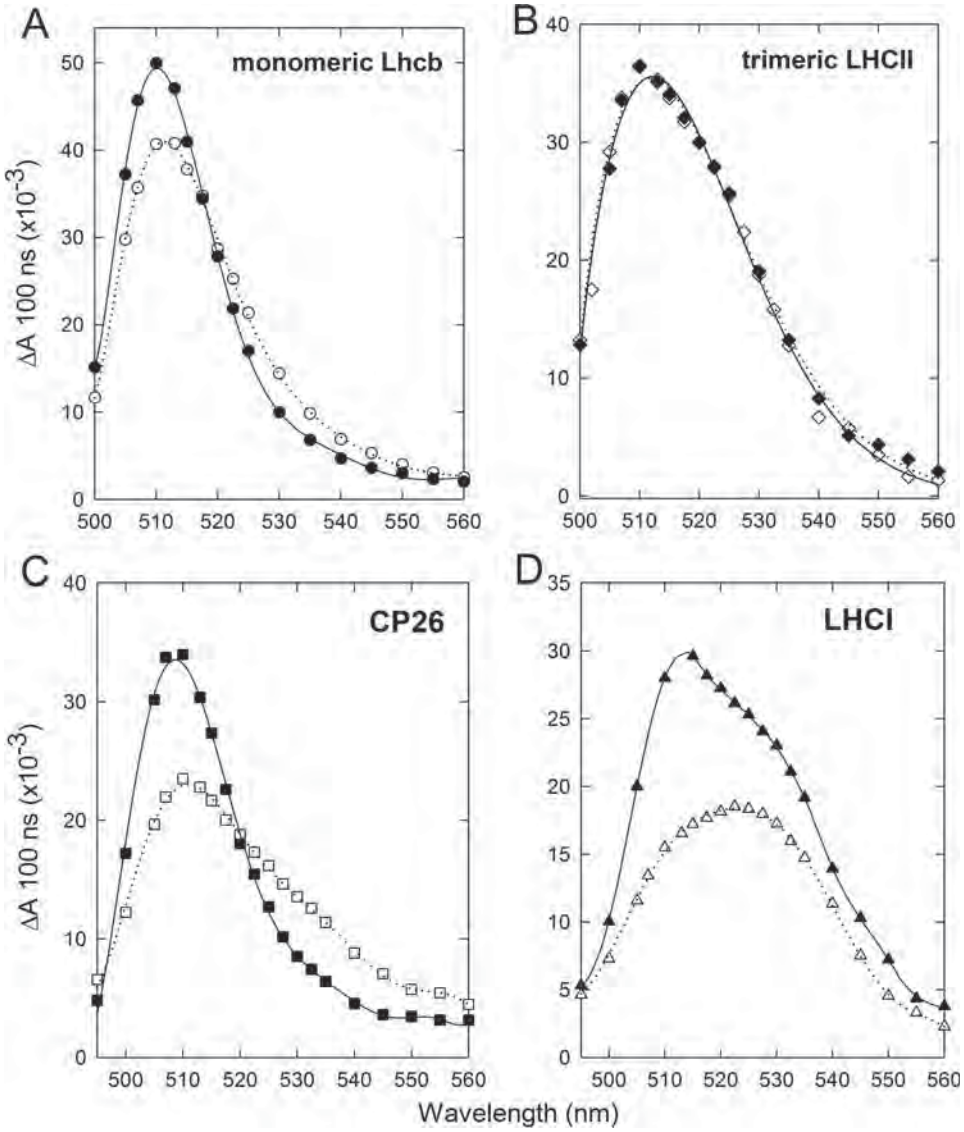

FIGURE 5. **Zea-induced red shift of the carotenoid triplet transition on isolated Lhc.** Spectral changes in the carotenoid triplet signal were detected in Lhc proteins isolated from *Arabidopsis* WT before and after EL exposure, leading to partial replacement of Vio by Zea in the protein complexes. Measurements were performed on either monomeric Lhcb (*A*), trimeric LHCII (*B*), the minor antenna CP26 (*C*), and the PSI-LHCI (*D*) proteins purified from dark-adapted (*closed symbols*) or EL-treated (*open symbols*) leaves.

^{3}Zea* form was necessary to fit the CP26-Zea TmS spectrum (Fig. 6, *A* and *B*).

The contributions of each xanthophyll to the total amount of ^{3}Car* formed were determined by using both the amplitudes in TmS spectra and ^{3}Car* extinction coefficients (ϵ_T) measured on isolated xanthophylls (Table 1) and are shown in Fig. 6*C*. In the CP26-Zea sample, the contributions of both ^{3}Vio* and ^{3}Lut* (which are reduced with respect to CP26-Vio sample) are compensated by formation of ^{3}Zea* (Fig. 6*C*).

To assess the kinetics of ^{3}Car* formation on purified CP26, time-resolved absorbance changes were recorded at two distinct wavelengths, corresponding to the maximum absorbance of ^{3}Vio* + ^{3}Lut* (510 nm) and ^{3}Zea* (530 nm). Similar half-times for both ^{3}Car* rise and decay (supplemental Fig. S5) were determined at both wavelengths, implying no differences in the ^{3}Chl* quenching capacity of CP26-bound Zea *versus* Vio.

In light of these findings, we attempted to verify the alternative hypothesis of direct modulation of ^{3}Chl* yield upon binding of Vio *versus* Zea independent from the quenching by xanthophylls. To this aim, we used FDMR. FDMR is a double resonance technique based on the principle that when a triplet steady state population is generated by illumination, application of a resonant electromagnetic field between a couple of spin sublevels of the triplet state induces a change in the steady state population of the triplet state itself due to anisotropy of the decay and population rates of the three spin sublevels. In FDMR experiments, the change induced in the triplet population is detected as a corresponding change in the emission of the system (60, 61). The activity of the carotenoids in quenching triplet states was investigated at low temperature (1.8 K), when the funneling of the excitation toward the low lying excited states of the Chl molecules is fast.

The low temperature emission spectrum of thylakoids from *Arabidopsis* WT showed the characteristic Chl *a* fluorescence bands peaking at 685–695 and 735 nm due to the different antenna pools belonging to PSII and PSI, in agreement with

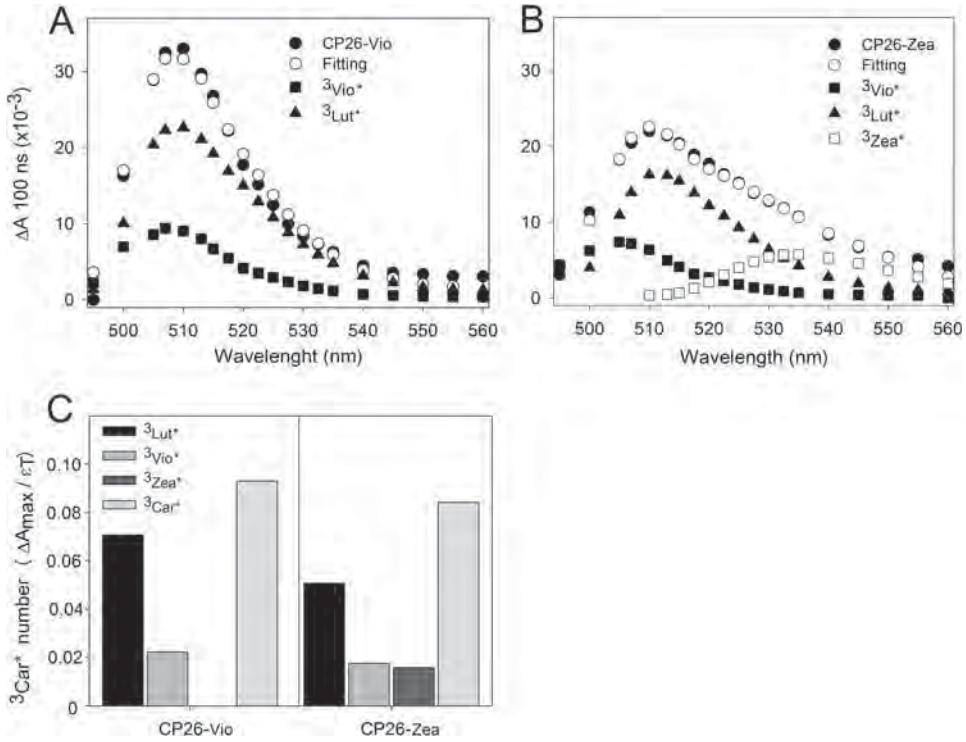

FIGURE 6. **Decomposition of CP26 TmS spectra.** Fitting of CP26 purified from leaves either dark-adapted (*A*) or treated with EL (*B*) was performed using absorption forms for xanthophyll triplets in protein environment. Components peaking at 507 and 510 nm were attributed to ^{3}Vio* and ^{3}Lut*, respectively, whereas the spectral form at 532 nm was attributed to ^{3}Zea*. In *panel C*, the amplitude of each spectral forms and the values of ϵ_T (Table 1) were used to calculate the number of triplet excited states formed upon excitation of Chl at 650 nm. The total carotenoid triplets (^{3}Car*) calculated from the spectral analysis were very similar in both samples.

literature data (data not shown). The FDMR signals, detected at 680–690 (PSII) and 720 nm (PSI), which represent transitions of ^{3}Chl* states, are shown in Fig. 7*A*. The three FDMR transitions with the polarization pattern usually found for ^{3}Car*, detected at 690 and 730 nm, are presented in Fig. 7*B* (44–46, 62). Two ^{3}Chl* components (visible in the 690 nm FDMR spectra), with $|D| - |E|/|D| + |E|$ transitions at about 725/945 and 742/965 MHz, have been previously assigned to the PSII outer antennae, whereas the 767/992-MHz component has been attributed to the core complex (45) (note that the signals have been reversed in sign compared with Ref. 48 for better representation). The ^{3}Car* states detected at 690 nm has been assigned to the PSII Lhcs (45). The negative signal at ~1000 MHz in the $|D| - |E|$ spectrum of ^{3}Car* in thylakoids (Fig. 7*B*) is the contribution of the ^{3}Chl* state from the PSII core complex (992 MHz component). The amplitude of this signal is enhanced due to the high frequency modulation (325 Hz) used for the ^{3}Car* measurement because of its fast decay (48). Other slower ^{3}Chl* components are not detected at this frequency (63).

The FDMR spectra of the thylakoids isolated from dark-adapted *npq1* leaves were identical to those of the sample from WT in the entire detection range explored (Fig. 7*C*). When measurements were performed on thylakoids isolated from WT EL-treated leaves (see supplemental Table S3 for pigment composition of thylakoids used), a decrease (−25%) in the intensity of the FDMR signals assigned to two ^{3}Chl* states belonging to PSII ($|D| - |E|$ transitions at 742 and 767 MHz) was observed. Also, a new component (719/992 MHz) appeared that can be assigned to the P_{680} recombination triplet state (64). Interestingly, in the thylakoids isolated from *npq1* EL-treated leaves, the intensity of the 742 MHz component did not undergo any decrease. A decreased amplitude was observed for the 767-MHz component, with a corresponding increase in the 720 MHz component (Fig. 7*C*). Except for the lack of the ^{3}P680* state formation, similar results were obtained on thylakoids isolated from dark-adapted WT and *npq1* leaves and de-epoxidated in the dark by incubating thylakoids at pH 5.2 (supplemental Fig. S6), implying that Zea itself, rather than the light treatment, is responsible for the spectral changes observed.

The FDMR signals of the ^{3}Car* states were sensitive to the treatments performed on the sample; the prolonged EL exposure induced a decrease of the intensity of the signals in WT thylakoids, whereas the effect was not evident in the *npq1* thylakoids (Fig. 7*D*). It should be noticed that carotenoids triplet states were observed in the presence of Zea, however, not with an increased yield. Lut and Zea contributions to the FDMR signal cannot be distinguished, as they have the same resonance frequencies as detected by comparing spectra from *npq2lut2* genotypes, containing Zea as the only carotenoid with the *npq2* containing Lute and Zea (not shown). Although FDMR cannot ascertain if Zea triplet states are or not populated at all, it is clear that the carotenoid triplet yield does not increase and does not correlate with the decrease of the ^{3}Chl* population in the presence of Zea. Once identified, the Zea-dependent effect on modulation of ^{3}Chl* populations in thylakoids was tracked to the individual pigment-protein components by performing the

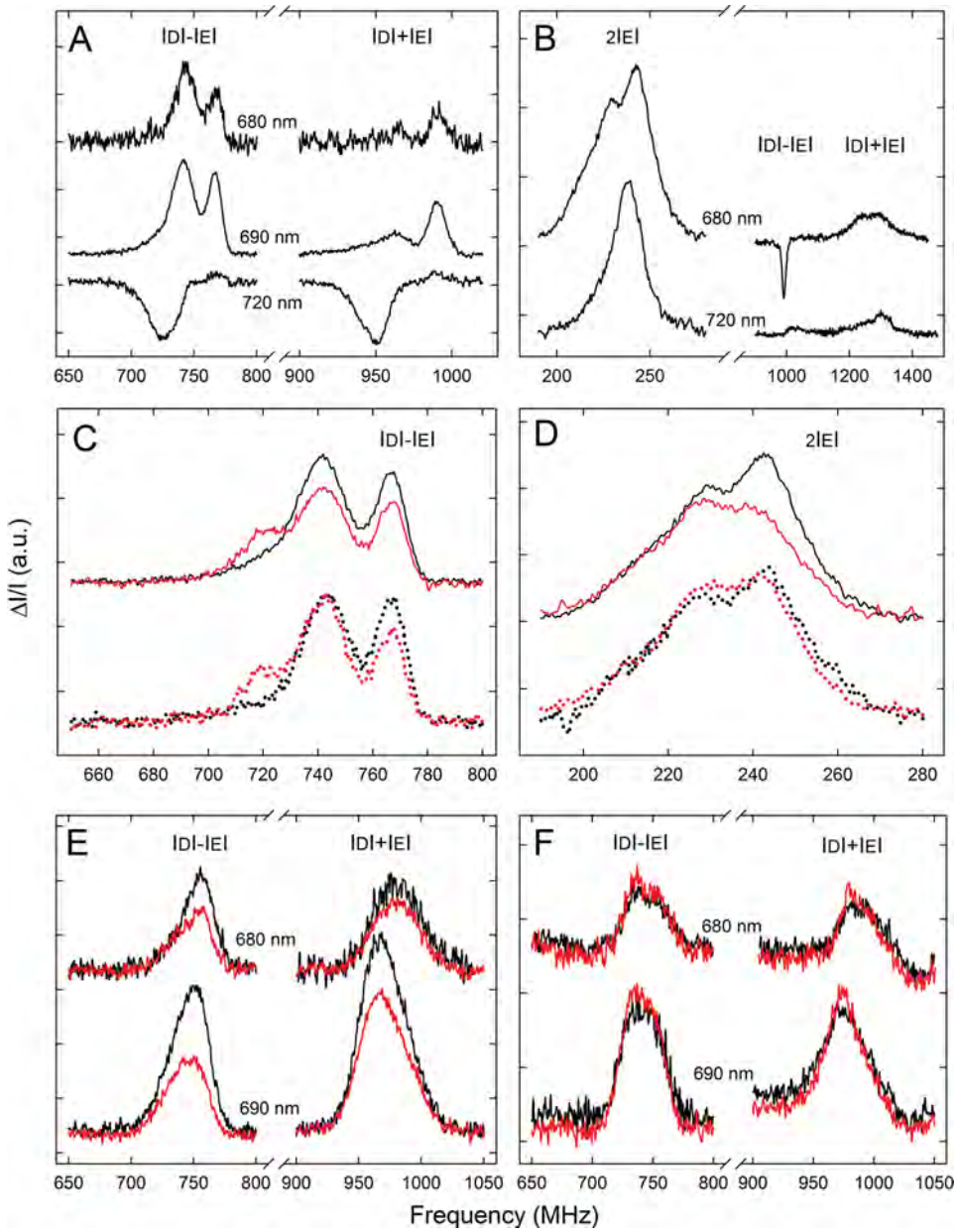

FIGURE 7. **Fluorescence detected magnetic resonance of the chlorophyll and carotenoid triplet states on thylakoids and isolated Lhc.** *A* and *B*, FDMR signals of the ^{3}Chl* states ($|D| - |E|$ and $|D| + |E|$ transitions) (*A*) and the ^{3}Car* states (*B*) observed in the WT thylakoid, dark-adapted sample, were detected at different wavelengths. *C*, $|D| - |E|$ transitions of the ^{3}Chl* states observed in the WT (*solid*) and *npq1* (*dotted*) thylakoids are shown. *Black*, dark-adapted; *red*, EL exposure. *a.u.*, absorbance units. *D*, shown are $2|E|$ transitions of the ^{3}Car* states, observed in the WT (*solid*) and in the *npq1* (*dotted*) thylakoids. *Black*, dark-adapted; *red*, EL exposure. *E*, FDMR signals of the ^{3}Chl* states of the minor antennae of WT detected at 680 and 690 nm are shown; dark-adapted samples are in *black*; samples isolated after EL irradiation are in *red*. *F*, FDMR signals of the ^{3}Chl* states of the trimeric LHCII of WT detected at 680 and 690 nm; dark-adapted samples are in *black*; samples isolated after EL irradiation are in *red*. Spectra have been vertically shifted for better comparison. Amplitude modulation frequency: 33 Hz (^{3}Chl* states) and 325 Hz, (^{3}Car* states), tc 600 ms, number of scans 20, mw power 500 milliwatt, temperature 1.8 K. *tc*, time constant; *mw*, microwaves.

same measurements on the different proteins isolated from WT leaves, either dark-adapted or treated with EL (Fig. 7*E*).

The ratio between the intensities of $|D| - |E|/|D| + |E|$ transitions of ^{3}Chl* are different in isolated Lhcs (Fig. 7*E*) with respect to thylakoids (Fig. 7*A*). Amplitudes of these transitions are sensitive to the environment of the triplet states; indeed ^{3}Chl* states show variable amplitudes in the two transitions due to changes in both populations and decay probabilities of the triplet sublevels. In thylakoids, the presence of interacting complexes creates a protein environment different than the detergent micelles of the isolated Lhcs. Moreover, FDMR spectra of thylakoids also contain the contribution from the PSII inner antenna subunits (767/992 MHz), absent in purified Lhcs.

Again, the Lhcbs affected by the light irradiation were the monomeric Lhcb4–6 proteins rather than the major LHCII complex. In Fig. 7*E*, the FDMR signals of ^{3}Chl* states detected at two different wavelengths show a decrease in intensity of 40% in the monomeric antenna fraction when binding Zea *versus* Vio. We did not observe any increase of the ^{3}Car* states correlated to the decrease of the ^{3}Chl* states. No change on the

triplet states FDMR signals was detected in the samples from *npq1,* and the FDMR spectra of isolated trimeric LHCII from WT and *npq1* were both insensitive to EL exposure of leaves previous to isolation (Fig. 7*F*). Establishing if the subset of chromophores-forming triplets is the same in both thylakoids and Lhcs is not straightforward. However, the effect of EL on the ^{3}Chl* yield is the same in both the minor Lhcbs and in thylakoids, suggesting these triplets have the same origin.

DISCUSSION

In this work we have scrutinized the mechanisms that contribute to the photoprotective effect of Zea, the xanthophyll specially synthesized in response to EL conditions. Previous work indicated that Zea synthesis has multiple effects. Earlier reports have emphasized the enhancing effect on qE, the PsbS-dependent thermal dissipation of ^{1}Chl* excited states (11, 14), and the uncoupler-resistant component called irreversible quenching or, more recently, qZ (51). A second photoprotective effect was reported to consist of a scavenging effect of lipid-free Zea for ROS released from Chl binding complexes (22, 29). A Zea-enhanced scavenging effect was also reported within Lhc proteins (30, 65). Although these functions contribute to the Zea photoprotective effect, genetic dissection showed that thermal dissipation of excess energy dissipation has a relatively small effect as assessed using the *npq4* mutant lacking qE (66) and likewise for the scavenging effect of lipid-free Zea with respect to the Lhc-bound fraction (Fig. 1). This implies that the Zea-dependent photoprotection effect is associated to the binding of Zea to Lhc proteins, where it has a strong effect in decreasing $^1O_2$ evolution during illumination. Here, we used high sensitivity laser spectroscopy to investigate changes in the optical properties of leaves associated with EL treatment. Illumination of *Arabidopsis* wild type plants induced a spectral red shift of the $T_2 \leftarrow T_1$ transition of ^{3}Car*. Using a range of *Arabidopsis* mutants, this spectroscopic feature was observed only in genotypes able to accumulate Zea, either upon EL exposure or constitutively (Fig. 5), irrespective of their the ability to perform qE (supplemental Fig. S4) and was coupled to a modulation of ^{3}Chl* yield, suggesting this mechanism is a component of photoprotection.

A Mechanism of Photoprotection Based on ^{3}Chl Down-regulation*—Because the TmS red shift involves the major ^{3}Car* transition, we first investigated if Zea had an enhanced ^{3}Chl* quenching capacity with respect to the pre-existing Viola, thus yielding a lower level of ^{3}Chl* formation. However, this was not confirmed by experimental evidences as (i) although not entirely resolved due to the 10 ns limitation in time resolution of our spectrophotometer, the kinetics of ^{3}Car* population was the same in Vio (510 nm) and Zea (530 nm) binding CP26 (supplemental Fig. 5), (ii) the relatively similar extinction coefficients of ^{3}Zea* and ^{3}Vio* (Fig. 6 and Table 1) imply that the decrease in the 510-nm band (^{3}Vio*) appears to be compensated by a similar increase of the 530-nm (^{3}Zea*) component in the spectra of Fig. 5*C* without a major difference in quenching efficiency between Zea and Vio, and (iii) a slight decrease in the ^{3}Car* level was detected by both laser spectroscopy (Fig. 6) and FDMR (Fig. 7*D*) in Zea *versus* Vio binding complexes. Rather, FDMR measurements showed that Zea binding to Lhc proteins induces a down-regulation of the ^{3}Chl* yield of the complexes (Fig. 7*E*) and whole thylakoids (Fig. 7*C*), likely through a mechanism different from the previously described triplet energy transfer to xanthophyll ligands (56, 67). The spectra are taken at 1.8 K; however, the samples adapted at RT were frozen by direct immersion on liquid helium into the cryostat, and therefore, the spectra are representative of the conformational distribution present at RT. It should be noted that the decrease in the concentration of ^{3}Chl* on both thylakoids and minor antennae cannot be ascribed to the residual quenching of ^{1}Chl* observed (68) upon EL treatment, as the procedure for thylakoid isolation is long enough to allow complete relaxation of NPQ induced by EL on leaves (19); the small quenching of ^{1}Chl* measured upon binding of Zea to minor antennae (about 10% than the corresponding sample from dark-adapted WT leaves, data not shown) cannot account for a 40% decrease in the concentration of ^{3}Chl* in these complexes (Fig. 7*E*). Moreover, FDMR signals are normalized to the amplitude of the steady state fluorescence. Thus, if the lower ^{3}Chl* yield was only due to the quenching of the corresponding singlet states, a decrease in the FDMR signal of the same level would be expected; instead, the decrease in the ^{3}Chl* yield in thylakoids upon EL treatment was ~25% (Fig. 7*C*) without a change in steady state fluorescence (not shown).

It is well known that CP26 and other Zea binding Lhc subunits undergo a conformational change upon exchange of Vio to Zea (51). We suggest that this conformational change, by affecting Chl-Chl and/or Chl-protein interactions, does modulate the triplet yield of the chlorophyll ligands and thus down-regulates the probability of reaction with O_2 and, subsequently, $^1O_2$ formation. Zea binding to Lhc proteins has at least two effects that may be correlated to each other or may not; that is, (*a*) quenching of ^{1}Chl* excited states and (*b*) decrease in ^{3}Chl* yield.

The relationship between the small change in fluorescence yield and the large change in triplet yield undergone by monomeric Lhc proteins upon binding of Zea is not clearly understood. An efficient thermal deactivation of ^{3}Chl* once they are formed appears unlikely because it requires intersystem crossing, making it a relatively slow process. A weak ^{1}Chl* quenching effect can be accounted for by an effect limited to a subset of chlorophylls in the pigment-protein complex. Such an effect could be produced by one of the following mechanisms; (i) the conformational change induced by Zea binding causes excitons in Chls bound to such a domain to be diverted from the sites where ^{3}Chl* are formed with higher yield (*i.e.* the red-most sites such as Chl A2, A4), possibly due to changes in the energy level of the former Chls (69), or (ii) alternatively, Chls generating triplet states with higher yield might become more readily quenched when still at their ^{1}Chl* state via thermal relaxation (70, 71). In such case, the singlet quenching would be limited to a subset of Chls of limited amplitude when refereed to the whole complex (52, 68, 72), whereas the effect on triplet state would be stronger.

Quenching of singlet states during short term light adaptation (qE) has been shown to be correlated to energy transfer from the Chl Q_y transition and the short-living ^{1}Car* state followed by thermal deactivation via the formation of a Chl^-/

Car^+ radical pair (18, 69). Such a mechanism could also favor $^3Chl^*$ to ^1Car energy transfer. However, the radical pair formation has been shown to require both the synthesis of Zea and the presence of a trans-membrane pH gradient, whereas its yield coefficient is far lower in isolated Lhc (18); this evidence is not consistent with the 40% reduction in $^3Chl^*$ yield detected in isolated pigment-protein complexes (Fig. 7).

Alternatively, the modulation of $^3Chl^*$ yield might be independent from the formation of radical pairs. Whatever the physical mechanism involved, the physiological effect is strong and produces effective photoprotection.

$^3Chl^*$ Down-regulation and PSII Supercomplex Organization—The search for fractions of thylakoid membranes exhibiting the red-shifted TmS spectrum and reduced FDMR $^3Chl^*$ signal yielded two major targets: monomeric Lhcb4–6 antenna subunits of PSII and LHCI. This is in agreement with previous work on Vio *versus* Zea exchange in different Lhc proteins during the operation of xanthophyll cycle (20, 53), as CP26 (Lhcb5), CP24 (Lhcb6), and Lhca4 were found to be the best "exchangers" among all Lhcs. Previous work with recombinant Lhc proteins (20) and *in vivo* (51) has shown that xanthophyll exchange is operated at the level of binding site L2 in both CP26 and LHCI. It would, therefore, appear that binding of Zea to Lhc proteins is sufficient for the modification of the triplet-state properties of the pigment-protein complexes, whereas the actual expression of this effect is controlled by the capacity for xanthophyll exchange in site L2 of the individual gene products. It should be noted that monomeric Lhcbs are located in between the PSII core complex and the outer antenna layer made by 2–4 copies of trimeric LHCII (75), each binding 42 Chls and 12 xanthophylls (26), implying most excitation energy collected by LHCII is funneled to the PSII reaction center through monomeric Lhcbs. Supplemental Fig. S2 clearly shows that, under EL conditions, Lhcb monomers get destroyed faster than LHCII unless they bind Zea that makes them more resistant to photodestruction.

A recent report demonstrated that, although xanthophyll ligands are very efficient in $^3Chl^*$ quenching, a limited fraction of $^3Chl^*$ cannot be quenched. In their original work, Mozzo *et al.* (56) measured a small amount of unquenched $^3Chl^*$ at physiological temperatures in LHCII. This is consistent with evidence that some Chls in purified LHCII, *e.g.* Chl 611 (26) were located too far apart from xanthophylls for efficient triplet transfer and can explain the bleaching of the complex when challenged with EL (76) (supplemental Fig. S2). In LHCII, ~5% of the triplets reside on Chls, corresponding to a 95% efficiency for Chl to Car triplet transfer (56); this value was lower for Lhcb5 and for Lhcb6 (52), reaching ~20% of unquenched $^3Chl^*$ in Vio binding complexes.

Results described here (Fig. 7) clearly show that even Chls in minor antennae, although active in singlet energy transfer (as assessed by fluorescence emission measurements), are not equally active in transferring triplets. It is well known that triplet transfer requires shorter distances between the chromophores than singlet transfer. The absence of a triplet transfer enhancement upon Zea synthesis on one hand and regulation of $^3Chl^*$ on the other, however, suggests that the binding of Zea in site L2 has an effect on the structure of the complex; it might result in an altered organization of protein domains to modulate the triplet yield of some chlorophylls rather than in a conformational change that reduces the proximity between unprotected chlorophylls and xanthophylls.

Why is Zea only present during stress conditions when it is effective in photoprotection? At least one reason, if not the only reason, is that massive binding of Zea to Lhc (such as in *npq2* mutant of *Arabidopsis*) is well known to strongly decrease the excited singlet state lifetime (77) of the plants. Therefore, plants that constitutively accumulate Zea can utilize less photons for charge separation, which decreases the growth rate in limiting light (51). We conclude that monomeric Lhcbs in WT PSII are present in two states, dark-adapted and EL, binding Vio and Zea, respectively, in their L2 sites. The dark-adapted state ensures a longer fluorescence lifetime and relatively high $^3Chl^*$ yield, which is not a problem due to efficient photochemical quenching in low light conditions. The EL state has a lower $^3Chl^*$ level and a shorter $^1Chl^*$ lifetime (68) than the dark-adapted state, which is well suited for photoprotection under these conditions. Besides Lhcbs, Zea also binds to Lhca polypeptides, which is so far unexplained under the widespread understanding that the major Zea function is to enhance qE due to the low level of excited states (short fluorescence lifetime) of PSI. Nevertheless, Lhca subunits host the red-most absorption forms that make a low energy trap for excitation energy before photochemical quenching by P700 (78). Because of the $^3Chl^*$ down-regulating effect of Zea, its binding to Lhcas may be understood as a photoprotection mechanism for highly localized excitons in Lhca3 and Lhca4, the red-most subunits in the PSI-LHCI supercomplex (79).

We have shown that Zea accumulation in chloroplasts under EL produced a red shift of the major carotenoid transition in the TmS spectra. These changes were measured on intact leaves and correlate with the amount of Zea accumulated in specific Lhc subunits located in between the major LHCII antenna complex and the reaction center in PSII supercomplexes and in LHCI. The resistance/sensitivity of these proteins to EL conditions indicated that the red shift is correlated with the dominant component of photoprotection, in absence of which monomeric Lhcbs are preferentially destroyed. The protection effect appears to consist with a direct down-regulation of $^3Chl^*$ without a corresponding triplet quenching enhancement by nearby xanthophylls. High resolution crystallography of Zea binding complexes will further assist with elucidating this new mechanism of photoprotection. After this manuscript was finished, the report by Carbonera *et al.* (73) was published, showing that $^3Chl^*$ concentration is strongly reduced upon high light treatment. Although this result is consistent with the present report, it refers to a component of photoprotection distinct from that discuss here. In fact, in Ref. 73 the protective effect was abolished by the *lhcsr1 lhcsr2 psbS* mutation abolishing qE. On the contrary, the zeaxanthin-dependent photoprotection component here described is fully active in the *npq4* mutant lacking PsbS (supplemental Fig. S4).

REFERENCES

1. Green, M. J., and Hill, H. A. (1984) Chemistry of dioxygen. *Methods Enzymol.* **105,** 3–22

2. Moan, J., and Berg, K. (1991) The photodegradation of porphyrins in cells can be used to estimate the lifetime of singlet oxygen. *Photochem. Photobiol.* **53,** 549–553
3. Girotti, A. W., and Kriska, T. (2004) Role of lipid hydroperoxides in photooxidative stress signaling. *Antioxid. Redox Signal.* **6,** 301–310
4. Martinez, G. R., Loureiro, A. P., Marques, S. A., Miyamoto, S., Yamaguchi, L. F., Onuki, J., Almeida, E. A., Garcia, C. C., Barbosa, L. F., Medeiros, M. H., and Di Mascio, P. (2003) Oxidative and alkylating damage in DNA. *Mutat. Res.* **544,** 115–127
5. Davies, M. J. (2004) Reactive species formed on proteins exposed to singlet oxygen. *Photochem. Photobiol. Sci.* **3,** 17–25
6. Harvaux, M., and Kloppstech, K. (2001) The protective functions of carotenoid and flavonoid pigments against excess visible radiations at chilling temperature investigated in *Arabidopsis npq* and *tt* mutants. *Planta* **213,** 953–966
7. Kok, B. (1956) On the inhibition of photosynthesis by intense light. *Biochim. Biophys. Acta* **21,** 234–244
8. Aro, E. M., Virgin, I., and Andersson, B. (1993) Photoinhibition of Photosystem-2. Inactivation, protein damage, and turnover. *Biochim. Biophys. Acta* **1143,** 113–134
9. Long, S. P., Humphries, S., and Falkowski, P. G. (1994) Photoinhibition of photosynthesis in nature. *Annu. Rev. Plant Physiol. Plant Mol. Biol.* **45,** 633–662
10. Frank, H. A., and Cogdell, R. J. (1996) Carotenoids in photosynthesis. *Photochem. Photobiol.* **63,** 257–264
11. Niyogi, K. K., Grossman, A. R., and Björkman, O. (1998) *Arabidopsis* mutants define a central role for the xanthophyll cycle in the regulation of photosynthetic energy conversion. *Plant Cell* **10,** 1121–1134
12. Mathis, P., Butler, W. L., and Satoh, K. (1979) Carotenoid triplet state and chlorophyll fluorescence quenching in chloroplasts and subchloroplasts particles. *Photochem. Photobiol.* **30,** 603–614
13. El-Agamey, A., Lowe, G. M., McGarvey, D. J., Mortensen, A., Phillip, D. M., Truscott, T. G., and Young, A. J. (2004) Carotenoid radical chemistry and antioxidant/pro-oxidant properties. *Arch. Biochem. Biophys.* **430,** 37–48
14. Demmig-Adams, B., Winter, K., Kruger, A., and Czygan, F.-C. (1989) in *Photosynthesis. Plant Biology* (Briggs, W. R., ed) Vol. 8, Alan R. Liss, New York
15. Bugos, R. C., and Yamamoto, H. Y. (1996) Molecular cloning of violaxanthin de-epoxidase from romaine lettuce and expression in *Escherichia coli*. *Proc. Natl. Acad. Sci. U.S.A.* **93,** 6320–6325
16. Arnoux, P., Morosinotto, T., Saga, G., Bassi, R., and Pignol, D. (2009) A structural basis for the pH-dependent xanthophyll cycle in *Arabidopsis thaliana*. *Plant Cell* **21,** 2036–2044
17. Niyogi, K. K., Bjorkman, O., and Grossman, A. R. (1997) Chlamydomonas xanthophyll cycle mutants identified by video imaging of chlorophyll fluorescence quenching. *Plant Cell* **9,** 1369–1380
18. Holt, N. E., Zigmantas, D., Valkunas, L., Li, X. P., Niyogi, K. K., and Fleming, G. R. (2005) Carotenoid cation formation and the regulation of photosynthetic light harvesting. *Science* **307,** 433–436
19. Nilkens, M., Kress, E., Lambrev, P., Miloslavina, Y., Müller, M., Holzwarth, A. R., and Jahns, P. (2010) Identification of a slowly inducible zeaxanthin-dependent component of non-photochemical quenching of chlorophyll fluorescence generated under steady-state conditions in *Arabidopsis*. *Biochim. Biophys. Acta* **1797,** 466–475
20. Morosinotto, T., Baronio, R., and Bassi, R. (2002) Dynamics of chromophore binding to Lhc proteins *in vivo* and *in vitro* during operation of the xanthophyll cycle. *J. Biol. Chem.* **277,** 36913–36920
21. Walters, R. G., and Horton, P. (1991) Resolution of components of non-photochemical chlorophyll fluorescence quenching in barley leaves. *Photosynth. Res.* **27,** 121–133
22. Havaux, M., and Niyogi, K. K. (1999) The violaxanthin cycle protects plants from photooxidative damage by more than one mechanism. *Proc. Natl. Acad. Sci. U.S.A.* **96,** 8762–8767
23. Külheim, C., Agren, J., and Jansson, S. (2002) Rapid regulation of light harvesting and plant fitness in the field. *Science* **297,** 91–93
24. Havaux, M., Dall'Osto, L., Cuiné, S., Giuliano, G., and Bassi, R. (2004) The effect of zeaxanthin as the only xanthophyll on the structure and function of the photosynthetic apparatus in *Arabidopsis thaliana*. *J. Biol. Chem.* **279,** 13878–13888
25. Caffarri, S., Croce, R., Breton, J., and Bassi, R. (2001) The major antenna complex of photosystem II has a xanthophyll binding site not involved in light harvesting. *J. Biol. Chem.* **276,** 35924–35933
26. Liu, Z., Yan, H., Wang, K., Kuang, T., Zhang, J., Gui, L., An, X., and Chang, W. (2004) Crystal structure of spinach major light-harvesting complex at 2.72 Å resolution. *Nature* **428,** 287–292
27. Jahns, P., Latowski, D., and Strzalka, K. (2009) Mechanism and regulation of the violaxanthin cycle. The role of antenna proteins and membrane lipids. *Biochim. Biophys. Acta* **1787,** 3–14
28. Morosinotto, T., Caffarri, S., Dall'Osto, L., and Bassi, R. (2003) Mechanistic aspects of the xanthophyll dynamics in higher plant thylakoids. *Physiol. Plant.* **119,** 347–354
29. Havaux, M., Dall'osto, L., and Bassi, R. (2007) Zeaxanthin has enhanced antioxidant capacity with respect to all other xanthophylls in *Arabidopsis* leaves and functions independent of binding to PSII antennae. *Plant Physiol.* **145,** 1506–1520
30. Dall'Osto, L., Cazzaniga, S., Havaux, M., and Bassi, R. (2010) Enhanced photoprotection by protein-bound *versus* free xanthophyll pools. A comparative analysis of chlorophyll *b* and xanthophyll biosynthesis mutants. *Mol. Plant* **3,** 576–593
31. Hartel, H., Lokstein, H., Grimm, B., and Rank, B. (1996) Kinetic studies on the xanthophyll cycle in barley leaves (influence of antenna size and relations to Nonphotochemical chlorophyll fluorescence quenching). *Plant Physiol.* **110,** 471–482
32. Havaux, M., Bonfils, J. P., Lütz, C., and Niyogi, K. K. (2000) Photodamage of the photosynthetic apparatus and its dependence on the leaf developmental stage in the *npq1 Arabidopsis* mutant deficient in the xanthophyll cycle enzyme violaxanthin de-epoxidase. *Plant Physiol.* **124,** 273–284
33. Casazza, A. P., Tarantino, D., and Soave, C. (2001) Preparation and functional characterization of thylakoids from *Arabidopsis thaliana*. *Photosynth. Res.* **68,** 175–180
34. Morosinotto, T., Bassi, R., Frigerio, S., Finazzi, G., Morris, E., and Barber, J. (2006) Biochemical and structural analyses of a higher plant photosystem II supercomplex of a photosystem I-less mutant of barley. Consequences of a chronic over-reduction of the plastoquinone pool. *FEBS J.* **273,** 4616–4630
35. Dainese, P., Hoyer-hansen, G., and Bassi, R. (1990) The resolution of chlorophyll *a*/*b*-binding proteins by a preparative method based on flat bed isoelectric focusing. *Photochem. Photobiol.* **51,** 693–703
36. Croce, R., and Bassi, R. (1998) in *Photosynthesis: Mechanisms and Effects* (Garab, G., ed) Vol. I, pp 421–424, Kluwer Academic Press, Dordrecht, The Netherlands
37. Gilmore, A. M., and Yamamoto, H. Y. (1991) Zeaxanthin formation and energy-dependent fluorescence quenching in pea chloroplasts under artificially mediated linear and cyclic electron transport. *Plant Physiol.* **96,** 635–643
38. León, R., Vila, M., Hernánz, D., and Vílchez, C. (2005) Production of phytoene by herbicide-treated microalgae *Dunaliella bardawil* in two-phase systems. *Biotechnol. Bioeng.* **92,** 695–701
39. Towbin, H., Staehelin, T., and Gordon, J. (1979) Electrophoretic transfer of proteins from polyacrylamide gels to nitrocellulose sheets. Procedure and some applications. *Proc. Natl. Acad. Sci. U.S.A.* **76,** 4350–4354
40. Beal, D., Rappaport, F., and Joliot, P. (1999) A new high-sensitive 10-ns time-resolution spectrophotometric technique adapted to *in vivo* analysis of the photosynthetic apparatus. *Rev. Sci. Instrum.* **70,** 202–207
41. Flors, C., Fryer, M. J., Waring, J., Reeder, B., Bechtold, U., Mullineaux, P. M., Nonell, S., Wilson, M. T., and Baker, N. R. (2006) Imaging the production of singlet oxygen *in vivo* using a new fluorescent sensor, singlet oxygen sensor green. *J. Exp. Bot.* **57,** 1725–1734
42. Driever, S. M., Fryer, M. J., Mullineaux, P. M., and Baker, N. R. (2009) Imaging of reactive oxygen species *in vivo*. *Methods Mol. Biol.* **479,** 109–116
43. de Bianchi, S., Betterle, N., Kouril, R., Cazzaniga, S., Boekema, E., Bassi, R., and Dall'Osto, L. (2011) *Arabidopsis* mutants deleted in the light-harvesting protein Lhcb4 have a disrupted Photosystem II macrostructure and are defective in photoprotection. *Plant Cell* **23,** 2659–2679

44. Carbonera, D., Giacometti, G., and Agostini, G. (1992) FDMR of carotenoid and chlorophyll triplets in light-harvesting complex LHCII of spinach. *Appl. Magn. Reson.* **3,** 361–368
45. Santabarbara, S., Bordignon, E., Jennings, R. C., and Carbonera, D. (2002) Chlorophyll triplet states associated with photosystem II of thylakoids. *Biochemistry* **41,** 8184–8194
46. Santabarbara, S., Agostini, G., Heathcote, P., and Carbonera, D. (2005) A fluorescence detected magnetic resonance investigation of the carotenoid triplet states associated with photosystem II of isolated spinach thylakoid membranes. *Photosynth. Res.* **86,** 283–296
47. Tanaka, A., Ito, H., Tanaka, R., Tanaka, N. K., Yoshida, K., and Okada, K. (1998) Chlorophyll a oxygenase (CAO) is involved in chlorophyll *b* formation from chlorophyll *a*. *Proc. Natl. Acad. Sci. U.S.A.* **95,** 12719–12723
48. Plumley, F. G., and Schmidt, G. W. (1987) Reconstitution of chloroform *a*/*b* light-harvesting complexes. Xanthophyll-dependent assembly and energy transfer. *Proc. Natl. Acad. Sci. U.S.A.* **84,** 146–150
49. Kim, E. H., Li, X. P., Razeghifard, R., Anderson, J. M., Niyogi, K. K., Pogson, B. J., and Chow, W. S. (2009) The multiple roles of light-harvesting chlorophyll *a*/*b*-protein complexes define structure and optimize function of *Arabidopsis* chloroplasts. A study using two chlorophyll *b*-less mutants. *Biochim. Biophys. Acta* **1787,** 973–984
50. Triantaphylidès, C., Krischke, M., Hoeberichts, F. A., Ksas, B., Gresser, G., Havaux, M., Van Breusegem, F., and Mueller, M. J. (2008) Singlet oxygen is the major reactive oxygen species involved in photooxidative damage to plants. *Plant Physiol.* **148,** 960–968
51. Dall'Osto, L., Caffarri, S., and Bassi, R. (2005) A mechanism of nonphotochemical energy dissipation, independent from Psbs, revealed by a conformational change in the antenna protein CP26. *Plant Cell* **17,** 1217–1232
52. Betterle, N., Ballottari, M., Hienerwadel, R., Dall'Osto, L., and Bassi, R. (2010) Dynamics of zeaxanthin binding to the photosystem II monomeric antenna protein Lhcb6 (CP24) and modulation of its photoprotection properties. *Arch. Biochem. Biophys.* **504,** 67–77
53. Wehner, A., Storf, S., Jahns, P., and Schmid, V. H. (2004) De-epoxidation of violaxanthin in light-harvesting complex I proteins. *J. Biol. Chem.* **279,** 26823–26829
54. Yakushevska, A. E., Jensen, P. E., Keegstra, W., van Roon, H., Scheller, H. V., Boekema, E. J., and Dekker, J. P. (2001) Supermolecular organization of photosystem II and its associated light-harvesting antenna in *Arabidopsis thaliana*. *Eur. J. Biochem.* **268,** 6020–6028
55. Dall'Osto, L., Lico, C., Alric, J., Giuliano, G., Havaux, M., and Bassi, R. (2006) Lutein is needed for efficient chlorophyll triplet quenching in the major LHCII antenna complex of higher plants and effective photoprotection *in vivo* under strong light. *BMC Plant Biology* **6,** 32
56. Mozzo, M., Dall'Osto, L., Hienerwadel, R., Bassi, R., and Croce, R. (2008) Photoprotection in the antenna complexes of photosystem II. Role of individual xanthophylls in chlorophyll triplet quenching. *J. Biol. Chem.* **283,** 6184–6192
57. Witt, H. T. (1979) Energy conversion in the functional membrane of photosynthesis. Analysis by light pulse and electric pulse methods. The central role of the electric field. *Biochim. Biophys. Acta* **505,** 355–427
58. Hiyama, T., and Ke, B. (1972) Difference spectra and extinction coefficients of P700*. *Biochim. Biophys. Acta* **267,** 160–171
59. Nielsen, B. R., Jorgensen, K., and Skibsted, L. H. (1998) Triplet-triplet extinction coefficients, rate constants of triplet decay, and rate constants of anthracene triplet sensitization by laser flash photolysis of astaxanthin, β-carotene, canthaxanthin, and zeaxanthin in deaerated toluene at 298 K. *J. Photochem. Photobiol. A Chem.* **112,** 127–133
60. Clarke, R. H. (1982) *Triplet State ODMR Spectroscopy. Techniques and Applications to Biophysical Systems* (Clarke, R. H., ed) Wiley, New York
61. Hoff, A. J. (1989) *Optically Detected Magnetic Resonance* (*ODMR*) *of triplet states in vivo* (Staehlin, L. A., ed) Elsevier, Amsterdam
62. Salvadori, E., Di Valentin, M., Kay, C. W., Pedone, A., Barone, V., and Carbonera, D. (2012) The electronic structure of the lutein triplet state in plant light-harvesting complex II. *Phys. Chem. Chem. Phys.* **14,** 12238–12251
63. Santabarbara, S., Jennings, R. C., and Carbonera, D. (2003) Analysis of photosystem II triplet states in thylakoids by fluorescence detected magnetic resonance in relation to the redox state of the primary quinone acceptor Q_A. *Chem. Phys.* **294,** 257–266
64. Carbonera, D., Giacometti, G., and Agostini, G. (1994) A well resolved ODMR triplet minus singlet spectrum of P680 from PSII particles. *FEBS Lett.* **343,** 200–204
65. Johnson, M. P., Havaux, M., Triantaphylidès, C., Ksas, B., Pascal, A. A., Robert, B., Davison, P. A., Ruban, A. V., and Horton, P. (2007) Elevated zeaxanthin bound to oligomeric LHCII enhances the resistance of *Arabidopsis* to photooxidative stress by a lipid-protective, antioxidant mechanism. *J. Biol. Chem.* **282,** 22605–22618
66. Li, X. P., Muller-Moule, P., Gilmore, A. M., and Niyogi, K. K. (2002) PsbS-dependent enhancement of feedback de-excitation protects photosystem II from photoinhibition. *Proc. Natl. Acad. Sci. U.S.A.* **99,** 15222–15227
67. Peterman, E. J., Dukker, F. M., van Grondelle, R., and van Amerongen, H. (1995) Chlorophyll *a* and carotenoid triplet states in light-harvesting complex II of higher plants. *Biophys. J.* **69,** 2670–2678
68. Moya, I., Silvestri, M., Vallon, O., Cinque, G., and Bassi, R. (2001) Time-resolved fluorescence analysis of the Photosystem II antenna proteins in detergent micelles and liposomes. *Biochemistry* **40,** 12552–12561
69. Ahn, T. K., Avenson, T. J., Ballottari, M., Cheng, Y. C., Niyogi, K. K., Bassi, R., and Fleming, G. R. (2008) Architecture of a charge-transfer state regulating light harvesting in a plant antenna protein. *Science* **320,** 794–797
70. Liao, P. N., Holleboom, C. P., Wilk, L., Kühlbrandt, W., and Walla, P. J. (2010) Correlation of Car S1 → Chl with Chl → Car S1 energy transfer supports the excitonic model in quenched light harvesting complex II. *J. Phys. Chem. B* **114,** 15650–15655
71. Liao, P. N., Pillai, S., Gust, D., Moore, T. A., Moore, A. L., and Walla, P. J. (2011) Two-photon study on the electronic interactions between the first excited singlet states in carotenoid-tetrapyrrole dyads. *J. Phys. Chem. A* **115,** 4082–4091
72. Wentworth, M., Ruban, A. V., and Horton, P. (2000) Chlorophyll fluorescence quenching in isolated light harvesting complexes induced by zeaxanthin. *FEBS Lett.* **471,** 71–74
73. Carbonera, D., Gerotto, C., Posocco, B., Giacometti, G. M., and Morosinotto, T. (2012) NPQ activation reduces chlorophyll triplet state formation in the moss *Physcomitrella patens*. *Biochim. Biophys. Acta* **1817,** 1608–1615
74. Deleted in proof
75. Caffarri, S., Kouril, R., Kereïche, S., Boekema, E. J., and Croce, R. (2009) Functional architecture of higher plant photosystem II supercomplexes. *EMBO J.* **28,** 3052–3063
76. Formaggio, E., Cinque, G., and Bassi, R. (2001) Functional architecture of the major light-harvesting complex from higher plants. *J. Mol. Biol.* **314,** 1157–1166
77. Gilmore, A. M., Shinkarev, V. P., Hazlett, T. L., and Govindjee (1998) Quantitative analysis of the effects of intrathylakoid pH and xanthophyll cycle pigments on chlorophyll a fluorescence lifetime distributions and intensity in thylakoids. *Biochemistry* **37,** 13582–13593
78. Croce, R., Dorra, D., Holzwarth, A. R., and Jennings, R. C. (2000) Fluorescence decay and spectral evolution in intact photosystem I of higher plants. *Biochemistry* **39,** 6341–6348
79. Croce, R., Morosinotto, T., Castelletti, S., Breton, J., and Bassi, R. (2002) The Lhca antenna complexes of higher plants photosystem I. *Biochim. Biophys. Acta* **1556,** 29–40
80. Britton, G., Liaaen-Jensen, S., and Pfander, H. (eds) (2004) *Carotenoids Vol. 1B: Spectroscopy*, pp. 57–61, Birkhauser Verlag, Basel, Switzerland

Supplemental data

Figure S1

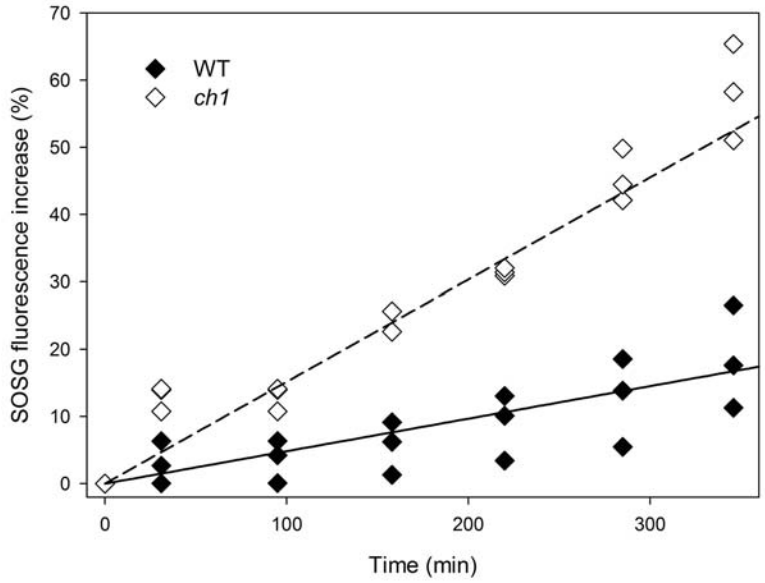

Figure S1. Photoprotective activity of Lhc subunits. Singlet oxygen release on intact leaves from WT and mutant *ch1*, lacking Lhc subunits, was quantified upon illumination (600<λ<750 nm, 1200 μmol photons m^{-2} s^{-1}, RT). The fluorescent probe SOSG was used in order to quantify light-dependent $^1O_2$ release, since its 530 nm emission band increases in proportion to the amount of $^1O_2$ released by the photosynthetic apparatus. Statistical analysis revealed that *ch1* leaves showed significantly higher $^1O_2$ release than WT leaves (Analysis of Covariance, $P < 0.01$).

Figure S2

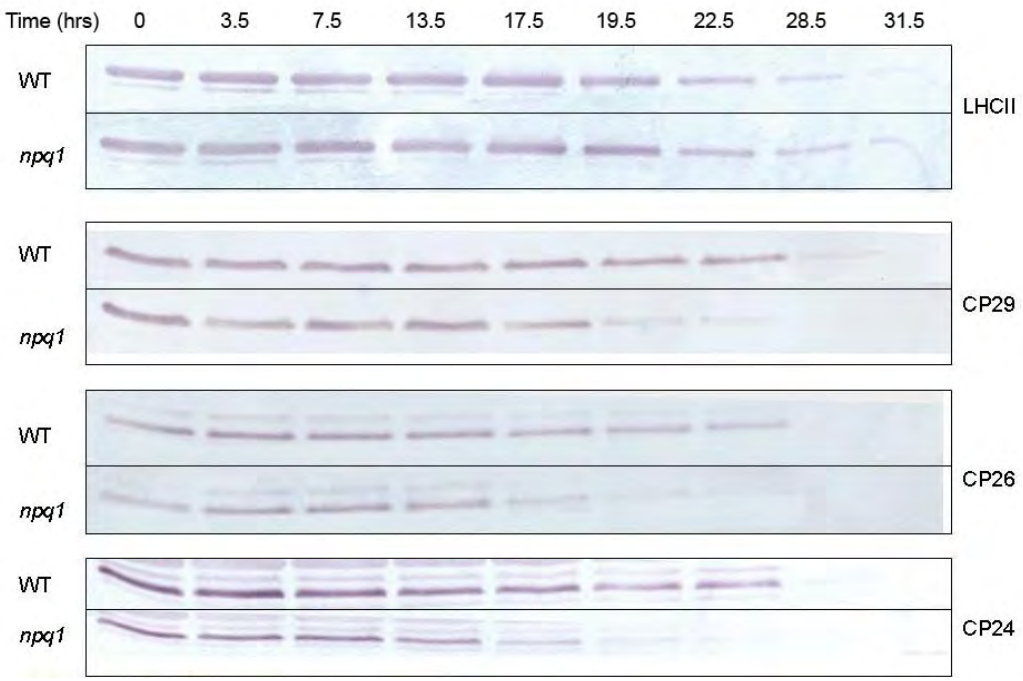

Figure S2. *In vivo* photo-oxidation of Lhcb exposed to EL stress. WT and *npq1* leaf discs floating on water were exposed to EL (2500 µmol photon m^{-2} s^{-1}, RT) for 31 hours. For the quantification of Lhcb subunits, frozen leaf discs were homogenized in liquid nitrogen and protein extracted. Immunoblot assays with antibodies against different polypeptides were performed, and samples were compared only when loaded in the same slab gel. Results show that, upon EL treatment, Lhcb content decays with a rate that is affected by zeaxanthin level; in particular, a much stronger effect of the *npq1* mutation was observed in the enhancement of minor antennae photodegradation, while lack of Zea only marginally affected LHCII decay rate.

Figure S3

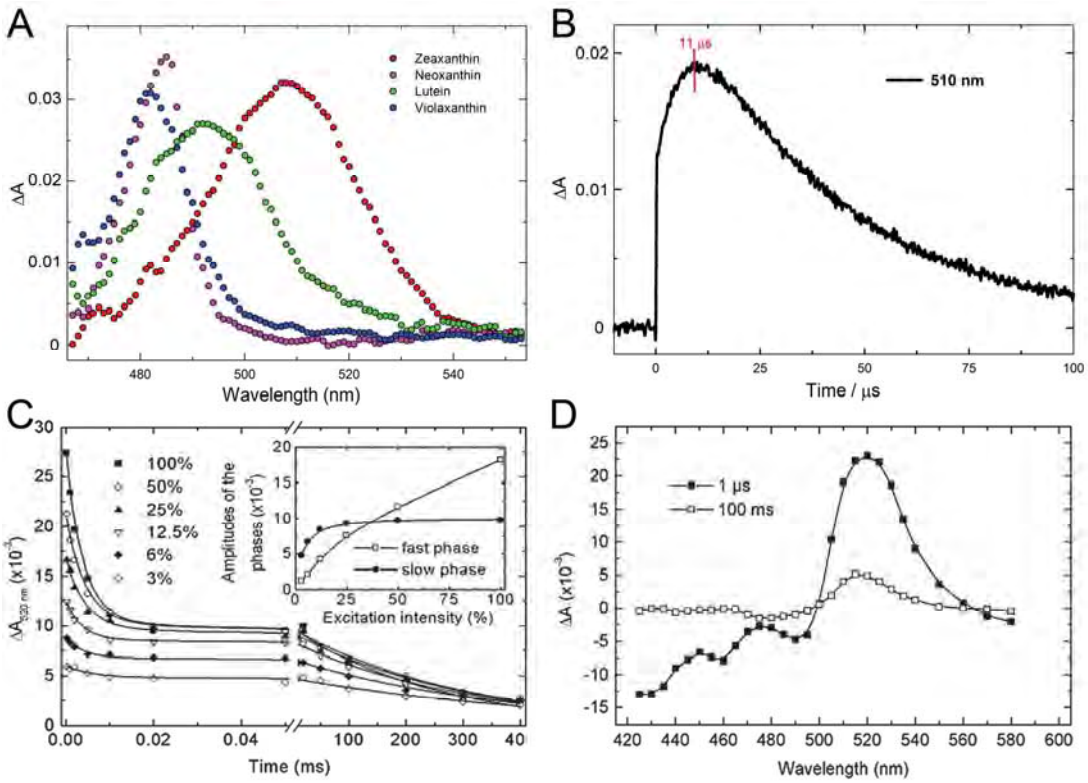

Figure S3. Time-resolved laser spectroscopy measurements of the Car triplet excited states after direct excitation of Chl on either purified pigments mix or intact leaves. (A) TmS spectra of purified zeaxanthin (red), neoxanthin (purple), lutein (green) and violaxanthin (blue). Solutions contained 2.4 µM Chl *a* and either 10 µM zeaxanthin, 11 µM neoxanthin, 13 µM lutein or 15 µM violaxanthin in ethanol (95%). Transient absorption spectra were recorded at RT; excitation pulse: 662 nm. (B) Kinetic trace of transient absorption of a solution containing Chl *a* and zeaxanthin, measured at 510 nm. The maximum triplet state absorption signal for zeaxanthin occurs at a delay time of 11 µs. (C) *In vivo* absorbance changes at 520 nm, induced by a flash of 650 nm light, 10 ns in an intact leaf of Arabidopsis WT. Insert shows the amplitude dependence of the slow and fast phases of the signal at 520 nm on the excitation energy: the slow phase saturates at the lower percentage range of the excitation intensity, whereas the fast phase increases linearly with excitation intensity. (D) Spectra of the flash-induced absorbance changes on WT Arabidopsis leaves at 100 ms (open symbols) and 1µs (closed symbols), corresponding to electrochromic changes and carotenoid triplet formation, respectively.

Figure S4

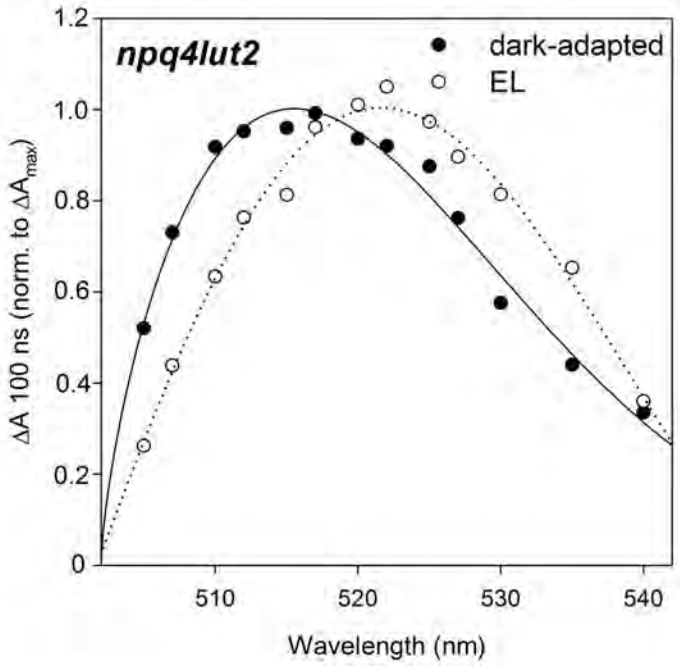

Figure S4. Light-induced red-shift of the carotenoid triplet transition on *npq4lut2* leaves. Carotenoid triplet signal (difference between the spectra at 100 ns and 30 µs) was measured on Arabidopsis *npq4lut2* leaves before and after illumination with a continuous red light, as described for Figure 4.

Figure S5

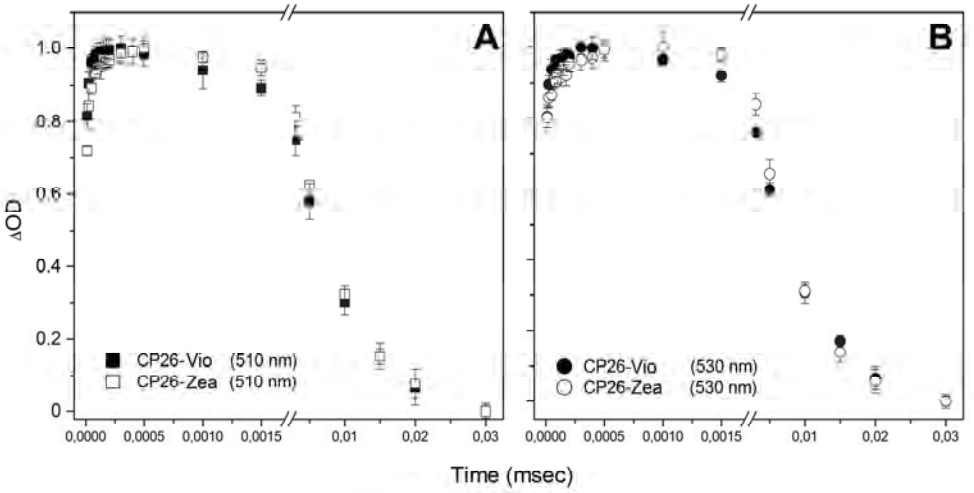

Figure S5. Flash-induced absorbance changes due to carotenoid triplet formation and decay in native CP26 proteins. Absorbance changes at 510 nm (contributions of ^{3}Vio* and ^{3}Lut*, panel A) and 530 nm (mainly ^{3}Zea* and ^{3}Lut*, panel B; see also Figure 6) are shown for CP26 purified from either dark-adapted (CP26-Vio) or EL-treated leaves (CP26-Zea). See Table S2, fraction 4, for Zea content of CP26-Z. Transient absorptions were normalized to the maximum amplitude.

Figure S6

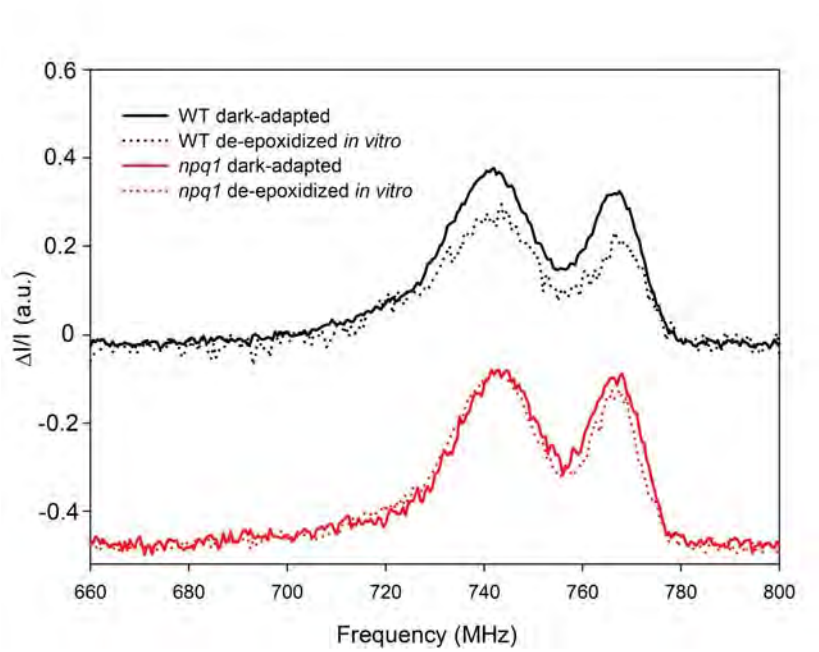

Figure S6. Fluorescence detected magnetic resonance (FDMR) of the chlorophyll triplet states on thylakoids. A. FDMR signals of the ^{3}Chl* states observed in thylakoids purified from WT (black) and *npq1* (red) dark-adapted leaves. Thylakoids were either kept at pH 7.5 (solid line) or de-epoxidized *in vitro* through incubation at pH 5.2 in the dark (dots) in order to maximize Zea accumulation. Detection wavelength: 690 nm. Spectra have been vertically shifted for better comparison. Amplitude modulation frequency: 33 Hz, tc 600 ms, number of scans 20, mw power 500 mW, temperature 1.8 K.

Table S1

	pigment content (mol/100 mol Chl)					
genotype	**neoxanthin**	**violaxanthin**	**antheraxanthin**	**lutein**	**zeaxanthin**	**β-carotene**
WT	4.8 ± 0.5	3.1 ± 0.5	-	13.5 ± 0.2	-	6.7 ± 0.8
	4.2 ± 0.6	1.5 ± 0.4	0.3 ± 0.1	12.8 ± 0.7	1.1 ± 0.3	6.2 ± 0.5
ch1	1.5 ± 0.4	6.7 ± 0.6	-	10.9 ± 1.0	-	15.6 ± 0.8
	1.6 ± 0.3	0.6 ± 0.2	0.7 ± 0.2	10.2 ± 1.4	6.0 ± 0.5	15.2 ± 1.1
npq1	5.1 ± 0.5	3.2 ± 0.5	-	14.5 ± 1.2	-	6.3 ± 0.8
	5.1 ± 0.2	3.9 ± 0.6	-	12.9 ± 0.3	-	6.5 ± 0.5
ch1npq1	1.6 ± 0.2	7.4 ± 0.7	-	11.6 ± 1.2	-	15.8 ± 1.1
	1.6 ± 0.4	6.6 ± 0.3	-	10.9 ± 0.4	-	15.4 ± 1.8
lut2	4.5 ± 0.3	11.8 ± 0.5	1.8 ± 0.3	-	0.9 ± 0.2	7.5 ± 0.7
	4.4 ± 0.3	6.6 ± 0.4	2.1 ± 0.5	-	3.3 ± 0.3	8.1 ± 0.6
ch1lut2	2.1 ± 0.6	9.2 ± 0.9	2.6 ± 0.5	-	0.7 ± 0.1	15.6 ± 2.1
	2.8 ± 0.1	1.4 ± 0.2	1.5 ± 0.7	-	8.6 ± 1.2	15.8 ± 1.2
npq1lut2	4.8 ± 0.5	12.0 ± 0.6	1.9 ± 0.3	-	0.9 ± 0.2	7.9 ± 0.7
	4.6 ± 0.2	12.1 ± 0.1	1.7 ± 0.2	-	0.9 ± 0.3	8.0 ± 0.6
npq2lut2	-	-	-	-	14.2 ± 0.8	6.8 ± 0.8
	-	-	-	-	14.8 ± 0.7	6.4 ± 0.6

Table S1. Carotenoid composition of leaf tissue from WT, *npq*, *lut2*, and *ch1* genotypes, used for measurements on Figures 1 and 4. Pigment content was quantified by HPLC on both dark-adapted (gray background) and EL-treated leaves (1200 μmol photons m^{-2} s^{-1}; white background) at RT. Data are normalized to 100 chlorophyll molecules and are expressed as means ± SD, n = 3. Abbreviation: Chl, chlorophyll.

Table S2

			pigment content (mol/100 mol Chl)						
		sample	neoxanthin	violaxanthin	antheraxanthin	lutein	zeaxanthin	β-carotene	DI
dark-adapted	*purified by sucrose gradient ultracentrifugation*	**Monomeric Lhcb**	6.3 ± 0.2	2.5 ± 0.3	-	14.6 ± 0.3	-	-	0
		Trimeric LHCII	7.7 ± 0.3	1.3 ± 0.2	-	18.6 ± 0.5	-	-	0
		LHCI	-	4.4 ± 0.3	-	11.4 ± 0.6	-	5.6 ± 0.2	0
		PSI-LHCI	-	2.0 ± 0.4	-	4.7 ± 0.2	-	11.9 ± 0.4	0
		PSII supercomplex	7.3 ± 0.6	1.6 ± 0.2	-	17.5 ± 0.5	-	4.3 ± 0.2	0
	purified by isoelectric focusing	**fraction 1**	6.9 ± 0.3	0.7 ± 0.1	-	14.7 ± 0.2	-	-	0
		fraction 2	2.7 ± 0.1	4.3 ± 1.3	-	13.6 ± 0.4	-	-	0
		fraction 3	7.5 ± 0.9	5.3 ± 0.1	-	12.8 ± 0.2	-	-	0
		fraction4	11.0 ± 2.3	2.7 ± 0.2	-	14.5 ± 0.1	-	-	0
EL-treated	*purified by sucrose gradient ultracentrifugation*	**Monomeric Lhcb**	6.0 ± 0.3	1.4 ± 0.2	0.4 ± 0.2	14.1 ± 0.4	2.0 ± 0.2	-	0.58 ± 0.01
		Trimeric LHCII	7.4 ± 0.3	0.3 ± 0.2	0.1 ± 0.1	17.9 ± 0.4	0.8 ± 0.2	-	0.71 ± 0.01
		LHCI	-	2.9 ± 0.4	0.5 ± 0.3	11.5 ± 0.5	0.9 ± 0.3	5.4 ± 0.4	0.27 ± 0.01
		PSI-LHCI	-	1.3 ± 0.3	0.1 ± 0.1	4.8 ± 0.2	0.5 ± 0.2	11.9 ± 0.5	0.29 ± 0.01
		PSII supercomplex	7.0 ± 0.5	0.6 ± 0.2	0.2 ± 0.1	16.8 ± 0.4	1.1 ± 0.3	4.3 ± 0.4	0.63 ± 0.01
	purified by isoelectric focusing	**fraction 1**	7.5 ± 0.3	0.7 ± 0.1	0.1 ± 0.1	14.9 ± 0.2	0.8 ± 0.1	-	0.61 ± 0.01
		fraction 2	2.0 ± 1.1	3.8 ± 0.6	0.6 ± 0.5	11.6 ± 0.3	2.1 ± 0.3	-	0.35 ± 0.01
		fraction 3	6.5 ± 0.1	5.1 ± 0.3	0.6 ± 0.1	11.6 ± 0.1	2.2 ± 0.1	-	0.32 ± 0.01
		fraction4	9.3 ± 0.5	2.7 ± 0.1	1.2 ± 0.4	14.0 ± 0.4	2.5 ± 0.1	-	0.52 ± 0.01

Table S2. Carotenoid content of pigment-protein complexes purified either by sucrose gradient ultracentrifugation or preparative isoelectric focusing. Complexes have been isolated from WT leaves, either dark-adapted or illuminated at 1200 μmol photons m^{-2} s^{-1}, RT for 1 hour (EL-treated). Pigment content was quantified on acetone extracts by HPLC. Zea content was expressed through the de-epoxidation index, calculated as (Zea + ½Antheraxanthin)/(Vio + Zea + Antheraxanthin). Lhcb fractions contain monomeric LHCII (fraction 1), or are enriched in minor antennae CP24 (fraction 2), CP29 (fraction 3) or CP26 (fraction 4). All these Lhcb from dark-adapted plants bind one molecule of Vio per monomer (1-4), respectively to the external site V1 in LHCII, and to the inner site L2 in the minor antennae; therefore, the de-epoxidation index represents the fraction of each specific complex that underwent Vio-Zea exchange. Data are expressed as means ± SD, n = 2. Abbreviations: DI, de-epoxidation index; Chl, chlorophyll.

Table S3

	pigment content (mol/100 mol Chl)					
genotype	**neoxanthin**	**violaxanthin**	**antheraxanthin**	**lutein**	**zeaxanthin**	**β-carotene**
WT	4.6 ± 0.1	1.6 ± 0.1	0.3 ± 0.1	13.7 ± 0.2	1.5 ± 0.1	6.1 ± 1.0
npq1	4.4 ± 0.2	3.4 ± 0.2	-	13.5 ± 0.3	-	5.8 ± 0.3

Table S3. Carotenoid content of thylakoids isolated from WT and *npq1* EL-treated leaves and used for FDMR measurements. Data are normalized to 100 chlorophyll molecules and are expressed as means ± SD, n = 3. Pigment content was quantified by HPLC. Abbreviation: Chl, chlorophyll.

Reference List

1. Liu, Z., Yan, H., Wang, K., Kuang, T., Zhang, J., Gui, L., An, X., and Chang, W. (2004) Crystal structure of spinach major light-harvesting complex at 2.72 A resolution. *Nature* **428,** 287-292

2. Pan, X., Li, M., Wan, T., Wang, L., Jia, C., Hou, Z., Zhao, X., Zhang, J., and Chang, W. (2011) Structural insights into energy regulation of light-harvesting complex CP29 from spinach. *Nat.Struct.Mol.Biol.* **18,** 309-315

3. Caffarri, S., Passarini, F., Bassi, R., and Croce, R. (2007) A specific binding site for neoxanthin in the monomeric antenna proteins CP26 and CP29 of Photosystem II. *FEBS Lett.* **581,** 4704-4710

4. Pagano, A., Cinque, G., and Bassi, R. (1998) In vitro reconstitution of the recombinant photosystem II light-harvesting complex CP24 and its spectroscopic characterization. *J.Biol.Chem.* **273,** 17154-17165

Section B.
Disturbed excitation energy transfer in *Arabidopsis thaliana* mutants lacking minor antenna complexes of photosystem II.

Biochimica et Biophysica Acta 1837 (2014) 1981–1988

Contents lists available at ScienceDirect

Biochimica et Biophysica Acta

journal homepage: www.elsevier.com/locate/bbabio

Disturbed excitation energy transfer in *Arabidopsis thaliana* mutants lacking minor antenna complexes of photosystem II

Luca Dall'Osto [a,1], Caner Ünlü [b,1], Stefano Cazzaniga [a], Herbert van Amerongen [b,c,*]

[a] Dipartimento di Biotecnologie, Università di Verona, 37134 Verona, Italy
[b] Laboratory of Biophysics, Wageningen University, 6703 HA Wageningen, The Netherlands
[c] MicroSpectroscopy Centre, Wageningen University, 6703 HA Wageningen, The Netherlands

ARTICLE INFO

Article history:
Received 21 May 2014
Received in revised form 28 September 2014
Accepted 29 September 2014
Available online 5 October 2014

Keywords:
Photosynthesis
Light-harvesting complex
Photosystem II
Time-resolved fluorescence spectroscopy
Thylakoid membrane

ABSTRACT

Minor light-harvesting complexes (Lhcs) CP24, CP26 and CP29 occupy a position in photosystem II (PSII) of plants between the major light-harvesting complexes LHCII and the PSII core subunits. Lack of minor Lhcs *in vivo* causes impairment of PSII organization, and negatively affects electron transport rates and photoprotection capacity. Here we used picosecond-fluorescence spectroscopy to study excitation-energy transfer (EET) in thylakoid membranes isolated from *Arabidopsis thaliana* wild-type plants and knockout lines depleted of either two (koCP26/24 and koCP29/24) or all minor Lhcs (NoM). In the absence of all minor Lhcs, the functional connection of LHCII to the PSII cores appears to be seriously impaired whereas the "disconnected" LHCII is substantially quenched. For both double knock-out mutants, excitation trapping in PSII is faster than in NoM thylakoids but slower than in WT thylakoids. In NoM thylakoids, the loss of all minor Lhcs is accompanied by an over-accumulation of LHCII, suggesting a compensating response to the reduced trapping efficiency in limiting light, which leads to a photosynthetic phenotype resembling that of low-light-acclimated plants. Finally, fluorescence kinetics and biochemical results show that the missing minor complexes are not replaced by other Lhcs, implying that they are unique among the antenna subunits and crucial for the functioning and macro-organization of PSII.

1. Introduction

Oxygenic photosynthesis is performed in the chloroplast by a series of reactions which transform sunlight energy into chemical energy [1]. Absorption of light, excitation energy transfer (EET) and electron transfer are the primary events of the photosynthetic light phase and take place in photosystems (PS) I and II [2–10]. PSII is a large supramolecular pigment–protein complex located in the thylakoid membranes of plants, algae and cyanobacteria. Its reaction center (RC) consists of several subunits carrying the cofactors for electron transport and forms, together with the proteins CP43 and CP47 a so-called core complex [11,12]. Core complexes form dimers (C_2), which bind a system of nuclear-encoded light-harvesting proteins (Lhcbs): CP29 and CP26 are monomeric antennae located in close connection to the core, and seem to mediate the binding of an LHCII trimer (the major antenna complex of PSII) called LHCII-S (strongly bound), thus forming the basic PSII supercomplex structure C_2S_2 [13]. Moreover, in higher plants another monomeric subunit (CP24) and one more trimeric LHCII (LHCII-M, "moderately" bound) bind the PSII core to extend the light-harvesting capacity of the supercomplex (called $C_2S_2M_2$). Besides light harvesting, the outer antenna of PSII plays a crucial role in photoprotective and regulatory mechanisms such as limiting the level of Chl triplet states [14–16], scavenging of reactive oxygen species [17] and activating non-radiative de-excitation pathways [18].

Excitations are used to induce primary charge separation (CS) within the RC, after which electrons are transferred in succession to the acceptors Q_A and Q_B, while the oxidizing equivalents in the Mn cluster are used to catalyze water splitting [1]. The quantum efficiency of CS depends on the rate constants of different molecular events, namely 1) EET from the outer antenna to the RC; 2) CS and charge recombination; 3) secondary electron transfer to Q_A, and 4) relaxation processes, such as intersystem crossing, internal conversion and fluorescence emission [19].

Among the antenna complexes of PSII, monomeric Lhcs CP24, CP26 and CP29 are of particular interest, because the location of these complexes in between LHCII and the RC makes them crucial for facilitating EET from LHCII, forming the major part of the antenna system, to the core subunits, although it seems that also direct EET

* Corresponding author at: Laboratory of Biophysics, Wageningen University, Dreijenlaan 3, 6703 HA Wageningen, The Netherlands. Tel.: +31 317482634; fax: +31 317482725.
E-mail address: herbert.vanamerongen@wur.nl (H. van Amerongen).
[1] Both authors equally contributed to this work.

http://dx.doi.org/10.1016/j.bbabio.2014.09.011

from LHCII-S to the core is possible [20,21]. Indeed, depletion of specific monomeric Lhcs *in vivo* was shown to impair the organization of photosynthetic complexes within grana partitions, and to negatively affect electron transport rates and photoprotection capacity [22]. Evidence that these gene products have been conserved over at least 350 million years of evolution [23] strongly indicates that each complex has a specific role in the PSII function over the highly variable conditions of the natural environment.

CS in the reaction centers of PSI and PSII occurs within tens to hundreds of picoseconds (ps) after light absorption. A great challenge in studying EET and charge separation in thylakoid membranes is to disentangle the kinetics related to both photosystems. Broess et al. [24] and Caffari et al. [20] recently provided a more detailed picture of EET in PSII membranes and supercomplexes of plants while van Oort et al. [25] investigated EET in entire thylakoids of WT and mutant *Arabidopsis* with the use of ps-fluorescence spectroscopy, using different combinations of excitation/detection wavelengths, in order to distinguish PSI and PSII kinetics. The exciton/radical-pair-equilibrium (ERPE) model has often been used to describe the kinetics of EET in PSII preparations with open RCs, *i.e.* with the electron acceptor Q_A fully oxidized [26,27]. This model assumes that EET to the RC is too fast to contribute substantially to the charge separation time [26]. To provide a more accurate description for grana-enriched membranes, the ERPE model was extended after analyzing ps-fluorescence measurements using different excitation wavelengths and applying a coarse-grained model to determine the excitation migration time to the RC [24]. Comparison of the fluorescence kinetics obtained for 412 nm (more excitations in the core) and 484 nm excitation (more excitations in the outer antenna), led to the conclusion that the average migration time of an excitation toward the RC contributes 20–25% to the average trapping time in PSII membranes and around 50% in full thylakoid membranes [25,28,29] and the overall migration time to the RC is around 150 ps in WT thylakoids, four times longer than for grana-enriched membranes [24] which is likely due to additional antenna complexes that are less well connected to the PSII RC [21,25,28–30] and that are lost during preparation of grana membranes [21]. Recently, also models were presented that assume excitation trapping the time of which is entirely dominated by migration of excitations to the RC [31,32].

Recent studies on EET dynamics focused on the behavior of specific pigment–protein complexes that constitute either PSI or PSII [33–35]. Reverse genetic approaches in model organisms such as *Arabidopsis thaliana* allowed to isolate knock-out lines devoid of specific components of PSII [36,37] and have been instrumental in order to dissect the function of each subunit *in vivo*. Hopefully, applying time-resolved spectroscopy on thylakoid membranes of different composition can provide new knowledge on the primary events of the light phase at the molecular level.

In this work, thylakoid membranes of *A. thaliana* have been studied with time-resolved fluorescence spectroscopy using different combinations of excitation and detection wavelengths, in order to (partly) separate PSI and PSII/LHCII contributions. In particular, PSII/LHCII fluorescence decay kinetics have been measured on thylakoids isolated from wild-type *Arabidopsis*, from the double knock-out mutants koCP26/24 and koCP29/24, and from a mutant depleted of all minor antennae (NoM). The main goal of this study was to investigate how the depletion of specific Lhcs affects the excitation- and electron-transfer parameters of PSII. In the absence of all minor Lhcs of PSII, the functional connection between LHCII from the PSII cores appears to be strongly impaired and LHCII is substantially quenched which is probably related to the fact that the NoM plants are strongly hampered in their growth as compared to WT plants. For double knock-out mutants, the outer antenna is better connected to the PSII core and the corresponding plants also grow significantly better than the NoM plants.

2. Materials and methods

2.1. Plant material and growth conditions

WT plants of *A. thaliana* ecotype Col-0 and mutants *koLhcb4.1*, *koLhcb4.2*, *koLhcb5* and *koLhcb6* were obtained as previously described [36,37]. Multiple mutants *koLhcb5 koLhcb6* (koCP26/24), *koLhcb4.1 koLhcb4.2* (koCP29/24) and *koLhcb4.1 koLhcb4.2 koLhcb5* (NoM) were isolated by crossing single mutant plants and by selecting the progeny through immunoblotting, using antibodies specific for the different Lhcb subunits. Double mutant *koLhcb4.1 koLhcb4.2* is devoid of both CP29 and CP24 minor antennae, since accumulation of CP24 is hampered when CP29 is missing, as previously reported [36]. Seedlings were grown for 5 weeks at 100 μmol photons m^{-2} s^{-1}, 23 °C, 70% humidity, and 8 h of daylight.

2.2. Membrane isolation

Dark-adapted leaves were rapidly homogenized using mortar and pestle, and stacked thylakoids were isolated as previously described [38], with the following modifications aimed at preserving thylakoid functionality: protease inhibitors (2 mM ε-aminocaproic acid, 2 mM benzamidine-hydrochloride, 0.5 mM PMSF) were added to the buffers; a maximum of 1 g of leaves was ground in 100 ml of GB; thylakoids were resuspended in B4 buffer (0.4 M sorbitol, 15 mM NaCl, 10 mM KCl, 5 mM $MgCl_2$, and 15 mM Hepes pH 7.8) before being frozen in liquid nitrogen.

2.3. Pigment analysis

Pigments were extracted from leaf disks with 85% acetone buffered with Na_2CO_3, then separated and quantified by HPLC [39].

2.4. In vivo fluorescence measurements

PSII maximal photochemical efficiency was measured through Chl fluorescence on dark-adapted leaves at room temperature with a PAM 101 fluorimeter (Walz, Germany); saturating light pulses (4500 μmol photons m^{-2} s^{-1}, 0.6 s) were supplied by a KL1500 halogen lamp (Schott, UK) (for results, please see Supplementary data).

2.5. Gel electrophoresis and immunoblotting

SDS-PAGE analysis was performed with the Tris–Tricine buffer system [40], with the addition of 7 M urea to the running gel when needed to separate Lhcb4 isoforms [36]. For fractionation of pigment–protein complexes, membranes corresponding to 500 μg of Chls were washed with 5 mM EDTA and then solubilized in 1 ml of 0.7% α-DM and 10 mM HEPES, pH 7.8. Solubilized samples were then fractionated by ultracentrifugation in a 0.1–1 M sucrose gradient containing 0.06% α-DM and 10 mM HEPES, pH 7.8 (22 h at 280,000 *g*, 4 °C). Non-denaturing Deriphat-PAGE was performed following the method developed in [41] with the modification described in [42]. The thylakoids concentrated at 1 mg/ml chlorophylls were solubilized with a final concentration of 1% α/β-DM, whereas 25 μg of Chls was loaded in each lane. Bands corresponding to trimeric LHCII and monomeric PSII core were excised from the gel, and purified complexes were then eluted by grinding gel slices in a buffer containing 10 mM Hepes pH 7.5 and 0.05% α-DM. LHCII/PSII core ratios were quantified by loading thylakoids (15 μg of Chls), PSII core (0.25–0.5–0.75–1.0 μg of Chls) and trimeric LHCII (1.0–2.0–3.0–4.0 μg of Chls) in the same slab gels. After staining with Coomassie blue, the signal amplitude of LHCII and CP43/CP47 bands were quantified ($n = 4$) by GelPro 3.2 software (Bio-Rad, USA). By using the pigment composition of the individual subunits [12,43] and the OD of each protein band, the number of LHCII trimers per monomeric PSII core was calculated. For immunotitration,

thylakoid samples corresponding to 0.1, 0.25, 0.5, and 1 μg of chlorophyll were loaded for each sample and electroblotted on nitrocellulose membranes; proteins were detected with alkaline phosphatase-conjugated antibody, according to Towbin et al. [44], and signal amplitude was quantified by densitometric analysis (n = 4). In order to avoid any deviation between different immunoblots, samples were compared only when loaded in the same slab gel.

2.6. Photosystem activity measured with artificial donors and acceptors

These measurements were performed as previously described [38]. PSI electron transport from the artificial donor ($TMPDH_2$, N,N,N,N-tetramethyl-p-phenylene-diamine, reduced form) to $NADP^+$ was measured at 22 °C on functional thylakoids in the dual-wavelength spectrophotometer Unicam AA (Thermo Scientific, USA), while PSII electron transport to DMBQ (dimethyl-benzoquinone) was measured following the O_2 evolution in a Clark-type oxygen electrode system (DW2/2, Hansatech Instruments, UK) both under red light illumination (200 μmol photons m^{-2} s^{-1}, λ > 600 nm). Concentrations used were as follows: 0.1 sorbitol, 5 mM $MgCl_2$, 10 mM NaCl, 20 mM KCl, 10 mM Hepes pH 7.8, 0.5 mM $NADP^+$, 10 μM Ferredoxin, either 300 mM DMBQ or 250 mM $TMPDH_2$ and thylakoids to a final Chl concentration of 10 μg/ml. When $TMPDH_2$ was used, the reaction mixture contained 5 mM ascorbic acid, and after 1.5 min of illumination 1 μM DCMU was added, followed by the artificial donor.

2.7. Time-resolved fluorescence

Time-correlated single photon counting (TCSPC) measurements were performed with a home-built setup [45,46]. In brief, samples were kept at room temperature (RT, 22 °C) in a flow cuvette coupled to a sample reservoir. The samples were flown from reservoir to cuvette with a speed of 2.5 ml/s and the optical path length of the cuvette was 3 mm. The samples were excited with 412 nm and 484 nm pulses of 0.2 ps duration at a repetition rate of 3.8 MHz. In order to avoid the closure of reaction centers the excitation intensity was kept low (0.5–1.5 μW) which resulted in a count rate of 30,000 photons per second or lower (see Supplementary data for details, Fig. S1). The diameter of the excitation spot was 2 mm. The instrument response function or IRF (70–80 ps FWHM) was obtained with pinacyanol iodide in methanol with a 6 ps fluorescence lifetime [47,48]. Measurements were done by collecting photons for 5 min. Fluorescence was detected at 679 nm, 701 nm and 720 nm using interference filters (15 nm width). The data were collected using a multichannel analyzer with a maximum time window of 4096 channels typically at 5 or 2 ps/channel. One complete experiment for a fluorescence decay measurement consisted of the recording of data sets of the reference compound, isolated thylakoid and again the reference compound, which was done at least three times in this order with a fresh sample for each condition, in order to check the reproducibility.

2.8. Data analysis

Data obtained with the TCSPC setup were globally analyzed using the "TRFA Data Processing Package" of the Scientific Software Technologies Center (Belarusian State University, Minsk, Belarus). Fluorescence decay curves were fitted to a sum of exponentials that was convoluted with the IRF. The quality of a fit was judged from the χ^2 value and by visual inspection of the residuals and the autocorrelation thereof. The number of exponentials was 5 in all cases, whereas one of these components was an artifact with a very fast lifetime (between 0.1 ps and 1 ps) which was mainly used to improve the fitting quality at early times. These artifacts are not further considered or discussed below.

3. Results

In order to isolate knock-out (KO) lines of *A. thaliana* lacking two or three minor antennae, kolhcb4.1, kolhcb4.2, kolhcb5 and kolhcb6 homozygous KO lines were identified in seed pools obtained from NASC by immunoblot analysis using specific antibodies raised against CP29, CP26 and CP24 antenna proteins, as previously described [36,37]. KO double mutants kolhcb5 kolhcb6 retain Lhcb4 (CP29) as the only minor antenna [37], while deletion of both CP29 isoforms in the kolhcb4.1 kolhcb4.2 double mutant results in a plant retaining CP26 as the only minor antenna, since accumulation of CP24 is hampered in this genotype [36]. Triple mutant kolhcb4.1 kolhcb4.2 kolhcb5 is lacking all minor antennae: indeed, deletion of both lhcb4.1 and lhcb4.2 yielded a plant devoid of CP29, and lack of CP29 hampered CP24 stability and accumulation [37]; thus the triple KO only retains subunits of the major antenna complex LHCII. In the following, we will refer to these genotypes as koCP26/24 (kolhcb5 kolhcb6), koCP29/24 (kolhcb4.1 kolhcb4.2) and NoM (kolhcb4.1 kolhcb4.2 kolhcb5). When grown in control conditions (100 μmol photons m^{-2} s^{-1}, 23 °C, 8/16 h day/night) for 4 weeks, koCP26/24 and koCP29/24 plants did not show significant reduction in growth with respect to the WT plants, while NoM plants were much smaller than WT plants (Fig. 1A). Thylakoid membranes were isolated from WT and mutant plants, and the lack of the corresponding gene product was confirmed by SDS-PAGE (Fig. 1B) and western blotting (see Supplementary data, Fig. S2). The pigment content of mutant thylakoids showed a significant decrease in the Chl *a*/Chl *b* ratio with respect to the membranes from WT (reflecting a relative increase of the amount of outer antenna

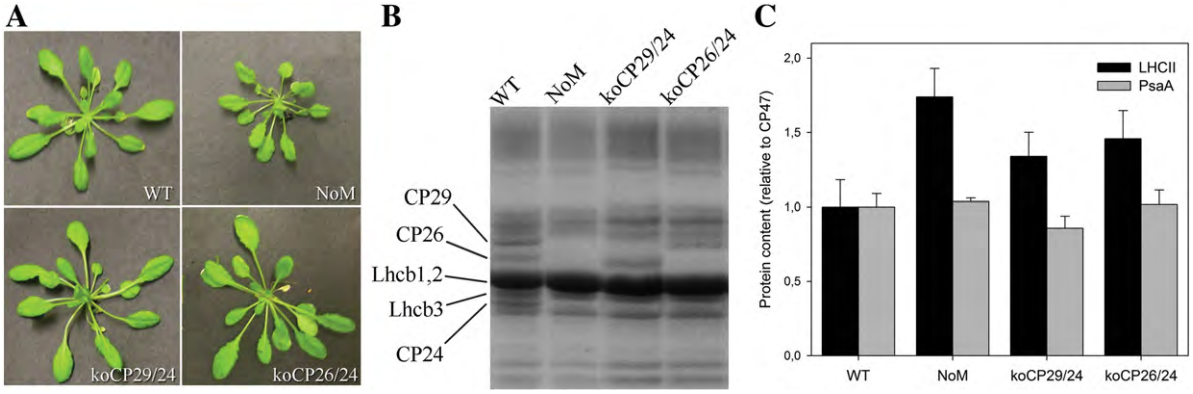

Fig. 1. Characterization of the KO mutants. (A) Phenotype of wild-type and mutant plants grown in control conditions (100 μmol photons m^{-2} s^{-1}, 23 °C, 8/16 h day/night) for 4 weeks. (B) SDS/PAGE analysis of wild-type and mutant thylakoid proteins. Selected apoprotein bands are marked. Fifteen micrograms of Chls were loaded in each lane. (C) Immunotitration of thylakoid proteins. Data of LHCII and PsaA subunits were normalized to the PSII core amount, CP47 content, and normalized to the corresponding WT content.

Table 1
Chlorophyll composition and LHCII content determined on thylakoids from wild-type and KO mutants.

Sample	Chl a/b	LHCII trimeric/PSII monomeric
WT	2.75 ± 0.05	4.2 ± 0.3
NoM	2.35 ± 0.04	6.1 ± 0.3
KoCP29/24	2.64 ± 0.03	4.8 ± 0.3
KoCP26/24	2.61 ± 0.02	5.1 ± 0.3

complexes): double mutants koCP26/24 and koCP29/24 showed a ratio of 2.61 and 2.64 respectively, *vs.* 2.75 for WT thylakoids. The lowest ratio (2.35) was observed for NoM (Table 1). In order to detect possible alterations in the relative amount of protein components of the photosynthetic apparatus upon removal of minor antennae, we determined the stoichiometry of the main subunits of both photosystems by immunoblotting titration, using antibodies specific for the subunits CP47 (PsbB, inner antenna of PSII core complex), PsaA (main subunit of PSI core complex) and LHCII (the major outer antenna of PSII). The PSI/PSII (PsaA/CP47) ratio was essentially the same in WT, koCP26/24 and NoM membranes, while a slight increase in CP47 relative content was detected for koCP29/24 as compared to WT. The LHCII/PSII ratio increased with the removing of monomeric antennae: both koCP26/24 and koCP29/24 had a significantly higher amount of LHCII with respect to WT, while the LHCII content was even higher in NoM (Fig. 1C). The stoichiometric ratio of trimeric LHCII and monomeric PSII core complex was determined by quantifying the Coomassie staining of the corresponding bands on an SDS/PAGE, by integrating the optical density of each band (see Supplementary data, Fig. S3; see Materials and methods for details). Results confirmed a far higher LHCII content in NoM (6.1 trimeric LHCII per monomeric PSII) with respect to the WT (4.2 trimers), while koCP29/24 and koCP26/24 showed an intermediate content (respectively, 4.8 and 5.1 trimers per monomeric PSII) (Table 1).

To analyze the organization of pigment–protein complexes, thylakoid membranes isolated from WT and KO mutants were solubilized with 0.7% dodecyl-α-D-maltoside (α-DM), then Chl-binding proteins were fractionated by sucrose gradient ultracentrifugation. The fractionation patterns are shown in Fig. 2. Six major green bands were obtained for the wild type: the PSI–LHCI complex was found as a major band in the lower part of the gradient, corresponding to a complex more stable than PSII that does not dissociate into smaller complexes upon mild solubilization of thylakoids; the PSII–LHCII components are visible as multiple green bands, namely PSII core complex, CP29–CP24–LHCII-M antenna supercomplex, trimeric LHCII and monomeric Lhcb; a large band with an apparent molecular mass higher than PSI–LHCI, which contained undissociated PSII supercomplexes of different LHCII compositions, was detected in the lower part of the gradient. The major difference detected in KO mutants with respect to the wild type was the lack of the antenna supercomplex CP29–CP24–LHCII. Moreover, PSII supercomplexes were differentially represented in these genotypes: faint bands of PSII supercomplexes were still detectable in the lower part of the gradient in both koCP29/24 and koCP26/24, although their amounts were strongly reduced as compared to WT, while NoM thylakoids were completely devoid of PSII supercomplexes.

To test the photosynthetic activity of both photosystems in our thylakoid preparations, artificial electron donors and acceptors were used. The rate of linear electron transport (ET) from H_2O to DMBQ, which accepts electrons at the Q_B site, was measured polarographically as the rate of O_2 evolution, while the ET capacity of PSI was measured spectrophotometrically as the rate of $NADP^+$ reduction, upon addition of the plastocyanin electron donor $TMPDH_2$ (see Materials and methods for details). Results reported in Table S1 show that all photosystems retained their ET capacity, which clearly indicates that all the preparations are active and can efficiently drive photosynthesis. However, a reduction in O_2 evolution and NADPH accumulation on a Chl basis was observed in the membranes of NoM mutants (respectively, −30% and −20% as compared with the WT); this result might be ascribed to a lower PSII efficiency due to the presence of badly connected LHCII in the NoM mutant as compared to WT.

Fluorescence decay curves were measured with the TCSPC setup stacked thylakoids from *A. thaliana*. This approach aimed to be close to the native situation and was preferred above measuring on grana-enriched membranes (BBYs), which are known to constitute a heterogeneous system and to retain a far lower amount of trimeric LHCII than the number generally reported to be bound per RC in thylakoid preparations. Either 412-nm laser pulses, exciting relatively more PSII core complexes, or 484 nm laser pulses, exciting relatively more outer antenna complexes, were used. For detection 679 nm-, 701 nm- and 720 nm-interference band filters were used. By combining the results for different excitation and detection wavelengths it is in principle possible to differentiate between PSI and PSII kinetics and to estimate the average migration time of excitations to the PSII reaction centers [25].

The fluorescence decay curves of thylakoid preparations from WT, NoM, koCP29/24 and koCP26/24 mutants were strikingly different from each other (Fig. 3). The decay of WT thylakoids was the fastest

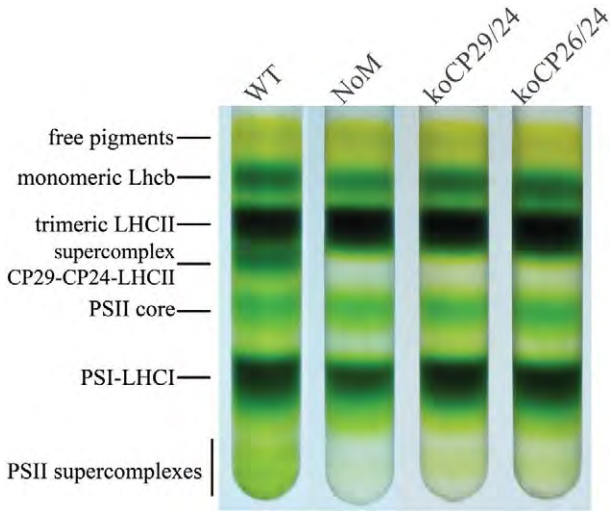

Fig. 2. Sucrose density gradient fractionation of wild-type and KO mutant solubilized thylakoids. Solubilization was performed with 0.7% α-DM. Composition of the green bands are indicated.

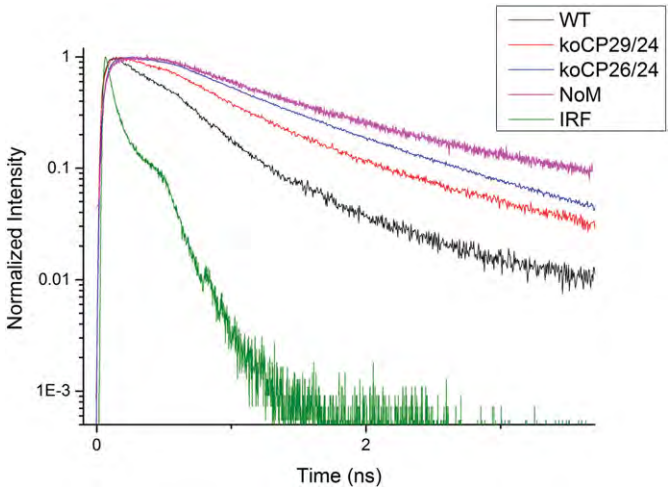

Fig. 3. Time-resolved fluorescence decays of thylakoid membranes from WT, KoCP29/24, KoCP26/24 and NoM strains. The excitation wavelength is 412 nm and the detection wavelength is 680 nm.

Table 2
Fitted lifetimes (and amplitudes in brackets) for thylakoids at room temperature with an excitation wavelength of 412 nm and a detection wavelength of 680 nm.

	WT	koCP2624	koCP29CP24	NoM
τ_1	52 ps (25%)	64 ps (23%)	66 ps (21%)	59 ps (30%)
τ_2	166 ps (32%)	273 ps (23%)	278 ps (23%)	294 ps (20%)
τ_3	409 ps (42%)	912 ps (53%)	732 ps (52%)	1.001 ns (48%)
τ_4	5.6 ns (1%)	2.8 ns (1%)	2.1 ns (4%)	2.9 ns (2%)

Confidence intervals of fluorescence lifetimes (τ) as calculated by exhaustive search were <5%; lifetimes were calculated from 2 to 6 repeats.

followed by those of koCP29/24, koCP26/24 and NoM, in that order. To get more quantitative information from the decay curves, they were fitted to a sum of exponential decay functions. The fitting results are given in Table 2 (more detailed results are given in Supplementary data, see Table S2, Table S3, Table S4 and Table S5).

The lifetime τ_1, which is in the range of 50 ps–70 ps, is largely due to PSI, although also PSII does contribute to some extent [25,28,49]. Because PSI fluorescence is red-shifted as compared to PSII fluorescence, the relative amplitude of this component increases upon going from detection wavelength 679 to 720 nm. The value of τ_1 and the corresponding amplitude only differ to a limited extent for the different thylakoid preparations. WT *Arabidopsis* shows the shortest value for τ_1 with 52 ps, whereas the τ_1 value for the NoM mutant is only 7 ps slower (59 ps). The τ_1 value is somewhat slower for koCP26/24 and koCP29/24 with 64 ps and 66 ps, respectively. The relative amplitude of τ_1 ranges from 21 to 30% for the different thylakoid preparations (for $\lambda_{exc} = 412$ nm, $\lambda_{det} = 679$ nm; more detailed results are given in Supplementary data; see Table S2, Table S3, Table S4 and Table S5).

The lifetimes τ_2 and τ_3 in Table 2 are mainly due to PSII–LHCII (and possibly some detached antenna with the highest amplitude at $\lambda_{det} = 679$ nm, as expected for PSII–LHCII) [25]. WT thylakoids show the lowest values for both τ_2 (166 ps) and τ_3 (409 ps). These lifetimes become considerably longer for the mutants. The τ_2 values for the various mutants are very similar to each other, ranging from 273 ps to 294 ps. On the other hand, the difference in τ_3 for the mutants is significantly more pronounced. τ_3 is 732 ps for the koCP29/24 mutant, whereas it is 905 ps for koCP26/24 and 1.00 ns for NoM. In comparison to WT, the amplitude for τ_3 becomes rather high in all mutants whereas the amplitudes for τ_2 decrease substantially. Finally, the slowest component (τ_4) can be ascribed to free chlorophyll and/or disconnected light-harvesting complexes with very low amplitudes and possibly some closed RCs although this is rather unlikely with the current excitation conditions (total amplitude is at most 4%) [25]. It should be noted that the amplitude for τ_4 is lower than 1% for WT thylakoids (detailed results are given in Supplementary data, see Table S2, Table S3, Table S4 and Table S5).

To estimate the PSII–LHCII kinetics, PSI and PSII kinetics were separated from each other using the method recently presented by van Oort et al. [25]. In brief, the PSII–LHCII contribution to the sub-100 ps component was determined by using different excitation and detection wavelengths [25] and together with the long lifetimes τ_2 and τ_3, which are solely attributed to PSII–LHCII, the kinetics of PSII–LHCII, with possibly some free LHCII, can be calculated [25]. The obtained PSII–LHCII kinetics differ considerably for WT and mutant thylakoids. For excitation at 412 nm, the WT preparation shows the fastest PSII–LHCII kinetics with an average lifetime of 259 ps, whereas the mutants are significantly slower; 523 for koCP29/24, 617 ps for koCP26/24, and 601 ps for NoM. For excitation at 484 nm, the PSII–LHCII kinetics of all mutant and WT preparations become slower. The PSII–LHCII average lifetime for WT cells is then 285 ps. For the mutant preparations, the average lifetimes are 565 ps, 687 ps and 771 ps for koCP29/24, koCP26/24 and NoM, respectively (Table 3).

The difference in PSII–LHCII average lifetime for different excitation wavelengths is approximately proportional to the average migration time of excitons needed to reach the RC for the first time, but the presence of detached antennae also affects this difference. The difference is 26 ps for WT thylakoids, whereas it becomes larger for the mutants: 41 ps and 70 ps for koCP29/24 and koCP26/24, respectively, whereas it is even 170 ps for NoM mutants. It should be noted that detached or loosely bound antennae cause a significant increase of the difference between PSII–LHCII kinetics for different excitation wavelengths (Table 3). In addition, it should be mentioned that the difference between overall average lifetimes (*i.e.* without correction for PSI) with different excitation wavelengths for WT and mutant strains has the same trend as the difference in PSII–LHCII average lifetime for different excitation wavelengths (see Supplementary data Table S2, Table S3, Table S4 and Table S5), which shows that the differences between corrected lifetimes upon different excitation wavelengths are not artificially created or exaggerated because of corrections and calculations. The calculated PSII–LHCII average lifetime values will be discussed hereafter.

Table 3
PSII–LHCII (with possible free LHCII) kinetics for thylakoid membranes.

Excitation	τ_{avg} (ps)		Difference (ps)
	412 nm	484 nm	
WT	259	285	26
KoCP29/24	523	565	42
KoCP26/24	617	687	70
NoM	601	778	178

The PSII–LHCII (with possible free LHCII) kinetics were derived from the kinetics of thylakoid membranes by removing the PSI contribution, as explained in van Oort et al. [25] before.

4. Discussion

The monomeric antennae CP24, CP26, and CP29 are three of the six light-harvesting subunits that compose the PSII peripheral antenna system of higher plants. They are the only Lhc subunits that can occupy the position between the inner antennae CP43/CP47 and the outer LHCII trimers within the PSII supercomplex [50] (Fig. 4). Although these pigment–protein complexes are homologous and are expected to share a common three-dimensional organization on the basis of the structural data available [43,51], they cannot be exchanged between each other in the supercomplexes [50].

Earlier work [52] has characterized *Arabidopsis* plants devoid of LHCII, and proposed a high degree of redundancy among Lhcb subunits; indeed, the PSII supercomplex organization was maintained in the absence of LHCII by over-accumulating Lhcb5. Instead, the knock-out of monomeric antennae leads to destabilization of PSII–Lhcb supercomplexes, meaning that the minor antennae are essential for PSII organization. This conclusion is supported by the fact that removal of two or more different monomeric Lhcbs increases the trapping time of excitons in the RCs substantially as compared to WT thylakoids, meaning that the absence of minor antenna complexes leads to badly connected or disconnected LHCII as will be discussed further below.

Recently, time-resolved fluorescence kinetic studies were performed on different knockout mutants of *A. thaliana*. It was shown that, in the absence of specific minor antenna complexes in most cases the overall average lifetimes become longer as compared to those of WT cells [25,30] and in particular the migration time of excitations to the RCs increases [25,30]. These results confirm that there are disruptions of the PSII–LHCII complex organization in the absence of minor antenna complexes resulting in the formation of badly connected or disconnected LHCII [25,30]. Among the mutants studied here, the most explicit slowdown of the fluorescence kinetics is observed for the NoM mutant as might have been expected since all minor antenna complexes are missing. For koCP26/24 the slowdown of the fluorescence kinetics is more pronounced than for koCP29/24. This observation is in good agreement with previous work in [30], which indicates that both double mutants have disconnected LHCII, but the koCP26/24

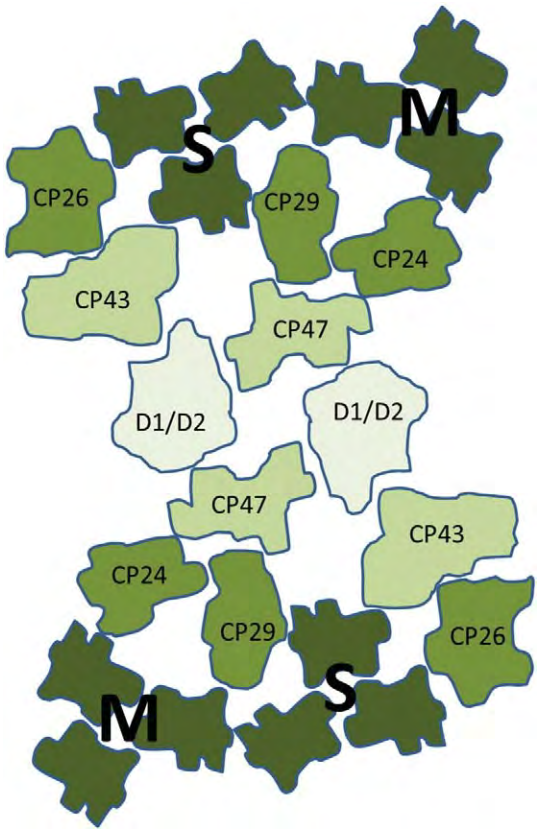

Fig. 4. Membrane organization of PSII in *Arabidopsis thaliana*. The core of PSII consists of the reaction center (D1/D2) together with CP47 and CP43. Minor antenna complexes (CP24, CP26 and CP29) with the major antenna complexes LHCII (dark green) form peripheral antenna that surrounds the core. The binding strength of trimeric LHCII at different locations is strong (S) or moderate (M). PSII structure is based on the study of Caffari et al. [22].

mutant has more, although the mutant that was lacking CP26 showed faster fluorescence kinetics than mutants lacking either CP24 or CP29 or both [25].

The most significant increase concerns the lifetimes of decay components 2 and 3 for all mutants, and this must originate from a reorganization or "disassembly" of PSII–LHCII, in agreement with earlier studies [25,30]. The increase in the lifetime of the PSII–LHCII components can be explained by the existence of badly connected or disconnected LHCII due to the absence of several minor antenna complexes. In the presence of disconnected LHCII, long-lived fluorescence components (around 4 ns) are expected, unless the LHCII complexes aggregate [48] which leads to a shortening of the fluorescence lifetime [48]. In a previous picosecond fluorescence study on thylakoid membranes from *A. thaliana*, it was shown that not only lifetime components 2 and 3 are responsible for the PSII–LHCII kinetics, but component 1 is also partly due to PSII–LHCII [25]. In that study, van Oort et al. used two excitation wavelengths in order to vary the relative amount of excitations in the core and outer antenna of PSII [25]. Applying this method, we find that the average lifetime of PSII–LHCII for the NoM mutant is 2.3 times longer than the average lifetime of PSII–LHCII for WT. This huge difference is attributed to the disruption of PSII supercomplexes and the presence of detached LHCII. Furthermore, from the biochemical analysis it is concluded that the LHCII/PSII ratio is increased by 50% in the NoM mutant as compared to WT cells, which means that the number of PSII pigments per RC in the NoM mutant is about 20% higher than in WT, since monomeric antennae are lacking. This should lead to an increase of the average lifetime of approximately 20% if all LHCII would be connected equally well to the PSII RC as in WT thylakoids [25]. To figure out the reason behind the increase of the average lifetime, the migration time for the WT and NoM mutant are calculated by the method van Oort et al. [25]. According to this method, the difference $\Delta\tau$ in the average lifetime of PSII for the two excitation wavelengths is approximately proportional to the migration time [25]. For WT cells we find $\Delta\tau = 26$ ps, whereas for the NoM mutant the value of $\Delta\tau$ is far larger, *i.e.* 170 ps. This dramatic increase cannot be explained by an increase of the migration time because of badly connected LHCII only but there should also be a significant fraction of disconnected LHCII (see also Van Oort et al. 2010). The (partial) detachment of LHCII is confirmed by the absence in NoM mutants of PSII supercomplexes containing LHCII-S, as shown upon mild solubilization of thylakoids and fractionation of pigment–protein complexes by ultracentrifugation (Fig. 2). Therefore, CP29 and CP26 play a crucial role in mediating the association of trimeric LHCII with the PSII complex. Moreover, the loss of all monomeric Lhcbs was accompanied by an over-accumulation of LHCII (+45% as compared to WT), suggesting compensation within the group of Lhcb proteins as a general regulatory mechanism for PSII antenna size. The phenotype of NoM is consistent with a recent study of *A. thaliana* acclimation to low- *vs.* high-light [53], which showed that LHCII is, among the Lhcbs, the major one responsible for the regulation of the PSII antenna size during acclimation.

The efficiency of light harvesting, directly related to the plastoquinone redox state, might play a role in antenna-size regulation. Indeed, the redox state is an indicator of the overall efficiency of photosynthetic electron transport, and it was suggested to play a key role in the modulation of antenna size through regulation of the Lhc genes expression [54]. More recent results [55] showed than upon long-term acclimation, despite a lack of Lhcb transcriptional regulation, the level of LHCII is tuned to environmental conditions, thus suggesting that the steady-state level of LHCII depends on post-transcriptional, rather than on transcriptional regulation, as assessed by the finding of a strong differential translational control on individual Lhcb mRNAs [56]. Thus, overaccumulation of LHCII in NoM would represent an adaptation response: depletion of minor antennae leads to reduced trapping efficiency in limiting light, and would trigger a compensative response leading to a photosynthetic phenotype with high LHCII/PSII ratio, namely resembling that of low light-acclimated leaves.

Accumulation of a large amount of disconnected antenna proteins in the NoM thylakoids suggests that LHCII is independently folded into membranes, irrespective from its assembly with the PSII core complex later on [57]. Therefore, even when assembly is prevented, LHCII is stable in the membrane and does not undergo proteolytic degradation. This evidence is consistent with the phenotype of PSII mutants such as *viridis-zd*^{69} of barley [58] and of lincomycin-treated plants [59], which revealed the stability of free LHCII in the thylakoids.

Isolation of the C_2S_2 supercomplex from koCP29/24 thylakoid membranes [36] has shown that LHCII-S can be associated with the core complex when CP26 is the only monomeric subunit present. This evidence is consistent with the isolation of a stable monomeric core with CP26 and the LHCII-S trimer [20]. In the absence of both CP29 and CP24, some $C_2S_2M_2$ complexes can assemble in grana membranes, but they are less stable and the molecular interactions are rather weak [36]. Moreover, koCP29/24 plants show a 15% increase in LHCII content with respect to the wild-type level (similar to the 20% for the koCP26/24 mutant). Thus, it is likely that a large part of the outer antenna is not directly bound to the PSII supercomplexes; rather, other trimers are interspersed among the C_2S_2 particles. This is confirmed by the time-resolved fluorescence data. The PSII–LHCII kinetics slows down significantly (average lifetime is almost doubled as compared to WT) while the value of $\Delta\tau$ is 42 ps as compared to 26 ps for WT. In a previous study, a CP29 antisense line was studied with the same method that we used here and the results are slightly different [25]. In that case $\Delta\tau$ was 30 ps instead of 42 ps [25]. However, it should be mentioned that in the CP29 antisense mutant CP29 expression was only partially blocked [60] as shown by detection of CP24 unlike the present mutant [36]. For koCP29/24 a large fraction of uncoupled LHCII is observed,

giving rise to a long lifetime of 732 ps (see τ_3 in Tables 2 and S3). In addition, after correcting for the PSI contribution and the 2 ns component the corresponding amplitude is around 65%, depending somewhat on excitation wavelength. For koCP26/24 the fitted lifetime is 912 ps with a similar amplitude around 64% after correcting for the PSI contribution. These amplitudes might correspond to the percentage of badly connected Chls *a* and since there are 5 LHCII trimers per PSII core in each mutant, this implies that at most one LHCII trimer plus one minor antenna, either CP29 or CP26 depending on the type of mutant, would be closely associated with the PSII core. This is in excellent agreement with earlier work in which it was shown that LHCII-S can be associated with the core complex when CP26 is the only monomeric subunit present [36]. Such an interpretation of the lifetime data would be in agreement with electron-microscopy observations, which show a high number of LHCII complexes interposed between rows of connected PSII cores in grana membranes [37]. These results would also be consistent with recent biochemical characterization of PSII supercomplexes in *Arabidopsis* [20], which indicates that LHCII-S binding is far less stable in a mutant devoid of CP26. The absence of a PSII supercomplex binding LHCII-M indicates that CP26 and CP24 have an important function in mediating the association of the $C_2S_2M_2$ complex.

A key consideration for the efficiency of primary productivity in plants and algae is the size of the light-harvesting system. Ort, Zhu and Melis have proposed antenna size reduction as a valuable strategy for the optimisation of the light reactions: theoretical simulation of net CO_2 uptake suggested that a smaller antenna size would significantly improve photosynthetic efficiency on crop canopies [61]. Even biomass yield of microalgal cultures at industrial scale is currently limited by several biological constraints, including the uneven light distribution into photobioreactors [62]; therefore, the successful implementation of biofuel production facilities requires domestication strategies, such as decreasing the absorption cross section to enhance light penetration and increase the size of metabolic sinks per chlorophyll [63,64].

However, strategies to improve light penetration must ensure that truncated antenna mutants are not photosynthetically impaired in ways other than reduced LHC content: indeed in higher plants, an extreme reduction in LHC complement leads to a lower photochemical yield and increases photoinhibition [65].

The present results show that depletion of even a sub-group of LHCs strongly affects the PSII light-harvesting efficiency and thus the photoautotrophic growth. To ensure that truncated-antenna strains will operate with improved light use efficiency, biotechnological approaches aimed at reducing antenna cross-section must focus on trimeric LHCII, rather than monomeric Lhcb, content: the latter leads to a strong impairment of PSII light-use efficiency, thus canceling out benefits of optical density reduction, although only for the NoM mutant this leads to strongly reduced growth under continuous-light conditions.

In summary, we have found in this study that in the absence of all minor antenna complexes of PSII, the functional connection of LHCII to the PSII cores is strongly diminished. A large part of this LHCII has a long excited-state lifetime although far shorter than the 4 ns of isolated LHCII trimers. Most likely, the detached LHCII is aggregated which leads to a shortening of the excited-state lifetime. In koCP26/24 and koCP29/24 mutants, it seems likely that only one LHCII trimer is directly (specifically) connected to the PSII core (or two LHCII trimers per PSII core dimer) whereas all other trimers are interspersed between the supercomplexes and still lead to relatively good EET, not hampering plant growth during continuous growth light conditions.

Acknowledgements

We thank Roberto Bassi for helpful discussions and support. This work was supported financially by the Netherlands Organization for Scientific Research (NWO) *via* the Council for Chemical Sciences (HvA) (Project number: 700.59.016).

Appendix A. Supplementary data

Supplementary data to this article can be found online at http://dx.doi.org/10.1016/j.bbabio.2014.09.011.

References

[1] N. Nelson, A. Ben-Shem, The complex architecture of oxygenic photosynthesis, Nat. Rev. Mol. Cell Biol. 5 (2004) 971–982.
[2] R. Croce, H. van Amerongen, Natural strategies for photosynthetic light harvesting, Nat. Chem. Biol. 10 (2014) 492–501.
[3] N. Nelson, C.F. Yocum, Structure and function of photosystems I and II, Annu. Rev. Plant Biol. 57 (2006) 521–565.
[4] J. Veerman, F.K. Bentley, J.J. Eaton-Rye, C.W. Mullineaux, S. Vasil'ev, D. Bruce, The PsbU subunit of photosystem II stabilizes energy transfer and primary photochemistry in the phycobilisome — photosystem II assembly of *Synechocystis* sp. PCC 6803, Biochemistry 44 (2005) 16939–16948.
[5] H. van Amerongen, R. Croce, Light harvesting in photosystem II, Photosynth. Res. 116 (2013) 251–263.
[6] G.H. Schatz, H. Brock, A.R. Holzwarth, Kinetic and energetic model for the primary processes in photosystem-II, Biophys. J. 54 (1988) 397–405.
[7] R. Croce, H. van Amerongen, Light-harvesting in photosystem I, Photosynth. Res. 116 (2013) 153–166.
[8] A. Busch, M. Hippler, The structure and function of eukaryotic photosystem I, Biochim. Biophys. Acta Bioenerg. 1807 (2011) 864–877.
[9] A.N. Melkozernov, S. Lin, R.E. Blankenship, Excitation dynamics and heterogeneity of energy equilibration in the core antenna of photosystem I from the cyanobacterium *Synechocystis* sp. PCC 6803, Biochemistry 39 (2000) 1489–1498.
[10] B. Gobets, R. van Grondelle, Energy transfer and trapping in photosystem I, Biochim. Biophys. Acta Bioenerg. 1507 (2001) 80–99.
[11] K.N. Ferreira, T.M. Iverson, K. Maghlaoui, J. Barber, S. Iwata, Architecture of the photosynthetic oxygen-evolving center, Science 303 (2004) 1831–1838.
[12] Y. Umena, K. Kawakami, J.R. Shen, N. Kamiya, Crystal structure of oxygen-evolving photosystem II at a resolution of 1.9 Angstrom, Nature 473 (2011) 55–60.
[13] E.J. Boekema, H. van Roon, J.F.L. van Breemen, J.P. Dekker, Supramolecular organization of photosystem II and its light-harvesting antenna in partially solubilized photosystem II membranes, Eur. J. Biochem. 266 (1999) 444–452.
[14] S.S. Lampoura, V. Barzda, G.M. Owen, A.J. Hoff, H. van Amerongen, Aggregation of LHCII leads to a redistribution of the triplets over the central xanthophylls in LHCII, Biochemistry 41 (2002) 9139–9144.
[15] M. Mozzo, L. Dall'Osto, R. Hienerwadel, R. Bassi, R. Croce, Photoprotection in the antenna complexes of photosystem II — role of individual xanthophylls in chlorophyll triplet quenching, J. Biol. Chem. 283 (2008) 6184–6192.
[16] V. Barzda, E.J.G. Peterman, R. van Grondelle, H. van Amerongen, The influence of aggregation on triplet formation in light-harvesting chlorophyll a/b pigment–protein complex II of green plants, Biochemistry 37 (1998) 546–551.
[17] N. Betterle, M. Ballottari, S. Zorzan, S. de Bianchi, S. Cazzaniga, L. Dall'Osto, T. Morosinotto, R. Bassi, Light-induced dissociation of an antenna hetero-oligomer is needed for non-photochemical quenching induction, J. Biol. Chem. 284 (2009) 15255–15266.
[18] P. Horton, A.V. Ruban, R.G. Walters, Regulation of light harvesting in green plants, Annu. Rev. Plant Physiol. Plant Mol. Biol. 47 (1996) 655–684.
[19] E.C.M. Engelmann, G. Zucchelli, F.M. Garlaschi, A.P. Casazza, R.C. Jennings, The effect of outer antenna complexes on the photochemical trapping rate in barley thylakoid photosystem II, Biochim. Biophys. Acta Bioenerg. 1706 (2005) 276–286.
[20] S. Caffarri, R. Kouril, S. Kereiche, E.J. Boekema, R. Croce, Functional architecture of higher plant photosystem II supercomplexes, EMBO J. 28 (2009) 3052–3063.
[21] S. Caffarri, K. Broess, R. Croce, H. van Amerongen, Excitation energy transfer and trapping in higher plant photosystem II complexes with different antenna sizes, Biophys. J. 100 (2011) 2094–2103.
[22] S. de Bianchi, M. Ballottari, L. Dall'Osto, R. Bassi, Regulation of plant light harvesting by thermal dissipation of excess energy, Biochem. Soc. Trans. 38 (2010) 651–660.
[23] D.G. Durnford, J.A. Price, S.M. McKim, M.L. Sarchfield, Light-harvesting complex gene expression is controlled by both transcriptional and post-transcriptional mechanisms during photoacclimation in *Chlamydomonas reinhardtii*, Physiol. Plant. 118 (2003) 193–205.
[24] K. Broess, G. Trinkunas, A. van Hoek, R. Croce, H. van Amerongen, Determination of the excitation migration time in photosystem II — consequences for the membrane organization and charge separation parameters, Biochim. Biophys. Acta Bioenerg. 1777 (2008) 404–409.
[25] B. van Oort, M. Alberts, S. de Bianchi, L. Dall'Osto, R. Bassi, G. Trinkunas, R. Croce, H. van Amerongen, Effect of antenna-depletion in photosystem II on excitation energy transfer in *Arabidopsis thaliana*, Biophys. J. 98 (2010) 922–931.
[26] G.H. Schatz, H. Brock, A.R. Holzwarth, Picosecond kinetics of fluorescence and absorbance changes in photosystem II particles excited at low photon density, Proc. Natl. Acad. Sci. U. S. A. 84 (1987) 8414–8418.
[27] R. Vangrondelle, Excitation-energy transfer, trapping and annihilation in photosynthetic systems, Biochim. Biophys. Acta 811 (1985) 147–195.
[28] E. Wientjes, H. van Amerongen, R. Croce, LHCII is an antenna of both photosystems after long-term acclimation, Biochim. Biophys. Acta 1827 (2013) 420–426.
[29] E. Wientjes, H. van Amerongen, R. Croce, Quantum yield of charge separation in photosystem II: functional effect of changes in the antenna size upon light acclimation, J. Phys. Chem. B 117 (2013) 11200–11208.

[30] Y. Miloslavina, S. de Bianchi, L. Dall'Osto, R. Bassi, A.R. Holzwarth, Quenching in *Arabidopsis thaliana* mutants lacking monomeric antenna proteins of photosystem II, J. Biol. Chem. 286 (2011) 36830–36840.
[31] D.I.G. Bennett, K. Amarnath, G.R. Fleming, A structure-based model of energy transfer reveals the principles of light harvesting in photosystem II supercomplexes, J. Am. Chem. Soc. 135 (2013) 9164–9173.
[32] J. Chmeliov, G. Trinkunas, H. van Amerongen, L. Valkunas, Light harvesting in a fluctuating antenna, J. Am. Chem. Soc. 136 (2014) 8963–8972.
[33] J.P. Dekker, R. Van Grondelle, Primary charge separation in photosystem II, Photosynth. Res. 63 (2000) 195–208.
[34] V.I. Novoderezhkin, E.G. Andrizhiyevskaya, J.P. Dekker, R. van Grondelle, Pathways and timescales of primary charge separation in the photosystem II reaction center as revealed by a simultaneous fit of time-resolved fluorescence and transient absorption, Biophys. J. 89 (2005) 1464–1481.
[35] M.K. Sener, C. Jolley, A. Ben-Shem, P. Fromme, N. Nelson, R. Croce, K. Schulten, Comparison of the light-harvesting networks of plant and cyanobacterial photosystem I, Biophys. J. 89 (2005) 1630–1642.
[36] S. de Bianchi, N. Betterle, R. Kouril, S. Cazzaniga, E. Boekema, R. Bassi, L. Dall'Osto, *Arabidopsis* mutants deleted in the light-harvesting protein Lhcb4 have a disrupted photosystem II macrostructure and are defective in photoprotection, Plant Cell 23 (2011) 2659–2679.
[37] S. de Bianchi, L. Dall'Osto, G. Tognon, T. Morosinotto, R. Bassi, Minor antenna proteins CP24 and CP26 affect the interactions between photosystem II subunits and the electron transport rate in grana membranes of *Arabidopsis*, Plant Cell 20 (2008) 1012–1028.
[38] A.P. Casazza, D. Tarantino, C. Soave, Preparation and functional characterization of thylakoids from *Arabidopsis thaliana*, Photosynth. Res. 68 (2001) 175–180.
[39] A.M. Gilmore, H.Y. Yamamoto, Zeaxanthin formation and energy-dependent fluorescence quenching in pea-chloroplasts under artificially mediated linear and cyclic electron-transport, Plant Physiol. 96 (1991) 635–643.
[40] H. Schagger, G. Vonjagow, Tricine sodium dodecyl-sulfate polyacrylamide-gel electrophoresis for the separation of proteins in the range from 1-kDa to 100-kDa, Anal. Biochem. 166 (1987) 368–379.
[41] G.F. Peter, J.P. Thornber, Biochemical-composition and organization of higher-plant photosystem-II light-harvesting pigment-proteins, J. Biol. Chem. 266 (1991) 16745–16754.
[42] M. Havaux, L. Dall'Osto, S. Cuine, G. Giuliano, R. Bassi, The effect of zeaxanthin as the only xanthophyll on the structure and function of the photosynthetic apparatus in *Arabidopsis thaliana*, J. Biol. Chem. 279 (2004) 13878–13888.
[43] Z.F. Liu, H.C. Yan, K.B. Wang, T.Y. Kuang, J.P. Zhang, L.L. Gui, X.M. An, W.R. Chang, Crystal structure of spinach major light-harvesting complex at 2.72 Angstrom resolution, Nature 428 (2004) 287–292.
[44] H. Towbin, T. Staehelin, J. Gordon, Electrophoretic transfer of proteins from polyacrylamide gels to nitrocellulose sheets — procedure and some applications, Proc. Natl. Acad. Sci. U. S. A. 76 (1979) 4350–4354.
[45] O.J.G. Somsen, L.B. Keukens, M.N. de Keijzer, A. van Hoek, H. van Amerongen, Structural heterogeneity in DNA: temperature dependence of 2-aminopurine fluorescence in dinucleotides, ChemPhysChem 6 (2005) 1622–1627.
[46] J.W. Borst, M.A. Hink, A. van Hoek, A.J.W.G. Visser, Effects of refractive index and viscosity on fluorescence and anisotropy decays of enhanced cyan and yellow fluorescent proteins, J. Fluoresc. 15 (2005) 153–160.
[47] B. van Oort, A. Amunts, J.W. Borst, A. van Hoek, N. Nelson, H. van Amerongen, R. Croce, Picosecond fluorescence of intact and dissolved PSI–LHCI crystals, Biophys. J. 95 (2008) 5851–5861.
[48] B. van Oort, A. van Hoek, A.V. Ruban, H. van Amerongen, Aggregation of Light-Harvesting Complex II leads to formation of efficient excitation energy traps in monomeric and trimeric complexes, FEBS Lett. 581 (2007) 3528–3532.
[49] R. Croce, H. van Amerongen, Light-harvesting and structural organization of photosystem II: from individual complexes to thylakoid membrane, J. Photochem. Photobiol. B Biol. 104 (2011) 142–153.
[50] H. van Amerongen, J.P. Dekker, Light harvesting in photosystem II, Light-harvesting antennas in photosynthesis, Kluwer Academic Publishers, 2003, pp. 219–251.
[51] X.W. Pan, M. Li, T. Wan, L.F. Wang, C.J. Jia, Z.Q. Hou, X.L. Zhao, J.P. Zhang, W.R. Chang, Structural insights into energy regulation of light-harvesting complex CP29 from spinach, Nat. Struct. Mol. Biol. 18 (2011) 309–315.
[52] A.V. Ruban, M. Wentworth, A.E. Yakushevska, J. Andersson, P.J. Lee, W. Keegstra, J.P. Dekker, E.J. Boekema, S. Jansson, P. Horton, Plants lacking the main light-harvesting complex retain photosystem II macro-organization, Nature 421 (2003) 648–652.
[53] M. Ballottari, L. Dall'Osto, T. Morosinotto, R. Bassi, Contrasting behavior of higher plant photosystem I and II antenna systems during acclimation, J. Biol. Chem. 282 (2007) 8947–8958.
[54] J.M. Escoubas, M. Lomas, J. Laroche, P.G. Falkowski, Light-intensity regulation of cab gene-transcription is signaled by the redox state of the plastoquinone pool, Proc. Natl. Acad. Sci. U. S. A. 92 (1995) 10237–10241.
[55] S. Frigerio, C. Campoli, S. Zorzan, L.I. Fantoni, C. Crosatti, F. Drepper, W. Haehnel, L. Cattivelli, T. Morosinotto, R. Bassi, Photosynthetic antenna size in higher plants is controlled by the plastoquinone redox state at the post-transcriptional rather than transcriptional level, J. Biol. Chem. 282 (2007) 29457–29469.
[56] M. Floris, R. Bassi, C. Robaglia, A. Alboresi, E. Lanet, Post-transcriptional control of light-harvesting genes expression under light stress, Plant Mol. Biol. 82 (2013) 147–154.
[57] N.H. Chua, P. Bennoun, Thylakoid membrane polypeptides of *Chlamydomonas reinhardtii* — wild-type and mutant strains deficient in photosystem 2 reaction center, Proc. Natl. Acad. Sci. U. S. A. 72 (1975) 2175–2179.
[58] O. Machold, D.J. Simpson, B.L. Moller, Chlorophyll-proteins of thylakoids from wild-type and mutants of barley (*Hordeum vulgare* L.), Carlsb. Res. Commun. 44 (1979) 235–254.
[59] L. Gaspar, E. Sarvari, F. Morales, Z. Szigeti, Presence of 'PSI free' LHCI and monomeric LHCII and subsequent effects on fluorescence characteristics in lincomycin treated maize, Planta 223 (2006) 1047–1057.
[60] J. Andersson, R.G. Walters, P. Horton, S. Jansson, Antisense inhibition of the photosynthetic antenna proteins CP29 and CP26: implications for the mechanism of protective energy dissipation, Plant Cell 13 (2001) 1193–1204.
[61] D.R. Ort, X.G. Zhu, A. Melis, Optimizing antenna size to maximize photosynthetic efficiency, Plant Physiol. 155 (2011) 79–85.
[62] P.G. Stephenson, C.M. Moore, M.J. Terry, M.V. Zubkov, T.S. Bibby, Improving photosynthesis for algal biofuels: toward a green revolution, Trends Biotechnol. 29 (2011) 615–623.
[63] J.E.W. Polle, S.D. Kanakagiri, A. Melis, tla1, a DNA insertional transformant of the green alga *Chlamydomonas reinhardtii* with a truncated light-harvesting chlorophyll antenna size, Planta 217 (2003) 49–59.
[64] H. Kirst, J.G. Garcia-Cerdan, A. Zurbriggen, T. Ruehle, A. Melis, Truncated photosystem chlorophyll antenna size in the green microalga *Chlamydomonas reinhardtii* upon deletion of the TLA3-CpSRP43 gene, Plant Physiol. 160 (2012) 2251–2260.
[65] C.E. Espineda, A.S. Linford, D. Devine, J.A. Brusslan, The AtCAO gene, encoding chlorophyll a oxygenase, is required for chlorophyll b synthesis in *Arabidopsis thaliana*, Proc. Natl. Acad. Sci. U. S. A. 96 (1999) 10507–10511.

Supplementary Information

Table S1. Photosynthetic capacity of PSII and PSI supercomplexes measured *in vitro* on thylakoids from WT and KO mutants. Effect of electron donors and acceptors on the electron transport rate of the supercomplex were assessed as described in "Material and Methods". Concentration used were: 250 μM DMBQ, PSII artificial electron acceptors; 250 μM $TMPDH_2$, PSI artificial electron donors. When $TMPDH_2$ was used, the reaction mixture contained 5 mM ascorbic acid, and after 1.5 min of illumination 1 μM DCMU was added, followed by the artificial donor. Data are expressed as mean ± SD (n = 3). Values marked with the same letters within the same column are not significantly different from each other (Student's *t* test, $P < 0.05$).

	μmol O_2 mg Chl^{-1} h^{-1} ($H_2O \rightarrow$ DMBQ, PSII)	μmol NADPH mg Chl^{-1} h^{-1} ($TMPDH_2 \rightarrow NADP^+$, PSI)
WT	53.2 ± 3.7 [a]	156.9 ± 6.5 [a]
NoM	37.0 ± 2.7 [b]	128.3 ± 7.3 [b]
koCP29/24	48.0 ± 1.7 [a]	141.6 ± 11.7 [a,b]
koCP26/24	47.8 ± 2.8 [a]	149.9 ± 7.8 [a]

Table S2. Fluorescence kinetics of PSII in thylakoids of WT *A. Thaliana*

	Excitation					
	412 nm			**484 nm**		
Detection	*680 nm*	*700 nm*	*720 nm*	*680 nm*	*700 nm*	*720 nm*
τ (ps)	%	%	%	%	%	%
52	24.8	43.7	51.8	13.6	29.5	42.3
166	32.2	25.1	26.6	35.5	31.9	28.0
409	42.1	30.6	21.1	49.9	37.9	29.3
5602	0.9	0.6	0.4	1.0	0.6	0.5
τ_{avg}(ps)	**287**	**221**	**181**	**324**	**257**	**214**

	PSII amplitudes from 166 ps DAS				PSII amplitudes from 409 ps DAS			
Wavelengths used for PSI removal	*700/680 nm*		*720/680 nm*		*700/680 nm*		*720/680 nm*	
Excitation	**412 nm**	**484 nm**	**412 nm**	**484 nm**	**412 nm**	**484 nm**	**412 nm**	**484 nm**
τ (ps)	%	%	%	%	%	%	%	%
52	17	9	19	9	17	9	18	9
166	36	38	35	38	36	38	35	38
409	47	53	46	53	47	53	46	53
τ_{avg} (ps)	**261**	**284**	**255**	**284**	**262**	**285**	**258**	**285**

	τ_{avg} for PSII		
Excitation	**412 nm**	**484 nm**	*Difference*
WT	259 ps	285 ps	*26 ps*

The kinetics were derived from the kinetics of thylakoid membranes by removing the PSI contribution, as explained in van Oort et al [23] before. Confidence intervals of fluorescence lifetimes (τ) were <5% (calculated by exhaustive search), standard errors of amplitudes were generally <5% (calculated from 2–6 repeats).

Table S3. Fluorescence kinetics of PSII in thylakoids of KoCP29/24 mutant of *A. Thaliana*

	Excitation					
	412 nm			**484 nm**		
Detection	*680 nm*	*700 nm*	*720 nm*	*680 nm*	*700 nm*	*720 nm*
τ (ps)	%	%	%	%	%	%
66	21.0	39.7	54.9	13.3	26.8	42.2
278	22.5	20.2	18.4	20.8	22.7	21.2
732	52.5	37.8	25.2	62.0	48.0	34.7
2099	4.0	2.3	1.6	4.0	2.5	1.9
τ_{avg} (ps)	**544**	**408**	**305**	**604**	**485**	**381**

	PSII amplitudes from 278 ps DAS				PSII amplitudes from 732 ps DAS			
Wavelengths used for PSI removal	*700/680 nm*		*720/680 nm*		*700/680 nm*		*720/680 nm*	
Excitation	**412 nm**	**484 nm**	**412 nm**	**484 nm**	**412 nm**	**484 nm**	**412 nm**	**484 nm**
τ (ps)	%	%	%	%	%	%	%	%
66	14	10	14	9	13	10	13	9
278	26	23	26	23	26	23	26	23
732	60	67	60	68	61	68	61	68
τ_{avg} (ps)	**521**	**561**	**520**	**566**	**525**	**565**	**525**	**569**

	τ_{avg} for PSII		
Excitation	**412 nm**	**484 nm**	*Difference*
KoCP29/24	523 ps	565 ps	*42 ps*

The kinetics were derived from the kinetics of thylakoid membranes by removing the PSI contribution, as explained in van Oort et al [23] before. Confidence intervals of fluorescence lifetimes (τ) were <5% (calculated by exhaustive search), standard errors of amplitudes were generally <5% (calculated from 2–6 repeats).

Table S4. Fluorescence kinetics of PSII in thylakoids of KoCP26/24 mutant of *A. Thaliana*

	Excitation					
	412 nm			**484 nm**		
Detection	*680 nm*	*700 nm*	*720 nm*	*680 nm*	*700 nm*	*720 nm*
τ (ps)	%	%	%	%	%	%
64	22.9	43.4	46.1	13.4	24.7	34.4
273	22.6	18.6	20.4	20.4	18.1	16.6
912	53.5	36.2	31.2	64.1	52.3	44.8
2800	0.9	1.8	2.3	2.1	4.9	4.2
τ_{avg} (ps)	**591**	**460**	**433**	**707**	**680**	**593**

	PSII amplitudes from 273 ps DAS				PSII amplitudes from 912 ps DAS			
Wavelengths used for PSI removal	*700/680 nm*		*720/680 nm*		*700/680 nm*		*720/680 nm*	
Excitation	**412 nm**	**484 nm**	**412 nm**	**484 nm**	**412 nm**	**484 nm**	**412 nm**	**484 nm**
τ (ps)	%	%	%	%	%	%	%	%
64	15	10	18	10	14	10	17	10
273	25	22	24	22	26	22	25	22
912	60	68	57	68	61	68	58	68
τ_{avg} (ps)	626	686	602	686	631	687	609	687

	τ_{avg} for PSII		
Excitation	**412 nm**	**484 nm**	*Difference*
KoCP26/24	617 ps	687 ps	*70 ps*

The kinetics were derived from the kinetics of thylakoid membranes by removing the PSI contribution, as explained in van Oort et al [23] before. Confidence intervals of fluorescence lifetimes (τ) were <5% (calculated by exhaustive search), standard errors of amplitudes were generally <5% (calculated from 2–6 repeats).

Table S5. Fluorescence kinetics of PSII in thylakoids of NoM mutant of *A. Thaliana*

	Excitation					
	412 nm			**484 nm**		
Detection	*680 nm*	*700 nm*	*720 nm*	*680 nm*	*700 nm*	*720 nm*
τ (ps)	%	%	%	%	%	%
59	30.0	43.4	53.8	17.2	29.1	40.1
294	19.9	21.3	21.1	12.0	13.8	15.0
1001	47.8	33.7	23.7	69.6	55.8	44.1
2862	2.2	1.5	1.3	1.3	1.3	0.8
τ_{avg} (ps)	**619**	**470**	**369**	**778**	**654**	**532**

	PSII amplitudes from 294 ps DAS				PSII amplitudes from 1001 ps DAS			
Wavelengths used for PSI removal	*700/680 nm*		*720/680 nm*		*700/680 nm*		*720/680 nm*	
Excitation	**412 nm**	**484 nm**	**412 nm**	**484 nm**	**412 nm**	**484 nm**	**412 nm**	**484 nm**
τ (ps)	%	%	%	%	%	%	%	%
59	28	15	27	15	25	14	25	13
294	21	12	21	13	22	13	22	13
1001	51	73	51	73	53	74	53	74
τ_{avg} (ps)	**590**	**771**	**594**	**775**	**608**	**782**	**610**	**786**

	τ_{avg} for PSII		
Excitation	**412 nm**	**484 nm**	*Difference*
NoM	601 ps	778 ps	*178 ps*

The kinetics were derived from the kinetics of thylakoid membranes by removing the PSI contribution, as explained in van Oort et al [23] before. Confidence intervals of fluorescence lifetimes (τ) were <5% (calculated by exhaustive search), standard errors of amplitudes were generally <5% (calculated from 2–6 repeats).

Table S6. Maximum quantum efficiency of PSII photochemistry determined on dark-adapted leaves of Arabidopsis WT and KO mutants. Data are expressed as mean ± SD (n = 6). Values marked with the same letters are not significantly different from each other (Student's *t* test, P < 0.05).

	F_v / F_m
WT	0.81 ± 0.01 [a]
NoM	0.56 ± 0.02 [b]
koCP29/24	0.75± 0.02 [c]
koCP26/24	0.74 ± 0.02 [c]

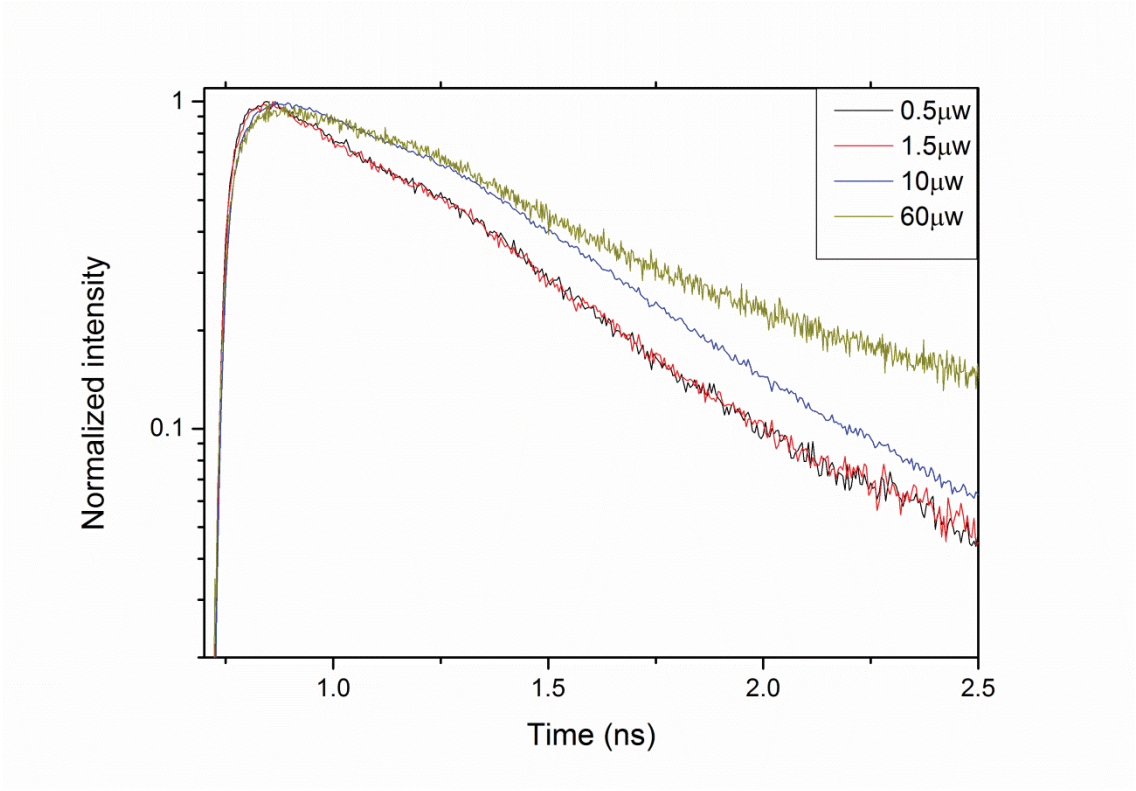

Figure S1. Fluorescence kinetics of thylakoid membranes of WT Arabidopsis Thaliana excited at 412 nm and detected at 680 nm at different excitation powers. The resulting decay curves were indistinguishable for excitation powers 0.5 μw and 1.5 μw, which are used for the experiments.

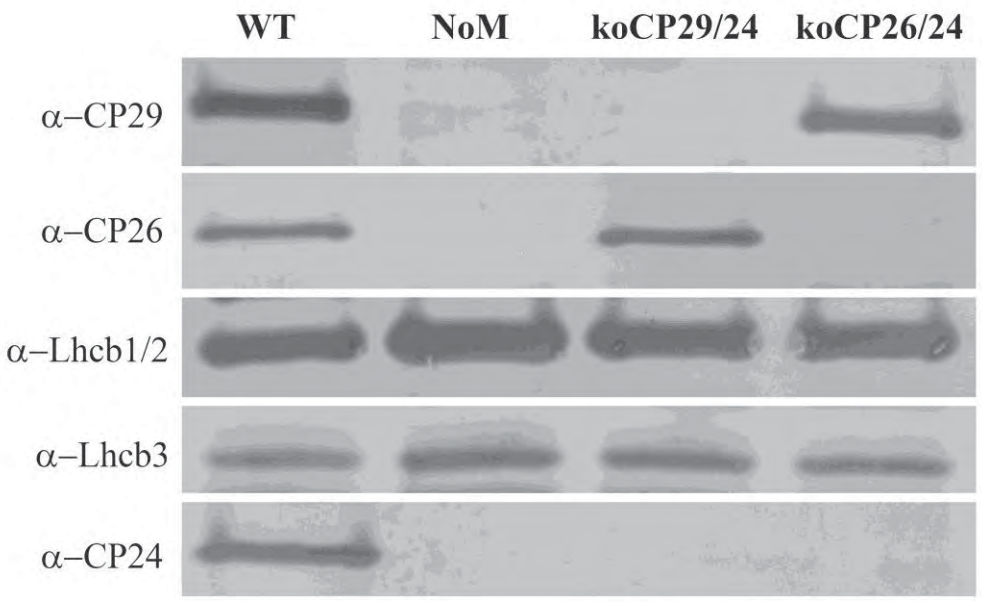

Figure S2. Polypeptide composition of thylakoids from WT and KO mutants. Immunoblot analysis was carried out with antibodies directed against Lhcb subunits. Thylakoids corresponding to 1 μg of Chls were loaded for each sample.

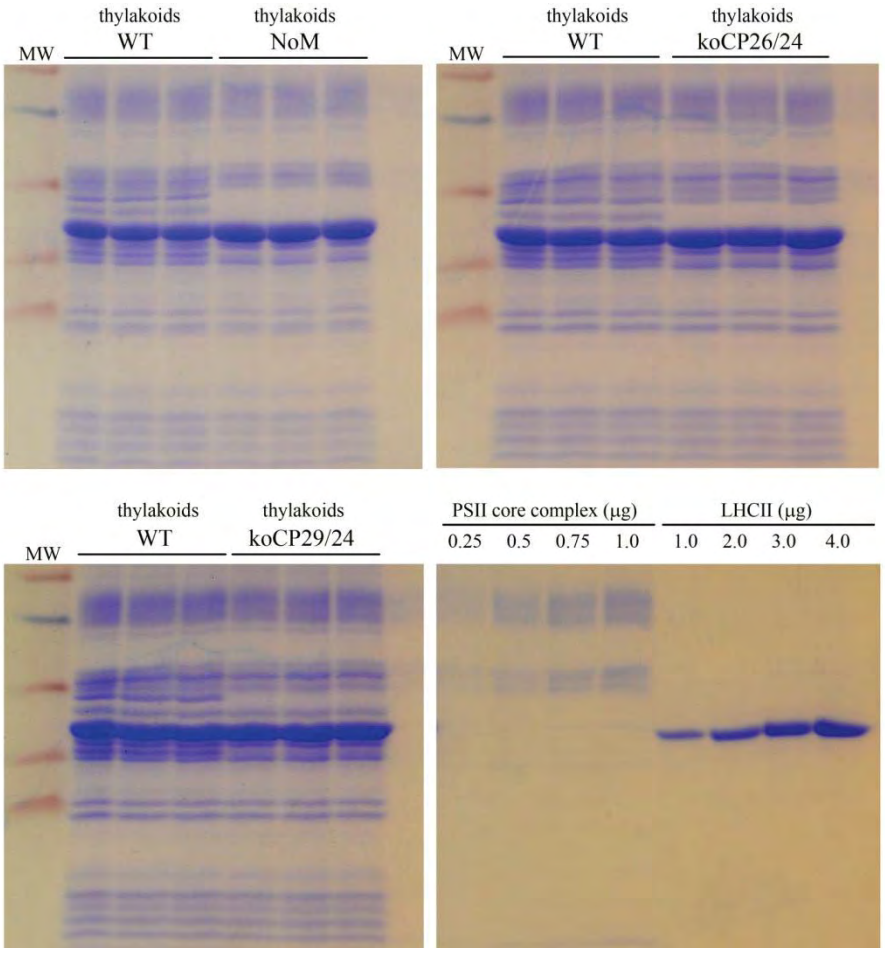

Figure S3. SDS-PAGE analysis of trimeric LHCII:monomeric PSII core stoichiometry in thylakoids from wild-type and KO mutants. Absolute contents of LHCII and PSII core were quantified by loading thylakoids (15 μg of Chls/lane), PSII core (0.25-0.5-0.75-1.0 μg of Chls) and trimeric LHCII (1.0-2.0-3.0-4.0 μg of Chls) in the same slab gels. After staining with coomassie blue, the signal amplitude of LHCII and CP43/CP47 bands were quantified by densitometric analysis (n=4). By using the pigment composition of the individual subunits and the OD of each protein band, the number of LHCII trimers per monomeric PSII core was calculated. MW, pre-stained molecular weight marker.

Section C.
Role of chloroplast relocation in photoprotection and its contribution in defining NPQ kinetic.

C1. Interaction between avoidance of photon absorption, excess energy dissipation and zeaxanthin synthesis against photooxidative stress in *Arabidopsis thaliana*.

the plant journal

SEB Society for Experimental Biology

The Plant Journal (2013) **76,** 568–579 doi: 10.1111/tpj.12314

Interaction between avoidance of photon absorption, excess energy dissipation and zeaxanthin synthesis against photooxidative stress in Arabidopsis

Stefano Cazzaniga[1,†], Luca Dall' Osto[1,†], Sam-Geun Kong[2], Masamitsu Wada[2] and Roberto Bassi[1,*]

[1]*Dipartimento di Biotecnologie, Università di Verona, 37134 Italy, and*

[2]*Department of Biology, Kyushu University, Fukuoka 812-8581, Japan*

Received 18 May 2013; revised 6 August 2013; accepted 12 August 2013; published online 3 October 2013.

*For correspondence (e-mail roberto.bassi@univr.it).

†Both authors contributed equally to this work.

SUMMARY

Plants evolved photoprotective mechanisms in order to counteract the damaging effects of excess light in oxygenic environments. Among them, chloroplast avoidance and non-photochemical quenching concur in reducing the concentration of chlorophyll excited states in the photosynthetic apparatus to avoid photooxidation. We evaluated their relative importance in regulating excitation pressure on photosystem II. To this aim, genotypes were constructed carrying mutations impairing the chloroplast avoidance response (*phot2*) as well as mutations affecting the biosynthesis of the photoprotective xanthophyll zeaxanthin (*npq1*) or the activation of non-photochemical quenching (*npq4*), followed by evaluation of their photosensitivity *in vivo*. Suppression of avoidance response resulted in oxidative stress under excess light at low temperature, while removing either zeaxanthin or PsbS had a milder effect. The double mutants *phot2 npq1* and *phot2 npq4* showed the highest sensitivity to photooxidative stress, indicating that xanthophyll cycle and qE have additive effects over the avoidance response. The interactions between non-photochemical quenching and avoidance responses were studied by analyzing the kinetics of fluorescence decay and recovery at different light intensities. *phot2* fluorescence decay lacked a component, here named as qM. This kinetic component linearly correlated with the leaf transmittance changes due to chloroplast relocation induced by white light and was absent when red light was used as actinic source. On these basis we conclude that a decrease in leaf optical density affects the apparent non-photochemical quenching (NPQ) rise kinetic. Thus, excess light-induced fluorescence decrease is in part due to avoidance of photon absorption rather than to a genuine quenching process.

Keywords: chloroplast avoidance movement, non-photochemical quenching, zeaxanthin, photoprotection, lipid peroxidation, *Arabidopsis thaliana*.

INTRODUCTION

In chloroplasts the absorbed light can easily exceed the capacity for photosynthetic electron transport due to changes in irradiance and/or physiological state. Excess light (EL) is harmful, because it increases the probability for population of chlorophyll (Chl) triplet excited states (^{3}Chl*) which can react with molecular oxygen to yield singlet oxygen ($^1O_2$). This is a reactive oxygen species (ROS) with a strong oxidative power towards lipids, nucleic acids and proteins (Triantaphylides and Havaux, 2009; Alboresi *et al.*, 2011).

During their lifetime, plants often experience environmental factors unbalancing the ratio between energy consumption and utilization that severely limit photosynthetic electron transport rate, leading to photoinhibition and thus reducing plant growth and fitness (Niyogi, 1999; Takahashi and Murata, 2008).

To avoid photoinhibition, a number of photoprotective responses can be activated in EL, aimed to either: (i) regulating the absorption of light; (ii) dissipating the excess of excited states; or (iii) scavenging ROS species eventually produced. NPQ is a major photoprotective response: it down-regulates ^{1}Chl* concentration in PSII light-harvesting complexes (LHC) by activating a heat dissipation channel, thus limiting ^{3}Chl* formation. NPQ includes components activated within different time spans. The fastest component is called qE and is fully dependent on thylakoid lumen

acidification (Horton *et al.*, 1996). Low lumenal pH is detected by the LHC-like subunit PsbS (Li *et al.*, 2004) and activates violaxanthin de-epoxidase, which transforms violaxanthin (Viola), present in dark or low light, into zeaxanthin (Zea) (Yamamoto and Kamite, 1972). The latter has a number of photoprotective effects, including amplification of qE (Niyogi *et al.*, 1998), down-regulation of ^{3}Chl* yield in LHC proteins (Dall'Osto *et al.*, 2012) and increased ROS scavenging (Havaux and Niyogi, 1999; Havaux *et al.*, 2007; Dall'Osto *et al.*, 2010). Besides relying in dissipative mechanisms located within the chloroplasts, plants can also avoid over-excitation by relocating chloroplasts within the cell: the 'avoidance response' relocates chloroplasts along side walls where they shade each other and decrease overall leaf photon absorption. In low light, instead, the 'accumulation response' directs chloroplasts toward the cytosolic layer along the periclinal cell walls maximizing light harvesting (Wada *et al.*, 2003). Accumulation and avoidance responses are mediated by blue light photoreceptors phototropins (phot1 and phot2 in *Arabidopsis thaliana*) (Jarillo *et al.*, 2001; Kagawa *et al.*, 2001; Sakai *et al.*, 2001). The *phot2* Arabidopsis mutant lacks the phot2, a membrane-bound serine/threonine kinase receptor activated by blue light, thus keeping chloroplasts aligned on periclinal cell walls regardless of light intensity, and making *phot2* plants exposed to EL more susceptible to photodamage than wild-type (WT) (Kasahara *et al.*, 2002; Sztatelman *et al.*, 2010).

Although the photoprotective action of either chloroplast avoidance, qE or Zea synthesis have been widely investigated, their relative contribution to photosynthetic efficiency in EL is unknown. In the present work, we evaluated their relative photoprotective effect under EL at low temperature. To this aim, we have produced double mutants impaired in the chloroplast avoidance movement (*phot2*) and in either the qE activity (*npq4)*, or the Zea synthesis (*npq1),* and analyzed their photoprotection performance *in vivo*. We found that the *phot2* mutation produces the strongest photodamage in EL. Interestingly, despite neither pigment composition nor qE amplitude were affected by the *phot2* mutation, the overall EL-induced fluorescence decay kinetics were different, with the loss of a kinetic component intermediate between qE and qI. We conclude that chloroplast relocation movement significantly influences the apparent kinetic of NPQ. This effect is rather due to a decreased photon absorption rate in WT versus *phot2* than to a change in the activity of quenching reactions.

RESULTS

Chloroplast avoidance movement and kinetic of NPQ

As chloroplast avoidance response significantly affects leaf optical absorption properties (Kasahara *et al.*, 2002; Sztatelman *et al.*, 2010), it appears reasonable that this mechanism might influence the fraction of incident light in excess with respect to the maximal capacity of energy utilization, thus affecting both the amplitude and the kinetics of NPQ rise and relaxation.

In order to verify this possibility, NPQ activity of both WT and *phot2* plants were measured upon exposure of dark-adapted leaves to white actinic light (400 μmol photons m^{-2} sec^{-1}, 22°C), for 60 min in order to allow all chloroplasts to attain the anticlinal cell walls (Kasahara *et al.*, 2002). In WT, NPQ showed an initial, rapid rise to a value of 1.6 within 5 min, after which the decrease of fluorescence was slower, the NPQ reaching a value of 2.4 after 60 min of illumination (Figure 1a). In the same conditions, the NPQ of *phot2* was clearly different: although the initial rapid rise to a value of 1.5 was similar to WT, no further increase of NPQ was observed in the following 55 min of illumination. Also, dark NPQ recovery was faster in *phot2* versus WT (Figure 1a, inset). Previous work (Jarillo *et al.*, 2001; Kagawa *et al.*, 2001; Sakai *et al.*, 2001) demonstrated that chloroplast relocation in higher plants is mediated by the phototropins that respond to blue light. In order to further verify the hypothesis that the action of phototropins was somehow involved in the change in NPQ kinetics observed, we repeated NPQ measurements by using red light ($600 < \lambda < 750$ nm, 350 μmol photons m^{-2} sec^{-1}, 22°C) as actinic source (Briggs and Christie, 2002). The light intensities for these experiments were chosen in order to produce the same value of qL, namely the same proportion of PSII reaction centres closed at steady-state photosynthesis (Baker, 2008), in both genotypes.

Result is shown in Figure 1b: upon induction of quenching by red actinic light, both WT and *phot2* leaves showed a rapid rise in NPQ followed by a plateau, thus matching the kinetic of *phot2* in white light. The slower NPQ kinetic of WT leaves, induced previously by white actinic light, was lacking in red light. Kinetic of dark relaxation of quenching was the same in both genotypes. The above results imply that a specific NPQ kinetic component is activated by actinic $\lambda < 600$ nm, while it is lacking at longer wavelengths, and is responsible for a large F_m' quenching in WT leaves (Figure 1c).

This quenching component, here named as qM, has been kinetically characterized by plotting the amplitude of the difference $F_{m'RL}$ (in red actinic light, RL)$-F_{m'WL}$ (in white actinic light, WL), measured on WT leaves at different time points during illumination and normalized to the corresponding F_m values. Data were then fitted with an exponential function. The kinetic analysis showed that the overall amplitude of the quenching component of F_m, lacking in red light, can be described by a single exponential phase, according to the equation $y = A \times (1-\exp(-t/\tau))$, showing a half-time τ of about 14 min (Figure 1d). Thus, kinetic analysis revealed that qM: (i) was clearly slower than the rapidly inducible qE process (which is completed

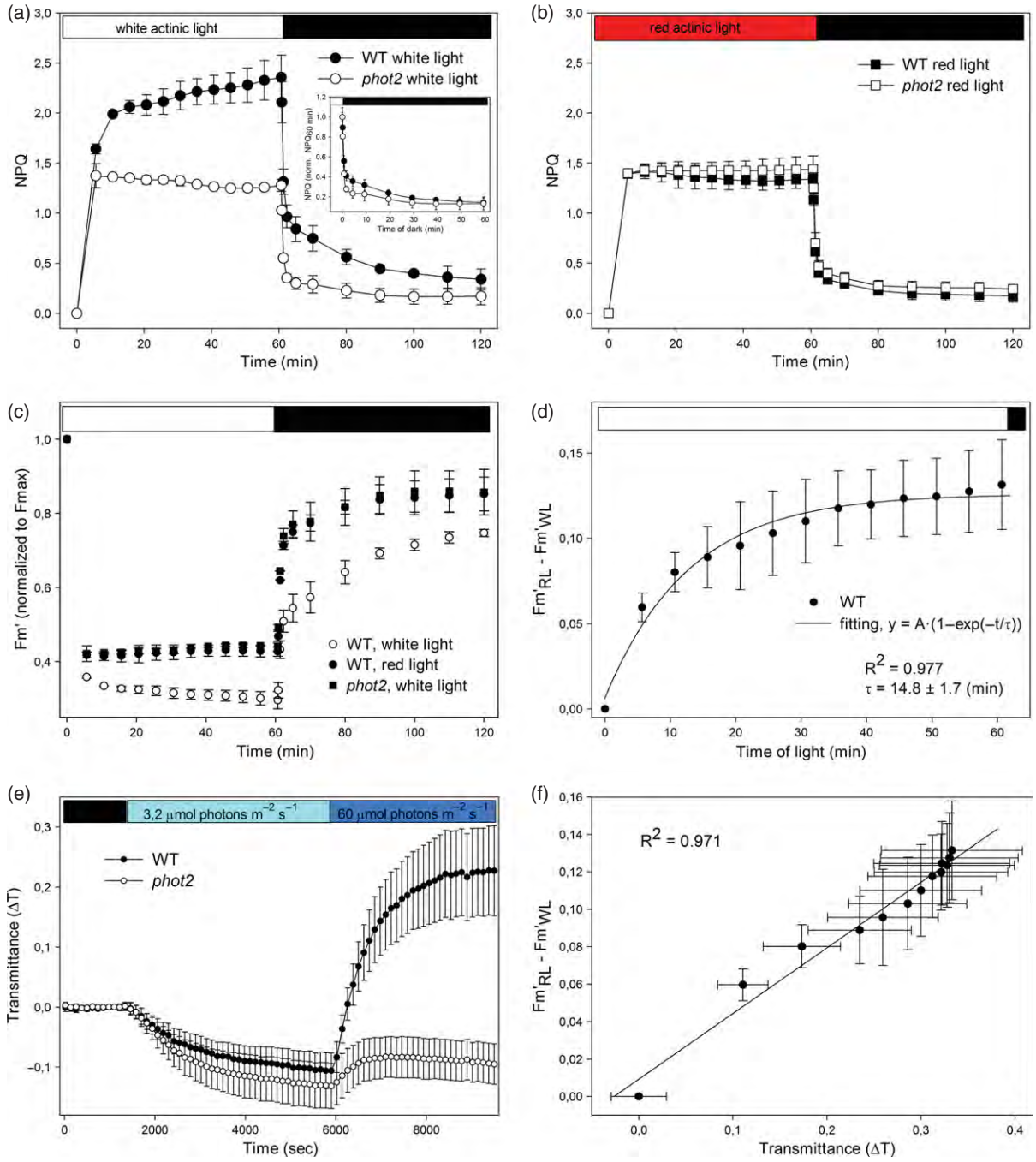

Figure 1. Kinetics of formation and relaxation of photoprotective energy dissipation in WT and *phot2* leaves.
(a, b) NPQ kinetics were measured on WT and *phot2* leaves upon illumination with either white actinic light (400 μmol photons m^{-2} sec^{-1}, 22°C (a), or red actinic light (350 μmol photons m^{-2} sec^{-1}, 600 < λ<750 nm, 22°C (b). Inset, kinetics of NPQ dark recovery in WT and *phot2*, after normalization to NPQ values at the end of the white light window.
(c) F_m' kinetics were measured on the same genotypes upon illumination with either white or red actinic light.
(d) Kinetic analysis of qM. The average data of $F_{m'RL}$ (in red actinic light, RL)−$F_{m'WL}$ (in white actinic light, WL), measured on WT leaves at different time points during illumination, were fitted by a single exponential function according to the equation $y = A \times (1-\exp(-t/\tau))$. The kinetic analysis showed that the overall F_m' amplitude can be described by a single exponential phase. Values of R^2 and half-time of the kinetic component (τ) are reported. Symbols and error bars show means ± standard deviation (SD) (n = 3).
(e) Changes in red light transmission accompanying the chloroplast photorelocation movement were recorded photometrically. Dark-adapted leaves of WT and *phot2* were exposed to blue light at low fluence rate (3.2 μmol photons m^{-2} sec^{-1}, λ = 470 nm, light blue bar) or high fluence rate (60 μmol photons m^{-2} sec^{-1}, λ = 470 nm, blue bar) in order to induce accumulation and avoidance responses, respectively. Symbols and error bars show means ± SD (n = 18).
(f) Correlation between the amplitude of F_m' quenching component induced by white light only (calculated as F_m' in red light−F_m' in white light) and ΔT change due to chloroplast photorelocation, measured at different time point. Line shows the best linear fitting of experimental points (R^2 value = 0.971).

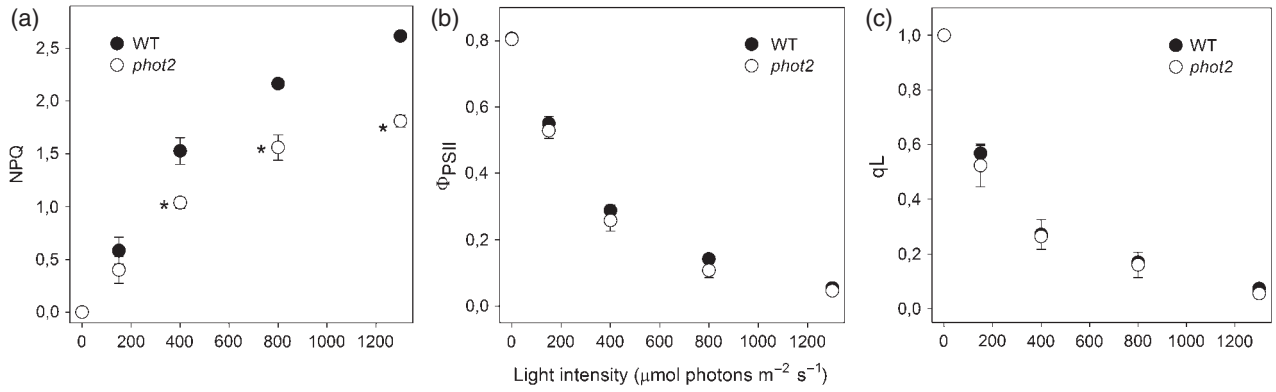

Figure 2. Analysis of room temperature Chl fluorescence during photosynthesis in WT and *phot2* plants.
(a) Dependence of NPQ; (b) PSII operating efficiency (Φ_{PSII}); and (c) amplitude of qL measured at different light intensities at 22°C; qL reflects the redox state of the primary electron acceptor Q_A, thus the fraction of open PSII centers. Steady-state photosynthesis was induced by white actinic light, parameters were measured after 25 min of illumination. Data are expressed as means ± standard deviation (SD) ($n = 4$). Values that are significantly different (Student's *t*-test, $P < 0.05$) from the wild-type are marked with an asterisk (*).

within 1–2 min upon illumination); and (ii) was developed independently from the induction of photoinhibition, indeed values of PSII operating efficiency at the end of the light induction were the same in both genotypes (Figure 2b).

Light transmittance has been used as a measure of the chloroplast positions in the cells of leaves illuminated by a light beam. These measurements showed that transmittance changes saturate within 30 min of illumination in WT with approximately 400 μmol photons m^{-2} sec^{-1} of white light, or approximately 60 μmol photons m^{-2} sec^{-1} of blue light; no transmittance changes were observed in leaves of *phot2* mutant under the same light regimes (Jarillo *et al.*, 2001; Kasahara *et al.*, 2002).

In order to quantify the rate of light-dependent chloroplast photorelocation, we followed changes in light transmittance (ΔT) over time in leaves of WT and *phot2* upon illumination with blue light, each light treatment lasting approximately 1 h. In both genotypes, ΔT decreases below zero at 3.2 μmol photons m^{-2} sec^{-1}; this decrease in transmittance corresponds to the accumulation response of chloroplasts. When illuminated with higher light intensity (60 μmol photons m^{-2} sec^{-1}), the ΔT of WT leaves showed a rapid rise in the first 18 min, followed by a slower rise, reaching a stable transmission after 60 min of illumination; rather, leaves from *phot2* did not show the light-dependent increase in transmittance (Figure 1e). For a more precise correlation of the quenching component activated by blue light with the chloroplast avoidance response, we compared the $F_m'_{RL}-F_m'_{WL}$ with ΔT due to chloroplast relocation (Figure 1f) showing that the two phenomena have the same time dependence.

Light harvesting and photosynthetic electron transport

PSII activity at steady-state photosynthesis was further investigated by Chl fluorescence in WT and *phot2* plants. NPQ amplitude was plotted as a function of the intensity of white actinic light (Figure 2a). A decrease in NPQ amplitude was measured in *phot2* with respect to WT at every actinic light intensity tested.

Differences in NPQ amplitude could be due to changes in either electron transport rate, pigment composition, lumen acidification, amplitude of state 1-state 2 transitions or PsbS accumulation level (Horton *et al.*, 1996; Li *et al.*, 2000; de Bianchi *et al.*, 2008, 2010). In order to exclude pleiotropic effects related to the lack of chloroplast relocation machinery, we performed a detailed analysis of thylakoid protein content, efficiency of linear electron transport and light-harvesting capacity in WT versus *phot2* plants.

Analysis of the fluorescence yield in dark-adapted leaves (Butler, 1978) showed the same PSII maximum quantum efficiency (F_v/F_m) in WT and *phot2* leaves (Table 1). Moreover, *phot2* leaves showed no significant differences with respect to WT plants either in the PSII photochemical efficiency (Φ_{PSII}) or in the Q_A redox state (qL) (Figure 2b,c), thus indicating no limitations in electron transport downstream of PSII.

The organization of pigment-protein complexes in WT and *phot2* was analyzed by non-denaturing Deriphat-PAGE (Figure 3a). No significant differences were observed in the Lhcb/PSII and PSI/PSII ratios in thylakoids from WT and *phot2*. Consistently, the PSII light-harvesting capacity, as estimated on leaves by measuring the rise time of Chl florescence in the presence of DCMU ($T_{2/3}^{-1}$), was not significantly affected by the *phot2* mutation. Chlorophyll content, Chl a/b and Chl/Car ratios were essentially the same in both genotypes (Table 1), as the Zea accumulated in EL (Table 1; Figure 3b); as de-epoxidation rate of Viola is dependent on low lumenal pH, this finding suggests that no significant differences in the efficiency of proton pumping into the chloroplast lumen were present in WT and *phot2*. Moreover, PsbS content was the same (Figure S1),

Table 1 Pigment content and Chl fluorescence induction parameters

Genotype	Chl content (μg cm^{-2})	Chl *a*/*b*	Chl/Car	Zeaxanthin (mol/100 mol Chl)	F_v/F_m	$T_{2/3}^{-1}$ ($\times 10^3$, ms^{-1})
WT	20.4 ± 1.3	3.1 ± 0.1	3.6 ± 0.1	1.1 ± 0.2	0.80 ± 0.01	5.1 ± 0.5
phot2	22.2 ± 0.7	3.1 ± 0.1	3.6 ± 0.1	1.1 ± 0.1	0.81 ± 0.01	5.0 ± 0.5
npq1	21.0 ± 2.7	3.1 ± 0.1	3.7 ± 0.1	–	0.81 ± 0.01	5.2 ± 0.5
npq4	21.3 ± 1.8	3.0 ± 0.1	3.7 ± 0.1	0.9 ± 0.1	0.80 ± 0.01	5.0 ± 0.6
phot2 npq1	20.3 ± 1.6	3.1 ± 0.1	3.7 ± 0.1	–	0.81 ± 0.01	5.1 ± 0.5
phot2 npq4	21.4 ± 2.1	3.1 ± 0.1	3.7 ± 0.1	1.1 ± 0.2	0.80 ± 0.01	5.5 ± 0.4

Measurements were done on dark-adapted leaves of Arabidopsis wild-type WT, single *npq* and double *phot2 npq* mutants. Data are expressed as mean ± standard deviation (SD) ($n > 3$). Chl, total chlorophylls; Car, total carotenoids. $T_{2/3}$, time corresponding to two-thirds of the induction fluorescence rise in DCMU-treated leaves; $T_{2/3}^{-1}$ is a measure of the functional antenna size of PSII. Values are not significantly different from each other within a column (Student's *t*-test, $P < 0.05$).

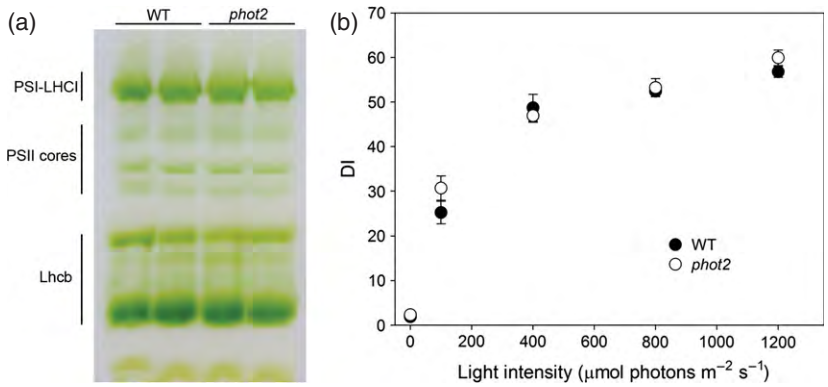

Figure 3. Composition of thylakoid membranes from WT and *phot2* plants.
(a) Thylakoid pigment-protein complexes were separated by non-denaturing Deriphat-PAGE upon solubilization with 0.7% β-dodecyl-maltoside. Thylakoids corresponding to 25 μg of chlorophylls were loaded in each lane. Composition of each band is indicated.
(b) Time course of de-epoxidation index (DI) in WT and *phot2* plants. Leaf discs from dark-adapted leaves were illuminated at different light intensities (white actinic light, 1200 μmol photons m^{-2} sec^{-1}) for 30 min, then discs were frozen in liquid nitrogen and total pigments extracted before HPLC analysis.

thus ruling out the hypothesis that a decrease in NPQ could be due to impaired ΔpH sensing. The amplitude and rate of state transitions (Jensen *et al.*, 2000) were the same in WT and *phot2* leaves, as well as the rate of the transition from state I to state II upon switching off far-red light (Figure S2).

On the basis of multiple measurements we could assess that *phot2* mutation does not affect organization and function of photosynthetic machinery, being mutants similar to the WT in term of light-harvesting capacity and efficiency of photosynthetic electron transport at all light intensities tested.

Photosensitivity to EL at chilling temperature

Upon crossing *npq1/4* and *phot2* plants and screening the F2 generation (Figure S3), it was possible to isolate double mutants *phot2 npq1* and *phot2 npq4*, lacking chloroplast avoidance response and either xanthophyll cycle (*npq1*) or qE (*npq4*), respectively.

All these mutants were identical to the corresponding control genotypes in term of organization of photosynthetic complexes (Figure S4), PSII photochemical yield and Q_A redox state (Figure S5), capacity for Zea accumulation in EL and functional antenna size (Table 1). Photometric measurements of chloroplast movement revealed that single *npq* mutants behaved similar to WT, showing the same kinetics of both chloroplast accumulation and avoidance responses (Figure 4a,b). Instead, all the double mutants were specifically depleted in the avoidance response.

The capacity for NPQ at steady-state photosynthesis, plotted as a function of the actinic light intensity, was significantly lower in *phot2* versus WT, *phot2 npq1* versus *npq1* and *phot2 npq4* versus *npq4* at light intensities ≥400 μmol photons m^{-2} sec^{-1} (Figure 4c,d). It is worth noting that the reduction in NPQ amplitude due to the lack of chloroplast photorelocation is lower when *phot2* mutation is coupled to a *npq* mutation. This finding can be ascribed to the non-linear relation between NPQ and F_m'. Indeed when F_m' values, rather than NPQ, are plotted as a function of the actinic light intensity, it appears that *phot2* mutation is responsible for the same increase in F_m' in all genetic backgrounds (Figure S6).

In order to investigate the relative contribution of xanthophyll cycle, qE and avoidance response on chloroplast

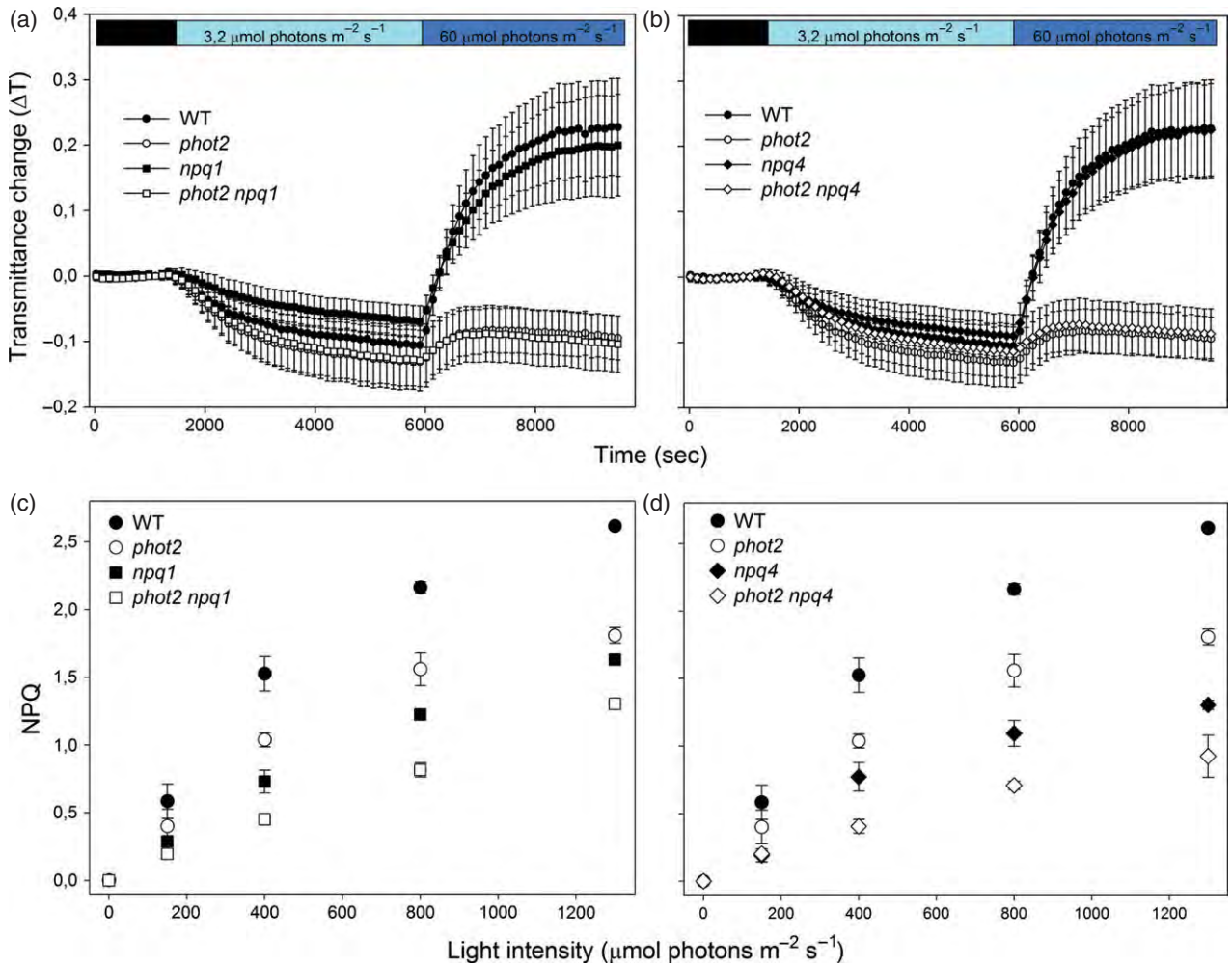

Figure 4. NPQ analysis of WT and mutant genotypes.
(a, b) Changes in red light transmission accompanying the chloroplast photorelocation movement, recorded photometrically. Dark-adapted leaves of WT, single *npq* and double *phot2 npq* mutants were exposed to blue light at low fluence rate (3.2 μmol photons m^{-2} sec^{-1}, light blue bar) or high fluence rate (60 μmol photons m^{-2} sec^{-1}, blue bar) in order to induce respectively accumulation and avoidance responses. Symbols and error bars show means ± standard deviation (SD) (n = 18).
(c, d) Dependence of NPQ to light intensity. NPQ amplitude were measured at steady-state photosynthesis, quenching was induced by white actinic light. Data are expressed as means ± SD (n = 4). For actinic light >200 μmol photons m^{-2} sec^{-1}, introduction of *phot2* mutation in either WT, *npq1* or *npq4* genetic background resulted in a significant reduction of NPQ amplitude at light intensities ≥400 μmol photons m^{-2} sec^{-1} (Student's *t*-test, $P < 0.05$).

photoprotection, WT and mutant plants were transferred to EL (650 μmol m^{-2} sec^{-1}, 8°C). The combination of low temperature and high light intensity is known to enhance the induction of both PSII photoinhibition and membrane photooxidation in Arabidopsis leaves (Havaux and Kloppstech, 2001). Then, the maximal photochemical yield of PSII (F_v/F_m) was monitored. Results are displayed on Figure 5. WT plants showed the highest resistance to PSII photoinhibition, while *phot2* plants were the most sensitive among single mutants; *npq1* and *npq4* showed an intermediate behavior between WT and *phot2*. Moreover, photoinhibition rate of *phot2* was enhanced to only a limited extent by addition of either *npq1* or *npq4* mutations. Thus, a higher level of light damage was observed in all genotypes carrying the *phot2* mutation. Instead, the effect of a disrupted xanthophyll cycle or qE was relatively less important.

To further investigate this point, the resistance to EL stress was measured from the extent of lipid peroxidation (Havaux *et al.*, 2005). WT, *npq1* and *npq4* leaves underwent a low level of photooxidative stress in the conditions used in this experiment (Figure 5). *phot2* genotypes showed enhanced photosensitivity. Indeed, EL treatment was accompanied by extensive lipid peroxidation in *phot2* and in the double mutants *phot2 npq1* and *phot2 npq4*. Moreover, an additive effects of both *npq1* and *npq4* mutations over *phot2* was observed, indicating that Zea, qE and avoidance response have additive effects in providing chloroplast photoprotection at low temperature.

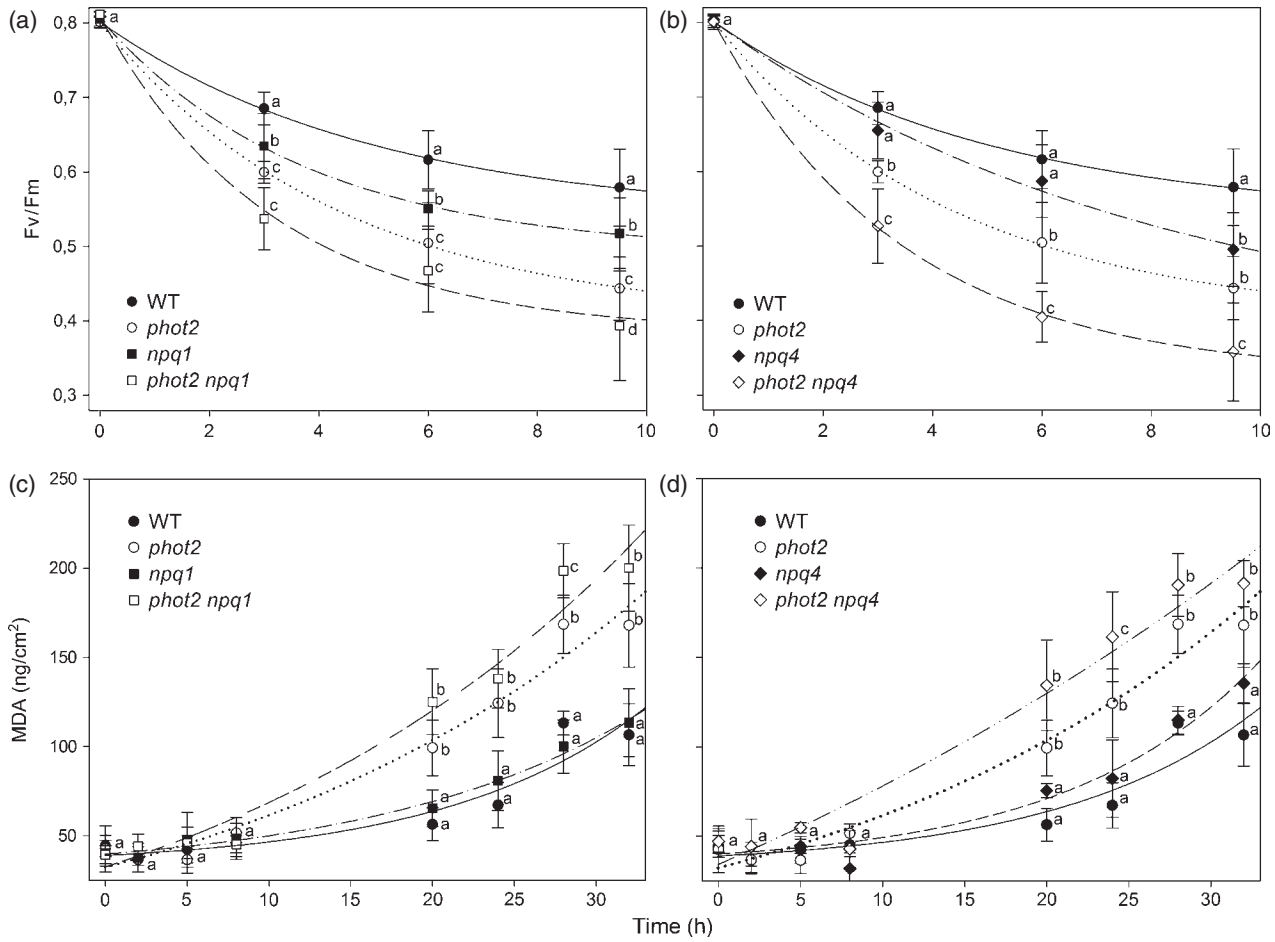

Figure 5. Photooxidation of Arabidopsis WT and mutants exposed to EL and low temperature.
(a, b) PSII photoinhibition (F_v/F_m decay) was followed in the wild-type (WT), *phot2*, *npq* and *phot2 npq* plants, treated at 650 μmol photons m^{-2} sec^{-1}, 8°C for 10 h. Symbols and error bars show means ± standard deviation (SD) ($n > 8$).
(c, d) Detached leaves floating on water were treated at 1500 μmol photons m^{-2} sec^{-1}, 8°C for 35 h, and kinetics of MDA formation were recorded. Symbols and error bars show means ± SD ($n = 5$). Values marked with the same letters are not significantly different from each other within the same time point (Student's *t*-test, $P < 0.05$).

DISCUSSION

Difference in NPQ kinetics of WT versus *phot2* evidenced a quenching component which tightly correlates with the leaf transmittance changes due to chloroplast photorelocation (Figure 1). The same contribution was induced in WT by white light but not by red light actinic excitation. Comparative analysis of different *npq* mutants showed that this kinetic component was not related to qE activity (Figure 4c, d) or to Zea accumulation (Figure 3b). Rather, it depends on the activity of the chloroplast relocation process mediated by the blue light receptors phototropins (Figure 4).

Suppression of the high light-induced chloroplast avoidance response enhanced oxidative stress in EL, while xanthophyll cycle or PsbS had a weaker effect in our experimental conditions. The double mutants *phot2 npq1* and *phot2 npq4* showed enhanced sensitivity to photooxidative stress with respect to the *phot2* plants, implying Zea, qE and avoidance response independently contribute to counteract photooxidative stress *in vivo*.

A slowly inducible component of NPQ is modulated by the chloroplast avoidance response

Early investigation on relaxation of Chl fluorescence quenching in barley (Walters and Horton, 1991) identified three kinetic components: a fast phase ($\tau_{½} \sim 1$ min), a middle phase ($\tau_{½} \sim 10$–20 min) and a slow phase ($\tau_{½} > 1$ h). These kinetic components had been ascribed to three different processes contributing to NPQ, namely: (i) the pH-dependent energy dissipation in the antenna of PSII (qE); (ii) the state 1-state 2 transitions (qT); and (iii) the photoinhibition of PSII (qI). As the rapidly-reversible qE component provides a major contribution to NPQ amplitude, it has been investigated more thoroughly (Holt *et al.*, 2005; Ruban *et al.*, 2007; Miloslavina *et al.*, 2008) than qT and qI components. Photoinhibitory quenching, or qI, has

been associated to a kinetic component whose relaxation is far slower than the decay of trans-thylakoid pH gradient upon light to dark transition and was attributed to processes involving damage of PSII, implying a reduction of the quantum yield of photosynthetic electron transport (Krause, 1988).

The intermediate kinetic component of NPQ, qT, is unlikely to be related to state 1-state 2 transitions, as: (i) these occur under low light only (Rintamaki *et al.*, 1997); and (ii) the Arabidopsis mutant *stn7* blocked in state transitions showed an unaltered amplitude of the three kinetic components of NPQ (Bellafiore *et al.*, 2005; Nilkens *et al.*, 2010). Rather, more recent results showed that Zea accumulation and its binding to LHC modulate the amplitude of the intermediate kinetic component of NPQ relaxation, thus renamed as qZ (Dall'Osto *et al.*, 2005; Nilkens *et al.*, 2010). This finding was consistent with the analysis of ultrafast Chl fluorescence quenching in intact leaves of Arabidopsis, that identified a Zea-dependent quenching site in the PSII antenna (Miloslavina *et al.*, 2008). Here, we show that the intermediate phase of NPQ kinetics strongly depends on the chloroplast avoidance movement (Figure 1d), while it is not affected by Zea synthesis. As the slow phase of NPQ induction is lacking in *phot2* plants, it suggests that chloroplast photorelocation, rather than xanthophyll cycle, is the main process contributing to the quenching component described previously as qZ (Nilkens *et al.*, 2010). Moreover, here we showed that the avoidance-dependent fluorescence decay component is not related to the rapidly induced qE activity: indeed the NPQ rise is the same in WT and *phot2* leaves within the first minute of illumination (Figure S7). Furthermore, it is neither related to photoinhibition processes (Figure 1) nor to altered state transitions (Figure S2). This kinetic component represents a light-induced decrease in photon absorption which yields into a decrease in fluorescence yield rather than the building up of a genuine quenching process. During illumination, chloroplast movement towards the anticlinal cell walls changes the distribution of pigments with the formation of areas with extremely high absorption due to the formation of localized chloroplast stacks. This produces a 'sieve effect' which reduces the photon dose absorbed by the ensemble of chloroplasts (McClendon and Fukshansky, 1990), thus yielding into a reduced Chl fluorescence emission. In fluorometry measurements this event can easily be interpreted as a fluorescence quenching.

It is worth noting that most Chl fluorometers do not measure homogeneously the emission of chloroplasts in the different cell layers within a leaf blade: light penetration is inhomogeneous throughout the mesophyll tissue, being dependent on several factors such as leaf anatomy, absorption cross section of the pigment-protein complexes, Chl content, distribution of chloroplasts across the leaf section and wavelength of the excitation light (Rappaport *et al.*, 2007). In a low light adapted leaf, we expect that periclinal cell surface is covered with chloroplasts (Jarillo *et al.*, 2001; Kagawa *et al.*, 2001; Sakai *et al.*, 2001; Wada *et al.*, 2003); under these conditions, by using white actinic light, largely absorbed by photosystems, fluorescence mainly arises from chloroplasts localized to the adaxial leaf face, while chloroplasts of deeper layers contributes far less to the fluorescence emission.

Thus, a progressive decrease in fluorescence intensity will accompany chloroplast photorelocation movements. This yields into an apparent F_m quenching component that adds to the fluorescence decrease due to NPQ defined as the activation of a ^{1}Chl* dissipation channel.

The photoprotective function of chloroplast avoidance mechanism

Although mutants *npq1*, *npq4* and *phot2* grown in low light did not show major differences in photosynthetic electron transport efficiency (Figure S5), they were clearly more sensitive to photoinhibition when exposed to EL at low temperature (Figure 5). The decline in the quantum efficiency of PSII (F_v/F_m), i.e. PSII photoinhibition, was higher in *phot2* plants with respect to *npq* mutants (Figure 5a,b), suggesting that chloroplast avoidance movement is more effective in photoprotection than NPQ or xanthophyll cycle and yet these mechanisms have been shown to provide important contributions to photoprotection (Havaux and Niyogi, 1999; Li *et al.*, 2002). The role of Zea in preventing photooxidative stress is more evident during prolonged light stress, perhaps when the capacity of other antioxidant network of the chloroplast are saturated (Muller-Moule *et al.*, 2003; Havaux *et al.*, 2007). Moreover, recent results showed that *npq4* plants, despite being depleted in the fast NPQ component, still develop a quenching activity, although at a slower rate than WT (Johnson and Ruban, 2010). Indeed, the decrease in fluorescence detected in *npq4* is slower than qE, thus less efficient in counteracting rapid fluctuations in light intensity. Consistently, *npq4* plants were only mildly affected by constant EL in growth chamber, while their fitness in natural environment, with rapid light intensity fluctuation during the day, was strongly reduced (Kulheim *et al.*, 2002). Photoprotection by qE is maximal when variation of incident light occurs on a timescale of seconds (Alter *et al.*, 2012). Here, we show that photoprotection by avoidance response is effective on EL and low temperature treatment over a period of hours (Figure 5); instead, *npq1 and npq4* mutants experienced lower level of photooxidative stress than *phot2*. The stress conditions applied in the present study cause imbalance between light absorption and energy utilization mainly at the onset of the EL treatment. Thus, qE depletion might have been compensated by the activation of slowly inducible quenching components, which alleviate over-excitation at longer times. Moreover,

longer-term acclimation responses lead to increased levels of antioxidant enzymes and scavenging agents. Indeed, previous results clearly pointed to a synergism between Zea and antioxidant molecules such as ascorbate and tocopherol (Muller-Moule *et al.*, 2003; Havaux *et al.*, 2005) as key element for chloroplast photoprotection.

Comparison of NPQ values during steady-state photosynthesis in WT and *phot2* leaves showed that the avoidance-dependent fluorescence decay component accounts for approximately 15% of global fluorescence decrease, thus a minor effect with respect to that caused by PsbS depletion in *npq4* (Figure 4d). We conclude that the reduced NPQ amplitude cannot be the only reason for the higher photosensitivity of *phot2* plants with respect to *npq* mutants. Moreover, it is worth noting that NPQ value is not a linear parameter, and photoprotection provided by NPQ and the amplitude of quenching are not linearly related as well. The fluorescence decay component here described is due to avoidance of photon absorption rather than to a genuine quenching process. Photoinhibition rate is proportional to light dose (Chow *et al.*, 2005). Thus, any mechanism leading to a decrease in total leaf absorption, will alter the rate of photodamage, namely the decrease of photon absorption due to chloroplast photorelocation.

The photoprotective effect of chloroplast photorelocation was first reported by Kasahara *et al.* (2002) based on prolonged experiments carried on at very high light (1400 μmol photons m^{-2} sec^{-1}, 22°C). We obtained consistent results using milder stress conditions at lower temperature in agreement with the observation that low temperature and EL are synergistic in eliciting photooxidative stress (Havaux *et al.*, 2005; Dall'Osto *et al.*, 2010; Cazzaniga *et al.*, 2012) and that chloroplast photorelocation is not inhibited at low temperature (Figure S3). Thus our results together with previous work (Kasahara *et al.*, 2002) highlight a crucial role of chloroplast photorelocation response in protection, as compared to other major protective mechanisms. This can be explained by the recent proposal that avoidance mechanism changes the distribution of photoinhibition profile through cell layers in leaf sections (Davis and Hangarter, 2012). Indeed, when chloroplasts were in an accumulation arrangement, a higher level of PSII photoinhibition occurred at the exposed leaf surface, while the avoidance arrangement allowed uniform distribution of PSII damage between adaxial and abaxial leaf surfaces. Therefore, chloroplast photorelocation is aimed to two targets: (i) maximize photosynthesis through higher light penetration; and (ii) distribute PSII damage among different leaf cell layers reduce the maximal extent of inhibition suffered by individual chloroplasts and prevent the depression of photosynthetic efficiency in a single cell.

Negative phototropism is a major photoprotection mechanism in *Chlamydomonas* (Harman Feinlein and Curry, 1971) which, together with complementary photoprotection responses localized into the chloroplast (Li *et al.*, 2009; Bonente *et al.*, 2011) ensure resistance from exposure to EL.

From an evolutionary perspective, chloroplast photorelocation movement is found in many species besides land plants (Suetsugu and Wada, 2007) while the basic mechanism of phototropin action is highly conserved, the diverse physiological significance of phototropin being confirmed in plants examined, including Arabidopsis, fern, moss, and algae (Kong and Wada, 2011) while negative phototropism was a photoprotective response in cyanobacteria (Song *et al.*, 2011) well before the establishment of xanthophyll cycle or LHC-proteins-associated NPQ (Li *et al.*, 2009; Peers *et al.*, 2009). Chloroplasts photorelocation in plants shows functional analogies with the phototactic behavior of flagellated green algae such as *Chlamydomonas reinhardtii*, able to move toward or away from the incident light in excess; phototrophic microorganisms switch between positive and negative phototaxis, upon light perception, in order to fluctuate under proper light conditions for photosynthesis (Wakabayashi *et al.*, 2011). Our results show that these mechanisms provide crucial photoprotection effect in EL conditions. Photosensitive phenotypes of mutants lacking chloroplast avoidance highlight the strong selection pressure that likely operated during the evolution leading from the ancestor flagella-dependent phototactic behavior, found in many green algae, to the current chloroplast photorelocation movement mediated by interaction with actin filaments (Kong and Wada, 2011). Both plastid photorelocation in plants and negative phototaxis in *Chlamydomonas* appear to involve the action of specialized plasma membrane domains containing photoreceptor proteins (Kong and Wada, 2011; Trippens *et al.*, 2012). This same selective pressure still operates to maintain chloroplast photorelocation, which has been shown to be optimal for light harvesting, NPQ and adaptation of plants to the changing irradiances in natural environment. In the absence of avoidance response, in fact, a strong decrease in fitness and fast selection would be expected, as shown in the case of Arabidopsis mutant devoid of avoidance response: indeed, *phot2* plants showed a strong photosensitivity to EL at low temperature, that the complementary photoprotective mechanism, such as qE and xanthophyll cycle, cannot fully compensate.

EXPERIMENTAL PROCEDURES

Plant material and growth conditions

Wild-type plants of *A. thaliana* ecotype Columbia and mutants *phot2*, *npq1* and *npq4* were obtained as previously reported (Kagawa *et al.*, 2001; Dall'Osto *et al.*, 2005). Individual mutants were crossed, and homozygous double mutant plants were selected through a chloroplast mobility assay (Kagawa *et al.*, 2001) and either immunoblotting with α-PsbS antibody (*phot2 npq4*) or HPLC (*phot2 npq1*). Plants were grown for 4 weeks on

Sundermisch potting mix (Gramoflor, http://www.gramoflor.com) in controlled conditions of 8 h light, 23°C/16 h dark, 20°C, with a light intensity of 100 μmol photons m^{-2} sec^{-1}.

Wild-type and mutants used for photometric analysis were sown on 0.8% (w/v) agar plates containing half-strength Murashige and Skoog medium supplemented with 1% sucrose. The plates were kept in the dark at 4°C for 72 h and subsequently transferred to a growth chamber under 16 h/8 h (day/night) periods at 23°C.

Thylakoids isolation

Stacked thylakoid membranes were isolated as described previously (Casazza *et al.*, 2001).

Pigment analyses

Pigments were extracted from leaves with 80% acetone, then separated and quantified by HPLC (Gilmore and Yamamoto, 1991).

Gel electrophoresis and immunoblotting

Non-denaturing Deriphat-PAGE was performed following the method described previously (Peter *et al.*, 1991) with modifications reported in Havaux *et al.* (2004). Thylakoids concentrated at 1 mg ml^{-1} Chl were solubilized with either 0.8% β-dodecylmaltoside, 30 μg of Chls were loaded in each lane. For immunotitration, thylakoid samples corresponding to 0.25, 0.5, 0.75, or 1 μg of chlorophyll were loaded for each sample and electroblotted on nitrocellulose membranes. Proteins were detected with alkaline phosphatase-conjugated antibody (Towbin *et al.*, 1979). To avoid any deviation between different immunoblots, samples were compared only when loaded in the same slab gel. Signal amplitude was quantified using the GELPRO 3.2 software (BIORAD, http://www.bio-rad.com).

Analysis of chlorophyll fluorescence

PSII function during photosynthesis was measured through Chl fluorescence on whole leaves at 22°C with a PAM 101 fluorometer (Heinz-Walz, http://www.walz.com/) (Andersson *et al.*, 2001). White actinic light (100–1200 μmol photons m^{-2} sec^{-1}) was supplied by a KL1500 halogen lamp (Schott, http://www.schott.com); red actinic light ($600 < \lambda < 750$ nm, 350 μmol photons m^{-2} sec^{-1}) was obtained by means of interference filter. NPQ, Φ_{PSII}, qP and qL were calculated according to the equations described in (Van Kooten and Snel, 1990; Baker, 2008). Calculation of ΔpH-dependent component of chlorophyll fluorescence quenching (qE) was performed as described previously (Walters and Horton, 1995). Fluorescence kinetics were measured with a home-built setup, in which leaves were vacuum-infiltrated with 3.0×10^{-5} M DCMU, 150 mM sorbitol and were excited with green light at 520 nm (Luxeon; Lumileds, http://www.philipslumileds.com/) while emission was measured in the near far-red (Rappaport *et al.*, 2007). The half-time of the fluorescence rise was taken as a measure of the functional antenna size of PSII (Malkin *et al.*, 1981). State transition measurements were performed on whole plants according to the previously described (Jensen *et al.*, 2000).

Determination of the sensitivity to photooxidative stress

For EL treatments, light was provided by 150-W halogen lamps (Focus 3, Prisma, http://www.pil-usa.com/). Short-term EL treatment was performed using actinic range between 100 and 1200 μmol photons m^{-2} sec^{-1} at 22°C to measure maximal Zea accumulation on detached leaves floating on water. Long-term EL treatment was performed at either 650 μmol photons m^{-2} sec^{-1}, 8°C (PSII photoinhibition) or 1500 μmol photons m^{-2} sec^{-1}, 8°C (lipid peroxidation) on whole plants. Decay kinetics of maximal quantum yield of PSII photochemistry (F_v/F_m) (Havaux *et al.*, 2004) was recorded during illumination to follow PSII photoinhibition. Photo-oxidative stress was assessed by measuring MDA formation as an indirect quantification of lipid peroxidation (Havaux *et al.*, 2005).

Photometric measurements of chloroplast movement

Photometric analysis of chloroplast movement was performed using a programmable plate reader by monitoring red light transmittance in response to different intensities of blue light (light-emitting diode with wavelength peak at 470 nm) as previously described (Wada and Kong, 2011).

Statistics

Significance analyses were performed using an analysis of variance with a pair-wise multiple comparison procedure in *Origin*. Error bars represent the standard deviation.

Accession numbers

Sequence data from this article can be found in the EMBL/GenBank data libraries under accession numbers At1g08550 (*npq1*), At1g44575 (*npq4*), At5g58140 (*phot2*).

ACKNOWLEDGEMENTS

This work was supported by the Marie Curie Actions–Networks for Initial Training Harvest (Grant PITN-GA-2009-238017) and Acclimphot (PITN-2012- 316427) and by Ministero delle Politiche Agricole, Alimentari e Forestali BioMassVal (Grant 2/01/140). This work was also partly supported by Grant-in-Aids for Young Scientists (B) (21770050 to S.G.K.), for Scientific Research (S) (20227001 to M.W.), and for Scientific Research on Innovative Areas (23120523 to M.W.).

SUPPORTING INFORMATION

Additional Supporting Information may be found in the online version of this article.

Figure S1. Immunotitration of PsbS subunit in WT and *phot2* thylakoids.

Figure S2. Measurement of state I–state II transition in the WT and *phot2*.

Figure S3. Screening for chloroplast avoidance mutants.

Figure S4. Analysis of pigment-protein complexes of the WT and mutants.

Figure S5. Analysis of room temperature Chl fluorescence during photosynthesis in WT, *npq* and *phot2* plants.

Figure S6. Analysis of F_m' during photosynthesis in WT, *npq* and *phot2* plants.

Figure S7. Kinetics of formation and relaxation of NPQ in WT and *phot2* leaves.

REFERENCES

Alboresi, A., Dall'Osto, L., Aprile, A., Carillo, P., Roncaglia, E., Cattivelli, L. and Bassi, R. (2011) Reactive oxygen species and transcript analysis upon excess light treatment in wild-type *Arabidopsis thaliana* vs a photosensitive mutant lacking zeaxanthin and lutein. *BMC Plant Biol.* **11**, 62.

Alter, P., Dreissen, A., Luo, F.L. and Matsubara, S. (2012) Acclimatory responses of *Arabidopsis* to fluctuating light environment: comparison of different sunfleck regimes and accessions. *Photosynth. Res.* **113**, 221–237.

Andersson, J., Walters, R.G., Horton, P. and Jansson, S. (2001) Antisense inhibition of the photosynthetic antenna proteins CP29 and CP26:

implications for the mechanism of protective energy dissipation. *Plant Cell*, **13**, 1193–1204.

Baker, N.R. (2008) Chlorophyll fluorescence: a probe of photosynthesis *in vivo*. *Annu. Rev. Plant Biol.* **59**, 89–113.

Bellafiore, S., Barneche, F., Peltier, G. and Rochaix, J.D. (2005) State transitions and light adaptation require chloroplast thylakoid protein kinase STN7. *Nature*, **433**, 892–895.

de Bianchi, S., Dall'Osto, L., Tognon, G., Morosinotto, T. and Bassi, R. (2008) Minor antenna proteins CP24 and CP26 affect the interactions between photosystem II subunits and the electron transport rate in grana membranes of *Arabidopsis*. *Plant Cell*, **20**, 1012–1028.

de Bianchi, S., Ballottari, M., Dall'Osto, L. and Bassi, R. (2010) Regulation of plant light harvesting by thermal dissipation of excess energy. *Biochem. Soc. Trans.* **38**, 651–660.

Bonente, G., Ballottari, M., Truong, T.B., Morosinotto, T., Ahn, T.K., Fleming, G.R., Niyogi, K.K. and Bassi, R. (2011) Analysis of LhcSR3, a protein essential for feedback de-excitation in the green alga *Chlamydomonas reinhardtii*. *PLoS Biol.* **9**, e1000577.

Briggs, W.R. and Christie, J.M. (2002) Phototropins 1 and 2: versatile plant blue-light receptors. *Trends Plant Sci.* **7**, 204–210.

Butler, W.L. (1978) Energy distribution in the photochemical apparatus of photosynthesis. *Annu. Rev. Plant Physiol.* **29**, 345–378.

Casazza, A.P., Tarantino, D. and Soave, C. (2001) Preparation and functional characterization of thylakoids from *Arabidopsis thaliana*. *Photosynth. Res.* **68**, 175–180.

Cazzaniga, S., Li, Z., Niyogi, K.K., Bassi, R. and Dall'Osto, L. (2012) The Arabidopsis szl1 mutant reveals a critical role of β-carotene in photosystem I photoprotection. *Plant Physiol.* **159**(4), 1745–1758.

Chow, W.S., Lee, H.Y., He, J., Hendrickson, L., Hong, Y.N. and Matsubara, S. (2005) Photoinactivation of photosystem II in leaves. *Photosynth. Res.* **84**, 35–41.

Dall'Osto, L., Caffarri, S. and Bassi, R. (2005) A mechanism of nonphotochemical energy dissipation, independent from Psbs, revealed by a conformational change in the antenna protein CP26. *Plant Cell*, **17**, 1217–1232.

Dall'Osto, L., Cazzaniga, S., Havaux, M. and Bassi, R. (2010) Enhanced photoprotection by protein-bound vs free xanthophyll pools: a comparative analysis of chlorophyll b and xanthophyll biosynthesis mutants. *Mol. Plant*, **3**, 576–593.

Dall'Osto, L., Holt, N.E., Kaligotla, S., Fuciman, M., Cazzaniga, S., Carbonera, D., Frank, H.A., Alric, J. and Bassi, R. (2012) Zeaxanthin protects plant photosynthesis by modulating chlorophyll triplet yield in specific light-harvesting antenna subunits. *J. Biol. Chem.* **287**, 41820–41834.

Davis, P.A. and Hangarter, R.P. (2012) Chloroplast movement provides photoprotection to plants by redistributing PSII damage within leaves. *Photosynth. Res.* **112**, 153–161.

Gilmore, A.M. and Yamamoto, H.Y. (1991) Zeaxanthin formation and energy-dependent fluorescence quenching in pea chloroplasts under artificially mediated linear and cyclic electron transport. *Plant Physiol.* **96**, 635–643.

Harman Feinlein, M.E. and Curry, G.M. (1971) The relationship between stimulus intensity and oriented phototactic response (topotaxis) in Chlamydomonas. *Physiol. Plant.* **25**, 346–352.

Havaux, M. and Kloppstech, K. (2001) The protective functions of carotenoid and flavonoid pigments against excess visible radiations at chilling temperature investigated in *Arabidopsis* npq and tt mutants. *Planta*, **213**, 953–966.

Havaux, M. and Niyogi, K.K. (1999) The violaxanthin cycle protects plants from photooxidative damage by more than one mechanism. *Proc. Natl Acad. Sci. USA*, **96**, 8762–8767.

Havaux, M., Dall'Osto, L., Cuine, S., Giuliano, G. and Bassi, R. (2004) The effect of zeaxanthin as the only xanthophyll on the structure and function of the photosynthetic apparatus in *Arabidopsis thaliana*. *J. Biol. Chem.* **279**, 13878–13888.

Havaux, M., Eymery, F., Porfirova, S., Rey, P. and Dormann, P. (2005) Vitamin E protects against photoinhibition and photooxidative stress in *Arabidopsis thaliana*. *Plant Cell*, **17**, 3451–3469.

Havaux, M., Dall'Osto, L. and Bassi, R. (2007) Zeaxanthin has enhanced antioxidant capacity with respect to all other xanthophylls in *Arabidopsis* leaves and functions independent of binding to PSII antennae. *Plant Physiol.* **145**, 1506–1520.

Holt, N.E., Zigmantas, D., Valkunas, L., Li, X.P., Niyogi, K.K. and Fleming, G.R. (2005) Carotenoid cation formation and the regulation of photosynthetic light harvesting. *Science*, **307**, 433–436.

Horton, P., Ruban, A.V. and Walters, R.G. (1996) Regulation of light harvesting in green plants. *Annu. Rev. Plant Physiol. Plant Mol. Biol.* **47**, 655–684.

Jarillo, J.A., Gabrys, H., Capel, J., Alonso, J.M., Ecker, J.R. and Cashmore, A.R. (2001) Phototropin-related NPL1 controls chloroplast relocation induced by blue light. *Nature*, **410**, 952–954.

Jensen, P.E., Gilpin, M., Knoetzel, J. and Scheller, H.V. (2000) The PSI-K subunit of photosystem I is involved in the interaction between light-harvesting complex I and the photosystem I reaction center core. *J. Biol. Chem.* **275**, 24701–24708.

Johnson, M.P. and Ruban, A.V. (2010) *Arabidopsis* plants lacking PsbS protein possess photoprotective energy dissipation. *Plant J.* **61**, 283–289.

Kagawa, T., Sakai, T., Suetsugu, N., Oikawa, K., Ishiguro, S., Kato, T., Tabata, S., Okada, K. and Wada, M. (2001) *Arabidopsis* NPL1: a phototropin homolog controlling the chloroplast high-light avoidance response. *Science*, **291**, 2138–2141.

Kasahara, M., Kagawa, T., Oikawa, K., Suetsugu, N., Miyao, M. and Wada, M. (2002) Chloroplast avoidance movement reduces photodamage in plants. *Nature*, **420**, 829–832.

Kong, S.G. and Wada, M. (2011) New insights into dynamic actin-based chloroplast photorelocation movement. *Mol. Plant*, **4**, 771–781.

Krause, G.H. (1988) Photoinhibition of photosynthesis. An evaluation of damaging and protective mechanisms. *Physiol. Plant.* **74**, 566–574.

Kulheim, C., Agren, J. and Jansson, S. (2002) Rapid regulation of light harvesting and plant fitness in the field. *Science*, **297**, 91–93.

Li, X.P., Bjorkman, O., Shih, C., Grossman, A.R., Rosenquist, M., Jansson, S. and Niyogi, K.K. (2000) A pigment-binding protein essential for regulation of photosynthetic light harvesting. *Nature*, **403**, 391–395.

Li, X.P., Muller-Moule, P., Gilmore, A.M. and Niyogi, K.K. (2002) PsbS-dependent enhancement of feedback de-excitation protects photosystem II from photoinhibition. *Proc. Natl Acad. Sci. USA*, **99**, 15222–15227.

Li, X.P., Gilmore, A.M., Caffarri, S., Bassi, R., Golan, T., Kramer, D. and Niyogi, K.K. (2004) Regulation of photosynthetic light harvesting involves intrathylakoid lumen pH sensing by the PsbS protein. *J. Biol. Chem.* **279**, 22866–22874.

Li, Z.R., Wakao, S., Fischer, B.B. and Niyogi, K.K. (2009) Sensing and responding to excess Light. *Annu. Rev. Plant Biol.* **60**, 239–260.

Malkin, S., Armond, P.A., Mooney, H.A. and Fork, D.C. (1981) Photosystem II photosynthetic unit sizes from fluorescence induction in leaves. Correlation to photosynthetic capacity. *Plant Physiol.* **67**, 570–579.

McClendon, J.H. and Fukshansky, L. (1990) On the interpretation of absorption spectra of leaves. II. The non-absorbed ray of the sieve effect and the mean optical pathlength in the remainder of the leaf. *Photochem. Photobiol.* **51**, 211–216.

Miloslavina, Y., Wehner, A., Lambrev, P.H., Wientjes, E., Reus, M., Garab, G., Croce, R. and Holzwarth, A.R. (2008) Far-red fluorescence: a direct spectroscopic marker for LHCII oligomer formation in non-photochemical quenching. *FEBS Lett.* **582**, 3625–3631.

Muller-Moule, P., Havaux, M. and Niyogi, K.K. (2003) Zeaxanthin deficiency enhances the high light sensitivity of an ascorbate-deficient mutant of *Arabidopsis*. *Plant Physiol.* **133**, 748–760.

Nilkens, M., Kress, E., Lambrev, P., Miloslavina, Y., Muller, M., Holzwarth, A.R. and Jahns, P. (2010) Identification of a slowly inducible zeaxanthin-dependent component of non-photochemical quenching of chlorophyll fluorescence generated under steady-state conditions in *Arabidopsis*. *Biochim. Biophys. Acta*, **1797**, 466–475.

Niyogi, K.K. (1999) Photoprotection revisited: genetic and molecular approaches. *Annu. Rev. Plant Physiol. Plant Mol. Biol.* **50**, 333–359.

Niyogi, K.K., Grossman, A.R. and Björkman, O. (1998) *Arabidopsis* mutants define a central role for the xanthophyll cycle in the regulation of photosynthetic energy conversion. *Plant Cell*, **10**, 1121–1134.

Peers, G., Truong, T.B., Ostendorf, E., Busch, A., Elrad, D., Grossman, A.R., Hippler, M. and Niyogi, K.K. (2009) An ancient light-harvesting protein is critical for the regulation of algal photosynthesis. *Nature*, **462**, 518–521.

Peter, G.F., Takeuchi, T. and Thornber, J.P. (1991) Solubilization and two-dimensional electrophoretic procedures for studying the

organization and composition of photosynthetic membrane polypeptides. *Methods*, **3**, 115–124.

Rappaport, F., Beal, D., Joliot, A. and Joliot, P. (2007) On the advantages of using green light to study fluorescence yield changes in leaves. *Biochim. Biophys. Acta*, **1767**, 56–65.

Rintamaki, E., Salonen, M., Suoranta, U.M., Carlberg, I., Andersson, B. and Aro, E.M. (1997) Phosphorylation of light-harvesting complex II and photosystem II core proteins shows different irradiance-dependent regulation *in vivo*. Application of phosphothreonine antibodies to analysis of thylakoid phosphoproteins. *J. Biol. Chem.* **272**, 30476–30482.

Ruban, A.V., Berera, R., Ilioaia, C., van Stokkum, I.H., Kennis, J.T., Pascal, A.A., Van Amerongen, H., Robert, B., Horton, P. and van Grondelle, R. (2007) Identification of a mechanism of photoprotective energy dissipation in higher plants. *Nature*, **450**, 575–578.

Sakai, T., Kagawa, T., Kasahara, M., Swartz, T.E., Christie, J.M., Briggs, W.R., Wada, M. and Okada, K. (2001) *Arabidopsis* nph1 and npl1: blue light receptors that mediate both phototropism and chloroplast relocation. *Proc. Natl Acad. Sci. USA*, **98**, 6969–6974.

Song, J.Y., Cho, H.S., Cho, J.I., Jeon, J.S., Lagarias, J.C. and Park, Y.I. (2011) Near-UV cyanobacteriochrome signaling system elicits negative phototaxis in the cyanobacterium Synechocystis sp PCC 6803. *Proc. Natl Acad. Sci. USA*, **108**, 10780–10785.

Suetsugu, N. and Wada, M. (2007) Chloroplast photorelocation movement mediated by phototropin family proteins in green plants. *Biol. Chem.* **388**, 927–935.

Sztatelman, O., Waloszek, A., Banas, A.K. and Gabrys, H. (2010) Photoprotective function of chloroplast avoidance movement: *in vivo* chlorophyll fluorescence study. *J. Plant Physiol.* **167**, 709–716.

Takahashi, S. and Murata, N. (2008) How do environmental stresses accelerate photoinhibition? *Trends Plant Sci.* **13**, 178–182.

Towbin, H., Staehelin, T. and Gordon, J. (1979) Electrophoretic transfer of proteins from polyacrylamide gels to nitrocellulose sheets: procedure and some applications. *Proc. Natl Acad. Sci. USA*, **76**, 4350–4354.

Triantaphylides, C. and Havaux, M. (2009) Singlet oxygen in plants: production, detoxification and signaling. *Trends Plant Sci.* **14**, 219–228.

Trippens, J., Greiner, A., Schellwat, J., Neukam, M., Rottmann, T., Lu, Y.H., Kateriya, S., Hegemann, P. and Kreimer, G. (2012) Phototropin influence on eyespot development and regulation of phototactic behavior in *Chlamydomonas reinhardtii*. *Plant Cell*, **24**, 4687–4702.

Van Kooten, O. and Snel, J.F.H. (1990) The use of chlorophyll fluorescence nomenclature in plant stress physiology. *Photosynth. Res.* **25**, 147–150.

Wada, M. and Kong, S.G. (2011) Analysis of chloroplast movement and relocation in *Arabidopsis*. *Methods Mol. Biol.* **774**, 87–102.

Wada, M., Kagawa, T. and Sato, Y. (2003) Chloroplast movement. *Annu. Rev. Plant Biol.* **54**, 455–468.

Wakabayashi, K., Misawa, Y., Mochiji, S. and Kamiya, R. (2011) Reduction-oxidation poise regulates the sign of phototaxis in *Chlamydomonas reinhardtii*. *Proc. Natl Acad. Sci. USA*, **108**, 11280–11284.

Walters, R.G. and Horton, P. (1991) Resolution of components of non-photochemical chlorophyll fluorescence quenching in barley leaves. *Photosynth. Res.* **27**, 121–133.

Walters, R.G. and Horton, P. (1995) Acclimation of *Arabidopsis thaliana* to the light environment: changes in photosynthetic function. *Planta*, **197**, 306–312.

Yamamoto, H.Y. and Kamite, L. (1972) The effects of dithiothreitol on violaxanthin deepoxidation and absorbance changes in the 500 nm region. *Biochim. Biophys. Acta*, **267**, 538–543.

Figure S1

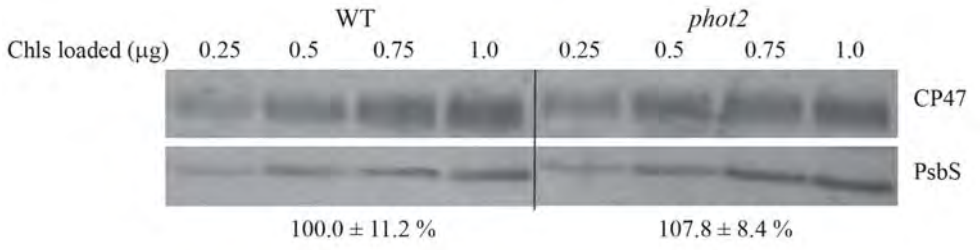

Figure S1. Immunotitration of PsbS subunit in WT and *phot2* thylakoids. Amounts of Chls loaded on the gel for each genotype were 0.1, 0.25, 0.5 and 1.0 µg. Amount of PsbS subunit was normalized to the CP47 content, and expressed as a percentage of the corresponding wild-type value. PsbS content in *phot2* thylakoids is not significantly different (Student's *t* test, $P < 0.05$) with respect to the WT.

Figure S2

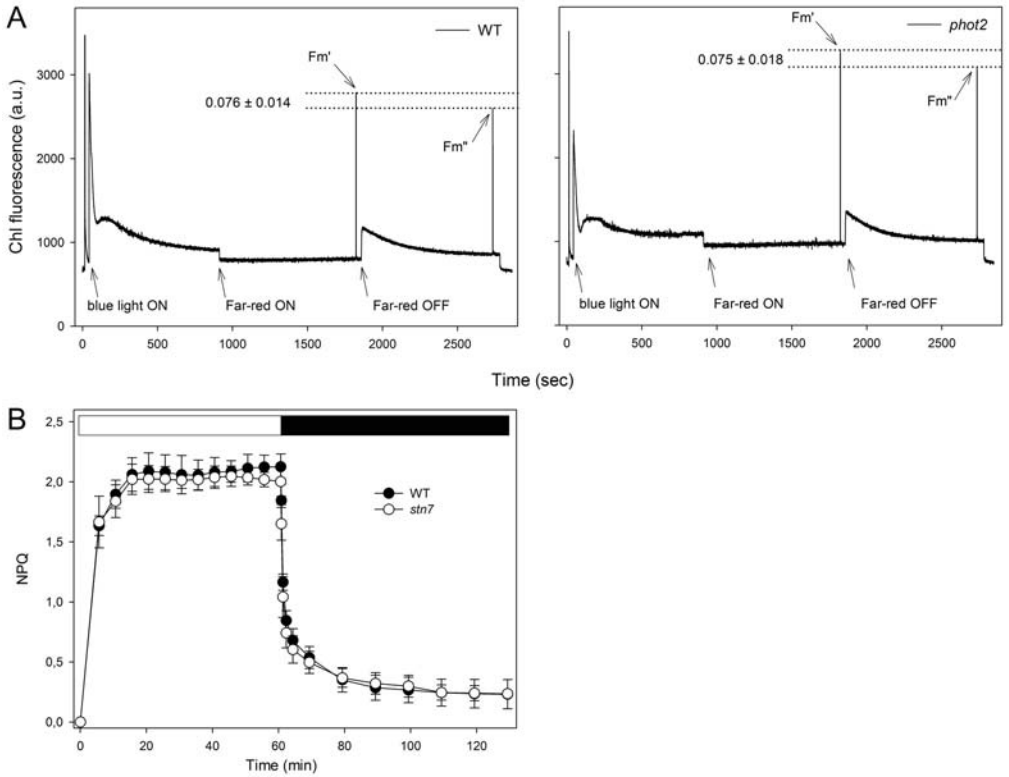

Figure S2. Measurement of state I–state II transition in the WT and *phot2*. (A) Upon 1 hour dark adaptation, plants were illuminated with blue light (60 µmol photons m^{-2} s^{-1}, λ < 500 nm) for 15 min to reach state II. A far-red light source was then superimposed on the blue light to induce a transition to state I. Values of F_m and F_m'/F_m" (where F_m'/F_m" are the maximal fluorescence yield in state I/II) were determined using light saturation pulses (4500 µmol photons m^{-2} s^{-1}, 0.6 s). The amplitude of state transition was evaluated by calculating the parameter qT (PSII cross-section changes) defined as (F_m'-F_m")/F_m'. a.u., arbitrary units. Statistical analysis (Student's *t* test, P < 0.05) did not revealed significant difference in qT values between WT and *phot2*. The ~15% lower values of F_m' and F_m" in WT *vs. phot2* reflect a quenching component induce by blue light and correlated to chloroplast photorelocation. (B) NPQ kinetics upon transition from the dark to EL (400 µmol photons m^{-2} s^{-1}, white actinic light) and subsequent relaxation in the dark, of WT and mutants *stn7*, devoid of the STN7 protein kinase responsible for state transitions.

Figure S3

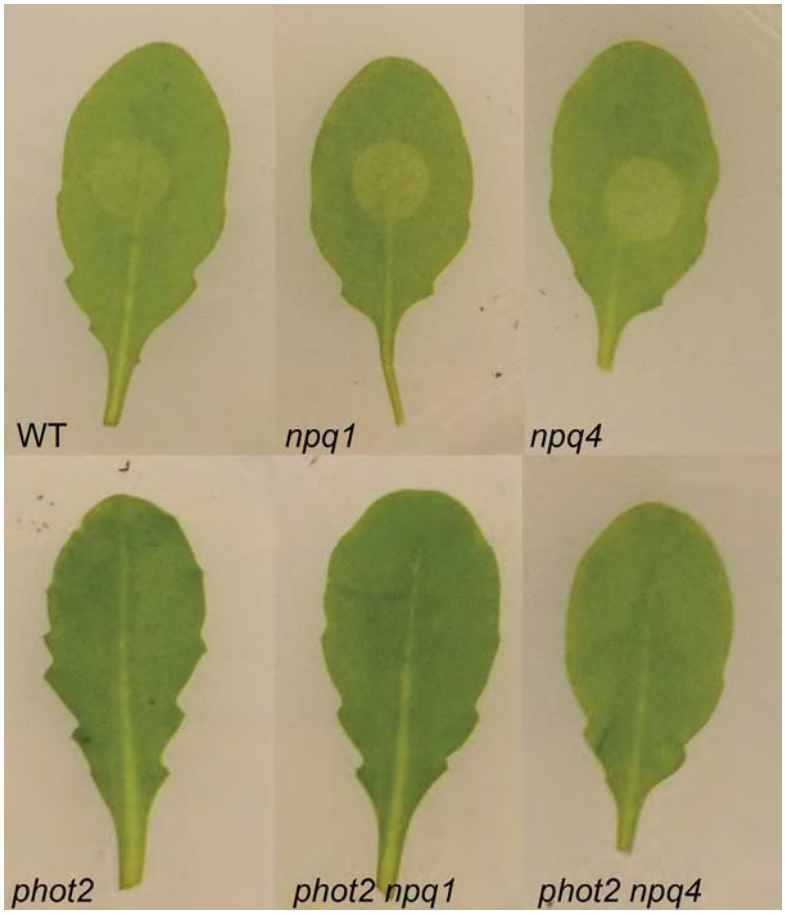

Figure S3. Screening for chloroplast avoidance mutants. Leaves of WT, *npq* and *phot2* mutants after partial irradiation with strong white light (1500 μmol photons m^{-2} s^{-1}, 8°C). Leaves were covered with a black plate with open hole were irradiated through the slits with strong cool white light for 3 hours. The irradiated area of the WT, *npq1* and *npq4* leaves changed from dark green to pale green, while in *phot2* leaves the area irradiated was indistinguishable from the rest of the blade. Individual mutants were crossed, and the same procedure of screening was used to isolate double mutants *phot2npq1* and *phot2npq4* in the F2 populations.

Figure S4

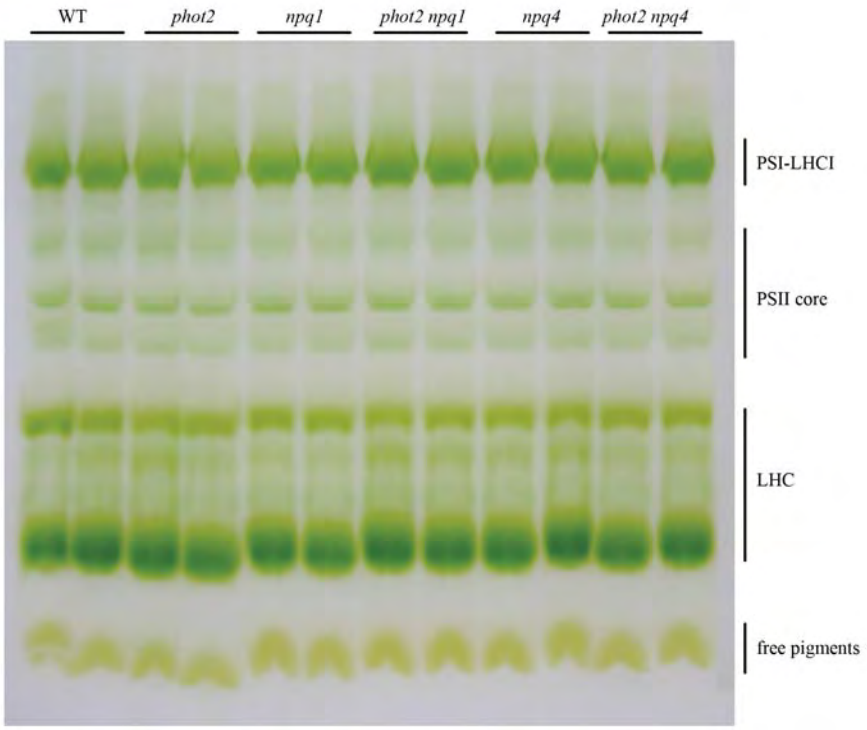

Figure S4. Analysis of pigment-protein complexes of the WT and mutants. Thylakoid pigment-protein complexes were separated by nondenaturing Deriphat-PAGE upon solubilization with 0.8% β-dodecyl-maltoside. Thylakoids corresponding to 25 µg of Chls were loaded in each lane. Composition of each band is indicated.

Figure S5

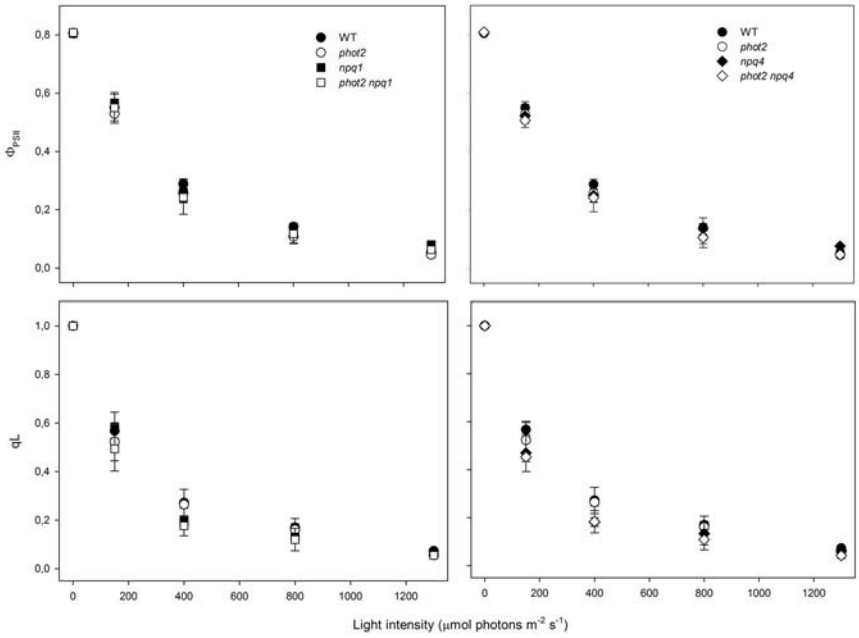

Figure S5. Analysis of room temperature Chl fluorescence during photosynthesis in WT, *npq* and *phot2* plants. (A,B) PSII operating efficiency (Φ_{PSII}) and (C,D) Q_A redox state (qL) were measured at different light intensities. Data are expressed as means ± SD (n=4). In both double mutants, values at each light intensity are not significantly different (Student's *t* test, $P < 0.05$) with respect to the corresponding *npq* control genotype.

Figure S6

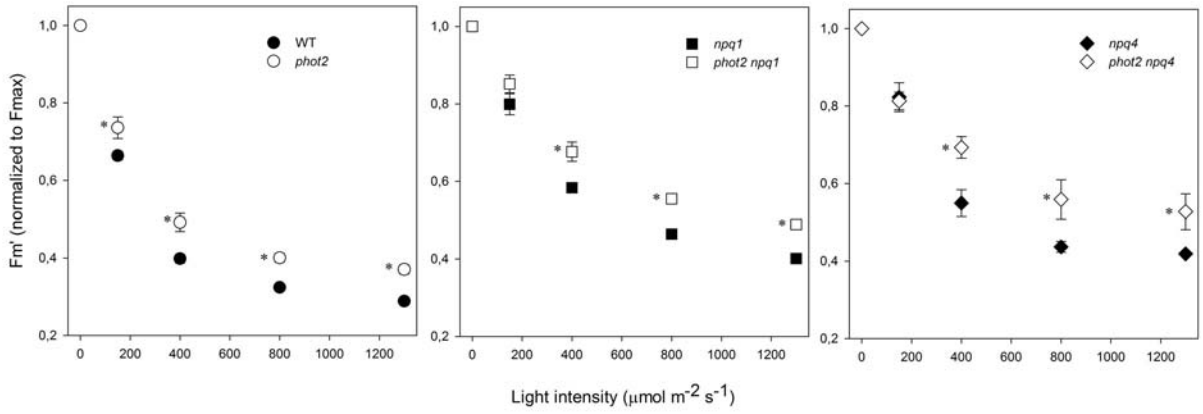

Figure S6. Analysis of F_m' during photosynthesis in WT, *npq* and *phot2* plants. F_m' values were measured on WT and mutant leaves upon illumination with white actinic light (150-1300 µmol photons m^{-2} s^{-1}, 22 °C, 30 min) and plotted upon normalization to the corresponding F_m values. Data are expressed as means ± SD (n=4). Values that are significantly different (Student's *t* test, $P < 0.05$) from the corresponding control genotype are marked with an asterisk (*).

Figure S7

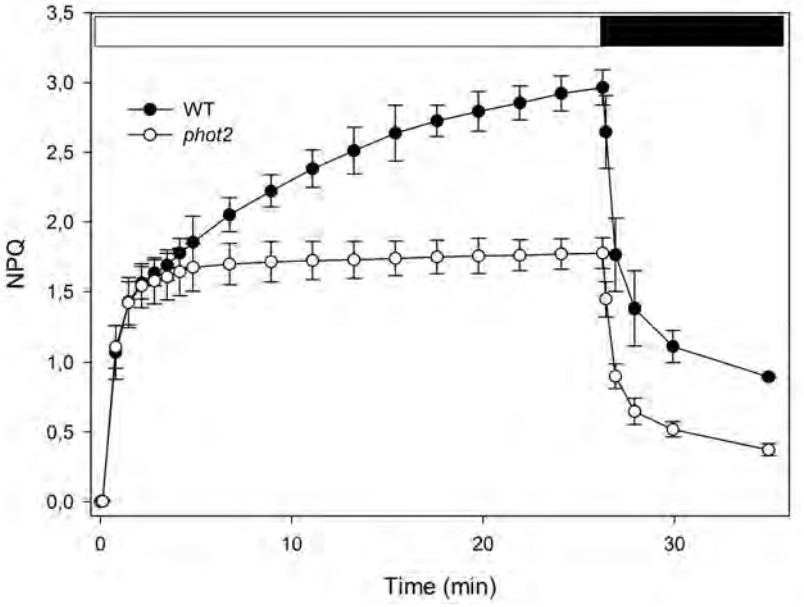

Figure S7. Kinetics of formation and relaxation of NPQ in WT and *phot2* leaves. Measurements of NPQ kinetics were performed on wild-type and *phot2* leaves, illuminated with 1200 µmol photons m^{-2} s^{-1} of white light, at 22°C.

C2. On the origin of a slowly reversible fluorescence decay component in the *Arabidopsis thaliana npq4* mutant.

PHILOSOPHICAL TRANSACTIONS OF THE ROYAL SOCIETY B

rstb.royalsocietypublishing.org

Research

Cite this article: Dall'Osto L, Cazzaniga S, Wada M, Bassi R. 2014 On the origin of a slowly reversible fluorescence decay component in the *Arabidopsis npq4* mutant. *Phil. Trans. R. Soc. B* **369**: 20130221.
http://dx.doi.org/10.1098/rstb.2013.0221

One contribution of 20 to a Theme Issue 'Changing the light environment: chloroplast signalling and response mechanisms'.

Subject Areas:
plant science, biophysics

Keywords:
energy dissipation, non-photochemical quenching, Lhcb, xanthophyll, photosynthesis, chloroplast avoidance

Author for correspondence:
Roberto Bassi
e-mail: roberto.bassi@univr.it

†These authors contributed equally to this study.

Electronic supplementary material is available at http://dx.doi.org/10.1098/rstb.2013.0221 or via http://rstb.royalsocietypublishing.org.

Royal Society Publishing

On the origin of a slowly reversible fluorescence decay component in the *Arabidopsis npq4* mutant

Luca Dall'Osto[1,†], Stefano Cazzaniga[1,†], Masamitsu Wada[2] and Roberto Bassi[1]

[1]Dipartimento di Biotecnologie, Università di Verona, Verona 37134, Italy
[2]Department of Biology, Kyushu University, Hakozaki 6-10-1, Fukuoka 812-8581, Japan

Over-excitation of photosynthetic apparatus causing photoinhibition is counteracted by non-photochemical quenching (NPQ) of chlorophyll fluorescence, dissipating excess absorbed energy into heat. The PsbS protein plays a key role in this process, thus making the PsbS-less *npq4* mutant unable to carry out qE, the major and most rapid component of NPQ. It was proposed that *npq4* does perform qE-type quenching, although at lower rate than WT *Arabidopsis*. Here, we investigated the kinetics of NPQ in PsbS-depleted mutants of *Arabidopsis*. We show that red light was less effective than white light in decreasing maximal fluorescence in *npq4* mutants. Also, the kinetics of fluorescence dark recovery included a decay component, qM, exhibiting the same amplitude and half-life in both WT and *npq4* mutants. This component was uncoupler-sensitive and unaffected by photosystem II repair or mitochondrial ATP synthesis inhibitors. Targeted reverse genetic analysis showed that traits affecting composition of the photosynthetic apparatus, carotenoid biosynthesis and state transitions did not affect qM. This was depleted in the *npq4phot2* mutant which is impaired in chloroplast photorelocation, implying that fluorescence decay, previously described as a quenching component in *npq4* is, in fact, the result of decreased photon absorption caused by chloroplast relocation rather than a change in the activity of quenching reactions.

1. Introduction

Plants use light as an energy source for their metabolism: solar energy is absorbed, and excitons rapidly transferred to the photosynthetic reaction centres by the light-harvesting complexes (LHC) of each photosystem (PS). These bind a large array of chlorophylls (Chls) that are tightly connected to yield more than 80% quantum efficiency of photochemical reactions [1]. Under stable light conditions, plants optimize the efficiency of photosynthetic machinery and yet light intensity changes during the day and the rapid fluctuations imposed by shading in the canopy or by clouds, easily result in over-excitation. Thus, quantum efficiency needs to be rapidly downregulated to decrease the probability of Chl *a* triplet (^{3}Chl*) and singlet oxygen formation [2,3]. This is performed by photoprotection mechanisms including leaf and chloroplast avoidance movement, reactive oxygen species (ROS) scavenging, and quenching of triplet and singlet Chl excited states [4–6]. The ability of plants to modulate light utilization efficiency in fluctuating light is crucial for plant fitness [7]. A major role for prevention of over-excitation is played by a set of inducible mechanisms referred to as non-photochemical quenching (NPQ) [8] that are triggered by a feedback loop in which excess light (EL) induces lumenal acidification, detected by the thylakoid protein PsbS, which in turn triggers qE, the most rapid component of NPQ, leading to dissipation of excess energy with a half-life of 1–2 min [5,9]. As PsbS is not a Chl-binding protein [10], its effect on Chl fluorescence must be achieved through interaction with the antenna system binding the xanthophylls zeaxanthin (Zea) and lutein (Lut) [11], in the absence of which quenching does not occur [12].

Besides qE, NPQ includes a slowly relaxing component ($\tau > 60$ min) qI, which is independent of lumenal pH and has been attributed to inactive PSII

centres produced by EL stress [13]. Additional quenching components with intermediate half-lives ($\tau = 10–15$ min) were originally attributed to state 1–state 2 transitions [8], and more recently to Zea binding to the LHC proteins, hence the names qT or qZ [14,15].

Two types of mechanism have been proposed for activation of quenching by PsbS: the first proposes a direct interaction of PsbS with a neighbour antenna protein, either LHCII or a monomeric complex, which causes a conformational change activating quenching site(s) within the antenna subunit itself [16,17] or through the trapping of a Zea molecule at the PsbS–LHCII interface [11]. The first type of mechanism relies on the notion that LHC proteins exist in two conformations with different fluorescence lifetimes [18], whose interconversion is controlled by changes in protein–protein interactions in the membrane, which are promoted by activation of PsbS [19,20]. The recent report that *npq4* plants lacking PsbS are competent in quenching, although longer exposure to EL is required than in WT plants [21], supports the first hypothesis.

In this work, we have studied the properties of light-induced fluorescence decrease in the *npq4* mutant, which develops a slow fluorescence decay. A component, qM, with the same amplitude and half-life, could also be deconvoluted from the kinetics of WT plants, was uncoupler-sensitive and unaffected by treatments inhibiting PSII repair or mitochondrial ATP production. Also it was induced by white light but not by red light. A targeted reverse genetic analysis showed that the *npq4phot2* double mutant which was impaired in chloroplast avoidance, was devoid of qM. On this basis, we propose that the fluorescence decay previously described as a quenching component in *npq4* is, in fact, the result of decreased photon absorption caused by chloroplast relocation rather than by a change in the activity of quenching reactions. This finding supports a direct role of PsbS in triggering the quenching reactions.

2. Experimental procedures

(a) Plant material

Arabidopsis thaliana T-DNA insertion mutants (Col-0) *npq1* (At1G08550) and *npq2* (At5G67030) were a kind gift of K.K. Niyogi (University of California at Berkeley). Mutant *lut2* (At5G57030) was obtained from the NASC collection, Salk line 005018. *koLhcb4*, *koLhcb5* and *koLhcb6* were obtained as described in [22,23]. Mutants *npq4* and *npq4ch1* were a kind gift of K. K. Niyogi, *stn7npq4* was provided by E.-M. Aro (University of Turku, Finland), and *phot2* by M. Wada (Kyushu University, Japan). Double mutants were obtained by crossing single mutant plants and selecting progeny either by pigment analysis, western blotting [22,23] or by the light-induced change in the green colour of leaf blades [24]. WT and mutant plants were grown on compost in a growth chamber for five weeks under controlled conditions (150 µmol photons $m^{-2}\,s^{-1}$, 23°C, 8 L/16 D cycle, 70% relative humidity).

(b) *In vivo* fluorescence and non-photochemical quenching measurements

NPQ of Chl fluorescence was measured on leaves at room temperature (RT; 23°C) with a PAM 101 fluorometer (Walz, Germany). NPQ was calculated according to Van Kooten & Snel [25]. When red actinic light was used, the light intensities for these experiments were chosen in order to produce the same value of qL in all genotypes. When indicated, fluorescence was measured on detached leaves infiltrated with 150 mM sorbitol containing either 50 µM nigericin [26], 100 µM lincomycin [27] or 2 µM myxothiazol [28].

(c) Pigment analysis

Pigments were extracted from leaf discs using 85% acetone buffered with Na_2CO_3. Separation and quantification of pigments were performed by HPLC [29].

(d) Measurement of chloroplast movement

Chloroplast avoidance response was induced in leaves by EL treatment. Before measurements, plants were adapted in darkness for 1 h, then detached leaves on wet paper were exposed to 400 µmol photons $m^{-2}\,s^{-1}$, white light at RT for 1 h. Distribution of chloroplasts in the mesophyll cells was determined by light microscopy. To take micrographs, we introduced the solution (150 mM sorbitol ± inhibitors) into intracellular spaces under weak negative pressure before EL treatment, and removed the upper epidermis from the leaves just before mounting the microscope slide.

3. Results

(a) Kinetics of non-photochemical quenching induction and relaxation in *npq4* versus wild-type leaves

Plants lacking PsbS are completely devoid of the fast quenching phase qE when illuminated for 8 min at 1200 µmol photons $m^{-2}\,s^{-1}$ (see electronic supplementary material, figure S1*a*), consistent with literature data [30]; the fluorescence quenching reached a maximum value four times lower than in WT plants. Dark relaxation of fluorescence quenching was clearly different between genotypes: *npq4* showed almost no relaxation, while WT recovered the most fluorescence quenching. Upon exposure to longer periods of actinic light, the quenching behaviour of *npq4* mutants showed a relative increase, reaching an NPQ value of 1.9, thus 45% with respect to WT plants (see electronic supplementary material, figure S1*b*). A major change was observed in the fluorescence recovery of *npq4* mutants in the dark, which showed a higher rate, although still slower than in WT plants. Thus, although the rapidly relaxing phase of the dominant qE component was missing in *npq4* mutants, a slowly reversible phase contributed to relaxation recovery, not only in WT plants but also in *npq4* mutants. Yet, the dark recovery was slower than in WT plants, yielding a higher qI.

The amplitude and kinetics of NPQ induction and relaxation were previously shown to be related to the activity of the xanthophyll cycle in EL [31]. We thus determined for Zea the extent of both EL-formation and dark-reconversion under the same experimental condition used to follow NPQ kinetics. Results in table S1 available in the electronic supplementary material show that the Zea content was the same in WT and *npq4* leaves for each condition. Both genotypes retained approximately 50% of the Zea produced upon in EL, upon 1 h dark recovery.

The NPQ kinetics of WT and *npq4* leaves were measured at different actinic intensities (figure 1*a–c*), showing similar behaviour of *npq4* leaves at all the light intensities used, including the rise in the light to half the amplitude of the WT leaves followed by a slow dark recovery.

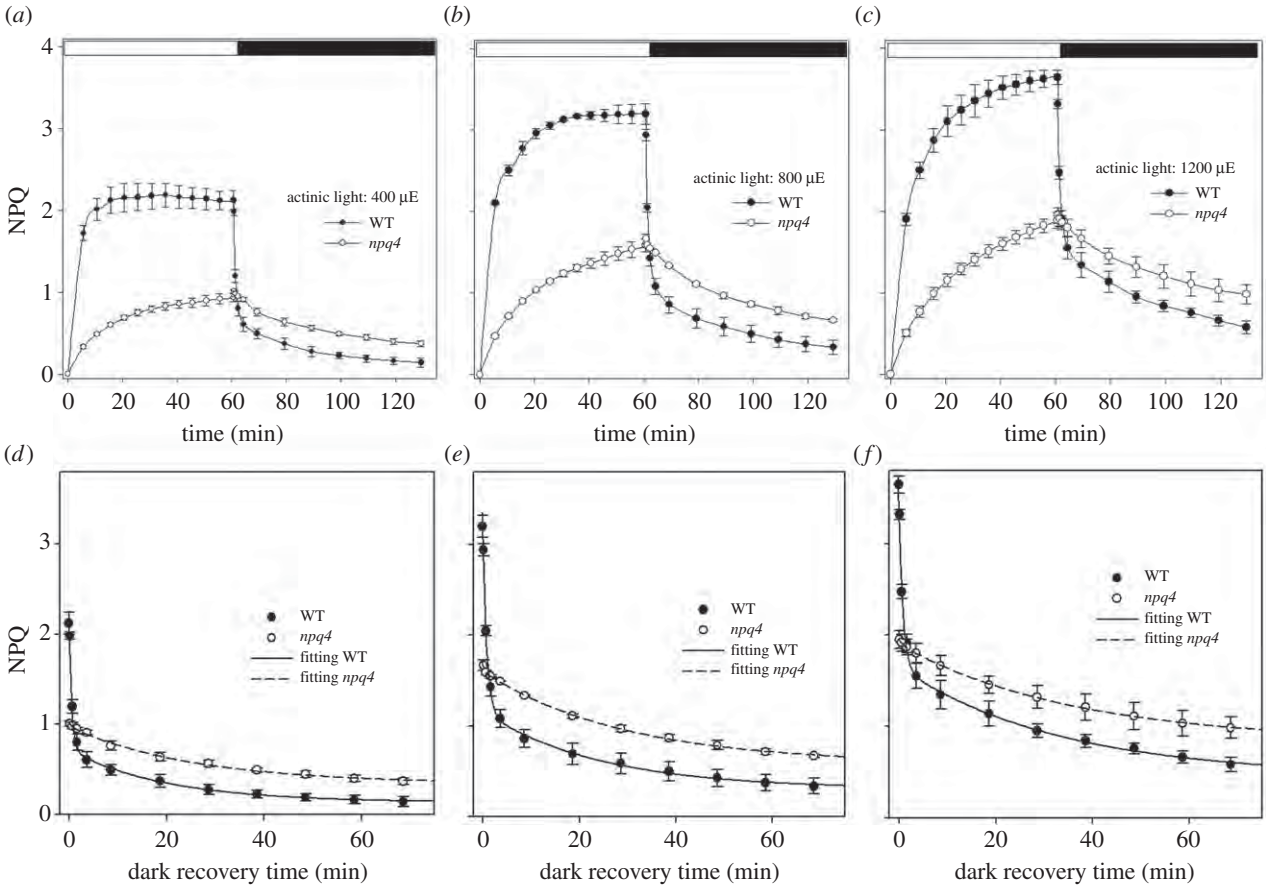

Figure 1. Kinetic deconvolution of NPQ dark relaxation of WT and *npq4* leaves. The dark recovery of NPQ was measured in intact leaves of *Arabidopsis* WT and *npq4* mutants upon illumination for 60 min with different intensities of white actinic light: (*a*) 400, (*b*) 800, (*c*) 1200 µmol photons m^{-2} s^{-1}. Symbols and error bars show mean ± s.d. ($n = 3$). Each dataset was fitted with a bi-exponential function $NPQ = A_{ql} + A_{qE}\, e^{(-t/\tau qE)} + A_{qM}\, e^{(-t/\tau qM)}$ (*d*–*f*) and the kinetics of qE and qM relaxation were assessed in the different genotypes (table 1).

Table 1. Kinetics of NPQ dark relaxation in WT and *npq4* leaves. The dark-recovery of NPQ was measured in intact leaves of *Arabidopsis* WT and *npq4* mutants upon 60 min illumination with different actinic intensities (400, 800 and 1200 µmol photons m^{-2} s^{-1}, white light, RT). Each dataset was fitted with a bi-exponential function $NPQ = A_{ql} + A_{qE}\, e^{(-t/\tau qE)} + A_{qM}\, e^{(-t/\tau qM)}$ and the kinetics of qE and qM relaxation were assessed in the different genotypes by comparing amplitudes of parameter A, which describes the slope of exponential functions. Significantly different values (Student's *t*-test) with respect to WT are marked with asterisks.

actinic intensity (µmol photons m^{-2} s^{-1})	genotype	τ_{qE} (min)	A_{qE}	τ_{qM} (min)	A_{qM}	A_{ql}
400	WT	0.56 ± 0.02	1.26 ± 0.05	19.9 ± 4.4	0.58 ± 0.04	0.14 ± 0.13
	npq4	—	—	25.7 ± 3.9	0.63 ± 0.03	0.39 ± 0.07*
800	WT	0.83 ± 0.04	1.73 ± 0.08	24.3 ± 6.8	0.85 ± 0.07	0.33 ± 0.09
	npq4			29.3 ± 2.2	1.02 ± 0.03*	0.67 ± 0.02*
1200	WT	0.81 ± 0.04	1.65 ± 0.08	33.3 ± 8.4	1.20 ± 0.10	0.58 ± 0.08
	npq4			35.8 ± 12.8	1.07 ± 0.13	1.01 ± 0.13*

The kinetic analysis of NPQ dark relaxation is frequently used as a tool for the characterization of quenching dynamics [15,32]. Thus, NPQ relaxation kinetics (figure 1*d*–*f*) were fitted with a bi-exponential decay function: $NPQ = A_1\, e^{(-t/\tau 1)} + A_2\, e^{(-t/\tau 2)} + A_3$. In WT plants, a fast decay component (τ_1, half-life of 35–50 s) represented the dominant component of NPQ under all light conditions (around 60% of total quenching), and could reasonably be attributed to qE. The residual quenching at the end of dark recovery (A_3) was due to processes that were essentially irreversible within the time range of the experiment ($\tau > 60$ min), fitting with the characteristics of the photo-inhibitory quenching, qI [33]. In *npq4* plants, the kinetics of NPQ relaxation were slowed down with respect to WT plants: a satisfactory fitting of NPQ dark relaxation could only be obtained with the introduction of an intermediate component with a decay rate intermediate between those of qE and qI (τ_2, half-life of 20–35 min). This component also improved the fitting of WT curves where it contributes to about 30% of total NPQ (figure 1*d*–*f* and table 1). From now on this component will be referred to as qM. The rapid (qE) kinetic component was missing in *npq4* mutants under all experimental conditions explored in this work. According to the

Table 2. Kinetics of qM dark relaxation in *npq4* leaves. The kinetic components qM and qI were deconvolved from dark recovery of NPQ in *npq4* leaves. Dark-adapted leaves were exposed to white actinic light for 60 min at 400 μmol photons m^{-2} s^{-1}, RT, following 60 min of dark recovery. (upper section) Before NPQ induction, leaves were vacuum-infiltrated with 150 mM sorbitol and either 50 μM nigericin (uncoupler, collapsed the ΔpH across the thylakoid membranes), 2 μM myxothiazol (respiratory chain inhibitor) or 100 μM lincomycin (chloroplast protein biosynthesis inhibitor). (middle section) The kinetic components qM and qI were measured in *npq4* double mutants lacking zeaxanthin (*npq4npq1*) or lacking lutein (*npq4lut2*). (lower section) Components qM and qI were measured in *npq4* double mutants depleted of Lhcb subunits CP26 and CP24 (*npq4koLhcb5/6*), CP29 and CP24 (*npq4koLhcb4/6*), lack the entire LHC (*npq4ch1*), or unable to activate state transition (*npq4stn7*) or chloroplast avoidance movement (*npq4phot2*). Each dataset was fitted with an exponential function $NPQ = A_{qI} + A_{qM}\ e^{(-t/\tau qM)}$ and the kinetics of qM relaxation were assessed in the different samples by comparing amplitudes of parameters A. Significantly different values (Student's *t*-test) with respect to WT are marked with asterisks.

	τ_{qM} (min)	A_{qM}	A_{qI}
npq4	28.4 ± 4.5	0.63 ± 0.03	0.35 ± 0.03
npq4 + nigericin	—	—	0.90 ± 0.03*
npq4 + myxothiazol	34.7 ± 13.9	0.52 ± 0.08	0.40 ± 0.09
npq4 + lincomycin	37.3 ± 6.3	0.58 ± 0.04	0.39 ± 0.04
npq4npq1	15.7 ± 1.3*	0.56 ± 0.02	0.34 ± 0.01
npq4lut2	27.7 ± 3.1	0.80 ± 0.03*	0.33 ± 0.03
npq4koLhcb5/6	22.8 ± 3.4	0.49 ± 0.03	0.28 ± 0.03
npq4koLhcb4/6	20.7 ± 3.5	0.49 ± 0.03	0.29 ± 0.03
npq4ch1	14.3 ± 1.2*	0.71 ± 0.03*	0.11 ± 0.03*
npq4stn7	14.2 ± 1.9*	0.55 ± 0.04	0.37 ± 0.06
npq4phot2	15.3 ± 5.8*	0.28 ± 0.05*	0.27 ± 0.09*

former attributions, exponential parameters used for fitting of NPQ dark relaxation will be hereafter called A_{qE} and τ_{qE} (qE amplitude and half-life, respectively), A_{qM} and τ_{qM} (qM amplitude and half-life), A_{qI} (qI amplitude).

Interestingly, the amplitude and half-life of the intermediate phase qM did not significantly differ between WT and *npq4* plants at 400 and 1200 μmol photons m^{-2} s^{-1}, while A_{qM} was only slightly higher in *npq4* than WT plants at 800 μmol photons m^{-2} s^{-1} (table 1); therefore, these data suggest that the component qM accounts for a fluorescence decay process, common to WT and *npq4* plants, activated upon prolonged illumination and distinct from qE and qI.

Increasing the actinic light intensity caused a linear increase of the slowly relaxing component qI (A_{qI}, table 1), that can reasonably be attributed to PSII photoinhibitory processes in both genotypes. In *npq4*, the parameter F_v/F_m (PSII maximal quantum efficiencies) reached lower values than WT upon illumination at intensities higher than 400 μmol photons m^{-2} s^{-1} (table S2 in the electronic supplementary material), thus showing that induction of PSII damage is more pronounced in *npq4* plants. However, the extent of PSII photoinhibition at 400 μmol photons m^{-2} s^{-1} was nearly identical to WT, which indicates that this light treatment did not cause differential PSII damage in the two genotypes; moreover, qM amplitude and kinetics were similar in WT and *npq4* plants using this light regime (table 1), thus showing that the middle decay phase is not influenced by qE and is not related to PSII photoinhibition. Therefore, the molecular basis of the component qM was further investigated under the optimal NPQ induction conditions of 400 μmol photons m^{-2} s^{-1}, 60 min.

(b) Effect of ΔpH and D1 turnover on qM

Build-up of trans-thylakoid ΔpH is the key event that triggers NPQ; indeed, ΔpH collapses upon treatment with the ionophore nigericin and the activation of thermal energy dissipation is prevented. *Npq4* leaves vacuum-infiltrated with the ionophore still maintained a rise of NPQ in the light, whose amplitude was comparable to that of untreated *npq4* leaves (figure 2*a*); nevertheless, NPQ relaxation in the dark was missing, thus suggesting that the quenching was mainly because of photoinhibition of PSII reaction centres (table 2). A recent report [34] suggested that the slow phase of NPQ relaxation in the dark would reflect the consumption of ATP accumulated in the light phase. To test this possibility, amplitude and kinetics of qM in *npq4* leaves were measured upon inhibition of the respiratory chain with myxothiazol: upon this treatment, cytoplasm is depleted in ATP in the dark, therefore acting as a sink for chloroplastic ATP, and accelerating NPQ relaxation [34]. However, myxothiazol treatment did not affect either qM amplitude or its half-life (figure 2*b* and table 2), thus indicating that the middle phase of NPQ decay was not related to slow ΔpH relaxation.

We further tested the possibility that turnover of D1 could account for qM; thus NPQ kinetics were measured on *npq4* leaves upon treatment with lincomycin, a plastid protein synthesis inhibitor. Results (figure 2*c* and table 2) show that lincomycin treatments failed to affect NPQ rise and decay in *npq4* leaves, indicating that turnover of the PSII reaction centre did not significantly contribute to qM.

To further investigate the molecular basis of qM, we used a targeted reverse genetic approach: we constructed a series of double and triple mutants combining *npq4* with mutations affecting mechanisms that are known to influence Chl fluorescence yield *in vivo*.

(c) Role of xanthophyll composition

Induction and relaxation of NPQ were measured on *Arabidopsis npq4* mutants with altered xanthophyll composition (figure 3).

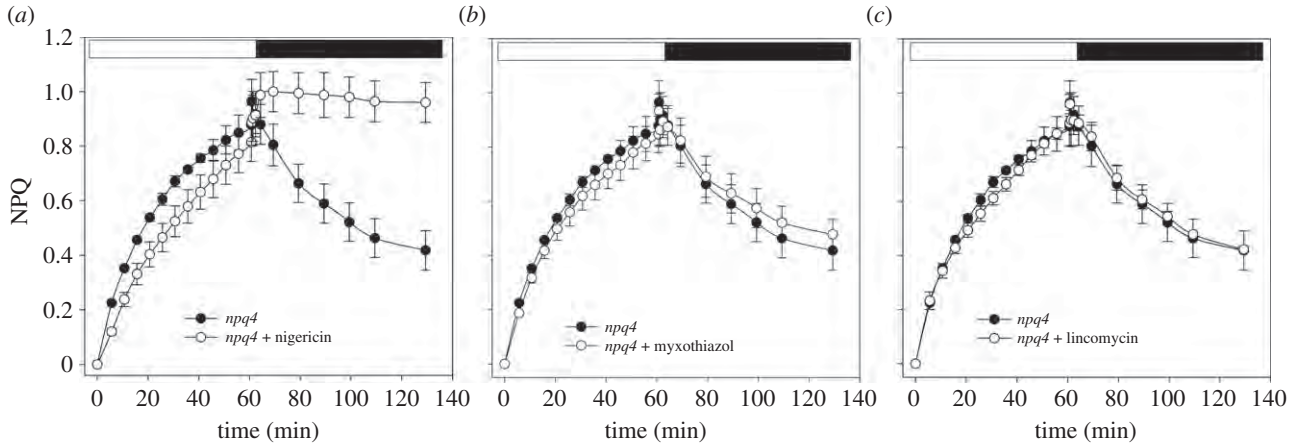

Figure 2. NPQ analysis of *npq4* leaves upon inhibition of trans-thylakoid ΔpH, PSII repair mechanism or mitochondrial ATP production. Kinetics of NPQ induction and relaxation were measured in dark-adapted leaves, upon 60 min illumination at 400 µmol photons m^{-2} s^{-1}, followed by a further 60 min of dark relaxation, in the absence or presence of 50 µM nigericin (*a*), 2 µM myxothiazol (*b*) or 100 µM lincomycin (*c*). Symbols and error bars show mean ± s.d. ($n = 3$).

The *npq1* mutant lacks violaxanthin de-epoxidase activity and is thus unable to convert Viola into Zea; qE in *npq1* has approximately 40% amplitude with respect to WT [12], showing that Zea synthesis is needed for full expression of qE. A comparison of quenching dynamics showed that qM kinetics are very similar in *npq4* and *npq4npq1* plants (figure 3*a*): although *npq4* showed a somewhat more rapid NPQ rise within the first minutes of illumination, prolonged treatment lead to overlapping amplitude in both genotypes (table 2); likewise, *npq4npq1* plants showed a dark recovery which was initially faster than in *npq4*, while the extent of reversible NPQ was similar in the two genotypes at the end of dark period. The half-life of fluorescence dark recovery is lower in *npq4npq1* than in *npq4*, suggesting that residual Zea in the dark could account for the different kinetics in dark recovery.

Long-term NPQ measurements were performed on *lut2*, an *Arabidopsis* mutant devoid of lutein (figure 3*b*). Lut, together with Zea, affects quenching dynamics by modulating qE [35]. Prolonged illumination leads to overlapping NPQ traces in *npq4* and *npq4lut2*, and qM half-life and amplitude were very similar in both genotypes (table 2), implying that qM is not affected by Lut depletion. In conclusion, the analysis of NPQ dark relaxation kinetics in *npq4* double mutants indicates that qM dynamics were only slightly affected, if at all, by mutations in xanthophyll composition.

(d) Role of light-harvesting complexes and state 1–state 2 transitions

As NPQ depends on the antenna proteins [14,22,23,36], we evaluated the capacity of *npq4* mutants, devoid of specific LHC gene products, to modulate qM.

In mutants devoid of both Lhcb5 and Lhcb6 subunits (figure 3*c* and table 2), the amplitude and relaxation of NPQ were essentially the same as observed in *npq4* mutants. Similar results were obtained upon removal of both Lhcb4 and Lhcb6 (figure 3*d* and table 2), thus ruling out the possibility that minor antennae modulate qM amplitude and kinetics. These data are consistent with the behaviour of *npq4ch1* that lacks Chl*b*, and is thus devoid of all LHCs [37,38]; the slow phase of NPQ relaxation was found to be independent of LHC composition, indeed qM amplitude was similar in *npq4* and *npq4ch1* mutants (figure 3*e* and table 2). State transitions lead to quenching of LHCII fluorescence by PSI [39] upon phosphorylation of LHCII, by STN7 kinase, driving its migration from PSII to PSI [40]; by using the mutant *npq4stn7*, we checked the possibility that state transition were involved in qM. The maximal amplitude of NPQ in *npq4stn7* was essentially the same as in *npq4* plants (figure 3*f*). The only difference was found in the kinetics of qM dark-recovery, which was faster in the double mutant than in the *npq4* mutant (τ about 15 min in *npq4stn7* versus 29 min in *npq4*; table 2).

(e) Role of chloroplast photorelocation

Previous reports showed that light-induced chloroplast movements could affect Chl fluorescence emission [41,42]. We thus determined the qM relaxation kinetics in a double mutant *npq4phot2*, lacking the phototropin PHOT2 which activates the blue-light-dependent chloroplast avoidance movement [24].

Although two different components of NPQ dark-relaxation (qM and qI) were still detected in *npq4phot2*, the kinetics of the qM component were faster than in *npq4* (figure 4*a* and table 2), and the amplitude of the middle phase was decreased by 50% compared with *npq4*.

To further verify the hypothesis that phototropins were involved in the modulation of qM, we repeated NPQ measurements by using red light ($600 < \lambda < 750$ nm, 350 µmol photons m^{-2} s^{-1}, 23°C) as actinic source. Results are shown in figure 4*b*: both *npq4* and *npq4phot2* matched the kinetics of *npq4phot2* in white light, implying that a specific fluorescence decay component is activated by actinic light $\lambda < 600$ nm but not by illumination with red light, and affects the amplitude of qM specifically. This point was further studied through the analysis of Chl fluorescence parameters F'_m and F'_0 during photosynthesis: we found that, upon illumination with white light at 400 µmol photons m^{-2} s^{-1}, *npq4* leaves underwent a decrease in both F'_m and F'_0 as the result of change in both quantum yield and leaf transmittance, respectively, while in *npq4phot2* only F'_m decreased upon irradiation (see electronic supplementary material, figure S2).

Thus, the chloroplast avoidance response is, among all the mechanisms examined, the only significant modulator of the concentration of Chl excited states independent of PsbS. To confirm the effect of the *phot2* mutation on the *npq4* background, we examined leaf cells by light microscopy (figure 4*c*). Upon irradiation with white light at 400 µmol photons m^{-2} s^{-1},

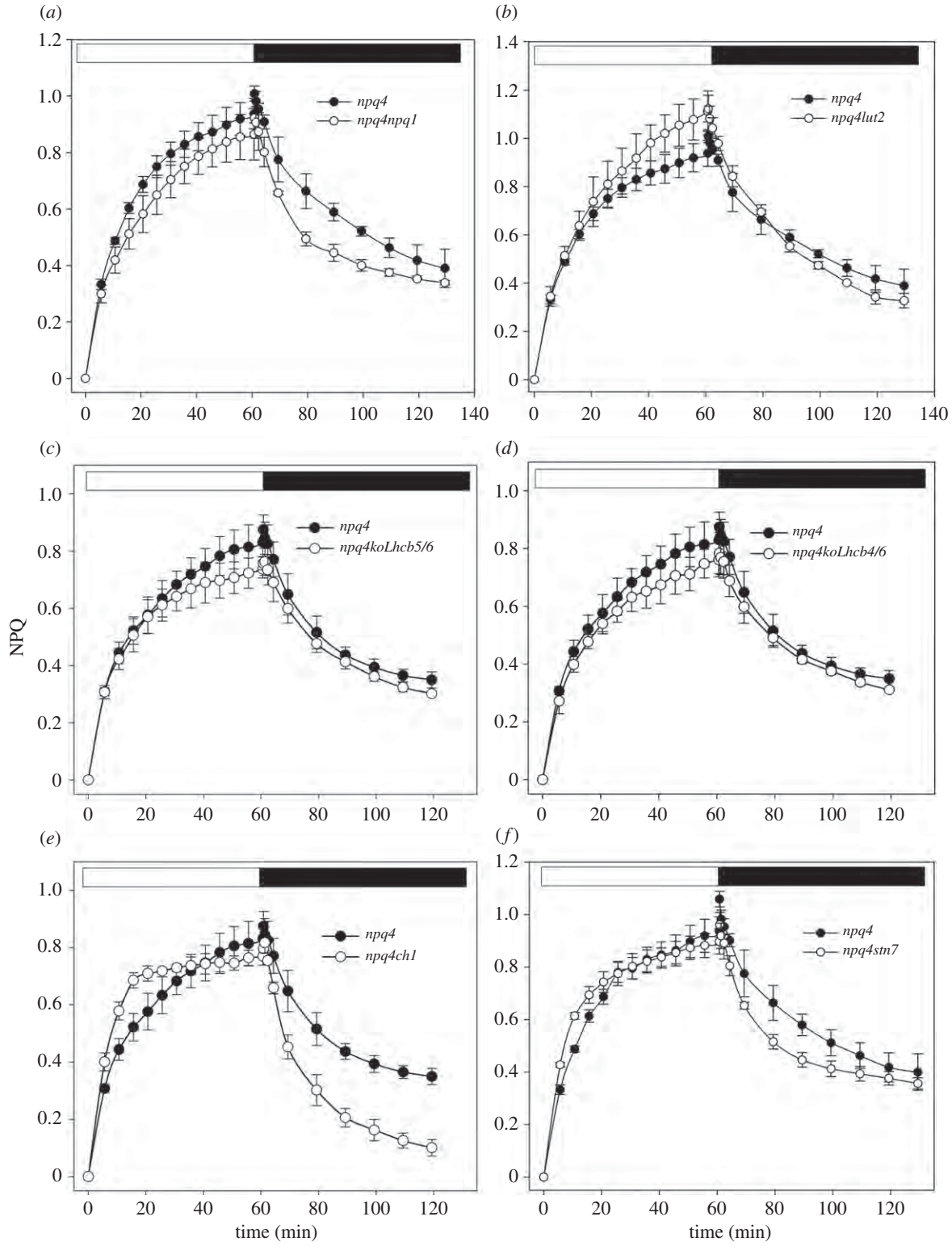

Figure 3. NPQ analysis of *npq4* leaves with altered xanthophyll compositions or depleted of either PSII LHCs or state transition. NPQ induction and relaxation were measured in dark-adapted *npq4* plants lacking zeaxanthin (*npq4npq1* (*a*)) or lutein (*npq4lut2* (*b*)), or devoid of either minor Lhcb CP26 and CP24 (*koLhcb5/6* (*c*)), CP29 and CP24 (*koLhcb4/6* (*d*)) or the entire LHC owing to mutation (*ch1* (*e*)), or blocked in state transitions (*npq4stn7* (*f*)). NPQ kinetics were measured in dark-adapted leaves, upon 60 min illumination at 400 μmol photons m^{-2} s^{-1}, followed by further 60 min of dark relaxation. Symbols and error bars show mean ± s.d. ($n = 3$).

npq4 leaves showed chloroplasts located at the anticlinal cell walls, thus indicating that they had undergone avoidance movement. Instead, the chloroplasts of the mutant *npq4phot2* retained their preferential association with the periclinal walls, as in leaves adapted to darkness for 1 h. Treatment with nigericin blocks the chloroplast avoidance response (figure 4*c*), consistent with the complete depletion of qM after treatment with the ionophore (figure 2*a*).

In conclusion, the analyses of quenching relaxation dynamics on a number of mutants in the *npq4* genetic background, identified a kinetically intermediate component of fluorescence decay, distinct from either qE or qI, called qM, the triggering of which requires uniquely formation of a transmembrane proton gradient, but which is not related to xanthophyll or LHC composition, PSII turnover, consumption of ATP accumulated in the light phase or state transitions. Based on its relaxation

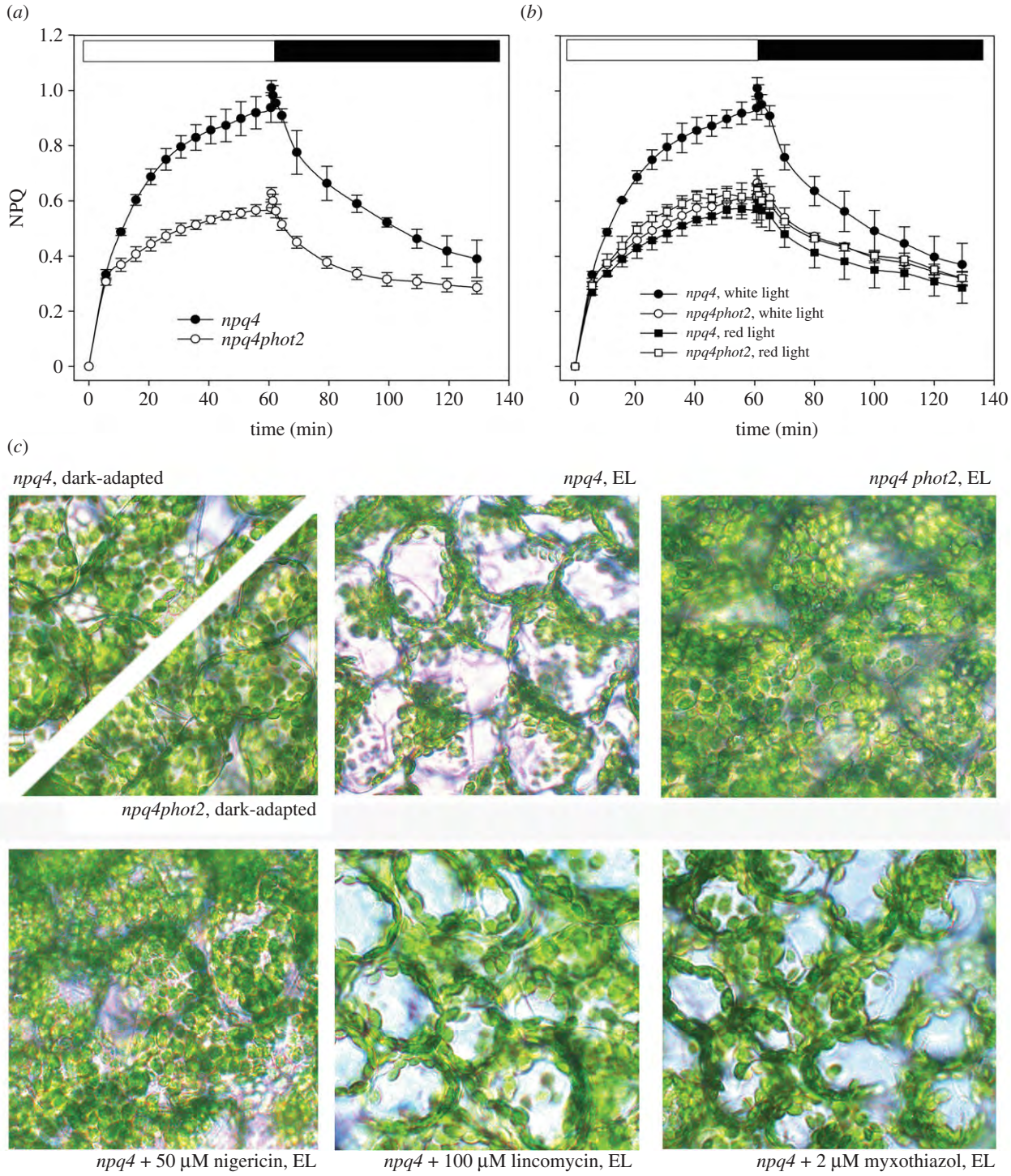

Figure 4. NPQ analysis of *npq4* leaves depleted of chloroplast avoidance movement. (*a*) PsbS-minus plants were crossed with *Arabidopsis* knock-out lines lacking the photoprotective mechanism of chloroplast avoidance movement (*phot2*). Kinetics of NPQ induction and relaxation of *npq4* and *npq4phot2* were measured in dark-adapted leaves, as described for figure 3. (*b*) NPQ kinetics were measured on *npq4* and *npq4phot2* leaves upon illumination with either white actinic light (400 µmol photons m^{-2} s^{-1}) or red light (350 µmol photons m^{-2} s^{-1}, $600 < \lambda < 750$ nm). Symbols and error bars show mean $\pm$ s.d. ($n = 3$). (*c*) Distribution of chloroplasts in the mesophyll cells of *npq4* and *npq4phot2* was determined by light microscopy. Leaves were dark-adapted for 1 h and then irradiated with white light at 400 µmol m^{-2} s^{-1} for 1 h. Prior to light treatment, detached leaves were infiltrated with 150 mM sorbitol containing either 50 µM nigericin, 100 µM lincomycin or 2 µM myxothiazol. (Online version in colour.)

kinetics, the mechanism of chloroplast photorelocation accounts for nearly 50% of qM amplitude.

4. Discussion

Here, we have investigated the light-induced decline of Chl fluorescence and its relaxation dynamics in the *npq4* mutant of *Arabidopsis*, lacking the PsbS subunit essential for qE activity, in order to assess the basis for its residual light-induced fluorescence decline activity. Kinetic analysis of fluorescence dark recovery *in vivo* allowed an NPQ component to be identified which relaxes in the dark within the time range 16–25 min, intermediate between the fast qE component (1–2 min) and inhibitory quenching qI (more than 1 h). This component, qM, showed similar amplitude and

half-life in WT and *npq4* plants (figure 1 and table 1) and is uncoupler-sensitive (figure 2*a*). To search for the molecular basis of this process, the *npq4* genotype was crossed with others, which affected photosynthetic components and mechanisms known to alter the characteristics of light-induced Chl fluorescence changes, and analysed the fluorescence quenching in each.

(a) The kinetic components of non-photochemical quenching dark relaxation in *npq4*

Analysis of NPQ dark relaxation of WT and *npq4* leaves identified three distinct kinetic components (figure 1 and table 1). The rapid phase (half-life 35–55 s) detected in WT but not in *npq4* leaves, can be safely assigned to qE [8]. The long-term relaxing component, whose half-life is longer than 60 min, can be assigned to photoinhibitory processes based on its amplitude dependence of photon fluency and increased incidence in *npq4* [13]. The third, intermediate kinetic component (half-life 20–35 min), can be detected with similar amplitude in both WT and *npq4* relaxation kinetics. Although the existence of a middle-phase kinetic component of NPQ has been reported previously [8,43], its physiological origin is still debated.

The middle phase component, qM, is saturated at moderate light intensity, maintaining the same amplitude at 800 and 1200 μmol photons $m^{-2} s^{-1}$ (table 1). This suggests that qM is not related to PSII photoinhibition, as the amplitude of a photoinhibitory component is expected to increase with irradiance; indeed, the component here defined as qI increases from 0.67 at 800 μmol photons $m^{-2} s^{-1}$ to 1.01 at 1200 μmol photons $m^{-2} s^{-1}$ in *npq4* (figure 1 and table 1). At all light regimes tested, the *npq4* leaves showed higher qI than WT leaves, consistent with the photoprotective role of qE in short-term exposure to EL [44].

We used an actinic intensity of 400 μmol photons $m^{-2} s^{-1}$ as at this irradiance qM is almost saturated and photoinhibition in *npq4* is as low as in the WT leaves (table S2 available in the electronic supplementary material). Lincomycin treatment failed to affect NPQ decay in *npq4* leaves, implying that at 400 μmol photons $m^{-2} s^{-1}$ turnover of D1 did not significantly contribute to qM.

A slow phase of NPQ dark relaxation was reported to depend on the hydrolysis of ATP accumulated during a light phase [34]. However, myxothiazol treatment did not affect qM in *npq4* (figure 2*b* and table 2), thus ruling out the possibility that the qM decay component was related to slow ΔpH relaxation.

It is interesting to note that qM is sensitive to uncouplers: indeed, dark relaxation of fluorescence decline is prevented in leaves infiltrated with the ionophore nigericin. Besides the loss of qM, nigericin led to a strong increase in qI amplitude, implying that both qE and qM are crucial for PSII photoprotection in EL conditions (figure 2*a*). The intermediate component has been previously defined as qT or qZ for its possible dependence on state transitions or Zea biosynthesis, respectively [8,15,43]. However, data reported here show that blocking these processes with specific mutations does not interfere with qM as determined in the *npq4* strain. This mutant was chosen to avoid overlapping contribution of qE to the dark relaxation dynamics. In *npq4*, we could not detect qE type quenching ($\tau < 5$ min) under any conditions, even upon 60 min of illumination (table 1).

(b) Targeted reverse genetic analysis to identify the molecular basis for qM

NPQ kinetic of nigericin-treated leaves demonstrated that triggering of qM requires transmembrane proton gradient formation during the light phase. Among the effects of EL treatment is thylakoid lumen acidification and Zea synthesis, which are needed for full expression of qE in *Arabidopsis* [31]. Instead, the double mutant *npq4npq1*, which is depleted in both qE and Zea, showed the same kinetics and amplitude of qM as *npq4* (figure 3*a*). Therefore, unlike qE, Zea depletion did not prevent full expression of qM, which indeed reaches maximum value (although much lower than in WT) in both *npq4* and *npq4npq1* plants (table 2). The kinetics of Zea epoxidation in *npq4* do not fit with those of NPQ dark recovery, the former being far slower than the kinetic relaxation of qM [15]. We conclude that the xanthophyll cycle, one of the most efficient modulators of qE [14,31], does not affect the amplitude of qM but only slowed the dark relaxation rate (figure 3*a*). Similar considerations can be applied to Lut; indeed, the amplitude and kinetics of qM are essentially the same in both *npq4* and *npq4lut2* plants (figure 3*b*). qE is located in the antenna system, and an important role in NPQ was attributed to Lhcb4 and Lhcb5 [36,45]. Nevertheless, light-induced fluorescence decline was essentially the same in *npq4*, *npq4koLhcb4/6* and *npq4koLhcb5/6* leaves. Moreover, no significant differences were found when comparing *npq4* versus *npq4ch1* leaves depleted in all LHC proteins, including LHCII (table 2) [37], suggesting that these changes were not the result of qE type quenching. Finally, we examined the hypothesis of the involvement of state 1–state 2 transitions in PsbS-independent fluorescence decline; however, the similar behaviour of *npq4* and *npq4stn7* leaves (figure 3*f*) excludes this possibility.

(c) Chloroplast avoidance response and qM

Among all the mutations introduced into the *npq4* genetic background, *phot2* was the only one that affected qM (figure 4*a*). Differences in *npq4* versus *npq4phot2* NPQ kinetics showed that the fluorescence recovery component is affected by chloroplast photorelocation. This process is mediated by the blue light receptors, phototropins. Consistently, we verified that the same effect on NPQ kinetics was obtained by using red light rather than white actinic light (figure 4*b*). Moreover, upon illumination with white light at 400 μmol photons $m^{-2} s^{-1}$, *npq4* leaves underwent a decrease in both F'_m and F'_0, as expected for concomitant changes in PSII quantum yield and leaf absorption, respectively, while in *npq4phot2* leaves only F'_m was decreased upon irradiation (see the electronic supplementary material, figure S2). Thus, an avoidance response, causing chloroplast movement towards cell walls parallel to incident light, affects the apparent kinetics of NPQ, particularly the slower components. This is consistent with reports showing that light-induced chloroplast movements could affect Chl fluorescence emission [41], and with recent results which highlighted, in *phot2*, the lack of a fluorescence decay kinetic component, qM, intermediate between qE and qI [46]. The similar amplitude and half-life of the qM component in WT and *npq4* leaves (table 1), and its reduction in a mutant devoid of chloroplast photorelocation (table 2; see also [46]), strongly support the view that chloroplast relocation significantly influences the apparent kinetics of NPQ by decreasing the photon absorption of leaves, rather than changing the activity of quenching reactions.

It should be noted, however, that this effect arises from decreased photon absorption which gives a lower fluorescence yield, rather than from a genuine quenching process. In fact, during illumination, chloroplast relocation induces a change in the distribution of pigments within the cell, with the formation of localized chloroplast stacks along anticlinal cell walls. This effect reduces the overall optical density of the cell because of a 'sieve effect' resulting from the formation of highly transmitting paths across the periclinal cell surfaces while increasing the optical density beyond linearity in the vicinity of the anticlinal cell walls [47]. Thus, the fraction of excited, fluorescence emitting chloroplasts is decreased because of shading by neighbouring, ones. It is worth noting that the kinetics and timescale of qM formation and relaxation at 400 µmol photons m^{-2} s^{-1} of white light (table 1) fits with that described for the chloroplast avoidance response under similar irradiance [48]. Light microscopy analysis (figure 4*c*) confirmed that movement of chloroplasts was inhibited in the presence of nigericin, consistent with the depletion in qM. The chloroplast avoidance response probably relies on the cytosolic Ca^{2+} signal for its activation [49]. Maintenance of a low cytosolic Ca^{2+} level requires an electrogenic pump which exploits, protonmotive force to actively extrude Ca^{2+} [50]. Phototropin signal transduction involves transient depolarization of the plasma membrane which, in turn, triggers cytosolic Ca^{2+} intake. Nigericin wrecks all the transmembrane electrochemical gradients, thus blocking several signal transduction events. The double effect of nigericin in collapsing the thylakoid pH gradient and in blocking chloroplast relocation (figure 4*c*) can easily lead to misinterpretation of qM as a slow qE response in the absence of PsbS.

Although chloroplast relocation is the major factor affecting the amplitude of qM in *npq4* (figure 4a,*b*), the fluorescence recovery kinetics of *npq4phot2* are not completely devoid of qM. The residual component accounts for about 18% of total reversible F'_m quenching in WT (tables 1 and 2) and reflects mechanism(s) sensitive to uncouplers (figure 2*a*) and yet distinct from the avoidance response, as it is still active in *npq4phot2*. Previous work led to different proposals for mechanisms leading to fluorescence recovery components with intermediate half-life between qE and qI. First, it was attributed to state 1–state 2 transitions [43]; second to PSII photoinhibition [51]; third to a slowly developing component of qE dependent on Zea [52]; fourth to light-induced dissociation of the complex Lhcb4-Lhcb6-LHCII-M [19]. Here, we show that qM did not correlate with Zea accumulation nor was it related to qI. Although thylakoid membrane reorganization could well explain changes in chloroplast fluorescence yield since protein–protein interactions are responsible for nearly 50% of quenching [14,19], the need for PsbS to trigger domain reorganization [19,20] suggests this is not the source of residual qM. An interesting observation is that a substantial fraction of qM is retained in the absence of Lhcb in the *npq4ch1* mutant (figure 3*e*), although with a somewhat shorter half-life (table 2). This is consistent with the characteristics of Zea-independent NPQ localized in the PSII core complex [53].

Our results support the view that no qE occurs in *npq4* leaves within a wide range of actinic light intensities. Moreover light-induced fluorescence decline in *npq4* was always far lower than in WT plants, even upon 1 h of EL exposure (figure 1). Finally, the residual fluorescence decline in *npq4* leaves is due to avoidance of photon absorption, while quenching mechanisms can only be responsible for a minor component associated with the PSII core (figure 3*e*), rather than to reactions within the antenna system. Our results significantly differ from those of Johnson & Ruban [21], who reported that qE could be catalysed, although at a slower rate, in *npq4* plants. First, we found that the amplitude of fluorescence decline in *npq4* leaves did not match that observed in WT under any conditions, the fraction of reversible F'_m quenching in the absence of PsbS and triggered by lumen acidification being small (about 18%) (table 1). The photoprotective effect of fluorescence decline was consistently low, as shown from the higher amplitude of qI in *npq4* leaves under EL conditions (table 1). Second, we found that uncouple sensitivity is the result of the disruption of chloroplast relocation, also involving a proton gradient for signal transduction upon blue light activation of phototropins [49]. Overall, these results point to a crucial role of PsbS in the modulation of NPQ and show that sensing of trans-thylakoid ΔpH by protonable residues in the LHC is not enough to induce WT levels of NPQ in the absence of PsbS. This conclusion is consistent with recent results showing that less than 0.5% of purified minor antennae underwent charge transfer quenching *in vitro*, whereas the fraction engaged in this process was more than 80 times higher in intact thylakoids with PsbS [36]. Thus, PsbS is indispensable for qE, within the trans-thylakoid ΔpH that can be obtained by light treatment of leaves, rather than being only a modulator of the proton–antenna association constant, p*K*, of qE activation [54].

References

1. Croce R, Van Amerongen H. 2011 Light-harvesting and structural organization of photosystem II: from individual complexes to thylakoid membrane. *J. Photochem. Photobiol. B* **104**, 142–153. (doi:10.1016/j.jphotobiol.2011.02.015)
2. Krieger-Liszkay A. 2005 Singlet oxygen production in photosynthesis. *J. Exp. Bot.* **56**, 337–346. (doi:10.1093/jxb/erh237)
3. Alboresi A, Dall'Osto L, Aprile A, Carillo P, Roncaglia E, Cattivelli L, Bassi R. 2011 Reactive oxygen species and transcript analysis upon excess light treatment in wild-type *Arabidopsis thaliana* vs a photosensitive mutant lacking zeaxanthin and lutein. *BMC. Plant Biol.* **11**, 62. (doi:10.1186/1471-2229-11-62)
4. Wada M, Kagawa T, Sato Y. 2003 Chloroplast movement. *Ann. Rev. Plant Biol.* **54**, 455–468. (doi:10.1146/annurev.arplant.54.031902.135023)
5. Niyogi KK. 2000 Safety valves for photosynthesis. *Curr. Opin. Plant Biol.* **3**, 455–460. (doi:10.1016/S1369-5266(00)00113-8)
6. Dall'Osto L, Holt NE, Kaligotla S, Fuciman M, Cazzaniga S, Carbonera D, Frank HA, Alric J, Bassi R. 2012 Zeaxanthin protects plant photosynthesis by modulating chlorophyll triplet yield in specific light-harvesting antenna subunits. *J. Biol. Chem.* **287**, 41 820–41 834. (doi:10.1074/jbc.M112.405498)
7. Kulheim C, Agren J, Jansson S. 2002 Rapid regulation of light harvesting and plant fitness in the field. *Science* **297**, 91–93. (doi:10.1126/science.1072359)
8. Walters RG, Horton P. 1991 Resolution of components of non-photochemical chlorophyll fluorescence quenching in barley leaves. *Photosynth. Res.* **27**, 121–133. (doi:10.1007/BF00033251)
9. Briantais J-M, Vernotte C, Picaud M, Krause GH. 1980 Chlorophyll fluorescence as a probe for the determination of the photoinduced proton gradient in isolated chloroplasts. *Biochim. Biophys. Acta* **591**, 198–202. (doi:10.1016/0005-2728(80)90233-9)
10. Dominici P, Caffarri S, Armenante F, Ceoldo S, Crimi M, Bassi R. 2002 Biochemical properties of the PsbS subunit of photosystem II either purified from

chloroplast or recombinant. *J. Biol. Chem.* **277**, 22 750–22 758. (doi:10.1074/jbc.M200604200)

11. Wilk L, Grunwald M, Liao PN, Walla PJ, Kuhlbrandt W. 2013 Direct interaction of the major light-harvesting complex II and PsbS in nonphotochemical quenching. *Proc. Natl Acad. Sci. USA* **110**, 5452–5456. (doi:10.1073/pnas.1205561110)
12. Niyogi KK, Shih C, Chow WS, Pogson BJ, DellaPenna D, Björkman O. 2001 Photoprotection in a zeaxanthin- and lutein-deficient double mutant of *Arabidopsis*. *Photosynth. Res.* **67**, 139–145. (doi:10.1023/A:1010661102365)
13. Anderson JM, Park YI, Chow WS. 1997 Photoinactivation and photoprotection of photosystem II in nature. *Physiol. Plant.* **100**, 214–223. (doi:10.1111/j.1399-3054.1997.tb04777.x)
14. Dall'Osto L, Caffarri S, Bassi R. 2005 A mechanism of nonphotochemical energy dissipation, independent from PsbS, revealed by a conformational change in the antenna protein CP26. *Plant Cell* **17**, 1217–1232. (doi:10.1105/tpc.104.030601)
15. Nilkens M, Kress E, Lambrev P, Miloslavina Y, Muller M, Holzwarth AR, Jahns P. 2010 Identification of a slowly inducible zeaxanthin-dependent component of non-photochemical quenching of chlorophyll fluorescence generated under steady-state conditions in *Arabidopsis*. *Biochim. Biophys. Acta* **1797**, 466–475. (doi:10.1016/j.bbabio.2010.01.001)
16. Ahn TK, Avenson TJ, Ballottari M, Cheng YC, Niyogi KK, Bassi R, Fleming GR. 2008 Architecture of a charge-transfer state regulating light harvesting in a plant antenna protein. *Science* **320**, 794–797. (doi:10.1126/science.1154800)
17. Ruban AV *et al*. 2007 Identification of a mechanism of photoprotective energy dissipation in higher plants. *Nature* **450**, 575–578. (doi:10.1038/nature06262)
18. Kruger TPJ, Novoderezhkin VI, Ilioaia C, van Grondelle R. 2010 Fluorescence spectral dynamics of single LHCII trimers. *Biophys. J.* **98**, 3093–3101. (doi:10.1016/j.bpj.2010.03.028)
19. Betterle N, Ballottari M, Zorzan S, de Bianchi S, Cazzaniga S, Dall'Osto L, Morosinotto T, Bassi R. 2009 Light-induced dissociation of an antenna hetero-oligomer is needed for non-photochemical quenching induction. *J. Biol. Chem.* **284**, 15 255–15 266. (doi:10.1074/jbc.M808625200)
20. Johnson MP, Goral TK, Duffy CD, Brain AP, Mullineaux CW, Ruban AV. 2011 Photoprotective energy dissipation involves the reorganization of photosystem II light-harvesting complexes in the grana membranes of spinach chloroplasts. *Plant Cell* **23**, 1468–1479. (doi:10.1105/tpc.110.081646)
21. Johnson MP, Ruban AV. 2010 *Arabidopsis* plants lacking PsbS protein possess photoprotective energy dissipation. *Plant J.* **61**, 283–289. (doi:10.1111/j.1365-313X.2009.04051.x)
22. de Bianchi S, Dall'Osto L, Tognon G, Morosinotto T, Bassi R. 2008 Minor antenna proteins CP24 and CP26 affect the interactions between photosystem II subunits and the electron transport rate in grana membranes of *Arabidopsis*. *Plant Cell* **20**, 1012–1028. (doi:10.1105/tpc.107.055749)
23. de Bianchi S, Betterle N, Kouril R, Cazzaniga S, Boekema E, Bassi R, Dall'Osto L. 2011 *Arabidopsis* mutants deleted in the light-harvesting protein Lhcb4 have a disrupted photosystem II macrostructure and are defective in photoprotection. *Plant Cell* **23**, 2659–2679. (doi:10.1105/tpc.111.087320)
24. Kagawa T, Sakai T, Suetsugu N, Oikawa K, Ishiguro S, Kato T, Tabata S, Okada K, Wada M. 2001 *Arabidopsis* NPL1: a phototropin homolog controlling the chloroplast high-light avoidance response. *Science* **291**, 2138–2141. (doi:10.1126/science.291.5511.2138)
25. Van Kooten O, Snel JFH. 1990 The use of chlorophyll fluorescence nomenclature in plant stress physiology. *Photosynt. Res.* **25**, 147–150. (doi:10.1007/BF00033156)
26. Gilmore AM, Shinkarev VP, Hazlett TL, Govindjee G. 1998 Quantitative analysis of the effects of intrathylakoid pH and xanthophyll cycle pigments on chlorophyll *a* fluorescence lifetime distributions and intensity in thylakoids. *Biochemistry* **37**, 13 582–13 593. (doi:10.1021/bi981384x)
27. Aro E-M, Virgin I, Andersson B. 1993 Photoinhibition of photosystem II - inactivation, protein damage and turnover. *Biochim. Biophys. Acta* **1143**, 113–134. (doi:10.1016/0005-2728(93)90134-2)
28. Garmier M, Carroll AJ, Delannoy E, Vallet C, Day DA, Small ID, Millar AH. 2008 Complex I dysfunction redirects cellular and mitochondrial metabolism in *Arabidopsis*. *Plant Physiol.* **148**, 1324–1341. (doi:10.1104/pp.108.125880)
29. Gilmore AM, Yamamoto HY. 1991 Zeaxanthin formation and energy-dependent fluorescence quenching in pea chloroplasts under artificially mediated linear and cyclic electron transport. *Plant Physiol.* **96**, 635–643. (doi:10.1104/pp.96.2.635)
30. Li XP, Bjorkman O, Shih C, Grossman AR, Rosenquist M, Jansson S, Niyogi KK. 2000 A pigment-binding protein essential for regulation of photosynthetic light harvesting. *Nature* **403**, 391–395. (doi:10.1038/35000131)
31. Niyogi KK, Grossman AR, Björkman O. 1998 *Arabidopsis* mutants define a central role for the xanthophyll cycle in the regulation of photosynthetic energy conversion. *Plant Cell* **10**, 1121–1134.
32. Johnson MP, Davison PA, Ruban AV, Horton P. 2008 The xanthophyll cycle pool size controls the kinetics of non-photochemical quenching in *Arabidopsis thaliana*. *FEBS Lett.* **582**, 262–266. (doi:10.1016/j.febslet.2007.12.016)
33. Krause GH. 1988 Photoinhibition of photosynthesis. An evaluation of damaging and protective mechanisms. *Physiol. Plant.* **74**, 566–574. (doi:10.1111/j.1399-3054.1988.tb02020.x)
34. Joliot PA, Finazzi G. 2010 Proton equilibration in the chloroplast modulates multiphasic kinetics of nonphotochemical quenching of fluorescence in plants. *Proc. Natl Acad. Sci. USA* **107**, 12 728–12 733. (doi:10.1073/pnas.1006399107)
35. Li Z *et al*. 2009 Lutein accumulation in the absence of zeaxanthin restores nonphotochemical quenching in the *Arabidopsis thaliana npq1* mutant. *Plant Cell* **21**, 1798–1812. (doi:10.1105/tpc.109.066571)
36. Avenson TJ, Ahn TK, Zigmantas D, Niyogi KK, Li Z, Ballottari M, Bassi R, Fleming GR. 2008 Zeaxanthin radical cation formation in minor light-harvesting complexes of higher plant antenna. *J. Biol. Chem.* **283**, 3550–3558. (doi:10.1074/jbc.M705645200)
37. Havaux M, Dall'Osto L, Bassi R. 2007 Zeaxanthin has enhanced antioxidant capacity with respect to all other xanthophylls in *Arabidopsis* leaves and functions independent of binding to PSII antennae. *Plant Physiol.* **145**, 1506–1520. (doi:10.1104/pp.107.108480)
38. Dall'Osto L, Cazzaniga S, Havaux M, Bassi R. 2010 Enhanced photoprotection by protein-bound vs free xanthophyll pools: a comparative analysis of chlorophyll *b* and xanthophyll biosynthesis mutants. *Mol. Plant* **3**, 576–593. (doi:10.1093/mp/ssp117)
39. Galka P, Santabarbara S, Khuong TTH, Degand H, Morsomme P, Jennings RC, Boekema EJ, Caffarri S. 2012 Functional analyses of the plant photosystem I–light-harvesting complex II supercomplex reveal that light-harvesting complex II loosely bound to photosystem II is a very efficient antenna for photosystem I in state II. *Plant Cell* **24**, 2963–2978. (doi:10.1105/tpc.112.100339)
40. Bellafiore S, Barneche F, Peltier G, Rochaix JD. 2005 State transitions and light adaptation require chloroplast thylakoid protein kinase STN7. *Nature* **433**, 892–895. (doi:10.1038/nature03286)
41. Brugnoli E, Bjorkman O. 1992 Chloroplast movements in leaves—influence on chlorophyll fluorescence and measurements of light-induced absorbance changes related to DeltapH and zeaxanthin formation. *Photosynth. Res.* **32**, 23–35. (doi:10.1007/BF00028795)
42. Davis PA, Hangarter RP. 2012 Chloroplast movement provides photoprotection to plants by redistributing PSII damage within leaves. *Photosynt. Res.* **112**, 153–161. (doi:10.1007/s11120-012-9755-4)
43. Quick WP, Stitt M. 1989 An examination of factors contributing to non-photochemical quenching of chlorophyll fluorescence in barley leaves. *Biochim. Biophys. Acta* **977**, 287–296. (doi:10.1016/S0005-2728(89)80082-9)
44. Li XP, Muller-Moule P, Gilmore AM, Niyogi KK. 2002 PsbS-dependent enhancement of feedback de-excitation protects photosystem II from photoinhibition. *Proc. Natl Acad. Sci. USA* **99**, 15 222–15 227. (doi:10.1073/pnas.232447699)
45. Miloslavina Y, de Bianchi S, Dall'Osto L, Bassi R, Holzwarth AR. 2011 Quenching in *Arabidopsis thaliana* mutants lacking monomeric antenna proteins of photosystem II. *J. Biol. Chem.* **286**, 36 830–36 840. (doi:10.1074/jbc.M111.273227)
46. Cazzaniga S, Dall'Osto L, Kong SG, Wada M, Bassi R. 2013 Interaction between avoidance of photon absorption, excess energy dissipation and zeaxanthin synthesis against photoxidative stress

in *Arabidopsis*. *Plant J.* **76**, 568–579. (doi:10.1111/tpj.12314)

47. Davis PA, Caylor S, Whippo CW, Hangarter RP. 2011 Changes in leaf optical properties associated with light-dependent chloroplast movements. *Plant Cell Environ.* **34**, 2047–2059. (doi:10.1111/j.1365-3040.2011.02402.x)
48. Kasahara M, Kagawa T, Oikawa K, Suetsugu N, Miyao M, Wada M. 2002 Chloroplast avoidance movement reduces photodamage in plants. *Nature* **420**, 829–832. (doi:10.1038/nature01213)
49. Suetsugu N, Wada M. 2007 Chloroplast photorelocation movement mediated by phototropin family proteins in green plants. *Biol. Chem.* **388**, 927–935. (doi:10.1515/BC.2007.118)
50. Ettinger WF, Clear AM, Fanning KJ, Peck ML. 1999 Identification of a $Ca2^{+}/H^{+}$ antiport in the plant chloroplast thylakoid membrane. *Plant Physiol.* **119**, 1379–1386. (doi:10.1104/pp.119.4.1379)
51. Ruban AV, Horton P. 1995 An investigation of the sustained component of nonphotochemical quenching of chlorophyll fluorescence in isolated chloroplasts and leaves of spinach. *Plant Physiol.* **108**, 721–726.
52. Horton P. 1996 Nonphotochemical quenching of chlorophyll fluorescence. In *Light as an energy source and information carrier in plant physiology* (ed. RC Jennings), pp. 99–111. New York, NY: Plenum Press.
53. Finazzi G, Johnson GN, Dall'Osto L, Joliot P, Wollman FA, Bassi R. 2004 A zeaxanthin-independent nonphotochemical quenching mechanism localized in the photosystem II core complex. *Proc. Natl Acad. Sci. USA* **101**, 12 375–12 380. (doi:10.1073/pnas.0404798101)
54. Johnson MP, Ruban AV. 2011 Restoration of rapidly-reversible photoprotective energy dissipation in the absence of PsbS protein by enhanced ΔpH. *J. Biol. Chem.* **286**, 19 973–19 981. (doi:10.1074/jbc.M111.237255)

Figure S1

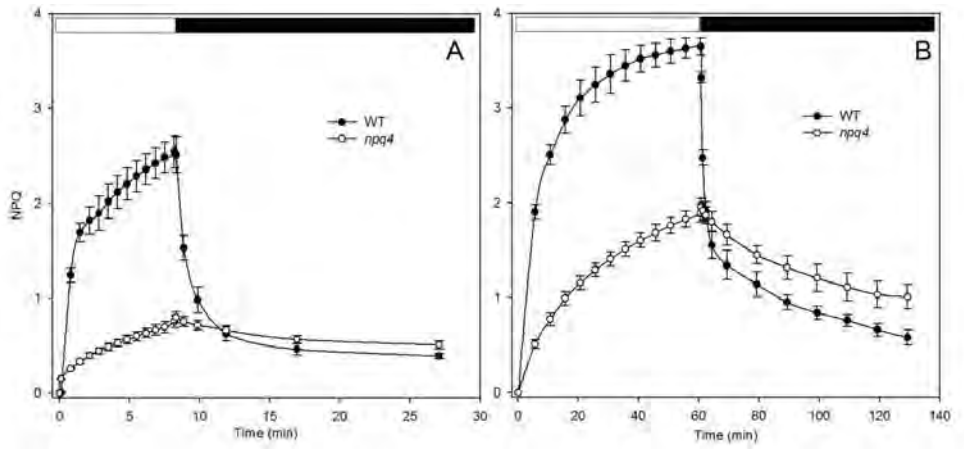

Figure S1. NPQ analysis of wild-type and *npq4* leaves. Kinetics of NPQ induction and relaxation were recorded with a pulse amplitude modulated fluorometer. Chlorophyll fluorescence was measured in intact, dark-adapted leaves, during either 8 min (**A**) or 60 min (**B**) of illumination at 1200 µmol photons m^{-2} s^{-1}, followed by dark relaxation. Symbols and error bars show mean ± SD (n = 3).

Figure S2

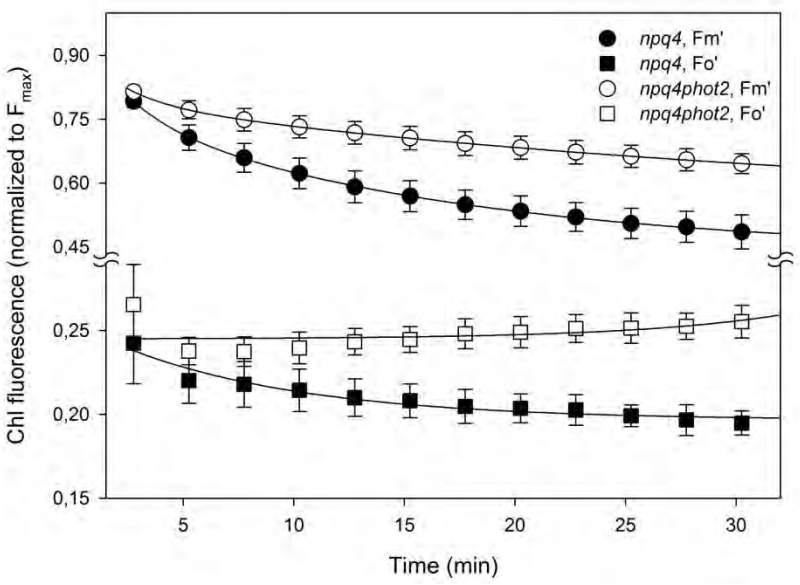

Figure S2. Analysis of F_0' and F_m' changes during photosynthesis. Chlorophyll fluorescence parameters F_m' (circles) and F_0' (squares) were monitored in *npq4* and *npq4 phot2* leaves upon induction of fluorescence quenching by white actinic light (400 μmol photons m^{-2} s^{-1}, RT). Fluorescence values were normalized to the corresponding F_{max} value. Data are expressed as means ± SD (*n* = 3).

Additional Table I. Zeaxanthin content of WT and *npq4* leaves. Zeaxanthin content was measured on leaf discs, either upon 60 min illumination of dark-adapted leaves with different actinic intensities (400, 800 or 1200 µmol photons m^{-2} s^{-1}, white light, RT) or upon further 60 min dark-relaxation following actinic light. At different times, discs were frozen in liquid nitrogen, and total pigments were extracted and quantified by HPLC.

	400 µmol photons m^{-2} s^{-1}		**800 µmol photons m^{-2} s^{-1}**		**1200 µmol photons m^{-2} s^{-1}**	
	60' light	**60' dark-recovery**	**60' light**	**60' dark-recovery**	**60' light**	**60' dark-recovery**
WT	1.30 ± 0.09	0.59 ± 0.11	2.19 ± 0.16	0.95 ± 0.12	2.60 ± 0.13	1.47 ± 0.15
npq4	1.39 ± 0.30	0.77 ± 0.16	1.94 ± 0.14	0.90 ± 0.17	2.46 ± 0.20	1.53 ± 0.08

Additional Table II. Maximum quantum efficiency of PSII photochemistry of the WT and *npq4*. F_v/F_m values were determined on intact leaves, either dark adapted (t_0) or treated with EL for 60 min and then relaxed in the dark for 60 min (t=120').

	400 µmol photons m^{-2} s^{-1}		**800 µmol photons m^{-2} s^{-1}**		**1200 µmol photons m^{-2} s^{-1}**	
	F_v/F_m (t_0)	**F_v/F_m (t=120')**	**F_v/F_m (t_0)**	**F_v/F_m (t=120')**	**F_v/F_m (t_0)**	**F_v/F_m (t=120')**
WT	0.81 ± 0.01	0.75 ± 0.01	0.81 ± 0.01	0.71 ± 0.01	0.81 ± 0.01	0.68 ± 0.01
npq4	0.80 ± 0.01	0.72 ± 0.02	0.81 ± 0.01	0.66 ± 0.01 *	0.81 ± 0.01	0.59 ± 0.01 *

Appendix A.
Domestication of the green alga *Chlorella sorokiniana*: reduction of antenna size improves light-use efficiency in a photobioreactor.

Cazzaniga et al. Biotechnology for Biofuels 2014, 7:157
http://www.biotechnologyforbiofuels.com/content/7/1/157

Biotechnology for Biofuels

RESEARCH ARTICLE Open Access

Domestication of the green alga *Chlorella sorokiniana*: reduction of antenna size improves light-use efficiency in a photobioreactor

Stefano Cazzaniga[1†], Luca Dall'Osto[1†], Joanna Szaub[2], Luca Scibilia[1], Matteo Ballottari[1], Saul Purton[2] and Roberto Bassi[1*]

Abstract

Background: The utilization of biomass from microalgae for biofuel production is one of the key elements for the development of a sustainable and secure energy supply. Among the different microalgae, *Chlorella* species are of interest because of their high productivity, high lipid content, and resistance to the high light conditions typical of photobioreactors. However, the economic feasibility of growing algae at an industrial scale is yet to be realized, in part because of biological constraints that limit biomass yield. A key issue is the inefficient use of light due to uneven light distribution, and the dissipation of excess absorbed light as heat. The successful implementation of biofuel production facilities requires the development of algal strains with enhanced light use efficiency in photobioreactors. Such domestication strategies include decreasing the absorption cross section in order to enhance light penetration, increasing the size of metabolic sinks per chlorophyll and minimizing feedback energy dissipation.

Results: In this work we applied random mutagenesis and phenotypic selection to the thermotolerant, fast-growing *Chlorella* species, *C. sorokiniana*. Truncated antenna mutants (TAMs) were selected that exhibited a lower fluorescence yield than the wild-type (WT) strain. Six putatively interesting mutants were selected by high throughput fluorescence video imaging, two of which, TAM-2 and TAM-4, were found to have approximately half the chlorophyll content per cell and LHCII complement per PSII with respect to the WT. In batch culture, TAM-2 showed an increased photon use efficiency, yielding a higher P_{max} at saturating irradiances with respect to the WT. Cultivation of TAM-2 in both laboratory-scale and outdoor photobioreactors showed higher productivity than WT, with a 30% higher biomass yield in dense cell suspensions typical of industrial photobioreactors.

Conclusions: These results suggest that generation of mutants with low chlorophyll content can significantly improve the light-to-biomass conversion efficiency of *C. sorokiniana* under mass culture conditions. However, owing to the lack of sexual reproduction in this species, the presence of additional mutations might affect growth rate, suggesting that selection should include evaluation of multiple independent mutants for each desired phenotype.

Keywords: *Chlorella sorokiniana*, Photosynthesis, Photobioreactor, Biomass, Biofuel, Antenna size, Light-use efficiency

* Correspondence: roberto.bassi@univr.it
†Equal contributors
[1]Dipartimento di Biotecnologie, Università di Verona, Strada Le Grazie, Verona 15-37134, Italy
Full list of author information is available at the end of the article

Background

In the last decades, the use of microalgae as a viable energy alternative to fossil fuels has attracted great attention, and efforts have been made to improve the mass culture yield using sunlight as the energy source. Microalgae have significant potential for biomass accumulation and biodiesel production when compared to crops, due to their higher productivity per surface and avoidance of competition for arable land for food production [1,2]. Due to their simple cellular structure, microalgae have a faster growth rate and are productive all year round; therefore, their biomass yield per area greatly exceeds that of the best crops [3]. Algae can grow in a broad range of temperature, salinity, and pH, and their ability to carry out photosynthesis under high CO_2 concentrations [4] enhances the economic impact of algal-based technologies, due to their potential for CO_2 mitigation [5].

Among the many candidate algal strains for biotechnological applications, a genus of considerable interest is *Chlorella*. Several freshwater species of *Chlorella* have been extensively used commercially over the past 40 years as a food and feed supplement on account of their rapid growth and tolerance over a wide range of temperature and culture conditions [6]. Cultures of *Chlorella vulgaris* grown in suitable outdoor photobioreactors (PBRs) can produce up to 40% of lipid per dry cell weight [7,8].

So far, algal-based industrial facilities have focused on the production of bioactive or dietary supplements due to their high product values [9], rather than on biofuels whose production is considered economically unfavorable [10]. An improvement in the biomass yield of microalgae in PBR conditions is therefore of primary importance and requires development of strains that overcome the biological constraints that limit intensive cultivation.

One of the most critical factors for biomass production is the efficiency of light utilization. Indeed, although photosynthesis has been optimized over three billion years of evolution, it remains inefficient at converting solar energy into chemical energy and biomass. The theoretical photoconversion efficiency of about 27% drops to 6% due to reductions in the efficiency of photon utilization and biomass accumulation [11]. Indeed, although the theoretical maximum productivity of microalgae is estimated to be around 170 to 190 g DW m^{-2} d^{-1} [11], the reported efficiencies in ponds or PBRs ranged from 20 to 35 g DW m^{-2} d^{-1} [12,13] with the present technology and available strains.

The reasons for this efficiency drop in dense culture conditions are rooted in the very structural organization of the photosynthetic apparatus. Oxygenic photosynthesis is performed by four multisubunit membrane-protein complexes in the thylakoid membrane: two photosystems (PSI and PSII), cytochrome b_6f, and ATPase [14]. Each photosystem includes a core complex that binds cofactors involved in electron transport together with additional chlorophyll (Chl) *a* and β-carotene as antenna pigments. Associated with the photosystems is an array of antenna complexes called light harvesting complexes (LHCs) which bind Chl *a*, *b* and xanthophylls, and enhance photon absorption and transfer excitation energy for photochemical reactions [15,16]. LHCs also have essential roles in photoprotection, through the dissipation of excess light as heat (non-photochemical energy dissipation, NPQ), and in reactive oxygen species (ROS) scavenging [17-20]. A reduction in pigment content per cell and a reduction in antenna size are targets for optimizing the photosynthetic yield of unicellular algae under mass culture [21,22]. Indeed, the light use efficiency of microalgae in PBRs is limited by the steep light gradient due to the strong optical density of the near-molar concentration of Chls in cells. Microalgae have evolved in natural environments where light and inorganic elements, particularly iron, are often limiting, leading to a low cell density. As a survival strategy, large antennae were developed around photosystems in order to maximize their capacity to collect photons per unit of iron content [23]. Thus, cells in surface-exposed layers of PBRs absorb far more photons than they can use in electron transport and yet cell density and light intensity need to be high in order to increase productivity per unit of an installed facility [7]. Indeed, due to their huge optical density, the surface layers of microalgae easily reach saturation (and hence, photoinhibition) of photosynthesis [24], while the inner layers are light limited [25]. This non-homogeneous light penetration results in a low productivity of the system. Optimization of the light quality and intensity within the culture volume can alleviate these constraints. This can be done by selecting a mutant strain with a reduced pigment content per cell resulting either from a truncated antenna size or a lower overall density of photosynthetic units per cell [22,26]. The resulting decrease in optical density per biomass unit would mitigate the steepness of the light gradient typical of cultures of wild-type (WT) strains in ponds or PBRs, with cells located in surface layers absorbing less photons and those in inner layers receiving more light, altogether resulting in a higher rate of growth [27].

In this work we report the isolation of truncated antenna mutants of *Chlorella sorokiniana* following UV mutagenesis. This species was chosen for its very high growth rates [28] and tolerance to temperatures as high as 42°C [29], parameters that offer clear advantages for large-scale production in PBRs [22]. Our characterization of six potential mutants identified TAM-2 and TAM-4 as having a reduced antennae size and Chl content per cell. However, only TAM-2 showed an increased photon use

efficiency, giving higher P_{max} at saturating irradiances with respect to the WT. Importantly, cultivation experiments in both laboratory-scale and outdoor PBRs consistently showed higher biomass productivity with TAM-2 (30% higher than WT) in dense suspensions of cells.

Results

Isolation of truncated antenna mutants (TAMs) of *Chlorella sorokiniana*

C. sorokiniana mutants that exhibited a lower Chl fluorescence yield than WT when exposed to a saturating pulse of light were identified following UV mutagenesis using a fluorescence video-imaging system (Additional file 1: Figure S1). Approximately 3,000 mutagenized lines were screened for retained photoautotrophy, but with a lower value of F_{max}, which is expected to correlate with a smaller antenna size [16]. Six independent mutants were identified as putatively affected in antenna size (**t**runcated **a**ntenna **m**utants) and named TAM-1 to TAM-6. As shown in Figure 1, all six mutants are capable of phototrophic growth, but they display various levels of reduction in fluorescence, with TAM-2 and TAM-4 the most pronounced.

The pigment composition of the mutants and the WT strain were determined after five days of growth, as shown in Additional file 1: Table S1. Two of the mutants (TAM-2 and TAM-4) showed a significant reduction of Chl content per cell when grown in minimal medium, while the other mutants had a Chl content per cell similar to that of WT. Furthermore, the analysis showed that the Chl *a/b* ratio was significantly higher in TAM-2 and TAM-4 with values of 3.36 and 3.40, respectively versus 2.62 in WT, while the Chl/Car ratio was significantly lower in TAM-1, TAM-2, and TAM-4 with respect to the WT. These data suggest a depletion in the Chl *b*-rich light-harvesting antenna complexes in TAM-2 and TAM-4, and so these mutants were chosen for further study. Additional HPLC analysis of the carotenoid composition of DMFA-acetone cell extracts (Additional file 1: Table S2) revealed that TAM-2 and TAM-4 accumulate lower levels of neoxanthin and lutein on a Chl basis compared to WT, while both β-carotene and xanthophyll cycle pigments (violaxanthin, antheraxanthin, and zeaxanthin) were more abundant.

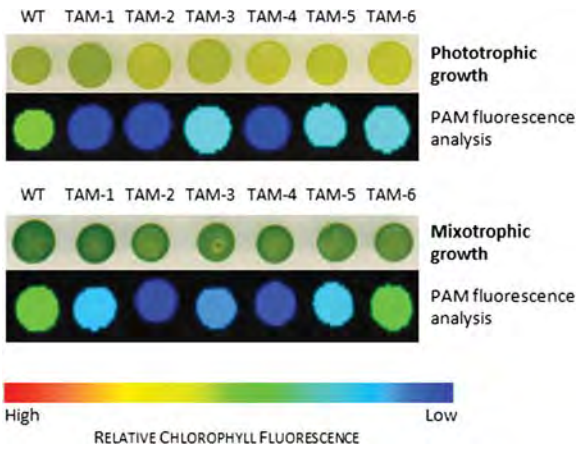

Figure 1 Growth and fluorescence analysis of six putative truncated antenna mutants (TAM1-6) of *Chlorella sorokiniana*. Culture samples were spotted onto minimal medium (upper panels: phototrophic growth) or acetate-containing medium (lower panels: mixotrophic growth), grown in continuous light (50 μmol photons m^{-2} s^{-1}) for seven days, and then dark-adapted for pulse amplitude modulation (PAM) fluorescence analysis. False color images reveal that all six mutants have lower fluorescence emissions compared to the wild ype (WT), with TAM-2 and TAM-4 the most pronounced.

Organization and stoichiometry of pigment-protein complexes

Pigment-protein complexes from WT, TAM-2, and TAM-4 were separated by non-denaturing Deriphat-PAGE following solubilization of thylakoid membranes with dodecyl-β-D-maltoside. All three strains showed similar electrophoretic profiles with five major green bands resolved, as shown in Figure 2a. However, densitometric analysis of the Deriphat-PAGE showed differences in the TAM-2 and TAM-4 profiles with respect to the WT: namely a reduced level of trimeric LHCII and a higher relative abundance of PSII core complexes in both mutants. The level of selected thylakoid proteins was determined by immunotitration and expressed relative to WT on a Chl basis (Figure 2b): the LHCII content was reduced in both TAM mutants, amounting to about 48% of WT values in TAM-2 and about 35% in TAM-4. Moreover, the PSI/PSII ratio was reduced in both mutants, reaching approximately 50% with respect to the WT level (Figure 2c).

The biochemical results were further confirmed through antenna size estimation for both photosystems. The PSII light harvesting cross section was measured by *in vivo* Chl fluorescence induction on cell suspensions in the presence of 3-(3,4-dichlorophenyl)-1,1-dimethylurea, (DCMU) (Figure 3a, Additional file 1: Figure S2). The $T_{2/3}$ of the Chl fluorescence rise is inversely related to the functional antenna size of PSII [30] and was reduced by about 45% in both TAM-2 and TAM-4 mutants with respect to WT (Table 1, Additional file 1: Table S1). For PSI, the estimation of the functional antenna size was carried out by light-induced P700 absorption changes at 705 nm on thylakoid suspensions (Figure 3b). The antenna size was expressed by the $T_{1/2}$ value, namely the time needed to oxidize 50% of the P700 in the sample. Results (Table 1, Additional file 1: Figure S2) show that there was no significant difference in $T_{1/2}$ in the WT and TAM samples, suggesting that the PSI antenna size was unaffected by the reduction of Chl content per cell in the mutants.

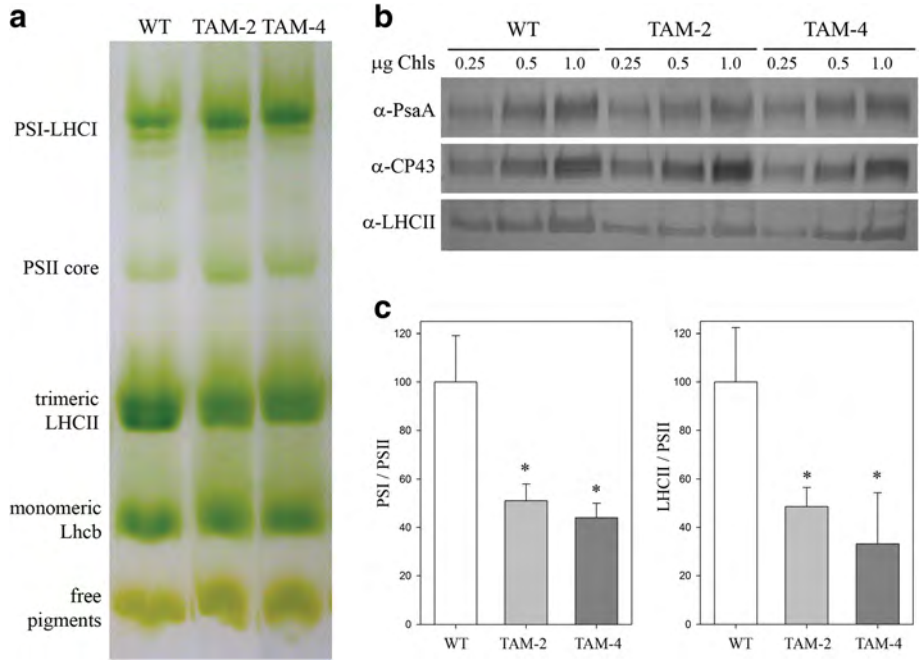

Figure 2 Polypeptide composition of thylakoid membranes from wild-type, TAM-2, and TAM-4 mutants. (a) Thylakoid pigment-protein complexes were separated by nondenaturing Deriphat PAGE upon solubilization with 1% β-DM. Thylakoids corresponding to 25 mg of chlorophylls were loaded in each lane. The composition of each band is indicated. **(b)** Immunoblotting used for the quantification of photosynthetic subunits in the wild-type (WT) and TAM thylakoids. Immunoblot analysis was performed with antibodies directed against individual gene products: LHCII, the major light harvesting complex of PSII; the PSII core subunit PsbC (CP43); the PSI core subunit (PsaA). Thylakoids corresponding to 0.25, 0.5, and 1 µg of Chls were loaded for each sample. All samples were loaded on the same SDS-PAGE slab gel. **(c)** Results of the immunotitration of thylakoid proteins. Data of PSII antenna subunits (left panel) and PSI core subunit (right panel) were normalized to the PSII core amount (PsbB content) and expressed as a percentage of the corresponding wild-type content ± SD. Significantly different values from wild type are marked with an asterisk.

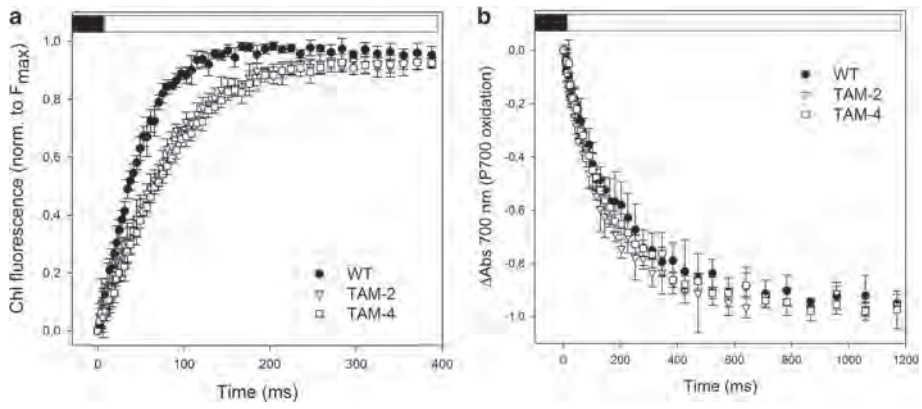

Figure 3 Functional antenna size of PSII and PSI measured in wild-type and mutants TAM-2 and TAM-4. (a) Variable Chl fluorescence was induced with a green light of 15 µmol photons m^{-2} s^{-1}, on dark-adapted cells (about $1.0 \cdot 10^7$ cells/ml) in BG-11 medium supplemented with 50 µM DCMU. The reciprocal of time corresponding to two-thirds of the fluorescence rise ($T_{2/3}$) was taken as a measure of the PSII functional antenna size. **(b)** The kinetics of P700 oxidation (ΔAbs at 705 nm) were measured on thylakoid suspension (75 µg Chl/ml) treated with 50 µM 2,5-dibromo-3-methyl-6-isopropylbenzoquinone (DBMIB) and 1 mM methylviologen, upon illumination with a 10-s pulse of red actinic light (λ =630 nm, 560 µmol photons m^{-2} s^{-1}). Data are expressed as mean ± SD, n =7.

Table 1 Pigment content, maximum quantum yield of PSII, and functional antenna size of wild-type and mutants TAM-2 and TAM-4

Genotype	Chl/cell (pg)	Chl *a/b*	Chl/Car	F_v/F_m	PSII antenna size ($T_{2/3}^{-1} \cdot 10^3$, ms^{-1})	PSI antenna size ($T_{1/2}$, ms)
WT	0.49 ± 0.07^a	2.62 ± 0.02^a	3.43 ± 0.02^a	0.69 ± 0.02^a	18.2 ± 1.4^a	134.3 ± 26.8^a
TAM-2	0.30 ± 0.02^b	3.36 ± 0.03^b	3.07 ± 0.05^b	0.70 ± 0.01^a	10.5 ± 0.5^b	115.4 ± 23.5^a
TAM-4	0.34 ± 0.05^b	3.41 ± 0.03^b	3.18 ± 0.03^b	0.69 ± 0.03^a	9.4 ± 0.5^b	122.7 ± 14.4^a

Data are expressed as mean ± SD. Significantly different values (ANOVA, $P < 0.05$) with respect to the wild-type (WT), within the same column, are marked with different letters.

Light-saturation curve of photosynthesis

To investigate the functional properties of the photosynthetic machinery in the TAM mutants with respect to that in the WT, the efficiency of photosynthetic electron transport was measured for photoautotrophically grown cells. The maximal quantum yield of photosynthesis was found to be the same for the WT and TAM strains (Table 1), thus indicating no limitations in PSII charge separation. The light-saturation curve of photosynthesis was also measured in photoautotrophically grown cells (Figure 4, Additional file 1: Figure S3). The rates of O_2 release were shown to increase as a function of irradiance within the range of light intensities of 0 to 1,200 μmol photons m^{-2} s^{-1}. The increase was linear for WT and TAM mutants at irradiances below 200 μmol photons m^{-2} s^{-1}. The slope of the linear regressions of O_2 yield versus light intensity was 0.34 ± 0.04 and 0.39 ± 0.03 for TAM-2 and TAM-4, respectively, versus 0.28 ± 0.02 for WT cells, thus showing that the quantum yield of photosynthesis for both TAM mutants was significantly higher with respect to the WT. Moreover, this means that truncated antenna size mutants are not affected in the quantum yield of the photosynthetic apparatus. The intensity at which photosynthesis was half-saturated was similar in all the strains tested, at approximately 250 μmol photons m^{-2} s^{-1} (Table 2), and irradiances higher than 1,100 μmol photons m^{-2} s^{-1} did not lead to any further increase in the O_2 yield in either WT or TAM mutants (Figure 4). It is worth noting that no decrease in O_2 production was observed at very high light conditions (>3,000 μmol photons m^{-2} s^{-1}), suggesting that these strains are rather resistant to photo-oxidative stress.

The values of P_{max}, namely the maximum rate of light-induced oxygen evolution (photosynthesis net respiration) was measured at 2,000 μmol photons m^{-2} s^{-1} and was equal to 119 ± 7 μmol O_2 per mg Chl per h in the WT, 165 ± 7 in TAM-2, and 141 ± 12 in TAM-4 cells (Figure 4 and Table 2). Since the rate of O_2 production is normalized on the Chl content of the samples, the value of P_{max} is a measure of the productivity of Chl in the two strains. Interestingly, TAM-2 showed a significantly higher P_{max} than the WT (Table 2).

The dark respiration of the strains was measured and O_2 consumption normalized to the Chl content of the cells: the respiration rates were 6.2 ± 3.0 μmol O_2 per mg Chl per h in the WT, 10.4 ± 4.4 in TAM-2, and 16.4 ± 4.3 in TAM-4 (Table 2); when normalized to a per-cell basis, TAM-2 cells showed a lower (-16%) and TAM-4 a higher (+58%) oxygen consumption with respect to the WT. Consistent with the evidence of a higher respiration rate in the TAM-4 mutant was the value of light-saturated O_2 yield of this strain, which was not significantly higher than that for the WT (125 ± 11 μmol O_2 per mg Chl per h for TAM-4, compared with 114 ± 7 μmol O_2 per mg Chl per h for the WT, see Figure 4b). TAM-2 showed a 40% higher O_2 yield than the WT (Figure 4a).

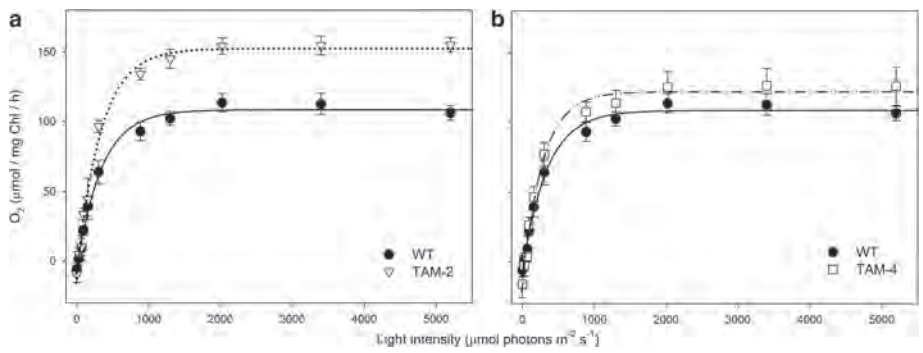

Figure 4 Light-saturation curves of photosynthesis. Curves were obtained with the *C. sorokiniana* wild-type and the TAM-2 **(a)** and TAM-4 **(b)** mutants. The light-saturated P_{max} was 1.5-fold higher in the TAM-2 mutant than in the wild type, suggesting a greater productivity on a per-Chl basis. In the TAM-4 mutant, the light-saturated O_2 yield was not significantly higher than that for the wild type. Data are expressed as mean ± SD, n =4.

Table 2 Photosynthesis and respiration rates

Parameters	WT	TAM-2	TAM-4
Half-saturation intensity (μmol photons m^{-2} s^{-1})	275 ± 48^{a}	259 ± 42^{a}	238 ± 51^{a}
P_{max} (μmol O_2 mg Chl^{-1} h^{-1})	119 ± 7.2^{a}	164 ± 7.3^{b}	141.5 ± 12.0^{a}
Respiration (μmol O_2 mg Chl^{-1} h^{-1})	6.2 ± 3.0^{a}	$10.4 \pm 4.4^{a,b}$	16.4 ± 4.3^{b}
Respiration (fmol oxygen $cell^{-1}$ h^{-1})	$3.1 \pm 1.5^{a,b}$	2.6 ± 1.2^{a}	5.6 ± 1.5^{b}
P_{max}/respiration (relative units)	19.3 ± 9.4^{a}	$15.8 \pm 6.7^{a,b}$	8.6 ± 2.4^{b}

Parameters were measured on a dark-adapted cell suspension of wild-type (WT), TAM-2, and TAM-4, at seven days of photoautotrophic growth in BG-11 medium in low light conditions (70 μmol photons m^{-2} s^{-1}, 25°C). O_2 evolution/consumption were measured with a Clark-type oxygen electrode. Data are expressed as mean ± SD (n >4). Significantly different values (ANOVA, P <0.05) with respect to the WT, within the same row, are marked with different letters.

Cultivation of WT and TAM strains in photobioreactors

The results presented above indicate that the mutant TAM-2 is likely to have enhanced efficiency of light energy conversion and photosynthetic productivity with respect to the WT strain. Therefore, TAM-2 was chosen for detailed analyses of growth rate and biomass productivity. Photoautotrophic growth was monitored over a period of 10 days in a laboratory-scale PBR, a semi-batch cultivation system composed of 1-L glass cylinders illuminated by white light diodes at a light intensity of 450 μmol photons m^{-2} s^{-1}. Cells were cultivated in minimal medium under a day:night cycle of 16:8 h. The system was fed with a flux of air and CO_2, whose relative abundance was regulated by the pH of the medium in order to keep within the range of 6.8 to 7.1.

The TAM-2 culture reached a cell concentration of about $8.3 \cdot 10^8$ cell/ml at day six versus $5.2 \cdot 10^8$ cell/ml in the WT (Figure 5a), with the specific growth rate (μ) for TAM-2 significantly higher than that for the WT (1.39 d^{-1} for TAM-2 and 1.28 d^{-1} for WT, Table 3). Moreover, the mutant showed a higher mean biomass productivity, equal to 380 mg per liter per day, that was significantly higher (+32%) than the corresponding value of 290 mg per liter per day for the WT (Table 3). In comparison, TAM-4 did not show any enhancement in either growth rate (1.30 d^{-1}) or biomass productivity (300 mg per liter per day) over the WT (Figure 5b, Table 3). Further upscaling of the cultures was performed in outdoor conditions. To this aim, the three genotypes were cultivated in triplicate within 7-L hanging bags exposed to full natural light during September 2012. The temperature and light conditions, reported in Additional file 1: Figure S5, ranged between 15 and 22°C and between 500 and 2,200 μmol photons m^{-2} s^{-1}. Figure 6 and Table 3 show that the final cellular concentration, the specific growth rate, and the daily biomass productivity were all significantly higher in the TAM-2 culture versus WT and TAM-4.

Discussion

The potential use of microalgal biomass for energy production has gained increasing attention in recent years, due to the many advantages over terrestrial crops [31]. However, algal biofuels are still more expensive than traditional fossil fuels because of a number of biological limitations [32]: among them is the inefficient conversion of solar energy into biomass under mass culture conditions. More than 80% of absorbed photons can thus be wasted at moderate to high irradiance, thus reducing photon use efficiencies and photosynthetic productivity [33]

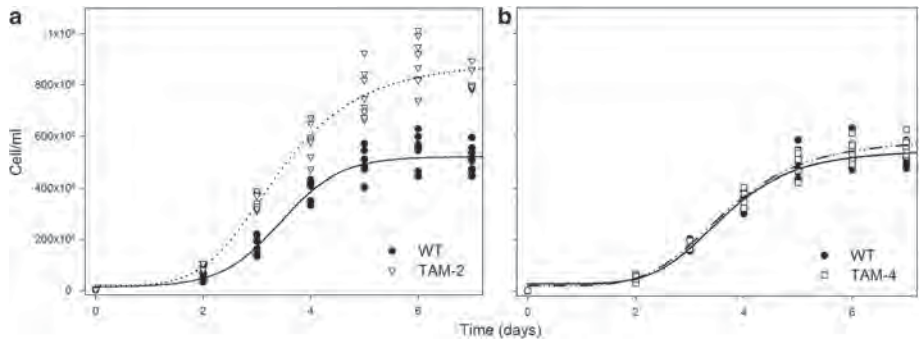

Figure 5 Growth curves of wild-type, TAM-2, and TAM-4 mutants under autotrophic conditions. Wild-type was grown with TAM-2 **(a)** or TAM-4 **(b)** and the cell content was measured once a day. All experiments were performed in 1-L cylinders, illuminated with 450 μmol photons m^{-2} s^{-1}, 25°C. Growths were performed in a semi-batch system fed with air/CO_2 mix; the CO_2 supply was modulated in order to keep the pH of the medium always below 7.1.

Table 3 Growth parameters of wild-type, TAM-2, and TAM-4, cultured in air/CO_2 bubbling systems

	Lab-scale, indoor PBR		Outdoor PBR	
Genotype	Mean increase of biomass (g L^{-1} day^{-1})	μ (day^{-1})	Mean increase of biomass (g L^{-1} day^{-1})	μ (day^{-1})
WT	0.29 ± 0.01	1.28 ± 0.05	0.22 ± 0.02	1.25 ± 0.04
TAM-2	0.38 ± 0.01*	1.39 ± 0.03*	0.28 ± 0.03*	1.33 ± 0.04*
TAM-4	0.30 ± 0.02	1.30 ± 0.03	0.18 ± 0.03	1.25 ± 0.06

Biomass increase was measured in both lab-scale and outdoor photobioreactors, by the determination of dry biomass accumulated after the cultivation period, divided by the number of days of cultivation. μ, the specific growth rate, was calculated from the slope of the logarithmic cell concentration curve. Data are expressed as mean ± SD, n = 6. Significant different values (Student's *t*-test, $P < 0.05$) are marked with an asterisk.

due to high optical density of the cell culture and the generation of a steep light gradient. Photosynthetic productivity can be improved with the design of new reactors with high surface-to-volume ratio [7] and the isolation of new strains with engineered optical properties.

In searching for mutants with improved optical properties we chose *Chlorella sorokiniana*, a robust species with a high market interest that offers the advantage of being able to carry out productivity tests at an industrial level. Although a reliable DNA transformation method has recently been developed for *C. sorokiniana* (Barbi T, Hiegle N, and Purton S, unpublished data), the targeted manipulation of specific genes such as *TLA1* [34] or *ARSA1* ([35]) that are known to be associated with antenna size, is not yet feasible for this species. Instead, a forward-genetic approach was adopted that involved random mutagenesis and screening for an altered fluorescence phenotype. The maximal level of fluorescence upon a pulse of saturating light is positively related to the number of Chl active in energy transfer to the PSII and is thus indicative of the antenna size of the strain [27]. Of the six putative mutants recovered from a screen of

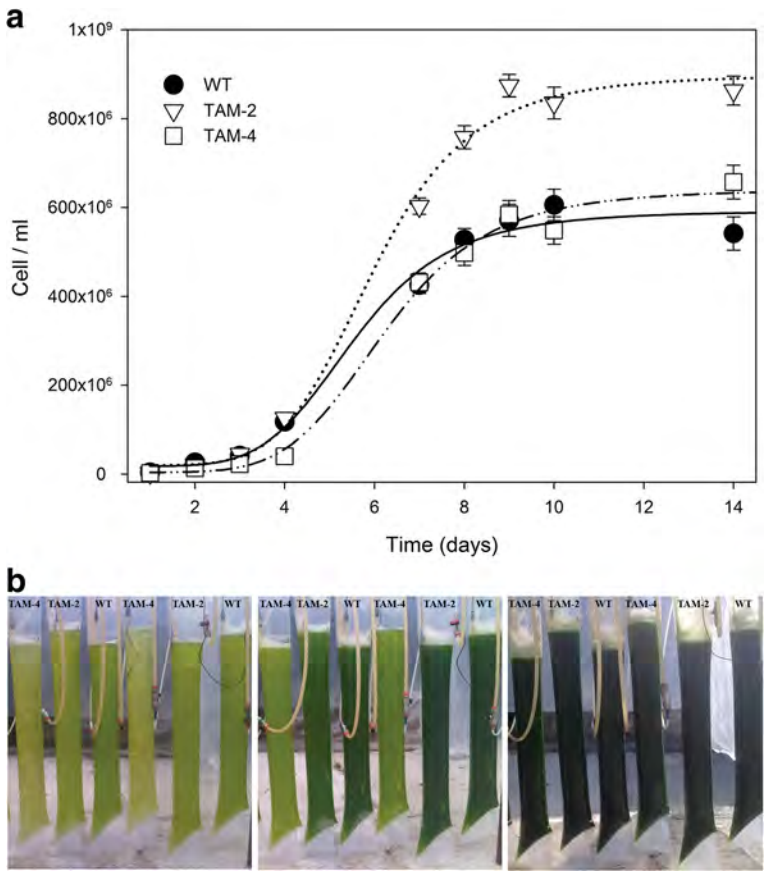

Figure 6 Growth curves of wild-type, TAM-2, and TAM-4 mutants in outdoor photobioreactor. (a) Time-dependent course of cell concentration. All experiments were performed in 7-L hanging bag reactors, fed with air/CO_2 mix modulated in order to keep the pH of the medium always below 7.1. Two runs with nine reactors, each operated in parallel, were prepared. Data are expressed as mean ± SD, n =9. **(b)** Picture of the outdoor plant with 7-L reactors, showing growth stage of WT and TAM after two (left), four (center), and eight (right) days from initial inoculum.

about 3,000 colonies, TAM-2 and TAM-4 showed a significant defect in PSII antenna size, as confirmed by the higher Chl *a*/*b* ratio. None of the six TAM mutants showed a reduced PSI antenna as expected, since the screening method using fluorescence induction at room temperature would not be selective for PSI antenna mutants.

The reduction in Chl content was similar in TAM-2 and TAM-4 (a reduction of about 39% with respect to WT Chl content/cell), and in both strains, the reduction was coupled to a modulation in the composition of the pigment-binding complexes with LHCII decreased to a similar extent (-49% in TAM-2, -38% in TAM-4). In contrast to the LHCII reduction, the amount of PSII per cell was found to be at WT levels, whereas the content of PSI was severely reduced, and to the same extent in both mutant strains (-34% compared to WT). Therefore, the two mutants, in addition to a reduced LHCII antenna content, also have a reduced content in PSI per cell, resulting in a photosynthetic phenotype resembling that of chloroplasts acclimated to excess light conditions [36].

Previous studies of *Chlamydomonas reinhardtii* chlorophyll-deficient mutants showed that a pale green phenotype could be due to different reasons rather than mutation affecting Lhcb-encoding genes, namely: mutations resulting in constitutive activation of NAB1, a repressor of the Lhc translation system in the cytoplasm [37], impairment in the mechanisms of protein import into the chloroplast [35] or Lhcb insertion in the thylakoids [27], mutations in Chl [35,38], or carotenoid biosynthesis pathways [39].

The observation that all six TAM mutants are resistant to high light (Figures 4 and 5) suggests that rather than defects in pigment biosynthesis, where lesions induce photosensitivity [40,41], mutations in the TAM lines likely affect chloroplast biogenesis steps such as those mediated by NAB1, ARSA1, or cpSRP [35,37,42]. Future work on the molecular analysis of such genes in the TAM mutants and complementation with the WT gene will confirm the causal link between antenna size and photosynthetic performance, and provide further insight into the basis of the phenotype. Furthermore, we cannot exclude that the lower PSI/PSII ratio derives from concomitant mutation(s) affecting their biosynthesis independently, but it is more likely that reduction of the PSI-LHCI complex is a secondary effect of PQ oxidation due to a decrease in PSII abundance/decrease in antenna size [43], as suggested from the unaffected stoichiometry between PSI and LHCI moieties of the complex (Figure 3b).

The measures of fluorescence induction in cells infiltrated with DCMU confirmed that, among the mutants, TAM-2 and TAM-4 have a marked reduction of the PSII antenna size as compared to WT, while PSI antenna size was unaffected.

Physiological characterization of WT and TAM-2 showed that photosynthetic yield was significantly enhanced in TAM-2. The linear phase of the light-saturation curve of O_2 yield (between 0 and 300 μmol photons m^{-2} s^1) showed the same slope, namely a similar quantum yield of photosynthesis in both strains under limiting light conditions, indicating that the decrease of antenna content and the differential reduction of the two photosystems did not negatively affect the efficiency of the photosynthetic apparatus. However, the P_{max} in TAM-2 was about 40% larger than in WT at saturating irradiances, indicating a higher productivity in high light. These results were consistent with the report that the *tla1* mutant of *C. reinhardtii* with a truncated antenna size has enhanced P_{max} [27]. Also, the *tla3* mutant showed enhanced photosynthetic productivity at saturating irradiances and a 60% reduction in the PSII functional antenna size caused by a defect in the insertion of chloroplast pre-proteins in thylakoids [42].

One might wonder if the depletion of antenna proteins and of photosystems could affect the photoautotrophic growth of strains. Under high irradiance, chloroplasts are particularly susceptible to photoinhibition [44], a phenomenon which impairs photosynthetic productivity. In higher plants, an extreme reduction in LHC proteins is obtained with the *ch1* mutation [45], in which assembly of LHC is prevented due to a lack of Chl *b*. Thylakoids isolated from *ch1* plants produce far more $^1O_2$ with respect to that from WT plants, and are more sensitive to photooxidation, thus implying that functional LHC complexes are essential for photoprotection [18,46]. Since LHC antenna proteins have a central role in photoprotection, their depletion in the TAM mutants could have reduced the photochemical yield and increased photoinhibition. However, the light-saturation curve of photosynthesis showed no decline of oxygen evolution even at very high light intensity (5,000 μmol photons m^{-2} s^{-1}). Moreover, the enhancement of photosynthetic yield by high light in TAM-2 with respect to WT suggests that phototolerance is not significantly affected. We conclude that a mutation that halves the LHC/PSII ratio and decreases the PSI content per cell does not result in photo-oxidative stress of *C. sorokiniana* cells under the growth conditions tested.

All the biochemical and spectroscopic analyses indicate that the TAM-2 is a good candidate for improved performance in a PBR system. To test this possibility, cell growth rates and biomass yield were measured in the long-term cultivation of dense algal suspensions under high irradiance. During seven days of growth TAM-2 showed a significant increase of productivity with respect to WT, both as biomass increment per day and maximal level of biomass reached at the end of the test period. The

increased light use efficiency of TAM-2 was maintained upon further up-scaling of the PBR to 7 liters and 16 cm diameter exposed to full sunlight and natural temperature. These findings suggest that the improved productivity of such reduced antenna mutants is translatable from the lab to the industrial setting. Furthermore, it was assessed that the mutation procedure did not significantly affect the capacity of strains to undergo variable light/temperature conditions typical of outdoor biomass production.

A possible mechanism underlying the enhancement of biomass productivity is the thermal dissipation of ^{1}Chl* in the bulk antenna, enhanced upon triggering the mechanisms of non-photochemical quenching (NPQ). A recent study on acclimation of *C. reinhardtii* to high light [47] showed that algal growth in high light unavoidably results in a reduction in the efficiency of light energy conversion into biomass, due to dissipation of a large fraction of photons absorbed as heat. Thus, unlike higher plants, in which the amplitude of NPQ is proportional to the actinic light intensity, algae dramatically upregulate their ability to perform NPQ even with moderate irradiances, thus leading to a strong reduction of photosynthetic efficiency [47]. The enhanced photosynthetic efficiency of TAM-2 suggested that this strain might be depleted in the heat dissipation response, thus showing an improved light energy conversion. Upon prolonged illumination of cells with the same intensity used for growth in lab-scale PBRs, the amplitude of NPQ at steady state was similar in WT and the TAM mutants. We conclude that the differential photosynthetic light use efficiency of WT versus TAM-2 was not due to differences in NPQ activity. It must be noted, however, that the NPQ amplitude observed with *Chlorella* was far below the level reported in *Chlamydomonas* [47], thus making any effect of NPQ level on productivity of limited impact.

From the characterization of TAM-2 strain we conclude that selection of strains by the reduction of optical cell density is a viable strategy to improve the light diffusion properties of the mass culture and to yield a higher productivity.

One question, however, is why reduction of both Chl content per cell and PSII antenna size did not improve photosynthetic productivity in TAM-4. In fact, the mutant showed a productivity far lower than TAM-2, consistent with the low P_{max} value measured, and yet a reduced LHC/PSII was observed as in TAM-2. One hypothesis is that imbalance in the PSII/PSI ratio could affect the photosynthetic electron transport rate [48]. However, the PSII/PSI ratio was increased by the same extent in both the TAM-2 and TAM-4 mutants, suggesting that the differential growth phenotype of TAM-2 versus TAM-4 is unlikely to be due to limitations in PSI and PSII electron transport rate. Since TAM-2 and TAM-4 have a similar Chl content per cell and PSII antenna size, their different performance implies that reducing antenna size and Chl per cell is not enough to obtain a better light use efficiency in dense cultures. This is consistent with results by [49] reporting on two low Chl/cell mutants of *Cyclotella sp.* which did not gain in productivity with respect to WT when grown in semi-continuous, laboratory-scale PBRs. A possible explanation can be proposed on the basis of the increased respiration rate of TAM-4 with respect to TAM-2. Mutants generated by random UV or chemical mutagenesis are likely to induce multiple mutations in any single cell. Some of these mutations could negatively affect the metabolic network of the cell, thus causing slower growth. A lower LHC content *per se* had no consequences on the respiration capacity of the cells [27]. Thus, an increased respiration rate in TAM-4 cells can be attributed to additional mutations, which adversely impact cell metabolism. Therefore, the distinctive parameter that needs to be assessed, beyond lower Chl content per cell and reduced PSII antenna size, is the P_{max}/respiration rate, which indeed was not significantly affected in TAM-2 cells, but was reduced by more than 50% in TAM-4. Thus, a full photosynthetic characterization of mutants obtained by chemical/UV mutagenesis is needed to ensure that mutants with a truncated antenna are not affected in their photosynthetic performance in ways other than reduced LHC content. The concept is consistent with that reported by the researchers of [27], who performed a screening of over 6,000 *C. reinhardtii* colonies from a library obtained through DNA insertional mutagenesis. Although the initial screen resulted in 129 putative truncated antenna mutants, only one showed an improvement in photosynthetic efficiency.

Further molecular characterization of the TAM mutants would allow the identification of genes which modulate the LHC content of algal cells. Indeed, new genome sequencing technologies provide an opportunity to identify such sites of mutation [50], and desired traits might then be transferred to other species of interest to the algal biotechnology industry, for CO_2 mitigation processes or production of biomass, biofuels, or high-value products [32,51-54].

Conclusions

Our results show that the modulation of antenna size to improve light penetration and enhance photosynthetic yield is a promising strategy in the development of domesticated microalgal strains for mass culture. However, it is important to consider that the optical path length of our growth facilities was short and likely to be significantly increased in industrial-scale outdoor PBRs, thus increasing the light gradient effect and further favoring the growth rate of TAM-2 with respect to WT. Furthermore, with this round of mutagenesis we selected only

six lines whose maximal reduction in LHC antenna proteins was 40% with respect to WT. Calculations suggest that a maximal P_{max} could be achieved in algal strains with Chl content/cell below 20% [22]; thus, even "paler" mutants than TAM-2 could further increase the photosynthetic performance in mass culture.

Methods

Cell cultivation

Chlorella sorokiniana 7-11-05 [55] was obtained from the UTEX Culture Collection (University of Texas, Austin, TX [http://web.biosci.utexas.edu/utex/]) as strain UTEX1230; maintained on BG-11 agar plates [56] and grown photoautotrophically in BG-11 medium in flasks at 25°C, 70 μmol photons m^{-2} s^{-1}, with a photoperiod of 16:8 h light:dark. Irradiance was provided by warm-white fluorescent lamps. For physiological measurements, cultures were harvested during the logarithmic growth phase (about $1\text{-}3 \cdot 10^7$ cells ml^{-1}).

Isolation of mutants

10 ml of a mid-log culture (about 10^8 cells) was subjected to UV irradiation using a 6-W UV bulb (254 nm), under predetermined conditions that yielded a 10% survival rate. The cells were left to recover in the dark for 2 h to prevent photoreactivation followed by plating at 100-fold dilution on acetate-containing (TAP) medium [57]. Single colonies appeared after seven days and approximately 3,000 were tooth-picked to fresh TAP medium. Mutants with low Chl fluorescence were identified by spotting cultures of each onto both TAP and minimal media; allowing growth in the light for seven days; dark-adapting for 10 min, and directly measuring *in vivo* fluorescence using a FluorCam 700MF (Photon Systems Instruments, Brno, Czech Republic). The F_{max} value was recorded following an 800-ms flash of saturating white light and displayed as a false-color image for each spot [27]. Strains still capable of phototrophic growth but showing significantly reduced fluorescence were retained for further analysis.

Cell count and pigment analysis

Cell density was measured using an improved Neubauer hemocytometer. Pigments were extracted from thylakoids with 85% acetone buffered with Na_2CO_3 or from intact cells with dimethylformamide. The supernatant of each sample was recovered after centrifugation (10 min at 15,000 g, 4°C); then the pigments were separated and quantified by HPLC [58].

Measurements of photosynthetic activity

The oxygen evolution activity of the cultures was measured at 25°C with a Clark-type O_2 electrode (Hansatech, Norfolk, UK), upon illumination with light from a halogen lamp (Schott, Germany). Samples of 2-ml cell suspension, $5 \cdot 10^6$ cell ml^{-1}, were loaded into the oxygen electrode chamber. $NaHCO_3$ (3 mM final concentration) was added to the cell suspension prior to the O_2 evolution measurements to ensure that electron transport was not limited by the carbon supply.

Isolation of thylakoid membranes

The cells were harvested by centrifugation at 1,500 g for 5 min at 4°C. The samples were resuspended with ice-cold grinding buffer (0.35 M sorbitol, 50 mM Tricine pH 7.9, 10 mM NaCl, 5 mM $MgCl_2$, 0.5% fat-free milk powder, 0.5 ml l^{-1} Antifoam A silicon polymer (Sigma), 1 mM aminocaproic acid, 1 mM aminobenzamidine, and 100 mM phenylmethylsulfonyl fluoride) at a final concentration of 10^8 cell ml^{-1}, and disrupted by passing three times through an ice-cold cell disruptor (Constant Systems, Northants, UK) at 1.48 kbar. The homogenate was then centrifuged at 1,500 g for 5 min, and the supernatant was further centrifuged at 30,000 g for 20 min at 4°C. The thylakoid membrane pellet was resuspended in a buffer containing 50% (w/v) glycerol, 20 mM Tricine pH 7.9, 10 mM NaCl, 5 mM $MgCl_2$, 1 mM aminocaproic acid, 1 mM aminobenzamidine, and 100 mM phenylmethylsulfonyl fluoride, and immediately used for analysis, or frozen in liquid nitrogen and stored at -80°C.

Gel electrophoresis and immunoblotting

SDS-PAGE analysis was performed with the Tris-Tricine buffer system [59]. Non-denaturing Deriphat-PAGE was performed following the method developed in [60] with the modification described in [36]. Thylakoids concentrated at 1 mg/ml Chls were solubilized with a final 1% β-DM, and 20 μg of Chls were loaded in each lane. For immunotitration, thylakoid samples corresponding to 0.25, 0.5, 0.75, and 1.0 μg of Chls were loaded for each sample and electroblotted on nitrocellulose membranes. Proteins were detected with alkaline phosphatase-conjugated antibody, according to [61]. The signal amplitude was quantified (n =3) using GelPro 3.2 software (Bio-Rad). In order to avoid any deviation between different immunoblots, samples were compared only when loaded on the same gel.

In vivo Chl fluorescence analysis

Fluorescence induction kinetics were recorded with a home-built apparatus, previously described [62]. For measurements of PSII functional antenna size, variable fluorescence was induced with a green light of 15 μmol photons m^{-2} s^{-1} on dark-adapted cells (about $1.0 \cdot 10^7$ cells/ml) in BG-11 medium supplemented with 50 μM DCMU. The F_0 values were subtracted from each curve, and the fluorescence inductions were normalized to the same F_v in order to estimate antenna size more accurately. The reciprocal of time corresponding to two-thirds of the fluorescence rise ($T_{2/3}$) was taken as a measure of the PSII functional

antenna size [30]. PSII function during photosynthesis was measured through Chl fluorescence on cell suspensions at room temperature with a PAM 101 fluorimeter (Heinz-Walz, Effeltrich, Germany), with a saturating light pulse of 4500 μmol photons m^{-2} s^{-1}, 0.6 s, and white actinic light of 500 μmol photons m^{-2} s^{-1}, supplied by a KL1500 halogen lamp (Schott). The NPQ values were calculated according to [63].

Analysis of P700 redox state

Spectroscopic measurements were performed on the thylakoids using an LED spectrophotometer (JTS-10, Bio-Logic Science Instruments, France) in which absorption changes are sampled by weak monochromatic flashes (10-nm bandwidth) provided by light emitting diodes (LEDs). The relative antenna size of PSI was determined by analyzing time courses of P700 photo-oxidation upon illumination of the thylakoid suspension with weak far-red light (12 μmol photons m^{-2} s^{-1}). The reaction mixture contained 20 mM Tricine pH 7.9, 10 mM NaCl, 5 mM $MgCl_2$, 50 μM 2,5-dibromo-3-methyl-6-isopropylbenzoquinone (DBMIB), 1 mM methylviologen, and thylakoid membranes corresponding to 75 μg Chls ml^{-1}.

Growth analysis/indoor PBR

The indoor growth experiments were performed at 25°C in home-built indoor photobioreactors (PBRs), composed of glass cylinders with a maximum light path of 8 cm and a working volume of 1 L each. The cultures were continuously mixed with a mixture composed of air and CO_2. The ratio of compressed air and CO_2 was automatically adjusted to keep the pH of the medium below 7.1. Each autotrophic batch cultivation was carried out in duplicate. The medium, cylinders and tubes were sterilized in an autoclave for 20 min at 121°C in order to prevent any contamination. Illumination was provided by a panel of warm-white LEDs, and the microalgae were exposed to an irradiance of 450 μmol photons m^{-2} s^{-1} with a photoperiod of 16:8 h light:dark. The parameters determined to monitor cell growth were cell number and dry biomass weight, for which the washed cell pellets were dried overnight in a lyophilizer.

Growth analysis/outdoor PBR

The outdoor growth experiments were performed in a PBR located in Sommacampagna (Verona, Italy) during September 2012. The plant consisted of nine cylindrical hanging bags with a diameter of around 16 cm and a reactor volume of 7 L. The gas flow rate was supplied through a perforated plastic hose at the bottom of the reactor, which allowed efficient intermixing of the cell suspension. The CO_2 flow rate was continuously adjusted by a controller unit and added to the air flow in order to maintain the pH of the medium below 7.1. The average light intensity and temperature measured during the course of the experiment are displayed in Additional file 1: Figure S5.

Additional file

Additional file 1: Figure S1. Schematic illustration of the mutagenesis and screening strategy used to isolate antenna mutants. **Figure S2.** Functional antenna size of PSII (A, B) and PSI (C, D) measured in wild-type and TAM mutants. See methods for details.. Data are expressed as mean ± SD, n =7. **Figure S3.** Light-saturation curves of photosynthesis. Curves were obtained with the *C. sorokiniana* wild-type and TAM mutants. Data are expressed as mean ± SD, n =4. **Figure S4.** Kinetics of formation and relaxation of photoprotective energy dissipation in wild-type and TAM mutants. See methods for details. Symbols and error bars show means ± SD (n =3). **Figure S5.** Daily mean irradiance on the reactors' surface (left panel) and atmospheric temperature (right panel), measured during the outdoor experiments. **Table S1.** Pigment composition of wild-type and TAM mutants. Data are expressed as mean ± SD. Significantly different values (ANOVA, P <0.05) with respect to the wild type, within the same column, are marked with different letters. **Table S2.** HPLC analysis of carotenoid composition of wild-type and TAM mutants. Data are expressed as mean ± SD and normalized to 100 Chls. Significantly different values (ANOVA, P <0.05) with respect to the wild type, within the same column, are marked with different letters. **Table S3.** Relative abundance of pigment-protein complex in the wild-type and TAM mutants. Amount of pigment-protein complexes per cell were calculated by densitometric analysis of native PAGE and by Chls content per cell, and expressed as a percentage of the corresponding wild-type values. Data are expressed as means ± standard deviation (n =3). Significantly different values (ANOVA, P <0.05) with respect to the wild type, within the same column, are marked with different letters.

Abbreviations

β-DM: dodecyl-β-D-maltoside; ^{1}Chl*: singlet excited state of Chl; Chl: chlorophylls; DCMU: 3-(3,4-dichlorophenyl)-1,1-dimethylurea; DBMIB: 2,5-dibromo-3-methyl-6-isopropylbenzoquinone; DW: dry weight; LHCI/II: light harvesting complex of PSI/II; NPQ: non-photochemical quenching; PBR: photobioreactor; PQ: plastoquinone; PSI/II: photosystem I/II; P700: reaction center of PSI; ROS: reactive oxygen species; TAM: truncated antenna mutant; WT: wild-type.

Competing interests

The authors declare that they have no competing interests.

Authors' contributions

JS performed identification and isolation of all the genotypes used; LD and SC carried out the biochemical and photosynthetic characterization of strains and drafted the manuscript; LS and MB carried out the outdoor PBR test; SP and RB conceived the study, participated in its design and coordination, and edited the manuscript. All authors read and approved the final manuscript.

Acknowledgements

Financial support for this work was provided by the Marie Curie Actions Initial Training Networks ACCLIPHOT (PITN-GA-2012-316427). LS thanks Fondo Sociale Europeo 2007-2013 - Reg. 1081/2006. Asse IV "Capitale Umano" Regione Veneto for financial support. JS was supported by a studentship from the UK's Biotechnology and Biological Sciences Research Council.

Author details

[1]Dipartimento di Biotecnologie, Università di Verona, Strada Le Grazie, Verona 15-37134, Italy. [2]Institute of Structural and Molecular Biology, University College London, London WC1E 6BT, UK.

Received: 25 June 2014 Accepted: 7 October 2014
Published online: 21 October 2014

References

1. Wijffels RH, Barbosa MJ: **An outlook on microalgal biofuels.** *Science* 2010, **329:**796–799.
2. Lee DH: **Algal biodiesel economy and competition among bio-fuels.** *Bioresour Technol* 2011, **102:**43–49.
3. Chisti Y: **Biodiesel from microalgae beats bioethanol.** *Trends Biotechnol* 2008, **26:**126–131.
4. Douskova I, Doucha J, Livansky K, Machat J, Novak P, Umysova D, Zachleder V, Vitova M: **Simultaneous flue gas bioremediation and reduction of microalgal biomass production costs.** *Appl Microbiol Biotechnol* 2009, **82:**179–185.
5. Putt R, Singh M, Chinnasamy S, Das KC: **An efficient system for carbonation of high-rate algae pond water to enhance CO_2 mass transfer.** *Bioresour Technol* 2011, **102:**3240–3245.
6. de Bashan LE, Trejo A, Huss VA, Hernandez JP, Bashan Y: ***Chlorella sorokiniana* UTEX 2805, a heat and intense, sunlight-tolerant microalga with potential for removing ammonium from wastewater.** *Bioresour Technol* 2008, **99:**4980–4989.
7. Munkel R, Schmid-Staiger U, Werner A, Hirth T: **Optimization of outdoor cultivation in flat panel airlift reactors for lipid production by *Chlorella vulgaris*.** *Biotechnol Bioeng* 2013, **110:**2882–2893.
8. Scott SA, Davey MP, Dennis JS, Horst I, Howe CJ, Lea-Smith DJ, Smith AG: **Biodiesel from algae: challenges and prospects.** *Curr Opin Biotechnol* 2010, **21:**277–286.
9. Ben-Amotz A: **Industrial production of microalgal cell-mass and secondary products: major industrial species *Dunaliella*.** In *Handbook of Microalgal Culture: Biotechnology and Applied Phycology*. Edited by Richmond A. Oxford, UK: Blackwell Publishing; 2007.
10. Stephenson PG, Moore CM, Terry MJ, Zubkov MV, Bibby TS: **Improving photosynthesis for algal biofuels: toward a green revolution.** *Trends Biotechnol* 2011, **29:**615–623.
11. Weyer KM, Bush DR, Darzins A, Willson BD: **Theoretical maximum algal oil production.** *Bioenerg Res* 2010, **3:**204–213.
12. Illman AM, Scragg AH, Shales SW: **Increase in *Chlorella* strains calorific values when grown in low nitrogen medium.** *Enzyme Microb Technol* 2000, **27:**631–635.
13. Rodolfi L, Chini Zittelli G, Bassi N, Padovani G, Biondi N, Bonini G, Tredici MR: **Microalgae for oil: strain selection, induction of lipid synthesis and outdoor mass cultivation in a low-cost photobioreactor.** *Biotechnol Bioeng* 2009, **102:**100–112.
14. Nelson N, Ben Shem A: **The complex architecture of oxygenic photosynthesis.** *Nature* 2004, **5:**1–12.
15. Croce R, Van Amerongen H: **Light-harvesting in photosystem I.** *Photosynt Res* 2013, **116:**153–166.
16. Van Amerongen H, Croce R: **Light-harvesting in photosystem II.** *Photosynt Res* 2013, **116:**251–263.
17. Horton P, Ruban AV, Walters RG: **Regulation of light harvesting in green plants.** *Annu Rev Plant Physiol Plant Mol Biol* 1996, **47:**655–684.
18. Havaux M, Dall'Osto L, Bassi R: **Zeaxanthin has enhanced antioxidant capacity with respect to all other xanthophylls in Arabidopsis leaves and functions independent of binding to PSII antennae.** *Plant Physiol* 2007, **145:**1506–1520.
19. Dall'Osto L, Holt NE, Kaligotla S, Fuciman M, Cazzaniga S, Carbonera D, Frank HA, Alric J, Bassi R: **Zeaxanthin protects plant photosynthesis by modulating chlorophyll triplet yield in specific light-harvesting antenna subunits.** *J Biol Chem* 2012, **287:**41820–41834.
20. Alboresi A, Dall'Osto L, Aprile A, Carillo P, Roncaglia E, Cattivelli L, Bassi R: **Reactive oxygen species and transcript analysis upon excess light treatment in wild-type *Arabidopsis thaliana* vs a photosensitive mutant lacking zeaxanthin and lutein.** *BMC Plant Biol* 2011, **11:**62.
21. Melis A: **Solar energy conversion efficiencies in photosynthesis: Minimizing the chlorophyll antennae to maximize efficiency.** *Plant Sci* 2009, **177:**272–280.
22. Formighieri C, Franck F, Bassi R: **Regulation of the pigment optical density of an algal cell: filling the gap between photosynthetic productivity in the laboratory and in mass culture.** *J Biotechnol* 2012, **162:**115–123.
23. Ort DR, Zhu XG, Melis A: **Optimizing antenna size to maximize photosynthetic efficiency.** *Plant Physiol* 2011, **155:**79–85.
24. Powles SB: **Photoinhibition of photosynthesis induced by visible light.** *Annu Rev Plant Physiol Plant Mol Biol* 1984, **35:**14–44.
25. Neale PJ, Melis A: **Algal photosynthetic membrane complexes and the photosynthesis-irradiance curve: a comparison of light-adaptation response in *Chlamydomonas reinhardtii* (Chlorophyta).** *J Phycol* 1986, **22:**531–538.
26. Nakajima Y, Ryohei U: **Improvement of photosynthesis in dense microalgal suspension by reduction of light harvesting pigments.** *J Appl Phycol* 1997, **9:**503–510.
27. Polle JEW, Kanakagiri SD, Melis A: **tla1, a DNA insertional transformant of the green alga *Chlamydomonas reinhardtii* with a truncated light-harvesting chlorophyll antenna size.** *Planta* 2003, **217:**49–59.
28. Sorokin C, Krauss RW: **Maximum growth rates of *Chlorella* in steady-state and in synchronized cultures.** *Proc Natl Acad Sci* 1959, **45:**1740–1744.
29. Kessler E: **Upper limits of temperature for growth in *Chlorella* (Chlorophyceae).** *Plant Syst Evol* 1985, **151:**67–71.
30. Malkin S, Armond PA, Mooney HA, Fork DC: **Photosystem II photosynthetic unit sizes from fluorescence induction in leaves. Correlation to photosynthetic capacity.** *Plant Physiol* 1981, **67:**570–579.
31. Day JG, Slocombe SP, Stanley MS: **Overcoming biological constraints to enable the exploitation of microalgae for biofuels.** *Bioresour Technol* 2012, **109:**245–251.
32. Jones CS, Mayfield SP: **Algae biofuels: versatility for the future of bioenergy.** *Curr Opin Biotechnol* 2012, **23:**346–351.
33. Neidhardt J, Benemann JR, Zhang LP, Melis A: **Photosystem-II repair and chloroplast recovery from irradiance stress: relationship between chronic photoinhibition, light-harvesting chlorophyll antenna size and photosynthetic productivity in *Dunaliella salina* (green algae).** *Photosynth Res* 1998, **56:**175–184.
34. Mitra M, Kirst H, Dewez D, Melis A: **Modulation of the light-harvesting chlorophyll antenna size in *Chlamydomonas reinhardtii* by TLA1 gene over-expression and RNA interference.** *Philo Trans Royal Soc B-Biol Sci* 2012, **367:**3430–3443.
35. Formighieri C, Cazzaniga S, Kuras R, Bassi R: **Biogenesis of photosynthetic complexes in the chloroplast of *Chlamydomonas reinhardtii* requires ARSA1, a homolog of prokaryotic arsenite transporter and eukaryotic TRC40 for guided entry of tail-anchored proteins.** *Plant J* 2012, **73:**850–861.
36. Havaux M, Dall'Osto L, Cuine S, Giuliano G, Bassi R: **The effect of zeaxanthin as the only xanthophyll on the structure and function of the photosynthetic apparatus in *Arabidopsis thaliana*.** *J Biol Chem* 2004, **279:**13878–13888.
37. Beckmann J, Lehr F, Finazzi G, Hankamer B, Wobbe L, Kruse O: **Improvement of light to biomass conversion by de-regulation of light-harvesting protein translation in *Chlamydomonas reinhardtii*.** *J Biotechnol* 2009, **142:**70–77.
38. Dall'Osto L, Piques M, Ronzani M, Molesini B, Alboresi A, Cazzaniga S, Bassi R: **The *Arabidopsis nox* mutant lacking carotene hydroxylase activity reveals a critical role for xanthophylls in photosystem I biogenesis.** *Plant Cell* 2013, **25:**591–608.
39. Tran PT, Sharifi MN, Poddar S, Dent RM, Niyogi KK: **Intragenic enhancers and suppressors of phytoene desaturase mutations in *Chlamydomonas reinhardtii*.** *PLoS One* 2012, **7:**e42196.
40. Baroli I, Gutman BL, Ledford HK, Shin JW, Chin BL, Havaux M, Niyogi KK: **Photo-oxidative stress in a xanthophyll-deficient mutant of *Chlamydomonas*.** *J Biol Chem* 2004, **279:**6337–6344.
41. Niyogi KK, Bjorkman O, Grossman AR: **The roles of specific xanthophylls in photoprotection.** *Proc Natl Acad Sci U S A* 1997, **94:**14162–14167.
42. Kirst H, Garcia-Cerdan JG, Zurbriggen A, Ruehle T, Melis A: **Truncated photosystem chlorophyll antenna size in the green microalga *Chlamydomonas reinhardtii* upon deletion of the TLA3-CpSRP43 gene.** *Plant Physiol* 2012, **160:**2251–2260.
43. Pfannschmidt T, Nilsson A, Allen JF: **Photosynthetic control of chloroplast gene expression.** *Nature* 1999, **397:**625–628.
44. Barber J, Andersson B: **Too much of a good thing - light can be bad for photosynthesis.** *Trends Biochem Sci* 1992, **17:**61–66.
45. Espineda CE, Linford AS, Devine D, Brusslan JA: **The AtCAO gene, encoding chlorophyll a oxygenase, is required for chlorophyll b synthesis in *Arabidopsis thaliana*.** *Proc Natl Acad Sci U S A* 1999, **96:**10507–10511.
46. Dall'Osto L, Cazzaniga S, Havaux M, Bassi R: **Enhanced photoprotection by protein-bound vs free xanthophyll pools: a comparative analysis of chlorophyll *b* and xanthophyll biosynthesis mutants.** *Mol Plant* 2010, **3:**576–593.
47. Bonente G, Pippa S, Castellano S, Bassi R, Ballottari M: **Acclimation of *Chlamydomonas reinhardtii* to different growth irradiances.** *J Biol Chem* 2012, **287:**5833–5847.

48. Lee YK: **Genetic and technological improvements with respect to mass cultivation of microalgae**. In *Microbiology Applications in Food Biotechnology*. Edited by Nga BH, Lee YK. New York: Elsevier Applied Science; 1990.
49. Huesemann MH, Hausmann TS, Bartha R, Aksoy M, Weissman JC, Benemann JR: **Biomass productivities in wild type and pigment mutant of *Cyclotella* sp. (Diatom).** *Appl Biochem Biotechnol* 2009, **157:**507–526.
50. Blanc G, Duncan G, Agarkova I, Borodovsky M, Gurnon J, Kuo A, Lindquist E, Lucas S, Pangilinan J, Polle J, Salamov A, Terry A, Yamada T, Dunigan DD, Grigoriev IV, Claverie JM, Van Etten JL: **The *Chlorella variabilis* NC64A genome reveals adaptation to photosymbiosis, coevolution with viruses, and cryptic sex.** *Plant Cell* 2010, **22:**2943–2955.
51. Yu WL, Ansari W, Schoepp NG, Hannon MJ, Mayfield SP, Burkart MD: **Modifications of the metabolic pathways of lipid and triacylglycerol production in microalgae.** *Microb Cell Fact* 2011, **10:**91.
52. Adarme-Vega TC, Lim DKY, Timmins M, Vernen F, Li Y, Schenk PM: **Microalgal biofactories: a promising approach towards sustainable omega-3 fatty acid production.** *Microb Cell Fact* 2012, **11:**96.
53. Christenson L, Sims R: **Production and harvesting of microalgae for wastewater treatment, biofuels, and bioproducts.** *Biotechnol Adv* 2011, **29:**686–702.
54. Sivakumar G, Xu JF, Thompson RW, Yang Y, Randol-Smith P, Weathers PJ: **Integrated green algal technology for bioremediation and biofuel.** *Bioresour Technol* 2012, **107:**1–9.
55. Sorokin C, Myers J: **A high temperature strain of *Chlorella*.** *Science* 1953, **117:**330–331.
56. Allen MM, Stanier MY: **Growth and division of some unicellular blue-green algae.** *J Gen Micro* 1968, **51:**199–202.
57. Harris EH: *Chlamydomonas Sourcebook, Vol. 1: Introduction to Chlamydomonas and its laboratory use.* San Diego: Academic Press; 2008.
58. Gilmore AM, Yamamoto HY: **Zeaxanthin formation and energy-dependent fluorescence quenching in pea chloroplasts under artificially mediated linear and cyclic electron transport.** *Plant Physiol* 1991, **96:**635–643.
59. Schägger H, von Jagow G: **Tricine-sodium dodecyl sulfate-polyacrylamide gel electrophoresis for the separation of proteins in the range from 1 to 100 kDa.** *Anal Biochem* 1987, **166:**368–379.
60. Peter GF, Takeuchi T, Thornber JP: **Solubilization and two-dimensional electrophoretic procedures for studying the organization and composition of photosynthetic membrane polypeptides.** *Methods: Comp Meth Enzymol* 1991, **3:**115–124.
61. Towbin H, Staehelin T, Gordon J: **Electrophoretic transfer of proteins from polyacrylamide gels to nitrocellulose sheets: procedure and some applications.** *Proc Natl Acad Sci U S A* 1979, **76:**4350–4354.
62. Rappaport F, Beal D, Joliot A, Joliot P: **On the advantages of using green light to study fluorescence yield changes in leaves.** *Biochim Biophys Acta* 2007, **1767:**56–65.
63. Van Kooten O, Snel JFH: **The use of chlorophyll fluorescence nomenclature in plant stress physiology.** *Photosynt Res* 1990, **25:**147–150.

doi:10.1186/s13068-014-0157-z
Cite this article as: Cazzaniga *et al.*: Domestication of the green alga *Chlorella sorokiniana*: reduction of antenna size improves light-use efficiency in a photobioreactor. *Biotechnology for Biofuels* 2014 **7**:157.

Supporting information

Figure S1. Schematic illustration of the mutagenesis and screening strategy used to isolate antenna mutants.

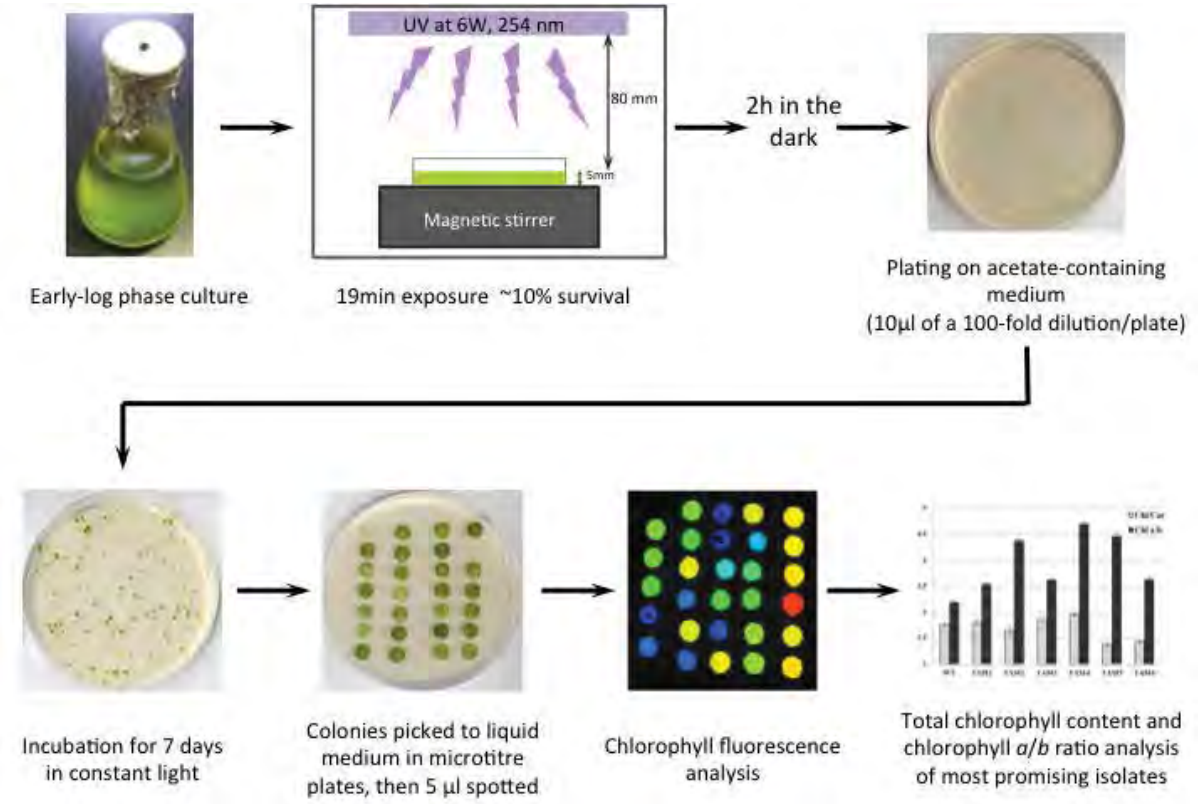

Figure S2. Functional antenna size of PSII and PSI measured in wild-type and TAM mutants (A) Variable Chl fluorescence was induced with a green light of 15 µmol photons m^{-2} s^{-1}, on dark-adapted cells (~$1.0 \cdot 10^7$ cells/ml) in BG-11 medium supplemented with 50 µM DCMU. The reciprocal of time corresponding to two-thirds of the fluorescence rise ($T_{2/3}$) was taken as a measure of the PSII functional antenna size. (B) The kinetics of P700 oxidation (ΔAbs at 705 nm) were measured on thylakoids suspension (75 µg Chl/ml) treated with 50 µM DBMIB and 1 mM methylviologen, upon illumination with a 10 s pulse of red actinic light (λ = 630 nm, 560 µmol photons m^{-2} s^{-1}). Data are expressed as mean ± SD, n = 7.

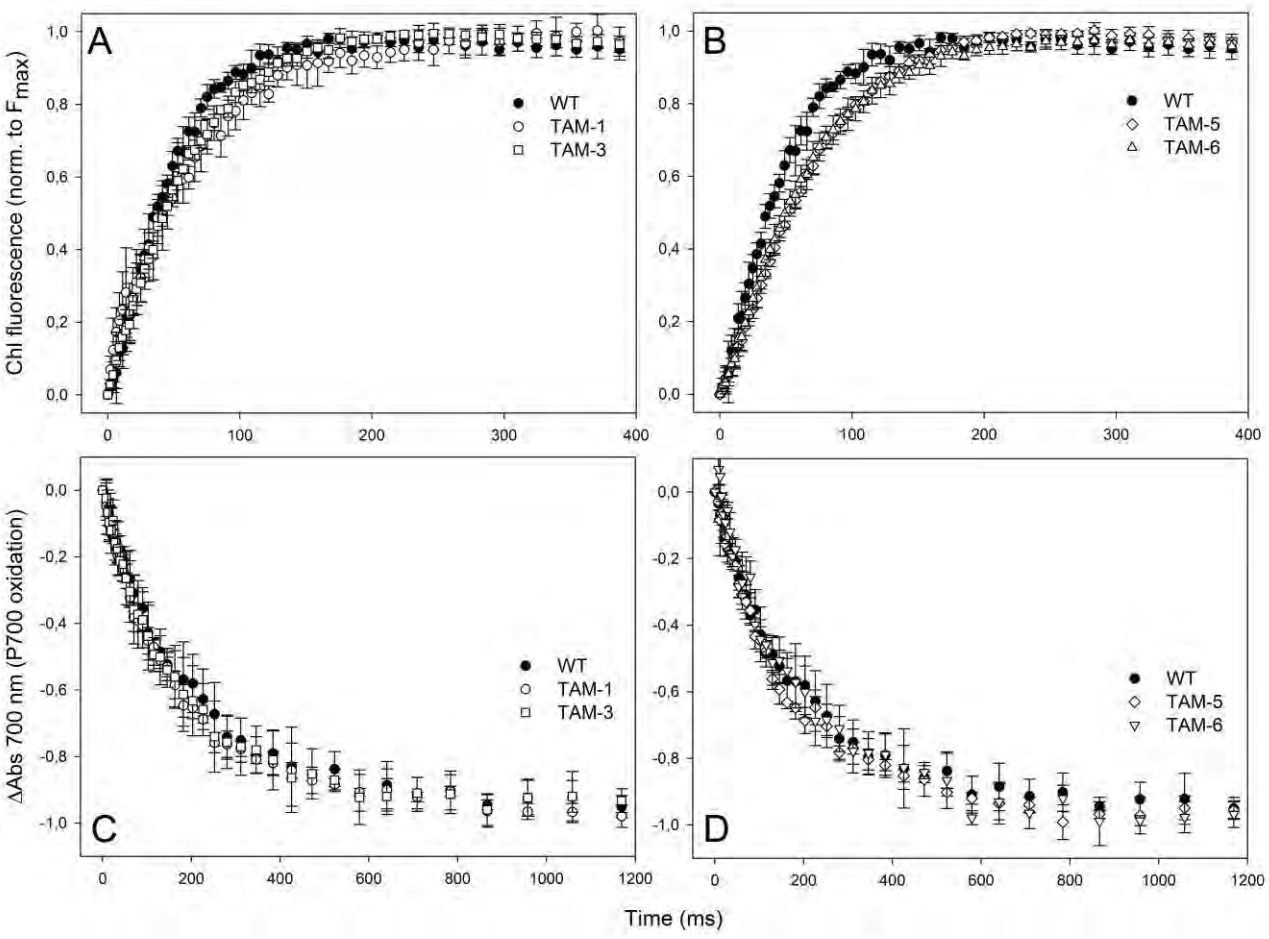

Figure S3. Light-saturation curves of photosynthesis. Curves were obtained with the *C. sorokiniana* wild-type and TAM mutants. Data are expressed as mean ± SD, n = 4.

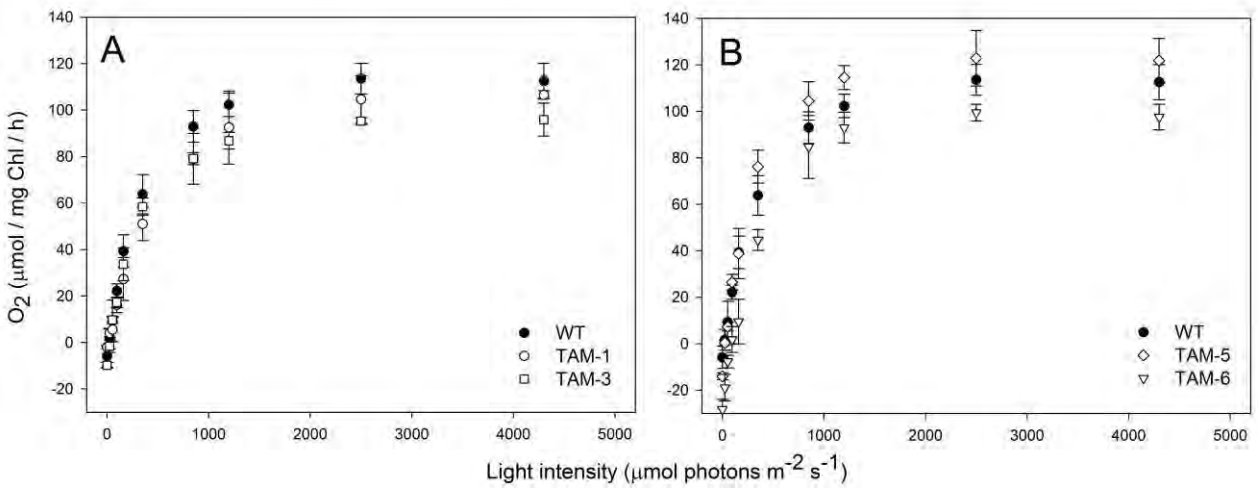

Figure S4. Kinetics of formation and relaxation of photoprotective energy dissipation in wild-type and TAM mutants. NPQ kinetics were measured on wild-type, TAM-2 and TAM-4 cells, grown photoautotrophically, upon illumination with 500 µmol photons m^{-2} s^{-1} of white actinic light. Symbols and error bars show means ± standard deviation (n = 3).

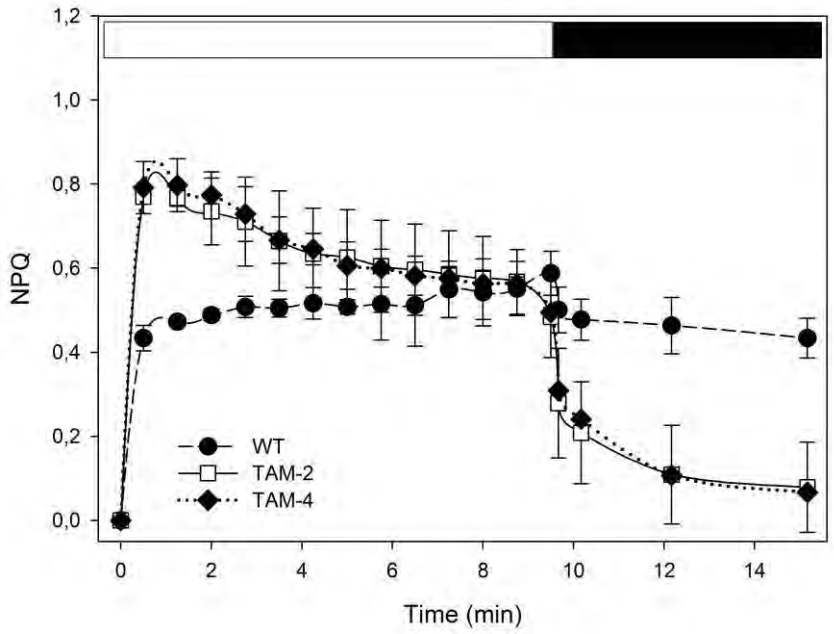

Figure S5

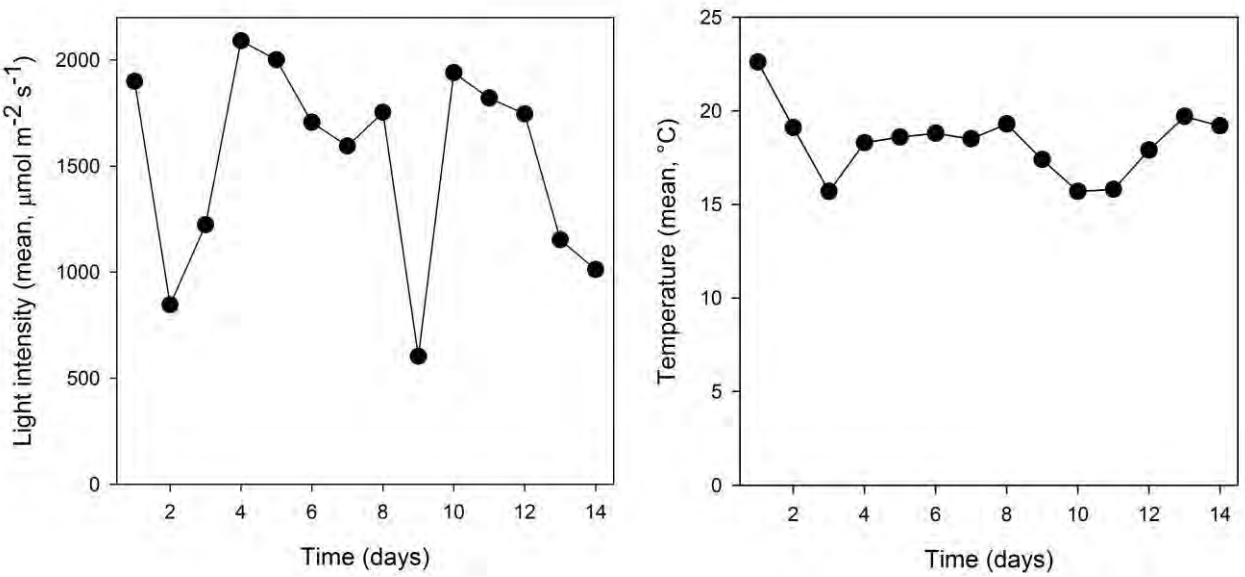

Figure S5. Daily mean irradiance on the reactors' surface (left panel) and mean atmospheric temperature (right panel) measured during the outdoor experiment.

Table S1. Pigment composition of wild-type and TAM mutants. Data are expressed as mean ± SD. Significantly different values (ANOVA, $P < 0.05$) with respect to the wild-type, within the same column, are marked with different letters.

genotype	Chl / cell (pg)	Chl *a* / *b*	Chl / Car	PSII antenna size ($T_{2/3}^{-1} \cdot 10^3$, ms^{-1})
WT	0.49 ± 0.07^{a}	2.62 ± 0.02^{a}	3.43 ± 0.02^{a}	18.2 ± 1.4^{a}
TAM-1	0.50 ± 0.09^{a}	2.92 ± 0.03^{b}	$3.16 \pm 0.02^{b,c}$	14.5 ± 1.6^{b}
TAM-2	0.30 ± 0.02^{b}	3.36 ± 0.02^{c}	3.07 ± 0.02^{b}	10.5 ± 0.5^{c}
TAM-3	0.58 ± 0.09^{a}	2.69 ± 0.12^{d}	3.47 ± 0.12^{a}	15.5 ± 0.5^{b}
TAM-4	0.34 ± 0.05^{b}	3.41 ± 0.03^{c}	$3.18 \pm 0.03^{b,c}$	9.4 ± 0.5^{c}
TAM-5	0.52 ± 0.08^{a}	2.84 ± 0.03^{b}	$3.30 \pm 0.04^{a,c}$	12.9 ± 0.5^{b}
TAM-6	0.51 ± 0.07^{a}	2.91 ± 0.02^{b}	3.35 ± 0.02^{a}	12.9 ± 0.8^{b}

Table S2. HPLC analysis of carotenoid composition of wild-type and TAM mutants. Cells were dark-adapted before pigment extraction in DMFA. Data are expressed as mean ± SD and normalized to 100 Chls. Significantly different values (ANOVA, $P < 0.05$) with respect to the wild-type, within the same column, are marked with different letters.

genotype	mol pigment / 100 mol Chls						
	neoxanthin	violaxanthin	antheraxanthin	lutein	zeaxanthin	α-carotene	β-carotene
WT	6.6 ± 0.2^{a}	1.5 ± 0.1^{a}	0.6 ± 0.1^{a}	17.3 ± 0.3^{a}	0.8 ± 0.1^{a}	0.5 ± 0.2^{a}	2.1 ± 0.2^{a}
TAM-1	6.2 ± 0.2^{a}	2.0 ± 0.1^{a}	0.5 ± 0.1^{a}	17.3 ± 0.1^{a}	1.1 ± 0.1^{a}	0.8 ± 0.2^{a}	2.1 ± 0.1^{a}
TAM-2	5.8 ± 0.2^{b}	5.9 ± 0.1^{b}	1.9 ± 0.1^{b}	10.3 ± 0.2^{b}	2.6 ± 0.2^{b}	0.2 ± 0.1^{a}	3.7 ± 0.3^{b}
TAM-3	6.5 ± 0.1^{a}	2.1 ± 0.1^{a}	1.2 ± 0.1^{c}	14.2 ± 0.3^{c}	2.2 ± 0.1^{b}	0.4 ± 0.2^{a}	2.3 ± 0.1^{a}
TAM-4	6.0 ± 0.1^{b}	6.9 ± 0.1^{c}	1.9 ± 0.1^{b}	9.6 ± 0.1^{d}	2.4 ± 0.2^{b}	0.2 ± 0.1^{a}	3.9 ± 0.2^{b}
TAM-5	6.7 ± 0.3^{a}	3.1 ± 0.1^{d}	2.8 ± 0.1^{d}	9.4 ± 0.2^{d}	3.7 ± 0.3^{c}	0.2 ± 0.1^{a}	2.8 ± 0.2^{c}
TAM-6	6.3 ± 0.2^{a}	3.6 ± 0.1^{d}	1.4 ± 0.1^{c}	13.2 ± 0.3^{c}	2.1 ± 0.1^{b}	0.4 ± 0.1^{a}	2.4 ± 0.2^{a}

Table S3. Relative abundance of pigment-protein complex in the wild-type and TAM mutants. Amount of pigment-protein complexes per cell were calculated by densitometric analysis of native PAGE and by Chls content per cell, and expressed as a percentage of the corresponding wild-type values. Data are expressed as means ± standard deviation (n = 3). Significantly different values (ANOVA, $P < 0.05$) with respect to the wild-type, within the same column, are marked with different letters.

Genotype	Relative abundance of pigment-protein complexes per cell		
	PSI-LHCI	PSII core	Lhcb
WT	100 ± 8^{a}	100 ± 9^{a}	100 ± 7^{a}
TAM-2	66 ± 4^{b}	102 ± 4^{a}	51 ± 3^{b}
TAM-4	66 ± 11^{b}	107 ± 6^{a}	62 ± 6^{b}

Appendix B.
Biogenesis of photosynthetic complexes in the chloroplast of *Chlamydomonas reinhardtii* requires ARSA1, a homolog of prokaryotic arsenite transporter and eukaryotic TRC40 for guided entry of tail-anchored proteins.

the plant journal

SEB Society for Experimental Biology

The Plant Journal (2012) doi: 10.1111/tpj.12077

Biogenesis of photosynthetic complexes in the chloroplast of *Chlamydomonas reinhardtii* requires ARSA1, a homolog of prokaryotic arsenite transporter and eukaryotic TRC40 for guided entry of tail-anchored proteins

Cinzia Formighieri[1], Stefano Cazzaniga[1], Richard Kuras[2] and Roberto Bassi[1,3,*]

[1]*Dipartimento di Biotecnologie, Università di Verona, 15, Strada Le Grazie, I-37134 Verona, Italy,*

[2]*Unité Mixte de Recherche (UMR) 7141, Centre National de la Recherche Scientifique (CNRS), Université Pierre et Marie Curie (UPMC – Paris 06), Institut de Biologie Physico-Chimique, 13 Rue Pierre et Marie Curie, F-75005 Paris, France, and*

[3]*IBG-2: Pflanzenwissenschaften, Forschungszentrum Jülich, 52425 Jülich, Germany*

Received 28 March 2012; revised 13 November 2012; accepted 15 November 2012.

*For correspondence (e-mail roberto.bassi@univr.it).

SUMMARY

***as1*, for antenna size mutant *1*, was obtained by insertion mutagenesis of the unicellular green alga *Chlamydomonas reinhardtii*. This strain has a low chlorophyll content, 8% with respect to the wild type, and displays a general reduction in thylakoid polypeptides. The mutant was found to carry an insertion into a homologous gene, prokaryotic arsenite transporter (*ARSA*), whose yeast and mammal counterparts were found to be involved in the targeting of tail-anchored (TA) proteins to cytosol-exposed membranes, essential for several cellular functions. Here we present the characterization in a photosynthetic organism of an insertion mutant in an *ARSA*-homolog gene. The ARSA1 protein was found to be localized in the cytosol, and yet its absence in *as1* leads to a small chloroplast and a strongly decreased chlorophyll content per cell. ARSA1 appears to be required for optimal biogenesis of photosynthetic complexes because of its involvement in the accumulation of TOC34, an essential component of the outer chloroplast membrane translocon (TOC) complex, which, in turn, catalyzes the import of nucleus-encoded precursor polypeptides into the chloroplast. Remarkably, the effect of the mutation appears to be restricted to biogenesis of chlorophyll-binding polypeptides and is not compensated by the other ARSA homolog encoded by the *C. reinhardtii* genome, implying a non-redundant function.**

Keywords: ARSA, tail-anchored proteins, TOC34, *Chlamydomonas*, protein targeting, chloroplast.

INTRODUCTION

The unicellular green alga *Chlamydomonas reinhardtii* is suitable for random nuclear genetic transformation, and the availability of nuclear genome sequence information (Merchant *et al.*, 2007) makes it an organism of choice for both forward and reverse genetic studies. In addition, the ability of *C. reinhardtii* to grow heterotrophically in the dark makes photosynthetic function dispensable and amenable to mutational analysis. Although the electron transport reactions associated with photosynthesis occur in the chloroplast, the multimeric thylakoid complexes contain only a few chloroplast-encoded polypeptides, the large majority being nuclear-encoded and needing to be imported into the plastid upon translation by cytosolic ribosomes. The enzymes catalyzing the synthesis of required cofactors are also nuclear-encoded; their expression and biogenesis must be strictly coordinated and controlled in order to optimally respond to developmental and external stimuli (Pogson *et al.*, 2008). Nuclear mutagenesis could therefore affect genes involved in or controlling the targeting of nucleus-encoded photosynthesis-related proteins to the chloroplast and the biogenesis of photosystems.

Random insertion mutagenesis of *C. reinhardtii* and phenotype screening identified a mutant severely affected in chlorophyll content, about 8% of the wild-type level, named *as1*, for antenna size mutant *1* (Bonente *et al.*, 2011). The light-harvesting antenna size of both photosystems is significantly reduced; this clear phenotype

of antenna versus reaction center reduction is confirmed by a higher β-carotene content and chlorophyll *a*/chlorophyll *b* ratio (Bonente *et al.*, 2011). The present work reports on further characterization of *as1*; in particular the 'pale green' phenotype is associated with an insertion mutation in an *ARSA*-homolog gene on chromosome 5.

ARSA proteins are found in bacteria where they have two ATPase domains within a single polypeptide chain and, together with the transmembrane partner ARSB, seem to be involved in active arsenite extrusion and resistance (Kuroda *et al.*, 1997; Zhou *et al.*, 2000; Borgese and Righi, 2010; Borgese and Fasana, 2011). ARSA homologs are conserved between archea and eukaryotes, where they have acquired a novel function in the targeting of tail-anchored (TA) proteins (Rabu *et al.*, 2009; Borgese and Righi, 2010; Borgese and Fasana, 2011). The TA proteins constitute a distinct class of integral membrane proteins, whose targeting information resides on the C-terminus rather than the N-terminus of the polypeptide. Since the only membrane-targeting sequence emerges from the ribosome upon completion of translation, TA proteins insert into their target membranes by post-translational mechanisms. The defining feature of a TA protein is the presence of a single transmembrane (TM) segment, typically of ~20 amino acids, very close to the C-terminus, at no more than 30 residues. This TM segment provides both the targeting signal for the delivery of the protein to the correct subcellular compartment and the anchor that retains the polypeptide in the lipid bilayer once integration has taken place (Kutay *et al.*, 1993; Borgese *et al.*, 2007), although targeting information may be additionally be located outside the tail anchor (Dhanoa *et al.*, 2010). Irrespective of the compartment in which they reside, TA proteins are oriented in the membrane such that the N-terminal region faces the cytosol where it can perform its biological function. As a consequence TA proteins are not embedded into the internal membranes of organelles (Kriechbaumer *et al.*, 2009; Rabu *et al.*, 2009). This protein group, present in all domains of life and in all cytosol-exposed membranes, performs essential cellular functions such as vesicle trafficking (e.g. the vesicle-associated membrane protein synaptobrevin-2), ubiquitination, apoptosis, protein translocation [e.g. Sec61β and Sec61γ subunits of the Sec61 translocon complex of the endoplasmic reticulum (ER)], signal transduction, transcription, enzymatic reactions and electron carrying (e.g. different isoforms of cytochrome b_5 targeted to the ER, mitochondria or plastids). Over 10 and 50 TA proteins are predicted to be expressed in prokaryotes (Borgese and Righi, 2010) and yeast (Beilharz *et al.*, 2003), respectively, while over 400 are predicted in humans (Kalbfleisch *et al.*, 2007) and plants (Kriechbaumer *et al.*, 2009). Studies performed in mammals (Mukhopadhyay *et al.*, 2006; Stefanovic and Hegde, 2007) and yeasts (Schuldiner *et al.*, 2008) have shown that ARSA homologs are involved in the delivery of TA proteins to target membranes. The mammalian ARSA homolog TRC40 interacts with newly synthesized Sec61β in cross-linking experiments and is peripherally associated with membranes (Stefanovic and Hegde, 2007). A homozygous knockout of the mouse *ASNA1* gene caused embryonic lethality (Mukhopadhyay *et al.*, 2006), suggesting that the ASNA1 pathway could be essential for the biogenesis of some strictly ASNA1-dependent TA proteins. The structure of the yeast homolog GET3 (Guided Entry of Tail-anchored proteins-3; Schuldiner *et al.*, 2008) was resolved, showing it to be a homodimer whose monomers, each carrying an ATPase domain and a methionine α-helical domain, are linked by two cysteine residues coordinating a zinc ion. In the active state, the dimer interface exposes a large hydrophobic groove implicated in TA binding (Hu *et al.*, 2009) and interacts with GET1 and GET2 membrane proteins to form a receptor (Schuldiner *et al.*, 2008) and with GET4 and GET5 in the cytosol to form the trans-membrane recognition complex (Jonikas *et al.*, 2009). The yeast *GET3* knockout, although presenting a reduced fitness, is viable, suggesting the existence of alternative routes for TA protein insertion in the absence of GET3 (Maggio *et al.*, 2007; Rabu *et al.*, 2009). Although there are bioinformatic predictions of over 400 TA proteins in Arabidopsis, including 138 TA proteins putatively localized in plastids (Kriechbaumer *et al.*, 2009), only a few plastidial TA proteins have been documented, including an isoform of cytochrome b_5 (Maggio *et al.*, 2007), TOC33 and TOC34 of the chloroplast outer membrane translocon (May and Soll, 1998; Qbadou *et al.*, 2003; Dhanoa *et al.*, 2010) and the novel outer envelope TA protein OEP9 of unknown function (Dhanoa *et al.*, 2010).While in yeast and human only one ARSA-homolog protein is encoded, two and three *ARSA* genes are present in *Chlamydomonas* and Arabidopsis, respectively. Different isoforms of ARSA could be required in photosynthetic eukaryotes where the presence of plastids, in addition to the other cellular compartments, could increase the level of complexity in TA protein targeting and biogenesis. In the present work we show that an insertional mutation in the *ARSA*-homolog gene on chromosome 5 of *C. reinhardtii* profoundly affects the biogenesis of photosynthetic complexes in the chloroplast and is not compensated by a different ARSA-homolog protein, encoded by a gene on chromosome 3, suggesting a non-redundant function. Despite the mutation strongly affecting chloroplast structure and function, the encoded protein was found to be located in the cytosol and to control the insertion of TOC34 which is a TA protein. These results suggest that *ARSA1* affects the biogenesis and activity of the macromolecular complex importing nuclear encoded chloroplast proteins.

RESULTS

Identification of an *arsa1* mutant of *Chlamydomonas reinhardtii*

Random insertion mutagenesis of the nuclear genome of a *cw15* strain of *C. reinhardtii* (also called wild type in the present paper) was performed with a linearized pSL18 plasmid containing the paromomycin resistance cassette, as described in Bonente *et al.* (2011). A mutant with a residual chlorophyll content of 8% of the wild-type level was isolated for a reduced yield of *in vivo* chlorophyll fluorescence and an altered pigment content (mutant formerly called *as1*) (Bonente *et al.*, 2011). To identify the insertion site, we proceeded to resequence the entire nuclear genome through an ILLUMINA® platform. The software SOAP v. 2.20 was used to align the ~100 bp reads against either the sequence of the pSL18 plasmid or the *C. reinhardtii* genome sequence available online on the NCBI website (Li *et al.*, 2009). The software BLAT was used to distinguish putative genomic regions flanking a plasmid sequence into a read and then aligned against all the reads to confirm the result. The insertion occurred in a predicted *ARSA*-homolog gene on chromosome 5 (*Cre05.g230350 Chlamydomonas reinhardtii* v4.3, g5570 v5.3). A second *ARSA*-homolog gene, *ARSA2*, not mutated in *as1*, is annotated on chromosome 3 (*Cre03.g204800*) (http://www.phytozome.net). Complementary DNA clones for *ARSA1* are available (Kazusa Institute, Tokyo, Japan), indicating that the gene is indeed expressed (the encoded amino acid sequence is reported in Figure S1 in the Supporting Information, aligned with those of homologous *Chlamydomonas* ARSA2, At3 g10350, At5 g60730 and At1 g01910 from *Arabidopsis thaliana*, ASNA1 from *Homo sapiens*, GET3 from *Saccharomyces cerevisiae* and ARSA from *Escherichia coli*). *Chlamydomonas reinhardtii* ARSA1 encodes a protein that has two ATPase domains within a single polypeptide and is not likely to require dimerization, similarly to bacterial counterparts. In contrast, ARSA2 of *Chlamydomonas*, as well as GET3, ASNA1 and predicted ARSA proteins from Arabidopsis, only have one ATPase domain (Figure 2). Remarkably, residues forming the hydrophobic groove for TM domain binding (Hu *et al.*, 2009) are conserved in *C. reinhardtii* ARSA1 differently to bacterial ARSA (marked in gray in the alignment in Figure S1). *Chlamydomonas reinhardtii* ARSA1 is likely to function in TA protein targeting like the other eukaryotic counterparts, as suggested by the phenotype of the present *as1* mutant (see below). The mutation in *as1* caused interruption of the coding sequence and deletion of the region encoding the second domain of the ARSA1 protein (Figure 1a), as confirmed by PCR on the genome (Figure 1b). No *ARSA1* transcript was detected in *as1* mutant (Figure 1c). Selected random progeny from the cross of *as1* with S34, a normally pigmented cell wall-containing strain, showed co-segregation between the mutant phenotype, unable to grow efficiently photoautotrophically in low light because of reduced light-harvesting capacity, and the paromomycin

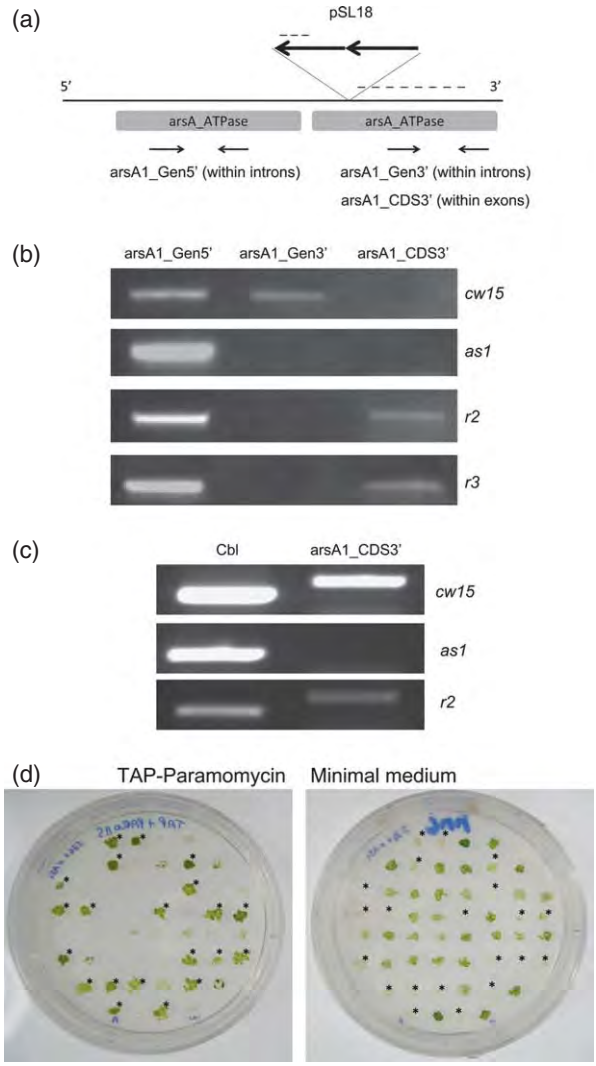

Figure 1. Mapping and characterization of the mutation in the *ARSA1* gene.
(a) Schematic representation of the insertion of the pSL18 cassette into the genomic sequence encoding for the second ARSA1_ATPase domain. The genome deletion caused by the insertion is marked by the dashed line. Arrows indicate primers used in (b) and (c). Also the pSL18 cassette itself underwent some rearrangements, including head-to-tail concatamerization and deletion of 899 bp close to the flanking border (dashed line).
(b) Polymerase chain reaction on genomic DNA from *cw15*, *as1* and two rescued clones (*r2*, *r3*). Primers were either designed to amplify a fragment at the 5′ end of the *ARSA1* gene, the 3′ end of the *ARSA1* gene or the ARSA1_CDS3′. The ARSA1_CDS3′ primer set was not able to amplify a 500 bp product on the wild-type genome due to the presence of introns.
(c) Reverse transcriptase-PCR, showing *ARSA1* expression at the transcript level only in the *cw15* and *r2* rescued clone, using the ARSA1_CDS3′ primer set as in (b). Expression of *CBL* is shown as a positive control.
(d) Random progeny analysis of the cross between cell wall-less *as1* mt– and the cell wall-containing wild type S34 mt +. Progeny colonies were tested on TRIS-acetate-phosphate (TAP) for resistance to paromomycin (15 μg ml^{-1}) and on minimal medium for photoautotrophy at 50 μM photons m^{-2} sec^{-1}. Of 52 progeny colonies, 21 colonies (left panel small stars) grew on TAP-paromomycin, while 31 died on minimal medium (right panel).

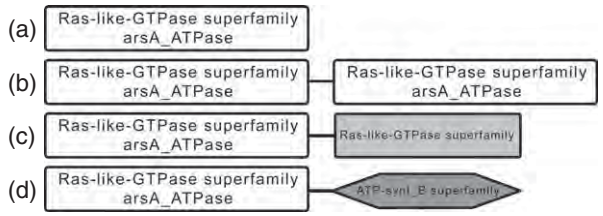

Figure 2. Structure of proteins with an ARSA-homolog domain.
Yeast and mammals have one ARSA-homolog protein with an ARSA_ATPase domain that has been proposed to form dimers *in vivo* (Hu *et al.*, 2009) (a). In contrast, more than one *ARSA* gene can be found in the genome of photosynthetic organisms. In most higher plants and algae the encoded proteins have one ARSA_ATPase domain (as in a). However, in *Chlamydomonas reinhardtii* (ARSA1, present work) and *Phaeodactylum tricornutum* CCAP 1055/1 (*PHATRDRAFT_32803*, gene ID 7197303) an *ARSA* gene encodes a protein that has two ARSA_ATPase domains within a single polypeptide, resembling the structure of bacterial ARSA proteins (b). In other cases, the single polypeptide contains an ARSA_ATPase domain and a shorter RAS-like-GTPase domain, such as in *Thalassiosira pseudonana* CCMP1335 (*THAPSDRAFT_1704*, gene ID 7445538) and in the cyanobacterium *Nostoc punctiforme PCC 73102* (*Npun_F2147*, gene ID 6251562) (c). Alternatively the ARSA_ATPase is fused to a distinct recognizable functional domain, such as the ATP synthase B subunit-like domain in *Ostreococcus tauri* (*Ot09 g01520*, gene ID 9831719) (d). These differences seem to be species- rather than genus-specific.

resistance carried by the insertion cassette, indicating a mutation tagged by the transforming DNA. An example of such genetic analysis is shown in Figure 1d. The mutant was then transformed with the *ARSA1* cDNA. Since photoautotrophy is compromised in *as1* at 50 μM photons m^{-2} sec^{-1}, a limiting light intensity considering the strongly reduced absorption cross-section of the mutant (Figures 1d and 6), selection of transformants was performed by directly selecting for a rescued phenotype in minimal medium at the aforementioned irradiance. No colonies were observed in the untransformed control, indicating absence of spontaneous revertants. Clones having the *ARSA1* cDNA cassette integrated in the genome and expressing the corresponding transcript (Figures 1b,c) showed rescue of the mutated phenotype (Figures 3, 4, 6 and 7), indicating that the observed pale green phenotype is indeed due to the insertion in the *ARSA1* gene.

The *arsa1* mutation affects the accumulation of photosystem polypeptides

as1 mutant has higher chlorophyll *a*/*b* ratio (6.4 versus 2.7 in *cw15*; Table 1) and a lower chlorophyll/carotenoid ratio (1.5 versus 3.2 in *cw15*; Table 1), suggesting a phenotype of antenna versus core complex reduction. Compared to the 8% chlorophyll content of *as1*, transformants for the *ARSA1* cDNA (Figure 1b, c) display different levels of chlorophyll content (from 46% in *r3* to 65 and 70% in *r1* and *r2*, respectively, as compared with the wild type). The expression of *ARSA1* in these clones is sufficient to recover chlorophyll *a*/*b* and chlorophyll/carotenoid ratios close to the wild-type level (Figure 3, Table 1).

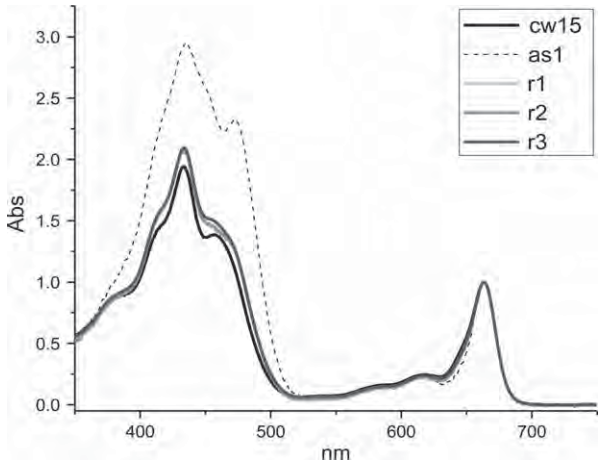

Figure 3. Rescue of pigmentation in clones *r1*, *r2*, *r3* obtained by transformation of *as1* with *ARSA1* cDNA.
Absorption (Abs) spectra of acetone-extracted pigments from *cw15*, *as1* and complemented clones (*r1*, *r2*, *r3*).

Since chlorophyll biosynthesis is coordinated to the expression of chlorophyll-binding proteins, the mutant is expected to have a reduced accumulation of such polypeptides in thylakoid membranes. Thylakoid proteins were thus separated by electrophoresis in denaturing conditions (SDS-PAGE), followed by Coomassie staining of the gel to give an overview of the polypeptide profile in thylakoids (Figure 4a). Annotation of protein bands is based on fractionation and immunoblotting as reported in Bassi and Wollman (1991). Moreover, a detailed investigation of several photosynthetic polypeptides was performed by immunoblotting with specific antibodies on total protein extract (on a per cell basis in Figure 4b and on a per chlorophyll basis in Figure S2). The mutant shows a general reduction in the level of thylakoid polypeptides per cell as compared with *cw15* (Figure 4a); in particular, the accumulation of photosystem II core subunits appears to be more affected than the accumulation of photosystem I core polypeptides, ATPase and cytochrome *f* of the cytochrome b_6f complex (Figures 4b and S2). In addition, light-harvesting chlorophyll *a*/*b*-binding (LHC) subunits of both photosystems are strongly reduced (Figure 4a, b). Among the LHCI polypeptides of the photosystem I antenna system, LHCA3 and LHCA9 were the most reduced, followed by LHCA4 and LHCA8 (Figure S2). However, the content of soluble chloroplast proteins such as ribulose 1,5-bisphosphate carboxylase/oxygenase (Rubisco) was significantly higher in the mutant versus *cw15* on a per cell basis. Markers for mitochondria and the ER (CPLX1 and BIP2, respectively) were present at the same level in both genotypes. We then proceeded to analyze cell organization by electron microscopy (Figure 5). We observed that in the wild type the chloroplast occupies most of the cell volume and is packed with thylakoid membranes. In contrast, *as1* cells exhibit

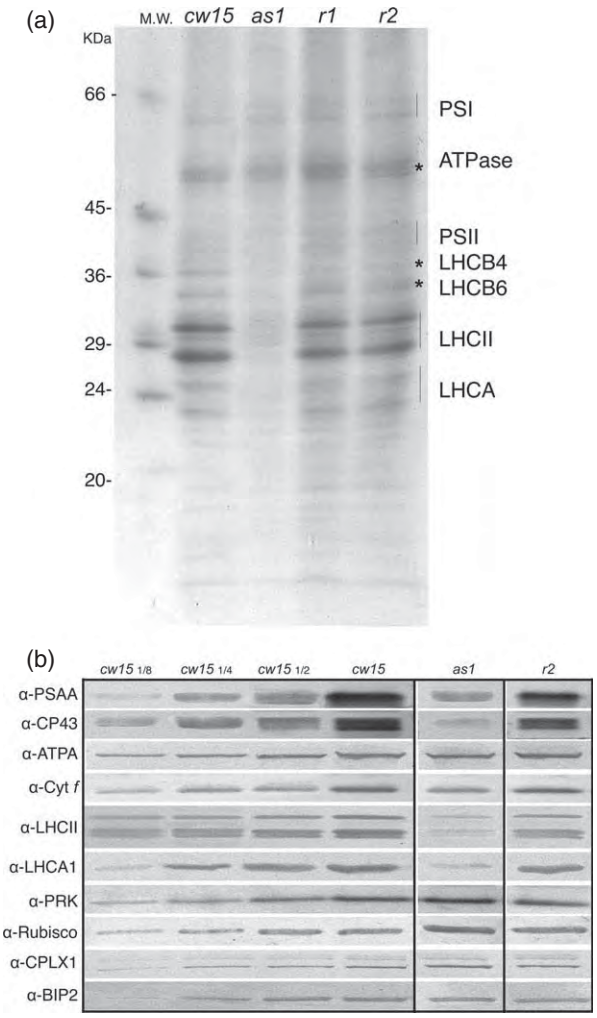

Figure 4. Polypeptide composition and immunological titration of selected proteins in the *as1* mutant as compared to *cw15* and the complemented clones (*r1*, *r2*).
(a) TRIS-sulfate SDS-PAGE 10–20% (Bassi and Wollman, 1991). Molecular weight markers are indicated on the left. Thylakoid polypeptides of *cw15*, *as1* and *r2* were loaded on a per cell basis (5×10^5).
(b) Immunoblot titration of selected chloroplast proteins performed on total protein cell extracts. Proteins extracted from 1.3×10^5 cells of *as1* and *r2* were loaded on the gel aside with the same cell number of *cw15* (100%) and three dilutions corresponding to 12.5, 25 and 50%.

much smaller chloroplasts with a lower density of thylakoid membranes, suggesting impaired biogenesis of chloroplast membrane structures.

The *arsa1* mutation compromises photoautotrophic but not heterotrophic growth

In order to verify the effect of the *arsa1* mutation on photosynthesis and photoautotrophy we compared growth on acetate-supplemented medium (TRIS-acetate-phosphate, TAP), allowing for heterotrophic growth, with growth on minimal medium (high salt, HS), selective for photoautotrophy. As shown in Figure 6, photoautotrophic growth on HS medium was severely impaired at 50 μM photons m^{-2} sec^{-1}, probably due to the very low chlorophyll level insufficient to sustain light harvesting and photosynthesis in limiting light. This phenotype was partially rescued at higher light (400 μM photons m^{-2} sec^{-1} in Figure 6), suggesting that the mutant is not light-sensitive, and almost completely rescued on TAP. Equal respiration rates were measured, expressed as oxygen uptake in the dark (18×10^2 μM O_2 10^{-6} $cells^{-1}$ h^{-1} versus 18.9 in *cw15*; Table 2), suggesting normal respiratory activity and thus unaffected mitochondrial biogenesis.

The *arsa1* mutation affects accumulation of the TOC34 subunit of the translocon of the outer chloroplast membrane (TOC) complex

Eukaryotic ARSA homologs have been proposed to target TA proteins to membranes, based on studies performed so far in yeast and mammals (Stefanovic and Hegde, 2007; Schuldiner *et al.*, 2008). The TA proteins are defined as integral membrane proteins exposed to the cytosol rather than embedded into the internal membranes of organelles (Kriechbaumer *et al.*, 2009; Rabu *et al.*, 2009). Therefore, thylakoid membranes do not comprise TA proteins. However, the outer chloroplast membrane is predicted to contain TA proteins (May and Soll, 1998; Qbadou *et al.*, 2003; Maggio *et al.*, 2007; Kriechbaumer *et al.*, 2009; Dhanoa *et al.*, 2010) that may also utilize different sorting pathways (Maggio *et al.*, 2007; Dhanoa *et al.*, 2010). In the present work we investigated the accumulation of TOC34, which is a TA protein (May and Soll, 1998; Qbadou *et al.*, 2003; Dhanoa *et al.*, 2010). By immunoblotting with a specific antibody raised against Arabidopsis TOC34, no reactivity was detected in the mutant in contrast to *cw15* (Figure 7). We verified that the anti-TOC34 antibody did not react with purified thylakoid membranes, while it did recognize a 44-kDa SDS-PAGE band in the intact chloroplast preparation, consistent with location of TOC34 in the chloroplast envelope membrane (Figure 7b). This result suggests a role for ARSA1 in the biogenesis of TOC34, which is a core component of the TOC complex. Consequently, accumulation of TOC34 is compromised in the *as1* mutant. The TOC complex has evolved to perform the physical task of transporting the nucleus-encoded precursor proteins across the chloroplast envelope (Li and Chiu, 2010) and represents the first step in the chloroplast protein targeting machinery. Impaired biogenesis of TOC34 could explain the reduced accumulation of photosynthetic complexes, due to reduced protein import activity, and the pale green/yellow phenotype of *as1* is consistent with the reported phenotype of an *Arabidopsis thaliana* mutant for the homolog TOC component (Jarvis *et al.*, 1998; Kubis *et al.*, 2003). Remarkably, TOC34 accumulation was restored to different extents in transformants for the *ARSA1* cDNA (*r2* and *r3* in Figure 7a). In particular, the higher level of TOC34

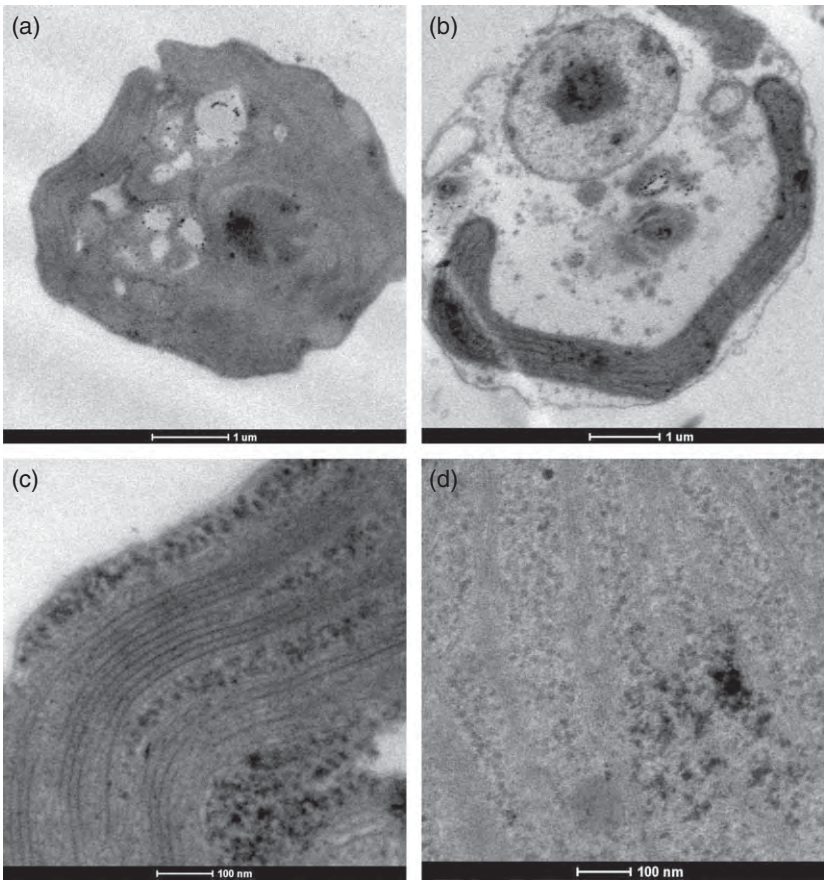

Figure 5. Results of transmission electron microscopy of cells and membranes.
Transmission electron microscopy of *cw15* (a) and *as1* mutant (b) cells showing that most of the cell volume is occupied by the electron-dense chloroplast in *cw15* which is much smaller in the mutant. Organization of the thylakoid membranes (c, d) showing that thylakoid membranes are more densely packed in *cw15* to respect to mutant. Scale bar: 1 μm (a, b) and 100 nm (c, d).

polypeptide in *r2* as compared with *r3* correlates to the extent of rescue of the wild-type phenotype, i.e. the chlorophyll content (Table 1). This result implies that absence of TOC34 in *as1* was indeed due to the *arsa1* mutation. We then proceeded to verify whether the inhibitory effect of the mutation was selective for the accumulation of TOC34 or if other TOC subunits were affected. To this aim we used antiserum raised against plant TOC159 which showed a good reaction in *Chlamydomonas* at the corresponding apparent molecular mass, implying TOC159 accumulated to the same level in *cw15* and *as1* on a cell basis (Figure 7c). Instead, the antiserum against plant TOC 75 showed no reaction on the extract from algae.

The ARSA1 protein is localized in the cytosol

TOC34 is localized in the outer chloroplast envelope membrane (Ferro *et al*., 2002); thus, the machinery for its insertion is expected to be cytosolic. In order to locate *ARSA1* in the *Chlamydomonas* cell we have produced an antibody by using as antigen the recombinant *ARSA1* protein expressed in *E. coli*. The antiserum recognized a single band around the molecular weight of 80 kDa in SDS-PAGE which was absent in *as1* and was present in *cw15* (Figure 8a). We then proceeded to fractionation of *C. reinhardtii* cells into intact chloroplasts and mitochondria, highly purified thylakoid membranes, microsomal and cytosol preparations as described in Experimental Procedures. Probing with antibodies directed against marker proteins (Figure 8b) confirmed the purity of the fractions: in fact, nitrite reductase was only found in intact chloroplasts, not in thylakoids, where the chlorophyll *a*/*b* binding protein LHCB4 was, instead, detected. CPLX1 (49-kDa subunit of mitochondrial complex I) was only found in the mitochondrial fraction while UGPase (UDP-glucose pyrophosphorylase) was detected in the cytosolic fraction. Finally, BIP2 (binding protein 2) was found in both the microsomal fraction and the cytosol, consistent with the partial loss of this soluble ER marker during the formation of right-side-out microsomal vesicles. All these antigens could be detected in the whole cell extract. When these fractions, loaded in the gel on a protein basis, were probed with anti-ARSA1 antibody, a signal was found in the cytosol fraction with a faint trace in microsomes (Figure 8b). In order to verify the possibility of an interaction between ARSA1 and microsomes, we proceeded to step centrifugation of the total cell extract at 20 000, 40 000 and 100 000 ***g*** and probed the pellet obtained after each centrifugation with respect to the whole cell extract and the 100 000 ***g*** supernatant loaded on a protein basis. Although the immunoblot signal was stronger in the soluble fraction and

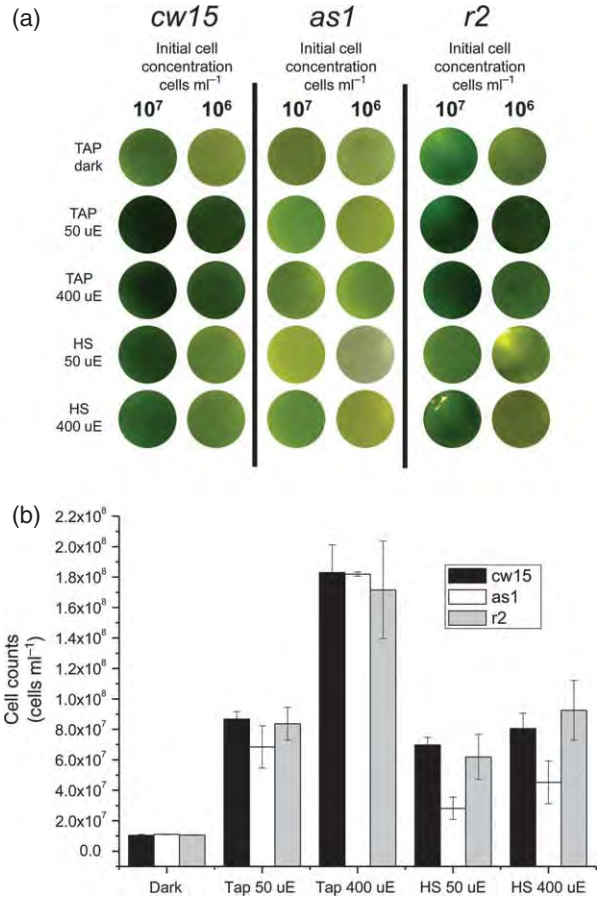

Figure 6. Growth test of *cw15*, *as1* and complemented clone (*r2*).
(a) Image of 3-ml microtiter wells grown for 4 days in different light and medium conditions from an initial inoculum of 10^6 or 10^7 cells ml^{-1}.
(b) Cell counts after 4 days of growth in minimal (high salt, HS) or rich (TRIS-acetate-phosphate, tap) media and different light conditions (0, 50 and 400 μE). Data are expressed as mean ± SD (n = 3). Inoculum was 10^7 cells ml^{-1}. (Results with 10^6 cells ml^{-1} were comparable.)

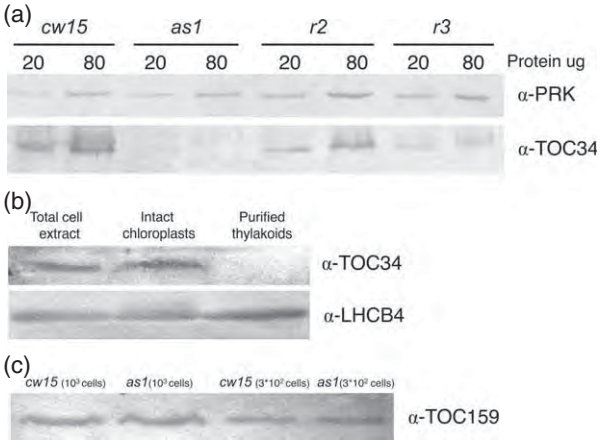

Figure 7. Accumulation of TOC34 subunit in *cw*15 and *as*1 mutant.
(a) Immunoblot analysis on a per protein basis of TOC34 polypeptide level in *cw15, as1* and complemented clones (*r2* and *r3*). Amounts of proteins loaded in each lane are indicated in micrograms. PRK reaction is reported as an internal control.
(b) Reactivity of α-TOC34 versus *cw15* total cell extract. Intact chloroplasts and purified thylakoid membranes (see Experimental Procedures). No reaction was observed with purified thylakoids. LHCB4, a pigment-binding protein integral of the thylakoid membrane was used as a marker.
(c) Reactivity of α-TOC159 with *cw15* and *as1* total cell extracts loaded on a per cell basis.

fainter in the pellets, a band was still detected in the 100 000 ***g*** pellet containing microsomes (figure S3). Thus, although ARSA1 is to a large extent soluble in the cytosol, we cannot exclude a low level of interaction with microsomes.

DISCUSSION

This study reports the identification and characterization of an *arsa1* mutant of *C. reinhardtii*, generated by random insertion mutagenesis of the nuclear genome and screened for an altered pigment content/composition and a lower chlorophyll fluorescent yield (mutant formerly called *as1*) (Bonente *et al.*, 2011). In bacteria, ARSA proteins are involved in active arsenite extrusion and resistance while *ARSA*-homolog genes have acquired a novel function in targeting of TA proteins in eukaryotes (Rabu *et al.*, 2009; Borgese and Fasana, 2011). So far ARSA-homologs have been studied in yeast and mammals (Mukhopadhyay *et al.*, 2006; Stefanovic and Hegde, 2007; Schuldiner *et al.*, 2008) while nothing is known about their function in plants. A homozygous knockout of the mouse *ASNA1* gene caused embryonic lethality (Mukhopadhyay *et al.*, 2006), suggesting the existence of some strictly ASNA1-dependent TA proteins fulfilling essential cellular functions. The homologous mutation in yeast didn't lead to lethality, indicating some redundancy in TA proteins targeting pathways, but all the same pleiotropic effects were observed (Schuldiner *et al.*, 2008). In eukaryotic photosynthetic organisms, in addition to TA proteins targeted to other cytosol-exposed membranes a specific plastidial set of TA proteins could increase the level of complexity in the biogenesis of TA proteins. Consistently, while a single *ARSA*-homolog is present in yeast and mammals, plants have more than one gene in the nuclear genome, i.e. two and three in *Chlamydomonas* and Arabidopsis, respectively. The present mutant for the *ARSA*-homolog gene on chromosome 5 of *C. reinhardtii* displays profound effects on the accumulation of chlorophyll-binding photosynthetic proteins in chloroplast thylakoids (Figure 4). ARSA1 seems to be specifically involved in chloroplast function and its mutation only mildly altered the function of other cellular compartments, if at all. As a matter of fact, the *arsa1* mutation had a much stronger effect on photoautotrophy than on heterotrophy (Figure 6). Moreover, respiration rate was unaltered, suggesting maintenance of mitochondrial function. This could reflect a major role of ARSA1 in the biogenesis and targeting of plastidial TA proteins. The

Table 1 Pigment content and composition of *Chlamydomonas reinhardtii cw15*, *as1* mutant and complemented *r1*, *r2*, *r3* clones. Data are expressed as mean ± SD (n = 4)

	cw15	*as1*	*r1*	*r2*	*r3*
μg chl/10^6 cells	3.72 ± 0.33	0.30 ± 0.04	2.44 ± 0.23	2.63 ± 0.23	1.72 ± 0.18
Chl *a*/chl/*b*	2.70 ± 0.22	6.40 ± 0.61	2.95 ± 0.28	3.20 ± 0.32	2.88 ± 0.29
Chl/Car	3.20 ± 0.34	1.50 ± 0.18	2.23 ± 0.22	2.32 ± 0.22	2.14 ± 0.21

Chl, chlorophyll; Car, carotenoid.

Table 2 Photosynthetic parameters extrapolated from light saturation curves, measured with a Clark-type electrode. Experimental data for oxygen exchange rates were curve-fitted with a hyperbolic tangent function (Falkowski and Raven, 1997) using the Microsoft Excel least-squares solver algorithm (Huesemann *et al.*, 2008). Data are expressed as mean ± SD (n = 4)

	cw15	*as1*
R_{dark} (10^2 μM O_2 10^{-6} $cell^{-1}$ h^{-1})	(−) 18.90 ± 1.51	(−) 18.00 ± 1.43
R_{dark} (μM O_2 mg chl^{-1} h^{-1})	(−) 18.90 ± 1.63	(−) 180.00 ± 14,4
P_{max} (10^2 μM O_2 10^{-6} $cell^{-1}$ h^{-1})	108.10 ± 8.94	85.80 ± 6.83
P_{max} (μM O_2 mg chl^{-1} h^{-1})	108.10 ± 8.62	858.60 ± 68.8
a	0.51 ± 0.01	0.31 ± 0.02
I_s (μM photons m^{-2} sec^{-1})	213.20 ± 17.01	276.90 ± 22.15
I_0 (μM photons m^{-2} sec^{-1})	37.60 ± 2.99	58.90 ± 4.71

R_{dark}, oxygen uptake in the dark by respiration; P_{max}, light-saturated maximum oxygen evolution rate; *a*, the slope of the initial linear increase of the light saturation curve that is a measure of the photon use efficiency; I_s, light intensity at which photosynthetic oxygen evolution saturates; I_0, light intensity at which oxygen uptake by respiration equals oxygen evolution by photosystem II, also known as the compensation point, Chl, chlorophyll.

mutation in *ARSA1* was not compensated by the distinct ARSA-homolog protein, encoded by a gene on chromosome 3, suggesting a non-redundant function. ARSA1 protein has two ATPase domains within a single polypeptide, in contrast to ARSA2 and ARSA-homologs found in other eukaryotic systems (Figures 2 and S1). In this respect, ARSA1 is more similar to prokaryotic ARSA proteins and could suggest an endosymbiotic origin.

Tail-anchored proteins are embedded in cytosol-exposed membranes, thus excluding thylakoids. As a consequence, polypeptides of photosynthetic complexes, that are reduced in the present mutant, cannot be direct substrates for ARSA1. However, the outer chloroplast membrane is predicted to contain TA proteins, including the TOC34 subunit of the translocon of the TOC (May and Soll, 1998; Qbadou *et al.*, 2003). It is generally accepted that the chloroplast arose from a photosynthetic prokaryote (a cyanobacterium) engulfed by a mitochondriate eukaryote (Raven and Allen, 2003). Since its endosymbiotic beginning, the chloroplast has become fully integrated into the biology of the host eukaryotic cell. The transfer of genetic information from the chloroplast genome to the host nuclear genome resulted in the loss of most plastid genes, whose function was assumed by nucleus-encoded proteins (Martin and Herrmann, 1998). New proteins were added to facilitate its biogenesis and coordinate its function. This process required evolution of a protein translocation system to facilitate the post-translational return of endosymbiont proteins back to the organelle. The translocon of the chloroplast performs the physical task of translocating the precursor proteins across the double membrane envelope of the chloroplast (Li and Chiu, 2010). The transit peptide, exposed by a precursor protein, is recognized at the chloroplast surface by two homologous GTPases, TOC159 and TOC34. Together with the channel TOC75, both TOC34 and TOC159 constitute the core components of the TOC complex, firmly interacting with each other (Waegemann and Soll, 1991). From the absence of any signal when assaying either whole cell extracts or membrane fractions using the antibody raised against Arabidopsis TOC34 in *as1*, while a band at the expected mobility was observed in *cw15* (Figure 7), we can hypothesize a role for ARSA1 in the targeting and biogenesis of TOC34. Critical in this respect is the cellular location of ARSA1 that was carefully assessed by raising a polyclonal antibody in rabbit using highly purified recombinant ARSA1 expressed in *E. coli* that we used for detection in cell fractions (Figure 8). Recovery of ARSA1 in the cytosolic fraction rather than in the chloroplast fraction or thylakoid membranes rules out the possibility that ARSA1 might reside in the chloroplast stroma to promote insertion of proteins into the thylakoid membrane. These findings are highly significant and consistent with ARSA1 being needed for the insertion of the TA protein TOC34 in the outer chloroplast membranes. Instead, accumulation of the non-TA protein TOC159 was unaffected (Figure 7c). In turn, the absence of TOC34 would impair the import of nucleus-encoded photosynthetic proteins. While photosystem core complexes (PSAA, D1, CP43, CP47; Figures 4 and S2) are encoded by the plastid genome, subunits of the light-harvesting antenna complexes (LHC) are encoded by the nucleus (LHCII, LHCB4-5 LHCA1-9; Figures 4 and S2) and then imported into the chloroplast where they are folded together with chlorophylls and carotenoid molecules.

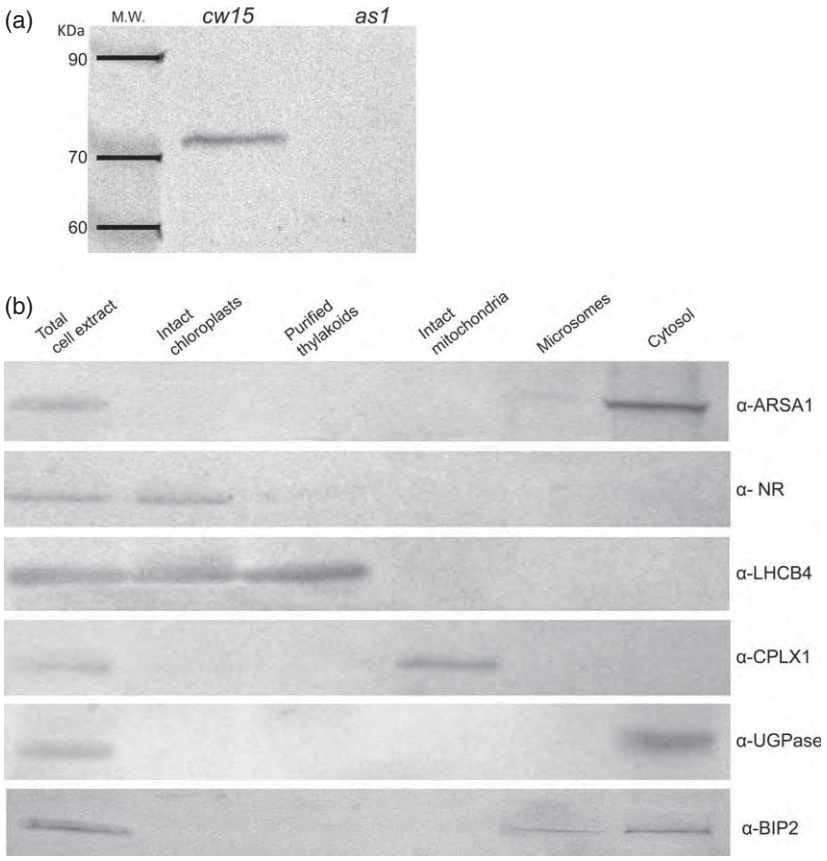

Figure 8. Localization of ARSA1 protein.
(a) Reaction of the α-ARSA1 antiserum (1:4000) versus *cw15* and *as1* total cell extract (10 μg protein per lane).
(b) Localization of ARSA1 in *Chlamydomonas reinhardtii* cell fractions. Samples from the cell fractionation procedure as described in Experimental Procedures (10 μg protein per lane) were run in a 12% Laemmli SDS-PAGE gel, blotted on a polyvinylidene difluoride membrane and revealed using specific antibodies directed to the following marker proteins: LHCB4 (thylakoid membranes); NR, nitrite reductase (chloroplast stroma); CPLX1 (mitochondria); BIP2 (endoplasmic reticulum); UDP-pyroglucosidase (cytosol).

The LHC polypeptides of both photosystems II and I are first recognized by translocases of the outer and inner chloroplast envelopes (TOC and TIC, respectively) (Li and Chiu, 2010) and once in the stroma, targeted to thylakoids thanks to a chloroplast signal recognition particle (SRP)-dependent pathway (Asakura *et al.*, 2004; Schunemann, 2004). Impaired biogenesis of TOC in the present *arsa1* mutant could explain the observed depletion of LHC polypeptides (Figure 4). Interestingly, plastid-encoded subunits of photosystem core complexes are also reduced in the mutant, especially those of photosystem II (Figure 4). Since plastid-encoded photosystem core subunits have no need for import machinery, the *arsa1* mutation could have an indirect effect by causing the reduced import of nucleus-encoded proteins of the transcription and translation machinery of the chloroplast (Gutensohn *et al.* 2004). Alternatively, this could be due to the lack of nuclear factors controlling specifically the assembly and stability of photosystem core complexes (Rochaix, 2011). In addition, import of enzymes involved in chlorophyll biosynthesis could be impaired (Reinbothe *et al.*, 2005), limiting the availability of chlorophyll for chlorophyll-binding protein folding.

It should be noted that TOC34 is present in a single copy in *C. reinhardtii* (Kalanon and McFadden, 2008) in contrast to Arabidopsis that has two paralogs (AtTOC33 and AtTOC34). Different paralogs exhibit distinct expression profiles and form functionally different TOC complexes, allowing the chloroplast to maintain import of non-abundant, housekeeping proteins while simultaneously importing highly abundant photosynthetic subunits (Bauer *et al.*, 2000). In Arabidopsis, TOC33 was proposed to be involved preferentially in the import of photosynthetic proteins, that are deficient in the *atTOC33* mutant, leading to a pale green phenotype especially in the early stages of leaf development when the capacity of plastids to import proteins has to be maximal to ensure the assembly of the photosynthetic apparatus (Jarvis *et al.*, 1998; Kubis *et al.*, 2003). TOC33 can substitute for TOC34 in the *atTOC34* mutant; however the double homozygous *TOC34*/*TOC33* mutation was found to be embryo lethal in Arabidopsis, suggesting an essential function provided by TOC34/TOC33 (Constan *et al.*, 2004). Differently, because of the presence of a single copy of TOC34 in wild-type *C. reinhardtii*, only one TOC complex is reasonably assembled. TOC34 is a core component of the TOC complex, firmly interacting with the other subunits (Waegemann and Soll, 1991). Impaired biogenesis of TOC34 in the *as1* mutant could thus compromise overall translocon function. However, the present *as1* mutant which has a pale green/yellow phenotype that resembles the reported phenotype of the

atTOC33 mutant rather than the double mutant *atTOC34/TOC33* (Gutensohn *et al.*, 2004), still accumulates 8% of the wild-type chlorophyll level and is photosynthetically active, particularly in high-light conditions. Interestingly, accumulation of phosphoribulose kinase (PRK), a nucleus-encoded chloroplast protein involved in the Calvin–Benson cycle, is largely unaffected in the mutant (Figure 4B). Similarly, the levels of some photosynthetic components, namely Rubisco as well as the cytochrome b_6f complex and ATP synthase, that comprise subunits encoded by both nuclear (Rubisco large chain) and chloroplast genes (ATPA, cytochrome *f*), are unaffected or reduced to a lesser extent than the observed depletion in chlorophyll-binding polypeptides of the photosystems (Figures 4 and S2), suggesting import of the required nucleus-encoded assembling partners, despite the *arsa1* mutation. Similar to the case of photosystems I and II, accumulation of these protein complexes is dependent on the presence of all assembling partners and the expression of chloroplast-encoded subunits is controlled by nucleus-encoded factors (Albus *et al.*, 2010; Rahire *et al.*, 2012). These results suggest residual chloroplast protein import to be the primary factor in determining the *as1* phenotype, that could derive from somehow lasting TOC activity catalyzed by TOC159, which is accumulated at similar level in *cw15* and *as1 (*Figure 7c). Alternatively, chloroplast protein import might be less dependent on TOC34 activity in algae than it is in plants (Constan *et al.*, 2004). Although the TOC/TIC translocon is the generally acknowledged import pathway into chloroplasts, an alternative import mechanism was reported for glycosylated proteins that are imported into plastids by first going through the endomembrane system (Chen *et al.*, 2004; Villarejo *et al.*, 2005; Nanjo *et al.*, 2006). This could be an ancient pathway used for delivering proteins from the host to the endosymbiont before the establishment of the TOC/TIC translocon (Reyes-Prieto *et al.*, 2007) and might account for the residual protein import into the plastid in *as1*. Other nucleus-encoded chloroplast proteins, although normally translocated by TOC/TIC, could be alternatively recognized by the ER receptor and delivered through the endomembrane system in particular conditions, such as in the presence of an impaired TOC function in *as1* mutant. This hypothesis would require further investigations but would also make the present mutant a valuable model for studying chloroplast protein import, that could shed light on unexpected complexity.

EXPERIMENTAL PROCEDURES

Chlamydomonas strains and culture conditions

The wild-type strain utilized was *cw15* mt– (mating type minus) (Harris,1989). Insertion mutagenesis was performed using *cw15* mt– as the genetic background, as described in Bonente *et al.* (2011). Wild-type S34 mt + , kindly provided by F. A. Wollman (UMR CNRS/UMPC Institut de Biologie Physico-Chimique, Paris, France) was employed for backcross analysis (Harris,1989). The *as1* mutant was transformed by electroporation (Shimogawara *et al.*, 1998) with *ARSA1* cDNA (accession AV644541, clone HCL090c04; Kazusa Institute, Tokyo, Japan) (Asamizu *et al.*, 2004), excised from pBluescript II SK- by digestion with *Kpn*I and *Bam*HI. All *C. reinhardtii* strains were grown at a controlled temperature of 25°C, with 45 r.p.m. agitation in a 16-h light/8-h dark photoperiod in TAP or minimal HS medium (Harris, 1989). For the growth tests in Figure 6,2 ml of 1×10^7 or 1×10^6 cells ml^{-1} were inoculated on TAP or HS medium and subjected to the light conditions indicated.

DNA extraction, sequencing and PCR analysis

Isolation of genomic DNA was performed according to the manufacturer's manual (Purification of total DNA from plant tissue, mini protocol, Qiagen, http://www.qiagen.com/). Primers ARSA1_Fw Gen5′ and ARSA1_Rv Gen5′ amplify a ~500 pb fragment at the 5′ end of the gene, ARSA1_Fw Gen3′ and ARSA1_Rv Gen3′ amplify a ~500 pb fragment at the 3′ end of the gene, which is deleted in the mutant, and were designed to include introns. Primers ARSA1_Fw CDS3′ and ARSA1_Rv CDS3′ were designed according to the coding sequence of the cDNA clone (Kazusa Institute, Tokyo, Japan) and used to confirm the transformants generated by the complementation experiment. For the sequence of the aforementioned primers see Table S1. Genomic DNAs from *Chlamydomonas* algae were extracted from nuclei using a modified protocol developed from Zhang *et al.* (1995) for plant nuclei. Library preparation was performed using Illumina DNA-seq Sample Preparation protocol (Illumina, Inc., http://www.illumina.com/) starting from 4 μg of nucleus-extracted genomic DNA. Libraries were quality tested and quantified using an Agilent 2100 Bioanalyzer (Agilent Technologies, http://www.agilent.com/), then processed with the Illumina Cluster Generation Station following the manufacturer's recommendations. Sequencing of the genomic DNA of *as1* was carried on using an ILLUMINA® platform as described. The Illumina Genome Analyzer IIx was programmed to run for 76 sequencing cycles in the pair-end set-up. Raw data were processed using Illumina Pipeline v. 1.5. The software SOAP v. 2.20 was used to align the ~100 bp reads against the *C. reinhardtii* genome sequence available online on the NCBI website (http://www.ncbi.nlm.nih.gov/) (Li *et al.*, 2009). The software BLAT was used to distinguish putative genomic regions flanking a pSL18 plasmid sequence into a read in order to identify insertion sites used to construct the map in Figure 1a.

Pigment analysis

Chlorophyll and carotenoids were extracted in 80% acetone. The absorbance spectrum was recorded using an Aminco DW-2000 spectrophotometer (Olis, http://www.olisweb.com) and fitted with spectra of individual pigments (Croce *et al.*, 2002).

Protein analysis

The unstacked thylakoids used for the SDS-PAGE in Figure 4a were obtained from cultures grown in TAP at 50 μM photons m^{-2} sec^{-1}. Cells were collected during the exponential phase, frozen in liquid nitrogen and resuspended in 0.1 M Tricine KOH pH 7.8, 0.5% milk powder before sonication (two cycles of 5 sec). The sample was centrifuged for 10 min at 10 000 ***g*** and the pellet was resuspended in 25 mM HEPES KOH pH 7.5, 10 mM EDTA. Debris was removed by centrifugation for 1 min at 500 ***g*** and finally thylakoids were collected at 10 000 ***g*** and resuspended in 25 mM HEPES KOH pH 7.5, 10 mM EDTA, 50% glycerol. Thylakoid

polypeptides were diluted in loading buffer (1% running buffer, 2% SDS, 5% β-mercaptoethanol, 10% glycerol), analysed by TRIS-sulfate SDS-PAGE 10–20% (Bassi and Wollman, 1991) and visualized by Coomassie staining. For immunoblots, total protein extracts were obtained from cells grown in TAP under 50 μM photons m^{-2} sec^{-1} illumination, collected and resuspended in loading buffer. Protein concentration was determined by colorimetric measurement with bicinchoninic acid (Pierce, http://www.piercenet.com/). The antibodies against Arabidopsis TOC34 and BiP2 were purchased from Agrisera (http://www.agrisera.com/).

Sample preparation for transmission electron microscopy

Chlamydomonas reinhardtii cells grown in TAP medium under 50 μM photons m^{-2} sec^{-1} illumination were harvested during the exponential growth phase and fixed with 3% glutaraldehyde in 0.1 M cacodylate buffer for 2 days at 4°C and rinsed three times for 30 min each with 0.1 M cacodylate buffer. Cells were then post-fixed for 2 h at 4°C using 1% osmium tetroxide in 0.1 M cacodylate buffer, dehydrated in increasing concentrations of ethanol (up to 100% ethanol) and embedded in araldite–dodecenylsuccinic anhydride. Ultrathin sections of 40 nm were examined with a FEI Tecnai T12 electron microscope operating at 100 kV accelerating voltage at the Department of Biology, University of Padova.

Recombinant protein expression, purification and antibody production

The *ARSA1* sequence encoding the mature protein was amplified by RT-PCR with the ARSA1_Fw*Bam*HI and ARSA1_Rv*Hin*dIII primers (Table S1) and cloned into the *Bam*HI and *Hin*dIII restriction sites of the pRSFduet-1 vector (Millipore, http://www.millipore.com/) for expression in BL21 *E. coli* strain. Expression was induced with isopropyl β-D-1-thiogalactopyranoside overnight at 37°C, the cell extract was loaded into a Ni + + column and the protein eluted with 250 mM imidazole. The ARSA1 recombinant protein was further purified from low-level contaminants by SDS-PAGE followed by electroelution of the excised Coomassie-stained band. In total, 100 μg of the purified protein was combined with Freund's adjuvant to form a stable emulsion that was injected subcutaneously into a rabbit. This procedure was repeated after 3 weeks, and 1 week after injection blood was collected from the central ear artery and the antibody's titer was checked by immunoblot.

Cell fractionation and immunoassay analysis

Cw15 cells were mildly broken by passing through a 27-gauge needle at a low flow rate (Mason *et al.*, 2006). Unbroken cells and chloroplasts were pelleted at 3000 ***g*** for 5 min while the supernatant was submitted to serial rounds of centrifugations at, respectively 20 000, 40 000 and 100 000 ***g*** in order to pellet different microsomal fractions. Intact chloroplasts and mitochondrial preparations were obtained according to the procedure described in Jans *et al.* (2008). Highly purified thylakoids were obtained as previously described (Bassi and Wollman, 1991).

The protein content of the cell fractions was determined by bicinchoninic acid protein assay (Pierce) and the same amounts of protein were loaded on 12% acrylamide gels for SDS-PAGE (Laemmli, 1970). Proteins were then transferred to polyvinylidene difluoride membranes and immunoassayed with different antibodies directed versus marker antigens for distinct cell compartments: LHCB4 (thylakoid membranes), nitrite reductase (chloroplast stroma), CPLX1 (mitochondria), BIP2 (endoplasmic reticulum), UDP-pyroglucosidase (cytosol).

ACKNOWLEDGEMENTS

The authors thank the Centro di Genomica Funzionale of the University of Verona for the help in analyzing ILLUMINA® genome sequence data obtained at the Institute of Applied Genomics, University of Udine, by Professor Michele Morgante. Professor Claire Remacle (Université de Liège) is thanked for help with isolation of intact chloroplasts and mitochondria and for the kind gift of Cplx1 antibody. Professor Juergen Soll (Ludwig Maximilian Universität München) is thanked for the kind gift of anti-TOC75 and TOC159 antibodies and Professor Rudolf Tishner (University of Göttingen) for the anti-nitrite reductase antibody. The FP7 EEC project 'SUNBIOPATH' and the CARIVERONA foundation for grant "BIOMASSE DI OGGI E DI DOMANI" are acknowledged for financial support.

SUPPORTING INFORMATION

Additional Supporting Information may be found in the online version of this article.

Figure S1. Sequence alignment of ARSA-homolog proteins. The cDNA of *Chlamydomonas reinhardtii* ARSA1.

Figure S2. Immunoblot analysis of photosynthetic polypeptides on thylakoid preparations of *cw15* and *as1* mutant, loaded on a per chlorophyll basis.

Figure S3. Reactivity of α-ARSA1 antiserum against fractions from differential centrifugation of *Chlamydomonas cw15* cells.

Figure S4. Reaction of the α-ARSA1 antiserum versus *cw15* and *as1* total cell extract and versus ARSA1 recombinant protein purified from *Escherichia coli* by Ni + + column.

Table S1. Primers used to characterize the *arsa1* mutation and for cloning and expression of recombinant ARSA1 in *Escherichia coli*.

REFERENCES

Albus, C.A., Ruf, S., Schottler, M.A., Lein, W., Kehr, J. and Bock, R. (2010) Y3IP1, a nucleus-encoded thylakoid protein, cooperates with the plastid-encoded Ycf3 protein in photosystem I assembly of tobacco and Arabidopsis. *Plant Cell,* **22**, 2838–2855.

Asakura, Y., Hirohashi, T., Kikuchi, S., Belcher, S., Osborne, E., Yano, S., Terashima, I., Barkan, A. and Nakai, M. (2004) Maize mutants lacking chloroplast FtsY exhibit pleiotropic defects in the biogenesis of thylakoid membranes. *Plant Cell,* **16**(1), 201–214.

Asamizu, E., Nakamura, Y., Miura, K. *et al.* (2004) Establishment of publicly available cDNA material and information resource of Chlamydomonas reinhardtii (Chlorophyta) to facilitate gene function analysis. *Phycologia,* **43**, 722–726.

Bassi, R. and Wollman, F.A. (1991) The Chlorophyll-a/b proteins of photosystem-II in Chlamydomonas-reinhardtii - isolation, characterization and immunological cross-reactivity to higher-plant polypeptides. *Planta,* **183**, 423–433.

Bauer, J., Chen, K.H., Hiltbunner, A., Wehrli, E., Eugster, M., Schnell, D. and Kessler, F. (2000) The major protein import receptor of plastids is essential for chloroplast biogenesis. *Nature,* **403**, 203–207.

Beilharz, T., Egan, B., Silver, P.A., Hofmann, K. and Lithgow, T. (2003) Bipartite signals mediate subcellular targeting of tail-anchored membrane proteins in Saccharomyces cerevisiae. *J. Biol. Chem.* **278**, 8219–8223.

Bonente, G., Formighieri, C., Mantelli, M., Catalanotti, C., Giuliano, G., Morosinotto, T. and Bassi, R. (2011) Mutagenesis and phenotypic selection as a strategy toward domestication of Chlamydomonas reinhardtii strains for improved performance in photobioreactors. *Photosynth. Res.* **108**, 107–120.

Borgese, N. and Fasana, E. (2011) Targeting pathways of C-tail-anchored proteins. *Biochim. Biophys. Acta.* **1808**, 937–946.

Borgese, N. and Righi, M. (2010) Remote origin of tail anchored proteins. *Traffic* **11**, 877–885.

Borgese, N., Brambillasca, S. and Colombo, S. (2007) How tails guide tail-anchored proteins to their destinations. *Curr. Opin. Cell Biol.* **19**, 368–375.

Chen, M.H., Huang, L.F., Li, H.M., Chen, Y.R. and Yu, S.M. (2004) Signal peptide-dependent targeting of a rice a-amylase and cargo proteins to plast-

ids and extracellular compartments of plant cells. *Plant Physiol.* **135**, 1367–1377.

Constan, D., Patel, R., Keegstra, K. and Jarvis, P. (2004) An outer envelope membrane component of the plastid protein import apparatus plays an essential role in Arabidopsis. *Plant J.* **38**, 93–106.

Croce, R., Canino, G., Ros, F. and Bassi, R. (2002) Chromophore organization in the higher-plant photosystem II antenna protein CP26. *Biochemistry,* **41**, 7334–7343.

Dhanoa, P.K., Richardson, L.G.L., Smith, M.D., Gidda, S.K., Henderson, M.P. A., Andrews, D.W. and Mullen, R.T. (2010) Distinct pathways mediate the sorting of tail-anchored proteins to the plastid outer envelope. *PLoS ONE,* **5**(4), e10098.

Falkowski, P.G. and Raven, J.A. (1997) *Aquatic photosynthesis*. Malden, Mass: Blackwell Science.

Ferro, M., Salvi, D., Riviere-Rolland, H., Vermat, T., Seigneurin-Berny, D., Grunwald, D., Garin, J., Joyard, J. and Rolland, N. (2002) Integral membrane proteins of the chloroplast envelope: identification and subcellular localization of new transporters. *Proc. Natl Acad. Sci. USA*, **99**, 11487–11492.

Gutensohn, M., Pahnke, S., Kolukisaoglu, U. *et al.* (2004) Characterization of a T-DNA insertion mutant for the protein import receptor atToc33 from chloroplasts. *Mol. Genet. Gen.* **272**, 379–396.

Harris, E.H. (1989) *The Chlamydomonas Sourcebook. A Comprehensive Guide to Biology and Laboratory Use*. San Diego: Academic Press.

Hu, J.B., Li, J.Z., Qian, X.G., Denic, V. and Sha, B.D. (2009) The crystal structures of yeast Get3 suggest a mechanism for tail-anchored protein membrane insertion. *PLoS ONE*. **4**, e8061.

Huesemann, M.H., Hausmann, T.S., Bartha, R., Aksoy, M., Weissman, J.C. and Benemann, J.R. (2008) Biomass productivities in wild type and pigment mutant of Cyclotella sp (Diatom). *Appl. Biochem. Biotechnol.* **157**, 507–526.

Jans, F., Mignolet, E., Houyoux, P.A., Cardol, P., Ghysels, B., Cuine, S., Cournac, L., Peltier, G., Remacle, C. and Franck, F. (2008) A type II NAD(P)H dehydrogenase mediates light-independent plastoquinone reduction in the chloroplast of Chlamydomonas. *PNAS* **105**, 20246–20551.

Jarvis, P., Chen, L.J., Li, H.M., Pete, C.A., Fankhauser, C. and Chory, J. (1998) An Arabidopsis mutant defective in the plastid general protein import apparatus. *Science,* **282**, 100–103.

Jonikas, M.C., Collins, S.R., Denic, V. *et al.* (2009) Comprehensive characterization of genes required for protein folding in the endoplasmic reticulum. *Science,* **323**, 1693–1697.

Kalanon, M. and McFadden, G.I. (2008) The chloroplast protein translocation complexes of Chlamydomonas reinhardtii: a bioinformatic comparison of Toc and Tic components in plants, green algae and red algae. *Genetics,* **179**, 95–112.

Kalbfleisch, T., Cambon, A. and Wattenberg, B.W. (2007) A bioinformatics approach to identifying tail-anchored proteins in the human genome. *Traffic,* **8**, 1687–1694.

Kriechbaumer, V., Shaw, R., Mukherjee, J., Bowsher, C.G., Harrison, A.M. and Abell, B.M. (2009) Subcellular distribution of tail-anchored proteins in Arabidopsis. *Traffic,* **10**, 1753–1764.

Kubis, S., Baldwin, A., Patel, R., Razzaq, A., Dupree, P., Lilley, K., Kurth, J., Leister, D. and Jarvis, P. (2003) The Arabidopsis ppi1 mutant is specifically defective in the expression, chloroplast import, and accumulation of photosynthetic proteins. *Plant Cell,* **15**, 1859–1871.

Kuroda, M., Dey, S., Sanders, O.I. and Rosen, B.P. (1997) Alternate energy coupling of ArsB, the membrane subunit of the Ars anion-translocating ATPase. *J. Biol. Chem.* **272**, 326–331.

Kutay, U., Hartmann, E. and Rapoport, T.A. (1993) A class of membrane proteins with a C-terminal anchor. *Trends Cell Biol.* **3**, 72–75.

Laemmli, U.K. (1970) Cleavage of structural proteins during the assembly of the head of bacteriophage T4. *Nature,* **15**(5259), 680–685.

Li, H.M. and Chiu, C.C. (2010) Protein transport into chloroplasts. *Annu. Rev. Plant Biol.* **61**(61), 157–180.

Li, R.Q., Yu, C., Li, Y.R., Lam, T.W., Yiu, S.M., Kristiansen, K. and Wang, J. (2009) SOAP2: an improved ultrafast tool for short read alignment. *Bioinformatics,* **25**, 1966–1967.

Maggio, C., Barbante, A., Ferro, F., Frigerio, L. and Pedrazzini, E. (2007) Intracellular sorting of the tail-anchored protein cytochrome b5 in plants: a comparative study using different isoforms from rabbit and Arabidopsis. *J. Exp. Bot.* **58**, 1365–1379.

Martin, W. and Herrmann, R.G. (1998) Gene transfer from organelles to the nucleus: how much, what happens, and why? *Plant Physiol.* **118**, 9–17.

Mason, C.B., Bricker, T.M. and Moroney, J.V. (2006) A rapid method for chloroplast isolation from the green alga Chlamydomonas reinhardtii. *Nat. Protoc.* **1** (5), 2227–2230.

May, T. and Soll, J. (1998) Positive charges determine the topology and functionality of the transmembrane domain in the chloroplastic outer envelope protein Toc34. *J. Cell Biol.* **141**, 895–904.

Merchant, S.S., Prochnik, S.E., Vallon, O. *et al.* (2007) The Chlamydomonas genome reveals the evolution of key animal and plant functions. *Science* **318**, 245–251.

Mukhopadhyay, R., Ho, Y.S., Swiatek, P.J., Rosen, B.P. and Bhattacharjee, H. (2006) Targeted disruption of the mouse Asna1 gene results in embryonic lethality. *FEBS Lett.* **580**, 3889–3894.

Nanjo, Y., Oka, H., Ikarashi, N., Kaneko, K., Kitajima, A., Mitsui, T., Munoz, F.J., Rodriguez-Lopez, M., Baroja-Fernandez, E. and Pozueta-Romero, J. (2006) Rice plastidial N-glycosylated nucleotide pyrophosphatase/phosphodiesterase is transported from the ER-Golgi to the chloroplast through the secretory pathway. *Plant Cell,* **18**, 2582–2592.

Pogson, B.J., Woo, N.S., Forster, B. and Small, I.D. (2008) Plastid signalling to the nucleus and beyond. *Trends Plant Sci.* **13**, 602–609.

Qbadou, S., Tien, R., Soll, J. and Schleiff, E. (2003) Membrane insertion of the chloroplast outer envelope protein, Toc34: constrains for insertion and topology. *J. Cell Sci.* **116**, 837–846.

Rabu, C., Schmid, V., Schwappach, B. and High, S. (2009) Biogenesis of tail-anchored proteins: the beginning for the end? *J. Cell Sci.* **122**, 3605–3612.

Rahire, M., Laroche, F., Cerutti, L. and Rochaix, J.D. (2012) Identification of an OPR protein involved in the translation initiation of the PsaB subunit of photosystem I. *Plant J.* **72**, 652–661.

Raven, J.A. and Allen, J.F. (2003) Genomics and chloroplast evolution: what did cyanobacteria do for plants? *Genome Biol.* **4**, 209.

Reinbothe, S., Pollmann, S., Springer, A., James, R.J., Tichtinsky, G. and Reinbothe, C. (2005) A role of Toc33 in the protochlorophyllide-dependent plastid import pathway of NADPH: protochlorophyllide oxidoreductase (POR) A. *Plant J.* **42**, 1–12.

Reyes-Prieto, A., Weber, A.P.M. and Bhattacharya, D. (2007) The origin and establishment of the plastid in algae and plants. *Annu. Rev. Genet.* **41**, 147–168.

Rochaix, J.D. (2011) Assembly of the Photosynthetic Apparatus. *Plant Physiol.* **155**, 1493–1500.

Schuldiner, M., Metz, J., Schmid, V., Denic, V., Rakwalska, M., Schmitt, H. D., Schwappach, B. and Weissman, J.S. (2008) The GET complex mediates insertion of tail-anchored proteins into the ER membrane. *Cell,* **134**, 634–645.

Schunemann, D. (2004) Structure and function of the chloroplast signal recognition particle. *Curr. Genet.* **44**, 295–304.

Shimogawara, K., Fujiwara, S., Grossman, A. and Usuda, H. (1998) High-efficiency transformation of Chlamydomonas reinhardtii by electroporation. *Genetics,* **148**, 1821–1828.

Stefanovic, S. and Hegde, R.S. (2007) Identification of a targeting factor for posttranslational membrane protein insertion into the ER. *Cell,* **128**, 1147–1159.

Villarejo, A., Buren, S., Larsson, S. *et al.* (2005) Evidence for a protein transported through the secretory pathway en route to the higher plant chloroplast. *Nat. Cell Biol.* **7**, 1224–1231.

Waegemann, K. and Soll, J. (1991) Characterization of the protein import apparatus in isolated outer envelopes of chloroplasts. *Plant J.* **1**, 149–158.

Zhang, H.B., Zhao, X., Ding, X., Paterson, A.H. and Wing., R.A. (1995) Preparation of megabase-size DNA from plant nuclei. *Plant J.* **7**, 175–184.

Zhou, T.Q., Radaev, S., Rosen, B.P. and Gatti, D.L. (2000) Structure of the ArsA ATPase: the catalytic subunit of a heavy metal resistance pump. *EMBO J.* **19**, 4838–4845.

Supplementary Information

Figure S1. Sequence alignment of ARSA-homolog proteins. C. r. ARSA1 protein sequence has been blasted in NCBI, blastp algorithm, non-redundant protein sequences (nr) database. The entries have then be multiply aligned, thus conserving informations on evolution divergences, by using ClustalW. First (A) and second (B) ARSA_ATPase domains of ARSA1 are aligned with C. r. ARSA2 sequence and with those from *Saccharomyces cerevisiae* (GET3), *Arabidopsis thaliana* (At3g10350, At5g60730, At1g01910), *Homo sapiens* (ASNA1) and *Escherichia coli* (Taxonomy ID: 562, PDB ID: 1F48). The amino acid residues are numbered at the right side of the alignment. The conserved cysteines of the zinc finger motif for dimerization and the conserved hydrophobic residues involved in forming the TM domain-binding groove, as proposed in GET3 (Hu et al., 2009), are labelled in green and grey, respectively. C) The cDNA of *C. reinhardtii* ARSA1 from which the aminoacid sequence is deduced, in grey the untranslated regions, in black the encoding sequence (from sequencing of the Kazusa clone HCL090c04, accession AV644541). Underlined is the region deleted in *as1* mutant, corresponding to the dashed line in figure 1A.

a

```
E.coli_ARSA     ------------------------------------------------------------
GET3            ------------------------------------------------------------
Chlamy_ARSA1    MALASGNRLGSARGQTCADASGRVAPRLLSRACSGSPLALGVLACLGAASSVKPHPRLPA 60
Chlamy_ARSA2    ------------------------------------------------------------
At3g10350       MATLSSYLLSSP------------------PLCKSRFSATSLVSGIDFISFSPRTTLSS 41
At5g60730       MAAL--LLLNRV------------------SRSTSSISLHRVAGTLGFNSFNAQIHGDR 39
At1g01910       ------------------------------------------------------------
ASNA1           ------------------------------------------------------------


E.coli_ARSA     --------------------------------MQFLQNIPP-----YLFFTGKGGVGKT 22
GET3            --MDLT-------------------------VEPNLHSLITSTTHKWIFVGGKGGVGKT 32
Chlamy_ARSA1    TTSAASAPLPARG----PAPCAAVPTVVTPDNATGVFEELAAGQQRKYIMISGKGGVGKT 116
Chlamy_ARSA2    MAADMP-------------------------DPTLQNVVDQKELKWIFVGGKGGVGKT 33
At3g10350       SSTVLPAILSLSVKHNRRRNSLQVKSVASPTETISEFDEMVSGTKRKYYMLGGKGGVGKT 101
At5g60730       ISGTL----------------FRVRSLATLAEGASHFNEMVSVNQRKYYLLGGKGGVGKT 83
At1g01910       MAADLP-------------------------EATVQNILDQESLKWVFVGGKGGVGKT 33
ASNA1           MAAGVAGWGVEAE---------EFEDAPDVEPLEPTLSNIIEQRSLKWIFVGGKGGVGKT 51
                                                . .:       : :. ********


E.coli_ARSA     SISCATAIRLAE--QGKRVLLVSTDPASNVGQVFSQTIG-NTIQAIASVPG-LSALEIDP 78
GET3            TSSCSIAIQMALSQPNKQFLLISTDPAHNLSDAFGEKFG-KDARKVTGMNN-LSCMEIDP 90
Chlamy_ARSA1    SLSASLAVKLAA--AGHTTLVVSTDPAHSLSDSLAQDVSGGRPVLLQGTDLPLWGLEIDP 174
Chlamy_ARSA2    TTSSSLAVALAESGTRNRVLIISTDPAHNLSDAFRQKFT-KTPTLVNGFTN-LFAMEVDP 91
At3g10350       SCAASLAVRFAN--NGHPTLVVSTDPAHSLSDSFAQDLTGGMLVPVEGPEAPLFALEINP 159
At5g60730       SCAASLAVKFAS--HGHPTIVVSTDPAHSLSDSFSQDLSGGVLKPVQGVDSPLLALEITP 141
At1g01910       TCSSILAICLAS--VRSSVLIISTDPAHNLSDAFQQRFT-KSPTLVQGFSN-LFAMEVDP 89
ASNA1           TCSCSLAVQLSK--GRESVLIISTDPAHNISDAFDQKFS-KVPTKVKGYDN-LFAMEIDP 107
                : :.  *: ::        :::***** .:.: : : .       : .    *  :*: *


E.coli_ARSA     QAAAQQYR---------------------ARIVDPIKGVLPDDVVSSINEQLSGACT-- 114
GET3            SAALKDMNDMA-------------VSRANNNGSDGQGDDLGSLLQGGALADLTGSIPGI 136
Chlamy_ARSA1    EEAKREFFEGSGAGQDGEAGGPSAASQVSDFMNRMGMGFVIDQLKELKLGELLNTPPPGL 234
Chlamy_ARSA2    QPDIGEM-----------------------EQLEWAQDSFLT--------ELAGSIPGI 119
At3g10350       EKAREEFRSAS--QMNGGTG-------VKDFMDGMGLGMLVEQLGELKLGELLDTPPPGL 210
At5g60730       EIMKDEIK-----RQTGDKS-------VKNMMDSMGLGMFAGELGDLNLEDMLNAASPGI 189
At1g01910       TVETDDM-----------------------AGTDG-MDGLFS--------DLANAIPGI 116
ASNA1           SLGVAEL-----------------------PDEFFEEDNMLSMGKK-MMQEAMSAFPGI 142
                     :                                                  . .
```

```
E.coli_ARSA     TEIAAFDEFTGLLTDAS--LLTRFDHIIFDTAPTGHTIRLLQLPGAWSSFIDSNPEGASC 172
GET3            DEALSFMEVMKHIKRQEQGEGETFDTVIFDTAPTGHTLRFLQLPNTLSKLLEKFGEITNK 196
Chlamy_ARSA1    DEAVAIAKVVQFVQAAE---YARFSRIVFDTAPTGHTLRLLALPDFVDASLAKVIRLRKK 291
Chlamy_ARSA2    DEAMSFAEVMKQVQTMD------YDTIVFDTAPTGHTLRLLNFPTILEKGLSKLVALKGA 173
At3g10350       DEAIAISKVIQFLESPE---YNMFTRIVFDTAPTGHTLRLLSLPDFLDASIGKILKLRQK 267
At5g60730       DEIAAISKVLQFMEAPE---YSRFTRIVFDTAPTGHTLRLLSLPDFYDSSISKITKLKKK 246
At1g01910       DEAMSFAEMLKLVQTMD------YATIVFDTAPTGHTLRLLQFPATLEKGLSKLMSLKSR 170
ASNA1           DEAMSYAEVMRLVKGMN------FSVVVFDTAPTGHTLRLLNFPTIVERGLGRLMQIKNQ 196
                 *  :  :.   :   .      :  ::*********:*:* :*   .  :

E.coli_ARSA     LGPMAG-------------------------LEKQREQYAYAVEALSDPKRTRLVLVAR 206
GET3            LGPMLN---SFMGAGNVDIS----------GKLNELKANVETIRQQFTDPDLTTFVCVCI 243
Chlamy_ARSA1    LNGATSVVRGLFGAGESQD--------EAVEKLELLQQRVRMVKALFRDKTQTEFIIATI 343
Chlamy_ARSA2    MGGMMGQVTRMLGGMAGGGEGAADLPDQLLGKVEGMLDVVRKVSAQFKDPLLTTFVAVCI 233
At3g10350       ITSATSAIKSVFGKEEKGP--------DAADKLEKLRERMVKVRELFRDTESTEFVIVTI 319
At5g60730       ITAAASAFKLVFGKKEIQQK-------ELPNELDQLKERMEKVRNVFRDVDTTEFVIVTI 299
At1g01910       FGGLMTQMSRMFGMEDEFGE------DALLGRLEGLKDVIEQVNRQFKDPDMTTFVCVCI 224
ASNA1           ISPFISQMCNMLGLGDMNAD-------QLASKLEETLPVIRSVSEQFKDPEQTTFICVCI 249
                :                                  ::           : *   * :: .

E.coli_ARSA     LQKSTLQEVARTHLELAAIGLKNQYLVINGVLPK--TEAANDTLAAAIWEREQEALANLP 264
GET3            SEFLSLYETERLIQELISYDMDVNSIIVNQLLFAENDQEHNCKRCQARWKMQKKYLDQID 303
Chlamy_ARSA1    PTYLGVNESSRLLQALRAEQIPCKRIIVNQIVGP---QQGD-AYLRMKMKDQIAALEMVA 399
Chlamy_ARSA2    PEFLSLYETERLVQELAKFEIDCRNIVINQIIFP--ESVGGSRLLDARVRMQQKYLDQFY 291
At3g10350       PTVMAVSESSRLSASLKKESVPVKRLIVNQLLPP---SSSDCKFCSIKRKDQMRALDMIR 376
At5g60730       PTVMAINESSRLHASLRKENVPVHRLIVNQLLPQ---SESDCKFCSIRRKEQTRVLGLIQ 356
At1g01910       PEFLSLYETERLVQELAKFEIDTHNIIINQVLYD--DEDVESKLLRARMRMQQKYLDQFY 282
ASNA1           AEFLSLYETERLIQELAKCKIDTHNIIVNQLVFP--DPEKPCKMCEARHKIQAKYLDQME 307
                     : *  *    *    :  . :::* ::               . :   *  .

E.coli_ARSA     --ADLAGLPTDTLFLQPVNMVGVSALSRLLSTQPVASPSSDEYLQQRP------------ 310
GET3            --ELYEDFHVVKMPLCAGEIRGLNNLTKFSQFLNKEYNPITDGKVIYELEDKE------- 354
Chlamy_ARSA1    NDPGLRPLRKVIAPMVDVEVR-------------------------------------- 420
Chlamy_ARSA2    --ELYEDFHILQLPLLEEEVRGPEALKAFAVNLLKPYVPAPPTDAAARQAALVSEVAALK 349
At3g10350       EDSELSALTLMEAPLVDMEIRGVPALRFLGDIIWK------------------------- 411
At5g60730       NDTELSGLKLIQSPLLDAEIRGVPALKFMGDLIWK------------------------- 391
At1g01910       --MLYDDFNITKLPLLPEEVTGVEALKAFSHKFLTPYHPTTSRSNVEELERKVHTLR-LQ 339
ASNA1           --DLYEDFHIVKLPLLPHEVRGADKVNTFSALLLEPYKPPSAQ---------------- 348
                       :      :   ::

E.coli_ARSA     --------------
GET3            --------------
Chlamy_ARSA1    --------------
Chlamy_ARSA2    KRVAELEAALAKK- 362
At3g10350       --------------
At5g60730       --------------
At1g01910       LKTAEEELERVKSG 353
ASNA1           --------------
```

b

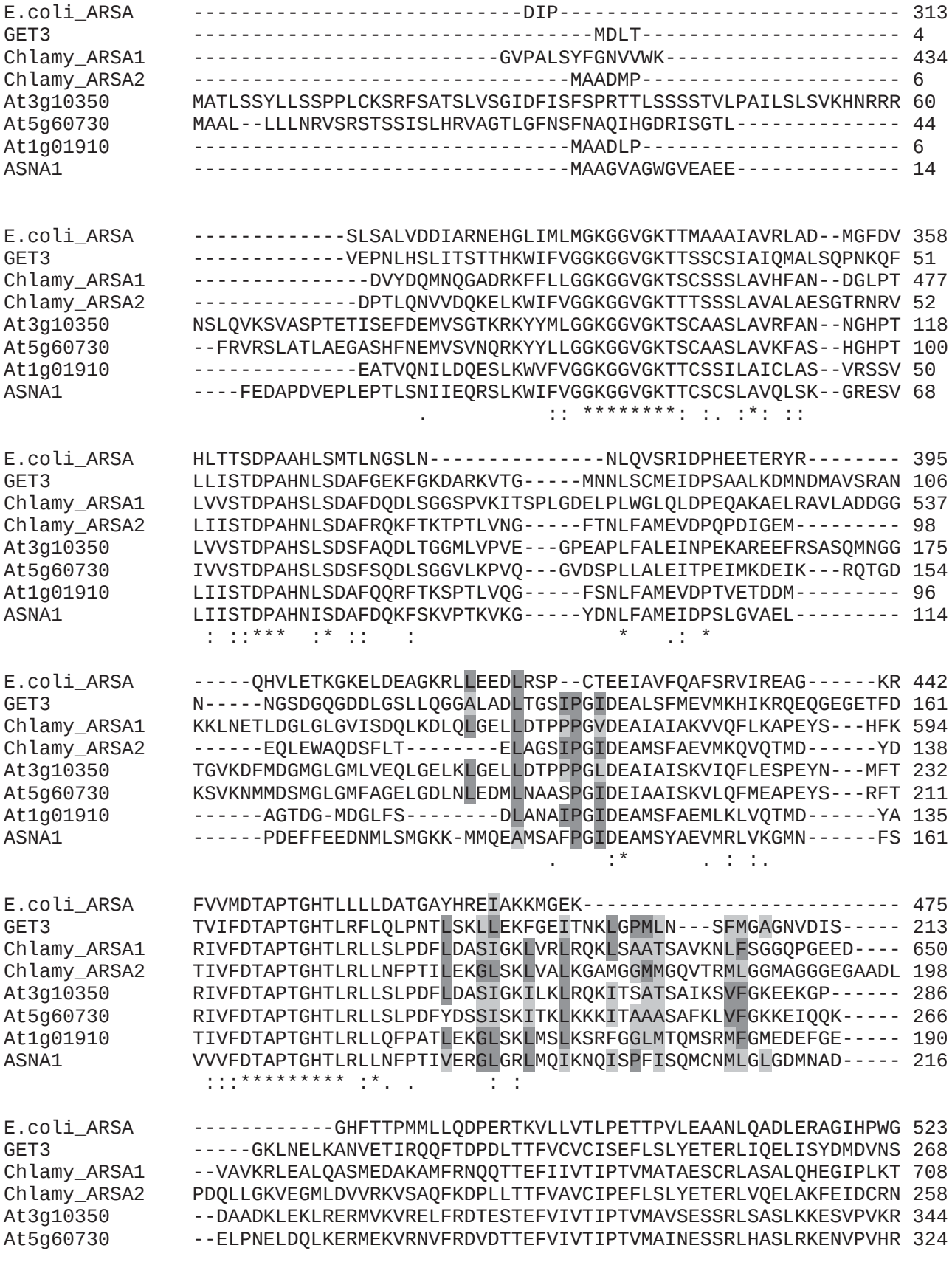
E.coli_ARSA ----------DIP---------- 313
GET3 ----------MDLT---------- 4
Chlamy_ARSA1 ----------GVPALSYFGNVVWK---------- 434
Chlamy_ARSA2 ----------MAADMP---------- 6
At3g10350 MATLSSYLLSSPPLCKSRFSATSLVSGIDFISFSPRTTLSSSSTVLPAILSLSVKHNRRR 60
At5g60730 MAAL--LLLNRVSRSTSSISLHRVAGTLGFNSFNAQIHGDRISGTL---------- 44
At1g01910 ----------MAADLP---------- 6
ASNA1 ----------MAAGVAGWGVEAEE---------- 14
E.coli_ARSA ----------SLSALVDDIARNEHGLIMLMGKGGVGKTTMAAAIAVRLAD--MGFDV 358
GET3 ----------VEPNLHSLITSTTHKWIFVGGKGGVGKTTSSCSIAIQMALSQPNKQF 51
Chlamy_ARSA1 ----------DVYDQMNQGADRKFFLLGGKGGVGKTSCSSSLAVHFAN--DGLPT 477
Chlamy_ARSA2 ----------DPTLQNVVDQKELKWIFVGGKGGVGKTTTSSSLAVALAESGTRNRV 52
At3g10350 NSLQVKSVASPTETISEFDEMVSGTKRKYYMLGGKGGVGKTSCAASLAVRFAN--NGHPT 118
At5g60730 --FRVRSLATLAEGASHFNEMVSVNQRKYYLLGGKGGVGKTSCAASLAVKFAS--HGHPT 100
At1g01910 ----------EATVQNILDQESLKWVFVGGKGGVGKTTCSSILAICLAS--VRSSV 50
ASNA1 ----FEDAPDVEPLEPTLSNIIEQRSLKWIFVGGKGGVGKTTCSCSLAVQLSK--GRESV 68
E.coli_ARSA HLTTSDPAAHLSMTLNGSLN----------NLQVSRIDPHEETERYR------- 395
GET3 LLISTDPAHNLSDAFGEKFGKDARKVTG-----MNNLSCMEIDPSAALKDMNDMAVSRAN 106
Chlamy_ARSA1 LVVSTDPAHSLSDAFDQDLSGGSPVKITSPLGDELPLWGLQLDPEQAKAELRAVLADDGG 537
Chlamy_ARSA2 LIISTDPAHNLSDAFRQKFTKTPTLVNG-----FTNLFAMEVDPQPDIGEM--------- 98
At3g10350 LVVSTDPAHSLSDSFAQDLTGGMLVPVE---GPEAPLFALEINPEKAREEFRSASQMNGG 175
At5g60730 IVVSTDPAHSLSDSFSQDLSGGVLKPVQ---GVDSPLLALEITPEIMKDEIK---RQTGD 154
At1g01910 LIISTDPAHNLSDAFQQRFTKSPTLVQG-----FSNLFAMEVDPTVETDDM--------- 96
ASNA1 LIISTDPAHNISDAFDQKFSKVPTKVKG-----YDNLFAMEIDPSLGVAEL--------- 114
E.coli_ARSA -----QHVLETKGKELDEAGKRLLEEDLRSP--CTEEIAVFQAFSRVIREAG------KR 442
GET3 N-----NGSDGQGDDLGSLLQGGALADLTGSIPGIDEALSFMEVMKHIKRQEQGEGETFD 161
Chlamy_ARSA1 KKLNETLDGLGLGVISDQLKDLQLGELLDTPPPGVDEAIAIAKVVQFLKAPEYS---HFK 594
Chlamy_ARSA2 ------EQLEWAQDSFLT--------ELAGSIPGIDEAMSFAEVMKQVQTMD------YD 138
At3g10350 TGVKDFMDGMGLGMLVEQLGELKLGELLDTPPPGLDEAIAISKVIQFLESPEYN---MFT 232
At5g60730 KSVKNMMDSMGLGMFAGELGDLNLEDMLNAASPGIDEIAAISKVLQFMEAPEYS---RFT 211
At1g01910 ------AGTDG-MDGLFS--------DLANAIPGIDEAMSFAEMLKLVQTMD------YA 135
ASNA1 ------PDEFFEEDNMLSMGKK-MMQEAMSAFPGIDEAMSYAEVMRLVKGMN------FS 161
E.coli_ARSA FVVMDTAPTGHTLLLLDATGAYHREIAKKMGEK---------- 475
GET3 TVIFDTAPTGHTLRFLQLPNTLSKLLEKFGEITNKLGPMLN---SFMGAGNVDIS----- 213
Chlamy_ARSA1 RIVFDTAPTGHTLRLLSLPDFLDASIGKLVRLRQKLSAATSAVKNLFSGGQPGEED---- 650
Chlamy_ARSA2 TIVFDTAPTGHTLRLLNFPTILEKGLSKLVALKGAMGGMMGQVTRMLGGMAGGGEGAADL 198
At3g10350 RIVFDTAPTGHTLRLLSLPDFLDASIGKILKLRQKITSATSAIKSVFGKEEKGP------ 286
At5g60730 RIVFDTAPTGHTLRLLSLPDFYDSSISKITKLKKKITAAASAFKLVFGKKEIQQK----- 266
At1g01910 TIVFDTAPTGHTLRLLQFPATLEKGLSKLMSLKSRFGGLMTQMSRMFGMEDEFGE----- 190
ASNA1 VVVFDTAPTGHTLRLLNFPTIVERGLGRLMQIKNQISPFISQMCNMLGLGDMNAD----- 216
E.coli_ARSA ----------GHFTTPMMLLQDPERTKVLLVTLPETTPVLEAANLQADLERAGIHPWG 523
GET3 -----GKLNELKANVETIRQQFTDPDLTTFVCVCISEFLSLYETERLIQELISYDMDVNS 268
Chlamy_ARSA1 --VAVKRLEALQASMEDAKAMFRNQQTTEFIIVTIPTVMATAESCRLASALQHEGIPLKT 708
Chlamy_ARSA2 PDQLLGKVEGMLDVVRKVSAQFKDPLLTTFVAVCIPEFLSLYETERLVQELAKFEIDCRN 258
At3g10350 --DAADKLEKLRERMVKVRELFRDTESTEFVIVTIPTVMAVSESSRLSASLKKESVPVKR 344
At5g60730 --ELPNELDQLKERMEKVRNVFRDVDTTEFVIVTIPTVMAINESSRLHASLRKENVPVHR 324

```
At1g01910       -DALLGRLEGLKDVIEQVNRQFKDPDMTTFVCVCIPEFLSLYETERLVQELAKFEIDTHN 249
ASNA1           --QLASKLEETLPVIRSVSEQFKDPEQTTFICVCIAEFLSLYETERLIQELAKCKIDTHN 274
                              .      : :   * .: * :.   .  *: .*   *    :

E.coli_ARSA     WIINNSLSI---ADTRSPLLRMRAQQELPQIESVKRQHAS------RVALVPVLASEPTG 574
GET3            IIVNQLLFAENDQEHNCKRCQARWKMQKKYLDQIDELYED-----FHVVKMPLCAGEIRG 323
Chlamy_ARSA1    IIVNQVVQA---NATD-KFLTARRADQARALHHLEEDTGPDGLASLQLIKAPLCDLEVRG 764
Chlamy_ARSA2    IVINQIIFP--ESVGGSRLLDARVRMQQKYLDQFYELYED-----FHILQLPLLEEEVRG 311
At3g10350       LIVNQLLPP---SSSDCKFCSIKRKDQMRALDMIREDSE---LSALTLMEAPLVDMEIRG 398
At5g60730       LIVNQLLPQ---SESDCKFCSIRRKEQTRVLGLIQNDTE---LSGLKLIQSPLLDAEIRG 378
At1g01910       IIINQVLYD--DEDVESKLLRARMRMQQKYLDQFYMLYDD-----FNITKLPLLPEEVTG 302
ASNA1           IIVNQLVFP--DPEKPCKMCEARHKIQAKYLDQMEDLYED-----FHIVKLPLLPHEVRG 327
                 ::*: :               :   :   :  .             :   *:   *  *

E.coli_ARSA     IDKLKQLAG------------------------------------------ 589
GET3            LNNLTKFSQFLNKEYNPITDGKVIYELEDKE--------------------- 354
Chlamy_ARSA1    VPALSYFGNVVWK--------------------------------------- 777
Chlamy_ARSA2    PEALKAFAVNLLKPYVPAPPTDAAARQAALVSEVAALKKRVAELEAALAKK- 362
At3g10350       VPALRFLGDIIWK--------------------------------------- 411
At5g60730       VPALKFMGDLIWK--------------------------------------- 391
At1g01910       VEALKAFSHKFLTPYHPTTSRSNVEELERKVHTLR-LQLKTAEEELERVKSG 353
ASNA1           ADKVNTFSALLLEPYKPPSAQ------------------------------ 348
                   :  :.
```

C

CTAAAAGACCCAGGTTCTATAAACACGCCATAAGACCTAGCAGCGCGCGGTTCTTGCT
GCTTTGCAATTGCCGACCAGCGCAACACCTCCATTTCGGCGACACCAGAAACTCTCCG
AATCCATCAACTTCTGGATTGGTAGAATGGCATTAGCCTCGGGGAATCGGCTGGGGTC
CGCGCGCGGACAGACGTGCGCGGATGCCTCTGGACGCGTTGCCCCTCGCTTGCTTTCCC
GGGCTTGCAGCGGCTCACCATTGGCGTTGGGAGTTCTCGCGTGTCTCGGTGCGGCATCA
AGCGTCAAGCCACACCCGCGCCTGCCCGCCACCACCTCCGCCGCGTCAGCACCGCTGC
CTGCTCGTGGGCCTGCGCCCTGCGCTGCCGTGCCGACGGTGGTGACGCCCGACAACGC
CACGGGCGTGTTTGAGGAGCTGGCCGCGGGGCAGCAGCGCAAGTACATCATGATCAGC
GGCAAGGGCGGCGTGGGCAAGACCAGCCTGTCCGCCTCCCTGGCCGTGAAGCTGGCGG
CGGCGGGTCACACCACCCTGGTGGTGTCCACCGACCCCGCCCACTCCCTCAGCGACTC
ACTGGCTCAGGACGTGAGCGGCGGCAGGCCTGTGCTGCTGCAGGGGACCGATCTGCCG
CTCTGGGGTCTGGAGATCGACCCTGAGGAGGCCAAGCGCGAGTTCTTTGAGGGCAGCG
GCGCGGGCCAGGACGGCGAGGCGGGGGGGCCCAGCGCGGCGTCGCAGGTCAGCGACT
TCATGAACCGCATGGGCATGGGCTTTGTCATCGACCAGCTCAAGGAACTGAAGCTGGG
CGAGCTGCTCAACACGCCGCCGCCAGGCCTGGATGAGGCGGTGGCCATTGCCAAGGTG
GTCCAGTTCGTGCAGGCGGCCGAGTACGCCCGCTTCAGCCGCATCGTGTTCGACACCG
CCCCCACTGGCCACACGCTGCGCCTGCTGGCGCTGCCCGACTTTGTGGATGCGTCGCTG
GCCAAGGTTATCCGGCTGCGCAAGAAGCTCAACGGCGCCACCTCCGTCGTGCGCGGCC
TGTTCGGAGCGGGCGAGAGCCAGGACGAGGCGGTTGAGAAGCTGGAGCTGCTGCAGC
AGCGTGTCCGCATGGTGAAGGCGCTGTTCCGCGACAAGACCCAGACCGAGTTCATCAT
CGCCACAATCCCCACCTACCTGGGAGTCAACGAGAGCAGCAGGCTGCTGCAAGCGCTG
CGGGCCGAGCAAATCCCCTGCAAGCGCATCATCGTGAACCAGATCGTGGGACCGCAGC
AGGGTGACGCCTACCTGCGCATGAAGATGAAGGACCAGATTGCGGCGCTGGAGATGGT
GGCGAACGACCCAGGGCTGAGGCCCCTGCGCAAGGTTATTGCGCCCATGGTGGACGTG
GAGGTTCGCGGCGTGCCCGCACTGTCCTACTTTGGCAACGTGGTGTGGAAGGATGTGT
ACGACCAGATGAACCAGGGCGCCGACCGCAAGTTCTTCCTGCTGGGCGGCAAGGGCGG
CGTGGGCAAGACCAGCTGCTCCTCATCGCTGGCGGTCCACTTCGCCAACGACGGCCTG
CCCACCCTGGTGGTGTCCACCGACCCCGCCCATTCCCTGAGCGACGCATTCGACCAGG

ACCTGTCCGGCGGCAGCCCCGTCAAGATCACCTCGCCGCTGGGTGACGAGCTGCCGCT
GTGGGGCCTGCAGCTGGACCCCGAGCAGGCCAAGGCGGAGCTGCGGGCGGTGCTTGC
GGACGACGGCGGCAAGAAGCTGAACGA**G**ACGCTGGACGGTCTTGGCCTGGGTGTGAT
CAGCGACCAGCTCAAGGACCTGCAGCTGGGCGAGCTGCTGGACACGCCGCCGCCCGGC
GTGGACGAGGCCATTGCCATCGCCAAGGTGGTCCAGTTCCTCAAGGCCCCCGAGTACT
CGCACTTCAAGCGCATCGTGTTCGACACCGCCCCCACTGGCCACACCCTGCGCCTGCTG
TCGTTGCCCGACTTCCTAGACGCCTCCATCGGCAAGCTGGTGCGGCTGCGCCAGAAGCT
GTCCGCCGCGACCTCGGCCGTGAAGAACCTGTTCAGCGGCGGCCAGCCGGGAGAGGA
GGACGTAGCGGTGAAGCGCCTGGAGGCGCTGCAGGCGAGCATGGAGGACGCCAAGGC
GATGTTCCGCAACCAGCAGACCACCGAGTTCATCATTGTCACCATTCCCACCGTCATGG
CCACAGCTGAGAGCTGCAGGCTGGCGTCGGCGCTGCAGCACGAAGGCATCCCGCTCAA
AACCATCATCGTCAACCAGGTGGTGCAGGCCAACGCAACAGACAAGTTCCTGACCGCA
CGCCGAGCAGACCAGGCCCGCGCGCTGCACCACCTGGAGGAGGACACGGGCCCGGAC
GGCCTGGCGTCGCTGCAGCTGATCAAGGCGCCGCTGTGCGACCTGGAAGTGCGCGGCG
TGCCCGCGCTGTCGTACTTCGGCAACGTGGTGTGGAAGTGAGGAGACTACTAGATGAG
GCGTGTGTGCGGTGCGTGCGGCTGACTGACGGGCTGACTGACCGACTGGATAACTGAC
AGATTGACTGCGCGGTACTGCGGCGTATGAAGCTAAGGGGCAGGACTTCCCGCGCCGC
AGGGAAGGCCGCCATGCCATGTGATTGTGCTGCATCGCGCATGGTTGCGTTGGTGGCT
ACTGGCTAGATGTGCATGTGCGTAAGTTTCCTCCGGCCTCCGGGCCGCCAGGCACAATT
GGAGCGTGCGCACGTGCAAAGCGCAGAGGAGGAGGAGGAAACGGGTGCGGAGGCGT
GGGAGGCAGGGCACCCTTGGTGGGAGGCTGAGTCCTCAGTCATTCTGTTGTATCCTCA
ACCATAGAAAAAAAAAAAAAAAAAAAA

Figure S2. Immunoblot analysis on a per chlorophyll basis of the indicated polypeptides on thylakoid preparations. Dilutions of 0.2-0.4-0.8-1.2 µg of chlorophylls were loaded for *cw15* and *as1* mutant.

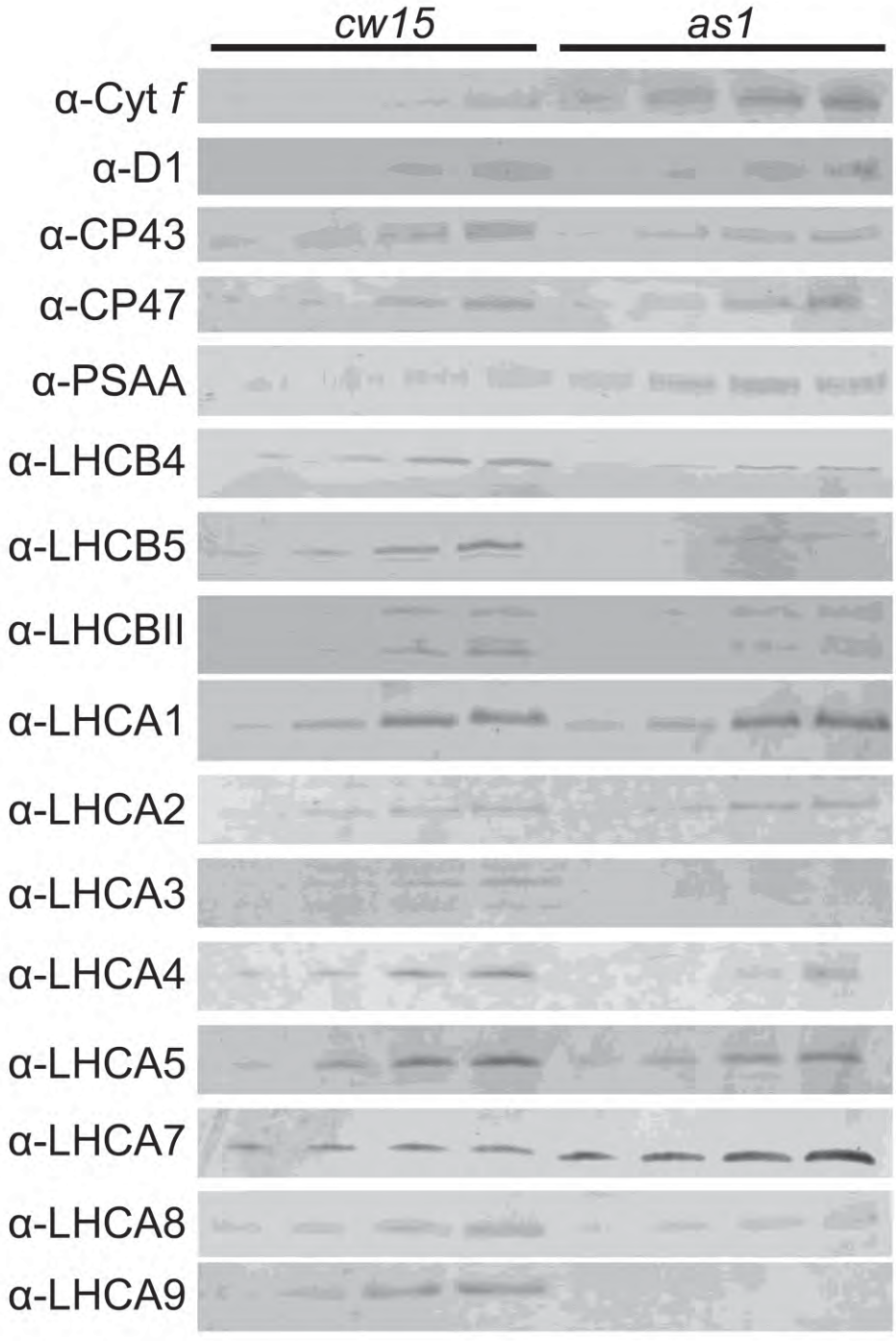

Figure S3. Reaction of the anti-ARSA1 antiserum against fractions from differential centrifugation upon disruption of *Chlamydomonas* cells as described in materials and methods. Each lane was loaded with 10 μg protein. The 3.000xg pellet also contains unbroken cells..

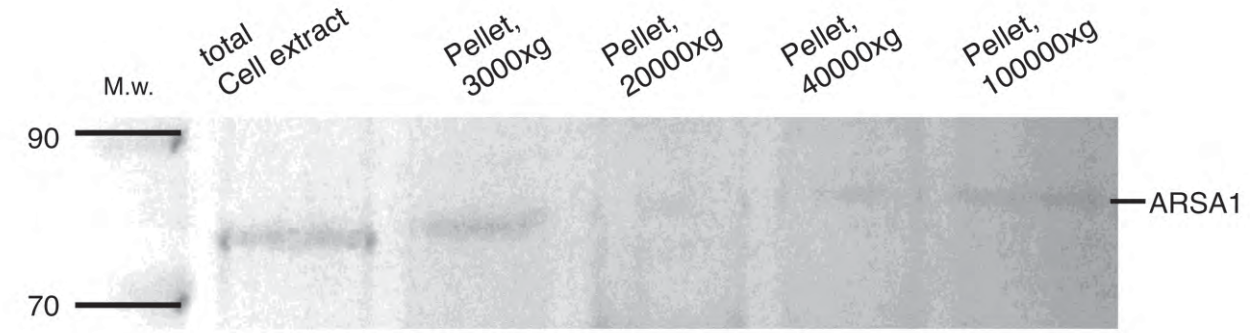

Figure S4. Reaction of the anti-ARSA1 antiserum (1:4000) versus *cw15* and *as1* total cell extract (10μg protein per lane) and versus ARSA1 recombinant protein (1 ug) purified from *E.coli* by Ni++ column. The band recognized by the antibody in the *cw15* has the same mobility of the ARSA1 recombinant protein.

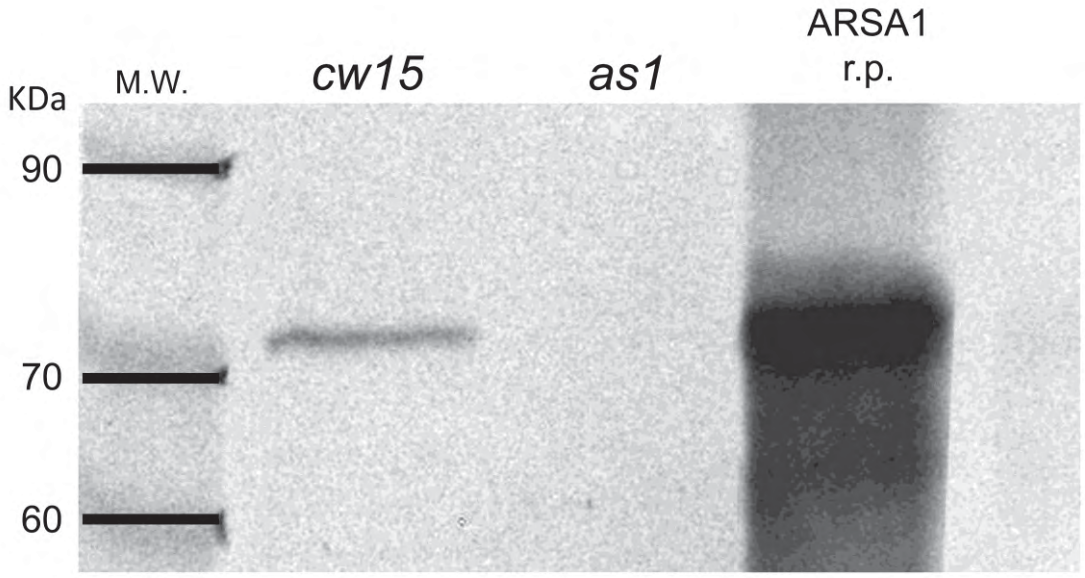

Table S1. primers used to characterise the *arsA1* mutation and for cloning and expression of recombinant ARSA1 in *E. coli*.

Oligo	**Sequence**
ARSA1_Fw CDS3’	5′- CGAGCATGGAGGACGCCAAGG-3′
ARSA1_Rv CDS3’	5′- GCCACCAACGCAACCATGCG-3′
ARSA1_Fw Gen5’	5′- CACAAGCGTCTTTCGTGCGGG -3′
ARSA1_Rv Gen5’	5′- GCAGCTTGTGGCTTCGCTAGGT -3′
ARSA1_Fw Gen3’	5'- CGCAACCAGCAGACCACCGA-3'
ARSA1_Rv Gen3’	5'- GGCGGGGGCAACTCAGCAAA-3'
ARSA1_FwBamHI	5’- AGGATCCGTGCGCTGCCGTGCCGACGGT-3’
ARSA1_RvHindIII	5’- TAAGCTTGTTGCCGAAGTACGACAGCG-3’

Conclusions

During my PhD I used reverse genetic on the model organism *A. thaliana* to identify and characterize components of the photoprotection machinery and determinant of thylakoid membrane organization that prevents photodamage. Among these mechanisms the thermal dissipation of energy absorbed in excess (NPQ) is of particular interest. Over the past decades many efforts have been made to elucidate the mechanisms underlying these processes and yet advancements proved difficult due to the complexity of the system. Nevertheless, I tried to shed light on photoprotection.

1. Role of carotenoids in photoprotection and biogenesis of photosynthetic complexes.

Mutant with altered composition or completely lacking xanthophylls were generated and analyzed to understand the role of these pigments in photoprotection and organization of photosynthetic complexes. These were also useful to further understand the catalytic activity of the enzymes involved in the downstream section of carotenoid biosynthesis pathway.

1.1 Reduced xanthophyll content negatively affects photoprotection and NPQ

A. thaliana mutants depleted in xanthophylls suffer from a strong photosensitivity. The *nox* mutant was lethal when seedlings were grown on soil and could survive in sucrose-supplemented medium under dim light only (20 µmol photons m^{-2} s^{-1}). The effect was stronger on PSI with respect to PSII. A major feature of these mutants is the depletion in LHC proteins, consistent with the evidence that xanthophylls are needed for folding of LHC complexes in vitro (Plumley and Schmidt 1987). The extreme photosensitive phenotype implies that functional LHC complexes are essential for photoprotection, consistent with previous reports (Dall'Osto et al. 2010). The *chy1chy2lut2lut5 and nox* mutants showed a stronger decrease in LHCB proteins *vs* PSII core, while LHCA assembly into PSI-LHCI is much less, or not at all, affected. This effect is likely due to the incapacity of LHCB proteins to fold in the absence of xanthophylls, while LHCA proteins can also bind β-carotene (Morosinotto et al. 2002, Mozzo et al. 2006). Having said so, the reduced LHC content cannot be the only reason for the extreme light sensitivity since *ch1* mutation (blocked in Chl *b* biosynthesis), although preventing assembly of LHCs allows for growth on soil and resists to moderate light (Havaux et al. 2007).

The capacity for excess energy dissipation into heat (qE mechanism) is strongly reduced in the absence of xanthophylls. Since the level of PSBS is not reduced with respect to wild type, qE depletion can thus be attributed to a lack of PSBS-interacting partners, namely, the LHCB proteins. These results support the correlation between xanthophyll content and qE amplitude, previously suggested on the basis of antisense inhibition of β-hydroxylation (Pogson and Rissler 2000). As for the role in photoprotection, the *npq4* mutation abolished qE in *A. thaliana* but has a modest impact on the photosensitivity in vivo, just a fraction of the effect observed upon decreasing the level of xanthophylls (Li et al. 2002). The differential resistance of wild type versus *nox* plants cannot be attributed to NPQ depletion or LHCB depletion. Rather, the decreased efficiency of photosynthetic electron transport, higher photoinhibition, and lethality in soil are to be ascribed to a severe deficiency in PSI.

1.2 Limitation in total xanthophyll availability affects light-harvesting complex content and PSI/PSII ratio

Immunotitration analysis on different genotypes impaired in carotenoids biosynthesis evidenced that the decrease in xanthophyll/carotenoid ratio causes a proportional decrease in the abundance of PSI core units with respect to PSII. This result was surprising, since there is no evident reason for the preferential effect of xanthophyll depletion on PSI with respect to PSII core complexes: in fact both PSII and PSI core complexes bind chlorophyll *a* and β-carotene as the only pigments (Nelson and Ben Shem 2004). These co-factors are not limiting in *all* genotypes carrying mutations affecting xanthophyll biosynthesis. This is especially evident in the *nox* mutant that is defective in PSI accumulation with a level of PSI of 10% with respect to wild type. Our results showed that the PSI depletion is not due limitations in Fe-S cofactor or to lack in protein subunits involved in PSI assembly.

One possibility is that xanthophylls, or their metabolites and catabolites, control either PSI synthesis or degradation. PSI genes in *nox* mutant were not impaired at transcriptional level, mRNA stability or intron splicing and RNA maturation. The reduction in PSAA/B post-transcriptional synthesis and its accelerated degradation both appear to be the major reasons for the absence of the PSI core complex in *nox*. At present, the functional target controlling the stoichiometric relation between impaired translation of PSAA/B and the lack of xanthophylls is still unclear. Nevertheless it is interesting to consider the implications that this regulation has on the function of the photosynthetic apparatus during acclimation to different light regimes:

a) The well known regulation of xanthophyll/carotene ratio in HL reflects into up-regulation of PSI level/activity thus preventing PQ over-reduction and protecting from photoinhibition (Chow et al. 1990, Ballottari et al. 2007);

b) While PSII reaction centres are subjected to rapid turn-over and their level readily adjusts to environmental conditions, PSI is much more stable, thus requiring specific mechanisms for its down-regulation in limiting light. LHCBs bind large amounts of xanthophylls and are strongly regulated depending on light intensity. Coupling PSI to xanthophyll levels provides a mechanism for coordinated regulation of PSII antenna size and PSI/PSII ratio (Dietzel et al. 2008).

1.3 LUT1 as a β-carotene hydroxylase

LUT1 was originally reported to be the only gene product required for the ε-ring hydroxylation of α-carotene (Kim et al. 2009). During my PhD we showed that, in the absence of α-carotene, LUT1 shows a major β-carotene hydroxylase activity, leading to the accumulation of substantial amounts of β-β-xanthophylls. This enzyme has a higher affinity towards ε-rings *vs*. β-rings and, when α-carotene is available, LUT1 performs mainly ε-ring hydroxylation; however, since no ε-ring-substrates are available in the *chy1chy2lut2lut5 mutant*, the β-ring substrates are processed, thus bringing out this minor activity of the enzyme. Conversely, in the absence of the main hydroxylases for β-rings CHY1, CHY2 and LUT5, all β-rings become available for LUT1 activity. A consequence of LUT1 operation on a less preferred substrate is its reduced overall catalytic rate that limits the level of xanthophylls accumulated. This evidence updates our knowledge on the molecular details of carotenoid hydroxylases, with respect to the view that LUT1 has only a low level of *in vivo* hydroxylase activity toward the β-carotene and a stronger activity towards α-carotene.

1.4 Role of β-Carotene in photosystem I photoprotection.

The *szl1* plants, which carry a point mutation in the Lcyb gene and thus a less-active β-cyclase than the wild type, have lower carotene content in both PSII and PSI with respect to wild-type plants (-40% and -30% respectively). Physiological characterization of the *szl1* mutant offered for the first time the possibility of probing carotene function in vivo differentially from the effect on xanthophylls complement.

Grown in control condition the *szl1* plants showed the same leaf morphology and development rate with respect to wild type. Carotene depletion does not affect photosynthetic transport rate since the ETR and ΔpH generation is similar to wild type. When challenged with HL and cold stress, *szl1* plants undergo more photodamage than the wild type. Fluorescence and spectroscopy analysis evidenced that the damage is higher within the PSI-LHCI complex as confirmed by thylakoids membrane fractionation and

single complex analysis. Comparison with the *chy1chy2* and *lut5* mutants, which share with *szl1* alterations in xanthophyll composition and α-carotene accumulation and qE reduction, showed that these features were not the major factors causing enhanced susceptibility to photoinhibition rather the carotene depletion in photosynthetic core complexes was the major source of photodamage.

In *szl1* plants, a general weakening of the PSI-LHCI structure would make the complex more susceptible to HL attack thus causing degradation. The recent improved model of PSI plant structure suggested that β-carotene molecules are coordinated by different subunits or different regions of the same subunit; therefore this pigment has a key role in preserving PSI structural integrity (Amunts et al. 2010). Besides β-carotene can act as an effective quencher and scavenger of singlet oxygen produced in the PSI core as it has been shown for PSII (Telfer et al. 1994, Ferreira et al. 2004), thus the decrease amount of this pigment in the *szl1* mutant can increase photodamage to PSI.

Alternatively, rather than the PSI core complex, the peripheral light-harvesting system might be more affected by carotene depletion. β-carotene is not only a ligand for the core but also for the LHCI. LHCA proteins play a dual role PSI photoprotection: first, a PSI with an intact antenna system is more resistant to HL because of a reduced production of reactive oxygen species and, second, antenna chlorophyll-proteins are the first target of HL damages (Alboresi et al. 2009). When photoprotection mechanisms become insufficient, the antenna proteins act as fuses: LHCI chlorophylls are degraded while the reaction centre photochemical activity is maintained. Recovery from PSI photoinhibition is an energetically demanding process, since it necessarily requires degradation and re-synthesis of the whole complex; thus, sacrificial photodamage of the antennae is a photoprotective strategy evolved to limit photo-oxidative damage into the PSI core moiety and preserve the integrity of iron-sulfur clusters. In the *szl1* mutant, impairing one of these functions by changing the occupancy of specific carotenoid binding sites through mutations in the biosynthetic pathway leads to photosensitivity, similar to what observed previously within PSII antenna system (Dall'Osto et al. 2007).

1.4 Photoprotective effect of zeaxanthin on modulation of chlorophyll triplet yield

During my PhD we have scrutinized the mechanism by which zeaxanthin exerts its photoprotective effect. Zea is the only xanthophyll species specially synthesized in response to HL conditions and previous work have emphasized its enhancing effect on qE (Niyogi et al. 1998) and the scavenging action of free Zea on the ROS released by chlorophylls upon excess irradiation (Havaux and Niyogi 1999). Although these functions contribute to the Zea photoprotective effect, genetic dissection using the *npq4* mutant lacking qE showed that thermal dissipation of excess energy has a relatively small effect (Li et al. 2002) as well as the scavenging effect of lipid-free Zea with respect to the LHC-bound fraction. This implies that the Zea-

dependent photoprotection effect is associated to the binding of Zea to LHC proteins, where it has a strong effect in decreasing $^1O_2$ evolution during illumination. We used high sensitivity laser spectroscopy to investigate changes in the optical properties of leaves associated with EL treatment. Illumination of *A. thaliana* wild type plants induced a spectral red shift of the $T_2 \leftarrow T_1$ transition of ^{3}Car*. Using a range of *A. thaliana* mutants, this spectroscopic feature was observed only in genotypes able to accumulate Zea, either upon EL exposure or constitutively, irrespective of their ability to perform qE.

Fractionation of thylakoids membranes allowed the detection of this signal changes were in specific minor LHC subunits and in LHCI but not in the major LHCII antenna complex. The resistance/sensitivity of these proteins to HL conditions showed that the red shift is correlated with the dominant component of photoprotection, in absence of which monomeric antennae are preferentially destroyed. These protective effect did not depend on an increased efficiency of ^{3}Chl* quenching by xanthophylls bound to LHCB proteins. Fluorescence-detected magnetic resonance showed that this photoprotective mechanism consist with a direct down-regulation of ^{3}Chl* production without a corresponding enhancement of carotenoid triplet quenching. Our laboratory previously showed that CP26 undergoes a conformational change after binding Zea (Dall'Osto et al. 2005). This conformational change, by affecting Chl/Chl interactions or Chl/protein interaction, can modulate the triplet yield. These results show that the high-light binding of Zea to specific antenna protein plays a major role in enhancing photoprotection by modulating the yield of potentially dangerous chlorophyll-excited states *in vivo* and preventing the formation of singlet oxygen.

2 Light energy transfer in Arabidopsis thaliana mutants lacking minor antenna complexes

The monomeric antennae CP24, CP26, and CP29 are three of the six light-harvesting subunits that compose the PSII peripheral antenna system of higher plants. Minor antennae are located between LHCII and the RC and are crucial for facilitating the energy transfer from LHCII to the core subunit (Caffarri et al. 2009). A long standing discussion has been developed on whether the site of the photoprotection mechanism, including protection from photo-oxidation and excitation energy quenching (NPQ), was located within the monomeric antenna proteins or in the major light harvesting complex (Horton et al. 2005, de Bianchi et al. 2008, de Bianchi et al. 2011). In order to investigate the role of individual monomeric LHCBs, we used a reverse genetic approach with the aim to obtain a mutant devoid of all the minor LHCB subunits, the *NoM*. In this thesis I present the first data on the characterization of this mutant.

Fluorescence kinetics and biochemical results show that the missing minor complexes are not replaced by other LHCs, implying that they are unique among the antenna subunits and crucial for the

functioning and macro-organization of PSII. Although these pigment-protein complexes are homologous and are expected to share a common three-dimensional organization (Pan et al. 2011), they cannot be exchanged between each other in the supercomplexes. In thylakoids of *NoM*, the loss of all minor LHCs is accompanied by an over-accumulation of LHCII, suggesting a compensating response to the reduced trapping efficiency in limiting light, which leads to a photosynthetic phenotype resembling that of low-light-acclimated plants. Accumulation of a large amount of disconnected antenna proteins suggests that LHCII is independently folded into membranes, irrespective from its assembly with the PSII core complex in further steps. Therefore, even when assembly is prevented, LHCII is stable in the membrane and does not undergo proteolytic degradation.

The pigment content of mutant thylakoids showed a significant decrease in the Chl *a*/Chl *b* ratio with respect to the membranes from wild type, reflecting the relative increase in outer antenna components (namely LHCII). The PSI/PSII ratio was essentially the same as in the wild type, while the LHCII/PSII showed an increase by 45%. The *NoM* mutant lacked the antenna complex CP29/CP24/LHCII and was completely devoid of PSII supercomplexes. Picosecond-fluorescence spectroscopy revealed that the removal of two or more different monomeric LHCBs increased the trapping time of excitons in the RCs substantially as compared to wild type thylakoids meaning that the absence of monomeric antenna complexes leads to badly connected or LHCII disconnected from PSII supercomplexes. A large part of this LHCII has a long excited-state lifetime although far shorter than the 4 ns of isolated LHCII trimers indicating that the detached LHCII is not equivalent to LHCII in detergent solution and that its environment induces a shortening of its excited-state lifetime. Among the mutants missing different combination of minor antennae, the most explicit slowdown of the fluorescence kinetics is observed for the *NoM* mutant. The average lifetime of PSII-LHCII for the *NoM* mutant is 2.3 times longer than the average lifetime of PSII-LHCII for wild type.

The disconnected LHCII in the *NoM* leads to a strong impairment of PSII light-use efficiency and a reduced growth under continuous-light conditions. In *koCP26/24* and *koCP29/24* mutants, it appears that only one LHCII trimer is directly connected to the PSII core whereas all other trimers are interspersed between the supercomplexes and still lead to relatively good excitation energy transfer (EET), not hampering plant growth. A key consideration for the efficiency of primary productivity in plants and algae is the size of the light-harvesting system that has to be reduced in order to decrease the absorption cross section to enhance light penetration and increases the size of metabolic sinks per chlorophyll unit. Our data show that depletion of the monomeric sub-type of LHCs strongly affects the PSII light-harvesting efficiency and thus the photoautotrophic growth. To ensure that truncated-antenna strains will operate with improved light use efficiency, biotechnological approaches aimed at reducing antenna cross-section must focus on trimeric LHCII, rather than monomeric LHCB.

3 Role of chloroplast relocation in photoprotection and its contribute in defining NPQ kinetic.

The *phot2* mutant lacks PHOT2, the blue-light photoreceptor responsible for chloroplast photorelocation, and its chloroplasts remains always aligned on periclinal cell walls regardless of light intensity (Kagawa et al. 2001). Although the photoprotective action of chloroplast avoidance, NPQ or Zea synthesis has been previously investigated, their relative contribution to photosynthetic efficiency in excessive light is unknown. I evaluated their relative photoprotective effect under excess light. During these analyses we also elucidated new aspects of the apparent NPQ kinetic as previously described by PAM fluorometry.

3.1 Photoprotective function of chloroplast avoidance with the respect to Zeaxanthin and NPQ.

The results presented in this thesis show that photorelocation provide a crucial photoprotection effect in HL conditions as compared to other major protective mechanisms. Suppression of the high light-induced chloroplast avoidance response enhanced oxidative stress under excess light, while removing either Zea or PSBS had a milder effect. This suggests that chloroplast avoidance movement is more effective in photoprotection than NPQ or xanthophyll cycle. The double mutants *phot2npq1* and *phot2npq4* showed the highest sensitivity to photooxidative stress, implying Zea, qE and avoidance response independently contribute to counteract photooxidative stress *in vivo*. The avoidance mechanism changes the distribution of photoinhibition profile through cell layers in leaf sections. Therefore, chloroplast photorelocation is aimed to two targets: maximize photosynthesis through higher light penetration and distribute PSII damage among different leaf cell layers reduce the maximal extent of inhibition suffered by individual chloroplasts and prevent the depression of photosynthetic efficiency in a single cell.

The NPQ kinetic of *phot2* lacked a component that is intermediate between the very fast qE phase ($\tau_{½}$ ~1 min) (Niyogi 2000) and the long qI phase ($\tau_{½}$ longer than 60 min) (Anderson et al. 1997). This kinetic component linearly correlated with the leaf transmittance changes due to chloroplast relocation induced by blue light. The same contribution was induced in wild type by white light but not by red light actinic excitation. Comparative analysis of different mutants showed that this kinetic component was not related to qE activity, to Zea accumulation or to altered state transitions. Rather, it depended on the activity of the chloroplast relocation process mediated by the blue light receptors phototropins. This kinetic component represents a light-induced decrease in photon absorption, which yields into a decrease in fluorescence yield, rather than the building up of a genuine quenching process. During illumination, chloroplast

movement towards the anticlinal cell walls changed the distribution of pigments with the formation of areas with extremely high absorption due to the formation of localized chloroplast stacks. This produces a 'sieve effect' which reduces the photon dose absorbed by the ensemble of chloroplasts, thus yielding into a reduced Chl fluorescence emission. In fluorometry measurements this event can easily be interpreted as a fluorescence quenching. In synthesis, a progressive decrease in fluorescence intensity will accompany chloroplast photorelocation movements. This yields into an apparent F_m quenching component that adds to the fluorescence decrease due to NPQ. We called this component as qM.

3.2 Analysis of the qM component in *npq4* mutants.

Although the existence of a middle-phase kinetic component of NPQ had been reported previously (Walters and Horton 1991, Nilkens et al. 2010), its physiological origin is still debated; we analyzed it in mutants depleted of PSBS, where the qE phase is absent thus easing the kinetic dissection.

qM exhibited the same amplitude in both wild type and *npq4* mutants; it was uncoupler-sensitive and unaffected by PSII repair or mitochondrial ATP synthesis inhibitors. Targeted reverse genetic analysis showed that traits affecting composition of the photosynthetic apparatus, carotenoid biosynthesis and state transitions did not affect qM. The intermediate component has been previously defined as qT or qZ for its possible dependence on state transitions or Zea biosynthesis, respectively. However, data reported here show that blocking these processes with specific mutations does not interfere with qM.

Among all the mutations introduced into the *npq4* genetic background, *phot2* was the only one that affected qM. Differences in *npq4 vs npq4phot2* NPQ kinetics showed that the fluorescence recovery component is affected by chloroplast photorelocation. Chloroplast relocation significantly influences the apparent kinetics of NPQ even if this effect arises from decreased photon absorption which gives a lower fluorescence yield, rather than from a genuine quenching process.

Light microscopy analysis confirmed that movement of chloroplasts was inhibited in the presence of nigericin, consistent with the depletion in qM. The chloroplast avoidance response probably relies on the cytosolic Ca^{2+} signal for its activation (Suetsugu and Wada 2007). Maintenance of a low cytosolic Ca^{2+} level requires an electrogenic pump which exploits, protonmotive force to actively extrude Ca^{2+} (Ettinger et al. 1999). Phototropin signal transduction involves transient depolarization of the plasma membrane which, in turn, triggers cytosolic Ca^{2+} intake. Nigericin wrecks all the transmembrane electrochemical gradients, thus blocking several signal transduction events. The double effect of nigericin in collapsing the thylakoid pH gradient and in blocking chloroplast relocation can easily lead to misinterpretation of qM as a slow qE response in the absence of PSBS.

Although chloroplast relocation is the major factor affecting the amplitude of qM in *npq4*, the fluorescence recovery kinetics of *npq4phot2* are not completely devoid of qM. The residual component accounts for about 18% of total reversible quenching in wild type and reflects mechanism(s) sensitive to uncouplers and yet distinct from the avoidance response.

It was previously proposed that *npq4* does perform qE-type quenching, although at lower rate than wild type (Johnson and Ruban 2010). Our results support the view that no qE occurs in *npq4* leaves within a wide range of actinic light intensities; light-induced fluorescence decline in *npq4* was always far lower than in wild type plants, even upon 1 h of EL exposure. Overall, these results point to a crucial role of PSBS in the modulation of NPQ and show that sensing of trans-thylakoid ΔpH by protonatable residues in the LHC antenna subunits is not enough to fully induce NPQ in the absence of PSBS. Thus, PSBS is indispensable for qE rather than being only a modulator of the proton-antenna association constant, p*K*.

4 Reduction of antenna size to improves light-use efficiency in a photobioreactor.

The study of photosynthetic membrane organization, photoprotection and the dissection of NPQ mechanism is not only academic curiosity; their regulation could become a key point in increasing stress resistance and productivity for food and fuels. A key consideration for the efficiency of primary productivity in plants and algae is the size of the light-harvesting system. Ort, and Melis have proposed antenna size reduction as a valuable strategy for the optimization of the light reactions (Ort et al. 2011). Biomass yield of microalgae cultures at industrial scale is currently limited by several biological constraints, including the uneven light distribution into photobioreactors (Weyer et al. 2010); therefore, the successful implementation of biofuel production facilities requires domestication strategies, such as decreasing the absorption cross section to enhance light penetration and increase the size of metabolic sinks per chlorophyll.

During my PhD we applied random mutagenesis and phenotypic selection to *C. sorokiniana*. Truncated antenna mutants (*TAMs*) were selected that exhibited a lower fluorescence yield than the wild type strain. The *TAM-2* mutant had approximately half of LHCII complement per PSII with respect to the wild type. In both laboratory-scale and outdoor photobioreactors this mutant showed higher productivity than wild type, with a 30% higher biomass yield in dense cell suspensions typical of industrial photobioreactors. This result suggest that rigorous application principles obtained from our knowledge of

breeding of oxygenic organisms actually provides a suitable pathway to improve photosynthetic efficiency, a plant function that has so far escaped improvement during domestication.

Reference list

Alboresi, A., M. Ballottari, R. Hienerwadel, G. M. Giacometti and T. Morosinotto (2009). "Antenna complexes protect Photosystem I from photoinhibition." BMC.Plant Biol. **9**: 71.

Amunts, A., H. Toporik, A. Borovikova and N. Nelson (2010). "Structure determination and improved model of plant Photosystem I." J.Biol Chem. **285**(5): 3478-3486.

Anderson, J. M., Y. I. Park and W. S. Chow (1997). "Photoinactivation and photoprotection of photosystem II in nature." Physiol.Plant. **100**(2): 214-223.

Ballottari, M., L. Dall'Osto, T. Morosinotto and R. Bassi (2007). "Contrasting behavior of higher plant photosystem I and II antenna systems during acclimation." Journal of Biological Chemistry **282**(12): 8947-8958.

Caffarri, S., R. Kouril, S. Kereiche, E. J. Boekema and R. Croce (2009). "Functional architecture of higher plant photosystem II supercomplexes." EMBO J. **28**: 3052-3063.

Chow, W. S., A. Melis and J. M. Anderson (1990). "Adjustments of photosystem stoichiometry in chloroplasts improve the quantum efficiency of photosynthesis." Proc.Natl.Acad.Sci.U.S.A **87**(19): 7502-7506.

Dall'Osto, L., S. Caffarri and R. Bassi (2005). "A mechanism of nonphotochemical energy dissipation, independent from Psbs, revealed by a conformational change in the antenna protein CP26." Plant Cell **17**(4): 1217-1232.

Dall'Osto, L., S. Cazzaniga, M. Havaux and R. Bassi (2010). "Enhanced photoprotection by protein-bound vs free xanthophyll pools: a comparative analysis of chlorophyll b and xanthophyll biosynthesis mutants." Mol.Plant **3**(3): 576-593.

Dall'Osto, L., A. Fiore, S. Cazzaniga, G. Giuliano and R. Bassi (2007). "Different roles of α- and β-branch xanthophylls in photosystem assembly and photoprotection." J.Biol.Chem. **282**(48): 35056-35068.

de Bianchi, S., N. Betterle, R. Kouril, S. Cazzaniga, E. Boekema, R. Bassi and L. Dall'Osto (2011). "*Arabidopsis* mutants deleted in the light-harvesting protein Lhcb4 have a disrupted Photosystem II macrostructure and are defective in photoprotection." Plant Cell **23**(7): 2659-2679.

de Bianchi, S., L. Dall'Osto, G. Tognon, T. Morosinotto and R. Bassi (2008). "Minor antenna proteins CP24 and CP26 affect the interactions between photosystem II subunits and the electron transport rate in grana membranes of Arabidopsis." Plant Cell **20**: 1012-1028.

Dietzel, L., K. Brautigam and T. Pfannschmidt (2008). "Photosynthetic acclimation: state transitions and adjustment of photosystem stoichiometry--functional relationships between short-term and long-term light quality acclimation in plants." FEBS J. **275**(6): 1080-1088.

Ettinger, W. F., A. M. Clear, K. J. Fanning and M. L. Peck (1999). "Identification of a Ca2+/H+ antiport in the plant chloroplast thylakoid membrane." Plant Physiol. **119**(4): 1379-1386.

Ferreira, K. N., T. M. Iverson, K. Maghlaoui, J. Barber and S. Iwata (2004). "Architecture of the photosynthetic oxygen-evolving center." Science **303**(5665): 1831-1838.

Havaux, M., L. Dall'Osto and R. Bassi (2007). "Zeaxanthin has enhanced antioxidant capacity with respect to all other xanthophylls in Arabidopsis leaves and functions independent of binding to PSII antennae." Plant Physiol **145**: 1506-1520.

Havaux, M. and K. K. Niyogi (1999). "The violaxanthin cycle protects plants from photooxidative damage by more than one mechanism." Proc.Natl.Acad.Sci.U.S.A **96**(15): 8762-8767.

Horton, P., M. Wentworth and A. Ruban (2005). "Control of the light harvesting function of chloroplast membranes: the LHCII-aggregation model for non-photochemical quenching." FEBS Lett. **579**(20): 4201-4206.

Johnson, M. P. and A. V. Ruban (2010). "Arabidopsis plants lacking PsbS protein possess photoprotective energy dissipation." Plant J. **61**(2): 283-289.

Kagawa, T., T. Sakai, N. Suetsugu, K. Oikawa, S. Ishiguro, T. Kato, S. Tabata, K. Okada and M. Wada (2001). "Arabidopsis NPL1: A phototropin homolog controlling the chloroplast high-light avoidance response." Science **291**(5511): 2138-2141.

Kim, J., J. J. Smith, L. Tian and D. DellaPenna (2009). "The evolution and function of carotenoid hydroxylases in Arabidopsis." Plant Cell Physiol **50**(3): 463-479.

Li, X. P., P. Muller-Moule, A. M. Gilmore and K. K. Niyogi (2002). "PsbS-dependent enhancement of feedback de-excitation protects photosystem II from photoinhibition." Proc.Natl.Acad.Sci.U.S.A **99**(23): 15222-15227.

Morosinotto, T., S. Castelletti, J. Breton, R. Bassi and R. Croce (2002). "Mutation analysis of Lhca1 antenna complex. Low energy absorption forms originate from pigment-pigment interactions." J.Biol.Chem. **277**(39): 36253-36261.

Mozzo, M., T. Morosinotto, R. Bassi and R. Croce (2006). "Probing the structure of Lhca3 by mutation analysis." Biochim.Biophys.Acta **1757**(12): 1607-1613.

Nelson, N. and A. Ben Shem (2004). "The complex architecture of oxygenic photosynthesis." Nature **5**: 1-12.

Nilkens, M., E. Kress, P. Lambrev, Y. Miloslavina, M. Muller, A. R. Holzwarth and P. Jahns (2010). "Identification of a slowly inducible zeaxanthin-dependent component of non-photochemical quenching of chlorophyll fluorescence generated under steady-state conditions in Arabidopsis." Biochim.Biophys.Acta **1797**(4): 466-475.

Niyogi, K. K. (2000). "Safety valves for photosynthesis." Curr.Opin.Plant Biol. **3**(6): 455-460.

Niyogi, K. K., A. R. Grossman and O. Björkman (1998). "Arabidopsis mutants define a central role for the xanthophyll cycle in the regulation of photosynthetic energy conversion." Plant Cell **10**: 1121-1134.

Ort, D. R., X. G. Zhu and A. Melis (2011). "Optimizing antenna size to maximize photosynthetic efficiency." Plant Physiol. **155**: 79-85.

Pan, X., M. Li, T. Wan, L. Wang, C. Jia, Z. Hou, X. Zhao, J. Zhang and W. Chang (2011). "Structural insights into energy regulation of light-harvesting complex CP29 from spinach." Nat.Struct.Mol.Biol. **18**(3): 309-315.

Plumley, F. G. and G. W. Schmidt (1987). "Reconstitution of chloroform a/b light-harvesting complexes: Xanthophyll-dependent assembley and energy transfer." Proc.Natl.Acad.Sci.U.S.A **84**: 146-150.

Pogson, B. and H. M. Rissler (2000). "Genetic manipulation of carotenoid biosynthesis and photoprotection." Phil.Trans.R.Soc.Lond.B **355**: 1395-1403.

Suetsugu, N. and M. Wada (2007). "Chloroplast photorelocation movement mediated by phototropin family proteins in green plants." Biol.Chem. **388**: 927-935.

Telfer, A., S. Dhami, S. M. Bishop, D. Phillips and J. Barber (1994). "β-carotene quenches singlet oxygen formed by isolated photosystem II reaction centers." Biochemistry **33**: 14469-14474.

Walters, R. G. and P. Horton (1991). "Resolution of components of non-photochemical chlorophyll fluorescence quenching in barley leaves." Photosynth.Res. **27**: 121-133.

Weyer, K. M., D. R. Bush, A. Darzins and B. D. Willson (2010). "Theoretical maximum algal oil production." Bioenerg.Res. **3**: 204-213.